frontiers | Research Topics

Community series in the role of angiogenesis and immune response in tumor microenvironment of solid tumor, volume II

Edited by
Xi Cheng, Ren Zhao and Xin Lu

Published in
Frontiers in Immunology

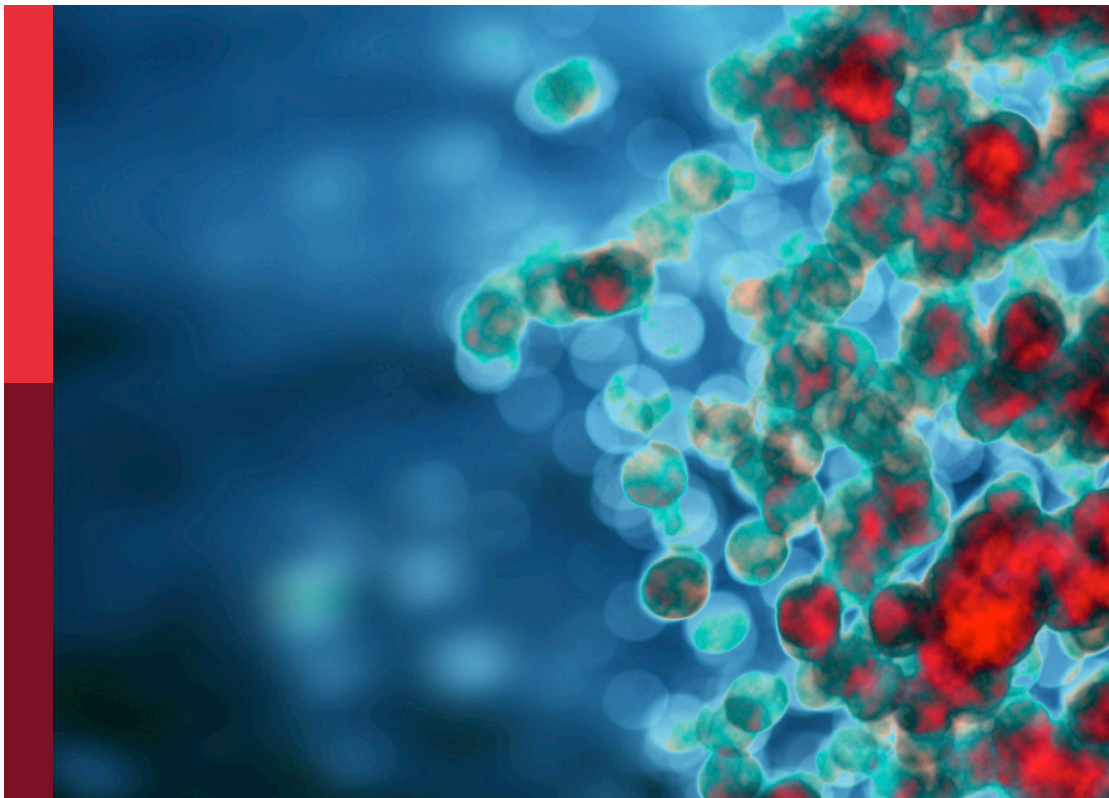

FRONTIERS EBOOK COPYRIGHT STATEMENT

The copyright in the text of individual articles in this ebook is the property of their respective authors or their respective institutions or funders. The copyright in graphics and images within each article may be subject to copyright of other parties. In both cases this is subject to a license granted to Frontiers.

The compilation of articles constituting this ebook is the property of Frontiers.

Each article within this ebook, and the ebook itself, are published under the most recent version of the Creative Commons CC-BY licence. The version current at the date of publication of this ebook is CC-BY 4.0. If the CC-BY licence is updated, the licence granted by Frontiers is automatically updated to the new version.

When exercising any right under the CC-BY licence, Frontiers must be attributed as the original publisher of the article or ebook, as applicable.

Authors have the responsibility of ensuring that any graphics or other materials which are the property of others may be included in the CC-BY licence, but this should be checked before relying on the CC-BY licence to reproduce those materials. Any copyright notices relating to those materials must be complied with.

Copyright and source acknowledgement notices may not be removed and must be displayed in any copy, derivative work or partial copy which includes the elements in question.

All copyright, and all rights therein, are protected by national and international copyright laws. The above represents a summary only. For further information please read Frontiers' Conditions for Website Use and Copyright Statement, and the applicable CC-BY licence.

ISSN 1664-8714
ISBN 978-2-8325-4082-4
DOI 10.3389/978-2-8325-4082-4

About Frontiers

Frontiers is more than just an open access publisher of scholarly articles: it is a pioneering approach to the world of academia, radically improving the way scholarly research is managed. The grand vision of Frontiers is a world where all people have an equal opportunity to seek, share and generate knowledge. Frontiers provides immediate and permanent online open access to all its publications, but this alone is not enough to realize our grand goals.

Frontiers journal series

The Frontiers journal series is a multi-tier and interdisciplinary set of open-access, online journals, promising a paradigm shift from the current review, selection and dissemination processes in academic publishing. All Frontiers journals are driven by researchers for researchers; therefore, they constitute a service to the scholarly community. At the same time, the *Frontiers journal series* operates on a revolutionary invention, the tiered publishing system, initially addressing specific communities of scholars, and gradually climbing up to broader public understanding, thus serving the interests of the lay society, too.

Dedication to quality

Each Frontiers article is a landmark of the highest quality, thanks to genuinely collaborative interactions between authors and review editors, who include some of the world's best academicians. Research must be certified by peers before entering a stream of knowledge that may eventually reach the public - and shape society; therefore, Frontiers only applies the most rigorous and unbiased reviews. Frontiers revolutionizes research publishing by freely delivering the most outstanding research, evaluated with no bias from both the academic and social point of view. By applying the most advanced information technologies, Frontiers is catapulting scholarly publishing into a new generation.

What are Frontiers Research Topics?

Frontiers Research Topics are very popular trademarks of the *Frontiers journals series*: they are collections of at least ten articles, all centered on a particular subject. With their unique mix of varied contributions from Original Research to Review Articles, Frontiers Research Topics unify the most influential researchers, the latest key findings and historical advances in a hot research area.

Find out more on how to host your own Frontiers Research Topic or contribute to one as an author by contacting the Frontiers editorial office: frontiersin.org/about/contact

Community series in the role of angiogenesis and immune response in tumor microenvironment of solid tumor, volume II

Topic editors

Xi Cheng — Shanghai Jiao Tong University, China

Ren Zhao — Shanghai Jiao Tong University, China

Xin Lu — University of Notre Dame, United States

Citation

Cheng, X., Zhao, R., Lu, X., eds. (2023). *Community series in the role of angiogenesis and immune response in tumor microenvironment of solid tumor, volume II*. Lausanne: Frontiers Media SA. doi: 10.3389/978-2-8325-4082-4

Table of contents

frontiers | Frontiers in Immunology

TYPE Editorial
PUBLISHED 22 November 2023
DOI 10.3389/fimmu.2023.1332519

Check for updates

OPEN ACCESS

EDITED AND REVIEWED BY
Juan José Lasarte,
University of Navarra, Spain

*CORRESPONDENCE
Xin Lu
xlu@nd.edu
Ren Zhao
rjzhaoren@139.com
Xi Cheng
drchengxi@126.com

†These authors have contributed equally to this work

RECEIVED 03 November 2023
ACCEPTED 16 November 2023
PUBLISHED 22 November 2023

CITATION
Li H, Yang Z, Lu X, Zhao R and Cheng X (2023) Editorial: Community series in the role of angiogenesis and immune response in tumor microenvironment of solid tumor: volume II. *Front. Immunol.* 14:1332519. doi: 10.3389/fimmu.2023.1332519

COPYRIGHT
© 2023 Li, Yang, Lu, Zhao and Cheng. This is an open-access article distributed under the terms of the Creative Commons Attribution License (CC BY). The use, distribution or reproduction in other forums is permitted, provided the original author(s) and the copyright owner(s) are credited and that the original publication in this journal is cited, in accordance with accepted academic practice. No use, distribution or reproduction is permitted which does not comply with these terms.

Editorial: Community series in the role of angiogenesis and immune response in tumor microenvironment of solid tumor: volume II

Haosheng Li[1,2†], Zheyu Yang[1,2†], Xin Lu[3*], Ren Zhao[1,2*] and Xi Cheng[1,2*]

[1]Department of General Surgery, Ruijin Hospital, Shanghai Jiao Tong University School of Medicine, Shanghai, China, [2]Shanghai Institute of Digestive Surgery, Ruijin Hospital, Shanghai Jiao Tong University School of Medicine, Shanghai, China, [3]Department of Biological Sciences, University of Notre Dame, Notre Dame, IN, United States

KEYWORDS

tumor microenvironment, angiogenesis, immune response, solid tumor, single cell sequence (scRNA-seq)

Editorial on the Research Topic:
Community series in the role of angiogenesis and immune response in tumor microenvironment of solid tumor: volume II

Introduction

As continually updated in "The Hallmarks of Cancer" by Hanahan and Weinberg, the tumor microenvironment (TME) is now widely recognized to play an indispensable role in tumorigenesis and malignant progression (1–3). This heterogeneous and interacting collective consists of cancer cells, cancer stem cells, and various recruited stromal cell types which include vascular cells, fibroblasts, diverse immune cells (lymphocytes, monocytes/macrophages, and inflammatory cells), and extracellular matrix (ECM) (4). Half a century ago, Folkman proposed that solid tumors rely on the formation of new blood vessels from the pre-existing vasculature within their tumor environment to provide adequate nutrients and oxygen supply, making anti-angiogenic therapy beneficial for cancer treatment (5). Subsequently, extensive research has identified anti-angiogenic therapy as a cornerstone of modern cancer therapy (6). Furthermore, research has continually revealed that tumor endothelial cells exhibit heterogeneity and plasticity, and angiogenic factors are closely associated with the inflammatory response during tumor development (7, 8). This complexity in tumor vasculature functionality implies a greater diversity of cell-cell interactions within the TME than initially expected (9). Regulatory immune cells also secrete various cytokines and pro-angiogenic factors, accelerating tumor progression (10). The advent of single-cell sequencing (scRNA-seq) provides a tool for

deciphering the tumor immune microenvironment. Compared to traditional methods, scRNA-seq can be employed to identify novel cell types and corresponding cellular states, deepening our understanding of the TME (11).

This special topic research, titled "Community Series in the Role of Angiogenesis and Immune Response in Tumor Microenvironment of Solid Tumor: Volume II", comprises 10 original research articles, 4 review articles, 1 case report, 1 method paper, and 1 perspective piece, totaling 17 original contributions. These articles elucidate the latest advances in tumor angiogenesis, the molecular mechanisms of tumor-infiltrating lymphocytes (TILs) in different malignancies, the functions and roles of other immune cells such as NK cells and regulatory T cells (Tregs), and the applications of scRNA-seq techniques. In this editorial, we will discuss these aspects, and aim to provide new insights into anti-tumor angiogenesis therapy, alterations in the immune microenvironment, as well as the regulation of immune responses.

Combining anti-angiogenic and immunotherapeutic approaches

Anti-angiogenic therapy stands as a viable tool for restoring immune cell infiltration within solid tumors, with combined therapies achieving greater success in immune-excluded and immune-desert tumors (12). Hu et al. provide an overview of the synergistic effects when anti-angiogenic agents are combined with immunotherapy in solid tumors, leading to improved drug resistance and cooperative inhibition of tumor growth and progression. Notably, this effect is observed in non-small-cell lung cancer, hepatocellular carcinoma, and renal cell carcinoma, as opposed to breast cancer, glioblastoma, and pancreatic ductal adenocarcinoma. To address efficacy concerns, the identification of sensitive biomarkers and the determination of appropriate combination dosages are imperative. These actions aim to augment immune cell infiltration and, consequently, enhance the effectiveness of immunotherapy. Shamshiripour et al. delve into the molecular mechanisms of abnormal angiogenesis in glioblastoma, discussing the applications and limitations of monoclonal antibodies, tyrosine kinase inhibitors, and aptamers in anti-angiogenic immunotherapy. Moreover, utilizing nanoparticles to deliver small interfering RNA (siRNA) across the blood-brain barrier represents a promising approach for the next generation of anti-angiogenic therapy, particularly in targeted brain delivery. Zhang et al. have identified a novel prognostic signature comprising four angiogenesis-related genes, AAG-related long non-coding RNAs (lncRNAs), including AC093278.2, NNT-AS1, CYTOR, and NUP50-DT, which serve as potential prognostic factors in clear cell renal cell carcinoma (KIRC). These lncRNAs show promise as independent prognostic indicators for KIRC patients. In a case report by Li et al., they document the case of a metastatic HCC patient who experienced recurrence post-surgery, and subsequently received a combination therapy of anti-angiogenic treatment and immune checkpoint inhibitors (lenvatinib and toripalimab). After seven months of treatment, the patient achieved complete remission, a status maintained until the paper's submission, with a final calculation of progression-free survival at 24 months. The synergistic effects of anti-angiogenic therapy, intratumoral cryoablation, and immunotherapy have yielded highly favorable outcomes for the patient, although the precise mechanisms behind this synergistic treatment approach remain to be elucidated.

Function and role of TILs

Immunocytes constitute a pivotal component within the intricate TME (13). The types and densities of TILs hold significant relevance for cancer progression and immunotherapeutic responses (14). Xiao et al. introduced the Tumor-Infiltration Immune Cell Proportion Estimator (TICPE) to estimate the proportions of immune cells in colorectal cancer and melanoma. Performance evaluations, which employed mRNA mixture expression data, scRNA-Seq data, immunohistochemistry data, and simulated bulk RNA-Seq samples, demonstrated its markedly superior accuracy compared to other methods. Cheng et al. observed that TILs and tertiary lymphoid structures (TLS) independently serve as prognostic factors in EBV-negative gastric cancer (EBVnGC), offering auxiliary indicators for gastric cancer prognosis. They established a nomogram model combining TILs grade and TLS status with other established prognostic factors, exhibiting good performance in calibration and external validation. Penny et al. identified 120 HLA-I phosphopeptides from primary CRC tumors, CRC liver metastases, and CRC cell lines using mass spectrometry. They evaluated the immune capacity of these post-translationally modified tumor antigens within tumors. PTM tumor antigens, namely HLA-I phosphopeptides, emerged as potential optimal targets for future immunotherapies, as they are targets for tumor-resident CD8 T cells. Wang et al. discovered a significant correlation between serum SDF-1 expression and TIL abundance in triple-negative breast cancer (TNBC) patients who underwent neoadjuvant chemotherapy (NAC) following standard radical surgery. SDF-1, when considered in conjunction with TILs, aids in identifying patients who would benefit from chemotherapy, thereby enhancing the pathological complete response (pCR) rate and preventing disease recurrence in non-pCR patients. Regarding TIL-based cancer therapy, Aydin et al. underscore the indispensability of identifying patients with bladder cancer (BC) who generate the optimal quantity of active TILs. Tumors in both primary and lymph node metastases in BC patients can produce tumor-specific TIL responses, justifying clinical trials to validate TILs as a rational treatment strategy for BC patients. Elkoshi proposes an explanation for the inverse correlation between tumor-infiltrating Tregs and survival in various cancer types. The frequency or proportion of Tregs and CD8+ T cells at the tumor site in the TME is mutually correlated. Consequently, this ratio exhibits less variation in frequency compared to both

lymphocyte populations separately. However, if one of these lymphocyte populations experiences substantial frequency fluctuations, opting for the lymphocyte population with lower frequency variation can enhance survival rates, particularly when the intra-tumor frequencies of the two lymphocyte types are inversely related. Selecting such optimal prognostic markers in this manner may also serve as the best predictive factor for cancer checkpoint inhibitor therapies.

ScRNA-seq reveals insights into the TME

ScRNA-seq technology enables a more comprehensive analysis of genetic and protein information differences between cells, allowing for the acquisition of individual cell genomic sequence information and a deeper investigation into the cellular characteristics and interactions within the TME (15). Wen et al. summarized the heterogeneity of the TME in colorectal cancer, highlighting the individualized and highly mutated nature of tumor epithelial cells in each patient. Various immune cells and inflammatory chemokines within the TME interact and influence one another, promoting tumor progression and thereby impacting tumor recurrence and treatment response. He et al. focused on the applications of scRNA-seq in revealing heterogeneity, microenvironment characteristics, and drug resistance in retinoblastoma (RB) and uveal melanoma (UM). This approach holds promise for identifying new biomarkers for diagnosis and targeted therapy. Ziblat et al. conducted phenotypic analysis of peripheral blood NK cells (PBNK) and tumor-infiltrating NK cells (TINK) from clear cell renal cell carcinoma (ccRCC) patients. PBNK in ccRCC patients exhibited an activated phenotype marked by the expression of CD25, CD69, and CD62L, while TINK showed reduced expression of DNAM-1, NKp30, NKp46, NKp80, and CD16, suggesting a more suppressive phenotype. Jiang et al. discovered that Galectin A-Related Protein (GARP) maintains Treg-mediated immune tolerance in gastric cancer. Upregulation of GARP was associated with increased FOXP3+ Treg and CD4+ T cell infiltration and positively correlated with CTLA-4 and PD-L1 expression. Furthermore, the role of CD4+ T cell immune signaling in premalignant gastric cancer may hold clinical significance, offering new insights into immune therapy approaches.

Emerging avenues in immunotherapy

Novel and advancing approaches in the field of immunotherapy are continually expanding, offering innovative avenues for the treatment of cancer (16). These emerging strategies encompass a diverse array of immunomodulatory techniques and novel therapeutic targets, promising the potential to enhance the effectiveness and precision of immunotherapeutic interventions (17). Zhang et al. identified the optimal single-chain variable fragment and investigated its biological functionality to further enhance the therapeutic potential of CAR-T cells targeting CEA-positive cancers. Proper affinity can improve the functionality of CAR-T cells based on different CAR-T types. Four CEA-targeting CAR-T cell sources were screened and compared, with M5A CAR-T cells demonstrating stable CAR expression, moderate affinity, cytokine secretion, and excellent anti-tumor capabilities both *in vitro* and *in vivo*. Xu et al. identified three distinct forms of programmed cell death in colorectal cancer, each associated with specific TME cell infiltration characteristics related to immune exclusion, immune desert, and immune-inflamed phenotypes. Patients with higher COPsig scores exhibited longer overall survival, lower immune cell and stromal infiltration, and a greater tumor mutational burden. Pan et al. discovered significant upregulation of soluble immune checkpoint-related proteins, BTLA, CD28, CD137, GITR, and LAG-3, in pancreatic ductal adenocarcinoma that were significantly associated with prognosis. Patients classified as having a soluble immune low subtype based on these biomarkers exhibited superior overall survival compared to those classified as having a soluble immune high subtype.

Summary and prospective

This topic emphasizes the multifaceted dynamics of the TME, underscoring the pivotal roles of angiogenesis and immune regulation in cancer therapy. By integrating these two distinct yet interconnected processes, the aim is to enhance our comprehension of cancer treatment modalities. Furthermore, we delve into the functional significance of TILs from a cancer biology perspective. The emergence of avenues such as scRNA-seq, CAR-T therapy, programmed cell death, soluble immune checkpoints, and others has opened new paths for deciphering the communication occurring within the TME and developing innovative approaches for therapy. We aspire to advance our understanding of the roles of these elements in cancer immunity and therapeutic strategies, thereby contributing to the development of novel approaches for cancer treatment.

In conclusion, the articles included in this topic provide a new direction for the development of angiogenesis and immune response in the TME. We would also like to express our sincere gratitude to all authors, reviewers, and the editorial team of *Frontiers in Immunology* for their devotion and assistance in the process of reviewing and publishing all these studies in this Research Topic. Simultaneously, we believe that with the tireless efforts of researchers worldwide, effective immune checkpoint targets like PD-1 and PD-L1 will continue to be discovered, offering new hope for cancer patients globally. The relentless exploration at the molecular level, facilitated by novel tools, holds the promise of a future where cancer can be effectively treated.

Author contributions

HL: Writing – original draft, Writing – review & editing. ZY: Writing – review & editing. XL: Writing – review & editing. RZ: Writing – review & editing. XC: Writing – review & editing.

Funding

The author(s) declare financial support was received for the research, authorship, and/or publication of this article. This study was supported by 82271766 (RZ); National Natural Science Foundation of China, 82002475 (XC); Shanghai Sailing Program, 20YF1427700 (XC); Shanghai "Rising Stars of Medical Talents" Youth Development Program, RC20220023 (XC).

Conflict of interest

The authors declare that the research was conducted in the absence of any commercial or financial relationships that could be construed as a potential conflict of interest.

Publisher's note

All claims expressed in this article are solely those of the authors and do not necessarily represent those of their affiliated organizations, or those of the publisher, the editors and the reviewers. Any product that may be evaluated in this article, or claim that may be made by its manufacturer, is not guaranteed or endorsed by the publisher.

References

1. Hanahan D, Weinberg RA. The hallmarks of cancer. *Cell.* (2000) 100(1):57–70. doi: 10.1016/s0092-8674(00)81683-9

2. Hanahan D, Weinberg RA. Hallmarks of cancer: the next generation. *Cell.* (2011) 144(5):646–74. doi: 10.1016/j.cell.2011.02.013

3. Hanahan D. Hallmarks of cancer: new dimensions. *Cancer Discovery* (2022) 12 (1):31–46. doi: 10.1158/2159-8290.CD-21-1059

4. de Visser KE, Joyce JA. The evolving tumor microenvironment: From cancer initiation to metastatic outgrowth. *Cancer Cell* (2023) 41(3):374–403. doi: 10.1016/j.ccell.2023.02.016

5. Folkman J. Tumor angiogenesis: therapeutic implications. *N Engl J Med* (1971) 285(21):1182–6. doi: 10.1056/NEJM197111182852108

6. Lopes-Coelho F, Martins F, Pereira SA, Serpa J. Anti-angiogenic therapy: current challenges and future perspectives. *Int J Mol Sci* (2021) 22(7):3765. doi: 10.3390/ijms22073765

7. Huijbers EJM, Khan KA, Kerbel RS, Griffioen AW. Tumors resurrect an embryonic vascular program to escape immunity. *Sci Immunol* (2022) 7(67): eabm6388. doi: 10.1126/sciimmunol.abm6388

8. Cabillic F, Corlu A. Regulation of transdifferentiation and retrodifferentiation by inflammatory cytokines in hepatocellular carcinoma. *Gastroenterology.* (2016) 151 (4):607–15. doi: 10.1053/j.gastro.2016.06.052

9. Blouw B, Song H, Tihan T, Bosze J, Ferrara N, Gerber HP, et al. The hypoxic response of tumors is dependent on their microenvironment. *Cancer Cell* (2003) 4 (2):133–46. doi: 10.1016/S1535-6108(03)00194-6

10. Munn DH, Sharma MD, Johnson TS. Treg destabilization and reprogramming: implications for cancer immunotherapy. *Cancer Res* (2018) 78(18):5191–9. doi: 10.1158/0008-5472.CAN-18-1351

11. Li PH, Kong XY, He YZ, Liu Y, Peng X, Li ZH, et al. Recent developments in application of single-cell RNA sequencing in the tumour immune microenvironment and cancer therapy. *Mil Med Res* (2022) 9(1):52. doi: 10.1186/s40779-022-00414-y

12. Perez-Gutierrez L, Ferrara N. Biology and therapeutic targeting of vascular endothelial growth factor A. *Nat Rev Mol Cell Biol* (2023) 24(11):816–34. doi: 10.1038/s41580-023-00631-w

13. Joyce JA. Therapeutic targeting of the tumor microenvironment. *Cancer Cell* (2005) 7(6):513–20. doi: 10.1016/j.ccr.2005.05.024

14. Zhang Y, Zhang Z. The history and advances in cancer immunotherapy: understanding the characteristics of tumor-infiltrating immune cells and their therapeutic implications. *Cell Mol Immunol* (2020) 17(8):807–21. doi: 10.1038/s41423-020-0488-6

15. Van de Sande B, Lee JS, Mutasa-Gottgens E, Naughton B, Bacon W, Manning J, et al. Applications of single-cell RNA sequencing in drug discovery and development. *Nat Rev Drug Discovery* (2023) 22(6):496–520. doi: 10.1038/s41573-023-00688-4

16. Melero I, Castanon E, Alvarez M, Champiat S, Marabelle A. Intratumoural administration and tumour tissue targeting of cancer immunotherapies. *Nat Rev Clin Oncol* (2021) 18(9):558–76. doi: 10.1038/s41571-021-00507-y

17. Khalil DN, Smith EL, Brentjens RJ, Wolchok JD. The future of cancer treatment: immunomodulation, CARs and combination immunotherapy. *Nat Rev Clin Oncol* (2016) 13(5):273–90. doi: 10.1038/nrclinonc.2016.25

frontiers in Immunology

ORIGINAL RESEARCH
published: 25 February 2021
doi: 10.3389/fimmu.2021.628063

The Factors Affecting Expansion of Reactive Tumor Infiltrating Lymphocytes (TIL) From Bladder Cancer and Potential Therapeutic Applications

*Ahmet Murat Aydin[1], Brittany L. Bunch[2], Matthew Beatty[2], Ali Hajiran[1], Jasreman Dhillon[3], Amod A. Sarnaik[2,4], Shari Pilon-Thomas[1,2,4] and Michael A. Poch[1]**

[1] Department of Genitourinary Oncology, Moffitt Cancer Center, Tampa, FL, United States, [2] Department of Immunology, Moffitt Cancer Center, Tampa, FL, United States, [3] Department of Pathology, Moffitt Cancer Center, Tampa, FL, United States, [4] Department of Cutaneous Oncology, Moffitt Cancer Center, Tampa, FL, United States

OPEN ACCESS

Edited by:
Mustafa Diken,
Johannes Gutenberg-Universität Mainz, Germany

Reviewed by:
Isabel Christina Poschke,
German Cancer Research Center (DKFZ), Germany
Daniel Olive,
Aix Marseille Université, France

***Correspondence:**
Michael A. Poch
Michael.poch@moffitt.org

Specialty section:
This article was submitted to Cancer Immunity and Immunotherapy, a section of the journal Frontiers in Immunology

Received: 10 November 2020
Accepted: 14 January 2021
Published: 25 February 2021

Citation:
Aydin AM, Bunch BL, Beatty M, Hajiran A, Dhillon J, Sarnaik AA, Pilon-Thomas S and Poch MA (2021) The Factors Affecting Expansion of Reactive Tumor Infiltrating Lymphocytes (TIL) From Bladder Cancer and Potential Therapeutic Applications. Front. Immunol. 12:628063. doi: 10.3389/fimmu.2021.628063

Tumor infiltrating lymphocytes (TIL) therapy was shown to provide durable objective response in patients with metastatic melanoma. As a fundamental first step to bring TIL therapy to clinical use, identification of patients whose tumors yield optimal numbers of reactive TIL is indispensable. We have previously shown that expansion of tumor reactive TIL from primary bladder tumors and lymph node metastases is feasible. Here, we performed TIL harvesting from additional surgical specimens (additional 31 primary tumors and 10 lymph nodes) to generate a heterogenous cohort of 53 patients with bladder cancer (BC) to evaluate the tumor characteristics that lead to tumor-reactive TIL expansion. Among a total of 53 patients, overall TIL growth from tumor samples were 37/53 (69.8%) and overall anti-tumor reactive TIL were 26/35 (74.3%). Mixed urothelial carcinoma is associated with higher anti-tumor reactivity of expanded TIL than pure urothelial carcinoma (89.5% vs. 56.3%, p=0.049). The anti-tumor reactivity of expanded TIL from primary tumors previously treated with BCG immunotherapy were lower (33.3% vs. 82.6%, p=0.027) although T-cell phenotype (CD3+, CD4+, CD8+, and CD56+) was similar regardless prior of BCG therapy. Addition of agonistic 4-1BB antibody in culture media with IL-2 improved the number of expanded TIL from primary tumors previously treated with BCG immunotherapy. There was no significant difference between basal and luminal subtype tumors in terms of viable and reactive TIL growth. Our study demonstrates that TIL expansion is feasible across all BC patients and BC subtypes, and we suggest that TIL therapy can be a reasonable treatment strategy for various manifestations of BC.

Keywords: adoptive cellular immunotherapy, Bacillus Calmette–Guerin, molecular subtypes, bladder cancer, tumor-infiltrating lymphocytes

INTRODUCTION

Bladder cancer (BC) is the 10th most common form of cancer worldwide with a significantly high mortality rate in men (3.2 vs. 0.9, per 100.000) (1). In the US alone, the estimated number of new BC cases and deaths in 2019 were 80.470 and 17.670, respectively (2). Immunotherapy has been utilized for treatment of BC for more than four decades since the start of utilization of intravesical Bacillus Calmette-Guerin (BCG) for treatment of non-muscle invasive bladder cancer (NMIBC) (3). Nonetheless, about 20% to 45% of high-risk NMIBC progress to muscle-invasive bladder cancer (MIBC) despite endoscopic tumor resection and BCG immunotherapy (4). Moreover, about 20 to 40% of patients with MIBC experiences disease recurrence within 5 years of neoadjuvant chemotherapy (NAC) and radical cystectomy (RC) (5). Metastatic BC is a very lethal disease with an overall survival of approximately 12 months (6). In the past 5 years, immune checkpoint blockade (ICB) has been utilized for management of metastatic BC. Single agent checkpoint inhibitors provided objective responses in about only one fifth of the patients after first-line therapy (7). Therefore, there is still an unmet need of novel effective therapies for management of BC across all stages.

Adoptive cell therapy (ACT) has become a real prospect for treatment of solid tumors (8). TIL therapy is a form of ACT, which is composed of extraction of TILs from human tumor samples, *ex vivo* expansion, and reinfusion of expanded autologous lymphocytes into patients following non-myeloablative chemotherapy (9–13). It has been proven an effective anticancer therapy in cervical cancer, ovarian cancer, and particularly in metastatic melanoma (9–13).

Feasibility of TIL expansion from bladder cancer was recently shown by our institution (14). However non-metastatic BC is a heterogenous spectrum of disease ranging from indolent papillary lesions to locally advanced tumors and it represents genomically diverse tumors (15). Proper selection of BC patients with tumors that yield optimal numbers of tumor-reactive TIL has a paramount importance for the success of TIL therapy. In this study, we aimed to evaluate the impact of clinicopathological parameters, molecular subtype (basal vs. luminal) and previous BCG immunotherapy on viable and tumor-reactive TIL expansion.

MATERIAL AND METHODS

Patient Selection and Data Collection

Patients older than 18 years of age with previously confirmed pathological diagnosis of BC were included in the study. All patients treated with RC also underwent bilateral pelvic lymph node dissection concurrently. Only patients treated with ≥6 cycles of BCG immunotherapy and completed induction BCG course was considered as BCG-treated. Our previous inclusion criteria was expanded to include patients treated with RC for bladder tumors smaller than 2 cm in size and any bladder lesions/tumors obtained by transurethral resection of bladder tumor (TURBT). The original protocol was amended and approved by the Institutional Review Board (MCC18142). Informed consent was obtained from all patients prior to tissue collection.

TIL Expansion Protocol

TIL were expanded as previously described (14). Primary bladder tumors or lymph node metastases were minced into ~1–3 mm^3 fragments and plated in TIL media consisting of RPMI 1640, 2.05 mM L–glutamine (HyClone, Thermo Fisher Scientific, Waltham, MA), 10% heat-inactivated human AB serum (Omega Scientific, Tarzana, CA), 55 μM 2-mercaptoethanol (Invitrogen), 50 μg/ml gentamicin (Invitrogen), 100 I.U./ml penicillin, 100 μg/ml streptomycin, and 10 mM HEPES Buffer (Mediatech, Manassas, VA) in 24- or 48-well plates with 6000 I.U./ml rhIL-2 (Prometheus). Some cultures were supplemented with 1 ug/ml anti-CD137 agonistic antibody (Urelumab, BMS-663513). All cultures were expanded for 4 weeks and confluent wells were split into additional wells. TIL from each independent fragment was counted. Remaining tumor material was mechanically and enzymatically digested using media containing 2% Collagenase Type IV and a GentleMACS Dissociator (Miltenyi, 130–093-235). Cells were counted by trypan blue exclusion and subjected to subsequent analysis or cryopreserved as functional assay targets. Positive TIL growth was defined as confluency and expansion of the primary well into 2 wells.

Evaluation of TIL Reactivity and Immunophenotyping of Expanded TIL

Flow cytometric analysis of TIL from each fragment was performed. Expanded TIL was stained with fluorescent antibodies for CD3, CD4, CD8, and CD56 (BD Biosciences, BDB555516). All cells were stained with a Live/Dead Near-IR viability stain (Invitrogen, L10119) and fixed in 2% paraformaldehyde. Data were acquired on an LSR II flow cytometer and analyzed using FlowJo software (TreeStar, Inc.). TIL and autologous tumor cells from enzymatic digestion were cultured at a 1:1 ratio (1×10^5 cells each) overnight in round bottom 96-well plates. Supernatants were collected after 24 h. IFN-gamma was measured using a Human IFNg Quantikine ELISA Kit (R&D Systems, SIF50). Optical density of each well was measured at 450 nm and IFN-γ concentration was calculated from the standard curve. IFN-γ concentration ≥100 pg/ml was the cut-off for reactivity.

Molecular Subtyping

Tumor blocks were retrieved from pathology archive and whole tissue sections were used for immunohistochemistry. Slides were stained using a Ventana Discovery XT automated system (Ventana Medical Systems, Tucson, AZ) as per manufacturer's protocol with proprietary reagents. Immunohistochemical staining was performed utilizing primary rabbit anti-CD3 antibody (790-4341, Ventana; a predilute concentration), primary rabbit anti-GATA3 antibody (#5852, Cell Signaling Technologies, Danvers, MA; at a 1:200 concentration in Dako antibody diluent, Carpenteria, CA), and mouse monoclonal anti-CK5/6 antibody (790-4554, Ventana; a predilute concentration). The detection system used was the Ventana ChromoMap kit and

slides were then counterstained with Hematoxylin. The immunohistochemical results were semi-quantitatively assessed and scored by one pathologist as follows: 0, negative (<1% staining of T cells); 1+, weak (1%–25% staining of T cells); 2+, moderate (26%–64% staining of T cells); and 3+, strong (≥65% staining of T cells).

Molecular characterization of MIBC tumors was performed in primary tumors to identify luminal and basal subtypes *via* immunohistochemistry as previously described by Dadhania et al. (16). Briefly, immunohistochemistry slides stained for GATA3, and CK5/6 were scanned using an Aperio AT2 digital pathology system (Leica Biosystems Inc., Vista, California) with a 20X 0.7NA objective lens. The luminal marker was GATA3 and basal marker was CK5/6. Matching H&E slides were also scanned. Whole slide images were viewed with Aperio Imagescope software and regions of interest (ROIs) were annotated to identify tumor regions. All ROIs were analyzed with Aperio eSlide Manager software using nucleus (GATA3) and membrane (CK5/6) detection algorithms and percent positive values for each sample was calculated. Twenty percent of tumor tissue positivity and 20% of tumor nuclei positivity were cut-off expression levels of the signature basal and luminal markers (**Figure 1**).

Statistical Analysis

Data represented as scatter plots show individual patient data points as well as error bars representing median values and interquartile range (IQR). The association for categorical and continues variables were evaluated using Fisher's exact, Chi-square, Mann–Whitney U and Wilcoxon signed rank tests where indicated. The statistical analyses were performed using SPSS version 22.0 (IBM, Armonk, NY) and GraphPad Prism software. p values were two sided and $p < 0.05$ was considered statistically significant.

RESULTS

Patient Characteristics

A total of 51 primary tumors and 17 additional LN from 53 patients were included for the analysis of factors that are associated with overall TIL expansion as well as expansion of reactive TIL (**Table 1**). Briefly, 43 (81.1%) patients underwent RC while 10 (18.9%) patients underwent TURBT. Eleven samples (20.8%) were collected from patients who had received intravesical BCG immunotherapy and 22 (41.5%) samples were

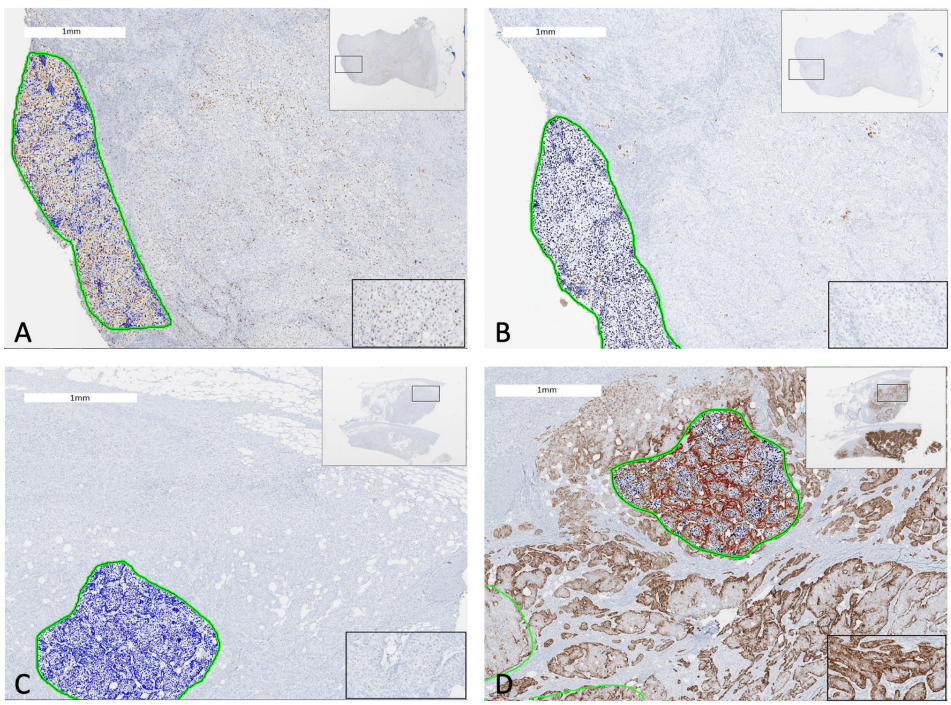

FIGURE 1 | Two cases of bladder cancer showing GATA3 and CK5/6 expression quantified by digital immunohistochemistry analysis. A luminal subtype bladder tumor with **(A)** GATA3 expression ≥20% and **(B)** CK5/6 expression <20% (Left: Anti-GATA3 Ab; Right: Anti-CK5/6 Ab). A basal subtype bladder tumor with **(C)** GATA3 expression <20% and **(D)** CK5/6 expression ≥20% (Left: Anti-GATA3 Ab; Right: Anti-CK5/6 Ab). The green circles represent tumor area analyzed by digital automated immunohistochemistry algorithm. Encircled blue cells/nuclei represents no staining with antibody whereas yellow, orange, brown, dark brown/red ones represent positive staining incremental to staining intensity. Views of whole tumor section at the right upper corner and of a magnified tumor area at the right lower corner.

TABLE 1 | Characteristics of 53 bladder cancer patients included in the analysis.

Variable	Patient number (%)
Age	
<60	8 (15.1)
60–69	16 (30.2)
70–79	21 (39.6)
≥80	8 (15.1)
Gender	
Female	14 (26.4)
Male	39 (73.6)
Ethnicity	
Non-hispanic white	51 (96.2)
Other	2 (3.8)
BMI	
18.5-24.9	17 (32.1)
25.0-29.9	17 (32.1)
≥30.0	15 (28.3)
Unknown	4 (7.5)
Surgery	
Radical cystectomy	43 (81.1)
Transurethral resection	10 (18.9)
Smoking status	
Never smoker	11 (20.7)
Ever smoker	32 (60.4)
Current smoker	10 (18.9)
pT stage	
Ta/Tis/T1	13 (24.5)
T2	15 (28.3)
T3	15 (28.3)
T4	10 (18.9)
pN stage (MIBC)	
N0	29 (67.5)
N1	6 (13.9)
N2	2 (4.7)
N3	6 (13.9)
Variant histology	
Pure	29 (54.7)
Mixed	24 (45.3)
Type of histology	
Pure urothelial carcinoma	29 (54.7)
Squamous differentiation	11 (20.8)
Plasmacytoid	4 (7.5)
Micropapillary	3 (5.7)
Sarcomatoid	2 (3.8)
Other variants[a]	4 (7.5)
Molecular subtype of MIBC	
Basal	10 (25.0)
Luminal	25 (62.5)
N/A	5 (12.5)
Prior BCG immunotherapy	11 (20.8)
Prior neoadjuvant chemotherapy	22 (41.5)

BCG, Bacillus Calmette-Guerin; BMI, body mass index; MIBC, muscle-invasive bladder cancer; pN, pathological lymph node; pT, pathological tumor; Tis, carcinoma in-situ; TIL, tumor-infiltrating lymphocytes; N/A, not applicable/evaluable.

[a]*One glandular differentiation, one microcystic, one clear cell, and one squamous cell carcinoma.*

collected from patients who had received NAC. Among 40 (71.4%) patients with MIBC, 10 patients were found to have basal tumors whereas 25 patients had luminal tumors.

TIL Growth and Reactivity

In our previous study, we showed TIL expansion from 70% of primary bladder tumors as well as TIL expansion from all LNs (20 primary tumors and 7 LN from 20 patients) (14). In this study, we collected tumor fragments from an additional 33 patients (31 primary tumors and 10 LN) and confirmed that TIL growth could be achieved in 37 out of 53 (69.8%) patients using primary tumors and/or LN (**Table 2**). In this study, autologous tumor was available for TIL samples in 29 patients. Co-culture of autologous tumor with expanded TIL was performed and production of IFN-gamma was measured. Expanded TIL from primary tumors and/or LNs showed anti-tumor reactivity in 20 out of 29 (69.0%) patients, thus overall reactivity of expanded TIL per patient was 74.3% (26/35 patients; six patients from the previous study).

TIL growth was achieved from additional nine out of 10 LN samples in the present study, thus the rate of TIL growth from LN samples was 94.1% (16/17 LNs; 7 LNs from the previous study). Co-culture with autologous tumor was feasible in 12 expanded TIL from LNs, and 10 expanded TIL showed anti-tumor reactivity (83.4%). The median number of expanded TIL from primary tumors and LN was 1.86E+07 and 4.73E+07 in 33 and 16 patients, respectively.

Factors Associated With Expansion and Anti-Tumor Reactivity of TIL

We next evaluated the factors associated with TIL expansion and tumor-reactivity of TIL among a total of 53 patients (20 patients from previous study and additional 33 patients). TIL growth was feasible across all patient subgroups (**Table 3**). The number of expanded TIL from primary tumors and LN were similar between patients regardless of age, gender, smoking status, BMI, type of surgery, pathological tumor/LN stage, histology, molecular

TABLE 2 | Expansion of tumor-reactive TIL in 53 bladder cancer patients.

Variable	Number
Overall TIL growth per patient	
Yes	37 (69.8%)
No	16 (30.2%)
TIL growth from PT	
Yes	33 (64.7%)
No	18 (35.3%)
Median TIL number from PT [a]	1.86E+07 (1.60E+06 - 3.09E+08)
TIL growth from LN	
Yes	16 (94.1%)
No	1 (5.9%)
Median TIL number from LN [b]	4.73E+07 (4.40E+06 - 2.86E+08))
Overall reactivity of TIL per patient	
Yes	26 (74.3%)
No	9 (25.7%)
N/A	2
Reactivity of TIL from PT	
Yes	18 (60.0%)
No	12 (40.0%)
N/A	3
Reactivity of TIL from LN	
Yes	10 (83.4%)
No	2 (16.6%)
N/A	4

LN, lymph node; PT, primary tumor; TIL, tumor-infiltrating lymphocytes; N/A, not applicable/evaluable.

[a]*Median (range) number of TIL that grew from 33 primary tumor fragments.*

[b]*Median (range) number of TIL grew from 16 lymph node fragments.*

TABLE 3 | Factors affecting growth and reactivity of TIL harvested from primary tumors and/or lymph nodes in 53 patients.

Variable	TIL Growth			TIL Reactivity[1]		
	No, n(%)	Yes, n(%)	P value	No, n(%)	Yes, n(%)	P value
Patients	16 (30.2)	37(69.8)	–	9 (25.7)	26 (74.3)	–
Age, yr.[2]	72.5 [57.6;88.4]	70.0 [51.8;91.9]	0.461	77.0 [65.0;90.5]	68.5 [51.8;91.9]	0.026
Gender			0.510			0.685
Male	13 (33.3)	26 (66.7)		7 (29.2)	17 (70.8)	
Female	3 (21.4)	11 (78.6)		2 (18.1)	9 (81.9)	
BMI[2]	26.1 [20.1;36.7]	26.8 [19.2;49.2]	0.834	26.8 [19.2;36.8]	27.6 [19.7;49.2]	0.558
Smoking status			0.470			0.191
Never	2 (18.2)	9 (81.8)		4 (44.4)	5 (55.6)	
Ever/Current	14 (33.3)	28 (66.7)		5 (19.2)	21 (80.8)	
Type of surgery			0.050			0.267
Radical cystectomy	10 (23.3)	33 (76.7)		7 (22.6)	24 (77.4)	
TURBT	6 (60.0)	4 (40.0)		2 (50.0)	2 (50.0)	
pT stage			0.234			0.353
Ta/Tis/T1	6 (46.2)	7 (53.8)		3 (42.8)	4 (57.2)	
T2	5 (33.3)	10 (66.7)		3 (30.0)	7 (70.0)	
T3/4	5 (20.0)	20 (80.0)		3 (16.6)	15 (83.4)	
pN stage (MIBC)			0.703			1.000
N0	6 (20.7)	23 (79.3)		5 (21.7)	18 (78.3)	
N+	4 (28.6)	10 (71.4)		2 (25.0)	6 (75.0)	
Variant histology			0.073			0.049
Pure	12 (41.4)	17 (58.6)		7 (43.7)	9 (56.3)	
Mixed	4 (16.6)	20 (83.4)		2 (10.5)	17 (89.5)	
Molecular subtype[3]			0.999			0.130
Basal	2 (20.0)	8 (80.0)		0	8 (100.0)	
Luminal	7 (28.0)	18 (72.0)		5 (31.2)	11 (68.8)	
Prior NAC			0.768			1.000
No	10 (31.2)	21 (68.8)		5 (26.3)	14 (73.7)	
Yes	6 (29.1)	16 (70.9)		4 (25.0)	12 (75.0)	
Prior intravesical BCG			0.716			0.027
No	12 (37.5)	30 (62.5)		5 (17.4)	24 (82.6)	
Yes	4 (36.4)	7 (63.6)		4 (66.7)	2 (33.3)	
Tumor weight, gr.[2]	0.60 [0.17;8.56]	1.17 [0.04;5.06]	0.150	0.66 [0.34;1.64]	1.48 [0.34;5.06]	0.102
Sample used[4]			0.026			0.276
Primary tumor	18 (35.3)	33 (64.7)		12 (40.0)	18 (60.0)	
Lymph node	1 (5.5)	16 (94.1)		2 (16.6)	10 (83.4)	

BCG, Bacillus Calmette-Guerin; BMI, Body mass index; MIBC, muscle-invasive bladder cancer; NAC, Neoadjuvant chemotherapy; Tis, carcinoma in-situ; pN, pathological lymph node; pT, pathological tumor; TIL, tumor-infiltrating lymphocytes; TURBT, Transurethral resection of bladder tumor

[1]TIL reactivity could not be measured due to lack of autologous tumor in 2 patients.

[2]Values are presented as median and range (min; max).

[3]Molecular subtyping was performed for MIBC. Tissue was not available in 5 patients with MIBC.

[4]Autologous tumor was not available for measurement of reactivity for 3 TIL samples grown from primary tumor and 4 TIL samples grown from lymph node.

subtype, previous NAC and weight of fragment (data now shown) with the exception of previous BCG immunotherapy.

Anti-tumor reactivity of expanded TIL was lower in primary tumors treated with BCG immunotherapy compared to those without (33.3% vs. 82.6%, p= 0.027). Other significant finding of the reactivity analysis included the age of patients and tumor histology. The median age of patients yielding tumor reactive TIL was significantly younger than the median age of patients with expanded TIL showing no anti-tumor reactivity (68.5 [51.8;91.9] vs. 77.0 [65.0;90.5], p=0.026). However the surgical specimen from the oldest patient in our cohort yielded higher amounts of reactive TIL (4.06E+07). Thus, age might not be a limiting factor for expansion of TIL although it warrants further investigation with additional specimens.

TIL reactivity from mixed urothelial tumors was significantly higher than pure urothelial carcinoma (89.5% vs. 56.3%, p=0.049). Basal subtype tumors yielded higher TIL growth (80%) with more anti- tumor reactivity (100%) compared to luminal subtype (72% TIL growth and 68.8% tumor-reactive TIL) albeit statistically not significant (p=0.999 and p=0.130). Thus, we identified a subset of BC tumors (mixed histology and BCG-naïve tumors) with enhanced TIL reactivity.

Previous BCG Immunotherapy and Tumor-Reactive TIL Expansion

The number of expanded TIL was lower than overall median TIL number (1.86E+07) in all (6/6) primary tumors previously treated with BCG compared to those from primary tumors without previous BCG exposure (10/27 (37.0%), p=0.007, **Figure 2**). This was not due to a lack of T cells in tumors since all primary tumors displayed moderate to strong infiltration of CD3+ tumor-infiltrating lymphocytes (scores ≥2+) regardless of history of BCG immunotherapy (**Figure 3**). The sample weight, and the percent of tumor fragments that grew TIL were also

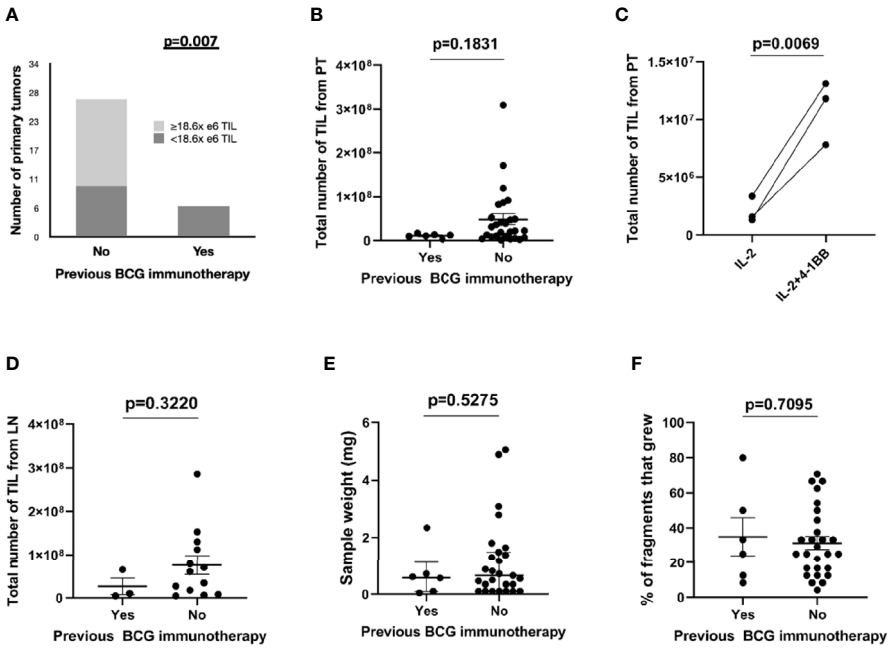

FIGURE 2 | Expansion of TIL from bladder tumors stratified by BCG immunotherapy. The total number of TIL expanded from bladder or LN tumor fragments was measured at 4 weeks after initiation of culture. **(A)** TIL growth from primary tumors stratified by previous BCG immunotherapy and median number of expanded TIL in 33 patients. Fisher's exact test. **(B)** Total number of expanded TIL from BCG-naïve primary tumors (27 patients) and from primary tumors with previous exposure to BCG immunotherapy (six patients). Each point represents the total TIL per patient (the sum of all TIL that was generated from each fragment within an individual patient). Median and interquartile range. Mann-Whitney test. **(C)** Total numbers of expanded TIL from three primary tumors previously treated with BCG immunotherapy. Fragments of the surgical specimens were cultured either in IL-2 (6000 IU/ml) only or in IL-2 (6000 IU/ml) + 4-1BB (10 ug/ml). Wilcoxon-signed rank test. **(D)** Total number of expanded TIL from BCG-naïve lymph nodes (13 patients) and from lymph nodes with previous exposure to BCG immunotherapy (three patients). Each point represents the total TIL per patient (the sum of all TIL that was generated from each fragment within an individual patient). Median and interquartile range. Mann-Whitney test. **(E)** The sample weight (mg) of primary tumors sent to the lab for expansion of TIL (six BCG-treated samples and 27 BCG-naive samples). Median and interquartile range. Mann–Whitney test. **(F)** The percentage of fragments that grew TIL from the total number of fragments plated (six samples from BCG-treated primary tumors and 27 samples from BCG-naive primary tumors). Median and interquartile range. Mann–Whitney test.

comparable between each group. To attempt to improve TIL expansion in these cultures, we added agonistic anti-4-1BB antibodies to culture media as it was previously found to enhance the expansion of TIL in malignant melanoma and bladder cancer treated with NAC by our institution (14, 17). Tumor fragments of three primary tumors were cultured in IL-2 (6000 IU/ml) + anti-4-1BB antibody (10 ug/ml) and these fragments yielded higher numbers of expanded TIL compared to fragments of the same tumors cultured only in IL-2 (6000 IU/ml) (p=0.006). There were no significant difference in composition of CD3+, CD4+, CD8+, and CD56+ T cells in expanded TIL regardless of BCG exposure or agonism with anti-4-1BB antibodies (**Figure 4**).

DISCUSSION

BC is morphologically and genomically a heterogenous malignancy and unique owing to utilization of immunotherapy for treatment of both early and late stage tumors (18). Moreover, BC has the third highest tumor mutational burden among all cancer types, which was associated with high neoantigen load and enrichment of activated immune cells within tumor site (19). Recently, our group demonstrated that TIL expansion from BC was feasible (70%) in a homogenous cohort of 20 patients treated with RC for bladder tumors larger than 2 cm (14). In the present study, we included an additional 33 patients, including patients who had smaller RC tumors (<2 cm) and patients who were treated with TURBT. We also measured anti-tumor reactivity of all expanded TIL if autologous tumors were available. In this expanded cohort of patients with BC, the success of viable TIL growth was 69.8%, which was consistent with our preliminary report (70%) and those reported for patients with malignant melanoma (ranging between 75% and 85%) (20). Moreover, we were able to utilize metastatic LN sent together with primary tumors in RC specimens for TIL expansion. Overall, TIL growth was feasible across all subgroups of BC patients. The rate of reactivity of expanded TIL against autologous tumors was 74.3% in our study, comparable to that reported for malignant melanoma (67%) (21).

Overall TIL reactivity from tumor samples of variant histology or squamous/glandular differentiation (mixed histology) was significantly higher than that of pure urothelial carcinoma (89.5% vs. 56.3%). Presence of variant histology in

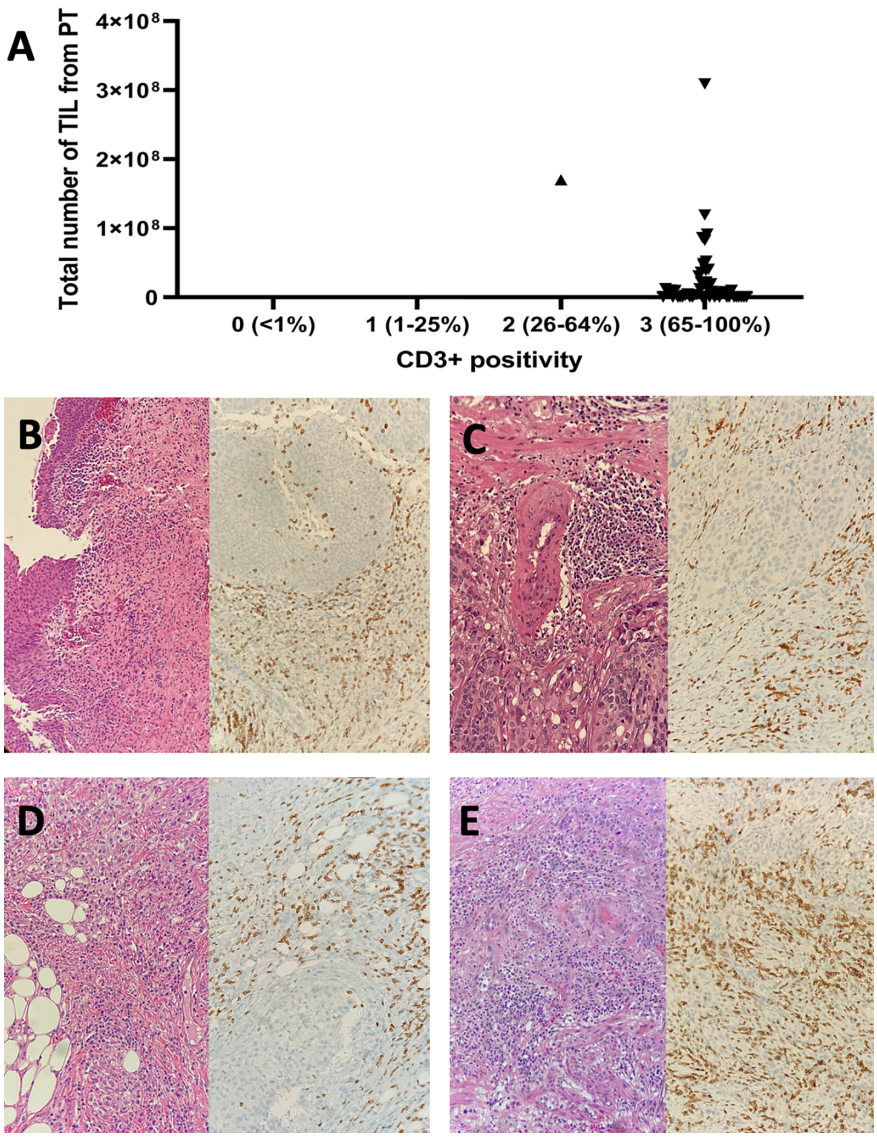

FIGURE 3 | The CD3+ tumor infiltrating lymphocyte infiltration within tumor microenvironment and expansion of TIL from primary bladder tumors. **(A)** Expansion of TIL was achieved in 33 out of 51 primary tumors, of which 50 and one displayed strong and moderate CD3+ T cell infiltration, respectively. **(B)** A pTis bladder tumor (pure urothelial call carcinoma) previously treated with BCG immunotherapy (Left: H-E x 100; Right: Anti-CD3 Ab x 200). **(C)** A pT2 bladder tumor (pure urothelial cell carcinoma) previously treated with BCG immunotherapy (Left: H-E x 200; Right: Anti-CD3 Ab x 200). **(D)** A pT3 bladder tumor (pure urothelial carcinoma) with no previous exposure to intravesical BCG (Left: H-E x 200; Right: Anti-CD3 Ab x 200). **(E)** A pT2 bladder tumor (squamous differentiation) with no previous exposure to intravesical BCG (Left: H-E x 200; Right: Anti-CD3 Ab x 200). H-E, hematoxylin and eosin; Ab, antibody; pT, pathological tumor stage.

NMIBC is considered as a high risk feature for progression to a higher stage disease and early RC is recommended for these cases (18). The therapeutic options for MIBC with variant histology is limited and response to NAC is modest without increase in overall survival (22). In contrast, preliminary reports suggest a substantial benefit from immunotherapy for MIBC with variant histology, downstaging to pT1 or less was achieved after neoadjuvant ICB in about half of the patients harboring such muscle-invasive disease (23). Particular variants of urothelial cell carcinoma have unique gene expression profiles and some characterized by enrichment with genomic signatures predictive for immunotherapy response or high PD-L1 expression (23–25). Based on anti-tumor reactivity of expanded TIL from mixed histology tumors in our study, we suggest that TIL therapy might have a potential to address the unmet need of perioperative systemic therapy for these tumors.

Interestingly, anti-tumor reactivity of expanded TIL from primary tumors previously treated with BCG immunotherapy was lower than those without (33% vs. 83%). Likewise, the number of expanded TIL appeared to be lower from such tumors. Of note, the number of BCG cycles and the interval time between last BCG instillation and TIL expansion varied

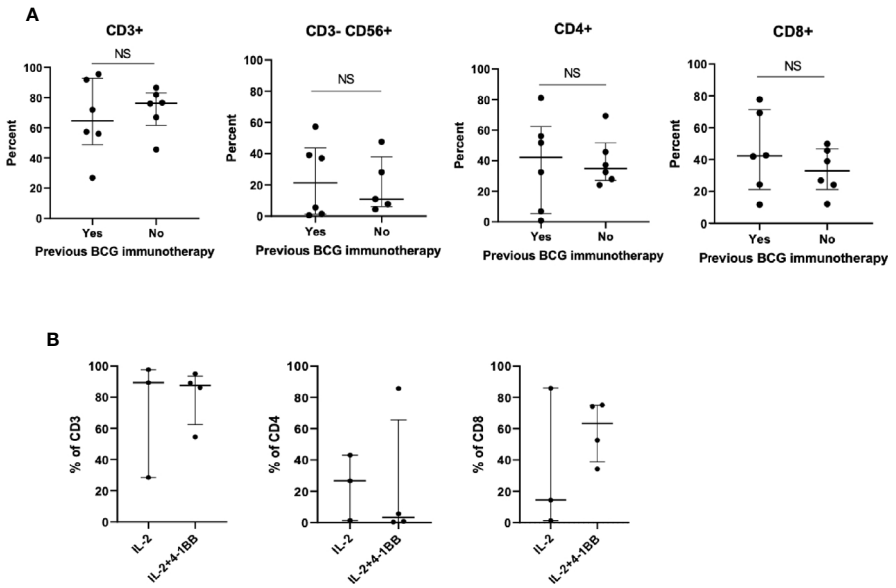

FIGURE 4 | Phenotype of TIL expanded from primary bladder tumors previously treated with BCG immunotherapy. **(A)** Six BCG-treated patients whose primary bladder tumors yielded TIL were matched with six BCG-untreated patients (1:1) in terms of patient age, tumor histology, tumor stage and molecular subtype of bladder cancer. At 4 weeks after the initiation of TIL cultures, TIL were collected from each fragment and the percentage of CD3+ T cells, CD4+ T cells, CD8+ T cells, and CD3-CD56+ NK cells was measured by flow cytometry. Each point represents the mean percentage of cells per patient (the mean of all TIL that was generated from each fragment within an individual patient). Wilcoxon-signed rank test. **(B)** Tumor fragments of three primary tumors previously treated with BCG immunotherapy were cultured either in IL-2 (6000 IU/ml) + 4-1BB (10 ug/ml) or in only IL-2 (6000 IU/ml). Percentage of CD3+ T cells, CD4+ T cells, and CD8+ T cells was measured by flow cytometry. Each point represents the percentage of cells generated from each tumor fragment. Median and interquartile range.

across the patients, however additional maintenance BCG was not found to further decrease TIL reactivity after induction BCG (data not shown). The decrease in anti-tumor reactivity might be due to BCG-related indirect mechanisms mediated by other components of tumor microenvironment such as MDSCs, regulatory T cells or increased expression of particular cytokines after exposure to BCG. Likewise, Chevalier et al. reported lower T cell-to-monocytic myeloid-derived suppressor cells (MDSC) ratios, higher frequencies of group 2 innate lymphoid cells, and detectable levels of IL-13, an inducer for suppressive functions in monocytes, in the urine of patients who failed intravesical BCG (26). Whether BCG exhausted TIL in the tumor microenvironment prior to harvesting was not clear and it warrants further investigation. However, the overall CD3+ T cell concentrations in primary tumors appeared similar across the patients in our study. The percentages of CD4+, CD8+, and CD3-CD+56 T cells in expanded TILs appeared to be not effected by previous BCG therapy, consistent with animal studies evaluating effect of BCG on T cell phenotype (27). Moreover, we could effectively multiply the number of expanded TIL from BCG treated primary tumors with agonistic anti-4-1BB. Thus, the effect of previous BCG immunotherapy on tumor-reactive TIL expansion warrants further investigation.

Unsurprisingly, an accurate predictive biomarker for expansion of viable and reactive TIL is invaluable. Particular molecular subtypes of BC were found to have predictive value and associate with significant immunological signatures (28). Basal subtype bladder tumors were associated with higher infiltration of CD8+ T cells and NK cells, advanced disease stage and lower median overall survival compared to luminal subtype tumors (1.2 years vs. 1.8–4.0 years). Patients with basal subtype tumors with high RNA-based immune signature had a 100% 2-year progression-free survival after neoadjuvant pembrolizumab therapy in a phase II MIBC trial (29). In our study, we did not observe any significant association between molecular subtype and viable and reactive TIL growth although basal subtype bladder tumors appeared to yield more reactive TIL, which warrants further investigation. For molecular subtyping, we used a validated immunohistochemistry method and quantitative scoring to improve reproducibility. Although basal tumors were shown to be almost exclusively basal, luminal subtypes appeared to consist of a more heterogenous group of tumors (16). A comprehensive genomic analysis would enable identification of other molecular subtypes such as luminal-papillary, luminal-unstable and neuroendocrine-like and a more reproducible molecular subtype profiling (28). Nonetheless, the value of molecular characterization as a predictive biomarker in BC appears to be limited due to significant tumor heterogeneity and impact of previous treatments (30). TCGA molecular subtype did not appear to be a strong predictor of response to Atezolizumab in patients with refractory metastatic urothelial cancer (31). We are currently exploring the diversity of T cell populations and neoantigen-specific T cells in expanded TIL from bladder tumors to identify predictive biomarkers for TIL expansion. Moreover, reliable identification of metastatic LNs in the operating room,

further optimization of TIL culture conditions, and comprehensive *in vitro* measurement of anti-tumoral T cell activity can further increase the success of tumor-reactive TIL expansion, which warrant further investigation.

The observed success in TIL expansion increases the potential to implement clinical trial of TIL therapy for BC patients in the near future. Conventional TIL therapy strategies focusing on treatment of metastatic cancer consists of systemic infusion of expanded TIL in patients preconditioned with non-myeloablative chemotherapy (such as cyclophosphamide and fludarabine) (32, 33). We demonstrated that expansion of tumor-reactive TIL is feasible from bladder tumor samples obtained *via* TURBT. TIL therapy can potentially be a novel treatment option in the non-metastatic setting including patients with BCG-naïve NMIBC. Clinical trials of intravesical TIL therapy with or without intravesical IL-2, alone or in combination with systemic PD-1 inhibitor or intravesical BCG appears reasonable. Acknowledging our imperfect ability to detect all tumor recognition *in vitro*, the polyclonal nature of TIL therapy, and demonstrated feasibility of TIL growth from BCG-treated tumor samples, a subset of BCG-unresponsive NMIBC may also benefit from TIL therapy.

CONCLUSIONS

Tumor fragments of both primary tumor and LN can yield TIL with tumor-specific reactivity in BC patients. Specifically, we identified a subset of BC patients with improved TIL reactivity including patients with mixed histology and BCG-naïve tumors. Nonetheless, TIL therapy appears to be feasible for any patient with BC, and our findings suggest feasibility for TIL clinical trials for management of BC.

DATA AVAILABILITY STATEMENT

The raw data supporting the conclusions of this article will be made available by the authors, without undue reservation.

ETHICS STATEMENT

The studies involving human participants were reviewed and approved by the Institutional Review Board (MCC18142). The patients/participants provided their written informed consent to participate in this study.

AUTHOR CONTRIBUTIONS

AA, BB, MB, SP-T, and MP designed the study. AA and MP procured the biological specimen. JD was in charge of the pathology. AA, BB, MB, and SP-T performed the experimental work. AA, BB, MB, SP-T, and MP analyzed and interpreted the data. All authors contributed to the article and approved the submitted version.

FUNDING

This work was funded in part by Iovance Biotherapeutics, Swim Across America, and the Dr. Miriam and Sheldon G. Adelson Medical Research Foundation. AS was supported by NCI-5K23CA178083. SP-T was supported by an American Cancer Society—Leo and Anne Albert Charitable Foundation Research Scholar Grant (RSG-16-117-01-LIB). The funder bodies were not involved in the study design, collection, analysis, interpretation of data, the writing of this article or the decision to submit it for publication.

ACKNOWLEDGMENT

This work was supported in part by the Tissue Core, Analytic Microscopy Core and the Flow Cytometry Core at the Moffitt Cancer Center, and in part by the Cancer Center Support Grant P30 CA076292 and a CCSG supplement P30 CA076292-18S5 from the National Cancer Institute.

REFERENCES

1. Bray F, Ferlay J, Soerjomataram I, Siegel RL, Torre LA, Jemal A. Global cancer statistics 2018: GLOBOCAN estimates of incidence and mortality worldwide for 36 cancers in 185 countries. *CA Cancer J Clin* (2018) 68(6):394–424. doi: 10.3322/caac.21492
2. Siegel RL, Miller KD, Jemal A. Cancer statistics, 2019. *CA Cancer J Clin* (2019) 69(1):7–34. doi: 10.3322/caac.21551
3. Morales A, Eidinger D, Bruce AW. Intracavitary Bacillus Calmette-Guerin in the treatment of superficial bladder tumors. *J Urol* (1976) 116(2):180–3. doi: 10.1016/S0022-5347(17)58737-6
4. Sylvester RJ, van der Meijden AP, Witjes JA, Kurth K. Bacillus calmette-guerin versus chemotherapy for the intravesical treatment of patients with carcinoma in situ of the bladder: a meta-analysis of the published results of randomized clinical trials. *J Urol* (2005) 174(1):86–91. doi: 10.1097/01.ju.0000162059.64886.1c
5. Mari A, Campi R, Tellini R, Gandaglia G, Albisinni S, Abufaraj M, et al. Patterns and predictors of recurrence after open radical cystectomy for bladder cancer: a comprehensive review of the literature. *World J Urol* (2018) 36(2):157–70. doi: 10.1007/s00345-017-2115-4
6. Bellmunt J, Theodore C, Demkov T, Komyakov B, Sengelov L, Daugaard G, et al. Phase III trial of vinflunine plus best supportive care compared with best supportive care alone after a platinum-containing regimen in patients with advanced transitional cell carcinoma of the urothelial tract. *J Clin Oncol* (2009) 27(27):4454–61. doi: 10.1200/JCO.2008.20.5534
7. Boegemann M, Aydin AM, Bagrodia A, Krabbe LM. Prospects and progress of immunotherapy for bladder cancer. *Expert Opin Biol Ther* (2017) 17(11):1417–31. doi: 10.1080/14712598.2017.1366445
8. Wong YNS, Joshi K, Pule M, Peggs KS, Swanton C, Quezada SA, et al. Evolving adoptive cellular therapies in urological malignancies. *Lancet Oncol* (2017) 18(6):e341–e53. doi: 10.1016/S1470-2045(17)30327-3
9. Besser MJ, Shapira-Frommer R, Treves AJ, Zippel D, Itzhaki O, Hershkovitz L, et al. Clinical responses in a phase II study using adoptive transfer of short-term cultured tumor infiltration lymphocytes in metastatic melanoma patients. *Clin Cancer Res* (2010) 16(9):2646–55. doi: 10.1158/1078-0432.CCR-10-0041
10. Pilon-Thomas S, Kuhn L, Ellwanger S, Janssen W, Royster E, Marzban S, et al. Efficacy of adoptive cell transfer of tumor-infiltrating lymphocytes after lymphopenia induction for metastatic melanoma. *J Immunother* (2012) 35(8):615–20. doi: 10.1097/CJI.0b013e31826e8f5f

11. Radvanyi LG, Bernatchez C, Zhang M, Fox PS, Miller P, Chacon J, et al. Specific lymphocyte subsets predict response to adoptive cell therapy using expanded autologous tumor-infiltrating lymphocytes in metastatic melanoma patients. *Clin Cancer Res* (2012) 18(24):6758–70. doi: 10.1158/1078-0432.CCR-12-117
12. Stevanovic S, Draper LM, Langhan MM, Campbell TE, Kwong ML, Wunderlich JR, et al. Complete regression of metastatic cervical cancer after treatment with human papillomavirus-targeted tumor-infiltrating T cells. *J Clin Oncol* (2015) 33(14):1543–50. doi: 10.1200/JCO.2014.58.9093
13. Fujita K, Ikarashi H, Takakuwa K, Kodama S, Tokunaga A, Takahashi T, et al. Prolonged disease-free period in patients with advanced epithelial ovarian cancer after adoptive transfer of tumor-infiltrating lymphocytes. *Clin Cancer Res* (1995) 1(5):501–7.
14. Poch M, Hall M, Joerger A, Kodumudi K, Beatty M, Innamarato PP, et al. Expansion of tumor infiltrating lymphocytes (TIL) from bladder cancer. *Oncoimmunology* (2018) 7(9):e1476816. doi: 10.1080/2162402X.2018.1476816
15. Tan TZ, Rouanne M, Tan KT, Huang RY, Thiery JP. Molecular Subtypes of Urothelial Bladder Cancer: Results from a Meta-cohort Analysis of 2411 Tumors. *Eur Urol* (2019) 75(3):423–32. doi: 10.1016/j.eururo.2018.08.027
16. Dadhania V, Zhang M, Zhang L, Bondaruk J, Majewski T, Siefker-Radtke A, et al. Meta-Analysis of the Luminal and Basal Subtypes of Bladder Cancer and the Identification of Signature Immunohistochemical Markers for Clinical Use. *EBioMedicine* (2016) 12:105–17. doi: 10.1016/j.ebiom.2016.08.036
17. Chacon JA, Sarnaik AA, Chen JQ, Creasy C, Kale C, Robinson J, et al. Manipulating the tumor microenvironment ex vivo for enhanced expansion of tumor-infiltrating lymphocytes for adoptive cell therapy. *Clin Cancer Res* (2015) 21(3):611–21. doi: 10.1158/1078-0432.CCR-14-1934
18. *National Comprehensive Cancer Network guidelines: bladder cancer V 6.2029* (2020). Available at: https://www.nccn.org/professionals/physician_gls/pdf/bladder.pdf.
19. Chalmers ZR, Connelly CF, Fabrizio D, Gay L, Ali SM, Ennis R, et al. Analysis of 100,000 human cancer genomes reveals the landscape of tumor mutational burden. *Genome Med* (2017) 9(1):34. doi: 10.1186/s13073-017-0424-2
20. Rosenberg SA, Yang JC, Sherry RM, Kammula US, Hughes MS, Phan GQ, et al. Durable complete responses in heavily pretreated patients with metastatic melanoma using T-cell transfer immunotherapy. *Clin Cancer Res* (2011) 17(13):4550–7. doi: 10.1158/1078-0432.CCR-11-0116
21. Goff SL, Smith FO, Klapper JA, Sherry R, Wunderlich JR, Steinberg SM, et al. Tumor infiltrating lymphocyte therapy for metastatic melanoma: analysis of tumors resected for TIL. *J Immunother* (2010) 33(8):840–7. doi: 10.1097/CJI.0b013e3181f05b91
22. Vetterlein MW, Wankowicz SAM, Seisen T, Lander R, Loppenberg B, Chun FK, et al. Neoadjuvant chemotherapy prior to radical cystectomy for muscle-invasive bladder cancer with variant histology. *Cancer* (2017) 123(22):4346–55. doi: 10.1002/cncr.30907
23. Necchi A, Raggi D, Gallina A, Madison R, Colecchia M, Luciano R, et al. Updated Results of PURE-01 with Preliminary Activity of Neoadjuvant Pembrolizumab in Patients with Muscle-invasive Bladder Carcinoma with Variant Histologies. *Eur Urol* (2020) 77(4):439–46. doi: 10.1016/j.eururo.2019.10.026
24. Batista da Costa J, Gibb EA, Bivalacqua TJ, Liu Y, Oo HZ, Miyamoto DT, et al. Molecular Characterization of Neuroendocrine-like Bladder Cancer. *Clin Cancer Res* (2019) 25(13):3908–20. doi: 10.1158/1078-0432.CCR-18-3558
25. Cheng L, Zhang S, Alexander R, Maclennan GT, Hodges KB, Harrison BT, et al. Sarcomatoid carcinoma of the urinary bladder: the final common pathway of urothelial carcinoma dedifferentiation. *Am J Surg Pathol* (2011) 35(5):e34–46. doi: 10.1097/PAS.0b013e3182159dec
26. Chevalier MF, Trabanelli S, Racle J, Salome B, Cesson V, Gharbi D, et al. ILC2-modulated T cell-to-MDSC balance is associated with bladder cancer recurrence. *J Clin Invest* (2017) 127(8):2916–29. doi: 10.1172/JCI89717
27. Kates M, Nirschl T, Sopko NA, Matsui H, Kochel CM, Reis LO, et al. Intravesical BCG Induces CD4(+) T-Cell Expansion in an Immune Competent Model of Bladder Cancer. *Cancer Immunol Res* (2017) 5(7):594–603. doi: 10.1158/2326-6066.CIR-16-0267
28. Kamoun A, de Reynies A, Allory Y, Sjodahl G, Robertson AG, Seiler R, et al. A Consensus Molecular Classification of Muscle-invasive Bladder Cancer. *Eur Urol* (2020) 77(4):420–33. doi: 10.1016/j.eururo.2019.11.011
29. Necchi A, Raggi D, Gallina A, Ross JS, Fare E, Giannatempo P, et al. Impact of Molecular Subtyping and Immune Infiltration on Pathological Response and Outcome Following Neoadjuvant Pembrolizumab in Muscle-invasive Bladder Cancer. *Eur Urol* (2020) 77(6):701–10. doi: 10.1016/j.eururo.2020.02.028
30. Todenhofer T, Seiler R. Molecular subtypes and response to immunotherapy in bladder cancer patients. *Transl Androl Urol* (2019) 8(Suppl 3):S293–S5. doi: 10.21037/tau.2019.06.21
31. Rosenberg JE, Hoffman-Censits J, Powles T, van der Heijden MS, Balar AV, Necchi A, et al. Atezolizumab in patients with locally advanced and metastatic urothelial carcinoma who have progressed following treatment with platinum-based chemotherapy: a single-arm, multicentre, phase 2 trial. *Lancet* (2016) 387(10031):1909–20. doi: 10.1016/S0140-6736(16)00561-4
32. Weber J, Atkins M, Hwu P, Radvanyi L, Sznol M, Yee C, et al. White paper on adoptive cell therapy for cancer with tumor-infiltrating lymphocytes: a report of the CTEP subcommittee on adoptive cell therapy. *Clin Cancer Res* (2011) 17(7):1664–73. doi: 10.1158/1078-0432.CCR-10-2272
33. Rohaan MW, van den Berg JH, Kvistborg P, Haanen J. Adoptive transfer of tumor-infiltrating lymphocytes in melanoma: a viable treatment option. *J Immunother Cancer* (2018) 6(1):102. doi: 10.1186/s40425-018-0391-1

Conflict of Interest: Moffitt Cancer Center has licensed Intellectual Property (IP) related to the proliferation and expansion of tumor infiltrating lymphocytes (TILs) to Iovance Biotherapeutics. SP-T and AS are inventors on such Intellectual Property. SP-T and AS are listed as co-inventors on a patent application with Provectus Biopharmaceuticals. Moffitt has also licensed IP to Tuhura Biopharma, and SP-T is an inventor on such Intellectual Property.

The remaining authors declare that the research was conducted in the absence of any commercial or financial relationships that could be construed as a potential conflict of interest.

Copyright © 2021 Aydin, Bunch, Beatty, Hajiran, Dhillon, Sarnaik, Pilon-Thomas and Poch. This is an open-access article distributed under the terms of the Creative Commons Attribution License (CC BY). The use, distribution or reproduction in other forums is permitted, provided the original author(s) and the copyright owner(s) are credited and that the original publication in this journal is cited, in accordance with accepted academic practice. No use, distribution or reproduction is permitted which does not comply with these terms.

frontiers in Immunology

METHODS
published: 14 May 2021
doi: 10.3389/fimmu.2021.672031

A Cancer-Specific Qualitative Method for Estimating the Proportion of Tumor-Infiltrating Immune Cells

Huiting Xiao[1†], Jiashuai Zhang[1†], Kai Wang[1,2†], Kai Song[1], Hailong Zheng[1], Jing Yang[1], Keru Li[1], Rongqiang Yuan[1], Wenyuan Zhao[1] and Yang Hui[2*]*

[1] Department of Systems Biology, College of Bioinformatics Science and Technology, Harbin Medical University, Harbin, China, [2] Department of Biochemistry and Molecular Biology, Harbin Medical University, Harbin, China

OPEN ACCESS

Edited by:
Alexandr Bazhin, LMU Munich University Hospital, Germany

Reviewed by:
Rainer Christoph Miksch, Ludwig Maximilian University of Munich, Germany
Florent Petitprez, University of Edinburgh, United Kingdom

***Correspondence:**
Wenyuan Zhao
zhaowenyuan@ems.hrbmu.edu.cn
Yang Hui
huiyang79@126.com

[†]These authors have contributed equally to this work and share first authorship

Specialty section:
This article was submitted to Cancer Immunity and Immunotherapy, a section of the journal Frontiers in Immunology

Received: 25 February 2021
Accepted: 22 April 2021
Published: 14 May 2021

Citation:
Xiao H, Zhang J, Wang K, Song K, Zheng H, Yang J, Li K, Yuan R, Zhao W and Hui Y (2021) A Cancer-Specific Qualitative Method for Estimating the Proportion of Tumor-Infiltrating Immune Cells. Front. Immunol. 12:672031. doi: 10.3389/fimmu.2021.672031

Tumor-infiltrating immune cells are important components in the tumor microenvironment (TME) and different types of these cells exert different effects on tumor development and progression; these effects depend upon the type of cancer involved. Several methods have been developed for estimating the proportion of immune cells using bulk transcriptome data. However, there is a distinct lack of methods that are capable of predicting the immune contexture in specific types of cancer. Furthermore, the existing methods are based on absolute gene expression and are susceptible to experimental batch effects, thus resulting in incomparability across different datasets. In this study, we considered two common neoplasms as examples (colorectal cancer [CRC] and melanoma) and introduced the Tumor-infiltrating Immune Cell Proportion Estimator (TICPE), a cancer-specific qualitative method for estimating the proportion of tumor-infiltrating immune cells. The TICPE was based on the relative expression orderings (REOs) of gene pairs within a sample and is notably insensitive to batch effects. Performance evaluation using public expression data with mRNA mixtures, single-cell RNA-Seq (scRNA-Seq) data, immunohistochemistry data, and simulated bulk RNA-seq samples, indicated that the TICPE can estimate the proportion of immune cells with levels of accuracy that are clearly superior to other methods. Furthermore, we showed that the TICPE could effectively detect prognostic signals in patients with tumors and changes in the fractions of immune cells during immunotherapy in melanoma. In conclusion, our work presented a unique novel method, TICPE, to estimate the proportion of immune cells in specific cancer types and explore the effect of the infiltration of immune cells on the efficacy of immunotherapy and the prognosis of cancer. The source code for TICPE is available at https://github.com/huitingxiao/TICPE.

Keywords: tumor microenvironment, relative expression orderings, signature genes, prognosis, immunotherapy

INTRODUCTION

Immune cells are critical components in the complex tumor environment (TME). Tumor-infiltrating immune cells (TIICs) can have either tumor-promoting or tumor-suppressive effects on tumor development and progression, depending on the specific type of cancer involved (1). The types and densities of TIICs not only have predictive value in patient survival, they also affect tumor responses to therapy, particularly immunotherapy (2, 3). For instance, an increase in CD8+ T cells is generally associated with improved clinical outcomes, whereas regulatory T cells (Tregs) and tumor-associated macrophages (TAMs) are often associated with a poor prognosis (4, 5). In addition, immune checkpoint blockade (ICB) antibodies reinvigorate anti-tumor immunotherapy responses by disrupting co-inhibitory T-cell signaling, a pathway that has demonstrated clinical activity in several malignancies (6). Evidence has shown that CD4+ and CD8+ memory T cell subsets, as well as NK cell subsets, correlated with a clinical response to immunotherapy in patients with melanoma (7, 8). As such, an assessment of TIICs is of critical importance in biomedical research as well as clinical pathology (9).

Previous studies concerning alterations in the composition of immune cells in human cancers have predominantly relied on immunohistochemistry (IHC) or flow cytometry. However, these techniques are compromised by the limited set of available molecular markers and are cumbersome to apply to large panels of tumors; furthermore, in the case flow cytometry, fresh or frozen tissue is required (10, 11). An abundance of transcriptomics data provide an ideal resource for large-scale immune landscape analysis and have been used to develop many computational methods that have been mainly classified into two categories: deconvolution-based approaches and methods that are based on marker genes (12). The deconvolution methods, which include CIBERSORT (13), TIMER (14), EPIC (15), and quanTIseq (16), estimate the cell fractions leveraging on a reference matrix composed of representative expression signatures for specific immune cells. Techniques that are based on marker genes, including MCP-counter (17), xCell (18), and ImmuCellAI (19), utilize a list of genes characterized for each immune cell type to compute an enrichment score and allow for inter-sample comparisons of the same immune cell type. However, these methods have been developed for the enumeration of immune cells from bulk transcriptome data from multiple cancer types that masked inter-tumor heterogeneity between different tumor types; this would affect accuracy, at least to some extent (20). In addition, all of these methods were based on absolute gene expression, thus resulting in incomparability across different datasets. Some of these techniques require data normalization, a process that is susceptible to experimental batch effects and can even distort real biological signals (21). In contrast, our research team has proven that qualitative information derived from relative gene expression is highly robust with regards to batch effects and does not necessarily require normalization (22, 23). It is therefore imperative to develop a cancer-specific qualitative method to estimate the proportion of tumor-infiltrating immune cells.

In this study, we considered colorectal cancer and melanoma as examples and constructed Tumor-infiltrating Immune Cell Proportion Estimator (TICPE), a qualitative method based on the relative expression orderings (REOs) of gene pairs within a sample, to estimate the proportion of immune cells in a TME. These cell proportions could then be used to directly compare the proportion of the corresponding immune cells across samples within a cohort or different cohorts. TICPE was extensively validated in human solid tumors *via* publicly available IHC data, mRNA mixtures, single-cell RNA-Seq (scRNA-Seq) data from colorectal and melanoma tumors, and simulated bulk samples. Moreover, the immune cell proportions estimated by TICPE could be used for prognostic analysis and associated with treatment status and the efficacy of immunotherapy response to melanoma.

MATERIALS AND METHODS

Dataset Preparation

We downloaded gene expression datasets from the Gene Expression Omnibus (GEO, http://cancergenome.nih.gov/) and RNA sequencing data from The Cancer Genome Atlas (TCGA) by the University of California Santa Cruz (UCSC) Xena website (https://xena.ucsc.edu/). The processed gene expression profiles of 97 datasets were divided into three sections (see **Supplementary Table 1**). Eighty-one of these datasets contained eight types of human immune cells and cancer cell lines; normal samples were used to generate signature genes and develop the TICPE. Five datasets were used for to assess the performance of the TICPE. Dataset 1 was derived from an *in vitro* RNA mixture experiment, GEO accession GSE64385. These mixtures contained different immune populations that were purified from the peripheral blood from healthy donors with variable concentrations and were further diluted in a fixed amount of a solution containing mRNA extracted from HCT-116, a CRC cell line (**Supplementary Table 2A**). Dataset 2 contained a large series of 566 CRC tumors and 19 non-tumoral colorectal mucosas, GEO accession GSE39582. Of the 566 tumors, 33 patients also had immunohistochemistry data relating to CD3, CD8, and CD68 (Aurélien de Reyniès, Personal Communication). The other three datasets (Accession numbers GSE146771, GSE115978, and GSE72056) were scRNA-Seq data, and corresponded to 10 colon cancer samples, and 31 and 19 patients with melanoma, respectively (see **Supplementary Tables 2B–D**). The remaining datasets that were associated with clinical information were used to investigate prognosis and response to immunotherapy. The response categories of the melanoma patients were defined by the RECIST classification scheme (Response Evaluation Criteria in Solid Tumors) as a complete response (CR) and partial response (PR) for responders, or stable disease (SD) and progressive disease (PD) for non-responders (24).

For the data downloaded from GEO, we mapped the probe ID to the Entrez gene ID using the corresponding platform annotation file. Data were discarded if a probe had no or

multiple corresponding Entrez gene IDs. If multiple probes shared the same Entrez gene ID, then the arithmetic mean of the expression values of these probes was used as the final expression value of the gene. For the RNA-Seq data, profiles of fragments per kilobase million (FPKM) were directly downloaded from the TCGA. For scRNA-Seq data, the reconstructed bulk samples from each donor were identified by aggregating expression profiles from all cell barcodes of the given donor. The cell ratio per cell type in a donor was then calculated by the cell number of a specific cell type divided by the total number of cells (19).

Marker Gene Preparation

For each immune cell type, we integrated a list of marker genes obtained from the literature and other analytical methods, such as xCell and MCP-counter. Most of these were overexpressed relative to other immune cells, and a total of 2,034 marker genes were acquired (see **Supplementary Table 3**).

Highly Stable Pairs in Cancer Cell Lines

For each cancer cell, pairwise comparisons were performed for the expression level of all genes. For each gene pair (G_i, G_j), with only two possible REO outcomes (the gene expression of $G_i > G_j$ or $G_i < G_j$), we retained the gene pair with a certain REO ($G_i > G_j$ or $G_i < G_j$) in at least 99% cancer cells, defined as a highly stable gene pair (SPairs).

The TICPE Development Pipeline

This cancer-specific method can be used for a variety of cancer types. Here, we took colorectal cancer as an example to describe the process in detail, the flowchart for TICPE is described in **Figure 1**.

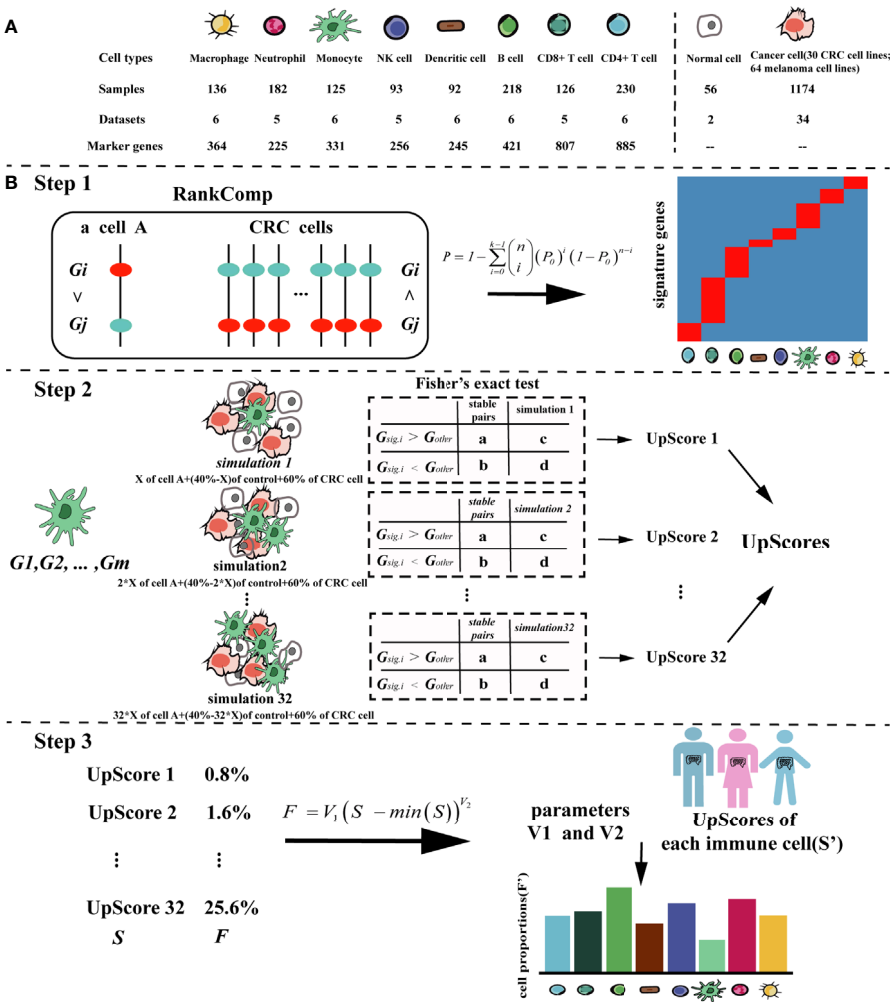

FIGURE 1 | The pipeline of the TICPE algorithm. **(A)** Summary of the data sources used in the study to develop the TICPE. **(B)** The pipeline of the TICPE algorithm. RankComp algorithm was used to identify robust signature genes compared with cancer cells for each type of immune cell from the known marker genes. The upregulated score was the reversal significance of all signature genes corresponding to the cell type. Using the simulated model for each cell type, we derived a transformation pipeline for the scores. For each queried sample, calculated upregulated scores and transformed them to estimated cell proportions using learned parameters.

Identifying Signature Genes Compared With CRC Cells

Since cell-type-specific signatures can vary depending on cancer type, there is a need to identify cancer-type specific marker genes for each immune cell type. We take immune cell type *A* with *n* cells as an example to illustrate the process that can be used to identify the corresponding signature genes among reported marker genes. Firstly, we used the RankComp algorithm (25) to identify individual-level differentially upregulated marker genes (up-DEGs) for each immune cell compared with the SPairs in the CRC cell lines. The p-values of RankComp were adjusted using the Benjamini and Hochberg method (26). Secondly, the cumulative binomial distribution model was used to identify up-DEGs shared by a non-random high proportion of samples and the *P* value determined whether a marker gene was differentially upregulated at the population level. Then, the *P* values were also adjusted for multiple testing to control the false discovery rate (FDR). The significance was calculated as shown in Equation (1).

Equation (1):

$$P = 1 - \sum_{i=0}^{k-1} \binom{n}{i} (P_0)^i (1 - P_0)^{n-i}$$

In Equation (1), P_0 represents the probability of observing a marker gene being differentially upregulated in a sample by chance (P_0 = 0.5), n and k represent the total number of samples of the immune cell type *A* and the number of samples with the marker gene being differentially upregulated, respectively. Next, when a marker gene's adjusted P-value was <0.05, it would be reserved. We finally removed the up-DEGs included in more than one type of immune cell to reduce the dependencies between closely related cell types, and the remained up-DEGs were defined as signature genes (Step 1).

Calculating Upregulated Scores Based on Signature Genes

Based on the signature genes for each immune cell type, we were able to compute the cell infiltration scores for each sample. However, the scores had different distributions between different signature genes and could not thus be compared across immune cell types in a sample. Thus, for each cell type, we conducted a simulated model using the immune cell (cell *A*) with an additional "control" cell type (a sample of normal colon) and a variety of CRC cell lines. Different types of CRC cell lines were used to reflect the heterogeneity of patients with the same cancer. For the simulated models, batch effects among the three types of dataset were removed using Combat (27). Then, we generated such simulations by using the median expression profile of the merged profile composed of three cell types: 60% of the CRC cell, X% of cell *A*, and 40–X% control (28). X% represents an arithmetic sequence with a range of 0.8 to 25.6% and an interval of 0.8%. We used this range because these interesting cell types had low fractions in the TME (18).

Taking the SPairs of CRC cell lines as the background, we calculated the cell infiltration scores of the simulations using *m* signature genes $\{G_{sig.1}, G_{sig.2}, \ldots G_{sig.m}\}$, as described below. We were able to calculate the numbers of gene pairs (the gene pair was constructed by G_{sig} and G_{other}) belonging to SPairs with ordering patterns ($G_{sig.i} > G_{other}$) and ($G_{sig.i} < G_{other}$) in cancer cells, which were denoted *a* and *b*. Similarly, *c* and *d* denoted the corresponding numbers of gene pairs with ordering patterns ($G_{sig.i} > G_{other}$) and ($G_{sig.i} < G_{other}$) in a simulation sample. When simulations involved an increasing proportion of immune cells, there were more stable pairs with the ordering patterns ($G_{sig.i} > G_{other}$). Using Fisher's exact test, we were able to determine the degree of cell infiltration by calculating the reversal significance, also known as the upregulated score (UpScore) for each simulation sample (Step 2).

Transforming UpScores to Estimate Cell Proportions

We designed a transformation pipeline for the UpScores of each cell type to enable the estimated proportions to be compared across cell types, and not just across samples. A simulation containing 0.8% of immune cells was considered to barely result in reversal significance. Therefore, for the simulated model of cell *A*, we first shifted the UpScores to 0 using the minimal UpScore (which corresponded to the simulation containing 0.8% of cell *A*) and fitted a power function to the UpScores that corresponded to proportions of 0.8 to 25.6%. The transformed parameters (V_1 and V_2) were acquired by Equation (2). For each immune cell type, we could get a pair of transformed parameters.

Equation (2):

$$F_i = V_{1i}(S_i - \min(S_i))^{V_{2i}}$$

In Equation (2), *F* represents the proportions of 0.8 to 25.6% and *S* represents the corresponding UpScores of cell *A*.

It was recommended that an expression dataset should contain as many signature genes as possible. The UpScores of different immune cell types were calculated based on their different signature genes. Subsequently, using the parameters corresponding to immune cells, the UpScores were transformed into estimated cell proportions for each sample (Step 3).

The Generation of Simulated Data

We simulated bulk RNA-seq data with different tumor purity values and immune infiltrates by mixing malignant cells with different immune cells from a scRNA-seq dataset. There were 100 simulated samples and each of these was composed of 1,000 cells that were randomly selected, as follows: (i) Cancer cells form the majority of a simulated samples, a fraction f of them was constrained to the interval [0.5, 0.99], and the remaining fraction $1 - f$ was randomly assigned to the other immune cell types; (ii) the fraction was multiplied by 1,000 to obtain cell counts for different cell types; (iii) the corresponding number of cells was randomly selected from the single cell dataset. If one cell type was available from the scRNA-seq dataset with only a few cells available, then, the same single cell sample would be selected multiple times for the artificial bulk sample.

Performance Assessment of the TICPE

The performance of the TICPE was evaluated using both microarray and RNA-Seq datasets and compared with that of previously published methods (CIBERSORT, EPIC, xCell,

MCP-counter, and ImmuCellAI). For a given immune cell type, the accuracy and sensitivity of each method were measured using Pearson's correlation between the results of *in silico* methods and the true proportions, as measured by immunohistochemistry or scRNA-Seq. Furthermore, we introduced a correlation deviation (19) for all cell types to measure the global performance of each method; this strategy took the sample size and overall accuracy into consideration. A smaller correlation deviation might suggest that the predicted cell fractions agree better with the true composition, as shown in Equation (3).

Equation (3):

$$correlation\ deviation = \sqrt{\frac{1}{n}\sum_{i=1}^{n}(1 - r_i)^2}$$

In Equation (3), n represents the number of immune cell types detected in samples and r_i represents the Pearson correlation coefficient of immune cell type i.

Statistical Analysis

The correlation between estimated proportion and true composition was evaluated by Pearson's correlation. The ROC analysis was performed to assess the validity of the TICPE and was completed by pROC R Package. The statistical significance of comparisons between two groups or more than two groups was estimated by the Wilcoxon rank-sum test or the Kruskal–Wallis test, respectively. The overall survival curves were estimated by the Kaplan–Meier method, and the differences between survival distributions were evaluated by the two-sided log-rank test (29). The Venn diagram was used to analyze the signature genes were different between CRC and melanoma by ggvenn R Package. All statistical analyses were performed using R program (version 4.0.2). P-values were two-sided, and P <0.05 was considered to be statistically significant (4).

RESULTS

Development of the TICPE Algorithm

We designed a method, called TICPE, to estimate the proportions of eight important tumor-infiltrating immune cells (B cells, $CD4^+$ T cells, $CD8^+$ T cells, dendritic cells (DC), monocytes, macrophages, natural killer (NK) cells, and neutrophils) in a specify type of cancer. We integrated marker genes for these different cell types from publications and obtained expression profiles for immune cells, cancer cell lines, and normal tissues, from the GEO database (**Figure 1A**; **Table 1**). Taking colorectal cancer as an example, a three-step strategy of the core algorithm of TICPE is shown in **Figure 1B**; the detailed algorithm is described in the *Materials and Methods* section. Since the marker genes were screened relative to other immune cells, but not to tumor cells, the genes for a specific type of cancer needed to be filtered. We applied the RankComp algorithm to detect overexpressed marker genes in a given immune cell compared with CRC cells (*FDR* <5%). We then created a specific gene set from overexpressed marker genes as signature genes; this included 218 genes from the eight immune cell types (Binomial test, *FDR* <5%) (**Table 2**) (Step 1). We were then able to compute the cell infiltration scores for each sample based on the signature genes (Fisher's exact test) (Step 2). However, the scores exhibited different distributions between different signature genes and could not therefore be compared across cell types in a given sample. For each immune cell type, we thus conducted a simulated model using the immune cells, CRC cells, and normal colon samples, and calculated the UpScores based on signature genes. Next, we designed a transformation pipeline for the UpScores and acquired a pair of transformed parameters for each cell type. For CRC samples, we were able to calculate the UpScores for each immune cell type and transform these into the estimated cell proportions with the acquired parameters corresponding to immune cells (Step 3).

The Performance of the TICPE in CRC and Melanoma Samples

Firstly, we calculated the proportion of immune cells in CRC samples with three independent publicly available datasets, and simulated RNA-seq data, to evaluate the TICPE. In the *in vitro* RNA mixture experiment (GSE64385), we observed that the estimated cell proportions were highly correlated with the cell proportions for the populations introduced in the mixtures ($\rho = 0.99$ and $P = 4.2 \times 10^{-13}$ for B cells, $\rho = 0.82$ and $P = 9.9 \times 10^{-4}$ for monocytes, $\rho = 0.96$ and $P = 3.3 \times 10^{-7}$ for NK cells,

TABLE 1 | Datasets used in developing TICPE for colorectal cancer.

Cell Type	Accession	Samples#	Marker Gene#
CRC cells	GSE11618, GSE13059, GSE110425, GSE14103, GSE16648, GSE122985, GSE18560, GSE24795, GSE115716, GSE35566, GSE55624, GSE59196, GSE63252, GSE112282, GSE50841, GSE116528, GSE90085, GSE59883, GSE59857, GSE116529, GSE75205, GSE106073, GSE72544, GSE50791, GSE119197, GSE120993	687	–
B cells	GSE24736, GSE19599, GSE12366, GSE49910, GSE120367, GSE75007	218	422
CD4+ T cells	GSE11292, GSE36769, GSE32959, GSE50175, GSE103527, GSE71956	230	885
CD8+ T cells	GSE84251, GSE93683, GSE98640, GSE84331, GSE71956	126	807
NK cells	GSE27838, GSE8059, GSE21774, GSE35330, GSE75091	93	256
Macrophages	GSE102117, GSE100129, GSE7568, GSE16385, GSE13670, GSE24897	136	364
Monocytes	GSE38351, GSE39840, GSE35683, GSE6054, GSE60199, GSE98480	125	331
DCs	GSE7509, GSE10316, GSE23618, GSE23371, GSE87494, GSE85305	92	245
Neutrophils	GSE22103, GSE39889, GSE8668, GSE18810, GSE70044	182	225

#, number; CRC, colorectal cancer; NK cells, natural killer cells; DCs, dendritic cells.

TABLE 2A | A specific gene set compared with CRC cells for per cell type was selected and used in TICPE.

Cell Type	Gene Number	Signature Genes
B cells	24	*BLK, CD19, CD79A, CD79B, IGLL1, TCL1A, TLR7, FCRL2, BANK1, CPNE5, KLHL14, LINC00926, FCRL5, EBF1, ARHGAP25, CLECL1, TNFRSF17, FCRLA, HLA-DOB, NCF1, P2RY10, PNOC, TLR9, FCRL4*
CD4+ T cells	65	*ANK1, CD40LG, CD69, CD72, CHI3L2, CCR4, CCR8, DGKA, FYN, GATA3, GPR18, GPR19, IL2RA, IL6R, IL9R, IL12RB2, TNFRSF9, ITGA4, ITGB2, JAK3, LCK, LTB, MAL, CD200, NPAT, P2RX5, PDCD1, PLCL1, PTPRC, RGS1, SELPLG, STAT4, STAT5A, STAT5B, TXK, WIPF1, SOCS3, AIM2, HS3ST3B1, TLR6, CD226, PASK, PLCL2, ANKRD12, STAP1, ZBTB32, LAT, PNMA3, FOXP3, ASB2, LRRN3, LAX1, RNF125, PARP11, PLXDC1, MAN1C1, HIVEP3, BCL11B, PVRIG, ANKRD55, TRIM46, LIMD2, SIGLEC10, RCSD1, PIK3IP1*
CD8+ T cells	42	*ABCD2, RUNX3, CD8A, CD8B, LYST, TSC22D3, GPR183, FLT3LG, HLA-DPB1, IFI16, INPP4A, POU6F1, PTGER4, RAB27A, ATXN7, ZBTB16, EOMES, IL18R1, SLC16A7, ITM2A, AKAP5, TOX, SPOCK2, ZEB2, PLXNC1, CA5B, IKZF2, PTPN22, PBXIP1, IGFLR1, APOL3, KIAA1109, SLA2, SLFN11, JAML, TC2N, TTC39C, TMIGD2, TMEM71, HAPLN3, PYHIN1, JAKMIP1*
DCs	15	*SLAMF8, CCL17, CD1B, CD1E, CLIC2, CD1C, CD209, DNASE1L3, IL3RA, SAMSN1, FABP4, C1QC, SLAMF9, THBD, FAM49A*
Macrophages	18	*CHIT1, CD14, APOC1, HAMP, VSIG4, SDS, SIGLEC7, ADAMDEC1, CCL18, CCL8, CCR1, CMKLR1, CSF1, HS3ST2, MMP19, CPM, ENG, MS4A7*
Monocytes	26	*TLR8, ASGR2, IRAK3, CD33, CFP, CLEC4A, CLEC4E, CXorf21, DOK2, DOK3, FCN1, HCK, LILRA1, LILRA5, LILRB2, MNDA, MYO1F, NCF4, PILRA, PLEK, POU2F2, PSTPIP1, QKI, RETN, CD300LF, SRGN*
NK cells	16	*KIR2DL3, NCR1, FGFBP2, KIR3DS1, PTGDR, LIM2, KIR3DL1, KIR2DS1, KIR3DL3, KIR2DS2, KIR2DS5, KIR2DL1, SH2D1B, KIR2DL4, PIK3CG, KIR2DS4*
Neutrophils	13	*FCGR3B, ALPL, VNN3, FFAR2, MMP25, TREM1, FPR1, LINC00528, CMTM2, PROK2, CLEC7A, CAMP, VNN2*

CRC, colorectal cancer; NK cells, natural killer cells; DCs, dendritic cells.

TABLE 2B | A specific gene set compared with melanoma cells for per cell type was selected.

Cell type	Gene Number	Signature Genes
B cells	15	*MS4A1, BLK, CD19, GNG3, SGCA, CD79A, CD79B, CD53, CD72, HTR3A, IGLL1, TCL1A, TLR7, VPREB3, AICDA*
CD4+ T cells	85	*LIMD2, TRAF1, NPAT, PIK3IP1, ANKRD12, AAK1, ACBD4, CD226, CUBN, GPSM3, GRAP2, IL16, INSL3, JAK3, KLHL3, KRT2, LAIR2, MLH3, MLXIP, NOL9, SELPLG, SORCS3, STAP1, TNK1, TSPAN32, ZNF780B, HS3ST3B1, FOXP3, LAX1, STAT5B, TTN, CCR3, NFATC3, IL2, GGT1, SYNGR3, IL12RB1, STAT4, ZBTB32, CSF2, DPP4, IL12RB2, IL22, EGFL6, IL4, GATA3, IL5, IL13, IL26, ANK1, MB, MICAL2, PHEX, PTGIS, IL1R1, RORC, IL21, IL1R2, IL17A, MAP4K1, SIK1, FOSB, PVRIG, CD69, BCL11B, CHI3L2, DGKA, LAT, LCK, MAP9, PASK, RGS1, SLC7A10, TCF7, TSHR, ZBTB10, TFAP4, COL5A3, ADCYAP1R1, DAB1, ERN1, FXYD7, PNMA3, ARHGEF5, DEFB126*
CD8+ T cells	43	*BLNK, HTR1B, SMCP, RRH, CCDC87, MOGAT2, GJB4, CALY, KIAA1109, CD248, RFX2, AMBN, MYL1, GPR52, CILP, TNFRSF10C, ITGAM, PTGDR2, PRDM1, MPO, RUNX3, APOL3, DUSP2, ZBTB16, CCND2, EOMES, ITM2A, SNX9, CXCL13, HAVCR2, LINC00299, MYO7A, TIGIT, TNFRSF1B, AKAP5, TOX, RGS2, GALM, SYNGR2, PTGER4, CCR6, ATR, GIPR*
DCs	28	*PTGIR, SLAMF8, SLC15A3, SYT17, CCL13, CCL17, CD1B, CD1E, CLIC2, MMP12, TREM2, PLA2G7, ALDH1A2, ALOX15, ALOX15B, BCL2L11, CCL23, CD1A, CD1C, CD209, CD80, DNASE1L3, FLT3, FUT7, GUCA1A, IL12B, IL3RA, KCNK13*
Macrophages	19	*CAMP, CHIT1, CD14, FCGR1A, HAMP, MSR1, VSIG4, SDS, SIGLEC7, TYROBP, ADAMDEC1, CCL7, CCR1, CD84, CMKLR1, CPNE6, CXCL9, CYBA, CYP19A1*
Monocytes	31	*CA1, TLR8, FOLR2, ASGR2, IRAK3, CD33, VCAN, AIF1, CD101, CD93, CEACAM4, CFP, CLEC4A, CXorf21, DOK2, DOK3, FCER1A, FCN1, FGL2, FOLR3, GPR183, HCK, KCNMB1, KDM6B, KSR1, LILRA1, LILRA5, LILRB1, LST1, LY86, LYL1*
NK cells	11	*KIR2DL3, NCR1, NCR3, PRR5L, KIR3DS1, PTGDR, HIPK1, LIM2, NMUR1, PRDM2, TNFSF11*
Neutrophils	19	*CXCR1, FCGR3B, S100A12, TREML2, TRPM6, SIGLEC5, CREB5, ALPL, CEACAM3, VNN3, CA4, CEACAM8, CYP4F3, FFAR2, HBB, MMP25, P2RY13, PGLYRP1, TGM3*

NK cells, natural killer cells; DCs, dendritic cells.

$\rho = 0.96$ and $P = 4.1 \times 10^{-7}$ for neutrophils; **Figure 2A**). Then, we used scRNA-Seq data from 10 colon cancer samples (GSE146771) and compared TICPE predictions with measured immune cell proportions. As shown in **Figure 2B**, the proportions of immune cells estimated by the TICPE showed a significantly positive correlation with the actual cell proportions ($P < 0.05$). We also observed a significant correlation between our predictions and the immunohistochemistry data from 33 colorectal cancer tumors ($P < 0.05$; **Figure 2C**). The number of samples available from published data was limited, so we further used the scRNA-Seq data of annotated immune cells to generate 100 simulated bulk RNA-seq samples (further details are given in the *Materials and Methods* section). The TICPE showed a high correlation between the known proportions and the estimated fractions in the simulated dataset ($P < 0.01$; **Figure 2D**). Furthermore, we used two scRNA-Seq datasets from melanoma patients (GSE115978; GSE72056) as benchmark resources for assessing the performance of the TICPE. The estimated proportion of each immune cell type was found to correlate with the true immune cell proportions that were calculated from single cell barcode information ($P < 0.05$; **Supplementary Figures 1A, B**). Similarly, we used one of the scRNA-seq datasets (GSE115978) from melanoma ecosystems to simulate bulk samples of known cell type proportions and observed a good agreement with our predictions ($P < 0.05$; **Supplementary Figure 1C**). Furthermore, we employed the receiver operating characteristic (ROC) curve and the area under the curve (AUC) to evaluate the performance of TICPE.

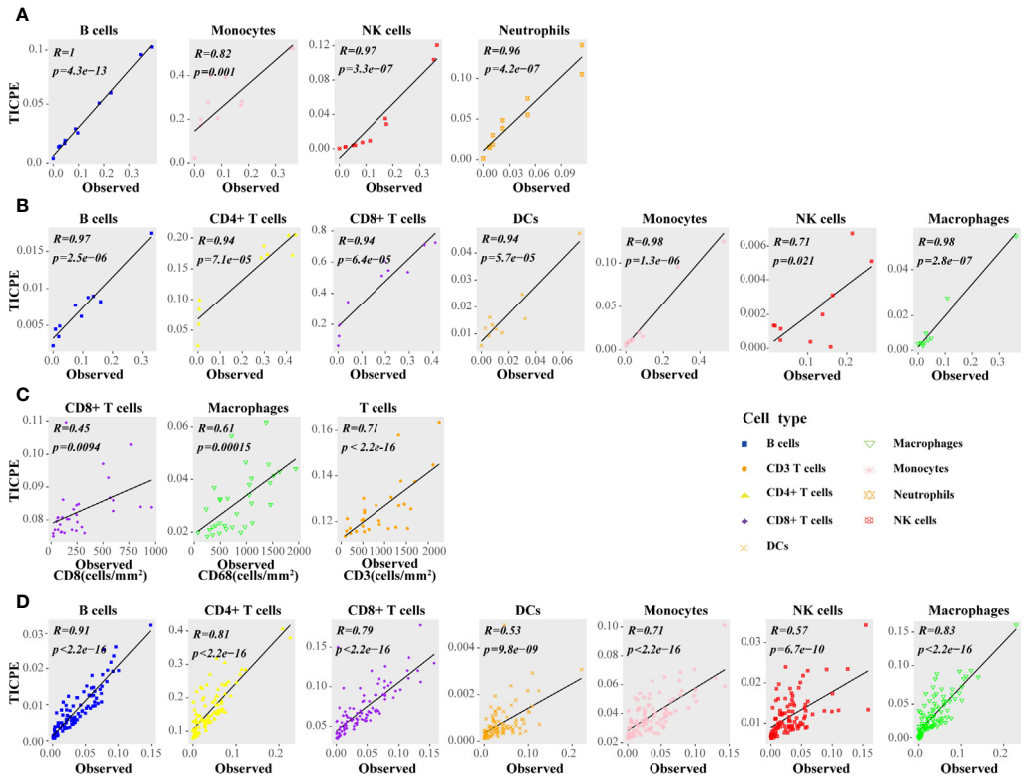

FIGURE 2 | Performance assessment of the TICPE in solid tumors. **(A)** Correlation of the TICPE predictions with the cell proportions for the populations introduced in the mixtures. **(B)** Comparison with single-cell RNA-Seq data from colon samples. **(C)** Correlation of the TICPE predictions with corresponding cell densities measured by immunohistochemistry from colon cancer primary tumors. **(D)** Correlation of the TICPE predictions versus known cell type fractions on 100 simulated bulk samples generated from scRNA-seq from colon samples. Correlations were based on Pearson correlation. Proportions of cells observed experimentally were given in **Supplementary Table 2**.

We used the median true cell proportions as the cutoff for each cell type, and found the TICPE estimates had an AUC value ranging from 0.667 to 1 on publicly available datasets (**Supplementary Figure 2**).

We hypothesized that the high correlation values resulted, at least in part, from the robust signature genes for a specific type of cancer. Therefore, we respectively collated sets of marker genes, as reported by Angelova et al. (30), Aran et al. (18), and Manoharan et al. (31), and used the same pipeline to estimate the cell proportions to compare the representativeness of the signature genes selected by the TICPE and those in specific types of cancer. Using these public validation datasets with different cell types, we evaluated the performance of the signature gene sets on independent datasets. We observed that, in most cases, the selected signature genes in our study showed better performance in terms of the estimated cell proportions than the marker genes from previously published methods (**Figure 3A**). In general, and not only for colorectal cancer and melanoma, the TICPE can also be developed to estimate the proportions of infiltrating immune cells in other types of cancer when collect relevant cancer cells and normal cells are tested within the same development pipeline. Moreover, the more robust cell type-specific genes we attained, the better performance we saw in the TICPE.

A Comparison of the TICPE With Previously Published Methods

We utilized the public validation datasets and simulated RNA-seq data to benchmark a range of other methods (CIBERSORT, EPIC, MCP-counter, xCell, and ImmuCellAI) in order to predict immune cell proportions. Compared to the other methods used currently in CRC validation datasets, the TICPE did not obtain the highest correlations across all cell types; however, it did provide the most consistent performance of all the assessments (**Figure 3B**). The majority of cell types measured by TICPE showed higher correlations with the observed cell fractions than the other methods for both scRNA-Seq datasets from melanoma patients and simulated samples (**Figure 3C**). Performance of TICPE and previous computational methods was assessed with all validation datasets by cell type. We chose the cell type that was analyzed in more than three datasets. The TICPE robustly obtained positive correlations across all cell types and data sets and scored the high performers in the assessments (**Supplementary Figure 3A**). In addition, the TICPE showed

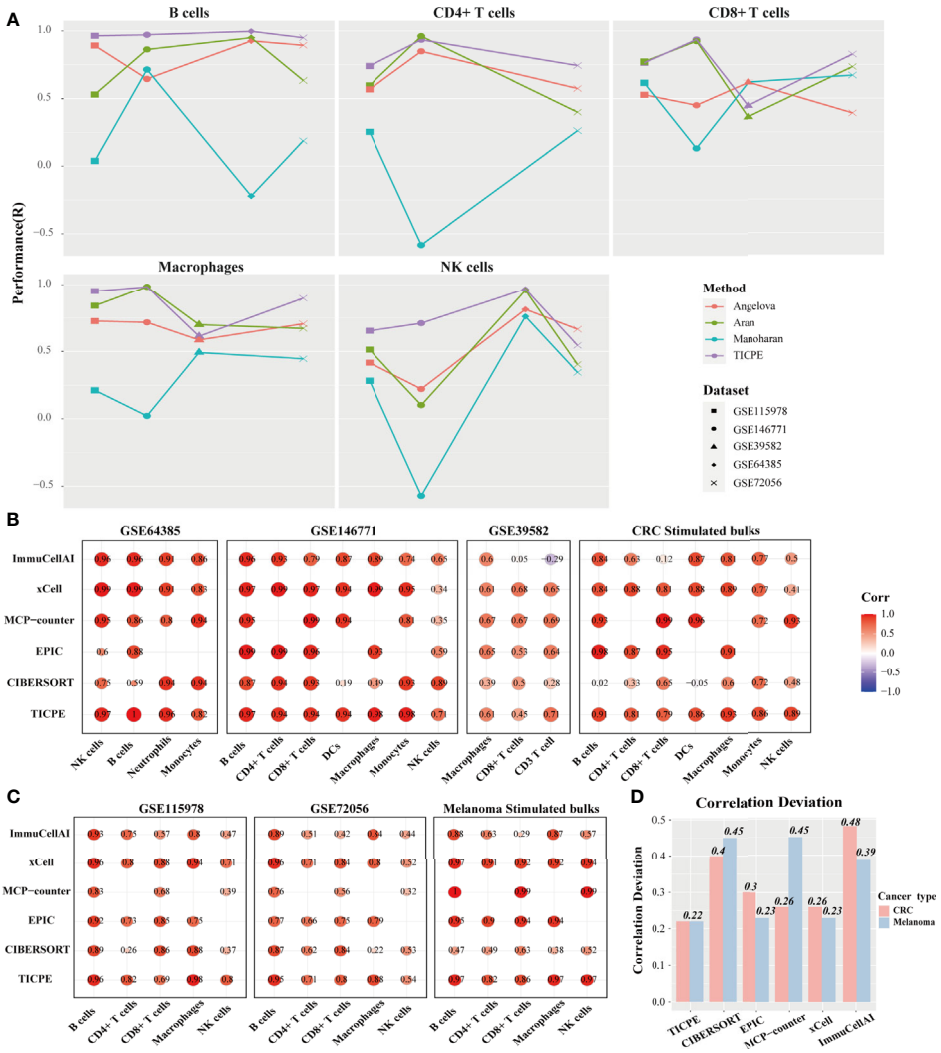

FIGURE 3 | Performance comparison with other methods. **(A)** Scatter plot organized by cell type showing the performance of different marker gene sets identified from four sources. Methods performance was quantified using Pearson's correlation (R). Different colors represented marker genes collated from different methods and different datasets had corresponding shapes. **(B, C)** Performance of TICPE and other methods on CRC and melanoma validation cohorts, respectively. Here rows corresponded to methods and columns showed the Pearson correlation coefficient for the corresponding cell type in each dataset. **(D)** Correlation deviation of each method in both CRC and melanoma validation datasets.

the least correlation deviation for the publicly available datasets for CRC and melanoma (**Figure 3D**).

It is also worth noting that the available methods for estimating immune cell contents are based on quantitative expression measurements of reference profiles or signature genes, thus resulting in incomparability across different datasets. In contrast, our method was based on the relative ordering of gene expression and was developed to estimate cell proportions in every individual tumor sample; this strategy was more flexible than the other methods. We analyzed the cell infiltration of two scRNA-Seq datasets for melanoma and compared the results of *in silico* methods with the true proportions. With the exception of macrophages (Wilcoxon test; $P = 0.017$), we found that there was no significant difference in the actual cell fractions when compared between the two datasets for melanoma. The TICPE estimates, had a similar trend to the actual proportions and showed no statistical significance between the two datasets except for macrophages (Wilcoxon test; $P = 0.02$; **Supplementary Figure 3B**). However, the majority of cell contents estimated by xCell and ImmuCellAI between the two datasets were significantly different and differed from the actual proportions. These results showed that the TICPE is a robust approach that supports the comparisons of the same cell type across different datasets at the same time and shows high levels of accuracy and robustness to estimate the proportion of immune cells of tumor samples.

TICPE Revealed That Immune Cell Infiltration Has Prognostic Value

TIICs are indispensable components of the tumor microenvironment and have been demonstrated to be highly valuable in determining the prognosis of multiple cancers. We accessed data from the GEO and TCGA to investigate whether TIICs had prognosis value for melanoma patients. We employed the TICPE to systematically estimate the eight infiltrated immune cells and stratified patients into a high infiltration subtype and a low infiltration subtype by using the median cell proportions as the cutoff. The results of Kaplan–Meier analysis of 79 metastatic melanoma specimens (GSE54467) and a unique set of 51 treatment-naive primary melanoma samples (GSE98394) both indicated that higher fractions of CD4+ T, CD8+ T cells, and NK cells might be associated with better survival over those with low proportions (P <0.05; **Figure 4**). In addition, RNA-seq data from 472 SKCM patients and OS data for 468 patients were downloaded from the TCGA database. In addition, 323 patients with a blank therapy type were posited without chemo/radiotherapy. We only selected these patients to reduce the treatment affecting patient prognosis and also found that melanoma patients with a high density of NK cells had a better prognosis (P = 0.0021; **Figure 4**). Furthermore, the TICPE was able to estimate cell proportions in every individual tumor sample. Therefore, we combined 57 melanoma patients with lymphnode (GSE22153) and subcutaneous metastases, along with 20 melanoma patients with liver and lymphnode metastases (GSE22154), who were treated in the same clinical center. Melanoma patients with a higher abundance of B cells, CD4+ T, and CD8+ T cells had a longer overall survival with or without combining the 20 patients with liver and lymphnode metastases (**Supplementary Figure 4**).

We also applied the TICPE to four cohorts of CRC patients to investigate the relationship between cell infiltrations and patient prognosis. In a cohort of 160 stage II and III CRC tissue samples that were treated surgically (GSE24551), patients with high levels of CD8+ T cell infiltration were significantly associated with a better DFS (disease-free survival) compared with those with a low infiltration subtype (P = 0.041). In a large series of CRC patients who had not received adjuvant chemotherapy (GSE39582), and a

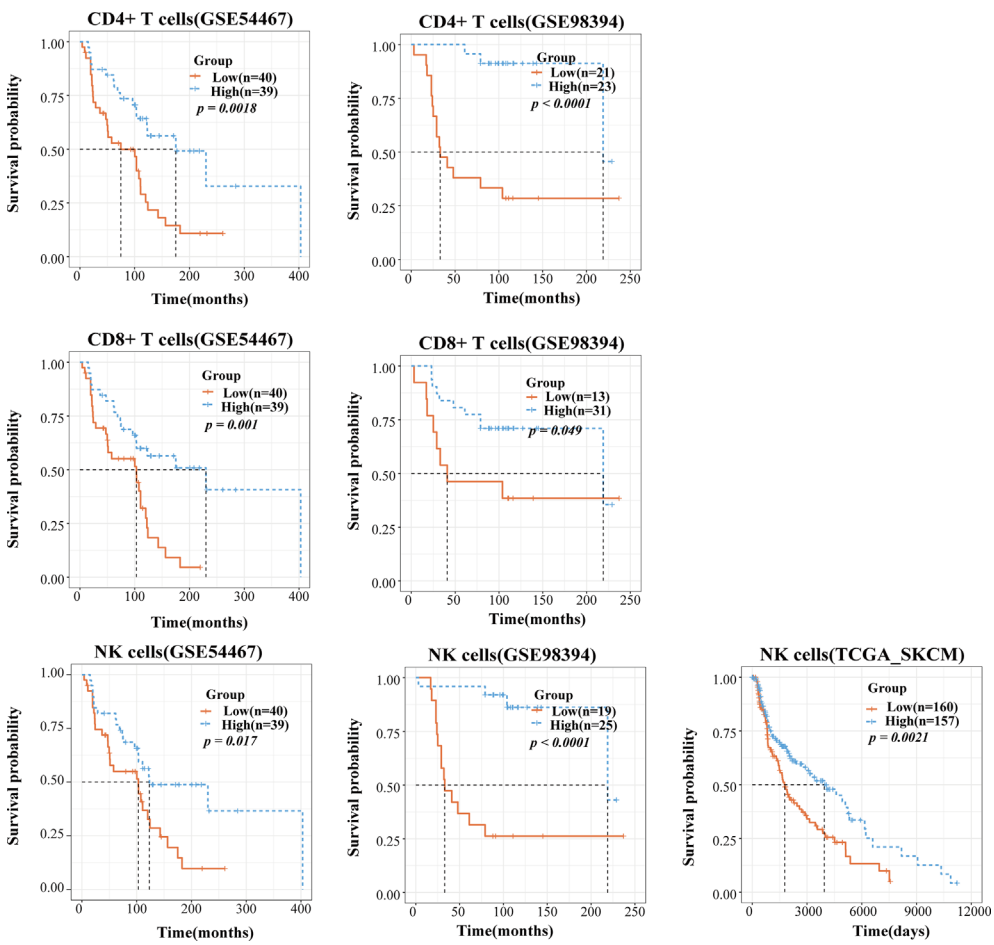

FIGURE 4 | The application of TICPE on prognostic analysis for melanoma. Survival high CD4+ T/CD8+ T/NK cells and low CD4+ T/CD8+ T/NK cells groups in melanoma patients, respectively. *P* values comparing two groups were calculated with the log-rank test.

cohort comprising 232 colorectal cancer patients (GSE17538), we found that a higher proportion of NK cells indicated a prolonged period of patient survival (P = 0.0079; P = 0.018) while an increased number of CD8+ T cells was associated with a better prognosis, although this was not statistically significant in either of the datasets. Furthermore, in a cohort of 232 colorectal cancer patients (GSE17538), despite the fact that macrophage infiltration was not statistically significant, a higher proportion of macrophages was associated with a dismal prognosis (P = 0.17). We also observed the same tendency in 171 surgically resected CRC specimens without chemo/radiotherapy (GSE14333); relatively poor DFS was correlated with an increased fraction of macrophages (P = 0.06; **Supplementary Figure 5**). Taken together, CD8+ T cells and NK cells were shown to play favorable roles in the survival of CRC and melanoma patients and the data obtained using the TICPE for several cohorts suggested that immune cell proportions can serve as an effective prognostic indicator for tumors.

TICPE Detected Changes in the Proportions of Immune Cells During Immunotherapy for Melanoma

An increasing number of research studies has revealed that an elevation in the levels of CD8+ T cells and NK cells is associated with an immunotherapy response in anti-PD-1 treatment (32, 33). We applied the TICPE to a melanoma dataset (GSE91061) to investigate the impact of immune cell proportions on cancer immunotherapy. The estimated fractions of CD8+ T cells and NK cells in pre-treatment and on-treatment samples showed a substantial increment in the complete and partial response group (CR & PR) (Kruskal-Wallis test; $P < 0.05$) than the other groups (**Figure 5A**). With regards to pre-treatment data, the immune cell fractions across different groups showed no statistical differences. Notably, there was no statistically significant difference between paired pre-treatment *versus* on-treatment immune cell proportions in responders. However, there was an increasing trend for changes in immune cell proportions during

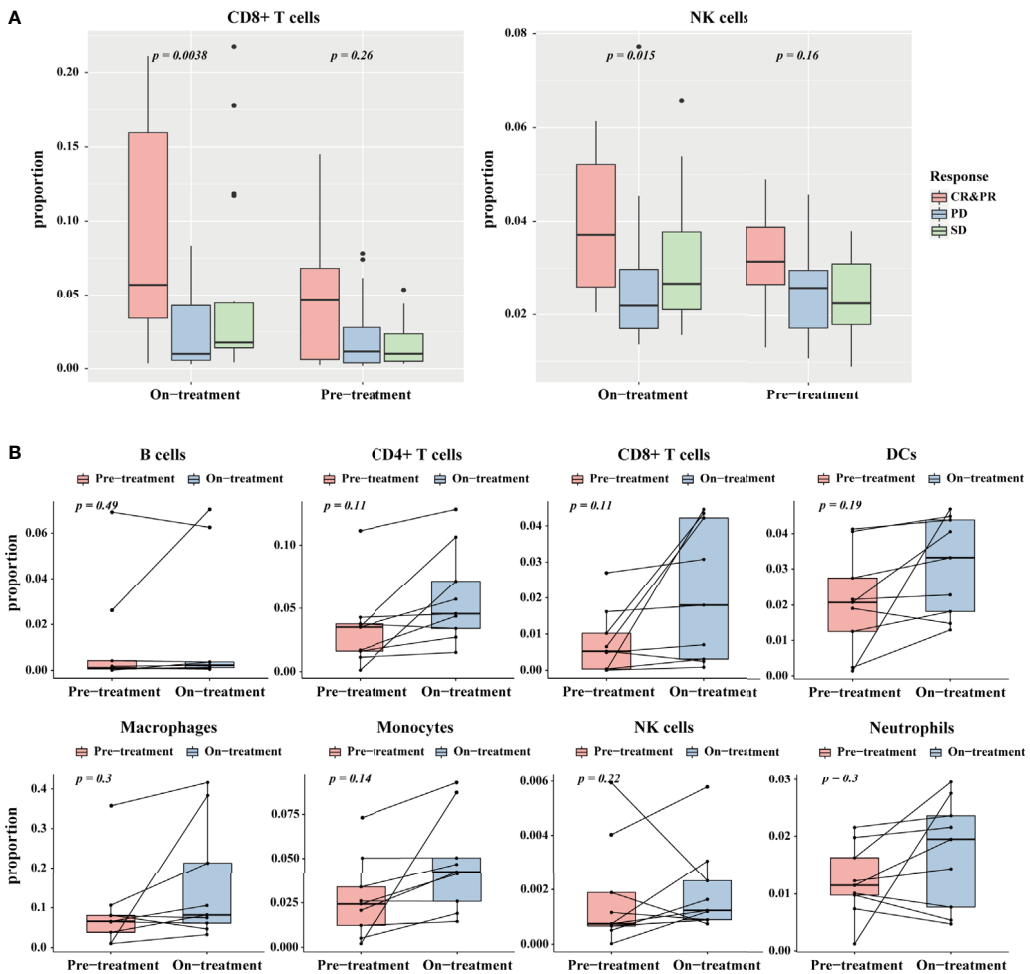

FIGURE 5 | The application of TICPE on immunotherapy for melanoma. **(A)** The significant proportion differences of CD8+ T cells (left)/NK cells (right) in different response groups at pre- and on-treatment (anti-PD1) time point. **(B)** Change of the estimated immune cell proportions between pre-treatment and on-treatment time point in paired responders.

anti-PD-1 treatment; this indicated that these immune cells were associated with a favorable response to PD-1 inhibition (**Figure 5B**; Wilcoxon test). These results suggested that TICPE could provide important insights on the dynamic immune cell infiltration during immunotherapy and offer valuable indicators for immunotherapy response during treatment.

DISCUSSION

In this study, we developed the TICPE, a cancer-specific qualitative method based on REOs, to estimate the proportion of eight different immune cells. The results of our extensive validation using immunohistochemistry data, mRNA mixtures *in vitro*, scRNA-Seq data, and simulated bulk RNA-seq samples, demonstrated that the TICPE could effectively infer immune cell fractions from transcriptome profiles. Of note, the TICPE does not only apply for colorectal cancer and melanoma, the TICPE could also be developed to estimate the infiltrating immune cells in any type of cancer as long as relevant data is available, such as cancer cells and normal samples. We had a straightforward comparison tumor microenvironment between colorectal cancer and melanoma utilizing data compiled by TCGA. The results showed that melanoma was highly infiltrated by CD4+ T cells, NK cells, dendritic cells, and neutrophils but poorly by cells of B cells, CD8+ T cells, monocytes, and macrophages in comparison with colorectal cancer (**Supplementary Figure 6A**). Moreover, the TICPE could be broadly employed to other components of the tumor microenvironment with the increased availability of public data by using the proposed pipeline. In the further work, with the gradual accumulation of relevant data of other cancer types and cell types, we will develop the TICPE for each neoplasm. Then we will estimate the abundance of immune cell populations in samples across multiple cancer types from The Cancer Genome Atlas (TCGA), and propose a global analysis of immune landscape across human cancers.

The key step in constructing the TICPE involved accurately identifying a list of genes characterized by a cell type. Compared to other methods based on marker genes, our method was more reliable due to the fact that it incorporated a group of signature genes for each cell type that was acquired from a comprehensive literature search and featured differentially expressed genes when compared with cancer cells. As shown the Venn diagram of **Supplementary Figure 6B**, there were some shared cell type-specific genes in both CRC and melanoma, but the majority of signature genes for each cell type were cancer type-specific in our study (**Supplementary Table 4**), which also indicated the gene expression of immune cell varied across different tissues. On the other hand, we chose to apply a gene signature approach over deconvolution methods because of the several advantages that the former provides. First, we did not require a reference expression matrix and could treat immune cells independently; this supported inter-sample comparisons and avoided issues relating to multicollinearity. Second, the TICPE was based on the rank of gene expression rather than the actual gene expression value and was therefore suitable for cross-platform transcriptomic measurements and comparisons. Finally, gene signatures are simple and can easily be adjusted. Furthermore, the procedure for developing TICPE was based on REOs so that it was agnostic to monotonic data normalization or concerns related to experimental batch effects; these effects rendered our technique more robust to both technical and biological noise.

The TICPE was reliable and could stratify a cohort of similar tumors based on the composition of their immune microenvironments, and could follow proportional changes of the microenvironment during the course of immunotherapy. In this investigation, CD8+ T cells and NK cells were shown to play favorable roles in the survival of CRC and melanoma patients. CD8+ T cells are the most potent cytolytic cell subset and NK cells also exert cytolytic functions (34, 35). CD8+ T cells are able to exert a directly killing effect on tumors cells and have been linked to a better prognosis in several types of cancer (36). In parallel with CD8+ T cells, NK cells can recognize and kill neoplastic cells and play pivotal roles in innate and adaptive immune responses and tumor immunosurveillance (37). In addition, our study also showed that the abundance of macrophages may serve as an unfavorable prognostic marker for CRC. Macrophages are conventionally classified into M1 and M2 subtypes. M2 macrophages secrete Interleukin 10 (IL-10), transforming growth factor-β(TGF-β), and other mediators that stimulate tumor-related angiogenesis and inhibit antitumor immune response (4, 38). On the other hand, although limited in sample size, our analysis detected an association between anti-PD-1 immunotherapy response and elevated CD8+ T cell and NK cell levels and revealed the potential of TICPE for providing important insights into dynamic immune cell infiltration during immunotherapy. The TIICs found in our study make a significant contribution to patient survival and treatment and our findings are corroborated by previous studies (17, 39). Overall, the proportions of immune cells measured by the TICPE could serve as a prognostic factor or a potential predictive model for the response to immune checkpoint blockade therapy in solid tumors.

Despite the utility of our method for estimating the tumor immune contexture for a particular type of cancer, several issues require further investigation. First, the TICPE was a cancer specific model and only focused on a very narrow range of cell types from the tumor microenvironment as our research involved publicly available datasets and gene sets that were characterized by each type of immune cell. Further efforts are required to collect more relevant information to extend the technique to other cell types (e.g., cancer-associated fibroblasts) and should be expanded to include more cancer types. Moreover, the inferences were strictly upregulated scores which could be compared with cancer cell and could not be interpreted as proportions. Thus, while we attempted to calibrate our method to resemble proportions, this strategy was hindered by conducting simulations to real-world datasets; the reliability of the technique needs to be improved. Furthermore, the final estimates were not normalized to sum up to one; therefore, the estimates could not be interpreted directly as cell fractions. Consequently, further improvement of our method is certainly warranted, including the reselection of signature genes from genome-wide

genes to extend to other cell types and the selection of a large cohort of real-world datasets with cell proportions to conduct simulated models.

In summary, the TICPE is a cancer-specific qualitative method for estimating the tumor immune contexture using public RNA-Seq and microarray datasets. The TICPE can estimate the proportion of infiltrating immune cells in CRC and melanoma but could also be extended to other types of cancer. Furthermore, the TICPE was based on REOs and can estimate the proportions of tumor-infiltrating immune cells in individual tumor samples. Therefore, the TICPE showed good comparability across different datasets and was only weakly affected by batch effects. We anticipate that this method will assist in the discovery of novel prognostic and predictive response biomarkers for both conventional and immunotherapy by taking immune cell composition into account.

DATA AVAILABILITY STATEMENT

The datasets presented in this study can be found in online repositories. The names of the repository/repositories and accession number(s) can be found in the article/ **Supplementary Material**.

AUTHOR CONTRIBUTIONS

WZ and YH conceived of, designed, and supervised the study. HX, JZ, and KW drafted the manuscript. HX and JZ implemented the source code of TICPE. KW participated in the study design and result validation. KS, HZ, JY, KL, and RY contributed to the design of TICPE. All authors contributed to the article and approved the submitted version.

FUNDING

This work was supported by the National Natural Science Foundation of China under Grant: 81872396.

ACKNOWLEDGMENTS

We thank all the individuals who participated in this study and gave helpful discussion. We thank Etienne Becht and their colleagues, for providing us with additional data relating to their published studies. We would like to express oue gratitude to EditSprings (https://www.editsprings.com/) for the expert linguistic services provided. We would also like to acknowledge the resources at GEO that facilitated this research.

SUPPLEMENTARY MATERIAL

The Supplementary Material for this article can be found online at: https://www.frontiersin.org/articles/10.3389/fimmu.2021.672031/full#supplementary-material

REFERENCES

1. Petitprez F, Meylan M, de Reynies A, Sautes-Fridman C, Fridman WH. The Tumor Microenvironment in the Response to Immune Checkpoint Blockade Therapies. *Front Immunol* (2020) 11:784. doi: 10.3389/fimmu.2020.00784
2. Galon J, Costes A, Sanchez-Cabo F, Kirilovsky A, Mlecnik B, Lagorce-Pages C, et al. Type, Density, and Location of Immune Cells Within Human Colorectal Tumors Predict Clinical Outcome. *Science* (2006) 313 (5795):1960–4. doi: 10.1126/science.1129139
3. Sideras K, Galjart B, Vasaturo A, Pedroza-Gonzalez A, Biermann K, Mancham S, et al. Prognostic Value of Intra-Tumoral CD8(+) /FoxP3(+) Lymphocyte Ratio in Patients With Resected Colorectal Cancer Liver Metastasis. *J Surg Oncol* (2018) 118(1):68–76. doi: 10.1002/jso.25091
4. Lan J, Sun L, Xu F, Liu L, Hu F, Song D, et al. M2 Macrophage-Derived Exosomes Promote Cell Migration and Invasion in Colon Cancer. *Cancer Res* (2019) 79(1):146–58. doi: 10.1158/0008-5472.CAN-18-0014
5. Nishikawa H, Sakaguchi S. Regulatory T Cells in Cancer Immunotherapy. *Curr Opin Immunol* (2014) 27:1–7. doi: 10.1016/j.coi.2013.12.005
6. Maibach F, Sadozai H, Seyed Jafari SM, Hunger RE, Schenk M. Tumor-Infiltrating Lymphocytes and Their Prognostic Value in Cutaneous Melanoma. *Front Immunol* (2020) 11:2105. doi: 10.3389/fimmu.2020.02105
7. Subrahmanyam PB, Dong Z, Gusenleitner D, Giobbie-Hurder A, Severgnini M, Zhou J, et al. Distinct Predictive Biomarker Candidates for Response to anti-CTLA-4 and anti-PD-1 Immunotherapy in Melanoma Patients. *J Immunother Cancer* (2018) 6(1):18. doi: 10.1186/s40425-018-0328-8
8. Tietze JK, Angelova D, Heppt MV, Reinholz M, Murphy WJ, Spannagl M, et al. The Proportion of Circulating CD45RO(+)CD8(+) Memory T Cells is Correlated With Clinical Response in Melanoma Patients Treated With Ipilimumab. *Eur J Cancer* (2017) 75:268–79. doi: 10.1016/j.ejca.2016.12.031
9. Fridman WH, Zitvogel L, Sautes-Fridman C, Kroemer G. The Immune Contexture in Cancer Prognosis and Treatment. *Nat Rev Clin Oncol* (2017) 14(12):717–34. doi: 10.1038/nrclinonc.2017.101
10. Chen Z, Wu A. Progress and Challenge for Computational Quantification of Tissue Immune Cells. *Brief Bioinform* (2021) bbaa358. doi: 10.1093/bib/bbaa358
11. Finotello F, Trajanoski Z. Quantifying Tumor-Infiltrating Immune Cells From Transcriptomics Data. *Cancer Immunol Immunother* (2018) 67 (7):1031–40. doi: 10.1007/s00262-018-2150-z
12. Sturm G, Finotello F, Petitprez F, Zhang JD, Baumbach J, Fridman WH, et al. Comprehensive Evaluation of Transcriptome-Based Cell-Type Quantification Methods for Immuno-Oncology. *Bioinformatics* (2019) 35(14):i436–45. doi: 10.1093/bioinformatics/btz363
13. Newman AM, Liu CL, Green MR, Gentles AJ, Feng W, Xu Y, et al. Robust Enumeration of Cell Subsets From Tissue Expression Profiles. *Nat Methods* (2015) 12(5):453–7. doi: 10.1038/nmeth.3337
14. Li B, Severson E, Pignon JC, Zhao H, Li T, Novak J, et al. Comprehensive Analyses of Tumor Immunity: Implications for Cancer Immunotherapy. *Genome Biol* (2016) 17(1):174. doi: 10.1186/s13059-016-1028-7
15. Racle J, de Jonge K, Baumgaertner P, Speiser DE, Gfeller D. Simultaneous Enumeration of Cancer and Immune Cell Types From Bulk Tumor Gene Expression Data. *Elife* (2017) 6:e26476. doi: 10.7554/eLife.26476
16. Finotello F, Mayer C, Plattner C, Laschober G, Rieder D, Hackl H, et al. Molecular and Pharmacological Modulators of the Tumor Immune Contexture Revealed by Deconvolution of RNA-seq Data. *Genome Med* (2019) 11(1):34. doi: 10.1186/s13073-019-0638-6
17. Becht E, Giraldo NA, Lacroix L, Buttard B, Elarouci N, Petitprez F, et al. Estimating the Population Abundance of Tissue-Infiltrating Immune and Stromal Cell Populations Using Gene Expression. *Genome Biol* (2016) 17 (1):218. doi: 10.1186/s13059-016-1070-5

18. Aran D, Hu Z, Butte AJ. xCell: Digitally Portraying the Tissue Cellular Heterogeneity Landscape. *Genome Biol* (2017) 18(1):220. doi: 10.1186/s13059-017-1349-1
19. Miao YR, Zhang Q, Lei Q, Luo M, Xie GY, Wang H, et al. Immucellai: A Unique Method for Comprehensive T-Cell Subsets Abundance Prediction and its Application in Cancer Immunotherapy. *Adv Sci (Weinh)* (2020) 7 (7):1902880. doi: 10.1002/advs.201902880
20. Frishberg A, Steuerman Y, Gat-Viks I. CoD: Inferring Immune-Cell Quantities Related to Disease States. *Bioinformatics* (2015) 31(24):3961–9. doi: 10.1093/bioinformatics/btv498
21. Lazar C, Meganck S, Taminau J, Steenhoff D, Coletta A, Molter C, et al. Batch Effect Removal Methods for Microarray Gene Expression Data Integration: A Survey. *Brief Bioinform* (2013) 14(4):469–90. doi: 10.1093/bib/bbs037
22. Patil P, Bachant-Winner PO, Haibe-Kains B, Leek JT. Test Set Bias Affects Reproducibility of Gene Signatures. *Bioinformatics* (2015) 31(14):2318–23. doi: 10.1093/bioinformatics/btv157
23. Qi L, Li T, Shi G, Wang J, Li X, Zhang S, et al. An Individualized Gene Expression Signature for Prediction of Lung Adenocarcinoma Metastases. *Mol Oncol* (2017) 11(11):1630–45. doi: 10.1002/1878-0261.12137
24. Eisenhauer EA, Therasse P, Bogaerts J, Schwartz LH, Sargent D, Ford R, et al. New Response Evaluation Criteria in Solid Tumours: Revised RECIST Guideline (Version 1.1). *Eur J Cancer* (2009) 45(2):228–47. doi: 10.1016/j.ejca.2008.10.026
25. Wang H, Sun Q, Zhao W, Qi L, Gu Y, Li P, et al. Individual-Level Analysis of Differential Expression of Genes and Pathways for Personalized Medicine. *Bioinformatics* (2015) 31(1):62–8. doi: 10.1093/bioinformatics/btu522
26. Korthauer K, Kimes PK, Duvallet C, Reyes A, Subramanian A, Teng M, et al. A Practical Guide to Methods Controlling False Discoveries in Computational Biology. *Genome Biol* (2019) 20(1):118. doi: 10.1186/s13059-019-1716-1
27. Johnson WE, Li C, Rabinovic A. Adjusting Batch Effects in Microarray Expression Data Using Empirical Bayes Methods. *Biostatistics* (2007) 8 (1):118–27. doi: 10.1093/biostatistics/kxj037
28. Aran D, Sirota M, Butte AJ. Systematic Pan-Cancer Analysis of Tumour Purity. *Nat Commun* (2015) 6:8971. doi: 10.1038/ncomms9971
29. Bland JM, Altman DG. The Logrank Test. *BMJ* (2004) 328(7447):1073. doi: 10.1136/bmj.328.7447.1073
30. Angelova M, Charoentong P, Hackl H, Fischer ML, Snajder R, Krogsdam AM, et al. Characterization of the Immunophenotypes and Antigenomes of Colorectal Cancers Reveals Distinct Tumor Escape Mechanisms and Novel Targets for Immunotherapy. *Genome Biol* (2015) 16:64. doi: 10.1186/s13059-015-0620-6
31. Manoharan M, Mandloi N, Priyadarshini S, Patil A, Gupta R, Iyer L, et al. A Computational Approach Identifies Immunogenic Features of Prognosis in Human Cancers. *Front Immunol* (2018) 9:3017. doi: 10.3389/fimmu.2018.03017
32. Eroglu Z, Zaretsky JM, Hu-Lieskovan S, Kim DW, Algazi A, Johnson DB, et al. High Response Rate to PD-1 Blockade in Desmoplastic Melanomas. *Nature* (2018) 553(7688):347–50. doi: 10.1038/nature25187
33. Iraolagoitia XL, Spallanzani RG, Torres NI, Araya RE, Ziblat A, Domaica CI, et al. NK Cells Restrain Spontaneous Antitumor CD8+ T Cell Priming Through PD-1/PD-L1 Interactions With Dendritic Cells. *J Immunol* (2016) 197(3):953–61. doi: 10.4049/jimmunol.1502291
34. de Wolf C, van de Bovenkamp M, Hoefnagel M. Regulatory Perspective on In Vitro Potency Assays for Human T Cells Used in Anti-Tumor Immunotherapy. *Cytotherapy* (2018) 20(5):601–22. doi: 10.1016/j.jcyt.2018.01.011
35. Guo L, Wang C, Qiu X, Pu X, Chang P. Colorectal Cancer Immune Infiltrates: Significance in Patient Prognosis and Immunotherapeutic Efficacy. *Front Immunol* (2020) 11:1052. doi: 10.3389/fimmu.2020.01052
36. Oh S, Perera LP, Terabe M, Ni L, Waldmann TA, Berzofsky JA. IL-15 as a Mediator of CD4+ Help for CD8+ T Cell Longevity and Avoidance of TRAIL-mediated Apoptosis. *Proc Natl Acad Sci USA* (2008) 105(13):5201–6. doi: 10.1073/pnas.0801003105
37. Bruni D, Angell HK, Galon J. The Immune Contexture and Immunoscore in Cancer Prognosis and Therapeutic Efficacy. *Nat Rev Cancer* (2020) 20 (11):662–80. doi: 10.1038/s41568-020-0285-7
38. Fridman WH, Pages F, Sautes-Fridman C, Galon J. The Immune Contexture in Human Tumours: Impact on Clinical Outcome. *Nat Rev Cancer* (2012) 12 (4):298–306. doi: 10.1038/nrc3245
39. Tang D, Park S, Zhao H. NITUMID: Nonnegative Matrix Factorization-Based Immune-TUmor Microenvironment Deconvolution. *Bioinformatics* (2020) 36(5):1344–50. doi: 10.1093/bioinformatics/btz748

Conflict of Interest: The authors declare that the research was conducted in the absence of any commercial or financial relationships that could be construed as a potential conflict of interest.

Copyright © 2021 Xiao, Zhang, Wang, Song, Zheng, Yang, Li, Yuan, Zhao and Hui. This is an open-access article distributed under the terms of the Creative Commons Attribution License (CC BY). The use, distribution or reproduction in other forums is permitted, provided the original author(s) and the copyright owner(s) are credited and that the original publication in this journal is cited, in accordance with accepted academic practice. No use, distribution or reproduction is permitted which does not comply with these terms.

frontiers in Immunology

ORIGINAL RESEARCH
published: 04 June 2021
doi: 10.3389/fimmu.2021.681615

Circulating and Tumor-Infiltrating NK Cells From Clear Cell Renal Cell Carcinoma Patients Exhibit a Predominantly Inhibitory Phenotype Characterized by Overexpression of CD85j, CD45, CD48 and PD-1

Andrea Ziblat[1†], Ximena Lucía Raffo Iraolagoitia[1†], Sol Yanel Nuñez[1†], Nicolás Ignacio Torres[1], Florencia Secchiari[1], Jessica Mariel Sierra[1], Raúl Germán Spallanzani[1†], Agustín Rovegno[2], Fernando Pablo Secin[2†], Mercedes Beatriz Fuertes[1], Carolina Inés Domaica[1] and Norberto Walter Zwirner[1,3]*

[1] Laboratorio de Fisiopatología de la Inmunidad Innata, Instituto de Biología y Medicina Experimental (IBYME-CONICET), Buenos Aires, Argentina, [2] Centro de Educación Médica e Investigaciones Clínicas "Norberto Quirno" (CEMIC), Servicio de Urología, Buenos Aires, Argentina, [3] Departamento de Química Biológica, Facultad de Ciencias Exactas y Naturales, Universidad de Buenos Aires, Buenos Aires, Argentina

Although natural killer (NK) cells infiltrate clear cell renal cell carcinomas (ccRCC), the most frequent malignancy of the kidney, tumor progression suggests that they become dysfunctional. As ccRCC-driven subversion of NK cell effector functions is usually accompanied by phenotypic changes, analysis of such alterations might lead to the identification of novel biomarkers and/or targets in immuno-oncology. Consequently, we performed a phenotypic analysis of peripheral blood NK cells (PBNK) and tumor-infiltrating NK cells (TINK) from ccRCC patients. Compared to HD, PBNK from ccRCC patients exhibited features of activated cells as shown by CD25, CD69 and CD62L expression. They also displayed increased expression of DNAM-1, CD48, CD45, MHC-I, reduced expression of NKG2D, and higher frequencies of CD85j$^+$ and PD-1$^+$ cells. In addition, compared to PBNK from ccRCC patients, TINK exhibited higher expression of activation markers, tissue residency features and decreased expression of the activating receptors DNAM-1, NKp30, NKp46, NKp80 and CD16, suggesting a more inhibitory phenotype. Analysis of The Cancer Genome Atlas (TCGA) revealed that CD48, CD45, CD85j and PD-1 are significantly overexpressed in ccRCC and that their expression is associated with an NK cell infiltration signature. Calculation of z-scores revealed that their expression on PBNK, alone or combined, distinguished ccRCC patients from HD. Therefore, these molecules emerge as novel potential biomarkers and our results suggest that they might constitute possible targets for immunotherapy in ccRCC patients.

Keywords: NK cells, renal cell carcinoma, CD85j, CD45, CD48, PD-1

OPEN ACCESS

Edited by:
Eyad Elkord,
University of Salford, United Kingdom

Reviewed by:
Emilie Picard,
Health Sciences North Research Institute (HSNRI), Canada
Natalia Aptsiauri,
University of Granada, Spain

****Correspondence:***
Norberto Walter Zwirner
nzwirner@ibyme.conicet.gov.ar
orcid.org/0000-0001-7098-359X

[†]Present address:
Andrea Ziblat, Department of Pathology, University of Chicago, Chicago, IL, United States
Ximena Lucia Raffo Iraolagoitia, Cancer Research UK Beatson Institute, Glasgow, United Kingdom
Sol Yanel Nuñez, Centre de Recherche Institut Curie - INSERM U932, Immunité et Cancer, Centre immunothérapie, Paris, France
Raúl Germán Spallanzani, Department of Immunology, Harvard Medical School, Boston, MA, United States
Fernando Pablo Secin, Facultad de Medicina, Universidad de Buenos Aires, Buenos Aires, Argentina

Specialty section:
This article was submitted to Cancer Immunity and Immunotherapy, a section of the journal Frontiers in Immunology

Received: *16 March 2021*
Accepted: *18 May 2021*
Published: *04 June 2021*

INTRODUCTION

Renal cell carcinomas (RCC) constitute a malignancy of the kidney that, according to GLOBOCAN (https://gco.iarc.fr/), exhibited an incidence of 4.5 cases per 100,000 individuals in 2018. The most frequent RCC is clear cell RCC (ccRCC, 70-75% of all RCC), followed by papillary RCC and chromophobe RCC (cancer.gov). RCC patients diagnosed early have a good prognosis (81% of five-year survival for stage I tumors and 74% of five-year survival for stage II tumors). However, patients diagnosed at advanced stages have a dramatic drop in five-year survival (53% of five-year survival for stage III tumors and 8% of five-year survival for stage IV tumors). RCC patients can be treated by partial or radical nephrectomy or kinase inhibitors. Also, immunotherapy with checkpoint inhibitors that target the PD-1/PD-L1 axis recently emerged as a treatment option in advanced disease (1, 2). However, most of them are diagnosed at later stages and exhibit recurrence and metastases, without further therapeutic options (3, 4). Therefore, it is of major interest to discover novel targets for immunotherapy and to identify biomarkers that might indicate recurrence or the efficacy of a certain treatment. Eradication of tumor cells is mainly executed by NK cells and cytotoxic $CD8^+$ T lymphocytes (CTL) through direct cytotoxicity against tumor cells and secretion of IFN-γ and other proinflammatory cytokines (5, 6). NK cells recognize specific ligands expressed on tumor cells that promote the engagement of an array of activating receptors such as DNAM-1, NKG2D, 2B4, NKG2C, the Natural Cytotoxicity Receptors (NCR) NKp30, NKp44, NKp46 and NKp80, and others (5). However, NK cell activation is counterbalanced by the engagement of an array of inhibitory receptors such as CD85j (ILT2), KIR, NKG2A, and TIGIT, and NK cell activity is also regulated by coinhibitory molecules such as PD-1 (5, 7).

Human PBNK comprise 2 major subsets, according to the expression of CD56 (8). Approximately 90% of PBNK exhibit a $CD3^-CD56^{dim}$ phenotype and a robust cytotoxic activity. The other 5-10% of PBNK display a $CD3^-CD56^{bright}$ phenotype, are abundant in secondary lymph nodes, display poor cytotoxic activity and mainly produce IFN-γ and other cytokines in response to different stimuli (8–10). Activation of $CD56^{dim}$ NK cells induces several changes that include the up-regulation of the expression of CD25 and CD69, and the downregulation of the expression of CD62L and CCR7 (8, 11–13). Moreover, during activation of NK cells, downregulation of CD62L and CCR7 prevents their egress from the tissue and migration into lymph nodes, and therefore their downregulation is considered a feature of tissue residency (8, 11, 12). In addition, upregulation of CD69, traditionally associated with activation, has been recently associated with tissue residency features (8, 11–13). Also, acquisition of CD57 expression by human NK cells has been associated with terminal differentiation (8, 13–15).

The mechanism of action of NK cells in the control of human hematologic malignancies is relatively well understood (16, 17). However, their role in the control of solid tumors is less known. Although NK cells and CTL infiltrate RCC tumors (18), tumors manage to grow and metastasize mainly due to the existence of an immune suppressive tumor microenvironment (TME). Through local and systemic effects, TME may generate dysfunctional NK cells with an altered phenotype, and the detection of such abnormal phenotypic characteristics of PBNK and TINK may result in the identification of novel targets for immunotherapy and/or biomarkers.

It was observed that TINK from ccRCC patients exhibit a diverse expression of KIR, CD85j and NKG2A (19), and that the extent of NK cell infiltration and the expression of CD16 and lytic mediators is associated with the functional capacity of these TINK (19, 20). Reduced expression of NKp46 was also described in TINK from ccRCC patients (21). Also, it has been observed that a lower frequency of TINK express the activating receptors NKp46, NKG2D, NKG2C, and a higher frequency of TINK express the inhibitory receptors NKG2A, CD158a and CD158b (22). Moreover, TINK from ccRCC display impaired degranulation (21, 22) and cytokine production (22). Others also described an abnormal phenotype of PBNK in RCC patients (84% of which were ccRCC) such as an increased expression of PD-1 that correlated with disease stage and was significantly reduced after surgical removal of the tumor (23). Phenotypic alterations of NK cells might be different in PBNK compared to TINK because TINK establish a close interaction with the TME while PBNK are only exposed to systemic effects of the TME. However, the comparative characteristics of PBNK and TINK from ccRCC remain mostly ill-defined. Such studies may unravel phenotypic alterations of NK cells that may represent useful prognostic, therapeutic and follow-up biomarkers and/or lead to the discovery of new candidates for immunotherapy, especially considering that immunotherapies aimed at reinvigorating NK cells in RCC constitute promising approaches (24).

Therefore, the aim of this work was to perform a phenotypic analysis of previously poorly explored markers expressed by PBNK and TINK from ccRCC patients to elucidate if systemic and local effects affect these cells critically involved in the elimination of tumor cells. We complemented these studies with bioinformatic analyses of TCGA data to establish whether the overexpression of inhibitory receptors detected in this work on NK cells from ccRCC patients is a general characteristic of ccRCC tumor samples and is associated with a NK cell signature.

MATERIALS AND METHODS

Patients and Samples

Peripheral blood mononuclear cells (PBMC) were isolated from blood of healthy donors (HD, provided by the Blood Bank of the Hospital Churruca-Visca of Buenos Aires) or kidney cancer patients (drawn just before nephrectomy) by Ficoll-Paque™ Plus (GE Life Sciences) centrifugation. Blood and nephrectomies were provided by the urology service from the Centro de Educación Médica e Investigaciones Clínicas "Norberto Quirno" (CEMIC) from the city of Buenos Aires. The characteristics of the patients are listed in **Table 1**. A total of 12 patients with ccRCC and 13 HD were included in the study. This study was conducted according to the guidelines of the Declaration of Helsinki, and approved by the Institutional Ethics Committee of IBYME (protocol CE003-03/2014, date of approval: March 20, 2014). Also, informed consent was obtained from all subjects involved in the study.

TABLE 1 | Patients with ccRCC included in the study.

Patient	Gender	Age	Stage	Type of nephrectomy*
1	M	74	Fuhrman II	P
2	M	74	Fuhrman II	R
3	M	67	Furhman II (pT3bpN0)	R
4	M	61	Fuhrman II	P
5	M	63	Fuhrman II	P
6	M	67	Fuhrman II/III	R
7	F	59	Fuhrman II	R
8	M	59	Fuhrman II	R
9	M	74	Fuhrman II	P
10	M	73	Fuhrman IV	R
11	M	71	Fuhrman II	R
12	F	72	Fuhrman II	P

P, partial; R, radical.

Preparation of Tumor Cell Suspensions

Surgical biopsies of human RCC were obtained from patients subjected to partial or radical nephrectomy and used for the preparation of single cell suspensions. Briefly, tumors were cut into small pieces and subjected to mechanical dissociation and filtration through nylon mesh (0.45 μm) in the presence of phosphate-buffered saline. After washing with saline solution, immune cells were enriched by Ficoll-Paque™ Plus (GE Life Sciences) centrifugation. All procedures were performed on ice. Diagnosis of each RCC was confirmed by the pathology service and only data corresponding to ccRCC were presented in this study.

Antibodies and Reagents

The following mAb were used for flow cytometry (FC): APC anti-CD56 (N901) from Beckman Coulter; PE/Cy7 anti-CD3 (UCHT1) from TONBO; FITC anti-DNAM-1 (DX11) from BD; FITC anti-CD85j (292305), AlexaFluor488 anti-TRAIL (71908), PE anti-NKG2A (131411) and AlexaFluor488 anti-NKG2C (134591) from Biotechne; FITC anti-CD16 (3G8); FITC anti-CD69 (FN50); PE anti-CD25 (BC96); PE anti-CD62L (DREG-56); PE anti-NKG2D (1D11), PE anti-NKp30 (P30-15); PE anti-NKp46 (9E2); PE anti-NKp80 (5D12); PE anti-2B4 (C1.7); FITC anti-CD48 (BJ40); APC/Cy7 anti-CD45 (HI30); AlexaFluor488 anti-PD-1 (29E.2A3); FITC anti-HLA class I (W6/32); PE anti-FasL (NOK-1); PE anti-NKp44 (9E2); FITC anti-CD57 (HCD57); FITC anti-CCR7 (G043H7); FITC anti-CD27 (M-T271); and PE anti-TIGIT (A15153G) from Biolegend.

Flow Cytometry

FC was performed as described (25, 26). Non-specific staining was blocked with 10% normal mouse serum. Cells were analyzed in a FACSCanto II flow cytometer (BD). Data were analyzed using FlowJo X software (BD) and results were expressed as geometric mean fluorescence intensity (MFI), as relative MFI (rMFI) calculated as the MFI of the specific mAb divided by the MFI of the "fluorescence minus one" (FMO) control or as percentage of positive cells. For comparison of PBNK with TINK, we used rMFI because the FMO of the tumor samples was higher than the FMO of the blood samples.

Bioinformatic Analysis

The Tumor IMmune Estimation Resource (TIMER, http://timer.cistrome.org/) (27) and the Gene Expression Profiling Interactive Analysis 2 (GEPIA2, http://gepia2.cancer-pku.cn/) (28) were used to analyze publicly available RNAseq data from The Cancer Genome Atlas (TCGA). TIMER was used to study the differential expression between ccRCC tumor and adjacent normal tissues datasets for the different genes of interest, and the statistical significance was computed by differential analysis (edgeR). GEPIA2 was used for correlation analysis between a multi-gene NK cell signature (*NCR1, XCL2, IL2RB, KLRF1, KIR2DL4, KLRC3, XCL1, NKG7, CTSW, NCR3* and *IL18RAP*) and the genes of interest (29, 30).

Statistical Analysis

Principal component analysis (PCA) of scaled data was conducted in R (version 4.0.3) (31) with missMDA (32) to compute missing values. For the comparison of PBNK from HD with PBNK from ccRCC patients (**Figure 1A**), the MFI of CD56, CD62L, CCR7, CD16, CD25, CD69, FasL, TRAIL, CD48, CD27, CD45, MHC-I, PD-1, DNAM-1, NKG2D, NKp30, NKp44, NKp46, NKp80, NKG2C, 2B4, NKG2A, and TIGIT on $CD56^{bright}$ and $CD56^{dim}$ NK cells, and the MFI of CD85j and CD57 on $CD56^{dim}$ cells were used. For the comparison of PBNK with TINK from ccRCC patients (**Figure 3A**), the rMFI of the following markers were used: CD62L, CCR7, CD16, CD25, CD69, FasL, TRAIL, CD48, CD27, CD57, MHC-I, PD-1, DNAM-1, NKG2D, NKp30, NKp44, NKp46, NKp80, NKG2C, 2B4, NKG2A, TIGIT, and CD85j. Plots were generated using the package factoextra (33). z-scores for CD85j, CD45 and CD48 expression were calculated using the formula $z=(x-\mu)/\sigma$, where z is the "z-score", x is the MFI of CD45 expression or the frequency of $CD85j^+$ or $CD48^+$ from total PBNK in each individual sample, μ is the mean of the MFI of CD45 expression or the mean of the frequency of $CD85j^+$ or $CD48^+$ PBNK cells in the HD population, and σ is the standard deviation of each set of these data in the HD population. The sum of z-scores was calculated for patients for whom data were available for each parameter (receptors). To compare PBNK from HD with PBNK from ccRCC patients, a two-sided unpaired t-test with Welch´s correction (when samples passed the normality test) or with Mann-Whitney´s correction (when samples did not pass the normality test) was used. To compare PBNK with TINK from ccRCC patients, a two-sided paired t-test was used when samples passed the normality test, and a two-sided paired t-test with Wilcoxon rank test was used when samples did not pass the normality test. D´Agostino-Pearson was used as normality test. Data were analyzed using Prism 6.0 software (GraphPad).

RESULTS

PBNK From ccRCC Patients Exhibit an Activated Phenotype With an Altered Balance of Activating and Inhibitory Receptors

First, we phenotyped PBNK from ccRCC patients and HD (the characteristics of the patients are detailed in **Table 1**). NK cells

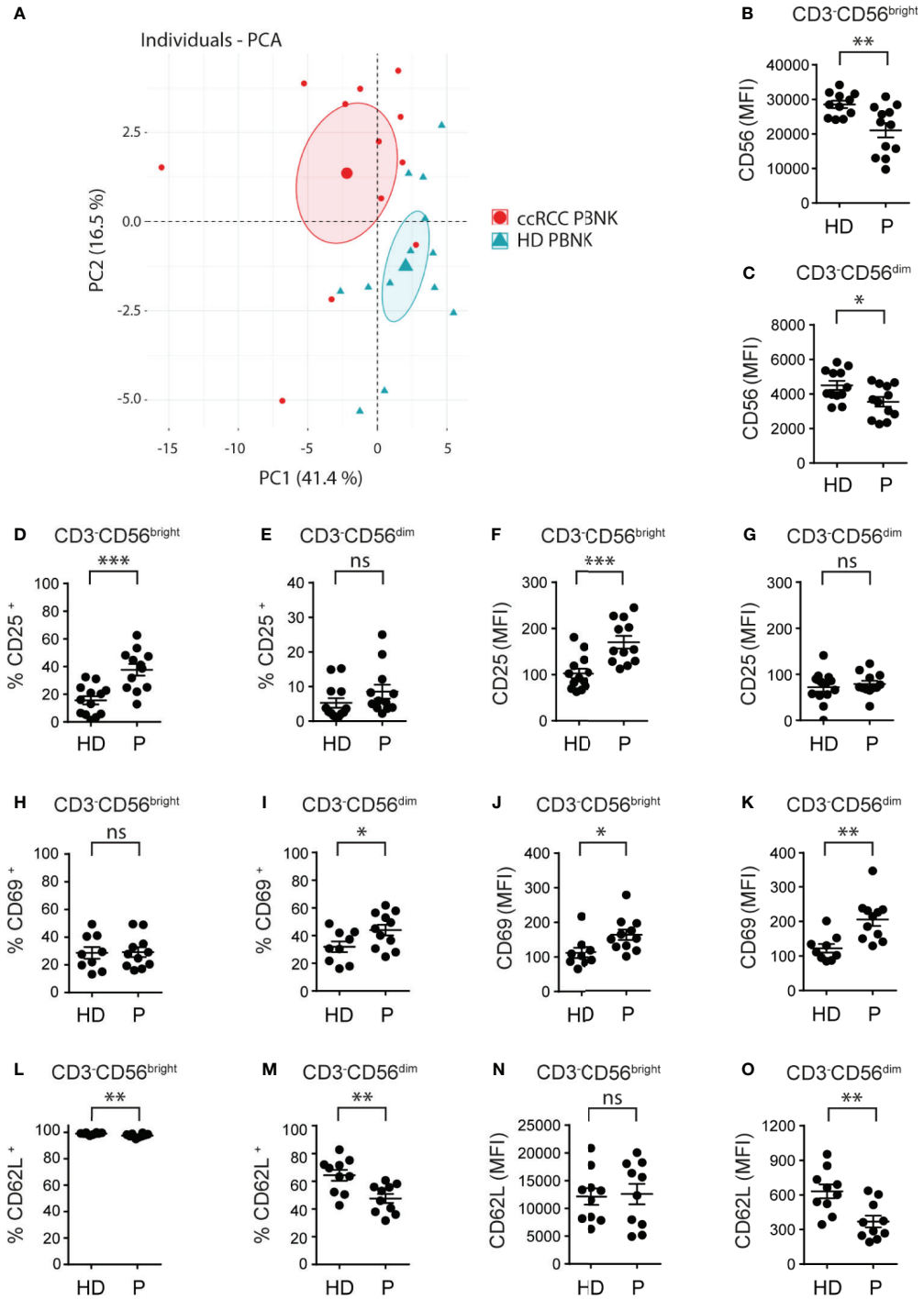

FIGURE 1 | Cell surface markers differentiate ccRCC patients from HD and indicate that PBNK from ccRCC patients exhibit an activated phenotype. MFI of the molecules analyzed on $CD3^-CD56^{bright}$ and $CD3^-CD56^{dim}$ cells of HD and ccRCC PBNK were used to perform a PCA **(A)**. The graph of individuals with the confidence ellipse is shown. Also, PBNK cells from healthy donors (HD) and ccRCC patients (P) were analyzed by FC to compare the intensity of expression of CD56 on $CD3^-CD56^{bright}$ **(B)** and on $CD3^-CD56^{dim}$ NK cells **(C)**, the frequencies of $CD25^+$ cells in $CD3^-CD56^{bright}$ **(D)** and in $CD3^-CD56^{dim}$ NK cells **(E)**, the intensity of expression of CD25 on $CD3^-CD56^{bright}$ **(F)** and on $CD3^-CD56^{dim}$ NK cells **(G)**, the frequencies of $CD69^+$ cells in $CD3^-CD56^{bright}$ **(H)** and in $CD3^-CD56^{dim}$ NK cells **(I)**, the intensity of expression of CD69 on $CD3^-CD56^{bright}$ **(J)** and on $CD3^-CD56^{dim}$ NK cells **(K)**, the frequencies of $CD62L^+$ cells in $CD3^-CD56^{bright}$ **(L)** and in $CD3^-CD56^{dim}$ NK cells **(M)**, and the intensity of expression of CD62L on $CD3^-CD56^{bright}$ **(N)** and on $CD3^-CD56^{dim}$ NK cells **(O)**. For HD: n=11 **(B)**, n=12 **(C)**; n=13 **(D–G)**; n=9 **(H–K)** and n=10 **(L–O)**. For P: n=12 **(B–G)**, n=11 **(H–K)**, and n=10 **(L–O)**. A two-sided unpaired t-test with Welch's correction was used in **(B–D, F–I, K–O)**. A two-sided unpaired t-test with Mann-Whitney's correction was used in **(E, J)**. ns, not significant; $^*p < 0.05$; $^{**}p < 0.01$; $^{***}p < 0.001$.

were defined as $CD3^-CD56^+$ cells and NK cell subsets were further characterized as $CD3^-CD56^{bright}$ and $CD3^-CD56^{dim}$ cells using the gating strategy described in **Supplementary Figure 1**. A PCA of cell surface markers used to analyze NK cells phenotype demonstrated that, according to PC1 and PC2, PBNK from ccRCC patients segregated together and separated from HD (**Figure 1A**). Therefore, as PBNK from ccRCC patients and HD could be discriminated with these markers, we explored the expression of these receptors and molecules in more detail.

Compared to HD, ccRCC patients exhibited similar frequencies of PBNK and distribution of $CD3^-CD56^{bright}$ and $CD3^-CD56^{dim}$ cells (*not shown*) but with lower amounts of CD56 expression in both NK cell subsets (**Figures 1B, C**). Moreover, $CD3^-CD56^{bright}$ but not $CD3^-CD56^{dim}$ cells from ccRCC patients showed a significant increased frequency of $CD25^+$ cells (**Figures 1D, E**) and they expressed significantly higher amounts of CD25 (**Figures 1F, G**). In addition, only $CD3^-CD56^{dim}$ cells but not $CD3^-CD56^{bright}$ cells from ccRCC patients displayed a significant increased frequency of $CD69^+$ cells (**Figures 1H, I**), and both subsets from ccRCC patients expressed significantly higher amounts of CD69 (**Figures 1J, K**). Moreover, $CD3^-CD56^{bright}$ and $CD3^-CD56^{dim}$ NK cells from ccRCC patients presented a lower frequency of $CD62L^+$ cells, a finding that was most notorious in $CD3^-CD56^{dim}$ cells (**Figures 1L, M**) and was accompanied by significantly lower expression of CD62L only on $CD3^-CD56^{dim}$ NK cells (**Figures 1N, O**). Also, we did not observe differences in the expression of CCR7, CD27 and CD57 on either subpopulation of PBNK from ccRCC patients compared to HD (*not shown*). Overall, our results show that PBNK from RCC patients display features of activated NK cells.

Next, we analyzed the expression of a set of activating and inhibitory receptors that regulate NK cell activity in $CD3^-CD56^{bright}$ and $CD3^-CD56^{dim}$ NK cells from ccRCC patients compared to HD. Among the activating receptors analyzed, we observed that there were no differences in the frequency of $CD16^+$ NK cells (**Figure 2A**). However, we observed an increased expression of DNAM-1 (**Figure 2B**), a reduced expression of NKG2D (**Figure 2C**), and no changes in the expression of NKp30 (**Figure 2D**), NKp46 (**Figure 2E**), NKp80 (**Figure 2F**), NKG2C (*not shown*), 2B4 (*not shown*) and NKp44 (*not shown*) in both subsets of PBNK. We also detected a higher frequency of NK cells that expressed the 2B4 ligand CD48 (**Figure 2G**) in the $CD3^-CD56^{bright}$ and $CD3^-CD56^{dim}$ NK cell subsets from ccRCC patients compared to HD. Both subsets of PBNK from ccRCC also exhibited increased amounts of CD48 (**Figure 2H**). In addition, among the inhibitory receptors and other molecules involved in negative signaling, we did not observe differences in the expression of NKG2A and TIGIT in $CD3^-CD56^{bright}$ and $CD3^-CD56^{dim}$ NK cells from ccRCC patients compared to HD (*not shown*). Also, we observed that $CD3^-CD56^{bright}$ did not express CD85j *(not shown)* but that $CD3^-CD56^{dim}$ cells from ccRCC patients exhibited higher frequencies of $CD85j^+$ cells but with similar amounts of expression compared to HD (**Figure 2I**). In addition, $CD3^-CD56^{bright}$ and $CD3^-CD56^{dim}$ NK cells from ccRCC patients exhibited a substantially higher expression of CD45 (**Figure 2J**), while only $CD3^-CD56^{dim}$ PBNK cells from ccRCC patients presented a higher frequency of PD-1^+ cells (**Figure 2K**) without changes in the amount of PD-1 expression (*not shown*). We also observed that $CD3^-CD56^{bright}$ and $CD3^-CD56^{dim}$ NK cells from ccRCC patients displayed higher expression of MHC-I (**Figure 2L**).

In addition, we did not observe differences in the frequency and amounts of expression of molecules involved in the cytotoxic function of NK cells *via* the death receptor pathway, such as FasL and TRAIL, in both subsets of PBNK from ccRCC patients compared to HD (*not shown*).

In summary, compared to HD, PBNK from ccRCC patients exhibit features of activated NK cells with a dysbalanced array of activating and inhibitory cell surface receptors skewed towards an inhibitory phenotype.

TINK Exhibit Activated and Tissue Residency Characteristics With a Balance of Activating and Inhibitory Receptors Even More Markedly Skewed Towards an Inhibitory Phenotype

To analyze the features of TINK and considering that $CD56^{bright}$ and $CD56^{dim}$ NK cell subsets could not be assessed separately within the tumor, we used the gating strategy described in **Supplementary Figure 2**. A PCA of the same cell surface markers used to analyze PBNK demonstrated that, according to PC1 and PC2, PBNK from ccRCC patients could be differentiated from TINK (**Figure 3A**). Hence, as with PBNK, we explored these differences in more detail.

Compared to PBNK from paired ccRCC patients, TINK exhibited similar amounts of expression of CD56 (*not shown*), and a higher frequency of $CD25^+$ (**Figure 3B**) with similar expression of CD25 (**Figure 3C**). TINK also displayed a higher frequency of $CD69^+$ cells (**Figure 3D**) and expressed higher amounts of CD69 (**Figure 3E**). In addition, they showed a lower frequency of $CD62L^+$ cells (**Figure 3F**) and expressed less CD62L (**Figure 3G**) than PBNK. Also, we did not find differences in the expression of CCR7, CD27 and CD57 (*not shown*). Thus, TINK from ccRCC patients also display features of activated NK cells with tissue residency characteristics.

The analysis of the expression of activating receptors revealed that TINK, compared to PBNK from ccRCC patients, exhibited a reduced frequency of $CD16^+$ cells (**Figure 4A**) and expressed less CD16 (**Figure 4B**). Similarly, TINK presented a reduced frequency of DNAM-1^+ cells (**Figure 4C**) and expressed less DNAM-1 (**Figure 4D**). TINK also exhibited reduced expression of NKp30 (**Figure 4E**), NKp46 (**Figure 4F**) and NKp80 (**Figure 4G**), but similar expression of NKG2D (**Figure 4H**) and frequencies and intensity of expression of NKp44 and NKG2C (*not shown*). Also, we did not observe differences in the frequency of $CD48^+$ NK cells (**Figure 4I**) or in the expression of CD48 (**Figure 4J**). In addition, the analysis of the expression of some inhibitory receptors demonstrated that there were no differences in the frequency of $CD85j^+$ (**Figure 4K**), $NKG2A^+$

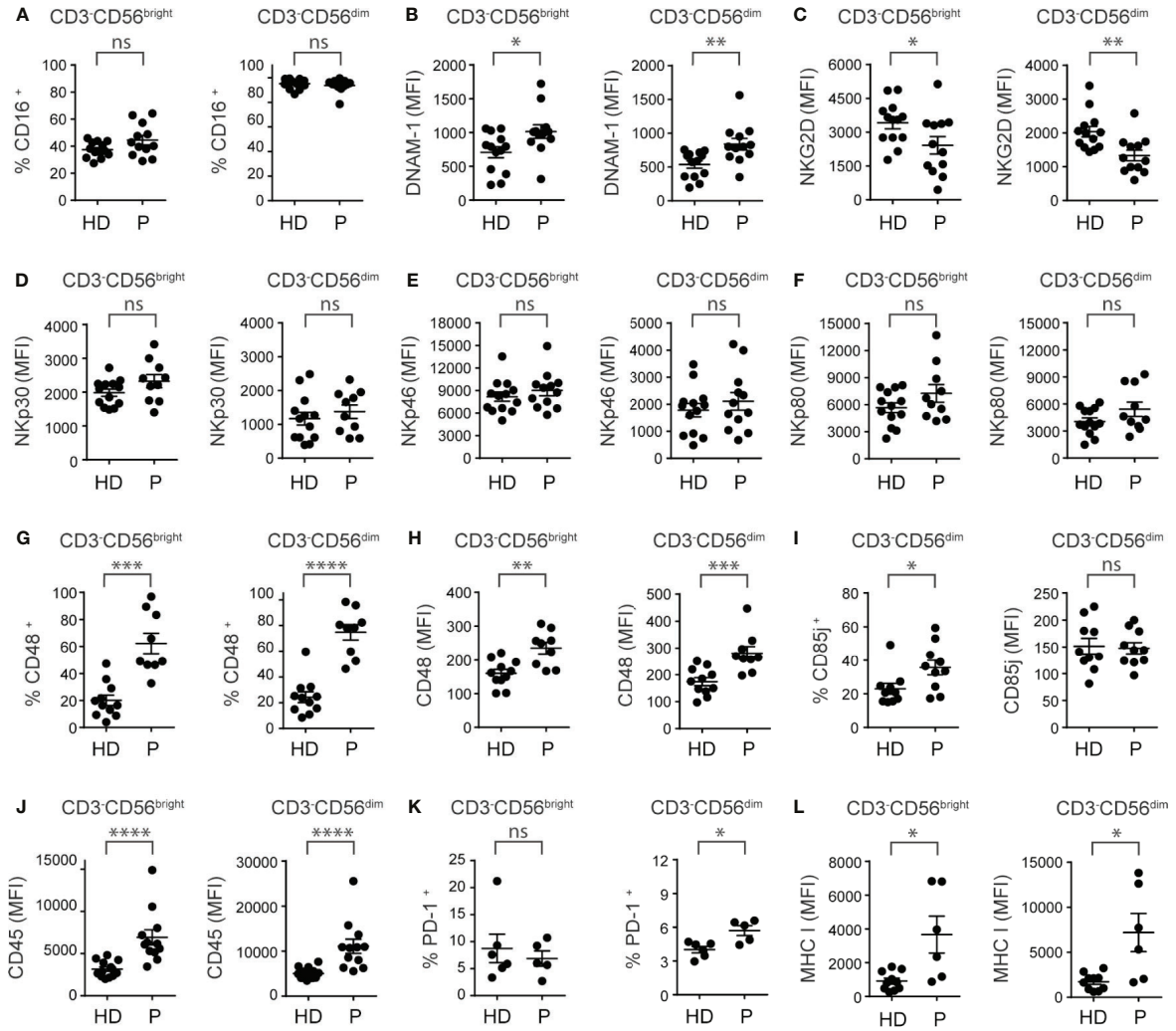

FIGURE 2 | PBNK from ccRCC patients exhibit an altered phenotype characterized by a dysregulation in the expression of activating and inhibitory receptors. PBNK cells from healthy donors (HD) and ccRCC patients (P) were analyzed by FC to compare, in the $CD3^-CD56^{bright}$ (*left graph*) and $CD3^-CD56^{dim}$ cells (*right graph*) subsets, the frequency of cells that expressed CD16 **(A)**, the intensity of expression of DNAM-1 **(B)**, NKG2D **(C)**, NKp30 **(D)**, NKp46 **(E)**, NKp80 **(F)**, the frequency of cells that expressed CD48 **(G)**, and the intensity of expression of CD48 **(H)**. Also, we analyzed the frequency of $CD85j^+$ cells (*left graph*) and the intensity of expression of CD85j (*right graph*) in $CD3^-CD56^{dim}$ cells **(I)**. In addition, in $CD3^-CD56^{bright}$ (*left graph*) and $CD3^-CD56^{dim}$ cells (*right graph*) we analyzed the intensity of expression of CD45 **(J)**, the frequency of $PD\text{-}1^+$ cells **(K)**, and the intensity of expression of MHC-I **(L)**. For HD: n=13 **(A–F, J)**, n=11 **(G, H)**, n=10 **(I, L)** and n=6 **(K)**. For P: n=12 **(A–C**, **E, J)**, n=1 **(D, F, I)**, n=9 **(G, H)**, n=5 **(K)** and n=6 **(L)**. A two-sided unpaired t-test with Welch´s correction was used in left graphs of **(A–C**, **G, H)**, in both graphs of **(D–F)**, and in right graph of **(I)** A two-sided unpaired t-test with Mann-Whitney´s correction was used in right graphs of **(A–C, G, H)**, in left graph of **(I)** and in both graphs of **(J–L)**. ns, not significant; $^*p < 0.05$; $^{**}p < 0.01$; $^{***}p < 0.001$; $^{****}p < 0.0001$.

and $TIGIT^+$ cells (*not shown*) or in the amount of these three molecules (*not shown*) or CD45 (**Figure 4L**) expressed by PBNK and TINK. Furthermore, there was a trend towards a higher frequency of $PD\text{-}1^+$ cells in TINK compared to PBNK that did not reach statistical significance (**Figure 4M**), while the amount of expression of MHC-I (**Figure 4N**) was similar in both NK cell compartments.

In addition, we observed no changes in the frequency of $FasL^+$ and $TRAIL^+$ TINK and in the intensity of expression of FasL and TRAIL compared to PBNK (*not shown*).

In summary, TINK exhibit features of activated NK cells with tissue residency characteristics and a pattern of activating and inhibitory receptors that is skewed towards an even more inhibitory phenotype than PBNK from ccRCC patients.

Bioinformatic Analyses Confirm That Overexpression of CD85j, CD45, CD48 and PD-1 in TINK Is Associated With a NK Cell Tumor Infiltration Signature in ccRCC

To interrogate whether the abnormal expression of NK cell receptors observed in our study is a general feature of patients with ccRCC, we performed a bioinformatic analysis using the TCGA database. We assessed whether inhibitory molecules that

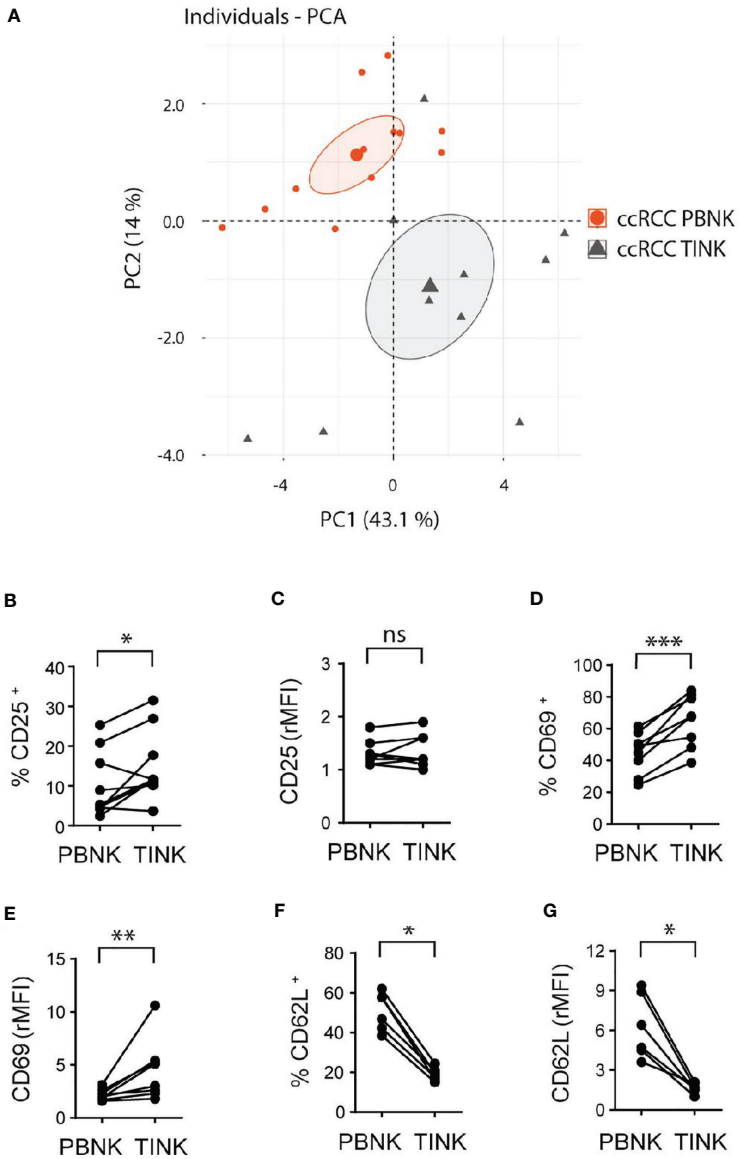

FIGURE 3 | Cell surface markers differentiate TINK from PBNK in ccRCC and indicate that TINK from ccRCC patients exhibit an activated phenotype. rMFI of the molecules analyzed on $CD3^{-}CD56^{+}$ cells from PBNK and TINK from ccRCC patients were used to perform PCA **(A)**. The graph of individuals with the confidence ellipse is shown. Also, PBNK and TINK from ccRCC patients were analyzed by FC to compare the frequency of $CD25^{+}$ cells **(B)**, the intensity of expression of CD25 **(C)**, the frequency of $CD69^{+}$ cells **(D)**, the intensity of expression of CD69 **(E)**, the frequency of $CD62L^{+}$ cells **(F)**, and the intensity of expression of CD62L **(G)**. In **(C, E, G)**, relative MFI (rMFI) was used instead of MFI because the FMO was different for PBNK and TINK. *n*=9 **(B, C)**; *n*=8 **(D, E)**; *n*=6 **(F, G)**. A two-sided paired t-test was used in **(B, D)** A two-sided paired t-test with Wilcoxon rank test was used in **(C, E–G)**. ns, not significant; $^{*}p < 0.05$; $^{**}p < 0.01$; $^{***}p < 0.001$.

exhibited overexpression in PBNK and TINK compared to HD *a)* were encoded by genes that exhibited altered expression in ccRCC compared to healthy kidney, and *b)* were associated with a NK cell infiltration signature in ccRCC samples. This signature was established by the overexpression of a group of 11 NK cell-associated genes that are not expressed or are weakly expressed on $CD8^{+}$ T cells: *NCR1, XCL2, IL2RB, KLRF1, KIR2DL4, KLRC3, XCL1, NKG7, CTSW, NCR3*, and *IL18RAP*. We observed that CD85j (**Figure 5A**), CD45 (**Figure 5B**), CD48 (**Figure 5C**) and PD-1 (**Figure 5D**) were significantly overexpressed in ccRCC. Moreover, expression of CD85j (**Figure 5E**), CD45 (**Figure 5F**), CD48 (**Figure 5G**) and PD-1 (**Figure 5H**) were strongly associated with a NK cell infiltration signature. Therefore, our results suggest that higher expression of CD45 on NK cells, increased frequencies of $CD85j^{+}$ and higher expression and frequency of $CD48^{+}$ NK cells (as detected by multicolor FC) might be a common characteristic of patients with ccRCC. Moreover, as their expression distinguishes ccRCC patients from HD, they also might emerge as potential candidates for immunotherapy.

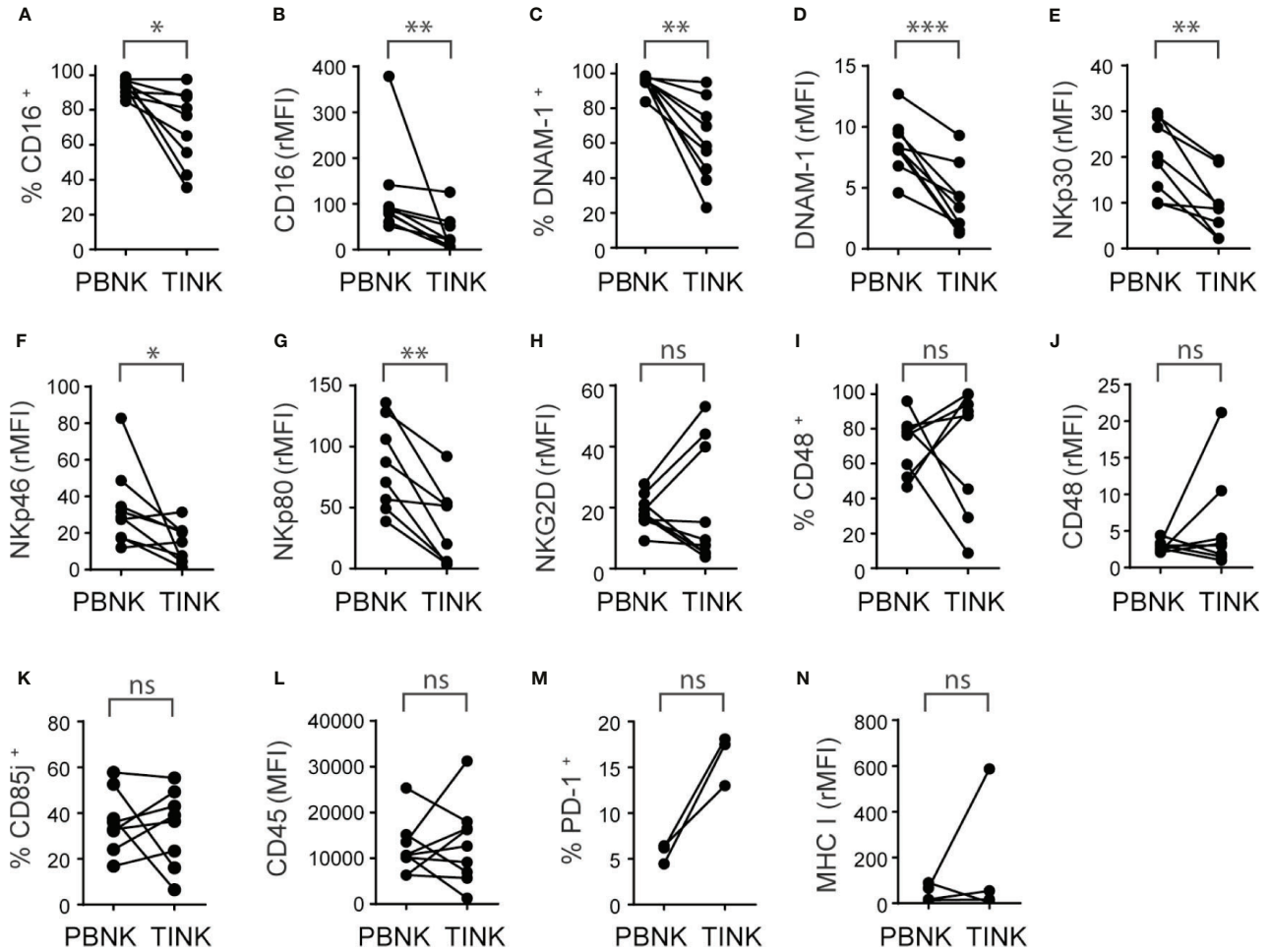

FIGURE 4 | TINK from ccRCC patients exhibit a similar increased expression of inhibitory receptors than PBNK and additional decreased expression of activating receptors. Peripheral blood NK cells (PBNK) and tumor-infiltrating NK cells (TINK) from ccRCC patients were analyzed by FC to compare the frequency of $CD16^+$ cells **(A)**, the intensity of expression of CD16 **(B)**, the frequency of DNAM-1^+ cells **(C)**, the intensity of expression of DNAM-1 **(D)**, the intensities of expression of NKp30 **(E)**, NKp46 **(F)**, NKp80 **(G)** and NKG2D **(H)**, the frequency of $CD48^+$ cells **(I)**, the intensity of expression of CD48 **(J)**, the frequency of $CD85j^+$ cells **(K)**, the intensity of expression of CD45 **(L)**, the frequency of PD-1^+ cells **(M)** and the intensity of expression of MHC-I **(N)**. In **(B, D–H, J, N)**, the relative MFI (rMFI) was used instead of MFI because the FMO was different for PBNK and TINK. *n*=9 **(A–D, F, H, L)**; *n*=8 **(E, G, I–K)**; *n*=3 **(M)**; *n*=4 **(N)**. A two-sided paired t-test was used in **(A, D, E, G–I)** and **(K)** A two-sided paired t-test with Wilcoxon rank test was used in **(B, C, F, J, L, N)**. ns, not significant; $^*p < 0.05$; $^{**}p < 0.01$; $^{***}p < 0.001$.

Calculation of z-Scores for CD85j, CD45 and CD48 Unravel Their Potential Use as Biomarkers

To explore if these inhibitory receptors could be part of a signature that might be used as biomarkers, we normalized our results calculating the z-scores for CD85j, CD45 and CD48, and we also combined these z-scores to explore if the behavior of PBNK from ccRCC differs from HD. We observed that z-scores from CD85j (**Figure 6A**), CD45 (**Figure 6B**) and CD48 (**Figure 6C**) in PBNK were significantly higher in ccRCC patients than in HD. Furthermore, the sum of z-scores by pairs of receptors improved the discrimination power between ccRCC patients and HD (**Figures 6D–F**). However, the most remarkable discrimination power was achieved with the sum of z-scores from the three receptors, as the mean for ccRCC patients was 9.5 standard deviations above the mean of HD and every single patient's value was at least 5 standard deviations above the mean of the HD (**Figure 6G**).

In summary, besides PD-1, which is an already known target for immunotherapy, our results suggest that expression of CD85j, CD45 and CD48 on NK cells from ccRCC patients constitute potential biomarkers and they might constitute candidates for therapeutic intervention that deserve further investigation.

DISCUSSION

Most patients with advanced ccRCC experience tumor recurrence and metastases (34). Notably, ccRCC is a tumor

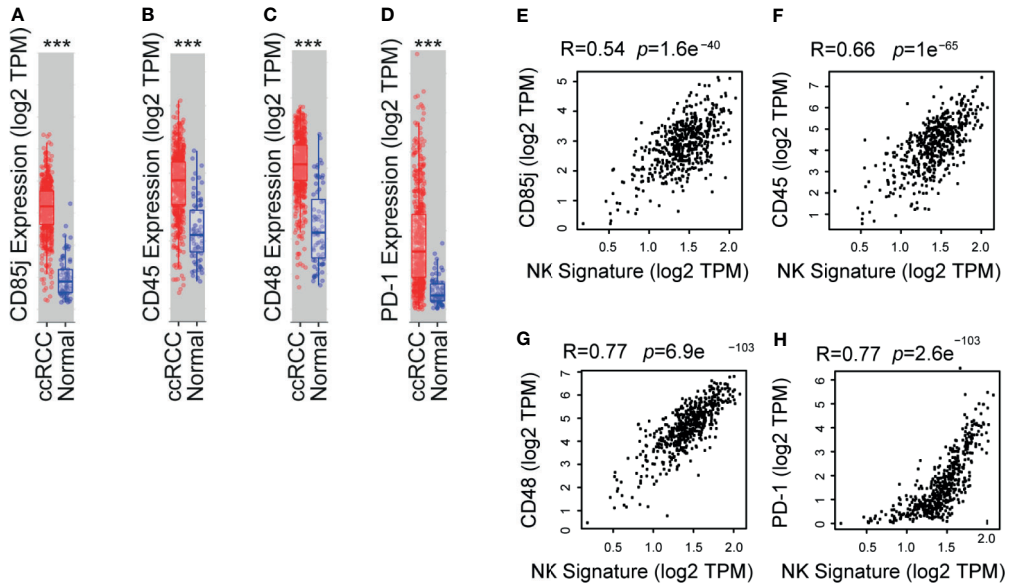

FIGURE 5 | TCGA analyses shows that CD85j, CD45, CD48 and PD-1 are overexpressed in ccRCC and associated with a NK cell signature. Analysis of expression of CD85j **(A)**, CD45 **(B)**, CD48 **(C)** and PD-1 **(D)** in ccRCC (*n*=533) compared to normal kidney (*n*=72) using the TIMER platform with data deposited in the TCGA. Also, a correlation analysis between the expression of CD85j **(E)**, CD45 **(F)**, CD48 **(G)** and PD-1 **(H)** and a NK cell signature (established by the overexpression of a group of 11 NK cell-associated genes that are not expressed or are weakly expressed on $CD8^+$ T cells: NCR1, XCL2, IL2RB, KLRF1, KIR2DL4, KLRC3, XCL1, NKG7, CTSW, NCR3, and IL18RAP) in ccRCC was performed using the GEPIA2 platform. ***$p < 0.001$.

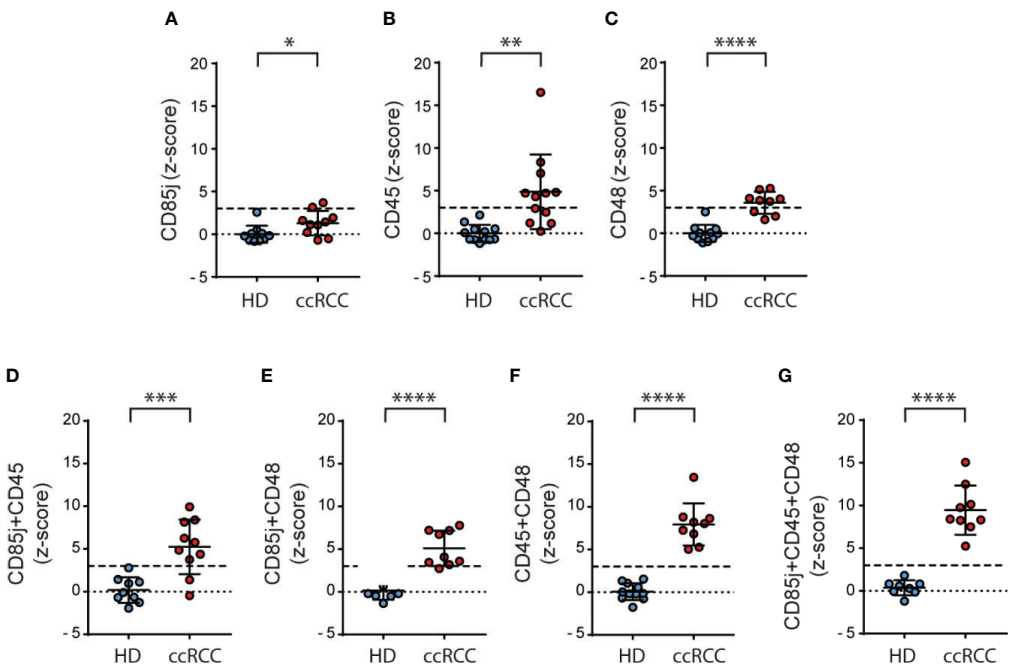

FIGURE 6 | Normalization of the expression of CD85j, CD45 and CD48 on NK cells significantly discriminates between ccRCC and HD samples. Normalization of the expression of CD85j, CD45 and CD48 in PBNK was performed calculating the respective z-scores and individual z-scores for CD85j **(A)**, CD45 **(B)** and CD48 **(C)** were depicted. Also, the sum of z-scores was calculated for the pairs of receptors CD85j and CD45 **(D)**, CD85j and CD48 **(E)**, and CD45 and CD48 **(F)** as well as the sum of z-scores of CD85j, CD45 and CD48 **(G)**. The dashed line in each graph indicates the value of the mean plus 3 SD. For HD: *n*=10 **(A)**, *n*=12 **(B)**, *n*=11 **(C, F)**, *n*=9 **(D)** and *n*=8 **(E, G)**. For P: *n*=10 **(A, D)**, *n*=12 **(B)** and *n*=9 **(C, E–G)**. *$p < 0.05$; **$p < 0.01$; ***$p < 0.001$; ****$p < 0.0001$.

that does not exhibit a high mutational burden (35) and therefore this finding might explain tumor progression even in the presence of high NK cell and CD8 T cell infiltration (36). However, patients with RCC treated with anti-PD-1 or anti-PD-L1 mAb respond relatively well and exhibit a higher objective response than the mean trend (37). Therefore, an immunosuppressive TME plays an important role in the generation of dysfunctional cytotoxic cells. Importantly, even though the administration of the immunological checkpoint inhibitors nivolumab and ipilimumab, alone or combined with other therapies, opened new therapeutic opportunities (38), most of the patients still do not benefit from these treatments. Therefore, the identification and validation of novel targets in immuno-oncology that, alone or combined with PD-1 blockade, may reinvigorate the function of cytotoxic cells becomes crucial but constitutes a formidable challenge. Bioinformatic analysis based mainly on RNA expression in whole tumor samples does not allow for discrimination of the different cells that constitute the TME. Additionally, such analysis does not account for post-translational modifications that may impact on cell surface expression of candidate molecules. Therefore, the analysis of the coding RNA may not mirror the protein expression. Consequently, the analysis of peripheral blood cells and paired tumor-infiltrating cells becomes a valuable tool in the path of identification and validation of novel predictive biomarkers and targets in immuno-oncology (39).

Given the relevant role of NK cells during tumor immunity and the promising pipelines in the field of NK cell therapies (40), we performed an exhaustive phenotypic analysis of NK cells from ccRCC patients with the aim to select candidates for further investigation of their potential use as biomarkers and/or targets for immunotherapy.

Interestingly, the panel of markers used in this work enabled us to discriminate ccRCC PBNK from HD, as shown by PCA. A more detailed analysis of the differences between HD and ccRCC PBNK phenotype revealed that compared to HD, PBNK from ccRCC patients exhibited features of activated NK cells shown by the increased frequency and expression of CD25 and CD69, and a decreased expression of CD62L (8, 41, 42). These PBNK did not exhibit alteration in their maturation or terminal differentiation status (according to the expression of CD27 and CD57, respectively) but displayed an abnormal array of activating and inhibitory receptors. The most notable change in the activating receptors was the decreased expression of NKG2D on PBNK from ccRCC patients. NKG2D is critical for tumor elimination (43, 44) and its down-regulation may arise as a consequence of the presence of soluble ligands such as MICA in plasma of cancer patients, a fact that contributes to tumor progression and immune escape (45, 46). Also, although there were no differences in the expression of the activating receptor 2B4, PBNK from ccRCC patients displayed increased frequencies and expression of its ligand CD48 (47). Notably, *cis* interaction between 2B4 and CD48 on NK cells has been reported to reduce the availability of 2B4 to interact with CD48 in *trans* on tumor cells, resulting in a heightened NK cell activation threshold (48). In addition, under certain circumstances 2B4-CD48 engagement leads to functional inhibition of NK cells (49). Moreover, CD48 can also bind to CD2 and this interaction and the effect of CD48 engagement on the cells that express it has not been properly studied yet. Therefore, up-regulation of CD48 on PBNK from ccRCC may contribute to tumor resistance to NK cell-mediated effector functions.

Other remarkable changes in PBNK from ccRCC patients were the increased frequencies of $CD3^{-}CD56^{dim}$ cells that expressed the inhibitory receptor CD85j and the coinhibitory molecule PD-1, and the expression of higher amounts of CD45 and MHC-I on both subsets of NK cells. CD85j engagement on NK cells limits their effector functions (26, 50) and its up-regulation in PBNK from triple negative breast cancer patients has been associated with impaired antibody-dependent cell-mediated cytotoxicity (ADCC) elicited by Cetuximab (51). HLA-G, which binds to CD85j with higher affinity than the classical MHC-I (35), is expressed in RCC cells (36, 37) and plays an inhibitory role on NK cell-mediated cytotoxicity against tumor cells (37). CD45 is a receptor with tyrosine phosphatase activity that participates in fine-tuning of cellular responses (52–54). Its phosphatase activity negatively controls the activation threshold of different cells from the immune system to diverse stimuli and alteration in such signaling has been involved in different pathological conditions. Regarding the upregulation of MHC-I observed on NK cells, such effect also may contribute to their inhibition as it was shown that cross-linking of MHC-I molecules on human NK cells inhibits their function (55, 56), while protecting them from self-killing (fratricide) through engagement of 2B4 (57). MHC-I expression on tumors cells might also play an important role in preventing NK cells activation through engagement of inhibitory receptors. Therefore, PBNK from ccRCC patients, besides exhibiting an activated status exhibited a phenotype skewed towards inhibition or higher activation threshold and could be clearly distinguished from PBNK from HD with the surface molecules analyzed in this work.

Moreover, performing a PCA we also demonstrated that PBNK from ccRCC patients differ from TINK. A more detailed phenotypic analysis revealed that TINK also exhibited an activated phenotype with tissue residency features characterized by a higher frequency of $CD25^{+}$ and of $CD69^{+}$ cells, higher expression of this last molecule, lower frequency of $CD62L^{+}$ and DNAM-1^{+} cells and lower expression of both molecules. Also, TINK did not exhibit alteration in their maturation or terminal differentiation status but exhibited a reduced frequency of $CD16^{+}$ cells and diminished expression of CD16, NKp30, NKp46 and NKp80, but conserved the reduced expression of NKG2D detected in PBNK. Such phenotype may not only impair direct tumor recognition by TINK through many activating receptors but also may weaken their ability to trigger ADCC through CD16. Regarding inhibitory receptors, TINK maintained the increased frequency of $CD85j^{+}$ and $CD48^{+}$ cells observed in PBNK from ccRCC patients. Moreover, each of the 3 patients analyzed for PD-1 expression exhibited increased frequency of PD-1^{+} cells in TINK compared to PBNK, but such increase was not significant likely due to the low number of

samples analyzed. TINK also exhibited similar heightened expression of CD45 and MHC-I as PBNK from ccRCC. Overall, our results indicate that TINK exhibit an activated phenotype with tissue residency characteristics that is even more skewed towards inhibition than PBNK from ccRCC patients. Coopting regulatory circuits that result in the upregulation of inhibitory receptors such as CD85j, CD45, CD48 and PD-1 may raise NK cell activation threshold, resulting in hyporesponsive NK cells. Such tumor-driven subversion of NK cells may impose restrictions to their effector functions to control tumor progression and metastases. In addition, within the TME, a concomitant downregulation of activating receptors also would desensitize NK cells to tumor cells that express the specific ligand, further facilitating tumor progression.

In addition, a bioinformatic analysis revealed that, compared to healthy kidneys, increased expression of CD85j, CD45, CD48 and PD-1 is a general characteristic of ccRCC and is strongly associated with an NK cell tumor infiltration signature in this type of tumor. Thus, besides the well-known role of PD-1 blockade on cytotoxic $CD8^+$ T cells, our results suggest that NK cells might also be involved in the efficacy of anti-PD-1/PD-L1 immunotherapy in ccRCC. Also, CD85j, CD45 and CD48 emerge as novel potential targets whose inhibition or blockade should be further examined as it may promote the reinvigoration of TINK. In addition, to evaluate the potential of these molecules as a signature capable of differentiating patients and HD, we calculated z-scores for each receptor and used them alone or combined. Remarkably, the sum of z-scores for CD85j, CD45 and CD48 exhibited a strong discrimination ability between ccRCC and HD samples. Therefore, we postulate their potential utility as peripheral biomarkers in ccRCC.

In summary, PBNK from ccRCC patients display an inhibitory profile characterized by overexpression of CD85j, CD45, CD48 and PD-1, while TINK exhibit additional alterations characterized by a decreased expression of several activating receptors. Therefore, our results suggest that CD85j, CD45 and CD48 expression represent interesting potential biomarkers in ccRCC and they might constitute possible candidates for immunotherapy whose blockade may result in their validation as novel targets in immuno-oncology.

DATA AVAILABILITY STATEMENT

The raw data supporting the conclusions of this article will be made available by the authors, without undue reservation.

ETHICS STATEMENT

The studies involving human participants were reviewed and approved by Institutional Ethics Committee of IBYME. The patients/participants provided their written informed consent to participate in this study.

AUTHOR CONTRIBUTIONS

AZ performed and designed most of the experiments and analyzed the data. XI, SN, NT, FS, JS, RS, MF, and CD contributed experimentally to the data presented in some figures. XI also performed the PCA analysis. AR and FS provided the nephrectomies and the data of the patients. NZ conceived, designed, and supervised the study and wrote the manuscript. All the authors reviewed the manuscript. All authors contributed to the article and approved the submitted version.

FUNDING

This work was funded with grants from the National Agency for Promotion of Science and Technology from Argentina (ANPCYT), the National Research Council of Argentina (CONICET) and the Trust in Science Program from GlaxoSmithKline (GSK), all to NZ. We also thank Fundación Williams and Fundación René Barón for providing financial assistance (donations) to our laboratory.

ACKNOWLEDGMENTS

We would like to thank to Dr. Gabriel A. Rabinovich for providing unlimited access to the FACSCanto II flow cytometer, to Dr. Nicolás Richards from the Centro de Educación Médica e Investigaciones Clínicas "Norberto Quirno" (CEMIC), Servicio de Urología for his assistance with the collection of medical records of some patients, and to Emily F. Higgs from the Department of Pathology of the University of Chicago for her assistance with the PCA.

SUPPLEMENTARY MATERIAL

The Supplementary Material for this article can be found online at: https://www.frontiersin.org/articles/10.3389/fimmu.2021.681615/full#supplementary-material

REFERENCES

1. Posadas EM, Limvorasak S, Figlin RA. Targeted Therapies for Renal Cell Carcinoma. *Nat Rev Nephrol* (2017) 13:496–511. doi: 10.1038/nrneph.2017.82
2. Rini BI, Battle D, Figlin RA, George DJ, Hammers H, Hutson T, et al. The Society for Immunotherapy of Cancer Consensus Statement on Immunotherapy for the Treatment of Advanced Renal Cell Carcinoma (RCC). *J Immunother Cancer* (2019) 7:354. doi: 10.1186/s40425-019-0813-8
3. Vesely MD, Kershaw MH, Schreiber RD, Smyth MJ. Natural Innate and Adaptive Immunity to Cancer. *Annu Rev Immunol* (2011) 29:235–71. doi: 10.1146/annurev-immunol-031210-101324
4. Mellman I, Coukos G, Dranoff G. Cancer Immunotherapy Comes of Age. *Nature* (2011) 480:480–9. doi: 10.1038/nature10673. nature10673.

5. Morvan MG, Lanier LL. NK Cells and Cancer: You Can Teach Innate Cells New Tricks. *Nat Rev Cancer* (2016) 16:7–19. doi: 10.1038/nrc.2015.5
6. Reading JL, Gálvez-Cancino F, Swanton C, Lladser A, Peggs KS, Quezada SA. The Function and Dysfunction of Memory CD8+ T Cells in Tumor Immunity. *Immunol Rev* (2018) 283:194–212. doi: 10.1111/imr.12657
7. Beldi-Ferchiou A, Lambert M, Dogniaux S, Vély F, Vivier E, Olive D, et al. PD-1 Mediates Functional Exhaustion of Activated NK Cells in Patients With Kaposi Sarcoma. *Oncotarget* (2016) 7:72961–77. doi: 10.18632/oncotarget.12150
8. Freud AG, Mundy-Bosse BL, Yu J, Caligiuri MA. The Broad Spectrum of Human Natural Killer Cell Diversity. *Immunity* (2017) 47:820–33. doi: 10.1016/j.immuni.2017.10.008
9. Moretta A, Marcenaro E, Parolini S, Ferlazzo G, Moretta L. NK Cells At the Interface Between Innate and Adaptive Immunity. *Cell Death Differ* (2008) 15:226–33:4402170. doi: 10.1038/sj.cdd.4402170
10. Michel T, Poli A, Cuapio A, Briquemont B, Iserentant G, Ollert M, et al. Human CD56bright Nk Cells: An Update. *J Immunol* (2016) 196:2923–31. doi: 10.4049/jimmunol.1502570
11. Shi F-D, Ljunggren H-G, La Cava A, Van Kaer L. Organ-Specific Features of Natural Killer Cells. *Nat Rev Immunol* (2011) 11:658–71. doi: 10.1038/nri3065
12. Peng H, Tian Z. Diversity of Tissue-Resident NK Cells. *Semin Immunol* (2017) 31:3–10. doi: 10.1016/j.smim.2017.07.006
13. Dogra P, Rancan C, Ma W, Toth M, Senda T, Carpenter DJ, et al. Tissue Determinants of Human Nk Cell Development, Function, and Residence. *Cell* (2020) 180:749–63. doi: 10.1016/j.cell.2020.01.022
14. Lopez-Verges S, Milush JM, Pandey S, York VA, Arakawa-Hoyt J, Pircher H, et al. CD57 Defines a Functionally Distinct Population of Mature NK Cells in the Human CD56dimCD16+ NK-Cell Subset. *Blood* (2010) 116:3865–74. doi: 10.1182/blood-2010-04-282301. blood-2010-04-282301.
15. Nielsen CM, White MJ, Goodier MR, Riley EM. Functional Significance of CD57 Expression on Human Nk Cells and Relevance to Disease. *Front Immunol* (2013) 4:422. doi: 10.3389/fimmu.2013.00422
16. Waldhauer I, Steinle A. NK Cells and Cancer Immunosurveillance. *Oncogene* (2008) 27:5932–43. doi: 10.1038/onc.2008.267
17. Dulphy N, Chrétien A-S, Khaznadar Z, Fauriat C, Nanbakhsh A, Caignard A, et al. Underground Adaptation to a Hostile Environment: Acute Myeloid Leukemia vs. Natural Killer Cells. *Front Immunol* (2016) 7:94. doi: 10.3389/fimmu.2016.00094
18. Chevrier S, Levine JH, Zanotelli VRT, Silina K, Schulz D, Bacac M, et al. An Immune Atlas of Clear Cell Renal Cell Carcinoma. *Cell* (2017) 169:736–749.e18. doi: 10.1016/j.cell.2017.04.016
19. Schleypen JS, Von Geldern M, Weiss EH, Kotzias N, Rohrmann K, Schendel DJ, et al. Renal Cell Carcinoma-Infiltrating Natural Killer Cells Express Differential Repertoires of Activating and Inhibitory Receptors and are Inhibited by Specific HLA Class I Allotypes. *Int J Cancer* (2003) 106:905–12. doi: 10.1002/ijc.11321
20. Schleypen JS, Baur N, Kammerer R, Nelson PJ, Rohrmann K, Grone EF, et al. Cytotoxic Markers and Frequency Predict Functional Capacity of Natural Killer Cells Infiltrating Renal Cell Carcinoma. *Clin Cancer Res* (2006) 12:718–25. doi: 10.1158/1078-0432.CCR-05-0857
21. Prinz PU, Mendler AN, Brech D, Masouris I, Oberneder R, Noessner E. NK-Cell Dysfunction in Human Renal Carcinoma Reveals Diacylglycerol Kinase as Key Regulator and Target for Therapeutic Intervention. *Int J Cancer* (2014) 135:1832–41. doi: 10.1002/ijc.28837
22. Xia Y, Zhang Q, Zhen Q, Zhao Y, Liu N, Li T, et al. Negative Regulation of Tumor-Infiltrating NK Cell in Clear Cell Renal Cell Carcinoma Patients Through the Exosomal Pathway. *Oncotarget* (2017) 8:37783–95. doi: 10.18632/oncotarget.16354
23. MacFarlane AW, Jillab M, Plimack ER, Hudes GR, Uzzo RG, Litwin S, et al. PD-1 Expression on Peripheral Blood Cells Increases With Stage in Renal Cell Carcinoma Patients and Is Rapidly Reduced After Surgical Tumor Resection. *Cancer Immunol Res* (2014) 2:320–31. doi: 10.1158/2326-6066.CIR-13-0133
24. Terrén I, Orrantia A, Mikelez-Alonso I, Vitallé J, Zenarruzabeitia O, Borrego F. Nk Cell-Based Immunotherapy in Renal Cell Carcinoma. *Cancers* (2020) 12 (2):316.. doi: 10.3390/cancers12020316
25. Ziblat A, Domaica CI, Spallanzani RG, Iraolagoitia XL, Rossi LE, Avila DE, et al. IL-27 Stimulates Human NK-Cell Effector Functions and Primes NK Cells for IL-18 Responsiveness. *Eur J Immunol* (2015) 45:192–202. doi: 10.1002/eji.201444699
26. Nuñez SY, Ziblat A, Secchiari F, Torres NI, Sierra JM, Raffo Iraolagoitia XL, et al. Human M2 Macrophages Limit Nk Cell Effector Functions Through Secretion of TGF-β and Engagement of CD85j. *J Immunol Baltim Md 1950* (2018) 200:1008–15. doi: 10.4049/jimmunol.1700737
27. Li T, Fan J, Wang B, Traugh N, Chen Q, Liu JS, et al. Timer: A Web Server for Comprehensive Analysis of Tumor-Infiltrating Immune Cells. *Cancer Res* (2017) 77:e108–10. doi: 10.1158/0008-5472.CAN-17-0307
28. Tang Z, Kang B, Li C, Chen T, Zhang Z. GEPIA2: An Enhanced Web Server for Large-Scale Expression Profiling and Interactive Analysis. *Nucleic Acids Res* (2019) 47:W556–60. doi: 10.1093/nar/gkz430
29. Cursons J, Souza-Fonseca-Guimaraes F, Foroutan M, Anderson A, Hollande F, Hediyeh-Zadeh S, et al. A Gene Signature Predicting Natural Killer Cell Infiltration and Improved Survival in Melanoma Patients. *Cancer Immunol Res* (2019) 7:1162–74. doi: 10.1158/2326-6066.CIR-18-0500
30. Böttcher JP, Bonavita E, Chakravarty P, Blees H, Cabeza-Cabrerizo M, Sammicheli S, et al. Nk Cells Stimulate Recruitment of cDC1 Into the Tumor Microenvironment Promoting Cancer Immune Control. *Cell* (2018) 172:1022–37.e14. doi: 10.1016/j.cell.2018.01.004
31. R: The R Project for Statistical Computing. Available at: https://www.r-project.org/ (Accessed January 4, 2021).
32. Josse J, Husson F. Missmda: A Package for Handling Missing Values in Multivariate Data Analysis. *J Stat Softw* (2016) 70:1–31. doi: 10.18637/jss.v070.i01
33. Kassambara A, Mundt F. *Factoextra: Extract and Visualize the Results of Multivariate Data Analyses* (2020). Available at: https://CRAN.R-project.org/package=factoextra (Accessed January 4, 2021).
34. Wong MCS, Goggins WB, Yip BHK, Fung FDH, Leung C, Fang Y, et al. Incidence and Mortality of Kidney Cancer: Temporal Patterns and Global Trends in 39 Countries. *Sci Rep* (2017) 7:15698. doi: 10.1038/s41598-017-15922-4
35. Shiroishi M, Tsumoto K, Amano K, Shirakihara Y, Colonna M, Braud VM, et al. Human Inhibitory Receptors Ig-like Transcript 2 (ILT2) and ILT4 Compete With CD8 for MHC Class I Binding and Bind Preferentially to HLA-G. *Proc Natl Acad Sci USA* (2003) 100:8856–61. doi: 10.1073/pnas.1431057100 1431057100
36. Rouas-Freiss N, LeMaoult J, Verine J, Tronik-Le Roux D, Culine S, Hennequin C, et al. Intratumor Heterogeneity of Immune Checkpoints in Primary Renal Cell Cancer: Focus on HLA-G/ILT2/ILT4. *Oncoimmunology* (2017) 6:e1342023. doi: 10.1080/2162402X.2017.1342023
37. Bukur J, Rebmann V, Grosse-Wilde H, Luboldt H, Ruebben H, Drexler I, et al. Functional Role of Human Leukocyte Antigen-G Up-Regulation in Renal Cell Carcinoma. *Cancer Res* (2003) 63:4107–11.
38. Ross K, Jones RJ. Immune Checkpoint Inhibitors in Renal Cell Carcinoma. *Clin Sci Lond Engl 1979* (2017) 131:2627–42. doi: 10.1042/CS20160894
39. Perez-Gracia JL, Sanmamed MF, Bosch A, Patiño-Garcia A, Schalper KA, Segura V, et al. Strategies to Design Clinical Studies to Identify Predictive Biomarkers in Cancer Research. *Cancer Treat Rev* (2017) 53:79–97. doi: 10.1016/j.ctrv.2016.12.005
40. Hoos A. Development of Immuno-Oncology Drugs - From CTLA4 to PD1 to the Next Generations. *Nat Rev Drug Discovery* (2016) 15:235–47. doi: 10.1038/nrd.2015.35
41. Juelke K, Killig M, Luetke-Eversloh M, Parente E, Gruen J, Morandi B, et al. CD62L Expression Identifies a Unique Subset of Polyfunctional CD56dim NK Cells. *Blood* (2010) 116:1299–307. doi: 10.1182/blood-2009-11-253286
42. Romee R, Foley B, Lenvik T, Wang Y, Zhang B, Ankarlo D, et al. NK Cell CD16 Surface Expression and Function Is Regulated by a Disintegrin and Metalloprotease-17 (Adam17). *Blood* (2013) 121:3599–608. doi: 10.1182/blood-2012-04-425397
43. Molfetta R, Zingoni A, Santoni A, Paolini R. Post-Translational Mechanisms Regulating NK Cell Activating Receptors and Their Ligands in Cancer: Potential Targets for Therapeutic Intervention. *Front Immunol* (2019) 10:2557. doi: 10.3389/fimmu.2019.02557
44. Bléry M, Vivier E. Nkg2d–Mica Interaction: A Paradigm Shift in Innate Recognition. *J Immunol* (2018) 200:2229. doi: 10.4049/jimmunol.1800176
45. Salih HR, Rammensee H-G, Steinle A. Down-Regulation of MICA on Human Tumors by Proteolytic Shedding. *J Immunol* (2002) 169:4098–102. doi: 10.4049/jimmunol.169.8.4098

46. Groh V, Wu J, Yee C, Spies T. Tumour-Derived Soluble MIC Ligands Impair Expression of NKG2D and T-Cell Activation. *Nature* (2002) 419:734–8. doi: 10.1038/nature01112
47. Veillette A. NK Cell Regulation by SLAM Family Receptors and SAP-related Adapters. *Immunol Rev* (2006) 214:22–34. doi: 10.1111/j.1600-065X.2006.00453.x
48. Claus M, Wingert S, Watzl C. Modulation of Natural Killer Cell Functions by Interactions Between 2B4 and CD48 in Cis and in Trans. *Open Biol* (2016) 6 (5):160010. doi: 10.1098/rsob.160010
49. Eissmann P, Beauchamp L, Wooters J, Tilton JC, Long EO, Watzl C. Molecular Basis for Positive and Negative Signaling by the Natural Killer Cell Receptor 2B4 (CD244). *Blood* (2005) 105:4722–9. doi: 10.1182/blood-2004-09-3796
50. Morel E, Bellón T. HLA Class I Molecules Regulate IFN-gamma Production Induced in NK Cells by Target Cells, Viral Products, or Immature Dendritic Cells Through the Inhibitory Receptor ILT2/CD85j. *J Immunol Baltim Md 1950* (2008) 181:2368–81. doi: 10.4049/jimmunol.181.4.2368
51. Roberti MP, Julia EP, Rocca YS, Amat M, Bravo AI, Loza J, et al. Overexpression of CD85j in TNBC Patients Inhibits Cetuximab-Mediated NK-Cell ADCC But Can Be Restored With CD85j Functional Blockade. *Eur J Immunol* (2015) 45:1560–9. doi: 10.1002/eji.201445353
52. Hermiston ML, Xu Z, Weiss A. CD45: A Critical Regulator of Signaling Thresholds in Immune Cells. *Annu Rev Immunol* (2003) 21:107–37. doi: 10.1146/annurev.immunol.21.120601.140946
53. Poggi A, Pardi R, Pella N, Morelli L, Sivori S, Vitale M, et al. CD45-Mediated Regulation of LFA1 Function in Human Natural Killer Cells. Anti-CD45 Monoclonal Antibodies Inhibit the Calcium Mobilization Induced Via LFA1 Molecules. *Eur J Immunol* (1993) 23:2454–63. doi: 10.1002/eji.1830231012
54. Starling GC, Hart DN. CD45 Molecule Cross-Linking Inhibits Natural Killer Cell-Mediated Lysis Independently of Lytic Triggering. *Immunology* (1990) 71:190–5.
55. Rubio G, Férez X, Sánchez-Campillo M, Gálvez J, Martí S, Verdú R, et al. Cross-Linking of MHC Class I Molecules on Human NK Cells Inhibits NK Cell Function, Segregates MHC I From the NK Cell Synapse, and Induces Intracellular Phosphotyrosines. *J Leukoc Biol* (2004) 76:116–24. doi: 10.1189/jlb.1103597
56. Petersson MG, Grönberg A, Kiessling R, Ferm MT. Engagement of MHC Class I Proteins on Natural Killer Cells Inhibits Their Killing Capacity. *Scand J Immunol* (1995) 42:34–8. doi: 10.1111/j.1365-3083.1995.tb03622.x
57. Betser-Cohen G, Mizrahi S, Elboim M, Alsheich-Bartok O, Mandelboim O. The Association of MHC Class I Proteins With the 2B4 Receptor Inhibits Self-Killing of Human NK Cells. *J Immunol Baltim Md 1950* (2010) 184:2761–8. doi: 10.4049/jimmunol.0901572

Conflict of Interest: The authors declare that the research was conducted in the absence of any commercial or financial relationships that could be construed as a potential conflict of interest.

Citation: *Ziblat A, Iraolagoitia XLR, Nuñez SY, Torres NI, Secchiari F, Sierra JM, Spallanzani RG, Rovegno A, Secin FP, Fuertes MB, Domaica CI and Zwirner NW (2021) Circulating and Tumor-Infiltrating NK Cells From Clear Cell Renal Cell Carcinoma Patients Exhibit a Predominantly Inhibitory Phenotype Characterized by Overexpression of CD85j, CD45, CD48 and PD-1.*
Front. Immunol. 12:681615. doi: 10.3389/fimmu.2021.681615

Copyright © 2021 Ziblat, Iraolagoitia, Nuñez, Torres, Secchiari, Sierra, Spallanzani, Rovegno, Secin, Fuertes, Domaica and Zwirner. This is an open-access article distributed under the terms of the Creative Commons Attribution License (CC BY). The use, distribution or reproduction in other forums is permitted, provided the original author(s) and the copyright owner(s) are credited and that the original publication in this journal is cited, in accordance with accepted academic practice. No use, distribution or reproduction is permitted which does not comply with these terms.

frontiers in Immunology

ORIGINAL RESEARCH
published: 01 July 2021
doi: 10.3389/fimmu.2021.692859

Prognostic Value of Tumor-Infiltrating Lymphocytes and Tertiary Lymphoid Structures in Epstein-Barr Virus-Associated and -Negative Gastric Carcinoma

Na Cheng[1†], Peng Li[2†], Huanhuan Cheng[3], Xiaoxiao Zhao[1,4], Min Dong[5], Yiwang Zhang[1], Peizhen Zhao[6], Jianning Chen[1] and Chunkui Shao[1*]*

[1] Department of Pathology, The Third Affiliated Hospital, Sun Yat-Sen University, Guangzhou, China, [2] Department of Histology and Embryology of Basic Medical Department, Guangdong Medical University, Dongguan, China, [3] Department of Ophthalmology, The Third Affiliated Hospital, Sun Yat-Sen University, Guangzhou, China, [4] Department of Pathology, The Central Hospital of Wuhan, Huazhong University of Science and Technology, Wuhan, China, [5] Department of Medical Oncology, The Third Affiliated Hospital, Sun Yat-Sen University, Guangzhou, China, [6] Dermatology Hospital, Southern Medical University, Guangzhou, China

Background: Tumor-infiltrating lymphocytes (TILs) are considered a manifestation of the host immune response against cancer and tertiary lymphoid structures (TLS) may contribute to lymphocytes recruitment. Both of them have been reported as potential prognostic parameters in some human malignancies. However, the roles of TILs, TLS, and their correlation in Epstein-Barr Virus-associated gastric carcinoma (EBVaGC) and EBV-negative gastric carcinoma (EBVnGC) are largely unknown.

Methods: To observe the correlation among TILs, TLS, and clinicopathological characteristics and their prognostic significance in EBVaGC and EBVnGC, respectively. TILs and TLS were assessed by morphology and/or immunohistochemistry, and accompanied by clinicopathological analysis from 846 gastric cancer patients in multiple institutions.

Results: Forty-two (5.0%) cases of EBVaGC and 804 cases of EBVnGC were identified by *in situ* hybridization, respectively. For EBVnGC, higher TILs grade was correlated with TLS-present. EBVnGC patients with high TILs grade and TLS-present exhibited survival benefits. TILs ($P = 0.001$) and TLS ($P = 0.003$), especially TILs & TLS ($P < 0.001$) were independent prognostic factors in EBVnGC. A nomogram was constructed and validated for predicting the probability of overall survival and performed well with a good calibration. No significant prognostic value was detected in EBVaGC.

Conclusion: TILs and TLS, especially TILs & TLS were promising prognostic indicators for overall survival in EBVnGC. TILs and TLS were highly overlapping in their extent and prognostic abilities, and may be considered as a coindicator of prognosis of gastric

OPEN ACCESS

Edited by:
Abbas Ghaderi, Shiraz University of Medical Sciences, Iran

Reviewed by:
Bing Luo, Qingdao University, China
Maria C. Ochoa, University of Navarra, Spain

***Correspondence:**
Chunkui Shao
shaochk@mail.sysu.edu.cn
Jianning Chen
chjning@mail.sysu.edu.cn

[†]These authors have contributed equally to this work and share first authorship

Specialty section:
This article was submitted to Cancer Immunity and Immunotherapy, a section of the journal Frontiers in Immunology

Received: *09 April 2021*
Accepted: *14 June 2021*
Published: *01 July 2021*

Citation:
Cheng N, Li P, Cheng H, Zhao X, Dong M, Zhang Y, Zhao P, Chen J and Shao C (2021) Prognostic Value of Tumor-Infiltrating Lymphocytes and Tertiary Lymphoid Structures in Epstein-Barr Virus-Associated and -Negative Gastric Carcinoma. Front. Immunol. 12:692859. doi: 10.3389/fimmu.2021.692859

cancer. The evaluations of TILs and TLS are simple and can be assessed routinely in pathological diagnosis.

Keywords: tumor-infiltrating lymphocytes, tertiary lymphoid structures, EBV-associated gastric carcinoma, EBV-negative gastric carcinoma, nomogram, prognosis

INTRODUCTION

Gastric carcinoma (GC) is the fourth leading cause of cancer-related mortality worldwide and the most prevalent cancer in Eastern Asia (1, 2). Immunity plays a key role in tumor initiation and progression, with immune modulation considered to be an important strategy for cancer therapy. As the major type of infiltrating immune cells, tumor-infiltrating lymphocytes (TILs) are a heterogeneous group containing T cells, B cells, and natural killer cells, which have been reported to be related to favorable prognosis in various tumors such as melanoma, breast and nasopharyngeal carcinomas (3–5). The low TILs density could predict regional lymph node metastasis and poor prognosis for recurrence free survival in GC (6). Some suggested that TILs may direct patient selection for immune checkpoint blockade therapy in GC (7, 8). However, a large proportion of patients do not respond to immunotherapy, suggesting other possible immune factors may play a certain role in tumor microenvironment (9, 10).

Tertiary lymphoid structures (TLS), characterized by ectopic aggregated lymphocytes with high endothelial venules, have gained attention because of its correlation with prolonged patient's survival in some tumors (11, 12). The formation and regulation of TLS involve the same chemokines and cytokines networks that orchestrate lymphoid organogenesis (13, 14). TLS have been reported to be associated with lymphocyte infiltration, represent a privileged area to provide a pathway for the recruitment of TILs, and generate the central-memory T and B cells to limit cancer progression (15, 16). Meanwhile, TLS could cooperate with TILs in a coordinated antitumor immune response (17). The exact prognostic role and the relationship between TILs and TLS in GC remain largely unknown.

Additionally, the association between Epstein-Barr virus (EBV) and GC is thought to be a predictive indicator for immunotherapy (18). Compared with EBV-negative GC (EBVnGC), EBV-associated GC (EBVaGC) has distinct clinicopathological features and most exhibit histology rich in lymphocyte infiltration and relatively favorable prognosis (19, 20).

The present study investigated TILs and TLS in the tumor tissues of patients with GC and evaluate their prognostic significance. In addition, the relationship between tumoral immune parameters such as TILs, TLS, TILs & TLS, and clinicopathological features in 42 EBVaGC and 804 EBVnGC patients was determined.

Abbreviations: TILs, tumor-infiltrating lymphocytes; TLS, tertiary lymphoid structures; GC, gastric carcinoma; EBVaGC, Epstein-Barr Virus-associated gastric carcinoma; EBVnGC, EBV-negative gastric carcinoma; ISH, *in situ* hybridization; EBER-1, EBV-encoded small RNA 1; H&E, hematoxylin and eosin; FDCs, follicular dendritic cells; AJCC, the American Joint Committee on Cancer; LAs, lymphoid aggregates.

MATERIALS AND METHODS

Patients and Specimens

Eight hundred forty-six cases of surgically resected GC were collected from multiple institutions including the First, Third, and Six Affiliated Hospitals of Sun Yat-sen University, from January 2001 to December 2013. An additional 86 GC patients from the Sun Yat-sen Memorial Hospital of Sun Yat-sen University (July 2008 to December 2011) were selected as a validation cohort for the nomogram. None of the patients underwent systematic chemotherapy or radiotherapy before surgery. Cases with cancer confined to mucosa were excluded because they have an excellent prognosis regardless of number of TILs.

Standard pathologic analyses were performed blindly by two experienced pathologists (CN, LP). Any discrepancy was reviewed to reach consensus at a multi-headed microscope. More than two H&E–stained section slides with tumor were obtained per case, and the mean number of slides was 4.72 (range, 3–14). In these slides, at least one slide contained the tumor invasive margin. Clinicopathological data were retrieved from the archives of the medical records and pathologic reports. All patients were restaged according to the American Joint Committee on Cancer (AJCC) Staging Manual, Seventh Edition (21).

Patients' clinical outcomes were followed up from the date of GC resection until death or December 31, 2016. The data of patients who were alive at the last follow-up date and of those died from a cause other than GC were regarded as censored data.

This study was approved by the Institute Research Ethics Committees of the First, Third, Six Affiliated Hospitals and Sun Yat-sen Memorial Hospital, Sun Yat-sen University. All participants provided written informed consents prior to surgery.

In Situ Hybridization for EBER-1

ISH assay was performed with an EBER-1 oligonucleotide probe (PanPath, Amsterdam, Netherlands), as previously described by Chen et al. (22). Dark brown nuclear staining was considered to be a positive signal. The known EBER-1-positive nasopharyngeal carcinoma tissues were used as the positive control and a sense probe for EBER-1 was used as the negative control.

Immunohistochemistry

Immunohistochemical staining was performed on 4-μm thick sections of tissue samples using an automatic staining device (Ventana Benchmark Ultra immunostainer, Ventana Medical Systems, Inc., Tucson, USA). Antibodies were as follows: mouse anti-CD3 (clone LN10, 1:100, Novocastra), mouse anti-CD20 (clone L26, 1:250, Novocastra), and mouse anti-CD21 (clone 2G9, prediluted, Novocastra). PBS was used as the negative control. A cervical lymph node served as the positive control.

Evaluation of TILs and TLS

No current consensus exists on the morphologic evaluation of TILs in GC, so we adopted and modified the TIL scoring recommendation used in previous studies (23–25). Briefly, global TILs are defined as the mean percentage of the invasive tumor area (including the tumor bed and peri-tumoral stroma) occupied by lymphocytes and plasma cells (23, 26), which was assessed by using a continuous scale as a semiquantitative parameter in 10% increments; if less than 10%, a 1 or 5% criteria was used. All available full-face tumor sections were evaluated, with no focus on hotspots. Area with necrosis, hemorrhage, or crush artifacts was excluded for TILs evaluation.

GC with lymphoid stroma, a rare histological variant of GC with prominent lymphocytic infiltration into the tumor and surrounding stroma, has distinctive clinicopathological and molecular features and is associated with a significantly better prognosis (24, 27). Therefore, patients with TILs level of >50% were classified as a separate group, and patients with TILs level of ≤50% were subdivided into two categories based on the mean value, which was determined as a threshold for survival analysis. As a whole, TILs were divided into three groups: grade 1 (minimal, ≤10%), grade 2 (moderate, 10–50%), and grade 3 (abundant, >50%).

All available sections were screened for the presence of TLS. First, the presence of lymphoid aggregates (LAs) was confirmed, as well as their patterns of organization at the tumor invasive margin and/or within the stroma of GC. Second, LAs with the visible germinal centers were considered as TLS. Third, LAs without visible germinal center were selectively stained by immunohistochemistry. The well-organized LAs with one or more $CD20^+$ B cells aggregations containing $CD21^+$ FDCs, surrounded by a $CD3^+$ T cells rich area were defined as TLS. LAs in the mucosa or submucosa of stomach were excluded (28).

Statistical Analysis

Comparisons among clinicopathologic features, EBV status, TILs, and TLS were performed by the Pearson Chi-Square test or Fisher's exact test. Pearson correlation analysis was used to examine the correlation between TILs and TLS. Survival distribution was compared using the Kaplan-Meier method and the log-rank test. Prognostic variables associated with overall survival were examined by univariate analyses using a Cox proportional hazards regression model. Only those variables which were significantly associated with survival were enrolled into multivariate regression analyses. A nomogram was generated by R software 3.3, with the discriminative ability assessed by the concordance index (C-index), which ranges from 0.5 (no discrimination at all) to 1.0 (perfect discrimination). Calibration plots were generated to compare the predicted probability of overall survival with the observed outcome. Furthermore, the precision of survival predictions was evaluated using the area under receiver operating characteristic (ROC) curve (AUC) in the validation cohort. Two-sided $P < 0.05$ was considered statistically significant. Statistical analyses were performed using SPSS 17.0 statistics software (SPSS Inc., Chicago, IL, USA).

RESULTS

Clinicopathological Features of EBVaGC and EBVnGC

According to the ISH results (**Figures 1A–D**), 42 of the 846 cases (5.0%) were identified as EBVaGC. As presented in **Table 1**, EBVaGC displayed distinct clinicopathological features, including younger age ($P = 0.010$), male predominance ($P = 0.003$), proximal stomach location ($P = 0.006$), bigger in tumor size ($P = 0.039$), Lauren diffuse type ($P = 0.043$), and higher grade of TILs ($P < 0.001$).

During a mean of 22.1 (range, 1–99) months of follow-up, 5 (12%) patients in EBVaGC and 309 (38%) ones in EBVnGC group died. Kaplan-Meier analysis revealed that patients of EBVaGC had significantly better overall survivals than that of EBVnGC ($P = 0.001$, **Figure 1E**). While stratified by tumor size and Lauren classification, EBVaGC exhibited better overall survivals than EBVnGC in patients with tumor size >5 cm ($P < 0.001$, **Figure 1G**) and Lauren diffuse type ($P = 0.001$, **Figure 1I**). No statistically significant difference was observed in EBVaGC and EBVnGC patients with tumor size <5 cm (**Figure 1F**), Lauren intestinal and mixed types (**Figures 1H, J**).

Comparison of Clinicopathologic Characteristics According to TILs

To identify the clinicopathological significance of TILs, we divided the specimens into three groups (grade 1 TILs ≤10%, grade 2 TILs 10–50%, and grade 3 TILs >50%) (**Figure 2A**). For EBVnGC, a summary of the clinicopathological characteristics according to the grade of TILs is shown in **Table 2**. The tumor with higher grade of TILs was bigger in size ($P = 0.028$). According to Lauren classification, there was a significant association between the TILs density and the diffuse/mixed type ($P < 0.001$).

For EBVaGC, no statistically significant difference was observed, except for gender. The patients with increasing TILs density were more likely to be male ($P = 0.046$; **Supplementary Table 1**). The proportion of TILs grade 2 and 3 in EBVaGC is 47.6%, significantly higher than that in EBVnGC (17.8%) ($P < 0.001$; **Table 1**).

Comparison of Clinicopathologic Characteristics According to TLS

TLS are highly organized structures with or without germinal center (**Figures 2B, C**). Among the total 804 EBVnGC patients, 563 (66.5%) cases showed the presence of TLS. Patients with the presence of TLS were younger age ($P = 0.010$), smaller in tumor size ($P = 0.013$), high pTNM stage ($P = 0.036$), poorly histologic differentiation ($P = 0.007$), Lauren diffuse type ($P = 0.009$), and WHO poorly differentiated type ($P = 0.007$) (**Table 2**).

For EBVaGC, no statistically significant difference was observed (**Supplementary Table 1**). However, the proportion of TLS-present patients was higher than that of TLS-absent ones (69.0% and 31.0%, respectively) (**Supplementary Table 1**).

Association Between TILs and TLS in EBVaGC and EBVnGC

The presence of TLS in EBVnGC was related with TILs ($P = 0.001$; **Table 3**). The proportion of TILs grade 2 and 3 in TLS-

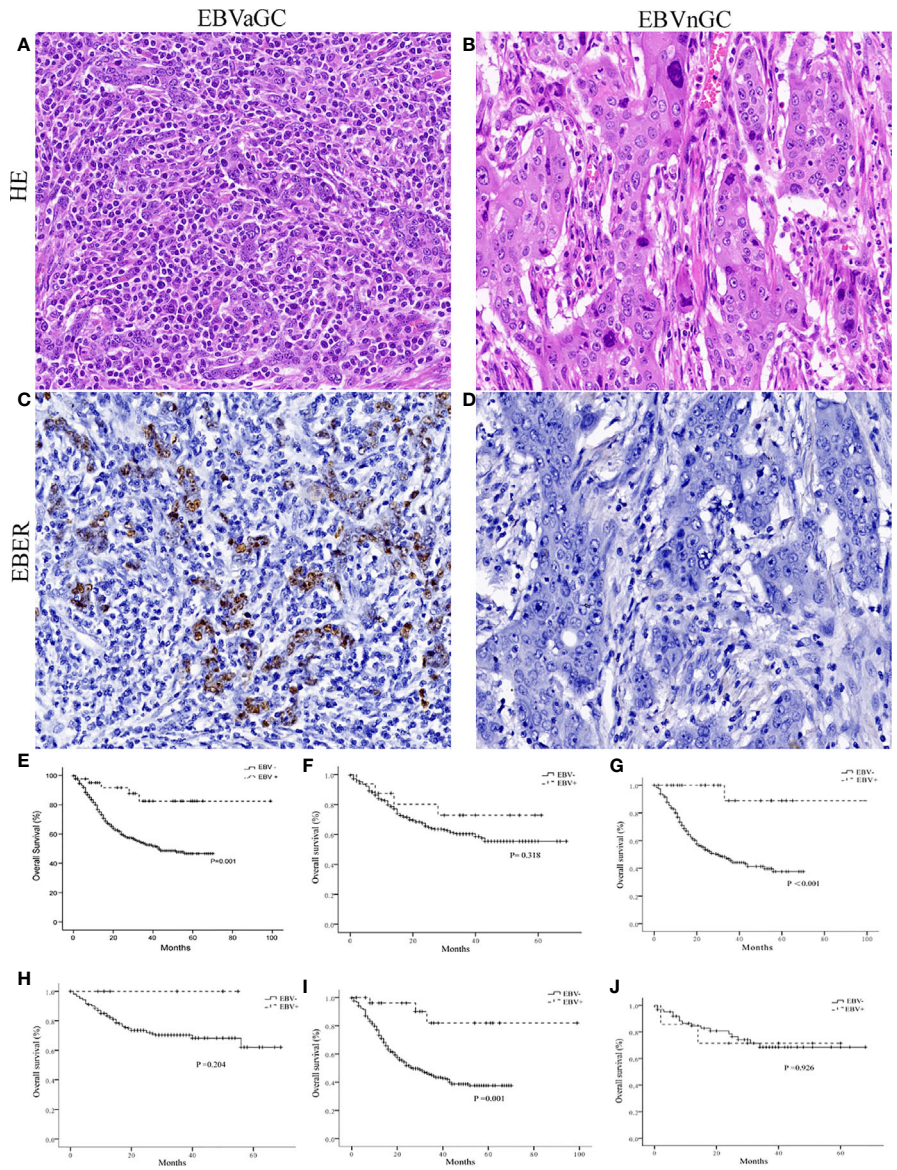

FIGURE 1 | Histology, EBER-1 ISH, and survival curves in EBVaGC and EBVnGC. Histology of the representative cases of EBVaGC **(A)** and EBVnGC **(B)** (×400). EBER-1 ISH revealed strong nuclear staining in EBVaGC **(C)**, but not in EBVnGC **(D)** (×400). **(E)** Kaplan-Meier survival curves for overall survival in 42 cases of EBVaGC and 804 cases of EBVnGC. EBVaGC had better prognosis than EBVnGC (P = 0.001, Log-rank test). When patients were stratified based on tumor size [<5 cm **(F)**; >5 cm **(G)**] and Lauren classification [Intestinal **(H)**, Diffuse **(I)**, Mixed **(J)**], EBVaGC exhibited longer overall survival than EBVnGC in patients with tumor size >5 cm (P < 0.001) and Lauren diffuse type (P = 0.001).

present patients was 21.2%, obviously higher than that in TLS-absent ones (9.9%) (**Table 3**). However, there was no significant association between TILs and TLS in EBVaGC (**Table 3**).

Prognostic Significance of TILs and TLS in EBVaGC and EBVnGC

We detected that EBVnGC patients with higher TILs grade and the presence of TLS showed survival benefits according to Kaplan-Meier survival analysis (**Figure 2D**). No significant prognostic value was detected in EBVaGC (**Figure 2E**).

In the univariate analysis of EBVnGC, the clinical parameters of tumor location, size, pTNM stage, lymphovascular invasion, perineural invasion, histologic differentiation, Lauren classification, WHO classification, TILs, and TLS were found to be significantly associated with overall survival (**Table 4**). The multivariate model revealed that pTNM stage (HR 5.025; 95% CI 3.745–6.743; $P < 0.001$), lymphovascular invasion (HR 2.053, 95% CI 1.571–2.684, $P < 0.001$), perineural invasion (HR 1.649, 95% CI 1.267–2.146, $P < 0.001$), histologic differentiation (HR 1.817, 95% CI 1.347–2.400, $P < 0.001$), Lauren classification

TABLE 1 | Clinicopathological characteristics of EBVaGC and EBVnGC.

Characteristics	All cases *n* (%)	EBVaGC *n* (%)	EBVnGC *n* (%)	*P* value
Total, *n*	846	42 (5.0)	804 (95.0)	
Age, y				0.010
<60	454 (53.7)	31 (73.8)	423 (52.6)	
≥60	392 (46.3)	11 (26.2)	381 (47.4)	
Mean ± SD	57.2 ± 12.7	53.2 ± 12.4	57.4 ± 12.6	
Gender				0.003
Male	585 (69.1)	38 (90.5)	547 (68.0)	
Female	261 (30.9)	4 (9.5)	257 (32.0)	
Location				0.006
Cardia, fundus	223 (26.4)	13 (31.0)	210 (26.1)	
Body	214 (25.3)	19 (45.2)	195 (24.3)	
Antrum	380 (44.9)	9 (21.4)	371 (46.1)	
Remnant/Multiple sites	29 (3.4)	1 (2.4)	28 (3.5)	
Size				0.039
<5 cm	457 (54.0)	16 (38.1)	441(54.9)	
≥5 cm	389 (46.0)	26 (61.9)	363 (45.1)	
pTNM stage*				0.339
I+II	375 (44.3)	22 (52.4)	353 (43.9)	
III+IV	471 (55.7)	20 (47.6)	451 (56.1)	
Lymphovascular invasion				0.138
Absent	701 (82.9)	31 (73.8)	670 (83.3)	
Present	145 (17.1)	11 (26.2)	134 (16.7)	
Perineural invasion				0.835
Absent	698 (82.5)	34 (81.0)	664 (82.6)	
Present	148 (17.5)	8 (19.0)	140 (17.4)	
Histologic differentiation				0.103
Well/Moderate	220 (26.0)	6 (14.3)	214 (26.6)	
Poor	626 (74.0)	36 (85.7)	590 (73.4)	
Lauren classification				0.043
Intestinal	221 (26.1)	6 (14.3)	215 (26.7)	
Diffuse	556 (65.7)	29 (69.0)	527 (65.5)	
Mixed	69 (8.2)	7 (16.7)	62 (7.7)	
WHO classification				0.073
Pap/tub	224 (26.5)	6 (14.3)	218 (27.1)	
Muc/por	622 (73.5)	36 (85.7)	586 (72.9)	
TILs				<0.001
Grade 1	683 (80.7)	22 (52.4)	661 (82.2)	
Grade 2	146 (17.3)	15 (35.7)	131 (16.3)	
Grade 3	17 (2.0)	5 (11.9)	12 (1.5)	
TLS				0.893
Absent	254 (30.0)	13 (31.0)	241 (30.0)	
Present	592 (70.0)	29 (69.0)	563 (70.0)	

*EBVaGC, EBV-associated gastric carcinoma; EBVnGC, EBV-negative gastric carcinoma; por, poorly cohesive carcinoma; pap, papillary adenocarcinoma; tub, well and moderately differentiated tubular adenocarcinoma; muc, mucinous adenocarcinoma; TILs, tumor-infiltrating lymphocytes; TLS, tertiary lymphoid structures. *The 7th AJCC TNM staging system.*

(HR 1.782, 95% CI 1.323–2.662, $P < 0.001$), WHO classification (HR 1.798, 95% CI 1.337–2.416, $P < 0.001$), TILs (HR 1.830, 95% CI 1.295–2.586, $P = 0.001$), and TLS (HR 1.558, 95% CI 1.228–1.977, $P = 0.003$) were independent prognostic factors for overall survival (**Table 4**).

For EBVnGC, even though TILs and TLS have a certain correlation (r = 0.139, $P < 0.001$), some tumors with moderate to abundant TILs did not show the presence of TLS. Therefore, we divided tumors into four groups according to TILs (grade 1 *vs* grade 2/3) and TLS (absent or present). As shown in **Figure 2F**, patients with higher grades of TILs and the presence of TLS had the significantly best overall survival than the other three groups. The univariate and multivariate analysis also confirmed that TILs and TLS was significantly and independently associated with better survival.

Prognostic Nomogram in EBVnGC and Validation of Predictive Accuracy of the Nomogram for Overall Survival

A prognostic nomogram was depicted to predict 1-, 3-, and 5-year individualized absolute risk for mortality based on significant factors among all EBVnGC patients (**Figure 3A**). Significant attributes were selected by the multivariate stepwise regression analysis, including location, pTNM stage, TILs, and TLS (all $P < 0.05$). Predictive accuracy of the nomogram was good, with the C-index being 0.751 (95% CI 0.724–0.779). Calibration curves for 1-, 3-, and 5-year survival prediction indicated good agreement between predicted probabilities and actual observations (**Figures 3B–D**).

For the external validation cohort, the mean follow-up time was 32.1 months (range 1–82 months). A summary of clinicopathological characteristics was shown in **Supplementary Table 2**. Predictive accuracy of the nomogram for overall survival was good, with the AUC value of 0.759 (95% CI, 0.641 to 0.848), indicating the nomogram was useful for predicting survival of patients with GC (**Figure 3E**).

DISCUSSION

In this study, TILs and TLS, especially TILs & TLS correlated with the clinical outcome of GC. Patients with higher TILs grade and TLS-present exhibited survival benefits in EBVnGC. TILs were associated with TLS and both were promising independent prognostic factors of EBVnGC. Moreover, we established a nomogram model that combined the TILs grade and TLS status as prognostic variables with other well-established prognostic factors in EBVnGC and found that the nomogram performed well for both calibration and external validation. The model may be the crucial determinants of clinical care for individual GC patients.

TILs were assessed on H&E sections and divided into three groups. EBVnGC patients with high TILs density showed markedly improved survival. The TILs grade was proved to be a promising independent prognostic indicator for overall survival in EBVnGC, which was in accordance with previous literature with regard to GC (23, 29) and other types of cancers (30–32). Generally, the predominance of TILs has been claimed to reflect an effective anti-tumor immune response, which was promoted by a dynamic and complex interaction between infiltrating immune cells and tumor cells, and this interaction is critical for tumor progression and clinical outcome (33, 34).

We found that the presence of TLS was a good, independent prognostic parameter for overall survival in EBVnGC. Despite heterogeneity in TLS-signatures and TLS-quantifying methods, most studies have consistently found the association between TLS and prolonged patients' survival, suggesting the occurrence of an active immune response within TLS to tumor microenvironment (35, 36). Conversely, limited studies have detected that the presence of TLS was a negative prognostic factor and associated with more

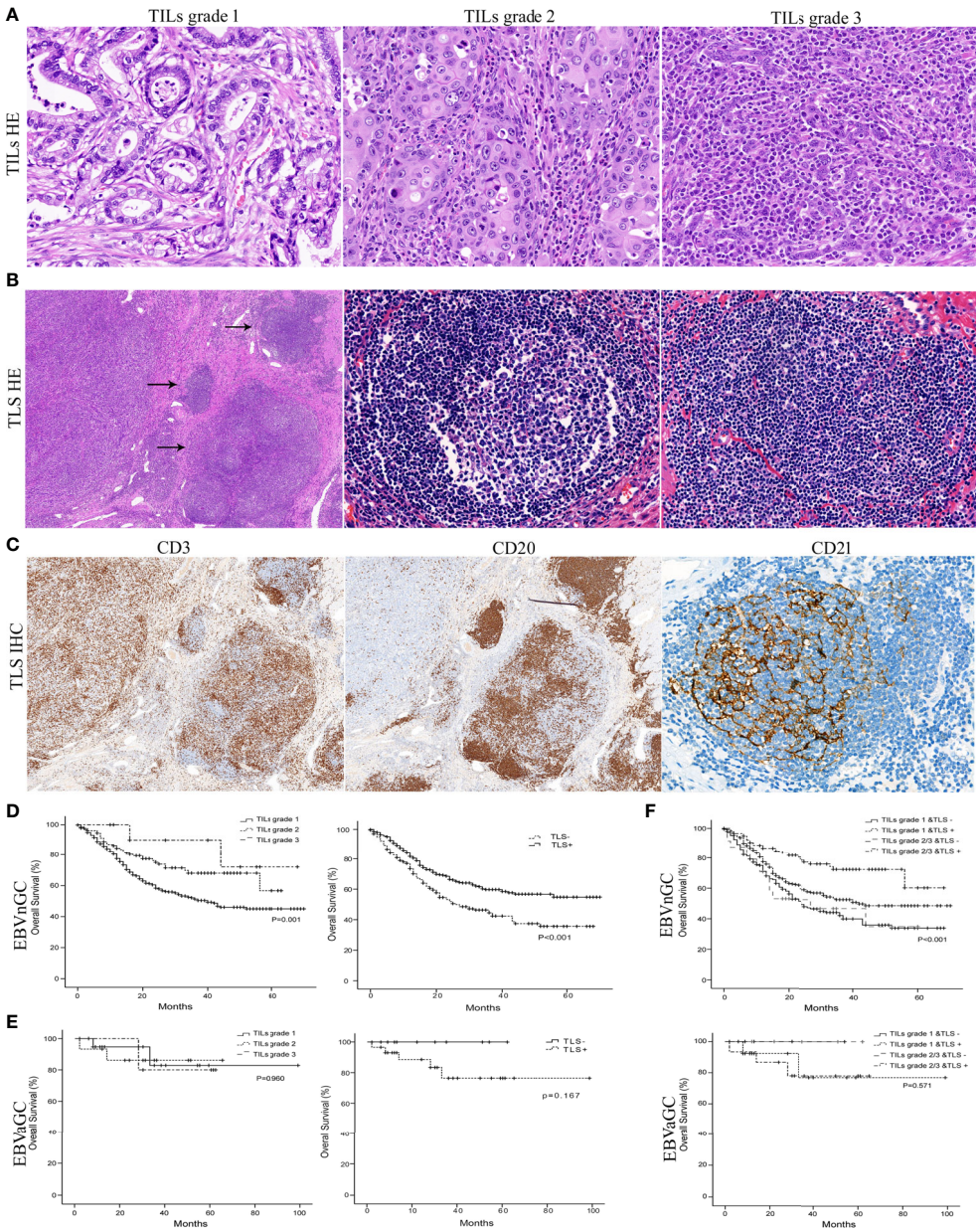

FIGURE 2 | Histology of the TILs grade, TLS, and survival curves in EBVaGC and EBVnGC. **(A)** The mean percentage of the stromal area occupied by lymphocytes and plasma cells within tumor was assessed as TILs grade 1 (minimal, ≤10%), grade 2 (moderate, 10–50%), and grade 3 (abundant, >50%) (H&E, ×400). **(B)** TLS (arrows) with or without germinal centers (center) were mainly localized at the invasive margin of cancer (left field) (H&E, left ×50, center ×400, right ×400). **(C)** Whether germinal centers were visible or not, clusters of $CD20^+$ B lymphocytes (×50) in TLS were surrounded by $CD3^+$ T cell areas (×50) and contained a network of $CD21^+$ FDCs (×400) by immunohistochemical staining. Kaplan-Meier survival analyses for overall survival were performed according to the TILs grade, TLS, or TILs & TLS in EBVnGC **(D, F)** top and EBVaGC **(E, F)** bottom.

advanced disease in colorectal, breast, and hepatocellular carcinomas (37–39). The possible reason for this discrepancy was that the maintenance and function of TLS dictated by their cellular composition and the surrounding immune contexture may vary in different tumors (36).

In our study, 42 (5.0%) patients were identified as EBVaGC, with distinct clinicopathological features and significantly better prognosis. The high TILs density and the presence of TLS may be the possible reasons. Kang et al. assessed the prognostic value of TILs amongst EBVaGC and found that the TILs density was an independent predictor for recurrence free survival (6). However, in our study, limited numbers of EBVaGC patients and the uneven distribution of cases within each TILs and TLS group made little internal difference, so no significant prognostic value

TABLE 2 | Correlation of the TILs grade and TLS with clinicopathological characteristics in EBVnGC.

Characteristics	All cases *n* (%)	TILs grade			*P* value	TLS		*P* value
		1	2	3		Absent	Present	
Total, *n*	804	661 (82.2)	131 (16.3)	12 (1.5)		241 (28.5)	563 (66.5)	
Age, y					0.089			0.010
<60	423 (52.6)	356 (53.9)	64 (48.9)	3 (25.0)		110 (45.6)	313 (55.6)	
≥60	381 (47.4)	305 (46.1)	67 (51.1)	9 (75.0)		131 (54.4)	250 (44.4)	
Mean ± SD	57.4 ± 12.6	57.0 ± 12.7	58.5 ± 12.1	64.3 ± 14.1		59.1 ± 12.9	56.7 ± 12.5	
Gender					0.100			0.411
Male	547 (68.0)	441 (66.7)	99 (75.6)	7 (58.3)		169 (70.1)	378 (67.1)	
Female	257 (32.0)	220 (33.3)	32 (24.4)	5 (41.7)		72 (29.9)	185 (32.9)	
Location					0.505			0.021
Cardia, fundus	210 (26.1)	173 (26.2)	32 (24.4)	5 (41.7)		60 (24.9)	150 (26.6)	
Body	195 (24.3)	164 (24.8)	27 (20.6)	4 (33.3)		50 (20.7)	145(25.8)	
Antrum	371 (46.1)	300 (45.4)	68 (51.9)	3 (25.0)		116 (48.1)	255 (45.3)	
Remnant/Multiple sites	28 (3.5)	24 (3.6)	4 (3.1)	0		15 (6.2)	13 (2.3)	
Size					0.028			0.013
<5 cm	441 (54.9)	366 (55.4)	73 (55.7)	2 (16.7)		116 (48.1)	325 (57.7)	
≥5 cm	363 (45.1)	295 (44.6)	58 (44.3)	10 (83.3)		125 (51.9)	238 (42.3)	
pTNM stage*					0.483			0.036
I+II	353 (43.9)	285 (43.1)	61 (46.6)	7 (43.9)		92 (38.2)	261 (46.4)	
III+IV	451 (56.1)	376 (56.9)	70 (53.4)	5 (41.7)		149 (61.8)	302 (53.6)	
Lymphovascular invasion					0.858			0.217
Absent	670 (83.3)	548 (82.9)	112 (85.5)	10 (83.3)		207 (85.9)	463 (82.2)	
Present	134 (16.7)	113 (17.1)	19 (14.5)	2 (16.7)		34 (14.1)	100 (17.8)	
Perineural invasion					0.051			0.761
Absent	664 (82.6)	537 (81.2)	115 (87.8)	12 (100)		201 (83.4)	463 (82.2)	
Present	140 (17.4)	124 (18.8)	16 (12.2)	0		40 (16.6)	100 (17.8)	
Histologic differentiation					0.411			0.007
Well/Moderate	214 (26.6)	182 (27.5)	30 (22.9)	2 (16.7)		80 (33.2)	134 (23.8)	
Poor	590 (73.4)	479 (72.5)	101(77.1)	10 (83.3)		161 (66.8)	429 (76.2)	
Lauren classification					<0.001			0.009
Intestinal	215 (26.7)	184 (27.8)	30 (22.9)	1 (8.3)		80 (33.2)	135 (24.0)	
Diffuse	527 (65.5)	441 (66.7)	78 (59.5)	8 (66.7)		149 (61.8)	378 (67.1)	
Mixed	62 (7.7)	36 (5.4)	23 (17.6)	3 (25.0)		12 (5.0)	50 (8.9)	
WHO classification					0.424			0.007
Pap/tub	218 (27.1)	185 (28.0)	31 (23.7)	2 (16.7)		81 (33.6)	137 (24.3)	
Muc/por	586 (72.9)	476 (72.0)	100 (76.3)	10 (83.3)		160 (66.4)	426 (75.7)	

*EBVnGC, EBV-negative gastric carcinoma; por, poorly cohesive carcinoma; pap, papillary adenocarcinoma; tub, well and moderately differentiated tubular adenocarcinoma; muc, mucinous adenocarcinoma; TILs, tumor-infiltrating lymphocytes; TLS, tertiary lymphoid structures. *The 7th AJCC TNM staging system.*

TABLE 3 | Association between TILs grade and TLS in EBVnGC and EBVaGC.

Variables	EBVnGC			*P* value	EBVaGC			*P* value
	n (%)	TLS-absent	TLS-present		*n* (%)	TLS-absent	TLS-present	
TILs				0.001				0.701
grade 1	661 (82.2)	217 (32.8)	444 (67.2)		22 (52.4)	8 (61.5)	14 (48.3)	
grade 2	131 (16.3)	22 (16.8)	109 (83.2)		15 (35.7)	4 (30.8)	11 (37.9)	
grade 3	12 (1.5)	2 (16.7)	10 (83.3)		5 (11.9)	1 (7.7)	4 (13.8)	
Total, *n*	804 (100.0)	241 (30.0)	563 (70.0)		42 (100.0)	13 (31.0)	29 (69.0)	

TILs, tumor-infiltrating lymphocytes; TLS, tertiary lymphoid structures.

was found in EBVaGC. Further large-scale validation studies remain to be done to fully understand the exact prognostic role of TILs and TLS in EBVaGC.

Of note, TLS and the TILs were highly overlapping in their extent and prognostic abilities. Combination of the two has prognostic power superior to each one individually. Comparing to patients with high TILs grade but the absence of TLS, the ones with high TILs grade and the presence of TLS showed improved survival, suggesting that TLS may actively license the prognostic value of TILs. Dendritic cells or plasma cells expressing markers of antigen-specific responses within TLS were reported to be associated with increased responses of TILs, which propose that TLS may educate TILs to control tumors better (15, 40). Some studies demonstrated that TLS were correlated with TILs, contributing to TILs

TABLE 4 | Cox proportional hazards regression models for the predictors of overall survival in EBVnGC.

Variables	Categories	Univariate analysis		Multivariate analysis	
		HR (95% CI)	*P* value	HR (95% CI)	*P* value
Age (y)	≥ 60 vs < 60	1.245 (0.988–1.568)	0.063		
Gender	female *vs* male	0.973 (0.761–1.244)	0.828		
Location	body *vs* cardia/fundus	0.945 (0.680–1.312)	0.735		
	antrum *vs* cardia/fundus	0.932 (0.701–1.238)	0.627		
	Remnant/multiple sites *vs* cardia/fundus	3.081 (1.859–5.106)	<0.001		
Size	≥5 cm *vs* <5 cm	1.419 (1.126–1.788)	0.003		
pTNM stage*	III+IV *vs* I+II	4.991 (3.722–6.694)	<0.001	5.025 (3.745–6.743)	<0.001
Lymphovascular invasion	present *vs* absent	2.120 (1.628–2.760)	<0.001	2.053 (1.571–2.684)	<0.001
Perineural invasion	present *vs* absent	1.771 (1.366–2.297)	<0.001	1.649 (1.267–2.146)	<0.001
Histologic differentiation	poor *vs* well/moderate	1.777 (1.322–2.389)	<0.001	1.817 (1.347–2.400)	<0.001
Lauren classification	diffuse/mixed *vs* intestinal	1.744 (1.300–2.340)	<0.001	1.782 (1.323–2.662)	<0.001
WHO classification	muc/por *vs* pap/tub	1.758 (1.313–2.354)	<0.001	1.798 (1.337–2.416)	<0.001
TILs	grade 1 *vs* grade 2/3	1.846 (1.306–2.607)	0.001	1.830 (1.295–2.586)	0.001
TLS	absent *vs* present	1.647 (1.300–2.085)	<0.001	1.558 (1.228–1.977)	0.003
TILs & TLS	grade 1&TLS– *vs* grade 2/3&TLS+	2.844 (1.864–4.340)	<0.001	2.683 (1.756–4.099)	<0.001
	grade 1&TLS+ *vs* grade 2/3&TLS+	2.039 (1.356–3.066)	0.001	2.005 (1.332–3.019)	0.001
	grade 2/3&TLS– *vs* grade 2/3&TLS+	2.879 (1.485–5.581)	0.002	2.411 (1.233–4.715)	0.010

*EBVnGC, EBV-negative gastric carcinoma; por, poorly cohesive carcinoma; pap, papillary adenocarcinoma; tub, well and moderately differentiated tubular adenocarcinoma; muc, mucinous adenocarcinoma; TILs, tumor-infiltrating lymphocytes; TLS, tertiary lymphoid structures; HR, hazard ratio; CI, confidence interval. *The 7th AJCC TNM staging system.*

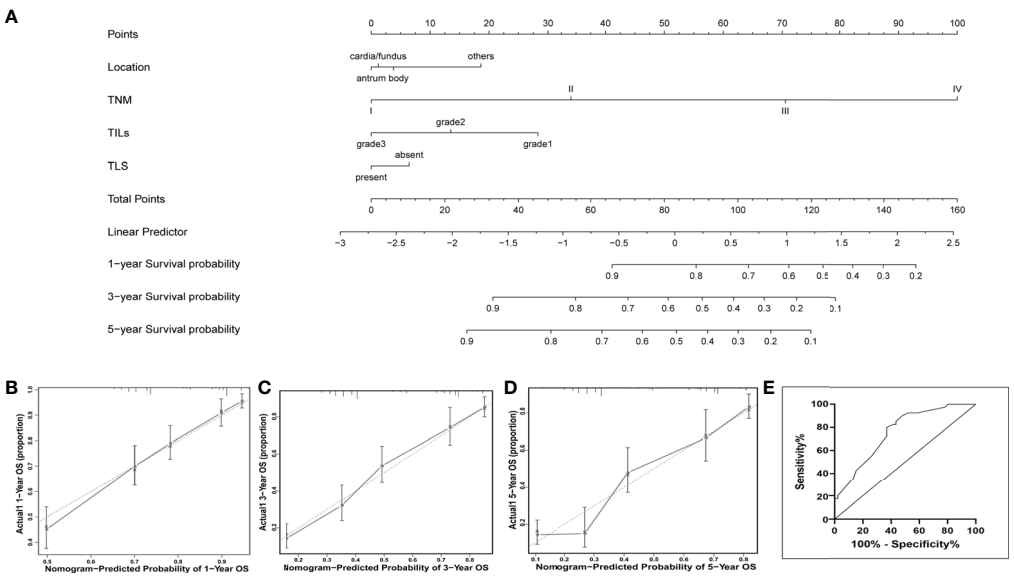

FIGURE 3 | Nomogram for predicting prognosis in patients with EBVnGC. **(A)** A predictive nomogram for 1-year, 3-year, and 5-year overall survival was generated by combining significant independent prognostic factors including location, TNM stage, TILs, and TLS. To estimate the survival in a given patient, the "Total Points" score is calculated by summing the respective "Points" values corresponding to each variable. Using this "Total Points" score, the survival probabilities at 1, 3, and 5 years can be predicted according to the lower scales. Calibration plots of the nomogram for 1-year **(B)**, 3-years **(C)**, and 5-years **(D)** overall survival. Dotted Line, ideal model; vertical bars, 95% confident interval. **(E)** Predictive accuracy of the nomogram for overall survival were confirmed in the external validation cohort, indicating the model was reliable.

recruitment and cooperating with TILs in antitumor immune response in colorectal cancer (17) and breast cancer (41). Hennequin et al. found a significant correlation between the density of B cell aggregates and Tbet$^+$ effector T cells in GC, which was also associated with better relapse-free survival, indicating that GC could be sustained through a complex network of tumor-infiltrating immune cells organized in TLS, allowing T/B cells coordination (42). The adhesion molecules, chemokines, and integrins may mediate migration of tumor-specific T cells into TLS. Meanwhile, TLS-serving HEVs may provide a gateway for the recruitment of circulating T lymphocytes into the tumor (43, 44).

Interestingly, we found a certain correlation between TILs and TLS, but some patients with moderate to abundant TILs did not develop TLS. The local tumor microenvironment including a series of signals or cytokines following the local cross-talk between TILs and resident stromal cells, may provide specific cues conducive to the formation of TLS (45, 46). We previously showed that $CD3^+$ and $CD8^+$ T lymphocytes as the predominant constituent cells of TILs in gastric cancer were associated with good prognosis (47), whereas tumor-infiltrating B cells especially when present in TLS, may be key players in anti-tumor immunity (48). Over half but not all diffuse type/genome stable GCs had enrichment of intratumoral TLS and exhibited different chemokine gene expression signature, reflecting signs of an initiated antitumor immune response and the different stages of lymphoid neogenesis (49). The presence of TLS may represent a privileged site where specific naïve B cells can undergo their final differentiation into effector B cells, such as memory B cells (48, 50). These suggest that TILs and TLS may interact with each other and play different roles in different stages of the anti-tumor immune response.

In conclusion, the present study indicated that high grade of TILs was associated with the presence of TLS and further elucidated that TILs and TLS, especially TILs & TLS were promising independent prognostic factors for overall survival in GC. TILs and TLS were highly overlapping in their extent and prognostic abilities, and could be considered as a coindicator of prognosis of gastric cancer. The evaluations of TILs and TLS are simple and can be assessed routinely in pathological diagnosis. TILs and TLS appear likely to be part of an adaptive immune response and may be helpful for understanding the immunobiology of the tumor microenvironment of gastric cancer.

DATA AVAILABILITY STATEMENT

The original contributions presented in the study are included in the article/**Supplementary Material**. Further inquiries can be directed to the corresponding authors.

ETHICS STATEMENT

The studies involving human participants were reviewed and approved by the Institute Research Ethics Committees of the First, Third, and Six Affiliated Hospital and Sun Yat-Sen Memorial Hospital, Sun Yat-Sen University. The patients/participants provided their written informed consent to participate in this study.

AUTHOR CONTRIBUTIONS

CS and JC prepared the study concept and design. NC, PL, JC, and CS wrote the paper. NC and PL performed standard pathologic analysis. XZ, MD, and YZ collected the cohort data and samples. HC and PZ did data analysis and interpretation. CS and JC supervised the project. All authors contributed to the article and approved the submitted version.

FUNDING

This work was supported by the National Natural Science Foundation of China (82073397), the Guangdong Basic and Applied Basic Research Foundation (2019A1515011455), the Natural Science Foundation of Guangdong Province (2018A030313650), the Guangzhou Science and Technology Project (202102010156, 202102010267), and the NSFC cultivating grant of The Third Affiliated Hospital, Sun Yat-sen University (2020GZRPYMS01, 2021GZRPYQN12), Guangdong Province, China.

ACKNOWLEDGMENTS

We thank Prof. Ling Xue from the First Affiliated Hospital, Sun Yat-Sen University, Prof. Yan Huang from the Sixth Affiliated Hospital, Sun Yat-Sen University, and Prof. Haigang Li from the Sun Yat-Sen Memorial Hospital of Sun Yat-Sen University for providing gastric carcinoma tissue samples used in this study.

SUPPLEMENTARY MATERIAL

The Supplementary Material for this article can be found online at: https://www.frontiersin.org/articles/10.3389/fimmu.2021.692859/full#supplementary-material

REFERENCES

1. Sung H, Ferlay J, Siegel RL, Laversanne M, Soerjomataram I, Jemal A, et al. Global Cancer Statistics 2020: GLOBOCAN Estimates of Incidence and Mortality Worldwide for 36 Cancers in 185 Countries. *CA Cancer J Clin* (2021) 71:209–49. doi: 10.3322/caac.21660
2. Smyth EC, Nilsson M, Grabsch HI, van Grieken NC, Lordick F. Gastric Cancer. *Lancet* (2020) 396:635–48. doi: 10.1016/S0140-6736(20)31288-5
3. Thomas NE, Busam KJ, From L, Kricker A, Armstrong BK, Anton-Culver H, et al. Tumor-Infiltrating Lymphocyte Grade in Primary Melanomas is Independently Associated With Melanoma-Specific Survival in the Population-Based Genes, Environment and Melanoma Study. *J Clin Oncol* (2013) 31:4252–9. doi: 10.1200/JCO.2013.51.3002
4. Lee HJ, Seo JY, Ahn JH, Ahn SH, Gong G. Tumor-Associated Lymphocytes Predict Response to Neoadjuvant Chemotherapy in Breast Cancer Patients. *J Breast Cancer* (2013) 16:32–9. doi: 10.4048/jbc.2013.16.1.32
5. Wang YQ, Chen YP, Zhang Y, Jiang W, Liu N, Yun JP, et al. Prognostic Significance of Tumor-Infiltrating Lymphocytes in Nondisseminated Nasopharyngeal Carcinoma: A Large-Scale Cohort Study. *Int J Cancer* (2018) 142:2558–66. doi: 10.1002/ijc.31279

6. Kang BW, Seo AN, Yoon S, Bae HI, Jeon SW, Kwon OK, et al. Prognostic Value of Tumor-Infiltrating Lymphocytes in Epstein-Barr Virus-Associated Gastric Cancer. *Ann Oncol* (2016) 27:494–501. doi: 10.1093/annonc/mdv610
7. Kawazoe A, Kuwata T, Kuboki Y, Shitara K, Nagatsuma AK, Aizawa M, et al. Clinicopathological Features of Programmed Death Ligand 1 Expression With Tumor-Infiltrating Lymphocyte, Mismatch Repair, and Epstein-Barr Virus Status in a Large Cohort of Gastric Cancer Patients. *Gastric Cancer* (2017) 20:407–15. doi: 10.1007/s10120-016-0631-3
8. Dai C, Geng R, Wang C, Wong A, Qing M, Hu J, et al. Concordance of Immune Checkpoints Within Tumor Immune Contexture and Their Prognostic Significance in Gastric Cancer. *Mol Oncol* (2016) 10:1551–8. doi: 10.1016/j.molonc.2016.09.004
9. Postow MA, Callahan MK, Wolchok JD. Immune Checkpoint Blockade in Cancer Therapy. *J Clin Oncol* (2015) 33:1974–82. doi: 10.1200/JCO.2014.59.4358
10. Topalian SL, Taube JM, Anders RA, Pardoll DM. Mechanism-Driven Biomarkers to Guide Immune Checkpoint Blockade in Cancer Therapy. *Nat Rev Cancer* (2016) 16:275–87. doi: 10.1038/nrc.2016.36
11. Sautes-Fridman C, Petitprez F, Calderaro J, Fridman WH. Tertiary Lymphoid Structures in the Era of Cancer Immunotherapy. *Nat Rev Cancer* (2019) 19:307–25. doi: 10.1038/s41568-019-0144-6
12. Gago DGC, van Baarsen L, Mebius RE. Tertiary Lymphoid Structures: Diversity in Their Development, Composition, and Role. *J Immunol* (2021) 206:273–81. doi: 10.4049/jimmunol.2000873
13. de Chaisemartin L, Goc J, Damotte D, Validire P, Magdeleinat P, Alifano M, et al. Characterization of Chemokines and Adhesion Molecules Associated With T Cell Presence in Tertiary Lymphoid Structures in Human Lung Cancer. *Cancer Res* (2011) 71:6391–9. doi: 10.1158/0008-5472.CAN-11-0952
14. Sautes-Fridman C, Lawand M, Giraldo NA, Kaplon H, Germain C, Fridman WH, et al. Tertiary Lymphoid Structures in Cancers: Prognostic Value, Regulation, and Manipulation for Therapeutic Intervention. *Front Immunol* (2016) 7:407. doi: 10.3389/fimmu.2016.00407
15. Goc J, Germain C, Vo-Bourgais TK, Lupo A, Klein C, Knockaert S, et al. Dendritic Cells in Tumor-Associated Tertiary Lymphoid Structures Signal a Th1 Cytotoxic Immune Contexture and License the Positive Prognostic Value of Infiltrating CD8+ T Cells. *Cancer Res* (2014) 74:705–15. doi: 10.1158/0008-5472.CAN-13-1342
16. Martinet L, Le Guellec S, Filleron T, Lamant L, Meyer N, Rochaix P, et al. High Endothelial Venules (Hevs) in Human Melanoma Lesions: Major Gateways for Tumor-Infiltrating Lymphocytes. *Oncoimmunology* (2012) 1:829–39. doi: 10.4161/onci.20492
17. Di Caro G, Bergomas F, Grizzi F, Doni A, Bianchi P, Malesci A, et al. Occurrence of Tertiary Lymphoid Tissue is Associated With T-cell Infiltration and Predicts Better Prognosis in Early-Stage Colorectal Cancers. *Clin Cancer Res* (2014) 20:2147–58. doi: 10.1158/1078-0432.CCR-13-2590
18. Naseem M, Barzi A, Brezden-Masley C, Puccini A, Berger MD, Tokunaga R, et al. Outlooks on Epstein-Barr Virus Associated Gastric Cancer. *Cancer Treat Rev* (2018) 66:15–22. doi: 10.1016/j.ctrv.2018.03.006
19. Shinozaki-Ushiku A, Kunita A, Fukayama M. Update on Epstein-Barr Virus and Gastric Cancer (Review). *Int J Oncol* (2015) 46:1421–34. doi: 10.3892/ijo.2015.2856
20. Nishikawa J, Yoshiyama H, Iizasa H, Kanehiro Y, Nakamura M, Nishimura J, et al. Epstein-Barr Virus in Gastric Carcinoma. *Cancers (Basel)* (2014) 6:2259–74. doi: 10.3390/cancers6042259
21. Edge S, Byrd DR, Compton CC, Fritz AG, Greene F, Trotti A. eds. *AJCC Cancer Staging Handbook*, 7th ed. New York: Springer-Verlag (2010).
22. Chen JN, Ding YG, Feng ZY, Li HG, He D, Du H, et al. Association of Distinctive Epstein-Barr Virus Variants With Gastric Carcinoma in Guangzhou, Southern China. *J Med Virol* (2010) 82:658–67. doi: 10.1002/jmv.21731
23. Zhang D, He W, Wu C, Tan Y, He Y, Xu B, et al. Scoring System for Tumor-Infiltrating Lymphocytes and Its Prognostic Value for Gastric Cancer. *Front Immunol* (2019) 10:71. doi: 10.3389/fimmu.2019.00071
24. Cho CJ, Kang HJ, Ryu YM, Park YS, Jeong HJ, Park YM, et al. Poor Prognosis in Epstein-Barr Virus-Negative Gastric Cancer With Lymphoid Stroma is Associated With Immune Phenotype. *Gastric Cancer* (2018) 21:925–35. doi: 10.1007/s10120-018-0820-3
25. Salgado R, Denkert C, Demaria S, Sirtaine N, Klauschen F, Pruneri G, et al. The Evaluation of Tumor-Infiltrating Lymphocytes (Tils) in Breast Cancer: Recommendations by an International Tils Working Group 2014. *Ann Oncol* (2015) 26:259–71. doi: 10.1093/annonc/mdu450
26. Buisseret L, Desmedt C, Garaud S, Fornili M, Wang X, Van den Eyden G, et al. Reliability of Tumor-Infiltrating Lymphocyte and Tertiary Lymphoid Structure Assessment in Human Breast Cancer. *Mod Pathol* (2017) 30:1204–12. doi: 10.1038/modpathol.2017.43
27. Gullo I, Oliveira P, Athelogou M, Goncalves G, Pinto ML, Carvalho J, et al. New Insights Into the Inflamed Tumor Immune Microenvironment of Gastric Cancer With Lymphoid Stroma: From Morphology and Digital Analysis to Gene Expression. *Gastric Cancer* (2019) 22:77–90. doi: 10.1007/s10120-018-0836-8
28. Hjelmstrom P. Lymphoid Neogenesis: De Novo Formation of Lymphoid Tissue in Chronic Inflammation Through Expression of Homing Chemokines. *J Leukoc Biol* (2001) 69:331–9.
29. Lee HE, Chae SW, Lee YJ, Kim MA, Lee HS, Lee BL, et al. Prognostic Implications of Type and Density of Tumour-Infiltrating Lymphocytes in Gastric Cancer. *Br J Cancer* (2008) 99:1704–11. doi: 10.1038/sj.bjc.6604738
30. Almangush A, Ruuskanen M, Hagstrom J, Hirvikoski P, Tommola S, Kosma VM, et al. Tumor-Infiltrating Lymphocytes Associate With Outcome in Nonendemic Nasopharyngeal Carcinoma: A Multicenter Study. *Hum Pathol* (2018) 81:211–9. doi: 10.1016/j.humpath.2018.07.009
31. Rakaee M, Kilvaer TK, Dalen SM, Richardsen E, Paulsen EE, Hald SM, et al. Evaluation of Tumor-Infiltrating Lymphocytes Using Routine H&E Slides Predicts Patient Survival in Resected non-Small Cell Lung Cancer. *Hum Pathol* (2018) 79:188–98. doi: 10.1016/j.humpath.2018.05.017
32. Huh JW, Lee JH, Kim HR. Prognostic Significance of Tumor-Infiltrating Lymphocytes for Patients With Colorectal Cancer. *Arch Surg* (2012) 147:366–72. doi: 10.1001/archsurg.2012.35
33. de Visser KE, Eichten A, Coussens LM. Paradoxical Roles of the Immune System During Cancer Development. *Nat Rev Cancer* (2006) 6:24–37. doi: 10.1038/nrc1782
34. Gooden MJ, de Bock GH, Leffers N, Daemen T, Nijman HW. The Prognostic Influence of Tumour-Infiltrating Lymphocytes in Cancer: A Systematic Review With Meta-Analysis. *Br J Cancer* (2011) 105:93–103. doi: 10.1038/bjc.2011.189
35. Dieu-Nosjean MC, Goc J, Giraldo NA, Sautes-Fridman C, Fridman WH. Tertiary Lymphoid Structures in Cancer and Beyond. *Trends Immunol* (2014) 35:571–80. doi: 10.1016/j.it.2014.09.006
36. Colbeck EJ, Ager A, Gallimore A, Jones GW. Tertiary Lymphoid Structures in Cancer: Drivers of Antitumor Immunity, Immunosuppression, or Bystander Sentinels in Disease? *Front Immunol* (2017) 8:1830. doi: 10.3389/fimmu.2017.01830
37. Bento DC, Jones E, Junaid S, Tull J, Williams GT, Godkin A, et al. High Endothelial Venules are Rare in Colorectal Cancers But Accumulate in Extra-Tumoral Areas With Disease Progression. *Oncoimmunology* (2015) 4:e974374. doi: 10.4161/2162402X.2014.974374
38. Finkin S, Yuan D, Stein I, Taniguchi K, Weber A, Unger K, et al. Ectopic Lymphoid Structures Function as Microniches for Tumor Progenitor Cells in Hepatocellular Carcinoma. *Nat Immunol* (2015) 16:1235–44. doi: 10.1038/ni.3290
39. Figenschau SL, Fismen S, Fenton KA, Fenton C, Mortensen ES. Tertiary Lymphoid Structures are Associated With Higher Tumor Grade in Primary Operable Breast Cancer Patients. *BMC Cancer* (2015) 15:101. doi: 10.1186/s12885-015-1116-1
40. Kroeger DR, Milne K, Nelson BH. Tumor-Infiltrating Plasma Cells Are Associated With Tertiary Lymphoid Structures, Cytolytic T-Cell Responses, and Superior Prognosis in Ovarian Cancer. *Clin Cancer Res* (2016) 22:3005–15. doi: 10.1158/1078-0432.CCR-15-2762
41. Lee HJ, Kim JY, Park IA, Song IH, Yu JH, Ahn JH, et al. Prognostic Significance of Tumor-Infiltrating Lymphocytes and the Tertiary Lymphoid Structures in HER2-Positive Breast Cancer Treated With Adjuvant Trastuzumab. *Am J Clin Pathol* (2015) 144:278–88. doi: 10.1309/AJCPIXUYDVZ0RZ3G
42. Hennequin A, Derangere V, Boidot R, Apetoh L, Vincent J, Orry D, et al. Tumor Infiltration by Tbet+ Effector T Cells and CD20+ B Cells is Associated With Survival in Gastric Cancer Patients. *Oncoimmunology* (2016) 5:e1054598. doi: 10.1080/2162402X.2015.1054598

43. Goc J, Fridman WH, Sautes-Fridman C, Dieu-Nosjean MC. Characteristics of Tertiary Lymphoid Structures in Primary Cancers. *Oncoimmunology* (2013) 2: e26836. doi: 10.4161/onci.26836
44. Dieu-Nosjean MC, Giraldo NA, Kaplon H, Germain C, Fridman WH, Sautes-Fridman C. Tertiary Lymphoid Structures, Drivers of the Anti-Tumor Responses in Human Cancers. *Immunol Rev* (2016) 271:260–75. doi: 10.1111/imr.12405
45. Fridman WH, Pages F, Sautes-Fridman C, Galon J. The Immune Contexture in Human Tumours: Impact on Clinical Outcome. *Nat Rev Cancer* (2012) 12:298–306. doi: 10.1038/nrc3245
46. Pipi E, Nayar S, Gardner DH, Colafrancesco S, Smith C, Barone F. Tertiary Lymphoid Structures: Autoimmunity Goes Local. *Front Immunol* (2018) 9:1952. doi: 10.3389/fimmu.2018.01952
47. Gong LP, Chen JN, Xiao L, He Q, Feng ZY, Zhang ZG, et al. The Implication of Tumor-Infiltrating Lymphocytes in Epstein-Barr Virus-Associated Gastric Carcinoma. *Hum Pathol* (2019) 85:82–91. doi: 10.1016/j.humpath.2018.11.002
48. Sakimura C, Tanaka H, Okuno T, Hiramatsu S, Muguruma K, Hirakawa K, et al. B Cells in Tertiary Lymphoid Structures are Associated With Favorable Prognosis in Gastric Cancer. *J Surg Res* (2017) 215:74–82. doi: 10.1016/j.jss.2017.03.033
49. Derks S, de Klerk LK, Xu X, Fleitas T, Liu KX, Liu Y, et al. Characterizing Diversity in the Tumor-Immune Microenvironment of Distinct Subclasses of Gastroesophageal Adenocarcinomas. *Ann Oncol* (2020) 31:1011–20. doi: 10.1016/j.annonc.2020.04.011
50. Germain C, Gnjatic S, Dieu-Nosjean MC. Tertiary Lymphoid Structure-Associated B Cells are Key Players in Anti-Tumor Immunity. *Front Immunol* (2015) 6:67. doi: 10.3389/fimmu.2015.00067

Conflict of Interest: The authors declare that the research was conducted in the absence of any commercial or financial relationships that could be construed as a potential conflict of interest.

Copyright © 2021 Cheng, Li, Cheng, Zhao, Dong, Zhang, Zhao, Chen and Shao. This is an open-access article distributed under the terms of the Creative Commons Attribution License (CC BY). The use, distribution or reproduction in other forums is permitted, provided the original author(s) and the copyright owner(s) are credited and that the original publication in this journal is cited, in accordance with accepted academic practice. No use, distribution or reproduction is permitted which does not comply with these terms.

frontiers in Immunology

ORIGINAL RESEARCH
published: 06 August 2021
doi: 10.3389/fimmu.2021.660397

GARP Correlates With Tumor-Infiltrating T-Cells and Predicts the Outcome of Gastric Cancer

Sutian Jiang[1,2†], Yifan Zhang[3†], Xiaojing Zhang[1], Bing Lu[1], Pingping Sun[1], Qianqian Wu[1], Xuzhong Ding[1] and Jianfei Huang[1,4]*

[1] Department of Clinical Biobank, Affiliated Hospital of Nantong University, Nantong, China, [2] Department of Pathology and Pathophysiology, School of Medicine, Nantong University, Nantong, China, [3] Clinical Medicine, Xian Medical University, Xi'an, China, [4] Translational Medicine Center, The Affiliated Kezhou People's Hospital of Nanjing Medical University, Kezhou, China

OPEN ACCESS

Edited by:
Jonathan Pol, Institut National de la Santé et de la Recherche Médicale (INSERM), France

Reviewed by:
Patrick P. Boor, Erasmus University Rotterdam, Netherlands
Rahul Roychoudhuri, University of Cambridge, United Kingdom
Charlotte Imianowski, University of Cambridge, United Kingdom, in collaboration with reviewer RR

****Correspondence:***
Jianfei Huang
jfhuang@ntu.edu.cn

[†]These authors have contributed equally to this work

Specialty section:
This article was submitted to Cancer Immunity and Immunotherapy, a section of the journal Frontiers in Immunology

Received: *29 January 2021*
Accepted: *04 May 2021*
Published: *06 August 2021*

Citation:
Jiang S, Zhang Y, Zhang X, Lu B, Sun P, Wu Q, Ding X and Huang J (2021) GARP Correlates With Tumor-Infiltrating T-Cells and Predicts the Outcome of Gastric Cancer. Front. Immunol. 12:660397. doi: 10.3389/fimmu.2021.660397

Accepting the crucial role of the immune microenvironment (TME) in tumor progression enables us to identify immunotherapeutic targets and develop new therapies. Glycoprotein A repetitions predominant (GARP) plays a vital part in maintaining regulatory T cell (Treg)-mediated immune tolerance. The impact of GARP in TME of gastric cancer is still worth exploring. We investigated public genomic datasets from The Cancer Genome Atlas and Gene Expression Omnibus to analyze the possible role of GARP and its relationship with TME of gastric cancer. Fluorescence-based multiplex immunohistochemistry and immunohistochemistry for T-cell immune signatures in a series of tissue microarrays were used to validate the value of GARP in the TME. We initially found that GARP expression was upregulated in gastric carcinoma cells, and diverse levels o3f immune cell infiltration and immune checkpoint expression were detected. Gene expression profiling revealed that GARP expression was related to the TME of gastric cancer. GARP upregulation was usually accompanied by increased FOXP3+ Treg and CD4+ T cell infiltration. In addition, GARP expression had positive relationships with CTLA-4 and PD-L1 expression in gastric cancer. Cox regression analysis and a nomogram highlighted that the probability of poor overall survival was predicted well by GARP or GARP+CD4+ T cell. Taken together, this research underlines the potential effect of GARP in regulating survival and tumor-infiltrating T-cells. In addition, the function of CD4+ T cell immune signatures in the prognosis can be clinically meaningful, thereby providing a new idea for the immunotherapeutic approach.

Keywords: GARP, mIHC, TMA, TME, gastric cancer

INTRODUCTION

Gastric cancer (GC) patients which received the conventional treatment at the same stage usually showed heterogeneous clinical prognosis (1, 2). Therefore, we need a prognostic signature that is different from the previous staging system to accurately predict the outcome of patients and better guide adjuvant therapy (2–4). Tumor-associated immune cells in the tumor microenvironment

have been demonstrated to play a vital part in tumor development and affect the clinical outcomes of patients (5, 6). Although remarkable progress has been made in cancer treatment through the blockade of CTLA-4 or PD-1 signaling using monoclonal antibodies (mAbs), most patients do not respond to immunotherapy because of primary or acquired drug resistance (7, 8). Therefore, a better understanding of the markers associated with T cells in the TME is meaningful for deciphering the mechanisms of immunotherapy and identifying new therapeutic targets (9, 10).

The transforming growth factor-β (TGF-β) superfamily is an important family of regulatory cytokines with multiple functions in development, immunity, and cancer (11). GARP (commonly known as leucine-rich repeat-containing 32) is a cell surface docking receptor for latent TGF-β, and also has been studied as a non-signal receptor on the surface of Tregs, platelets, and certain cancer cells (12–14). GARP forms a complex with integrin and releases active TGF-β from the cell surface, thereby enhancing the inhibitory phenotype of Tregs (15–17). It has been reported that GARP is overexpressed in colon, lung, and breast cancers, and patients with high GARP expression tend to have a poor prognosis (12, 18). Therefore, the roles of GARP in the immune microenvironment of gastric cancer and prognosis are worthy of further exploration. In the present study, we combined experiment and bioinformatic technique to further characterize the potential impact of GARP in regulating survival and the TME of gastric cancer, thereby finding TME-associated prognostic signature.

METHODS

Bioinformatic Analysis

Evidence From the Public Database

TCGA clinical and RNA-Seq data for GC patients, including 375 tumor samples, 27 paracancerous samples, and 32 normal samples, were download from Genome Data Commons (https://portal.gdc.cancer.Gov/). We excluded data missing key information, such as overall survival (seven cases), age (four cases), and lymph node metastasis (two cases). Our research meets the publishing requirements provided by TCGA. We also obtained an additional GEO dataset, GSE84437, which contained 434 GC patients with survival information (https://www.ncbi.nlm.nih.gov/geo/).

TISIDB Analysis

TISIDB is a website for comprehensive research on the immune microenvironment that integrates tumor immunology with multiple types of data resources (http://cis.hku.hk/TISIDB/) (19). In TISIDB, we can use literature mining and high-throughput data analysis to clarify the roles of genes of interest in tumor-immune interactions. We analyzed the effect of GARP expression on the prognosis of patients with gastric cancer and its connections with the clinicopathological parameters and immune subtypes of gastric cancer.

TIMER Database Analysis

TIMER (v.2.0.) used a deconvolution statistical method to infer the prevalence of tumor-infiltrating immune cells (TIICs) based on the gene expression profile (https://cistrome.shinyapps.io/timer/), The database used TCGA data from 10897 samples of 32 cancers to approximate the abundance of TIICs. We performed a gene module to assess the association between GARP expression in gastric cancer and TIICs, including B cells, CD4 + T cells, CD8 + T cells, neutrophils, macrophages, and dendritic cells.

CIBERSORT Estimation

CIBERSORT is an analytical tool for deconvolution of the expression matrix of immune cell subtypes based on the principle of linear support vector regression (https://cibersort.stanford.edu/index.php) (20). We used the CIBERSORT database to explore the infiltration levels of 22 immune cells in gastric cancer. Standard annotation files were utilized to generate gene expression datasets. CIBERSORT approximates the p-value *via* Monte Carlo sampling and deconvolution to determine the credibility of the results. We grouped the data downloaded from the TCGA database according to the immune subtypes obtained *via* single-sample Gene Set Enrichment Analysis (ssGSEA) to evaluate the infiltration of immune cells in different immune subtypes.

Gene Set Enrichment Analysis (GSEA) and Unsupervised Clustering

GSEA is a tool for analyzing genome-wide expression profiling data (21). The basic idea is to use a predefined set of genes, sort the genes according to the degree of differential expression between two sample types, and then test whether the predefined set of genes is enriched at the top or bottom of the sorted table. The samples were first grouped according to phenotypes, and then the differential gene sets were selected according to the group. GSEA determined which group the gene sets assembly chose. In this case, the gene sets were associated with the phenotypic grouping. We downloaded RNA-Seq data for gastric cancer from the TCGA database. Then, we performed GSEA using R (v.3.5.3) to identify signaling pathways that were differentially activated in gastric cancer. The threshold was determined using the following parameters: false-discovery rate (FDR) < 0.05 and P < 0.05.

The infiltration levels of the different immune cell populations were determined *via* single-sample GSEA (ssGSEA) using the R Bioconductor package Gene Set Variation Analysis with the default parameters. The ssGSEA algorithm is a rank-based method that defines a score representing the degree of absolute enrichment of a particular gene set in each sample. GSEA was performed on each sample using transcriptome data and clinical data downloaded from the TCGA database. We obtained the immune cells, immune-related gene sets, and immune-related pathways of each sample, thereby permitting the immune activity of each sample to be evaluated using the CIBERSORT and ESTIMATE algorithms. Unsupervised clustering classifies the samples into distinct subtypes according to the immune cell infiltration pattern of each sample. The unsupervised clustering "Pam" method in accordance with Euclidean and Ward's linkage was used in our analysis, executed by using the "ConsensuClusterPlus" R package, and repeated 1,000 times to ensure the classification stability.

Protein-Protein Interactions

STRING is a database of known and predicted protein-protein interactions (https://string-db.org/) (22). The interactions include direct (physical) and indirect (functional) associations. They stem from computational prediction, knowledge transfer between organisms, and interactions aggregated from other (primary) databases. We used the STRING database to build a protein network of interactions between GARP and related immune signatures.

Human Tissue Samples and Patient Clinical Information

The tissue microarray (TMA) (176 gastric cancer tissues, 52 normal gastric mucosa tissues) used in this research was prepared by the Department of Clinical Biobank of the Affiliated Hospital of Nantong University. A core on the TMA represents a sample with a diameter of 2 millimeters. We averaged the results of multiple samples from the same patient. This research retrospectively analyzed the clinicopathological features and prognoses of the patients. We collected clinicopathological information from the patients' medical records. The patients had not received radiotherapy, chemotherapy, or biological immunotherapy before surgery. This research protocol was approved by the Human Research Ethics Committee of the Affiliated Hospital of Nantong University (Jiangsu, China).

Immunohistochemistry (IHC)

Formalin-fixed, paraffin-embedded TMA sections were deparaffinized and rehydrated using alcohol and xylene. TMA sections were heated using a microwave in sodium citrate buffer (0.01 M, pH 6.0) to repair antigen. The sections were incubated with 5%BSA to quench endogenous peroxidase activity and then with rabbit anti-PD-L1 (13684S, Cell Signaling Technology) and mouse anti-CTLA-4 antibodies (NB10064849, NOVUS). An EliVision Plus DAB Kit (Kit-0015; Maxim Biotechnologies, Fuzhou, China) was used to analyze the result of antibody binding. The results of TMA staining were assessed using the semiquantitative H-score method by a pathologist who was blinded to the clinical information of the patients. The staining intensity score was multiplied by the percentage of positively stained cells to calculate the total score, which ranged from 0 to 300.

Fluorescence-Based Multiplex Immunohistochemistry (mIHC)

TMA sections were heated using a microwave in AR6 buffer (AR600, AKOYA) to repair antigen. MIHC staining was performed after the secondary antibody was added, and then the antigen was repaired *via* heat induction and cooling. The nucleus was stained with DAPI and sealed. The slides were scanned using the Vectra 3.0 automated quantitative pathology imaging system to detect and measure the positive rate of biomarkers. The cores containing both tumor and stroma were captured with a ×20 Olympus lens objective. Using inForm® Cell Analysis software, we train machine-learning algorithms to segment the images into tissue areas of cancerous cells and stromal cells, to segment individual cells by DAPI counterstaining, and to accurately identify and quantify the phenotypes of those cells in all high-power fields within the entire tissue section.

The following primary antibodies were used in this study: rabbit anti-GARP (orb36818, BIORBYT), rabbit anti-CD3 (85061S, Cell Signaling Technology), rabbit anti-CD4 (ab133616, Abcam), rabbit anti-CD8 (ab83278, Abcam), and mouse anti-FOXP3 (ab20034, Abcam). The secondary antibody was Opal™ polymer HRP Ms+Rb (ARH1001EA, Perkin Elmer). Fluoroshield with DAPI (F6057, Sigma) was used to stain nuclei and seal the slices.

Statistical Analysis

Student's ?-test was used to compare GARP protein expression between tumor and non-tumor tissue samples. Pearson's χ^2 test was performed to determine the correlation between GARP expression and clinicopathologic parameters. Cox regression models were used to identify prognostic factors. We used the "rms" R package to formulate nomograms, which can predict the probability of 1-year, 3-year, and 5-year overall survival for GC patients. R software (v.3.6.0), SPSS (v.17.0), GraphPad Prism (v.5.0), and Strawberry Perl (v.5.30.1) were used in the early data processing of this study. For all tests, $P < 0.05$ was considered statistically significant.

RESULTS

Immune Microenvironment Grouping of Patients With Gastric Cancer

TME is mainly composed of tumor-infiltrating immune cells, extracellular matrix, and secreted factors that are highly related to overall survival and treatment response (23). We used the CIBERSORT and ESTIMATE algorithms to evaluate each TCGA sample by scoring immune cells, stromal cells, and tumor purity. Besides, we divided TCGA samples into high and low immunity groups *via* the unsupervised clustering "Pam" method. Compared with that in the high immunity group, the immune score was significantly lower in the low immunity group, whereas the tumor score was higher in the low immunity group ($P < 0.05$) (**Figures 1A, B**). In addition, GARP expression was significantly increased in the high immunity group ($P < 0.001$) (**Figure 1C**). Then, we investigated the link between GARP expression and the markers of CD4+ T cells, CD8+ T cells, and Tregs in different immune groups. We found that GARP expression was related to CD4, CD8A, and FOXP3 expression, and the correlation was stronger in the high immunity group than in the low immunity group ($P < 0.05$) (**Figures 1D–F**). To determine whether GARP was involved in the activation of Treg in gastric cancer, we subdivided the GARP high/low group into a TGF-β1 low and high group, and then made a Kaplan-Meier curve with overall survival (**Supplementary Figure 1**). We also divided the GARP high/low group into a FOXP3 low and high group. However, the P-value of Kaplan-Meier curve with overall survival was no

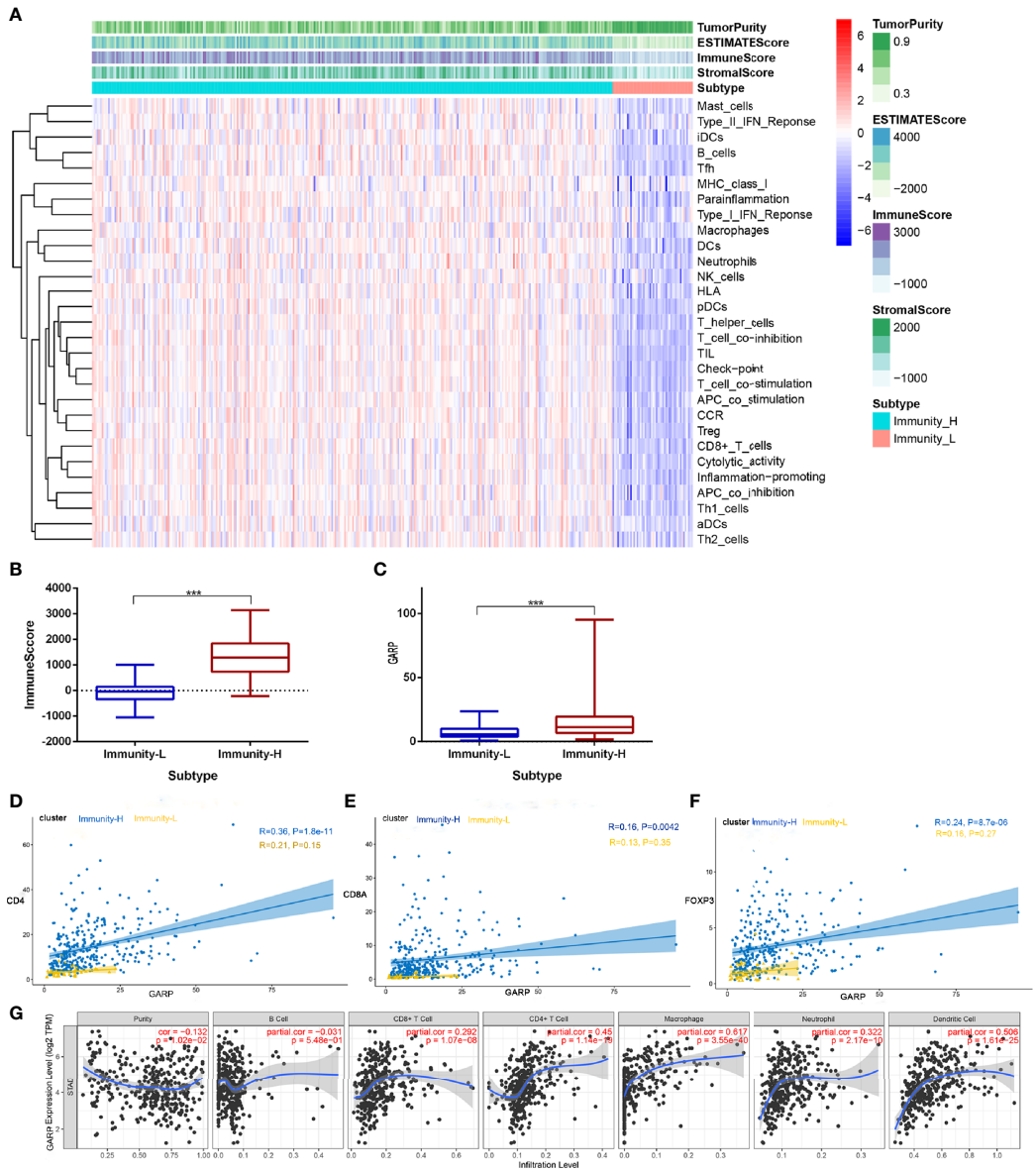

FIGURE 1 | **(A)** Immune cell score, stroma cell score, comprehensive scores of immune and stromal cells, and tumor purity score in different immunity groups. **(B)** Analysis of the difference of the immune score between the high and low immunity groups. **(C)** Analysis of the difference of glycoprotein A repetitions predominant (GARP) expression between the high and low immunity groups. **(D–F)** The relationships of GARP with CD4, CD8A, and forkhead box protein 3 (FOXP3) in different immune groups. Immunity-L, low immunity group; Immunity-H, high immunity group. ***, P < 0.001. **(G)** Correlations between GARP expression and immune cells infiltration levels in TIMER.

statistical significance. In TIMER database, there was a significant link between GARP expression and the levels of CD4+ T cells (Pearson correlation = 0.450, P < 0.05), CD8+ T cells (Pearson correlation = 0.290, P < 0.05), macrophages (Pearson correlation = 0.617, P < 0.05), neutrophils (Pearson correlation = 0.322, P < 0.05), and dendritic cells (Pearson correlation = 0.506, P < 0.05) (**Figure 1G**). These findings illustrated the relationship of GARP with the immune microenvironment in gastric cancer.

High Expression of GARP Is Associated With Clinicopathological Features

Although histological classification or clinical staging can well help to predict the prognosis of GC patients, other markers are needed to detect tumor progression. GARP expression was correlated with the tumor grade (P < 0.05) and stage (P < 0.05) (**Figures 2A, B**). In the TISIDB database, the samples were classified into distinct subtypes according to the median GARP mRNA levels. High GARP expression in patients with

gastric cancer was associated with a worse prognosis ($P < 0.05$) (**Figure 2C**). A great amount of transcriptomic data may not be translated into proteins. We next performed fluorescence-based mIHC using TMA and determined that GARP protein levels significantly differed between tumor and normal tissues ($P < 0.05$) (**Figure 2D**). MIHC staining was combined with multispectral image analysis to estimate the positive rate of GARP in a cohort of GC patients. Cytokeratin (CK) was used to identify epithelial cells in tumor samples and to define tumor and stroma, and DAPI was used to stain nuclei. Machine-learning algorithms were trained to distinguish between different tissues (tumor tissue, stroma, and no tissue) and cell phenotypes (tumor cell, and immune cell).

Then, we analyzed whether GARP expression levels were associated with clinicopathological features, including gender, age, tumor size (T), lymph node metastasis (N), distant metastasis (M), TNM stage, tumor differentiation, preoperative serum carcinoembryonic antigen (CEA) levels, and preoperative serum carbohydrate antigen 19-9 (CA19-9) levels. 176 GC patients were divided into the GARP-high group (88 cases) and GARP-low group (88 cases) based on the median GARP expression. From our analysis, we observed marked correlations of GARP expression with tumor size ($P < 0.05$), distant metastasis ($P < 0.05$), and TNM stage ($P < 0.001$) (**Table 1**). We performed Bonferroni adjustment for multiple comparisons of clinicopathologic characteristics in **Supplementary Table 1**.

The Relationship Between GARP and TIICs

We performed computational imaging techniques to evaluate multiple lymphocyte markers at the same time, allowing spatial analysis of different T cell populations in the same sample tissue section (**Figures 3E, F**). TMA sections were developed to visualize CD3, CD4, CD8, FOXP3, GARP, and CK simultaneously on a cohort of gastric cancer samples. These markers were indicated as signatures for T cells (CD3, CD4, CD8, and FOXP3). Our results demonstrated that nearly all samples had varying degrees of immune cell infiltration. Then, we analyzed whether TIIC counts differed between patients with gastric cancer according to GARP expression. Our samples were divided into two groups based on the median GARP expression level. CD3+ T cell infiltration was significantly suppressed in the high GARP expression group compared with that in the low GARP expression group ($P < 0.05$) (**Figure 3A**). In addition, CD4+ T cell ($P < 0.05$) and FOXP3+ Treg infiltration ($P < 0.05$) were obviously enhanced in the high expression group, whereas CD8+ T cell infiltration did not differ significantly between the two groups ($P = 0.728$) (**Figures 3B–D**). In addition, our analysis illustrated that the levels of immune cell infiltration were vastly correlated with tumor size (T) (**Figures 3G, H**). According to GARP high/low expression, we subdivided our data to reveal the effect of GARP within T groups on levels of immune cell infiltration. CD4+ T cell and FOXP3+ Treg infiltration were slightly higher in GARP high group (**Supplementary Figure 2**).

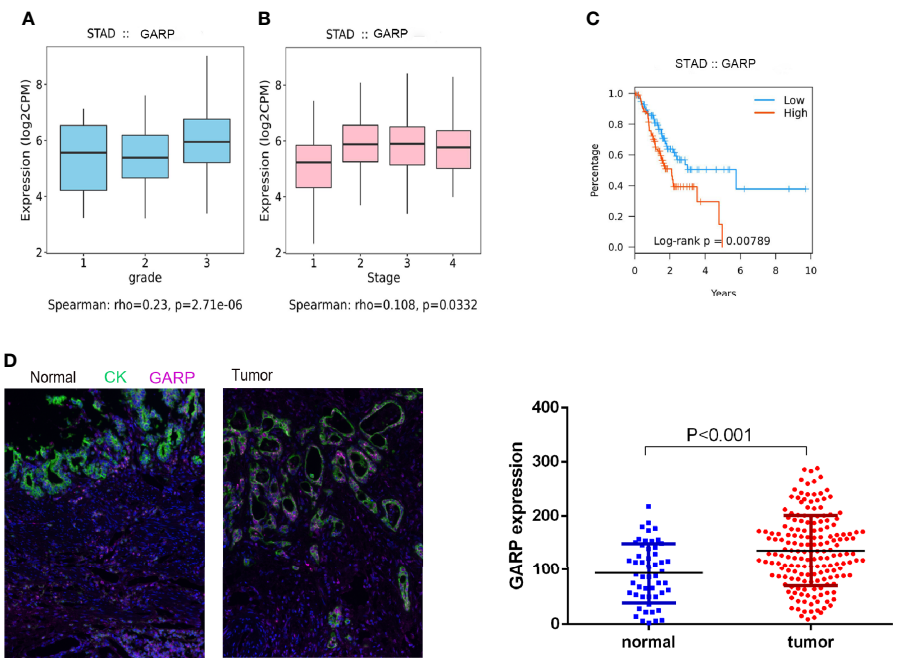

FIGURE 2 | **(A, B)** Increased GARP expression was significantly associated with unfavorable histologic grade and advanced clinical stage. **(C)** The Kaplan–Meier curve for overall survival in patients with gastric cancer in the TISIDB database. The cutoff point was based on the median. **(D)** Fluorescence-based multiplex immunohistochemistry revealed differences in glycoprotein A repetitions predominant (GARP) expression between tumor and normal samples. Cytokeratin (CK) was used to identify epithelial cells in tumor samples and to define tumor and stroma. All images were obtained using 20 × zoom and were scaled digitally.

TABLE 1 | Association of glycoprotein a repetitions predominant (GARP) expression levels with clinicopathological characteristics in patients with gastric cancer.

Characteristic	Total No.	Low or No Expression, No. (%)	High Expression, No. (%)	Pearson $\chi 2$	P-Value
Total No.	176	88 (50.00)	88 (50.00)		
Sex				1.031	0.398
Man	128	61 (47.66)	67 (52.34)		
Female	48	27 (56.25)	21 (43.75)		
Age (year)				0.211	0.760
≤60	73	38 (52.05)	35 (47.95)		
>60	103	50 (48.54)	53 (51.46)		
Differentiation				1.729	0.421
Well	9	5 (55.55)	4 (44.45)		
Middle	47	26 (55.32)	21 (44.68)		
Poor	97	43 (44.33)	54 (55.67)		
Unknown	23	14	9		
T				15.532	0.001*
Tis+T1	26	19 (73.08)	7 (26.92)		
T2	41	27 (65.85)	14 (34.15)		
T3	100	38 (38.00)	62 (62.00)		
T4	9	4 (44.44)	5 (55.56)		
N				5.311	0.150
N0	77	45 (58.44)	32 (41.56)		
N1	25	13 (52.00)	12 (48.00)		
N2	38	14 (36.84)	24 (63.16)		
N3	36	16 (44.44)	20 (55.56)		
M				5.724	0.032*
M0	164	86 (52.44)	78 (47.56)		
M1	12	2 (16.67)	10 (83.33)		
TNM				18.683	<0.001*
I	48	35 (72.92)	13 (27.08)		
II	56	28 (50.00)	28 (50.00)		
II	60	23 (38.33)	37 (61.67)		
IV	12	2 (16.67)	10 (83.33)		
Preoperative				2.666	0.143
CEA, ng/m1	76	46 (60.53)	30 (39.47)		
≤5	22	9 (40.91)	13 (59.09)		
>5	78	33	45		
Unknown					
Preoperative				1.569	0.332
CA199, u/ml	76	40 (52.63)	36 (47.37)		
≤37	11	8 (72.73)	3 (27.27)		
>37	89	40	49		
Unknown					

$P < 0.05$. T, tumor size; N, lymph node metastasis; M, distant metastasis; CEA, carcinoembryonic antigen; CA19-9, carbohydrate antigen 19-9.

From our exploration, we can conclude that GARP, as a surface molecule of Tregs, is associated with the infiltration of CD4+ T cell and FOXP3+ Treg but not that of CD8 + T cell.

GARP Upregulation or GARP+CD4+ T Cell Is an Independent Prognostic Factor for Poor Overall Survival

We utilized a cohort of 434 GC patients (GSE84437) to further comprehend the survival mechanism associated with the relationship between GARP and T-cell immune signatures. Cox regression analysis showed only GARP can be used as an independent factor affecting the prognosis of gastric cancer compared with other immune molecules ($P < 0.001$) (**Figures 4A, B**). In our research cohort, GARP upregulation in gastric cancer was a prognostic factor for poor overall survival ($P < 0.001$) (**Figures 4C, D**). We evaluated GARP expression levels in stroma and tumor cells, respectively. Immunofluorescence results showed the positive staining of GARP in CD4+ T cells (**Figures 4F, G**). Additionally, high proportions of GARP+CD4+ T cells from all T cells translated to the inferior outcome ($P < 0.05$) (**Figure 4E**). On the contrary, CD3+ T cell, CD4+ T cell, CD8+ T cell, and FOXP3+ Treg were not associated with the survival of gastric cancer.

Construction and Evaluation of a Nomogram for Overall Survival

Cox regression analyses were conducted to exhibited that GARP or GARP+CD4+ T cell could serve as an independent predictor of patients' overall survival after adjusted by TME-associated signatures in multiple GC cohorts (**Figure 4**). Based on logistic regression, we generated a nomogram that integrated GARP, GARP+CD4+ T cell, and other clinicopathological features, including tumor size, lymph node metastasis, distant metastasis, TNM stage, tumor differentiation to predict the probability of 1-year, 3-year, and 5-year overall survival for GC patients with the GSE84437 and the experimental cohort

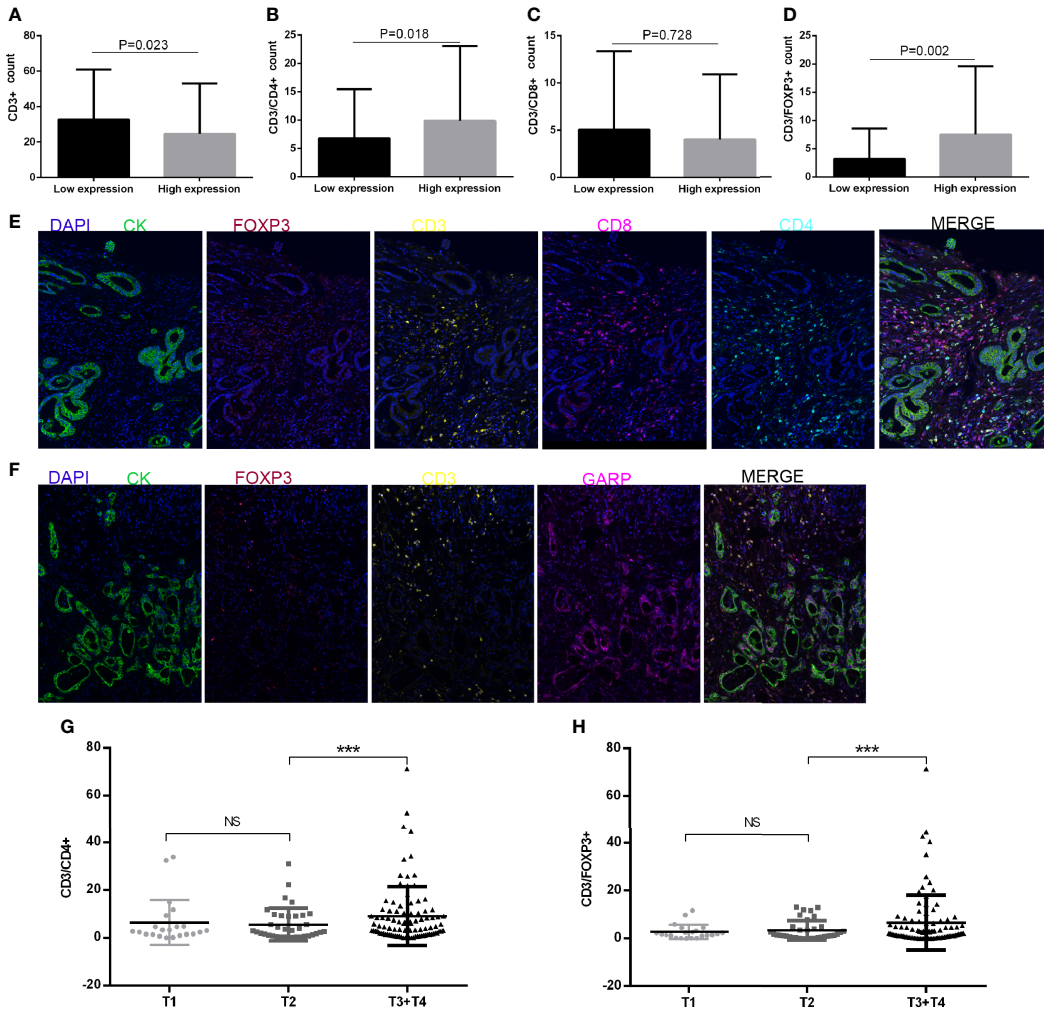

FIGURE 3 | **(A–D)** CD3+ T cell, CD4+ T cell, CD8+ T cell, and FOXP3+ regulatory T cell (Treg) infiltration levels in patients with low or high glycoprotein A repetitions predominant (GARP) expression. **(E, F)** Representative fluorescence-based multiplex immunohistochemistry images. **(E)** A staining panel was developed to visualize CD3, CD4, CD8, FOXP3, and CK simultaneously on the same tissue slide. **(F)** A staining panel was developed to visualize CD3, GARP, FOXP3, and CK simultaneously on the same tissue slide. **(G, H)** Tumor size (T) was associated with changes in CD4+ T cell and FOXP3+ Treg infiltration. Ns, $P > 0.05$; ***, $P < 0.001$.

(**Figures 5A, C**). The calibration plots revealed the probability of a 3-year survival rate is well predicted in the GSE84437 cohort and the experimental cohort (**Figures 5B, D**).

Exploration of the Molecular Mechanism of GARP

We investigated whether the prognostic effect of GARP is related to immune checkpoints in gastric cancer. IHC was performed to explore the expression of PD-L1 and CTLA-4 in gastric cancer and then analyzed their correlations with GARP expression. As presented in **Figures 6A–F**, GARP expression was associated with CTLA-4 ($P < 0.05$) and PD-L1 expression ($P < 0.05$). Meanwhile, a positive relationship between CTLA-4 and PD-L1 expression was noted in gastric cancer ($P < 0.05$).

As the surface receptor of Treg, CTLA-4 can bind CD80/CD86 on the antigen-presenting cells (APC) (24). Then, APC interacts with activated antigen-specific effector T cell, thereby transforming these cells into induced Tregs (25). Induced Treg exerts an immunosuppressive effect by secreting TGF-β and IL-10. In TISIDB, we found that GARP expression was correlated with CD80, CD86, and IL-10 expression (**Figures 6G–I**). We confirmed this correlation in the TCGA cohort (**Supplementary Figures 1E, F**). In addition, GARP, CTLA-4, PD-L1, FOXP3, CD80, CD86, and IL-10 formed a protein-protein network (**Figure 6J**).

We divided 176 GC patients into the GARP-high group and GARP-low group based on the median GARP expression. GSEA analysis screened the differential genes according to the sample groups, and then enriched the genes. The results showed that gene sets were enriched with GARP upregulation in GC samples. We selected 10 KEGG pathways with significant differences according to the normalized enrichment score (FDR < 0.25,

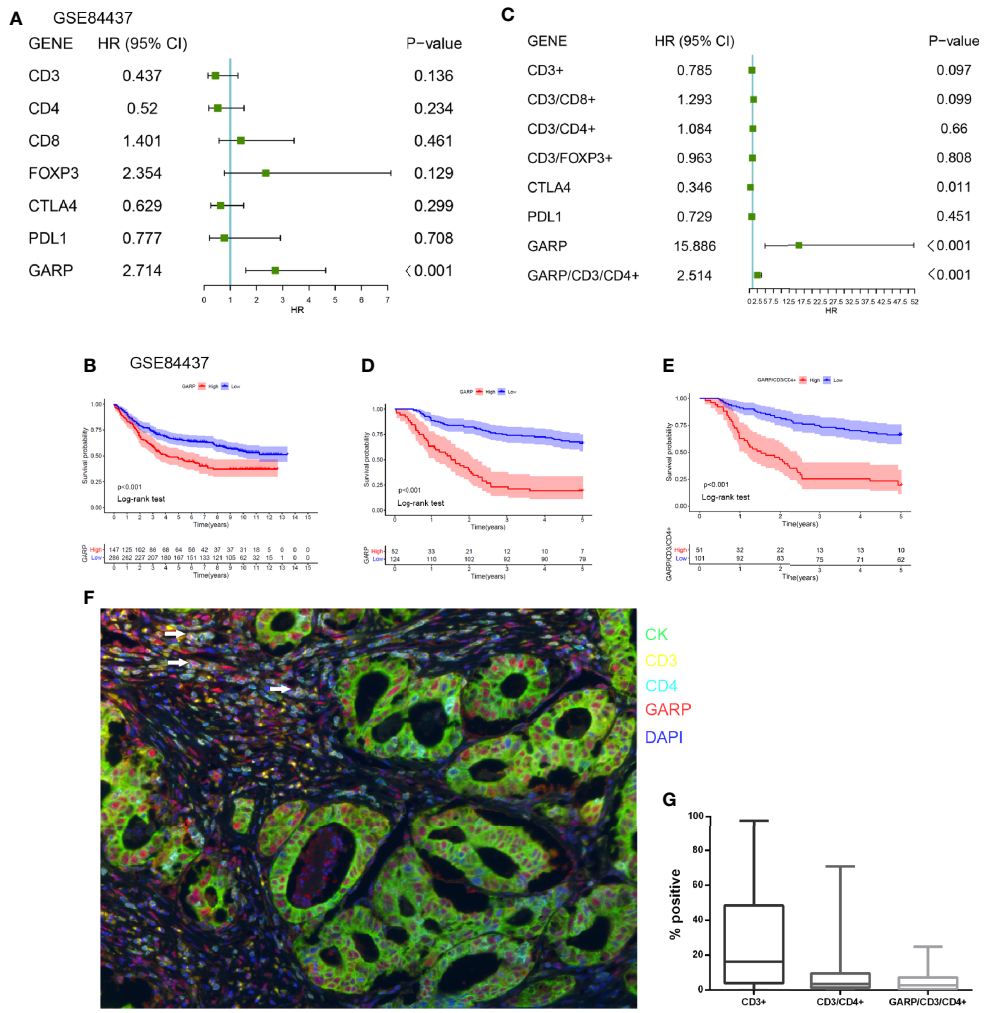

FIGURE 4 | **(A)** A forest plot visualizing the impact of the immune microenvironment (TME)-associated signatures and GARP on overall survival (OS) in the GSE84437, as evaluated using Cox univariate tests. **(B)** Kaplan–Meier curve for the high and low expression groups in the GSE84437. **(C)** A forest plot visualizing the impact of the immune microenvironment (TME)-associated signatures and GARP on overall survival (OS) in our cohort, as evaluated using Cox univariate tests. **(D)** Kaplan–Meier curve for the high and low expression groups in our cohort. **(E)** Kaplan-Meier plot visualizing survival associations of GARP+CD4+ T cell. The optimal cutoff point was obtained from X-tile 3.6.1 software. **(F)** Representative fluorescence-based multiplex immunohistochemistry images of the rate of positivity for GARP+CD4+ T cell in tissue microarray sections. **(G)** A plot shows the rate of positivity for CD3+ T cell, CD4+ T cell, and GARP+ CD4+ T cell. White arrows in the picture that point to the GARP+CD4+ cells.

NOM P < 0.05). Specifically, the following pathways were significantly enriched in the high expression phenotype: ECM-receptor interaction, GAP junction, leukocyte transendothelial migration, the JAK-STAT signaling pathway, the MAPK signaling pathway, pathways in cancer, the TGF-β signaling pathway, the Toll-like receptor signaling pathway, the intestinal immune network for IgA production, and natural killer cell-mediated cytotoxicity (**Figure 6K**).

DISCUSSION

The genome resources of the public database provide a unique platform for us to further explore the molecular characteristics of different cancers (24). Our research explored the relationship between GARP and the immune microenvironment of gastric cancer based on TCGA and GEO data. The success of cancer immunotherapy has revealed that immune cells, especially T cells, can be helpful in eliminating tumor cells (26). Wang Yu Cai et al. revealed that evaluating the TME components can predict survival time and provide a new idea for the immunotherapeutic approach of gastric cancer (GC) (27). Compared with a low density of T cells, a higher density of T cells in the TME can better predict the prognosis of gastric cancer (28, 29). Salem et al. demonstrated that GARP restrains antitumor immunity by adjusting the function of Tregs in colorectal cancer (30). our analysis illustrated that the significant connection between GARP and TME was still worth exploring.

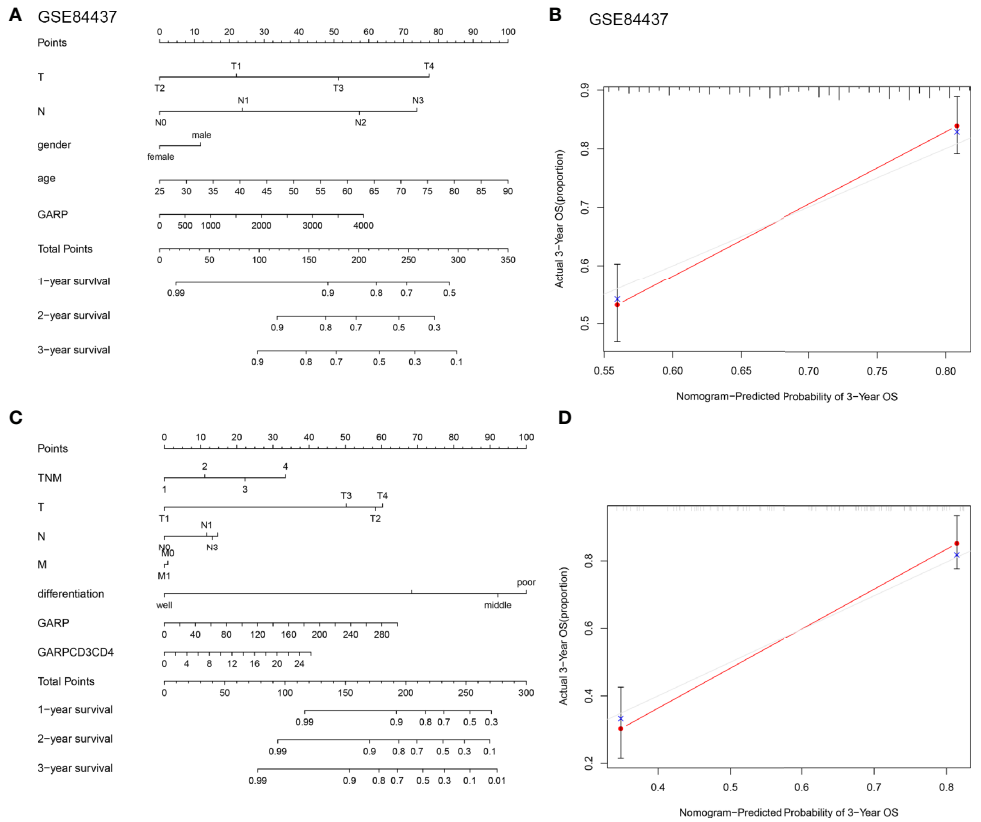

FIGURE 5 | **(A, C)** Nomograms were constructed with the GSE84437 and our research cohort for predicting the probability of 1-year, 3-year, and 5-year overall survival for GC patients. **(B, D)** Calibration plots of the nomograms for predicting the probability of overall survival at 3 years in the GSE84437 and our research cohort. The grey line represents the ideal nomogram, and the red line represents the observed nomogram.

T helper cells, cytotoxic T cells, and Tregs are associated with T cell-mediated immune responses in the TME (31). Bioinformatic analysis illustrated that GARP expression was relevant to the immune groups of gastric cancer. In the colon cancer model, the loss of GARP in Treg leads to spontaneous inflammation and enteritis with high activation of CD4+ and CD8+ T cell, which has an important impact on immune surveillance (30). Our research illustrated GARP expression correlated with FOXP3+ Treg and CD4+ T cell infiltration and CTLA-4, and PD-L1 expression, whereas GARP expression had no remarkable connection with CD8+ T cell infiltration. Lucas et al. reported that the enhancement of this combination therapy did not depend on increasing the number of CD8+ T cells (7). Our study undoubtedly provided evidence for this result and also raised a question, specifically whether the antineoplastic effect of GARP affects the infiltration of CD4 + T cells. Despite the high expression of T cell markers indicate the improvement of progress in many cancers, no statistically significant correlation was observed in gastric cancer (24). A recent report has shown that T cells expressing immune checkpoints such as LAG3, PD1 may represent exhausted T-cell (32). In our analysis, the levels of CD4+ T cell and FOXP3+ Treg infiltration were significantly higher in patients with T3 gastric cancer than patients with T1 and T2 gastric cancer. We further found the expression of GARP in CD4+ T cells and analyzed that GARP+CD4+ T cells play a significant role in the prognosis of gastric cancer. The nomogram also showed that GARP+CD4+ T cell can predict the survival rate of GC patients together with other clinicopathological parameters. CD4 positive cells are likely to annotate as Tregs, dendritic cells, macrophages, or NK cells (27, 33). GARP may identify a special subgroup of T cells related to inferior prognosis. The variations in the phenotype of tumor-infiltrating immune cells and their relationship with prognosis highlight the clinical significance of the crosstalk between tumor cells and TME (34). However, more efforts are needed to determine whether T cell dysfunction is associated with GARP expression and poor prognosis of GC patients.

By analyzing the STRING database and our study, we also found an interaction between GARP, PD-L1 and, CTLA-4 expression. Researches have also found a significant correlation between PD-1+PD-L1+ T cells and Tregs. In animal experiments, combined therapy targeting GARP and PD-1 has achieved positive results (7, 35). A recent report suggests that combining checkpoint inhibitors with chimeric antigen receptor T-cells may also be of great significance in the treatment of cancer (27). GARP upregulation was related to the TGF-β signaling pathway.

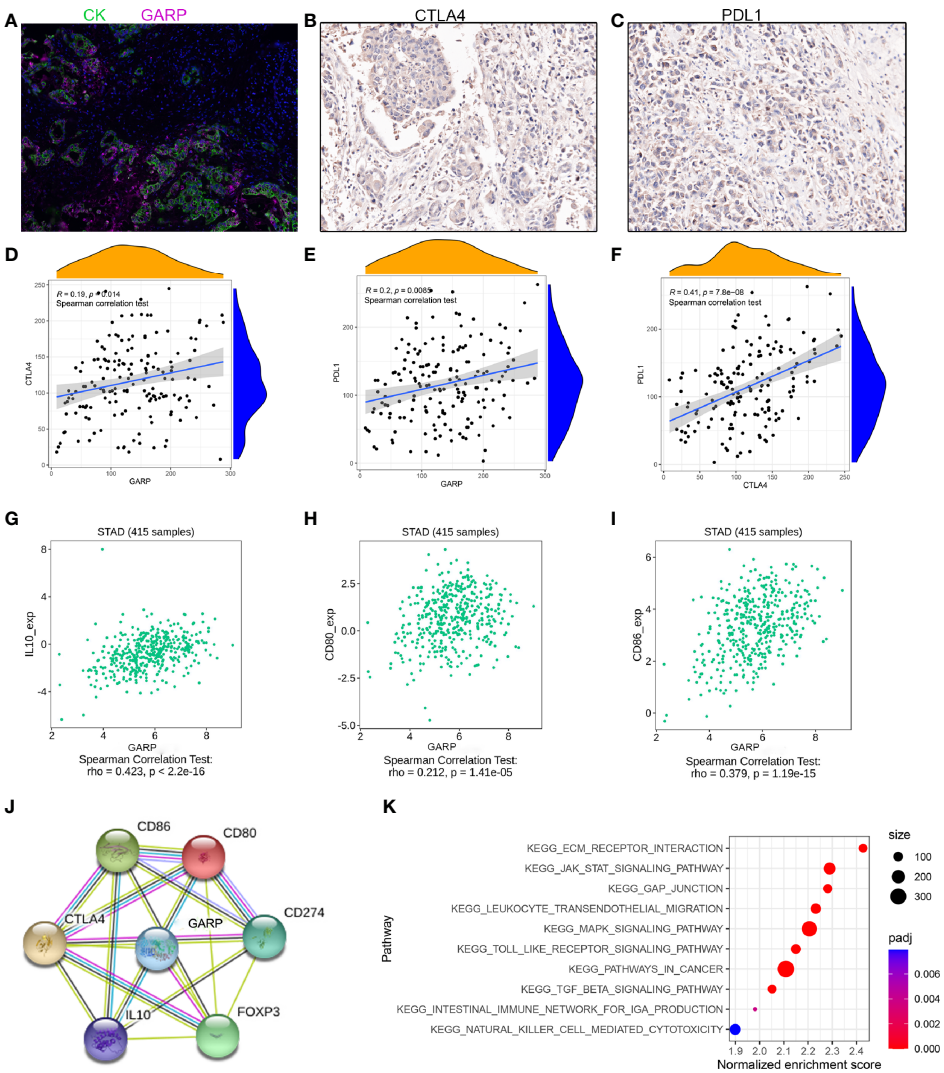

FIGURE 6 | **(A–C)** Representative images of GARP, PD-L1, and CTLA-4 staining in tissue microarray sections of tumor tissues. **(D–F)** The relationships between GARP and PD-L1 expression, GARP and CTLA-4 expression, and PD-L1 and CTLA-4 expression. **(G–I)** GARP expression was correlated with CD80, CD86, and IL-10 expression in the TISIDB database. **(J)** Protein interaction network in the STRING online database. CD274: PD-L1. **(K)** KEGG pathway analysis revealed 10 positively correlated pathways.

Evidence of TGF-β signaling in T cells has been found in melanoma specimens infiltrated by GARP-expressing T cells, indicating that inhibiting the activity of Treg-derived TGF-β1 using anti-GARP: TGF-β1 mAbs may effectively enhance CD8+ T cell-mediated antitumor immunity (7). Our study illustrated that the TGF-β signaling pathway was differentially enriched in the GARP high expression phenotype. Whether GARP affects the immune microenvironment of gastric cancer through the TGF-β signaling pathway is worthy of further exploration.

This study had several limitations. For example, the number of samples was limited, thus limiting the strength of our conclusions. In addition, we have not yet identified the regulatory pathway connecting GARP expression and CD4+ T cell, nor have we confirmed whether there are interactions among GARP, CTLA-4, and PD-L1. The combination of anti-GARP: TGF-β mAbs and PD-1 inhibitors can significantly enhance the effector ability of tumor T cells (36–38). Although remarkable progress has been made in cancer treatment by blocking CTLA-4 or PD-1 pathway with mAbs, most patients do not respond to therapy because of T cell-mediated primitive or acquired immune resistance to anti-tumor drugs (8, 39, 40). Combining checkpoint inhibitors with chimeric antigen receptor T-cell may also be of great significance in the treatment of cancer.

Taken together, our study proved that GARP is an independent influencing factor that is significantly upregulated in gastric cancer. We underlined the relationship between GARP and tumor-infiltrating T-cell. The phenotype of tumor-infiltrating immune cells was clinically meaningful, thereby

providing a new idea for the immunotherapeutic approach of gastric cancer (30, 41).

DATA AVAILABILITY STATEMENT

The datasets presented in this study can be found in online repositories. The names of the repository/repositories and accession number(s) can be found in the article/**Supplementary Material**.

AUTHOR CONTRIBUTIONS

Conceptualization, JH. Data acquisition, SJ, YZ, XZ, BL, and PS. Formal analysis, SJ and YZ. Funding acquisition, JH. Methodology, XD and QW. Supervision, XZ. Validation, BL and PS. Visualization, SJ. Writing – original draft, SJ and YZ. Writing – review & editing, SJ. All authors contributed to the article and approved the submitted version.

FUNDING

This work was supported by the National Natural Science Foundation of China (81874067), Jiangsu Provincial Department of Science and Technology (EB2018673), and the Scientific Research Project of Jiangsu Provincial Health Commission (H2017052).

ACKNOWLEDGMENTS

We sincerely appreciate all lab members.

SUPPLEMENTARY MATERIAL

The Supplementary Material for this article can be found online at: https://www.frontiersin.org/articles/10.3389/fimmu.2021.660397/full#supplementary-material

REFERENCES

1. Van Cutsem E, Sagaert X, Topal B, Haustermans K, Prenen H. Gastric Cancer. *Lancet* (2016) 388(10060):2654–64. doi: 10.1016/S0140-6736(16)30354-3
2. Shah MA, Ajani JA. Gastric Cancer–An Enigmatic and Heterogeneous Disease. *JAMA* (2010) 303(17):1753–4. doi: 10.1001/jama.2010.553
3. Kong R, Zhang EB, Yin DD, You LH, Xu TP, Chen WM, et al. Long Noncoding RNA PVT1 Indicates a Poor Prognosis of Gastric Cancer and Promotes Cell Proliferation Through Epigenetically Regulating P15 and P16. *Mol Cancer* (2015) 14:82. doi: 10.1186/s12943-015-0355-8
4. Jin Z, Jiang W, Wang L. Biomarkers for Gastric Cancer: Progression in Early Diagnosis and Prognosis (Review). *Oncol Lett* (2015) 9(4):1502–8. doi: 10.3892/ol.2015.2959
5. Fridman WH, Pagès F, Sautès-Fridman C, Galon J. The Immune Contexture in Human Tumours: Impact on Clinical Outcome. *Nat Rev Cancer* (2012) 12(4):298–306. doi: 10.1038/nrc3245
6. Ma Y, Pitt JM, Li Q, Yang H. The Renaissance of Anti-Neoplastic Immunity From Tumor Cell Demise. *Immunol Rev* (2017) 280(1):194–206. doi: 10.1111/imr.12586
7. de Streel G, Bertrand C, Chalon N, Liénart S, Bricard O, Lecomte S, et al. Selective Inhibition of TGF-β1 Produced by GARP-Expressing Tregs Overcomes Resistance to PD-1/PD-L1 Blockade in Cancer. *Nat Commun* (2020) 11(1):4545. doi: 10.1038/s41467-020-17811-3
8. Ribas A, Wolchok JD. Cancer Immunotherapy Using Checkpoint Blockade. *Science* (2018) 359(6382):1350–5. doi: 10.1126/science.aar4060
9. Zhang Y, Zhang Z. The History and Advances in Cancer Immunotherapy: Understanding the Characteristics of Tumor-Infiltrating Immune Cells and Their Therapeutic Implications. *Cell Mol Immunol* (2020) 17(8):807–21. doi: 10.1038/s41423-020-0488-6
10. Yang H, Yamazaki T, Pietrocola F, Zhou H, Zitvogel L, Ma Y, et al. Improvement of Immunogenic Chemotherapy by STAT3 Inhibition. *Oncoimmunology* (2016) 5(2):e1078061. doi: 10.1080/2162402X.2015.1078061
11. Batlle E, Massagué J. Transforming Growth Factor-β Signaling in Immunity and Cancer. *Immunity* (2019) 50(4):924–40. doi: 10.1016/j.immuni.2019.03.024
12. Stockis J, Dedobbeleer O, Lucas S. Role of GARP in the Activation of Latent TGF-β1. *Mol Biosyst* (2017) 13(10):1925–35. doi: 10.1039/C7MB00251C
13. Edwards JP, Thornton AM, Shevach EM. Release of Active TGF-β1 From the Latent TGF-β1/GARP Complex on T Regulatory Cells Is Mediated by Integrin β8. *J Immunol* (2014) 193(6):2843–9. doi: 10.4049/jimmunol.1401102
14. Stockis J, Liénart S, Colau D, Collignon A, Nishimura SL, Sheppard D, et al. Blocking Immunosuppression by Human Tregs In Vivo With Antibodies Targeting Integrin αvβ8. *Proc Natl Acad Sci USA* (2017) 114(47):E10161–8. doi: 10.1073/pnas.1710680114
15. Metelli A, Salem M, Wallace CH, Wu BX, Li A, Li X, et al. Immunoregulatory Functions and the Therapeutic Implications of GARP-TGF-Beta in Inflammation and Cancer. *J Hematol Oncol* (2018) 11(1):24. doi: 10.1186/s13045-018-0570-z
16. Wang R, Kozhaya L, Mercer F, Khaitan A, Fujii H, Unutmaz D, et al. Expression of GARP Selectively Identifies Activated Human FOXP3+ Regulatory T Cells. *Proc Natl Acad Sci USA* (2009) 106(32):13439–44. doi: 10.1073/pnas.0901965106
17. Wallace CH, Wu BX, Salem M, Ansa-Addo EA, Metelli A, Sun S, et al. B Lymphocytes Confer Immune Tolerance via Cell Surface GARP-TGF-β Complex. *JCI Insight* (2018) 3(7):e99863. doi: 10.1172/jci.insight.99863
18. Metelli A, Wu BX, Fugle CW, Rachidi S, Sun S, Zhang Y, et al. Surface Expression of Tgfβ Docking Receptor GARP Promotes Oncogenesis and Immune Tolerance in Breast Cancer. *Cancer Res* (2016) 76(24):7106–17. doi: 10.1158/0008-5472.CAN-16-1456
19. Ru B, Wong CN, Tong Y, Zhong JY, Zhong SSW, Wu WC, et al. TISIDB: An Integrated Repository Portal for Tumor-Immune System Interactions. *Bioinformatics* (2019) 35(20):4200–2. doi: 10.1093/bioinformatics/btz210
20. Chen B, Khodadoust MS, Liu CL, Newman AM, Alizadeh AA. Profiling Tumor Infiltrating Immune Cells With CIBERSORT. *Methods Mol Biol* (2018) 1711:243–59. doi: 10.1007/978-1-4939-7493-1_12
21. Subramanian A, Tamayo P, Mootha VK, Mukherjee S, Ebert BL, Gillette MA, et al. Gene Set Enrichment Analysis: A Knowledge-Based Approach for Interpreting Genome-Wide Expression Profiles. *Proc Natl Acad Sci USA* (2005) 102(43):15545–50. doi: 10.1073/pnas.0506580102
22. von Mering C, Huynen M, Jaeggi D, Schmidt S, Bork P, Snel B, et al. STRING: A Database of Predicted Functional Associations Between Proteins. *Nucleic Acids Res* (2003) 31(1):258–61. doi: 10.1093/nar/gkg034
23. Zhang X, Shi M, Chen T, Zhang B. Characterization of the Immune Cell Infiltration Landscape in Head and Neck Squamous Cell Carcinoma to Aid Immunotherapy. *Mol Ther Nucleic Acids* (2020) 22:298–309. doi: 10.1016/j.omtn.2020.08.030
24. Fakih M, Ouyang M, Wang C, Tu C, Gozo TY, Cho MC, et al. Immune Overdrive Signature in Colorectal Tumor Subset Predicts Poor Clinical Outcome. *J Clin Invest* (2019) 129(10):4464–76. doi: 10.1172/JCI127046
25. Bertolini TB, Biswas M, Terhorst C, Daniell H, Herzog RW, Piñeros AR, et al. Role of Orally Induced Regulatory T Cells in Immunotherapy and Tolerance. *Cell Immunol* (2021) 359:104251. doi: 10.1016/j.cellimm.2020.104251
26. Darvin P, Toor SM, Sasidharan Nair V, Elkord E. Immune Checkpoint Inhibitors: Recent Progress and Potential Biomarkers. *Exp Mol Med* (2018) 50(12):1–11. doi: 10.1038/s12276-018-0191-1

27. Autio M, Leivonen SK, Bruck O, Mustjoki S, Jorgensen JM, Karjalainen-Lindsberg ML, et al. Immune Cell Constitution in the Tumor Microenvironment Predicts the Outcome in Diffuse Large B-Cell Lymphoma. *Haematologica* (2020) 106(3):718–29. doi: 10.3324/haematol.2019.243626
28. Cai WY, Dong ZN, Fu XT, Lin LY, Wang L, Ye GD, et al. Identification of a Tumor Microenvironment-Relevant Gene Set-Based Prognostic Signature and Related Therapy Targets in Gastric Cancer. *Theranostics* (2020) 10 (19):8633–47. doi: 10.7150/thno.47938
29. Kim JW, Nam KH, Ahn SH, Park DJ, Kim HH, Kim SH, et al. Prognostic Implications of Immunosuppressive Protein Expression in Tumors as Well as Immune Cell Infiltration Within the Tumor Microenvironment in Gastric Cancer. *Gastric Cancer* (2016) 19(1):42–52. doi: 10.1007/s10120-014-0440-5
30. Salem M, Wallace C, Velegraki M, Li A, Ansa-Addo E, Metelli A, et al. GARP Dampens Cancer Immunity by Sustaining Function and Accumulation of Regulatory T Cells in the Colon. *Cancer Res* (2019) 79(6):1178–90. doi: 10.1158/0008-5472.CAN-18-2623
31. Ostroumov D, Fekete-Drimusz N, Saborowski M, Kühnel F, Woller N. CD4 and CD8 T Lymphocyte Interplay in Controlling Tumor Growth. *Cell Mol Life Sci* (2018) 75(4):689–713. doi: 10.1007/s00018-017-2686-7
32. Xiong H, Mittman S, Rodriguez R, Pacheco-Sanchez P, Moskalenko M, Yang Y, et al. Coexpression of Inhibitory Receptors Enriches for Activated and Functional CD8(+) T Cells in Murine Syngeneic Tumor Models. *Cancer Immunol Res* (2019) 7(6):963–76. doi: 10.1158/2326-6066.CIR-18-0750
33. O'Doherty U, Steinman RM, Peng M, Cameron PU, Gezelter S, Kopeloff I, et al. Dendritic Cells Freshly Isolated From Human Blood Express CD4 and Mature Into Typical Immunostimulatory Dendritic Cells After Culture in Monocyte-Conditioned Medium. *J Exp Med* (1993) 178(3):1067–76. doi: 10.1084/jem.178.3.1067
34. Zeng D, Li M, Zhou R, Zhang J, Sun H, Shi M, et al. Tumor Microenvironment Characterization in Gastric Cancer Identifies Prognostic and Immunotherapeutically Relevant Gene Signatures. *Cancer Immunol Res* (2019) 7(5):737–50. doi: 10.1158/2326-6066.CIR-18-0436
35. Cuende J, Liénart S, Dedobbeleer O, van der Woning B, De Boeck G, Stockis J, et al. Monoclonal Antibodies Against GARP/TGF-β1 Complexes Inhibit the Immunosuppressive Activity of Human Regulatory T Cells In Vivo. *Sci Transl Med* (2015) 7(284):284ra56. doi: 10.1126/scitranslmed.aaa1983
36. Hui E, Cheung J, Zhu J, Su X, Taylor MJ, Wallweber HA, et al. T Cell Costimulatory Receptor CD28 is a Primary Target for PD-1-Mediated Inhibition. *Science* (2017) 355(6332):1428–33. doi: 10.1126/science.aaf1292
37. Arasanz H, Gato-Cañas M, Zuazo M, Ibañez-Vea M, Breckpot K, Kochan G, et al. PD1 Signal Transduction Pathways in T Cells. *Oncotarget* (2017) 8 (31):51936–45. doi: 10.18632/oncotarget.17232
38. Dahan R, Sega E, Engelhardt J, Selby M, Korman AJ, Ravetch JV, et al. Fcγrs Modulate the Anti-Tumor Activity of Antibodies Targeting the PD-1/PD-L1 Axis. *Cancer Cell* (2015) 28(3):285–95. doi: 10.1016/j.ccell.2015.08.004
39. Zaretsky JM, Garcia-Diaz A, Shin DS, Escuin-Ordinas H, Hugo W, Hu-Lieskovan S, et al. Mutations Associated With Acquired Resistance to PD-1 Blockade in Melanoma. *N Engl J Med* (2016) 375(9):819–29. doi: 10.1056/NEJMoa1604958
40. Yang H, Xia L, Chen J, Zhang S, Martin V, Li Q, et al. Stress-Glucocorticoid-TSC22D3 Axis Compromises Therapy-Induced Antitumor Immunity. *Nat Med* (2019) 25(9):1428–41. doi: 10.1038/s41591-019-0566-4
41. Rachidi S, Metelli A, Riesenberg B, Wu BX, Nelson MH, Wallace C, et al. Platelets Subvert T Cell Immunity Against Cancer *via* GARP-Tgfβ Axis. *Sci Immunol* (2017) 2(11):eaai7911. doi: 10.1126/sciimmunol.aai7911

Conflict of Interest: The authors declare that the research was conducted in the absence of any commercial or financial relationships that could be construed as a potential conflict of interest.

Publisher's Note: All claims expressed in this article are solely those of the authors and do not necessarily represent those of their affiliated organizations, or those of the publisher, the editors and the reviewers. Any product that may be evaluated in this article, or claim that may be made by its manufacturer, is not guaranteed or endorsed by the publisher.

Copyright © 2021 Jiang, Zhang, Zhang, Lu, Sun, Wu, Ding and Huang. This is an open-access article distributed under the terms of the Creative Commons Attribution License (CC BY). The use, distribution or reproduction in other forums is permitted, provided the original author(s) and the copyright owner(s) are credited and that the original publication in this journal is cited, in accordance with accepted academic practice. No use, distribution or reproduction is permitted which does not comply with these terms.

frontiers in Immunology

ORIGINAL RESEARCH
published: 24 August 2021
doi: 10.3389/fimmu.2021.723566

Tumor Infiltrating Lymphocytes Target HLA-I Phosphopeptides Derived From Cancer Signaling in Colorectal Cancer

Sarah A. Penny[1], Jennifer G. Abelin[2], Stacy A. Malaker[2†], Paisley T. Myers[2], Abu Z. Saeed[1], Lora G. Steadman[1], Dina L. Bai[2], Stephen T. Ward[1,3], Jeffrey Shabanowitz[2], Donald F. Hunt[2,4] and Mark Cobbold[1,5†]*

[1] School of Immunity and Infection, University of Birmingham, Birmingham, United Kingdom, [2] Department of Chemistry, University of Virginia, Charlottesville, VA, United States, [3] Department of Colorectal Surgery, Queen Elizabeth Hospital, Birmingham, United Kingdom, [4] Department of Pathology, University of Virginia, Charlottesville, VA, United States, [5] Center for Cancer Immunology, Massachusetts General Hospital, Charlestown, MA, United States

OPEN ACCESS

Edited by:
Luis Alvarez-Vallina,
Aarhus University, Denmark

Reviewed by:
Robert Hawkins,
Victoria University of Manchester, United Kingdom
Anaïs Jiménez-Reinoso,
Research Institute Hospital 12 de Octubre, Spain

***Correspondence:**
Sarah A. Penny
s.a.penny@bham.ac.uk

†Present address:
Stacy A. Malaker,
Department of Chemistry, Yale University, New Haven, CT, United States;
Mark Cobbold,
AstraZeneca, Gaithersburg, MD, United States

Specialty section:
This article was submitted to Cancer Immunity and Immunotherapy, a section of the journal Frontiers in Immunology

Received: 10 June 2021
Accepted: 27 July 2021
Published: 24 August 2021

Citation:
Penny SA, Abelin JG, Malaker SA, Myers PT, Saeed AZ, Steadman LG, Bai DL, Ward ST, Shabanowitz J, Hunt DF and Cobbold M (2021) Tumor Infiltrating Lymphocytes Target HLA-I Phosphopeptides Derived From Cancer Signaling in Colorectal Cancer. Front. Immunol. 12:723566. doi: 10.3389/fimmu.2021.723566

There is a pressing need for novel immunotherapeutic targets in colorectal cancer (CRC). Cytotoxic T cell infiltration is well established as a key prognostic indicator in CRC, and it is known that these tumor infiltrating lymphocytes (TILs) target and kill tumor cells. However, the specific antigens that drive these CD8+ T cell responses have not been well characterized. Recently, phosphopeptides have emerged as strong candidates for tumor-specific antigens, as dysregulated signaling in cancer leads to increased and aberrant protein phosphorylation. Here, we identify 120 HLA-I phosphopeptides from primary CRC tumors, CRC liver metastases and CRC cell lines using mass spectrometry and assess the tumor-resident immunity against these posttranslationally modified tumor antigens. Several CRC tumor-specific phosphopeptides were presented by multiple patients' tumors in our cohort (21% to 40%), and many have previously been identified on other malignancies (58% of HLA-A*02 CRC phosphopeptides). These shared antigens derived from mitogenic signaling pathways, including p53, Wnt and MAPK, and are therefore markers of malignancy. The identification of public tumor antigens will allow for the development of broadly applicable targeted therapeutics. Through analysis of TIL cytokine responses to these phosphopeptides, we have established that they are already playing a key role in tumor-resident immunity. Multifunctional CD8+ TILs from primary and metastatic tumors recognized the HLA-I phosphopeptides presented by their originating tumor. Furthermore, TILs taken from other CRC patients' tumors targeted two of these phosphopeptides. In another cohort of CRC patients, the same HLA-I phosphopeptides induced higher peripheral T cell responses than they did in healthy donors, suggesting that these immune responses are specifically activated in CRC patients. Collectively, these results establish HLA-I phosphopeptides as targets of the tumor-resident immunity in CRC, and highlight their potential as candidates for future immunotherapeutic strategies.

Keywords: Immunopeptidomics, HLA-I phosphopeptides, tumor antigens, TIL (tumor infiltrating lymphocytes), CRC (colorectal cancer), signaling pathway

INTRODUCTION

Tumor infiltration by effector T cells has been confirmed by several large studies to be significantly associated with good prognosis in CRC, even in metastatic disease (1–5). Cytotoxic T cells recognize antigenic peptides presented by HLA-I complexes on the surface of cancer cells. These T cells release cytotoxic factors, which kill the transformed cells and thus can control tumor growth. However, the targets of CD8+ T cells are not yet well defined in CRC (6).

The use of immunotherapies, such as immune checkpoint blockade (ICB), is revolutionizing cancer treatment, but their use has been limited in the majority (86%) of CRC, which are microsatellite stable (MSS) (7). The remaining 14% of tumors that may respond to ICB therapies, have a defect in DNA mismatch repair, leading to microsatellite instability (MSI) and thus a high tumor mutational burden (TMB) (8, 9). Irrespective of therapy, MSI is predictive of favorable outcomes in CRC, associated with the extensive cytotoxic T cell infiltration into these tumors (9, 10); however, once the tumor has evaded T cell recognition and recurrence occurs, prognosis is poor (7). Preclinical studies have demonstrated that PD-1 blockade is only effective in the presence of fully primed and committed antigen-specific T cells (11). Therefore, it has been proposed that the T cells infiltrating MSI CRC are targeting the mutational neoantigens that arise from the high TMB in these tumors (12, 13). TMB does show a strong correlation with ICB-response (14, 15), yet it has proven controversial and challenging to implement as a response biomarker in clinical practice (16). Moreover, cytotoxic T cell infiltration has also been shown to be a significant predictor of prognosis in MSS CRC, even though these usually have a low to moderate TMB (9). Whilst some TILs may target mutational neoantigens in MSS CRC, it seems unlikely that T cell targeting of these limited antigens could fully explain the control of tumor growth in CRC; consequently, other classes of tumor antigens are almost certainly implicated (6).

Mutations in the Wnt, TGF-β and RAS signaling pathways are ubiquitous in CRC, often affecting critical kinases and phosphatases (17). Deregulation of these kinases can lead to the activation of several signaling cascades and increase the extent of protein phosphorylation within tumor cells (18). Therefore, we hypothesized that the infiltrating cytotoxic T cells in CRC may be targeting, not only mutated peptides, but also the phosphorylated peptides resulting from this dysregulated signaling. Phosphorylated peptides have already been defined as strong candidates for tumor-specific antigens in melanoma, renal cell carcinoma and hematological malignancies (19–21). Phosphorylation is preserved on peptides through antigen processing and presentation pathways (22), and can produce T cell epitopes that differ structurally from their unphosphorylated counterparts (23, 24). In some instances, this has been shown to be due to phosphorylation-induced conformational alterations in the peptide, facilitated by novel contacts with the HLA complex (23, 25). Yet, even when these conformational alterations are minimal, T cell receptor (TCR) recognition can be specific to the phosphorylated peptide form (23). These data suggest that phosphopeptide specific T cells may not be deleted by central tolerance in the same way as those targeting other non-mutational tumor-associated antigens (26). Phosphopeptide antigens also provide an advantage as potential immunotherapeutic targets because they are often shared across patients (19). We hypothesized that CRC-specific phosphopeptides may represent a subset of posttranslationally modified (PTM) tumor antigens targeted by the tumor-resident CD8 T cell response in CRC.

Previous efforts in defining the CRC immunopeptidome have focused on mutational neoantigens and cancer germline antigens (6). To identify putative PTM tumor associated antigens, we used CRC cell lines, primary CRC tumors and CRC liver metastases. From these we purified HLA-I peptides, enriched for phosphopeptides and then sequenced these using mass spectrometry (MS). We evaluated the responses of TILs taken from the same tumors that were used for phosphopeptide identification, and then broadened this to determine if the immunogenic phosphopeptides may represent public T cell targets in CRC. In addition, peripheral T cell responses targeting CRC phosphopeptides were compared between patients and healthy donors. Finally, the functional capacity of the TILs targeting phosphopeptides was assessed in killing assays. We hope that identifying these PTM tumor antigens, and understanding their role in tumor immunity, may support the development of future targeted tumor immunotherapies.

MATERIALS AND METHODS

Patient and Healthy Donor Samples and Cell Lines

Tumor and blood samples were obtained fresh from University Hospital Birmingham. Samples were received from the Human Biomaterials Resource Centre (HBRC) at the University of Birmingham (Ref 09/H1010/75) and *via* studies approved by research ethics committees local to the University of Birmingham (Ref: 06/Q2702/61 and 09/H1203/49). Informed written consent was obtained in accordance with the Declaration of Helsinki, in all cases. Fresh blood samples were collected from patients and healthy donors. 20-30 mL of blood was collected in vacutainers containing lithium heparin (BD, UK). CRC cell lines were grown up from laboratory stocks, originating from the European Collection of Cell Cultures and the American Type Culture Collection. All cells were stored in fetal bovine serum (FBS) with 10% DMSO at -80°C. The cells were managed in sterile conditions in a laminar airflow hood, at all times, and incubated at 37°C with 5% CO_2. Cell lines were grown in D-MEM (Dulbecco's Modified Eagle Medium (1X) liquid (High Glucose), 10% FBS, 1% penicillin/streptomycin) and the cells were grown in 25 cm^2, 75 cm^2, 175 cm^2 and 1720 cm^2 vented tissue culture flasks, with 20 mM HEPES buffer added. The cells were observed using a phase contrast microscope. Cell counts and viability were determined by the exclusion of Trypan blue dye by light microscopy. Mycoplasma infection was excluded in all cell lines, using the Lonza MycoAlert Mycoplasma Kit (Lonza, ME, USA).

TIL Isolation and Expansion

In a laminar flow hood, the tumor was sliced into small (2 mm x 2 mm) chunks and each one placed into 2 mL T cell medium, containing extra antibiotics to eliminate gut bacteria and yeast (AIM-V/10% Human serum/25 mM HEPES/6000 IU/mL IL-2/50 μg/mL neomycin/2 μg/mL micofungin/55 μM β-mercaptoethanol/15 μg/mL metronidazole/20 μg/mL vancomycin). The TILs were maintained at $1x10^6$ cells/mL in T cell medium in a 24-well plate for 14-21 days. The cells were subsequently FACS analyzed to determine the proportion of CD8+ TILs and aliquots frozen.

TILs were rapidly expanded using a standard rapid expansion protocol (REP), as described by Dudley and colleagues (27). Briefly, $1x10^6$ thawed TILs were added to REP medium ($2x10^8$ irradiated PBMCs/30 ng/mL OKT3/6000 IU/mL IL-2/50 mL RPMI 10% HS/50 mL AIM-V/50 μg/mL neomycin/2 μg/mL micofungin/55 μM β-mercaptoethanol/25 mM HEPES). Half of the medium was exchanged on day 5. On day 7 the TILs were counted and their density reduced to 0.5 million/mL. Cells were maintained at 0.5 million/mL until day 14 when aliquots of up to 30 million TILs were frozen.

Isolation of HLA-Associated Peptides

HLA class I molecules were immunoaffinity purified from samples, and their associated peptides were extracted as described previously (22, 28). Briefly, $1x10^9$ cells, or 1 g of tissue were lysed in 10 mL of 20 mM Tris-HCl pH 8.0/150 mM NaCl with 1% 3-[(3-cholamidopropyl) dimethylammonio]-1-propane sulfonate (CHAPS)/1 mM PMSF/5 μg/mL aprotinin/10 μg/mL leupeptin/10 μg/mL pepstatin A/and phosphatase inhibitor cocktails II and III (Sigma-Aldrich, UK) at 4°C. Tissues were homogenized, on ice. The lysate was subject to ultra-centrifugation at 100,000 *x g*, for 1 hour, at 4°C (Optima LE-8K (Ti70 rotor), Beckman-Coulter, UK). Supernatants were incubated overnight with W6/32 antibody-bound NHS sepharose beads, specific for HLA class I molecules (Amersham Pharmacia Biotech). The beads then underwent a series of washes in lysis buffer, TBS (20mM Tris-HCl/150 mM NaCl pH 8), TBS2 (20 mM Tris-HCl/1 M NaCl pH 8), and 20 mM Tris-HCl pH 8. Peptides were eluted from the MHC class I molecules with 10% acetic acid and isolated by ultrafiltration (Ultrafree-MC, Millipore).

HLA-I Phosphopeptide Enrichment by IMAC

As previously described (29), samples were initially passed through C18 microcapillary cleanup-columns to desalt, internal standards were added and the samples dehydrated. Prior to phosphopeptide enrichment using Fe^{+3}-immobilized metal affinity chromatography (IMAC), peptides were esterified to neutralize acidic groups on the peptides and prevent non-specific binding (29). IMAC columns, created in-house, as described previously (29), were used to enrich for phosphopeptides. These were eluted directly onto a C18 precolumn, and transferred to an analytical column containing irregular C18 packing material equipped with an electrospray emitter tip. Two further internal standard peptides, were loaded prior to analysis.

HPLC-ESI-MS/MS Analysis of IMAC Enriched Phosphopeptides

Enriched phosphopeptides were gradient eluted through an electrospray tip directly into a Thermo Scientific LTQ-FT-ion cyclotron resonance mass spectrometer equipped with an Agilent 1100 series binary HPLC. Mass spectra were acquired in the high-resolution Fourier transform mass analyzer, and the tandem MS spectra were acquired in the linear ion trap of the LTQ-FT-ion cyclotron resonance instrument using collision-activated dissociation (CAD) and electron transfer dissociation (ETD). Detailed methods have been previously described (29).

Data analysis was performed by using the Xcalibur software (Thermo Electron Corporation). The data files were searched against the RefSeq database (downloaded June 2009) using OMSSA (version 2.1.1) (30). An in house software program called "Neutral Loss Finder" was also used to identify phosphopeptides from their neutral loss of phosphoric acid (98 Da) in MS2 CAD spectra. OMSSA and neutral loss search results were used to guide the analysis, but all peptide sequences were determined by accurate mass measurement and manual interpretation of the MS2 spectra using theoretical peptide fragment ion masses (**Supplementary Figure 1**).

HLA Typing and Epitope Prediction

HLA sequences were obtained to 2 digits from the NHS clinical facility. The MHC-I binding predictions were made on 7/22/2017 using the IEDB analysis resource Consensus tool and the 6 predetermined HLA alleles for each patient (31).

Intracellular Cytokine Staining

CD8+ T cells were extracted from frozen stocks using magnetic cell separation (Miltenyi Biotec, Germany). TIL responses were expanded over 6 days. 100,000 irradiated CD8- TILs/well in TIL medium (50% AIM-V, 40% RPMI, 10% Human serum, 100 IU/mL penicillin, 100 μg/mL streptomycin, 100 mg/mL Neomycin, 2 mg/mL Micafungin, 7.5 μg/mL metronidazole, 2000 IU/mL IL-2) were pulsed with 10 μg/mL peptide overnight. These were washed and added to 200,000 CD8+ TILs/well of a 48-well plate in TIL medium. The positive control was stimulated with 1 μg/mL PHA. On day 6 the TILs were all washed twice in AIM-V and resuspended in TIL medium containing 5 μg/mL of Brefeldin A and monensin. Each well was restimulated overnight with CD8-TILs that had been peptide pulsed for 2 hours with 10 μg/mL of the relevant peptide. They were then harvested, washed with PBS and stained with a fixable viability dye (APC-Cy7) (eBiosciences) and the surface antibodies, anti-CD3 (APC) and anti-CD8 (PerCP) (Biolegend, Cambridge, UK). The cells were then washed in MACS buffer, fixed, using 2% paraformaldehyde, washed, permeablized using 0.5% saponin, and stained with anti-IFNγ (PE), anti-IL-2 (Pacific blue) and anti-TNFα (PE-Cy5.5) (BioLegend, Cambridge, UK) for 30 minutes at room temperature. Cells were washed again with MACS buffer and lightly fixed until they could be analyzed on the BD LSR-Fortessa flow cytometer (BD, Oxford, UK).

Immunohistochemistry

Sections of formalin fixed paraffin embedded tumor were baked at 60°, deparaffinized in xylene and rehydrated in descending gradient alcohols. The Leica Bond-max was used for staining, alongside Leica antibodies (Leica, UK). Endogenous peroxidase activity was blocked by incubation with 3% hydrogen peroxide for 5 min. Mouse monoclonal anti-human antibodies (Leica, UK) were applied as per manufacturer's instructions. Sections were then incubated with HRP polymer for 8 min, washed and then developed for 10 min using diaminobenzidine (DAB) solution. The sections were counterstained in hematoxylin, dehydrated in alcohol and xylene and mounted using an automated coverslipper (Leica, Germany).

Enzyme-Linked Immunospot Assay

A cultured ELISpot was used, as previously described (19). PBMCs were cultured in AIM-V medium (Invitrogen) for 6 days with 2 ug/mL peptide at $5x10^5$/mL. The ELISpot PRO for human IFNγ kit (Mabtech, Sweden) was used for these experiments. On day 6 cells were washed and transferred in AIM-V to the pre-washed polyvinylidene difluoriden (PVDF)-backed microplates coated with a monoclonal antibody specific for human IFNγ. The cells were restimulated with the relevant peptide at 2 μg/mL, and the CD3 monoclonal antibody (100 ng/mL) added to the positive control. The microplate was incubated for overnight at 37°C. The cells were then removed and the plate treated as per manufacturer's instructions. Once dry, the spots representing individual IFNγ secreting cells were counted using an ELISpot reader (AID ELISpot Reader HR XL, Advanced Imaging Devices GmbH, Germany) and images captured using the AID ELISpot Software 4.0 (AID GmbH, Germany).

Generation of Phosphopeptide-Specific T Cell Lines

CD8+ TILs were plated at $1x10^6$/mL in TIL medium and stimulated with 10 μg/mL of the relevant peptide. On days 7 and 10 TILs were adjusted to $5x10^5$/mL and half of the medium exchanged. On day 14 phosphopeptide-specific TILs were selected, using CD137 MACS (Miltenyi biotech). Half of the cells were peptide pulsed for 2 hours, washed and added to the other half overnight. These were then rapidly expanded, and used in a killing assay on day 24.

Killing Assay

A Europium release assay was used, which produces results that are similar to the classical chromium release assay (32). Target cells were washed in the relevant medium and resuspended to 1 million cells/mL. 2.5 μL/mL of the BATDA fluorescence enhancing ligand was added and the cells incubated for 30 minutes at 37°C, 5% CO2 in a humidified environment. The cells were washed five times in excess medium. 10,000 target cells were added to each well of a V-bottomed 96-well plate. T cells at varying effector to target (E:T) ratios were added to the test wells. Lysis buffer was added to the wells for maximal release. All well volumes were made up to 200 μL. The plate was incubated for 2-5 hours in a humidified 5% CO2 atmosphere at 37°C. 20 μL of each supernatant was transferred to a flat-bottomed, white, 96-well plate and 200 μL of Europium solution was added. This was incubated for 15 minutes, shaking, at room temperature. The fluorescence was measured in a time-resolved fluorometer (Tecan Infinite 200 PRO; Tecan, Switzerland).

Statistical Analysis

Statistical analysis was performed using Graphpad Prism 5.0. EulerAPE was used to produce the Euler diagrams (33). Weblogo was used to generate the sequence logos (34).

RESULTS

Tumor-Specific HLA-I Phosphopeptides Are Presented by CRC Cell Lines and Tumors

To identify tumor-specific phosphopeptides, we compared HLA-I phosphopeptides found on healthy colon tissue to those on tumor tissue. HLA-peptide complexes were affinity purified, the HLA-bound peptides eluted, and immobilized metal affinity chromatography (IMAC) was used to enrich for phosphopeptides, which were identified using liquid chromatography with tandem mass spectrometry (LC-MS/MS) (**Figure 1** and **Supplementary Figure 1**). Three primary tumors, two liver metastases and three CRC cell lines were used to identify a total of 198 phosphopeptides, of which 120 were tumor-associated in our cohort: 74 tumor-specific (identified only on tumor), 12 tumor-associated (at least 10-fold higher amounts identified on tumor than on healthy tissue), and 34 CRC cell line-associated phosphopeptides (**Supplementary Tables 1–5**). More phosphopeptides were identified on primary tumors than neighboring healthy colon tissue – 3.1 fold more, with 73% of phosphopeptides being assigned as tumor-specific (**Figures 2A, B**). Liver metastases presented even more tumor-specific phosphopeptides – 1.5 fold the number identified on the primary CRC tumors. Many more phosphopeptides were also seen in neighboring healthy liver tissue than healthy colon tissue, so the number of phosphopeptides identified on healthy liver tissue and CRC liver metastases were comparable (**Figure 1B**).

The phosphopeptides identified were predominately nine (63%) or ten (23%) amino acids long and contained phosphoserine (92%) at position four (71%) (**Supplementary Figure 2**). These phosphopeptides were predicted to be presented by 16 different HLA alleles, but nonetheless 23% were shared across multiple patients' samples in our cohort (**Figure 2C** and **Supplementary Figure 3**; **Supplementary Tables 3–5**). This proportion increased to 40% when looking at HLA-B*07, a commonly expressed HLA allele (n=3) that presents many phosphopeptides (**Figure 2C** and **Supplementary Figure 4**). The list of CRC-associated phosphopeptides was compared with published lists of leukemia and melanoma phosphopeptides (19, 20). Many of the CRC phosphopeptides have been identified on other malignancies - 11/19 (58%) of HLA-A*02, and 19/48 (40%) of HLA-B*07 phosphopeptides, with a subset being shared across all malignancies tested (**Figure 2D** and **Supplementary Table 6**). These shared

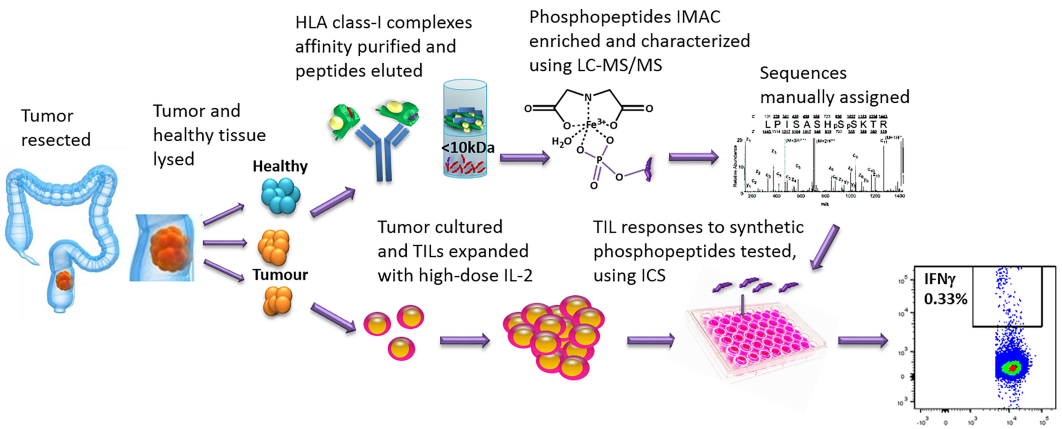

FIGURE 1 | The work-flow used to identify phosphopeptides from CRC tumors and to test TIL responses to the phosphopeptides identified. Tumor and neighboring healthy tissue samples were taken at resection. Some tumor was cultured and the TILs expanded, using high-dose IL-2. The remaining sample was homogenized in sample buffer and HLA-I complexes affinity purified with immobilized W6/32 antibody. The peptides were acid eluted, the phosphopeptides IMAC enriched and then characterized using LC-MS/MS. Synthetic phosphopeptides were used to test TIL responses to the phosphopeptides identified on the tumors using an intracellular cytokine staining assay.

epitopes may be representative of mitogenic signaling pathways shared across cancers. Therefore, we mapped the proteins to known CRC oncogenic pathways (35), and demonstrated that many of the tumor-specific HLA-I phosphopeptides derive from proteins involved in key signaling pathways, such as Wnt, MAP kinase, TGFβ and p53 (**Supplementary Figure 5**). Although we have denoted many of the phosphopeptides as tumor-specific, because we could not identify them on healthy tissue, there may be small amounts present on healthy cells that are below the limits of detection in mass spectrometry, or on other tissues that were not sampled. Regardless, the detection of PTM tumor antigens, which are associated with key signaling pathways, on CRC tumors hinted that they could be targeted by TILs.

Patient TILs Target Tumor-Specific HLA-I Phosphopeptides

Immunohistochemical analysis of patient tumors revealed T cell infiltration of the stroma in all cases, with functional cytotoxic T cell infiltration of the tumor apparent in the primary CRC tumor (**Figure 3A**). To assess whether patients harbored tumor-resident T cells capable of targeting the HLA-I phosphopeptides identified on autologous CRC tumor, TILs were extracted, expanded using cytokines, and frozen (27). Once the phosphopeptide analyses were complete, we selected the tumor-associated and tumor-specific phosphopeptides binding common HLA alleles for further study. After a 6-day culture with peptide, we quantitated immunity within the TILs against phosphopeptides, or control viral peptides (19), using intracellular cytokine staining (ICS) (**Figure 3B** and **Supplementary Figure 6**). We observed that multifunctional, memory TILs target many of the phosphopeptides identified in a CRC liver metastasis sample (CRCLM1) and a single phosphopeptide in primary CRC sample - CRC3 (RRIsDPQVF, which was predicted to bind HLA-C*06 in this patient), producing TNFα, IFNγ, and IL-2, but no TIL responses targeting phosphopeptides were detected in CRCLM2 (**Figures 3C–E** and **Supplementary Figures 6–8**). Considerable variability was observed in TIL responses, but despite this variation, clear TIL responses to a subset of the LC-MS/MS detected HLA phosphopeptides were seen. Surprisingly, phosphopeptides that were also present on adjacent healthy tissue could be targeted by TILs. Namely, those targeting RRIsDPQVF in CRC3, which was found at 18 times greater concentration on tumor than healthy colon tissue (**Supplementary Table 5** and **Figure 3E**), and two phosphopeptides identified on CRCLM1, though these were identified only at very low concentrations (<1fmol/g) on neighboring healthy liver tissue (**Supplementary Figure 9**). In this small cohort, all TIL responses to the HLA-I phosphopeptides were unique; therefore, we expanded our cohort of patients to investigate whether TIL responses to shared HLA-I phosphopeptides could be found more broadly in CRC patients.

T Cells Targeting CRC HLA-I Phosphopeptides Are Present in CRC Patient Tumors and Peripheral Blood

We have demonstrated that the same tumor-specific HLA-I phosphopeptides are presented on CRC tumors from different patients, and also on other malignancies. To evaluate if any CRC phosphopeptides are commonly targeted by CRC patient TILs, we selected a subset of phosphopeptides that were predicted to bind to commonly expressed HLA-I alleles - HLA-A*02, HLA-C*06 and HLA-C*07 - and have also been identified in other malignancies (19, Penny et al., unpublished). TIL responses were assessed, using ICS, in a small cohort of patients. In all of the patients tested, we found TILs targeting the CRC-associated HLA-I phosphopeptides, with moderate to strong responses against two peptides (**Figure 4A**). These TIL responses were detected against an HLA-A*02-associated phosphopeptide from tensin 3 (VMIGsPKKV) and an HLA-C*07-associated

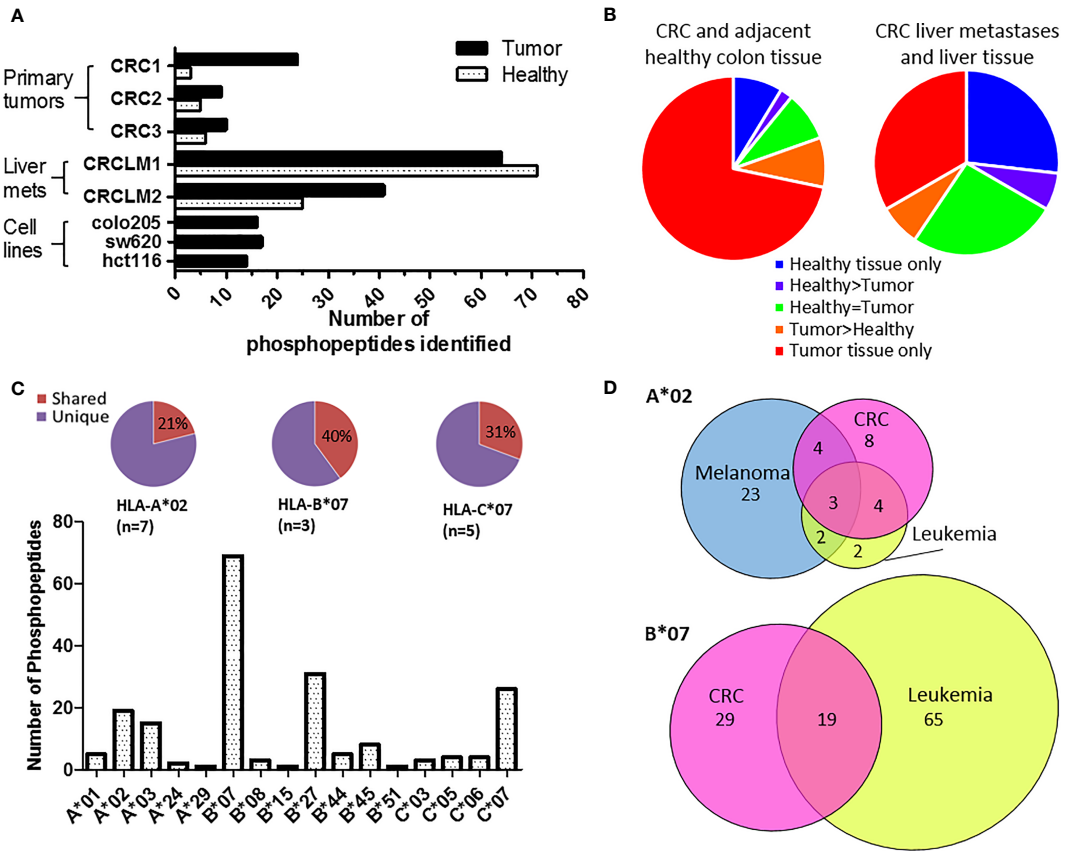

FIGURE 2 | Phosphopeptides identified from colorectal cancer samples – putative cancer antigens. **(A)** Comparison of phosphopeptides identified on tumors and healthy tissue from CRC patients with primary (n=3) and secondary (n=2) tumors and CRC cell lines (n=3). **(B)** Proportion of the phosphopeptides identified on primary and secondary tumors that were healthy specific (not detected on tumor) (blue), healthy associated (more detected on healthy than tumor tissue) (purple), equal (where equal was within one order of magnitude) (green), tumor associated (more detected on tumor than healthy tissue) (orange) and tumor specific (not detected on healthy tissue) (red). **(C)** The number of phosphopeptides identified predicted to bind to different HLA-I. Pie charts show the proportion of phosphopeptides shared (red) across multiple patients' samples for the most common HLA-alleles. **(D)** Overlap of HLA-A*02 and HLA-B*07 phosphopeptides identified on CRC (pink) with those found on other types of malignancy; melanoma (blue) and leukemia (yellow).

phosphopeptide from selenoprotein H (RRGsFEVTL), with responses comparable in magnitude to those targeting control viral antigens. Thus, we identified shared tumor-specific phosphopeptide antigens on CRC and demonstrate that these same phosphopeptides are targeted by TILs in tumors whose HLA peptidomes have not been characterized by LC-MS/MS.

To investigate whether the T cells that target HLA-I phosphopeptides could be found in the peripheral blood of CRC patients, we used cultured IFNγ ELISpot (**Supplementary Figure 10**), and compared responses between CRC patients and healthy donors. We detected T cells targeting HLA-I phosphopeptides in the peripheral blood of CRC patients (**Figures 4B, C** and **Supplementary Figure 11**). Interestingly, responses targeting some of the CRC-associated HLA-I phosphopeptides were absent in CRC patients, but present in healthy donors, as has been seen in other malignancies (19, Buettner et al., unpublished) (**Figures 4B, C**, denoted by filled red circles). However, there were also HLA-I phosphopeptides that elicited higher responses in CRC patients than their healthy counterparts (**Figures 4B, C**, open green circles), some significantly so - namely RAHSsPASL (p=0.032) a peptide from transcriptional coactivator YAP1, from the TGFβ signaling pathway (**Figure S4**) and TRKtPESFL (p=0.036) a peptide from Epsin-1. Of note, strong responses could also be seen in the circulating T cells of many CRC patients targeting HLA-A*02-associated peptides RVAsPTSGV and VMIGsPKKV (**Figure 4B**), and HLA-C*07-associated peptide RRGsFEVTL (**Figure 4C** and **Table 1**). Although interpretation of these results is limited by the small patient cohort, the peripheral T cell responses observed align with responses seen in other patients at the tumor site, and warrant future investigation in additional CRC patients, as there appears to be a clear role for phosphopeptide-specific T cells in CRC.

Phosphopeptide-Specific T Cells Can Kill, but May Become Dysfunctional

To test phosphopeptide-specific T cell functionality, T cell lines were established from primary CRC TILs and healthy donor peripheral blood mononuclear cells (PBMCs). Phosphopeptide-

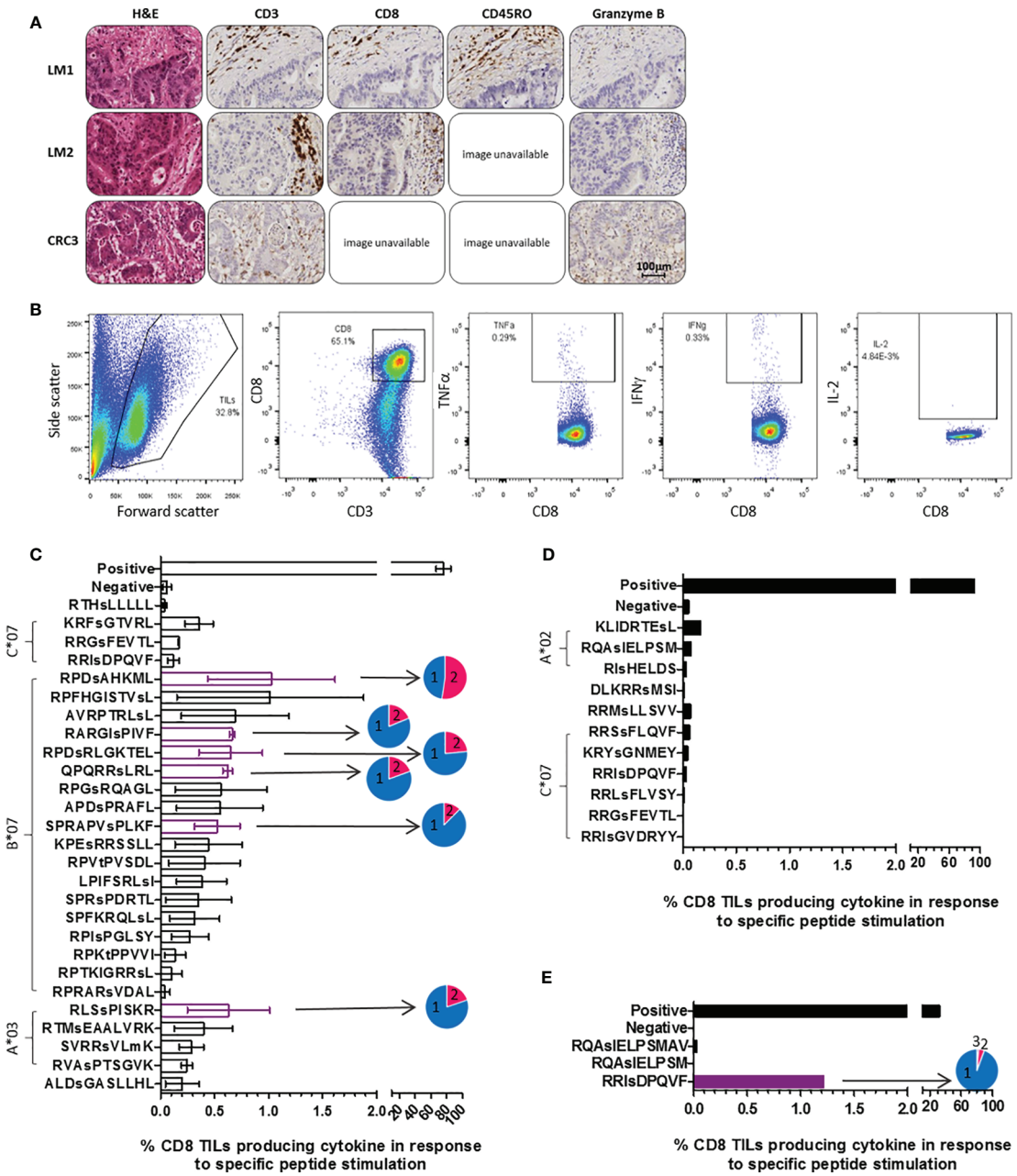

FIGURE 3 | TILs target phosphopeptides found on CRC tumors. **(A)** Immunohistochemistry (IHC) of the tumors that TILs were taken from, stained for CD3, CD8, CD45RO and Granzyme B (DAB staining in brown). Some slide images unavailable due to loss of section. **(B)** ICS gating strategy utilized in assessment of TIL phosphopeptide responses. **(C)** CRCLM1 TIL cytokine responses to phosphopeptides identified on CRCLM1 (results represent the assay repeated on 2 separate occasions, with differentially expanded TILs), pie charts show the proportion of T cells producing 1 (blue), 2 (pink) and 3 (purple) cytokines. Consistently strong responses are highlighted in purple. **(D)** CRCLM2 TIL cytokine responses to phosphopeptides identified on CRCLM2. **(E)** CRC3 TIL cytokine responses to phosphopeptides identified on CRC3, pie chart shows the proportion of T cells producing 1 (blue), 2 (pink) and 3 (purple) cytokines.

specific cells were enriched using magnetic cell sorting for activation marker CD137, after stimulation with phosphopeptide (**Supplementary Figure 12**). Surprisingly, when we evaluated cytotoxicity, the extensively expanded, phosphopeptide-specific TILs tested did not kill phosphopeptides pulsed target cells (**Figure 5A**). Nonetheless, some of the $CD8^+$ TILs were activated in response to phosphopeptide, but not its unphosphorylated counterpart, with 16.7% upregulating the T cell activation marker CD137 (**Figure 5B**). Thus proving the TILs specifically target the phosphopeptide, and not the unmodified peptide. Unlike the TILs, T cell lines grown from healthy donor PBMCs targeting VMIGsPKKV and RVAsPTSGV were functional and did kill, in a

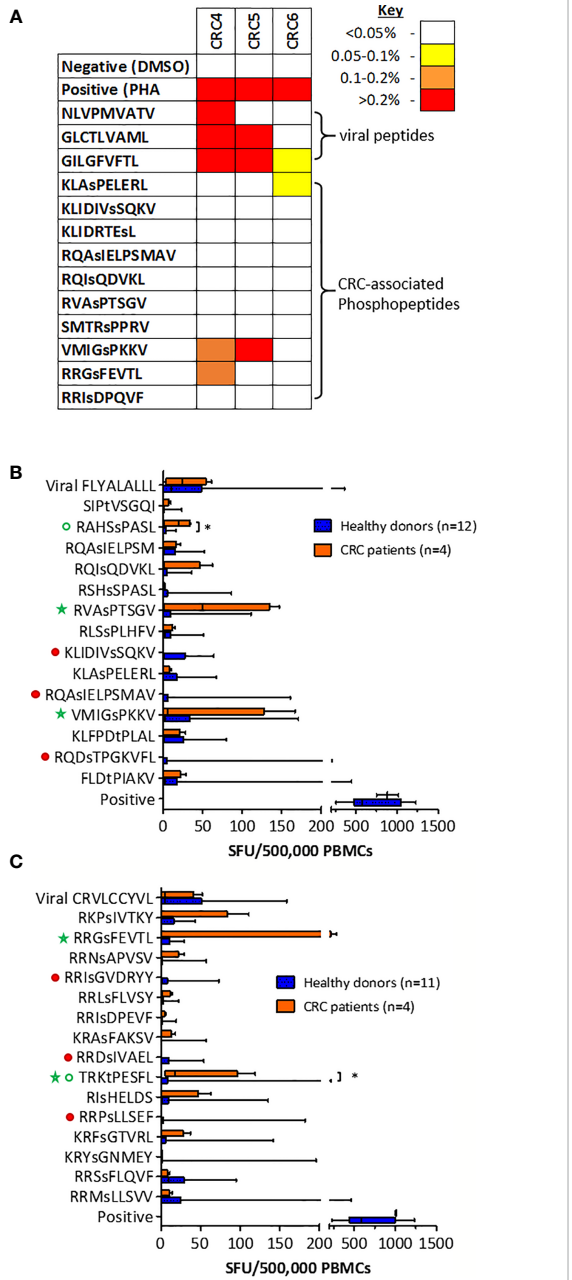

FIGURE 4 | T cells targeting CRC phosphopeptides are found in a number of patients. **(A)** Summary of CRC TIL cytokine responses to common phosphopeptides (n=3). Box and whisker plots comparing HD and CRC patient PBMC IFNg production targeting **(B)** HLA-A*02-associated phosphopeptides and **(C)** HLA-C*07-associated phosphopeptides; median, interquartile range (box) and minima to maxima (whiskers) are shown. Responses that were absent (red circles) in CRC patients are highlighted. Green circles highlight the responses that were significantly higher in CRC patients than HD (Mann-Whitney U, * denotes p<0.05). Green stars highlight the phosphopeptides to which at least one patient had a high PBMC response.

dose-dependent manner (**Figures 5C, D** and **Supplementary Figure 13**). These observations suggest a loss of functional competence in HLA-I phosphopeptide specific T-cell responses - either at the tumor site, or due to their extensive *ex vivo* expansion – as phosphopeptide-specific T cells can clearly target and kill CRC cells.

DISCUSSION

Despite T cell infiltration of CRC being well-established as the most important predictor of prognosis in CRC, the targets of these T cells remain ill-defined (1, 3, 5, 6, 9). This has limited the development of antigen targeted immunotherapies in CRC, especially as the vast majority of tumors are MSS and have a low to moderate TMB (6). Recently, case reports have demonstrated promising proof of concept for adoptive T cell (ATC) therapy - targeting a HLA-C*08 restricted mutational neoantigen (KRAS G12D) in metastatic CRC - showing it to be both safe and effective (36). However, targeting mutational neoantigens is limited by the low frequencies of public neoantigens combined with the highly polymorphic nature of HLA alleles (37). Here, we have identified 74 tumor-specific HLA-I bound phosphopeptide antigens from primary and secondary CRC tumors, which may represent targetable PTM tumor antigens in CRC. We have shown that CRC TILs target these phosphopeptides, implicating them in tumor immunity and thus indicating that they may be favorable candidate immunotherapeutic targets. Importantly, although HLA-restricted, these PTM tumor antigens are public and consequently afford the opportunity to develop "off-the-shelf" cell therapy approaches. Future immunotherapeutic strategies could include: ATC therapy, using phosphopeptide-specific T cells expanded *ex vivo*, or engineered TCRs; chimeric antigen receptor (CAR) T cells; the use of bispecific TCRs targeting phosphopeptides; a phosphopeptide vaccine; or a combination therapy, including ICB (38–40).

Our data indicate that HLA-I phosphopeptides may be favorable candidate immunotherapeutic targets for several reasons. Firstly, we have shown a link between cancer signaling and HLA-I phosphopeptide presentation, in that some HLA-I phosphopeptides are tumor specific, and their numbers increase with tumor stage progression (**Figures 2A, B**). This mirrors an increase in aberrant signaling as cancers progress and metastasize (18). However, although the number and amount of phosphopeptides presented appeared to correlate with malignancy, these differences could also have been attributed to the specific binding preferences of the expressed HLA alleles. For example, we show that both HLA-B*07 and HLA-B*27 present more phosphopeptides than other alleles (**Figure 2C** and **Supplementary Figure 4A**), as previously reported (41). This overrepresentation could be ascribed to the similarity of the HLA- and the kinase- binding motifs (**Supplementary Figure 4B**). Nonetheless, of the two HLA-B*07 samples (CRC1 and CRCLM1, from different patients), the liver metastasis sample presented more than twice the number of HLA-B*07 phosphopeptides, indicating that this increased presentation is actually driven by the metastatic status of the tumor. We show

TABLE 1 | Summary of responses to key CRC HLA-I phosphopeptides.

Phosphopeptide	RVAsPTSGV	VMIGsPKKV	RRGsFEVTL
Protein of Origin	IRS2	TNS3	SELH
HLA-binding	A*02	A*02	C*07
Samples	colo205 & hct116	sw620	CRC1, CRCLM1, CRCLM2
Other malignancies	Melanoma & Leukemia	Melanoma & Leukemia	
TIL responses	–	+++	++
HD PBMC responses	++	+++	+
CRC patient PBMC	+++	+++	+++

+ low, ++ moderate, +++ strong responses, - not detected.

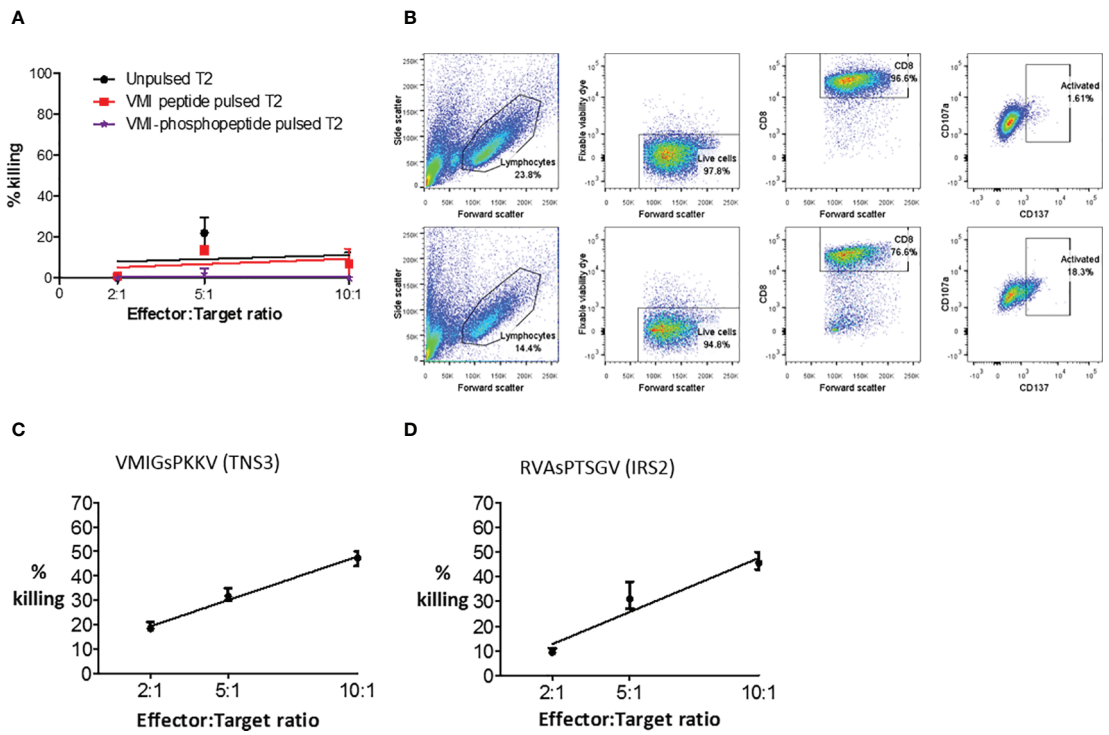

FIGURE 5 | Phosphopeptide-specific T cells can kill, but expanded TILs do not. **(A)** A europium release assay, using a VMI-specific T cell line grown from patient (CRC5) TILs to target T2 cells pulsed with phosphopeptide VMIGsPKKV, or unphosphorylated VMIGSPKKV. **(B)** Flow cytometry to show the activation and degranulation of VMI-specific CRC5 TILs when stimulated with unphosphorylated VMIGSPKKV (top) and phosphorylated VMIGsPKKV (bottom). Healthy donor T cell lines targeting **(C)** VMIGsPKKV and **(D)** RVAsPTSGV were used in a europium-release killing assay with a CRC cell line natively expressing the phosphopeptides (SW620).

that at least a quarter of these HLA-I phosphopeptides are derived from essential cancer signaling pathways, which may therefore limit the scope for tumor immune escape by loss of antigen (**Supplementary Figure 5**) (42). Since little is known about the effects of phosphorylation at the specific sites on most of the phosphopeptide source proteins (**Supplementary Tables 3–5**), it is difficult to reach firm conclusions about their contribution to the malignant state, creating the possibility that even more CRC phosphopeptides are implicated in cancer signaling than currently described.

Secondly, we have shown that these HLA-I phosphopeptides are public antigens, with up to 40% of the phosphopeptides presented by common HLA alleles found on more than one sample in our small cohort (**Figure 2C** and **Supplementary Figure 2C**). This would make any targeted therapies widely applicable at a population level, potentially against any malignancy. Of note, many of the phosphopeptides identified were attributed to HLA-C*07, a common allele (37-69%) across European and African populations and known to contribute significantly to tumor immunity (43, 44). Further examination of a larger CRC patient cohort is needed to confirm which phosphopeptides are most frequently presented. Promisingly, some of the identified phosphopeptides were predicted to bind different HLA-I alleles in different patients, suggesting that presentation may be not be limited by specific HLA-type, but apply across different HLA superfamilies (**Supplementary Tables 3–5**) (41).

Thirdly, we have shown that some of the tumor-resident immunity in CRC, which is known to be of prognostic significance, targets HLA-I phosphopeptides (**Figures 3** and **4**) (1, 3, 5, 9). This was true of TILs in the tumors in which we had identified the phosphopeptides (**Figure 3**), and in a further cohort of primary CRC tumors (**Figure 4A**). Previously, it has been suggested that many of the TILs in CRC are merely bystanders - not directly targeting the tumor (45). Indeed, viral responses were also assayed here, and these bystander responses were strong. However, we clearly demonstrate that at least some TILs are targeting phosphopeptides. The frequency of TILs targeting each individual phosphopeptide was low, but this has also been seen with other tumor antigen specific TILs (46). Taken together with the data from patient PBMCs, we can conclude that HLA-I phosphopeptide-specific TILs represent a subset of the tumor-resident immunity to CRC. We have also shown that phosphopeptide-specific T cells can target and kill tumor cells (**Figures 5C, D** and **Supplementary Figure 13**). Thus, these may prove ideal candidates for future immunotherapeutic strategies.

The use of phosphopeptides as immunotherapeutic targets would have limitations. Primarily, the presence of HLA-I phosphopeptides on other healthy tissues, which we discovered particularly on the "healthy" liver tissue, neighboring CRC liver metastases. This could be due to the presence of microscopic metastases; however, it may also be attributable to the role of the liver in tolerizing antigen from the gastrointestinal tract (47). There were TILs that targeted HLA-I phosphopeptides identified on healthy tissue. If this were not simply due to micrometastases, it might suggest a low T cell functional avidity, which would prevent auto-reactivity and enable targeting of tumor cells, where antigen density is much higher (48). Therefore, in these cases it would not be appropriate to use any therapeutic strategies that involve the modulation of TCR affinity, such as bispecifics (39). Strikingly, peripheral T cell responses were detected in heathy donors targeting most of the CRC phosphopeptides (**Figures 4B, C**). These responses may be initiated in healthy donors when pre-malignant transformation events occur, perhaps caused by infection with transforming viruses (19). In CRC, transforming events may also be initiated by bacteria, such as enterotoxigenic *Bacteroides fragilis* or *Fusobacterium nucleatum* (49, 50). The fact that some healthy donors have T cells targeting these phosphopeptides suggests that these phosphopeptides are not presented on other healthy tissues, since these donors are not showing symptoms of autoimmunity. Furthermore, phase I clinical trials using a phosphopeptide vaccine have proven safe in melanoma, which included one of the CRC phosphopeptides of interest RVAsPTSGV (40). Therefore, any therapy targeting these PTM tumor antigens should not be limited by off-target effects.

Another potential limitation of therapeutically targeting HLA-I phosphopeptide antigens is the lack of functional response seen in patient TILs *in vitro*. We show that phosphopeptide-specific T cell lines can kill CRC cell lines in a phosphopeptide-specific manner (**Figures 5C, D** and **Supplementary Figure 13**). This is in accordance with data from previous studies, where phosphopeptide-specific T cells were observed to kill *ex vivo* from leukemia patients and *in vivo* in a mouse melanoma model (19, 51). However, a line derived from CRC patient TILs, although activated, did not kill (**Figures 5A, B**). This difference in function may explain why the tumor is persisting in these patients - perhaps these T cells have become exhausted and no longer kill, or they may be functionally altered by the tumor microenvironment (52, 53). Recent studies in CRC have suggested roles for immune checkpoints other than PD-1, and exhaustion markers, such as CD39, CD73, TIM-3, LAG-3 and TIGIT (52). Limitations due to exhaustion or checkpoint blockade could be overcome using combination therapies with a checkpoint blockade inhibitor, or therapies targeting coinhibitory receptor molecules, or enhancing costimulatory immune checkpoint molecules, as has proven effective in preclinical vaccine models (54). An alternative explanation could be that the TILs lost function during the expansion *in vitro* (55), since using "young" TILs we observed phosphopeptide-specific upregulation of degranulation marker CD107a (**Figure S14**). These *in vitro* effects could be overcome using modified expansion protocols, to provide successful ATC therapies (56).

This study is too small to establish the clinical significance of patient T cell responses targeting HLA-I phosphopeptides. Previously, we observed that CLL patients without immunity to phosphopeptides did less well clinically (19). Although anecdotal at this stage, here we saw very few TILs targeting HLA-I phosphopeptides in the one CRC patient (CRC6) who did suffer recurrence (**Figure 4A**). A larger scale study in CRC is needed to determine whether having higher responses targeting tumor-specific phosphopeptides correlates with better patient outcomes. Intriguingly, we observed stronger peripheral T cell responses targeting many of the HLA-I phosphopeptides in CRC patients than healthy donors, whereas previously, in leukemia, we showed that a subset of patients have absent or impaired responses to phosphopeptides (19). The difference between the PBMC responses in CRC and leukemia patients may be due to the inherent difference between solid tumors and blood malignancies – that the tumor microenvironment can be controlled in a solid tumor, so whilst CRC patients may retain phosphopeptide-specific T cells their function may be impaired at the tumor site. Although there were also HLA-I phosphopeptides that did not elicit T cell responses from CRC patients (**Figures 4B, C**), given that CD8 T cells are known to control tumor growth in CRC, then the more interesting responses may be those that we have seen in tumor-resident T cells and observed to be higher in CRC patients' peripheral blood (1–3, 9). This approach is further supported by recent reports describing the presence of memory T cells in the peripheral blood of CRC patients that target tumor-associated antigens (57), and mutational neoantigens (58). Using T cells extracted from the peripheral blood in ATC therapies would have demonstrable benefits over the requirement for surgically obtained TILs.

In conclusion, we have shown that the targets of tumor-resident CD8 T cells include PTM tumor antigens, namely HLA-I phosphopeptides. Once these findings have been validated in a larger patient cohort, tumor-specific phosphopeptides may

provide an optimal target for future immunotherapeutics. Critically, these HLA-I associated phosphopeptides are public antigens - often shared across patients presenting the same HLA molecules. This would make any targeted therapies widely applicable at a population level, potentially against any malignancy. Our future efforts will be devoted to expanding this work into larger patient cohorts to further our understanding of phosphopeptide targeting by effector T cells, and to ultimately develop more efficacious immunotherapies for CRC.

DATA AVAILABILITY STATEMENT

The original contributions presented in the study are included in the article/**Supplementary Material**. Further inquiries can be directed to the corresponding author.

ETHICS STATEMENT

The studies involving human participants were reviewed and approved by ethics committees local to the University of Birmingham (Ref 09/H1010/75, 06/Q2702/61 and 09/H1203/49). The patients/participants provided their written informed consent to participate in this study.

AUTHOR CONTRIBUTIONS

SP was involved in the conception and design of the study, acquisition and analysis of data and wrote manuscript. JA designed and performed MS experiments, analysed data, and participated in manuscript writing. SM participated in manuscript writing. AS performed scientific experiments. PM performed MS experiment and analysed data. LS performed scientific experiments. SW assisted with sample collection. DB wrote in-house software and analysed MS data. DH and JS directed MS experiments and analysed MS data. MC was involved in conception of the work, directed experiments and participated in manuscript writing. All authors contributed to the article and approved the submitted version.

FUNDING

This work was supported by Queen Elizabeth Hospital Birmingham Charity grant RCDE13729 (to MC), NIH-AI033993 (to DH).

ACKNOWLEDGMENTS

We thank the whole MC and DH laboratories for suggestions and support at all stages of the project. Thanks also to the University of Birmingham Human Biomaterials Resource Centre and the patients who donated blood and tissue to this study.

SUPPLEMENTARY MATERIAL

The Supplementary Material for this article can be found online at: https://www.frontiersin.org/articles/10.3389/fimmu.2021.723566/full#supplementary-material

REFERENCES

1. Galon J, Costes A, Sanchez-Cabo F, Kirilovsky A, Mlecnik B, Lagorce-Pages C, et al. Type, Density, and Location of Immune Cells Within Human Colorectal Tumors Predict Clinical Outcome. *Science* (2006) 313:1960–4. doi: 10.1126/science.1129139
2. Ogino S, Nosho K, Irahara N, Meyerhardt JA, Baba Y, Shima K, et al. Lymphocytic Reaction to Colorectal Cancer Is Associated With Longer Survival, Independent of Lymph Node Count, Microsatellite Instability, and CpG Island Methylator Phenotype. *Clin Cancer Res an Off J Am Assoc Cancer Res* (2009) 15:6412–20. doi: 10.1158/1078-0432.CCR-09-1438
3. Pages F, Mlecnik B, Marliot F, Bindea G, Ou FS, Bifulco C, et al. International Validation of the Consensus Immunoscore for the Classification of Colon Cancer: A Prognostic and Accuracy Study. *Lancet* (2018) 391:2128–39.
4. Katz SC, Pillarisetty V, Bamboat ZM, Shia J, Hedvat C, Gonen M, et al. T Cell Infiltrate Predicts Long-Term Survival Following Resection of Colorectal Cancer Liver Metastases. *Ann Surg Oncol* (2009) 16:2524–30. doi: 10.1245/s10434-009-0585-3
5. Baldin P, Van den Eynde M, Mlecnik B, Bindea G, Beniuga G, Carrasco J, et al. Prognostic Assessment of Resected Colorectal Liver Metastases Integrating Pathological Features, RAS Mutation and Immunoscore. *J Pathol Clin Res* (2021) 7:27–41. doi: 10.1002/cjp2.178
6. Angelova M, Charoentong P, Hackl H, Fischer ML, Snajder R, Krogsdam AM, et al. Characterization of the Immunophenotypes and Antigenomes of Colorectal Cancers Reveals Distinct Tumor Escape Mechanisms and Novel Targets for Immunotherapy. *Genome Biol* (2015) 16:64. doi: 10.1186/s13059-015-0620-6
7. Guinney J, Dienstmann R, Wang X, de Reynies A, Schlicker A, Soneson C, et al. The Consensus Molecular Subtypes of Colorectal Cancer. *Nat Med* (2015) 21:1350–6.
8. Le DT, Uram JN, Wang H, Bartlett BR, Kemberling H, Eyring AD, et al. PD-1 Blockade in Tumors With Mismatch-Repair Deficiency. *New Engl J Med* (2015) 372:2509–20.
9. Mlecnik B, Bindea G, Angell HK, Maby P, Angelova M, Tougeron D, et al. Integrative Analyses of Colorectal Cancer Show Immunoscore Is a Stronger Predictor of Patient Survival Than Microsatellite Instability. *Immunity* (2016) 44:698–711. doi: 10.1016/j.immuni.2016.02.025
10. Gryfe R, Kim H, Hsieh ET, Aronson MD, Holowaty EJ, Bull SB, et al. Tumor Microsatellite Instability and Clinical Outcome in Young Patients With Colorectal Cancer. *New Engl J Med* (2000) 342:69–77. doi: 10.1056/NEJM200001133420201
11. Fife BT, Guleria I, Gubbels Bupp M, Eagar TN, Tang Q, Bour-Jordan H, et al. Insulin-Induced Remission in New-Onset NOD Mice Is Maintained by the PD-1-PD-L1 Pathway. *J Exp Med* (2006) 203:2737–47. doi: 10.1084/jem.20061577
12. Giannakis M, Mu XJ, Shukla SA, Qian ZR, Cohen O, Nishihara R, et al. Genomic Correlates of Immune-Cell Infiltrates in Colorectal Carcinoma. *Cell Rep* (2016) 17:1206. doi: 10.1016/j.celrep.2016.10.009
13. Castle JC, Uduman M, Pabla S, Stein RB, Buell JS. Mutation-Derived Neoantigens for Cancer Immunotherapy. *Front Immunol* (2019) 10:1856. doi: 10.3389/fimmu.2019.01856
14. Yarchoan M, Hopkins A, Jaffee EM. Tumor Mutational Burden and Response Rate to PD-1 Inhibition. *New Engl J Med* (2017) 377:2500–1. doi: 10.1056/NEJMc1713444

15. Buttner R, Longshore JW, Lopez-Rios F, Merkelbach-Bruse S, Normanno N, Rouleau E, et al. Implementing TMB Measurement in Clinical Practice: Considerations on Assay Requirements. *ESMO Open* (2019) 4:e000442. doi: 10.1136/esmoopen-2018-000442
16. Mlecnik B, Bifulco C, Bindea G, Marliot F, Lugli A, Lee JJ, et al. Multicenter International Society for Immunotherapy of Cancer Study of the Consensus Immunoscore for the Prediction of Survival and Response to Chemotherapy in Stage III Colon Cancer. *J Clin Oncol* (2020) 38:3638–51.
17. Cancer Genome Atlas N. Comprehensive Molecular Characterization of Human Colon and Rectal Cancer. *Nature* (2012) 487:330–7. doi: 10.1038/nature11252
18. Hanahan D, Weinberg RA. Hallmarks of Cancer: The Next Generation. *Cell* (2011) 144:646–74. doi: 10.1016/j.cell.2011.02.013
19. Cobbold M, de la Pena H, Norris A, Polefrone JM, Qian J, English AM, et al. MHC Class I-Associated Phosphopeptides Are the Targets of Memory-Like Immunity in Leukemia. *Sci Trans Med* (2013) 5:203ra125.
20. Zarling AL, Polefrone JM, Evans AM, Mikesh LM, Shabanowitz J, Lewis ST, et al. Identification of Class I MHC-Associated Phosphopeptides as Targets for Cancer Immunotherapy. *Proc Natl Acad Sci USA* (2006) 103:14889–94. doi: 10.1073/pnas.0604045103
21. Meyer VS, Drews O, Gunder M, Hennenlotter J, Rammensee HG, Stevanovic S. Identification of Natural MHC Class II Presented Phosphopeptides and Tumor-Derived MHC Class I Phospholigands. *J Proteome Res* (2009) 8:3666–74. doi: 10.1021/pr800937k
22. Zarling AL, Ficarro SB, White FM, Shabanowitz J, Hunt DF, Engelhard VH. Phosphorylated Peptides Are Naturally Processed and Presented by Major Histocompatibility Complex Class I Molecules *In Vivo*. *J Exp Med* (2000) 192:1755–62. doi: 10.1084/jem.192.12.1755
23. Mohammed F, Stones DH, Zarling AL, Willcox CR, Shabanowitz J, Cummings KL, et al. The Antigenic Identity of Human Class I MHC Phosphopeptides Is Critically Dependent Upon Phosphorylation Status. *Oncotarget* (2017) 8:54160–72. doi: 10.18632/oncotarget.16952
24. Petersen J, Wurzbacher SJ, Williamson NA, Ramarathinam SH, Reid HH, Nair AK, et al. Phosphorylated Self-Peptides Alter Human Leukocyte Antigen Class I-Restricted Antigen Presentation and Generate Tumor-Specific Epitopes. *Proc Natl Acad Sci USA* (2009) 106:2776–81. doi: 10.2210/pdb3fqn/pdb
25. Mohammed F, Cobbold M, Zarling AL, Salim M, Barrett-Wilt GA, Shabanowitz J, et al. Phosphorylation-Dependent Interaction Between Antigenic Peptides and MHC Class I: A Molecular Basis for the Presentation of Transformed Self. *Nat Immunol* (2008) 9:1236–43. doi: 10.1038/ni.1660
26. Raposo B, Merky P, Lundqvist C, Yamada H, Urbonaviciute V, Niaudet C, et al. T Cells Specific for Post-Translational Modifications Escape Intrathymic Tolerance Induction. *Nat Commun* (2018) 9:353. doi: 10.1038/s41467-017-02763-y
27. Dudley ME, Wunderlich JR, Shelton TE, Even J, Rosenberg SA. Generation of Tumor-Infiltrating Lymphocyte Cultures for Use in Adoptive Transfer Therapy for Melanoma Patients. *J Immunother* (2003) 26:332–42. doi: 10.1097/00002371-200307000-00005
28. Penny SA, Malaker SA. Isolation of Major Histocompatibility Complex (MHC)-Associated Peptides by Immunoaffinity Purification. *Methods Mol Biol* (2019) 2024:235–43. doi: 10.1007/978-1-4939-9597-4_14
29. Abelin JG, Trantham PD, Penny SA, Patterson AM, Ward ST, Hildebrand WH, et al. Complementary IMAC Enrichment Methods for HLA-Associated Phosphopeptide Identification by Mass Spectrometry. *Nat Protoc* (2015) 10:1308–18. doi: 10.1038/nprot.2015.086
30. Chi A, Huttenhower C, Geer LY, Coon JJ, Syka JE, Bai DL, et al. Analysis of Phosphorylation Sites on Proteins From Saccharomyces Cerevisiae by Electron Transfer Dissociation (ETD) Mass Spectrometry. *Proc Natl Acad Sci USA* (2007) 104:2193–8.
31. Kim Y, Ponomarenko J, Zhu Z, Tamang D, Wang P, Greenbaum J, et al. Immune Epitope Database Analysis Resource. *Nucleic Acids Res* (2012) 40: W525–530. doi: 10.1093/nar/gks438
32. von Zons P, Crowley-Nowick P, Friberg D, Bell M, Koldovsky U, Whiteside TL. Comparison of Europium and Chromium Release Assays: Cytotoxicity in Healthy Individuals and Patients With Cervical Carcinoma. *Clin Diagn Lab Immunol* (1997) 4:202–7. doi: 10.1128/cdli.4.2.202-207.1997
33. Micallef L, Rodgers P. eulerAPE: Drawing Area-Proportional 3-Venn Diagrams Using Ellipses. *PloS One* (2014) 9:e101717. doi: 10.1371/journal.pone.0101717
34. Crooks GE, Hon G, Chandonia JM, Brenner SE. WebLogo: A Sequence Logo Generator. *Genome Res* (2004) 14:1188–90. doi: 10.1101/gr.849004
35. Kanehisa M, Sato Y, Kawashima M, Furumichi M, Tanabe M. KEGG as a Reference Resource for Gene and Protein Annotation. *Nucleic Acids Res* (2016) 44:D457–462. doi: 10.1093/nar/gkv1070
36. Tran E, Robbins PF, Lu YC, Prickett TD, Gartner JJ, Jia L, et al. T-Cell Transfer Therapy Targeting Mutant KRAS in Cancer. *New Engl J Med* (2016) 375:2255–62. doi: 10.1056/NEJMoa1609279
37. Rech AJ, Vonderheide RH. T-Cell Transfer Therapy Targeting Mutant KRAS. *New Engl J Med* (2017) 376:e11. doi: 10.1056/NEJMc1616637
38. Rosenberg SA, Restifo NP. Adoptive Cell Transfer as Personalized Immunotherapy for Human Cancer. *Science* (2015) 348:62–8. doi: 10.1126/science.aaa4967
39. Lowe KL, Cole D, Kenefeck R, OKelly I, Lepore M, Jakobsen BK. Novel TCR-Based Biologics: Mobilising T Cells to Warm 'Cold' Tumours. *Cancer Treat Rev* (2019) 77:35–43. doi: 10.1016/j.ctrv.2019.06.001
40. Engelhard VH, Obeng RC, Cummings KL, Petroni GR, Ambakhutwala AL, Chianese-Bullock KA, et al. MHC-Restricted Phosphopeptide Antigens: Preclinical Validation and First-in-Humans Clinical Trial in Participants With High-Risk Melanoma. *J Immunother Cancer* (2020) 8. doi: 10.1136/jitc-2019-000262
41. Solleder M, Guillaume P, Racle J, Michaux J, Pak HS, Muller M, et al. Mass Spectrometry Based Immunopeptidomics Leads to Robust Predictions of Phosphorylated HLA Class I Ligands. *Mol Cell Proteomics MCP* (2020) 19:390–404. doi: 10.1074/mcp.TIR119.001641
42. Matsushita H, Vesely MD, Koboldt DC, Rickert CG, Uppaluri R, Magrini VJ, et al. Cancer Exome Analysis Reveals a T-Cell-Dependent Mechanism of Cancer Immunoediting. *Nature* (2012) 482:400–4. doi: 10.1038/nature10755
43. Ramskov S, Hansen KU, Saini KS, Sturm T, Borch A, Bjerregaard A-M, et al. HLA-C Restricted Neoepitopes Contribute Significantly to the Immune Recognition of Cancer. *Eur J Immunol* (2019) 49:O066.
44. Gonzalez-Galarza FF, McCabe A, Santos E, Jones J, Takeshita L, Ortega-Rivera ND, et al. Allele Frequency Net Database (AFND) 2020 Update: Gold-Standard Data Classification, Open Access Genotype Data and New Query Tools. *Nucleic Acids Res* (2020) 48:D783–8. doi: 10.1093/nar/gkz1029
45. Scheper W, Kelderman S, Fanchi LF, Linnemann C, Bendle G, de Rooij MAJ, et al. Low and Variable Tumor Reactivity of the Intratumoral TCR Repertoire in Human Cancers. *Nat Med* (2019) 25:89–94. doi: 10.1038/s41591-018-0266-5
46. Reissfelder C, Stamova S, Gossmann C, Braun M, Bonertz A, Walliczek U, et al. Tumor-Specific Cytotoxic T Lymphocyte Activity Determines Colorectal Cancer Patient Prognosis. *J Clin Invest* (2015) 125:739–51. doi: 10.1172/JCI74894
47. Yang R, Liu Q, Grosfeld JL, Pescovitz MD. Intestinal Venous Drainage Through the Liver Is a Prerequisite for Oral Tolerance Induction. *J Pediatr Surg* (1994) 29:1145–8. doi: 10.1016/0022-3468(94)90297-6
48. Vigano S, Utzschneider DT, Perreau M, Pantaleo G, Zehn D, Harari A. Functional Avidity: A Measure to Predict the Efficacy of Effector T Cells? *Clin Dev Immunol* (2012) 2012:153863. doi: 10.1155/2012/153863
49. Wu S, Morin PJ, Maouyo D, Sears CL. Bacteroides Fragilis Enterotoxin Induces C-Myc Expression and Cellular Proliferation. *Gastroenterol* (2003) 124:392–400. doi: 10.1053/gast.2003.50047
50. Rubinstein MR, Wang X, Liu W, Hao Y, Cai G, Han YW. Fusobacterium Nucleatum Promotes Colorectal Carcinogenesis by Modulating E-Cadherin/Beta-Catenin Signaling *via* Its FadA Adhesin. *Cell Host Microbe* (2013) 14:195–206. doi: 10.1016/j.chom.2013.07.012
51. Zarling AL, Obeng RC, Desch AN, Pinczewski J, Cummings KL, Deacon DH, et al. MHC-Restricted Phosphopeptides From Insulin Receptor Substrate-2 and CDC25b Offer Broad-Based Immunotherapeutic Agents for Cancer. *Cancer Res* (2014) 74:6784–95. doi: 10.1158/0008-5472.CAN-14-0043
52. Saleh R, Taha RZ, Toor SM, Sasidharan Nair V, Murshed K, Khawar M, et al. Expression of Immune Checkpoints and T Cell Exhaustion Markers in Early and Advanced Stages of Colorectal Cancer. *Cancer Immunol Immunother CII* (2020). doi: 10.1007/s00262-020-02593-w
53. Taylor ES, McCall JL, Girardin A, Munro FM, Black MA, Kemp RA. Functional Impairment of Infiltrating T Cells in Human Colorectal Cancer. *Oncoimmunology* (2016) 5:e1234573. doi: 10.1080/2162402X.2016.1234573
54. Duraiswamy J, Kaluza KM, Freeman GJ, Coukos G. Dual Blockade of PD-1 and CTLA-4 Combined With Tumor Vaccine Effectively Restores T-Cell Rejection Function in Tumors. *Cancer Res* (2013) 73:3591–603. doi: 10.1158/0008-5472.CAN-12-4100

55. Donia M, Junker N, Ellebaek E, Andersen MH, Straten PT, Svane IM. Characterization and Comparison of 'Standard' and 'Young' Tumour-Infiltrating Lymphocytes for Adoptive Cell Therapy at a Danish Translational Research Institution. *Scand J Immunol* (2012) 75:157–67. doi: 10.1111/j.1365-3083.2011.02640.x
56. Sakellariou-Thompson D, Forget M-A, Roszik J, Jackson KR, Kim YU, Crosby S, et al. Preclinical Development of Tumor-Infiltrating Lymphocyte Therapy for Metastatic Colorectal Cancer. *J Clin Oncol* (2018) 36:95–5.
57. Picard E, Martel A, Simard A, Le H-T, Verschoor C, Ma G, et al. 758 Identification of Tumor Antigen-Specific T Cells in the Peripheral Blood of Colorectal Cancer Patients. *J Immunother Cancer* (2020) 8:A454–5. doi: 10.1136/jitc-2020-SITC2020.0758
58. Cafri G, Yossef R, Pasetto A, Deniger DC, Lu YC, Parkhurst M, et al. Memory T Cells Targeting Oncogenic Mutations Detected in Peripheral Blood of Epithelial Cancer Patients. *Nat Commun* (2019) 10:449. doi: 10.1038/s41467-019-08304-z

Conflict of Interest: MC owns equity in Revitope Oncology and Gritstone Oncology and now is an employee of AstraZeneca. JS and DH own stock in Agenus. The discovery here makes up patent Target peptides for colorectal cancer therapy and diagnostics, WO2014/039675. 2014 Mar 13 with inventors MC, SP, DH, JS and JGA.

The remaining authors declare that the research was conducted in the absence of any commercial or financial relationships that could be construed as a potential conflict of interest.

Publisher's Note: All claims expressed in this article are solely those of the authors and do not necessarily represent those of their affiliated organizations, or those of the publisher, the editors and the reviewers. Any product that may be evaluated in this article, or claim that may be made by its manufacturer, is not guaranteed or endorsed by the publisher.

Copyright © 2021 Penny, Abelin, Malaker, Myers, Saeed, Steadman, Bai, Ward, Shabanowitz, Hunt and Cobbold. This is an open-access article distributed under the terms of the Creative Commons Attribution License (CC BY). The use, distribution or reproduction in other forums is permitted, provided the original author(s) and the copyright owner(s) are credited and that the original publication in this journal is cited, in accordance with accepted academic practice. No use, distribution or reproduction is permitted which does not comply with these terms.

frontiers in Immunology

CASE REPORT
published: 18 October 2021
doi: 10.3389/fimmu.2021.740790

Case Report: Antiangiogenic Therapy Plus Immune Checkpoint Inhibitors Combined With Intratumoral Cryoablation for Hepatocellular Carcinoma

Xin Li[1†], Jiahua Xu[1†], Xiaoqiang Gu[1†], Ling Chen[2†], Qing Wu[1], Hongwei Li[1], Haoran Bai[1], Jinzu Yang[1] and Jianxin Qian[1*]*

[1] Department of Oncology, Longhua Hospital Affiliated to Shanghai University of Traditional Chinese Medicine (TCM), Shanghai, China, [2] Department of Oncology, Yueyang Hospital of Integrated Traditional Chinese and Western Medicine Affiliated to Shanghai University of Traditional Chinese Medicine (TCM), Shanghai, China

Background: Hepatocellular carcinoma (HCC) is a common gastrointestinal malignancy with high incidence and poor prognosis. Common treatment methods include surgery, transcatheter arterial chemoembolization (TACE), ablation, and targeted therapy. In recent years, combination treatment with antiangiogenic therapy and immune checkpoint inhibitors has made great progress in the treatment of advanced HCC. Here, we report the case of a patient with HCC who achieved a durable benefit from anti-vascular therapy and immune checkpoint inhibitors combined with intratumoral cryoablation.

Main Body: A 38-year-old male patient initially presented with severe abdominal pain that was identified as an HCC rupture and hemorrhage by computed tomography (CT). The patient underwent emergency surgery and postoperative pathology confirmed HCC. The patient received prophylactic TACE after surgery. Unfortunately, three months after surgery, the patient developed multiple liver metastases. Subsequently, he received systemic anti-vascular therapy and immune checkpoint inhibitors combined with intratumoral cryoablation. After treatment, the patient achieved extensive tumor necrosis and the disease was effectively controlled.

Conclusions: Anti-angiogenic therapy and immune checkpoint inhibitors combined with cryoablation can induce a powerful and effective systemic anti-tumor immune response, which is worthy of further research.

Keywords: hepatocellular carcinoma, cryoablation, immune checkpoint inhibitors, antiangiogenic therapy, case report

OPEN ACCESS

Edited by:
Eyad Elkord,
University of Salford, United Kingdom

Reviewed by:
Chunxia Su,
Shanghai Pulmonary Hospital, China
Hong Zhu,
Sichuan University, China

****Correspondence:***
Jinzu Yang
kingzuy@126.com
Jianxin Qian
jianxinqiang3@163.com

[†]These authors have contributed equally to this work

Specialty section:
This article was submitted to Cancer Immunity and Immunotherapy, a section of the journal Frontiers in Immunology

Received: *13 July 2021*
Accepted: *04 October 2021*
Published: *18 October 2021*

Citation:
Li X, Xu J, Gu X, Chen L, Wu Q, Li H, Bai H, Yang J and Qian J (2021) Case Report: Antiangiogenic Therapy Plus Immune Checkpoint Inhibitors Combined With Intratumoral Cryoablation for Hepatocellular Carcinoma. Front. Immunol. 12:740790. doi: 10.3389/fimmu.2021.740790

INTRODUCTION

Liver cancer is a common gastrointestinal malignancy that is associated with a poor prognosis. Currently, among all cancers, liver cancer ranks 6th for incidence and 3rd for mortality globally (1). The two main liver cancer subtypes are hepatocellular carcinoma (HCC) and intrahepatic cholangiocarcinoma, of which HCC accounts for more than 90% of primary tumors of the liver. At present, treatment methods for HCC include surgical therapy, transcatheter arterial chemoembolization (TACE), ablation therapy, molecular targeted therapy and immunotherapy (2). However, a majority of patients with HCC are detected at an advanced stage that precludes surgical treatment and for patients able to undergo surgical intervention the postoperative recurrence rate is high. This limits the application of surgical therapy and contributes to the poor clinical prognosis for HCC.

For patients with advanced HCC with extrahepatic spread, treatment is usually based around the molecular targeted therapies sorafenib and lenvatinib. In recent years, the development of immunotherapies such as immune checkpoint inhibitors have also led to great progress in the treatment of HCC (3). In particular, based on the results of the IMbrave150 trial, combination treatment with atezolizumab (an immune checkpoint inhibitor) and bevacizumab (an anti-angiogenic agent) has been approved as a first-line treatment for advanced HCC and is recommended by the National Comprehensive Cancer Network treatment guidelines in this setting (4). However, although immune checkpoint inhibitors have achieved good outcomes in HCC, the application of immunotherapy in HCC still faces many challenges such as the relatively low response rate characteristic of this class of therapy and a lack of tumor biomarkers to identify treatment-sensitive patients.

Image-guided tumor ablation (radiofrequency, microwave or cryoablation) has been applied to numerous cancers, including renal cell carcinoma, prostate cancer, lung cancer, and liver cancer with promising short-term results. However, cryoablation has several comparative advantages over radiofrequency ablation and other thermal-based ablation approaches, including the ability to produce a larger and more precise ablation area, a more clearly identifiable therapeutic area, and the ability to stimulate immune regulation to produce ectopic tumor suppressive effects (5, 6).

Here, we report the case of a patient with HCC diagnosed as the result of tumor rupture and hemorrhage who experienced a sustained survival benefit following treatment with antiangiogenic and immunotherapy combined with intratumoral cryoablation after post-surgical tumor recurrence. To our knowledge, this treatment strategy has not been previously reported.

CASE DESCRIPTION

A 38-year-old Chinese male patient presented to the hospital in March 2019 with severe abdominal pain. Computed tomography (CT) imaging indicated that the patient had a ruptured liver tumor in the lower right lobe of the liver and was experiencing bleeding. The patient had a history of chronic viral hepatitis B (HBV) with no previous antiviral therapy. His mother and brother also had a history of chronic HBV. The patient had no family history of cancer. The patient underwent an emergency liver tumor resection on March 2019. A postoperative pathological diagnosis revealed HCC with tumor thrombus in the vessel (**Figure 1A**). Hepatic arteriography was performed one month after surgery, and no tumor staining was observed in the liver. In addition, Positron Emission Tomography-CT (PET-CT) indicated no systemic metastasis after resection of the tumor in the lower right lobe of the liver. A time course of the entire case is shown in **Figure 2**.

DIAGNOSTIC ASSESSMENT

On August 26, 2019, the patient underwent routine follow-up with an enhanced magnetic resonance imaging (MRI) of the upper abdomen, which revealed multiple metastatic tumors in the liver, the larger ones were around 6.3 x 4.3 x 4.7 cm, with hepatic hilar lymph node metastasis, suggesting that the patient's Barcelona Clinic Liver Cancer (BCLC) stage was stage C (**Figure 2**). At this time, the patient's alpha fetoprotein (AFP) was 6050 ng/mL. Subsequently, the patient underwent a liver tumor puncture biopsy and next generation sequencing (NGS) was performed on the puncture sample in a College of American Pathologists accredited laboratory (GeneCast Biotechnology Co, Beijing). The test results indicated that the patient had negative programmed cell death ligand 1 (PD-L1) expression, a microsatellite status of MS-Stable, and the tumor mutation burden (TMB) was 3 Muts/Mb. The gene mutation results are summarized in **Table 1**. The patient subsequently initiated treatment with lenvatinib (12 mg/day) in combination with tegafur gimeracil oteracil potassium capsules (60mg twice daily), but he developed severe nausea and vomiting.

The patient came to our hospital in early September 2019, and at this time, the patient's alpha fetoprotein (AFP) level was 90421.42 ng/mL (**Figure 3**). Considering that the nausea and vomiting may be mainly caused by the tegafur gimeracil oteracil potassium capsule, we suggested that the patient stop taking tegafur gimeracil oteracil potassium capsules, but continue to be treated with low dose lenvatinib (8 mg/day). On September 5, we performed CT-guided intratumoral cryoablation of one large metastatic tumor in the patient's liver (other lesions and lymph nodes did not receive cryoablation). A postoperative CT scan revealed complete ablation of the tumor. On the fourth day after cryoablation, we performed a CT-guided puncture biopsy on the metastatic liver tumor that had not received cryoablation, and performed NGS testing on the tissue sample and peripheral blood plasma at GeneCast Biotechnology Co. The NGS sequencing results showed negative PD-L1 expression with MS-Stable microsatellite status and TMB of 18.67 Muts/Mb. The gene mutation results are summarized in **Table 1**. On September 11, the patient initiated treatment with lenvatinib (8 mg/day) in combination with the immune checkpoint inhibitor toripalimab (240 mg IV infusion every 3 weeks), a

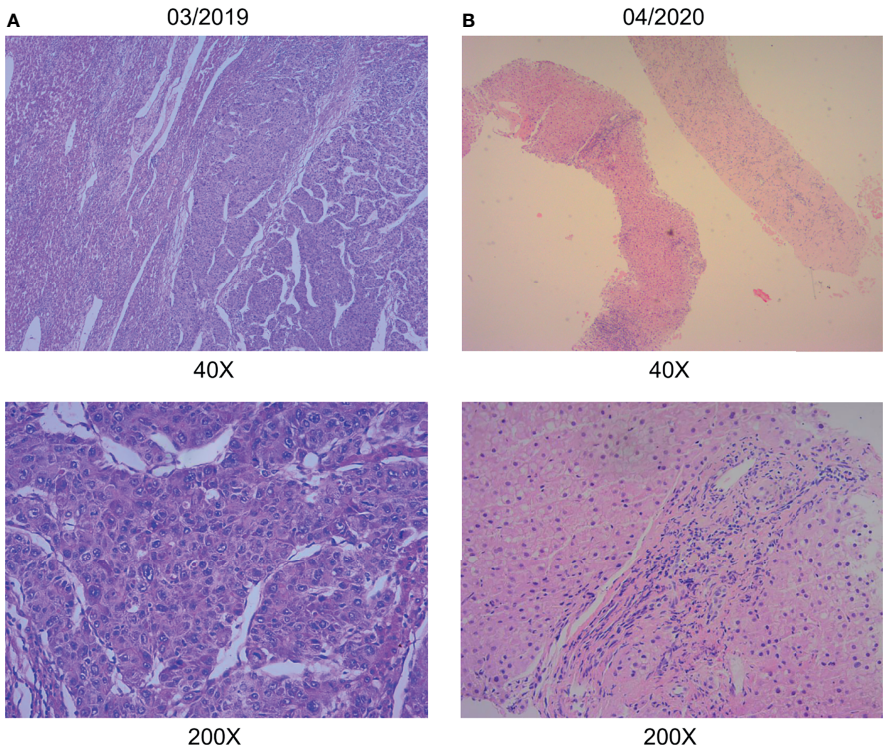

FIGURE 1 | Pathological data. **(A)** Hepatic surgery specimens showed histological characteristic of hepatocellular carcinoma. **(B)** Liver puncture specimens showed no histological characteristic of malignancy. (hematoxylin-eosin stain; original magnification 40×and 200×).

humanized monoclonal antibody targeting the programmed cell death 1 (PD-1) receptor. On October 8, the AFP of the patient dropped to 5025.00 ng/mL. An MRI of the upper abdomen indicated that after the comprehensive treatment of the liver tumors, there were multiple masses in the liver. Considering the partial survival of the tumor, the tumor necrosis was more obvious than that in the previous image.

Encouraged by these exceptional results, a decision was made to continue systemic treatment with combined lenvatinib (8 mg orally daily) and toripalimab (240 mg IV infusion every 3 weeks). In early December 2019, the patient's AFP level had dropped to 17.20 ng/mL. MRI of the upper abdomen showed multiple abnormal signals and partial abnormal enhancement in the liver. Considering most of the tumor necrosis and partial survival, the tumor volume was reduced compared with the previous images taken on 2019-10-09.

Thereafter, the patient continued lenvatinib and toripalimab. An upper abdominal MRI acquired in April 2020 revealed necrosis of the tumor and continued reductions in tumor volume. According to the modified response evaluation criteria in solid tumors (mRECIST), the patient had achieved a complete response (CR). In order to evaluate the extent of residual active tumor tissue in the liver of the patient, we conducted a puncture biopsy on the suspected active tumor under the guidance of B-ultrasound. Pathological assessment of the puncture biopsy samples revealed local hepatocyte hyperplasia with edema and degeneration, and fibrous tissue hyperplasia in some areas. No clear evidence of malignant tumor was found (**Figure 1B**). The patient has continued this combined treatment regimen until now (last treatment date July 11, 2021), and their AFP level in regular examinations has been consistently below the normal value (0-7 ng/mL). A PET-CT examination in August 2021 showed multiple nodules in the liver, decreased FDG metabolism indicating no active tumor in the liver, and no tumor metastasis in the whole body (**Supplementary Figure 1**).

During the whole treatment period, the patient had no obvious discomfort, no adverse events related to antiangiogenic therapy or immunotherapy, and their HBV replication level was well controlled.

DISCUSSION

Here, we present the case a patient with metastatic HCC who had disease recurrence following surgery and then received cryoablation followed by combined lenvatinib and toripalimab. The patient achieved a complete response after 7 months of treatment which has been sustained until the submission of this manuscript, giving a progression free survival of 24 months at the last calculation.

The tumor microenvironment is a highly heterogeneous microecosystem composed of tumor cells and their surrounding environment, which is characterized by tissue ischemia, hypoxia and low pH, and evolves with the development of tumor (7, 8).

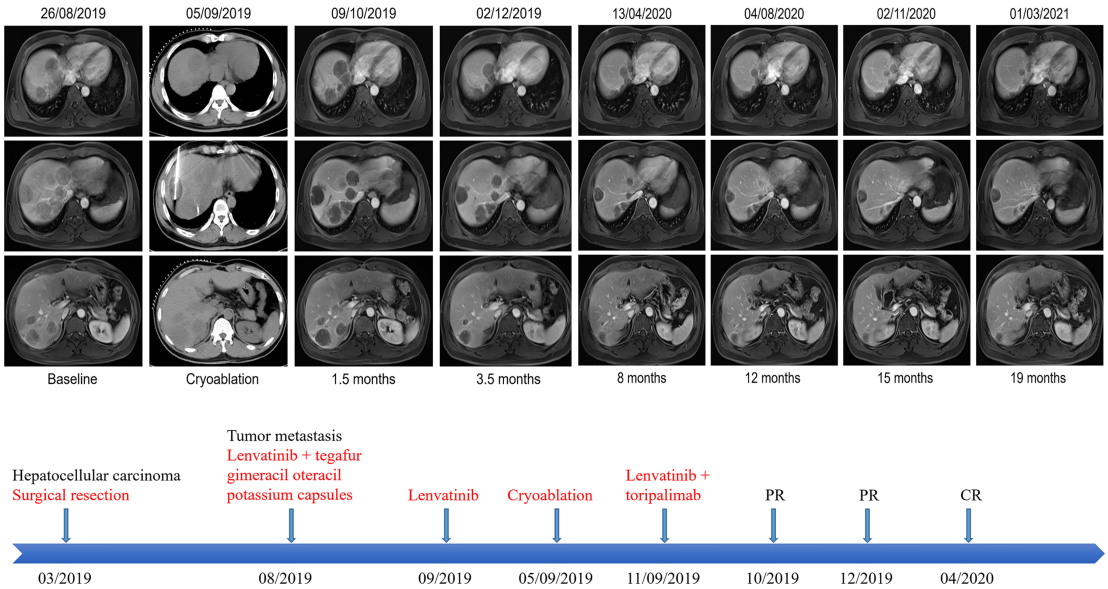

FIGURE 2 | Representative upper abdominal imaging showing changes in the liver tumor throughout the treatment period and the patient's course of treatment. After intratumoral cryoablation combined with antiangiogenic therapy plus immune checkpoint inhibitors, the patient's liver tumor was necrotic, with no obvious tumor activity, and some tumor lesions disappeared and shrank, which were evaluated as a complete response according to mRECIST.

TABLE 1 | Summary of genetic test results.

Pre-cryoablation			Post-cryoablation		
GENES	**Variations**	**Abundance**	**GENES**	**Variations**	**Abundance**
KLHL6	p.T328M	1.63%	ABCC1	p.C1479Y	0.57%
MLL2	p.L4575I	11.48%	ABCC4	p.A971T	0.55%
MLL2	p.T4110I	32.73%	AURKB	p.A329T	2.50%
MUTYH	Q253*		AXIN1	p.Q184Rfs*58	0.90%
NTRK	p.N218K	1.17%	CDK9	p.R188H	0.81%
RICTOR	amplification		CREBBP	p.R1347W	0.50%
TP53	p.R249S	5.56%	DOT1L	p.A1254T	1.13%
TSC2	loss		EGFR	p.A767V	0.54%
MSI	MS-stable		FH	p.V73M	0.53%
TMB	3 Muts/Mb		FLT3	p.G891D	1.53%
			FOXA1	p.E456G	0.54%
			GLI2	p.A43V	2.62%
			GLI2	p.R1470W	0.68%
			HGF	p.G396D	1.13%
			IRS2	p.A618V	1.61%
			KEAP1	p.Q20*	0.96%
			KMT2B	p.C1249Y	0.67%
			LZTR1	p.A512T	1.11%
			MUTYH	P.Q264*	
			NKX2-1	p.G134D	0.79%
			NOTCH4	p.P237S	0.57%
			NSD1	p.A955V	0.52%
			PARP4	p.T1170I	6.11%
			PRF1	p.G149D	0.86%
			RBM10	p.A717V	0.70%
			SLC16A7	p.L241P	3.82%
			SMARCA1	p.G889D	0.58%
			SOX9	p.A209V	0.51%
			TERT	p.A745V	0.55%
			MSI	MS-stable	
			TMB	18.67 Muts/Mb	

** stands for codon variation variation.*

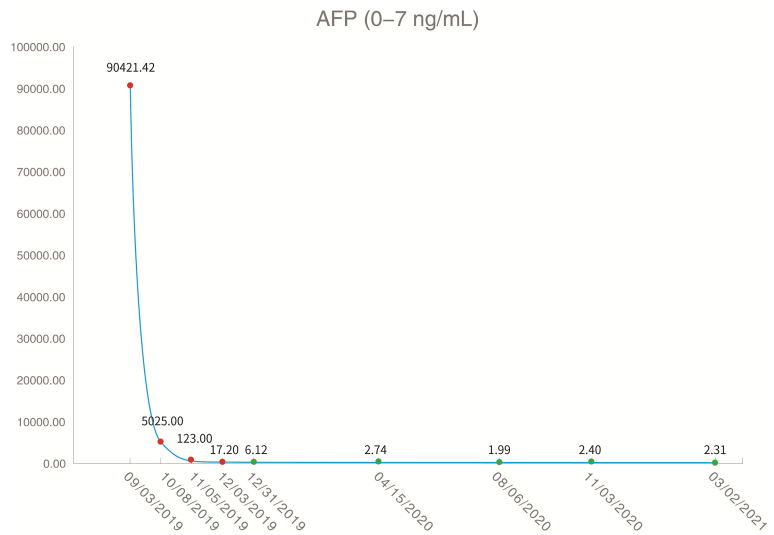

FIGURE 3 | Serum alpha fetoprotein levels throughout the treatment period (red dots indicate increased and green dots indicate normal levels).

Normalizing the tumor microenvironment to enhance anticancer therapy is currently a research topic of great interest. In particular, a large number of studies have demonstrated that antiangiogenic therapy combined with immunotherapy can normalize tumor vasculature and thus alleviate ischemia and hypoxia in the tumor microenvironment, increase the delivery of drugs and anti-tumor immune cells, and transform the tumor immunosuppressive microenvironment into an immune-supportive microenvironment (9–11). Based on the above mechanisms, anti-angiogenic therapy combined with immunotherapy (atezolizumab plus bevacizumab) has achieved breakthrough progress in the treatment of HCC, and has since been recommended as a first-line treatment for patients with advanced HCC (12). Lenvatinib is a small molecule targeted antiangiogenic agent that is approved for the first-line treatment of HCC. Toripalimab has also been shown to have excellent and durable antitumor activity against a variety of advanced or recurrent malignancies, including HBV-associated HCC (13, 14). Therefore, we treated this patient with lenvatinib combined with toripalimab with the expectation of a robust and durable therapeutic effect.

Cryoablation is a locoregional treatment for tumor lesions that is often used in patients with HCC. Studies have shown that cryoablation is safe and significantly improved local control of HCCs >2 cm in diameter compared with radiofrequency ablation and microwave ablation (15). More importantly, cryoablation can produce an abscopal effect, which is thought to affect cancer cells outside the primary ablation area. At present, the mechanism of abscopal effect in cryoablation is not clear. Cryoablation of the tumor tissue results in cell destruction by freezing. Contrary to heat-based ablative modalities, cryoablation induces tumor cell death by osmosis and necrosis. It is hypothesized that with necrosis, the intracellular contents of the cancer cells stay intact, and that these contents are mechanically similar to vaccination, where hundreds of unique tumor-derived self-antigens are released into circulation (16, 17). However, the release of tumor-derived self-antigens into the circulation alone may not be sufficient to overcome tumor immune escape. Simultaneous boosting of the immune response through the use of immune checkpoint inhibitors may therefore be the optimal treatment strategy to enable the immune system to recognize these novel circulating self-antigens. This hypothesis is supported by multiple studies showing that cryoablation can upregulate the expression of circulating PD-L1/PD-1 (18), and induce a more potent immune response compared with other local treatments such as radiofrequency ablation (19). Therefore, cryoablation combined with immune checkpoint inhibitors is considered to have a synergistic effect (20). Some preclinical and clinical evidence has shown that cryoablation combined with immunotherapy can produce synergies, generating an abscopal effect to distant lesions (21–24). However, this reaction is idealistic and is rarely observed in clinical practice. In the present case, the patient underwent NGS sequencing after cryoablation, and the results showed that the patient's TMB was significantly higher than observed following initial surgical resection, and the number of mutated genes was also significantly increased. We speculated that this may be a manifestation of novel cryoablated self-antigens formed by the intracellular contents of the cancer cells entering the circulation system after cryoablation.

There have been preliminary studies of the effect of cryoablation on the activation of the immune system, but the effect of cryoablation on tumor blood vessels is less well described. It has been reported that cryoablation of normal rat skin can stimulate local angiogenesis, but the resulting neovasculature may not be fully functional (25). Some studies have found that the expression of vascular endothelial growth factor (VEGF) is up-regulated in tumor tissue after cryoablation, and angiogenesis in residual tumor is significantly increased.

Anti-angiogenic therapy can downregulate the expression of VEGF, inhibit tumor angiogenesis, and therefore improve the inhibitory effect of cryoablation on tumors (26, 27). It is well known that in the tumor vascular system, the vascular structure is disordered, the morphology is abnormal, and the structure of vascular walls is incomplete, leading to leakage of the vascular wall, elevated interstitial fluid pressure, and elevated blood flow resistance (28). We therefore hypothesized that new blood vessels formed after cryoablation will also have these characteristics and therefore antiangiogenic therapy combined with cryoablation may also have a synergistic effect. However, the choice of dosage for antiangiogenic therapy is very important.

High-dose antiangiogenic therapy may over-prune tumor vessels, which may adversely affect the delivery of systemic therapies, while low-doses of antiangiogenic therapy can normalize tumor blood vessels, and increase the delivery of anti-tumor drugs and immune cells (29), and at the same time allow the cryoablated self-antigens to efficiently enter the circulation, thus stimulating strong tumor immunity. In addition, the order of drug administration also plays a very important role. Experiments have shown that sequential immunotherapy or chemotherapy after antiangiogenic therapy generates a vascular normalization window and has a better therapeutic effect (28, 30).

A key limitation of this case study is that the patient underwent an emergency surgical resection of HCC and may not represent the usual population of patients with HCC who undergo surgery. In summary, the patient in this case received intratumoral cryoablation after low-dose antiangiogenic therapy. We hypothesize that the normalized tumor blood vessels facilitated entry of cryoablated self-antigens into the circulation as well as promoting the formation of an immune-supportive tumor microenvironment, which was then followed by the administration of immunotherapy to the patient. The three synergistic effects of antiangiogenic therapy, intratumoral cryoablation, and immunotherapy resulted in a very positive outcome for the patient. However, the mechanism of this synergistic therapy is still unclear, and there are no clear criteria for the selection of drug dosage, sequence of drug administration and time point of cryoablation, which are worthy of further study.

PATIENT PERSPECTIVE

The written informed consent of the patient was obtained for the publication of this case report and any identifying information and images. He was happy to agree to publication of this case report in hopes of furthering medical knowledge in this area.

DATA AVAILABILITY STATEMENT

The raw data supporting the conclusions of this article will be made available by the authors, without undue reservation.

ETHICS STATEMENT

Ethical review and approval were not required for the study on human participants in accordance with the local legislation and institutional requirements. The patients/participants provided their written informed consent to participate in this study. Written informed consent was obtained from the individual(s) for the publication of any potentially identifiable images or data included in this article.

AUTHOR CONTRIBUTIONS

XL, JX, XG, and LC contributed equally to this work and are co-first authors. QW, JY, and JQ designed the study. XL and JX collected the data. XL and LC drafted the manuscript. XG, JX, and LC performed radiological data analysis and provided the imaging figures. HL and HB analyzed the data. All authors contributed to the article and approved the submitted version.

FUNDING

This work was partially supported by Genecast Cancer Research Project of Beijing CSCO Clinical Cancer Research Foundation (Y2019Genecast-074) and Natural Science Foundation of Shanghai (21ZR1463600). The funder was not involved in the study design, collection, analysis, interpretation of data, the writing of this article or the decision to submit it for publication.

ACKNOWLEDGMENTS

The authors wish to gratefully acknowledge the patient and his family for allowing us to publish his clinical case.

SUPPLEMENTARY MATERIAL

The Supplementary Material for this article can be found online at: https://www.frontiersin.org/articles/10.3389/fimmu.2021.740790/full#supplementary-material

Supplementary Figure 1 | PET-CT examination conducted in August 2021 showing multiple nodules in the liver and decreased FDG metabolism, indicating no active tumor in the liver.

REFERENCES

1. Sung H, Ferlay J, Siegel RL, Laversanne M, Soerjomataram I, Jemal A, et al. Global Cancer Statistics 2020: GLOBOCAN Estimates of Incidence and Mortality Worldwide for 36 Cancers in 185 Countries. *CA: Cancer J Clin* (2021) 71(3):209–49. doi: 10.3322/caac.21660
2. Hartke J, Johnson M, Ghabril M. The Diagnosis and Treatment of Hepatocellular Carcinoma. *Semin Diagn Pathol* (2017) 34(2):153–9. doi: 10.1053/j.semdp.2016.12.011
3. Jiang Y, Han QJ, Zhang J. Hepatocellular Carcinoma: Mechanisms of Progression and Immunotherapy. *World J Gastroenterol* (2019) 25 (25):3151–67. doi: 10.3748/wjg.v25.i25.3151

4. Finn RS, Qin S, Ikeda M, Galle PR, Ducreux M, Kim TY, et al. Atezolizumab Plus Bevacizumab in Unresectable Hepatocellular Carcinoma. *N Engl J Med* (2020) 382(20):1894–905. doi: 10.1056/NEJMoa1915745
5. Chu KF, Dupuy DE. Thermal Ablation of Tumours: Biological Mechanisms and Advances in Therapy. *Nat Rev Cancer* (2014) 14(3):199–208. doi: 10.1038/nrc3672
6. Hinshaw JL, Lee FTJr. Cryoablation for Liver Cancer. *Tech Vasc Interv Radiol* (2007) 10(1):47–57. doi: 10.1053/j.tvir.2007.08.005
7. Hanahan D, Weinberg RA. Hallmarks of Cancer: The Next Generation. *Cell* (2011) 144(5):646–74. doi: 10.1016/j.cell.2011.02.013
8. Quail DF, Joyce JA. Microenvironmental Regulation of Tumor Progression and Metastasis. *Nat Med* (2013) 19(11):1423–37. doi: 10.1038/nm.3394
9. Jain RK. Normalizing Tumor Microenvironment to Treat Cancer: Bench to Bedside to Biomarkers. *J Clin Oncol* (2013) 31(17):2205–18. doi: 10.1200/jco.2012.46.3653
10. Khan KA, Kerbel RS. Improving Immunotherapy Outcomes With Anti-Angiogenic Treatments and Vice Versa. *Nat Rev Clin Oncol* (2018) 15 (5):310–24. doi: 10.1038/nrclinonc.2018.9
11. van der Woude LL, Gorris MAJ, Halilovic A, Figdor CG, de Vries IJM. Migrating Into the Tumor: A Roadmap for T Cells. *Trends Cancer* (2017) 3 (11):797–808. doi: 10.1016/j.trecan.2017.09.006
12. Benson AB, D'Angelica MI, Abbott DE, Anaya DA, Anders R, Are C, et al. Hepatobiliary Cancers, Version 2.2021, NCCN Clinical Practice Guidelines in Oncology. *J Natl Compr Cancer Network JNCCN* (2021) 19(5):541–65. doi: 10.6004/jnccn.2021.0022
13. Chen J, Hu X, Li Q, Dai W, Cheng X, Huang W, et al. Effectiveness and Safety of Toripalimab, Camrelizumab, and Sintilimab in a Real-World Cohort of Hepatitis B Virus Associated Hepatocellular Carcinoma Patients. *Ann Trans Med* (2020) 8(18):1187. doi: 10.21037/atm-20-6063
14. Yang J, Dong L, Yang S, Han X, Han Y, Jiang S, et al. Safety and Clinical Efficacy of Toripalimab, a PD-1 mAb, in Patients With Advanced or Recurrent Malignancies in a Phase I Study. *Eur J Cancer (Oxford Engl 1990)* (2020) 130:182–92. doi: 10.1016/j.ejca.2020.01.028
15. Ei S, Hibi T, Tanabe M, Itano O, Shinoda M, Kitago M, et al. Cryoablation Provides Superior Local Control of Primary Hepatocellular Carcinomas of >2 Cm Compared With Radiofrequency Ablation and Microwave Coagulation Therapy: An Underestimated Tool in the Toolbox. *Ann Surg Oncol* (2015) 22 (4):1294–300. doi: 10.1245/s10434-014-4114-7
16. Aarts BM, Klompenhouwer EG, Rice SL, Imani F, Baetens T, Bex A, et al. Cryoablation and Immunotherapy: An Overview of Evidence on Its Synergy. *Insights Imaging* (2019) 10(1):53. doi: 10.1186/s13244-019-0727-5
17. Abdo J, Cornell DL, Mittal SK, Agrawal DK. Immunotherapy Plus Cryotherapy: Potential Augmented Abscopal Effect for Advanced Cancers. *Front Oncol* (2018) 8:85. doi: 10.3389/fonc.2018.00085
18. Zeng Z, Shi F, Zhou L, Zhang MN, Chen Y, Chang XJ, et al. Upregulation of Circulating PD-L1/PD-1 is Associated With Poor Post-Cryoablation Prognosis in Patients With HBV-Related Hepatocellular Carcinoma. *PLoS One* (2011) 6(9):e23621. doi: 10.1371/journal.pone.0023621
19. Jansen MC, van Hillegersberg R, Schoots IG, Levi M, Beek JF, Crezee H, et al. Cryoablation Induces Greater Inflammatory and Coagulative Responses Than Radiofrequency Ablation or Laser Induced Thermotherapy in a Rat Liver Model. *Surgery* (2010) 147(5):686–95. doi: 10.1016/j.surg.2009.10.053
20. Sidana A. Cancer Immunotherapy Using Tumor Cryoablation. *Immunotherapy* (2014) 6(1):85–93. doi: 10.2217/imt.13.151
21. Katzman D, Wu S, Sterman DH. Immunological Aspects of Cryoablation of Non-Small Cell Lung Cancer: A Comprehensive Review. *J Thorac Oncol* (2018) 13(5):624–35. doi: 10.1016/j.jtho.2018.01.017
22. Regen-Tuero HC, Ward RC, Sikov WM, Littrup PJ. Cryoablation and Immunotherapy for Breast Cancer: Overview and Rationale for Combined Therapy. *Radiol Imaging Cancer* (2021) 3(2):e200134. doi: 10.1148/rycan.2021200134
23. Yakkala C, Chiang CL, Kandalaft L, Denys A, Duran R. Cryoablation and Immunotherapy: An Enthralling Synergy to Confront the Tumors. *Front Immunol* (2019) 10:2283. doi: 10.3389/fimmu.2019.02283
24. Yakkala C, Denys A, Kandalaft L, Duran R. Cryoablation and Immunotherapy of Cancer. *Curr Opin Biotechnol* (2020) 65:60–4. doi: 10.1016/j.copbio.2020.01.006
25. Pimentel CB, Moraes AM, Cintra ML. Angiogenic Effects of Cryosurgery With Liquid Nitrogen on the Normal Skin of Rats, Through Morphometric Study. *An Bras Dermatol* (2014) 89(3):410–3. doi: 10.1590/abd1806-4841.20142249
26. Ma CH, Jiang R, Li JD, Wang B, Sun LW, Lv Y. Experimental Study on Residual Tumor Angiogenesis After Cryoablation. *Asian Pacific J Cancer Prev APJCP* (2014) 15(6):2491–4. doi: 10.7314/apjcp.2014.15.6.2491
27. Ma CH, Jiang R, Li JD, Wang B, Sun LW, Lv Y. Experimental Study of Endostar Injection Concomitant With Cryoablation on Lung Adenocarcinoma A549 Xenografts. *Asian Pacific J Cancer Prev APJCP* (2014) 14(11):6697–701. doi: 10.7314/apjcp.2013.14.11.6697
28. Liu M, Li H, Wang X, Jing L, Jiang P, Li Y. Experimental Study of the Vascular Normalization Window for Tumors Treated With Apatinib and the Efficacy of Sequential Chemotherapy With Apatinib in Lung Cancer-Bearing Mice and Patients. *Cancer Med* (2020) 9(8):2660–73. doi: 10.1002/cam4.2923
29. Huang Y, Yuan J, Righi E, Kamoun WS, Ancukiewicz M, Nezivar J, et al. Vascular Normalizing Doses of Antiangiogenic Treatment Reprogram the Immunosuppressive Tumor Microenvironment and Enhance Immunotherapy. *Proc Natl Acad Sci U S A* (2012) 109(43):17561–6. doi: 10.1073/pnas.1215397109
30. Farsaci B, Higgins JP, Hodge JW. Consequence of Dose Scheduling of Sunitinib on Host Immune Response Elements and Vaccine Combination Therapy. *Int J Cancer* (2012) 130(8):1948–59. doi: 10.1002/ijc.26219

Conflict of Interest: The authors declare that the research was conducted in the absence of any commercial or financial relationships that could be construed as a potential conflict of interest.

Publisher's Note: All claims expressed in this article are solely those of the authors and do not necessarily represent those of their affiliated organizations, or those of the publisher, the editors and the reviewers. Any product that may be evaluated in this article, or claim that may be made by its manufacturer, is not guaranteed or endorsed by the publisher.

Copyright © 2021 Li, Xu, Gu, Chen, Wu, Li, Bai, Yang and Qian. This is an open-access article distributed under the terms of the Creative Commons Attribution License (CC BY). The use, distribution or reproduction in other forums is permitted, provided the original author(s) and the copyright owner(s) are credited and that the original publication in this journal is cited, in accordance with accepted academic practice. No use, distribution or reproduction is permitted which does not comply with these terms.

frontiers in Immunology

REVIEW
published: 23 February 2022
doi: 10.3389/fimmu.2022.802846

The Research Progress of Antiangiogenic Therapy, Immune Therapy and Tumor Microenvironment

Haoyue Hu[1,2†], Yue Chen[3†], Songtao Tan[1†], Silin Wu[4], Yan Huang[1], Shengya Fu[1,5], Feng Luo[1] and Jun He[6*]*

[1] Lung Cancer Center, Cancer Center, State Key Laboratory of Biotherapy, West China Hospital of Sichuan University, Chengdu, China, [2] Department of Medical Oncology, Sichuan Cancer Hospital and Institute, Sichuan Cancer Center, Medicine School of University of Electronic Science and Technology, Chengdu, China, [3] Department of Pathology, Beijing Shijitan Hospital, Capital Medical University, Beijing, China, [4] School of Pharmacy, Southwest Medical University, Luzhou, China, [5] Second Department of Oncology, Sichuan Friendship Hospital, Chengdu, China, [6] Department of Oncology, The Third Hospital of Mianyang (Sichuan Mental Health Center), Mianyang, China

OPEN ACCESS

Edited by:
Alessandro Poggi,
San Martino Hospital (IRCCS), Italy

Reviewed by:
Vita Golubovskaya,
University of Oklahoma Health Sciences Center, United States
Zahid Pranjol,
University of Sussex, United Kingdom

***Correspondence:**
Feng Luo
luofeng66666@sina.com
Jun He
he-001jun@163.com

[†]These authors have contributed equally to this work

Specialty section:
This article was submitted to Cancer Immunity and Immunotherapy, a section of the journal Frontiers in Immunology

Received: 27 October 2021
Accepted: 01 February 2022
Published: 23 February 2022

Citation:
Hu H, Chen Y, Tan S, Wu S, Huang Y, Fu S, Luo F and He J (2022) The Research Progress of Antiangiogenic Therapy, Immune Therapy and Tumor Microenvironment. Front. Immunol. 13:802846. doi: 10.3389/fimmu.2022.802846

Anti-angiogenesis therapy, a promising strategy against cancer progression, is limited by drug-resistance, which could be attributed to changes within the tumor microenvironment. Studies have increasingly shown that combining anti-angiogenesis drugs with immunotherapy synergistically inhibits tumor growth and progression. Combination of anti-angiogenesis therapy and immunotherapy are well-established therapeutic options among solid tumors, such as non-small cell lung cancer, hepatic cell carcinoma, and renal cell carcinoma. However, this combination has achieved an unsatisfactory effect among some tumors, such as breast cancer, glioblastoma, and pancreatic ductal adenocarcinoma. Therefore, resistance to anti-angiogenesis agents, as well as a lack of biomarkers, remains a challenge. In this review, the current anti-angiogenesis therapies and corresponding drug-resistance, the relationship between tumor microenvironment and immunotherapy, and the latest progress on the combination of both therapeutic modalities are discussed. The aim of this review is to discuss whether the combination of anti-angiogenesis therapy and immunotherapy can exert synergistic antitumor effects, which can provide a basis to exploring new targets and developing more advanced strategies.

Keywords: antiangiogenic therapy, immune therapy, tumor microenvironment, cancer biology, progress

CURRENT STATUS OF ANTI-TUMOR ANGIOGENESIS THERAPY

In 1971, Folkman hypothesized that "neovascularization is critical for tumors growth". Since then, anti-tumor angiogenesis therapy has gained considerable attention, and is currently one of the most effective methods to treat cancer. Tumor blood vessels are fundamental for tumor growth and metastasis. Tumor angiogenesis is regulated by a variety of cytokines. The vascular endothelial growth factor (VEGF) family regulates the growth of blood vessels. In mammals, there are five

isoforms within the VEGF family, including VEGF-A, VEGF-B, VEGF-C, VEGF-D, and placental growth factor (PGF). These proteins correspond to three different tyrosine kinase receptors, known as VEGFR1, VEGFR2, and VEGFR3. Studies have demonstrated that VEGF is highly expressed in different types of tumors, including vascular endothelial growth factor receptor (VEGFR1), VEGFR2, and VEGFR3. VEGFR2 plays a significant role in angiogenesis. VEGFR2 can activate the MAPK and PI3K signal pathways, which, in turn, activates the downstream ERK1/2 or mTOR ligand, leading to tumor growth and angiogenesis (**Figure 1**). Therefore, most anti-angiogenic drugs target the VEGF signaling system (ligands, receptors, and intracellular downstream pathways). Over the past 20 years, dozens of antiangiogenic drugs have been granted approval for treatment of multiple cancer types. One meta-analysis of randomized phase II/III trials (1) showed that, compared to platinum-based chemotherapy alone, the combination of bevacizumab and chemotherapy significantly prolonged survival of previously untreated patients with advanced non-small-cell lung cancer (NSCLC) (HR = 0.90, 95% CI: 0. 81-0. 99, *P* = 20). In the phase III LUME - Lung1 trial, the combination of docetaxel and nintedanib increased the median overall survival (OS) of lung adenocarcinoma patients, who had relapsed within 9 months of first-line chemotherapy, from 7.9 months to 10. 9 months (HR = 0.75, 95% CI: 0.60- 0.92, *P* = 0. 0073) (2). In the second cohort, the combination treatment also provided a survival benefit (median OS of docetaxel + nintedanib group *vs* control group = 12.6 months *vs* 10.3 months; HR = 0.83, CI:0.70-0.99, *P* = 0. 0359). The phase III REVEL trial (3) compared the therapeutic effect of docetaxel alone, as well as in combination with ramucirumab, in advanced NSCLC patients recalcitrant to platinum-based dual-drug chemotherapy. The median survival duration of the combination treatment group was 10.5 months, while the docetaxel group was 9.9 months (HR = 0.86, 95% CI: 0.75-0.98, *P* = 0.023). Subsequently, docetaxel and ramucirumab were granted approval by both EMA and FDA for treating metastatic NSCLC.

However, anti-tumor angiogenesis therapy has shown limited efficacy, with survival benefits ranging from only a few weeks to months. On the other hand, other studies have reported tumor progression (4) during anti-angiogenesis treatment. For example, Kindler et al. (5) compared the therapeutic effect of gemcitabine alone and combined with bevacizumab on advanced pancreatic cancer patients, and found that the combination therapy did not improve OS. Similarly, a significant recurrence rate was seen among glioma patients treated with bevacizumab (6). Studies on xenograft models of melanoma or breast cancer (7) showed that sunitinib, in fact, increased metastasis and shortened the survival of the tumor-bearing mice. Recently, the China Food and Drug Administration (CFDA) approved the single agent anlotinib as a third-line treatment for patients with advanced NSCLC. Compared to placebo, anlotinib has been demonstrated to improve both progression-free survival (PFS) and overall survival (OS) in a phase III trial among patients with advanced non-small-cell lung cancer (NSCLC), despite progression of cancer after two lines of prior treatments.

THE RESISTANCE TO ANTIANGIOGENIC THERAPY

Among normal healthy human beings, angiogenic balance exists due to regulation of the vascular endothelial growth factors (VEGFs) - angiostatin and the angiogenic molecules. However, in tumors, this balance becomes converted to pro-angiogenesis. VEGFs, which play pivotal roles in wound healing and angiogenesis, consist of five members, VEGF A-E. VEGF works by binding to the vascular endothelial growth factor receptor (VEGFR), which is comprised of three tyrosine kinases. VEGA-A is up-regulated in most solid tumors, including breast cancer and

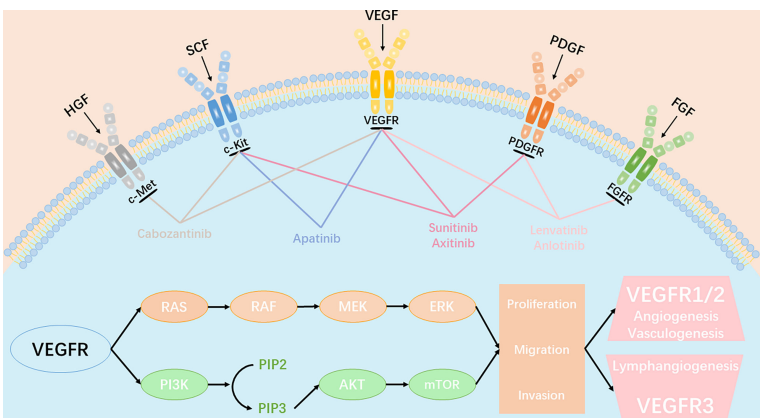

FIGURE 1 | Angiogenic signaling pathway and key anti-angiogenic targets in tumor angiogenesis. VEGFR、PDGFR、FGFR、c-kit、c-Met involved in the key molecular signal events(RAS-RAF-MEK-ERK signaling pathway and PI3K-AKT-mTOR signaling pathway) which plays a significant role in tumor proliferation, migration and invasion. All approved angiogenic tyrosine kinase inhibitors (TKIs) can target multiple receptors simultaneously and inhibit the transduction of downstream signaling.

lung cancer, which makes it a significant target of anti-angiogenesis drugs (8). The first FDA-approved anti-angiogenesis treatment was kinase inhibitors that targeted the VEGFR. Subsequently, antibodies against VEGF-Trap and VEGFR2 have been approved (9). Hepatocyte growth factor (HGF) promotes cell survival, enhances cell invasion ability, and facilitates epithelial-mesenchymal transition by activating the mesenchymal-epithelial transformation factor (c-MET) signaling pathway in endothelial cells. To date, researchers have discovered that c-MET and HGF are overexpressed in a number of tumors, which has led to abnormal gene amplification, activation of transcription or hypoxia microenvironment. Aberrant HGF/Met signaling is associated with poor prognosis in several tumor types. HGF/Met signaling stimulates several pathways, including MAPK signal pathway, which we mentioned above. PI3K signal pathway and Wnt/β-catenin pathways play significant roles in cell proliferation, survival, and angiogenesis. However, clinical efficacy of VEGF-targeted drugs has vital limitations. Although phase 3 trials have demonstrated that use of anti-angiogenic agents leads to significant improvements in overall survival (OS) for several cancers, such as advanced-stage CRC, RCC, and HCC, it is also associated with a failure to improve OS in other cancers, such as breast cancer, glioblastoma, pancreatic ductal adenocarcinoma (PDAC) and prostate cancer (10–13). Carvalho B et al. discovered that, in glioblastoma, c-Met overexpression is associated with a time-to-progression (TTP) after bevacizumab of 3 months (95% CI, 1.5–4.5), compared with a TTP of 7 months (95% CI, 4.6–9.4) among patients with low or no expression of c-Met (p = 0.05). VEGFR2 expression was associated with a TTP after bevacizumab treatment at 3 months (95% CI, 1.8–4.2) compared with a TTP at 7 months (95% CI, 5.7–8.3) among patients with no expression of VEGFR2 (p = 0.009). Concomitant c-Met/VEGFR2 overexpression was found to be associated with worse overall survival (13 months) compared to concomitant c-Met/VEGFR2 negative expression (19 months; p = 0.025). Their data indicates that c-Met and VEGFR2 overexpression play a significant role in the development of glioblastoma early resistance and may predict poorer responses to anti-angiogenic therapies (13).

Either anti-VEGFs or anti-VEGFRs or other nonspecific tyrosine kinase inhibitors ultimately shut down tumor blood supply and drive tumor necrosis. Necrosis usually occurs in the central part of the tumor, and the surrounding tumor cells remain alive as they are benefited by nutrition delivered by nearby normal blood vessels. As a result, most vascular disruptor therapy does not completely prevent tumor growth. This may be one of the reasons why antiangiogenic therapy improves therapeutic outcomes, while beneficial effects remain short (9). In addition, primary or acquired resistance contributes more to failure of anti-angiogenesis treatment. Tina Cascone used mouse-and human-specific profiling of human NSCLC xenografts in mice in order to investigate stromal and tumor cell changes that occur in tumors that acquire resistance to anti-angiogenesis treatment. Researchers found that changes in gene expression, particularly changes in expression of angiogenesis-related genes, occurred predominantly in stromal cells, but not in tumor cells. The observation reinforces the notion that tumor stroma may play an important and potentially dominant role, in at least some circumstances — in VEGF inhibitor resistance (14). Furthermore, extrinsic mechanisms have also been shown to be involved in resistance to antiangiogenic therapy, including changes in the tumor microenvironment (TME), the presence of cancer stem cells (CSCs), and tumor immunosuppression, which significantly limits their clinical value (15, 16).

TUMOR MICROENVIRONMENT AND ANTIANGIOGENIC THERAPY

The tumor microenvironment (TME) is composed of immune cells, stromal cells, extracellular matrix (ECM), blood vessels, tumor cells, lymphatic vessels and CSCs. The constant changes that occur in the various components of the TME result in its complexity and heterogeneity. TME is associated with multiple processes, including proliferation, angiogenesis, apoptosis, and immune surveillance. The stromal cells, particularly cancer-associated fibroblasts (CAFs), can promote tumor cell survival mainly by recruiting immune cells into the TME, and promote invasion by constructing a hypoxic environment. Tumor-driven hypoxia, increased inflammation, or MMPs overexpression in the TME induces alterations in the ECM, following the tumor biological behavior of evading apoptosis, elevating invasion and metastasis (17, 18). In addition, ECM components can regulate the cancer-immunity cycle. The above TME changes cause tumor progression and drug resistance (19). As tumors generally tend to be hypoxic, prolonged use of anti-angiogenesis drugs can often aggravate hypoxia (20, 21). As previously reported, the upregulation of hypoxic inducible factor 1a (HIF-1a) is also responsible for heterogeneity of breast cancer, lung cancer, cervical carcinoma, and gliomas (22–24). Hypoxia-induced upregulation of HIF-1a can mediate tumor cell de-differentiation into CSCs, which is a primary mechanism that underlies resistance to anti-angiogenesis therapy (25, 26). In addition, HIF-1a upregulates the expression of nuclear factor-kβ and leads to increased recruitment of monocytes and tumor-associated macrophages (TAMs), including polarization of the M2 phenotype TAMs, which promotes recurrence and metastasis (27). The immune system can have a dual effect in cancer biology, including pro-tumorigenic and anti-tumorigenic effect. The immune surveillance system identifies, kills, and removes tumor cells from the body. NK cells, CD8+ cytotoxic T cells and the major histocompatibility complex (MHC) class 1 molecules are known to play major roles in the function of immunosurveillance. Unsurprisingly, the host immune system is often disrupted and creates an immune imbalance among cancer patients. Tumor cells can camouflage themselves in order to hide from immune cells, thus avoiding being discovered. Numerous cellular and molecular mechanisms have been shown to be responsible for tumor evasion (28, 29). Immunosuppressive cells, such as T-regs, TAMs, and MDSCs frequently accumulate within the TME, which is associated with an

unfavorable prognosis. When there are a large number of immune cells in tumor tissues, such as T-regs, MDSCs, TAMs, and DCs, they can promote an immunosuppressive microenvironment and participate in immune escape. Anti-angiogenic therapy for VEGF or VEGF receptor-2 (VEGFR-2) can increase the transport of T cells to the tumor, thereby reducing immunosuppressive cytokines and T-regs, helping overcome resistance to the checkpoint inhibitors' medicinal properties (30) (**Figure 2**). Furthermore, tumor cells also secrete immunosuppressive cytokines, such as IL-10 and TGF-β, which are known to inhibit perforin and production by CD8+ T cells and inactivate cytotoxicity of NK cells (31–33).

Additionally, primary drug resistance due to a lack of tumor-infiltrating lymphocytes in the tumor should not be ignored. In addition to the VEGF pathway, angiogenesis can be induced by the angiopoietin (Ang1-2)/Tie-2 pathway. Studies have shown that patients that receive immunotherapy with higher Ang-2 expression tend to have poorer clinical outcomes. This suggests that the Ang-2 pathway is another cause of immunotherapy resistance (34, 35).

THE EFFICACY OF ANTI-CANCER IMMUNOTHERAPY

Under normal circumstances, the immune system can recognize and eliminate tumor cells within the tumor microenvironment. However, in order to survive, tumor cells can adopt different strategies in order to suppress the immune system and protect itself from CD8+ T cells. Immunotherapy has heralded a new era of oncotherapy and aims to either directly eliminate cancer cells or activate the host immune response. It is mediated through anti-cancer cell vaccines and antibodies, cytokines, adoptive immune cell transfer and immune checkpoint blockers (ICBs). Tumor immunotherapy is a treatment that restores the body's normal anti-tumor immune response by restarting and maintaining the tumor-immune cycle, thereby controlling and eliminating tumor cells. Tumor immunotherapy includes monoclonal antibody immune checkpoint inhibitors (36), therapeutic antibodies, cancer vaccines, cell therapy and small molecule inhibitors. In recent years, cancer immunotherapy has continued to progress. At present, this treatment method has shown strong anti-tumor activity in the treatment of solid tumors such as melanoma, NSCLC, kidney cancer, and prostate cancer. Furthermore, immunotherapy drugs have been approved by the US FDA (Food and Drug Administration) for clinical application (37). Moreover, increasing evidence has shown that overexpression of vascular growth factors can activate immunosuppressive cells directly and suppress immune effector cells to alter the immunosuppressive microenvironment.

COMBINATION OF IMMUNOTHERAPY AND ANTI-TUMOR ANGIOGENESIS

The relationship between angiogenesis and immune therapy is a complicated interplay. Anti-angiogenic agents can stimulate the immune system and improve the immunosuppressive environment, while immunotherapy can also have anti-angiogenesis effects. Therefore, there is a synergistic relationship between the two treatment methods (38, 39). Tumor cells can evade T cell-mediated killing by up-regulating the interaction of PD-L1 with the inhibitory receptor PD-1, which is expressed on tumor-infiltrating T-cells. Tumor cells can evade T cell-mediated killing by upregulating the interaction of ligands (such as PD-L1) with the inhibitory receptor PD-1, CTLA-4, and LAG-3, which are expressed on tumor-infiltrating T-cells (40). It is inevitable that patients will develop resistance to immune checkpoint inhibitors

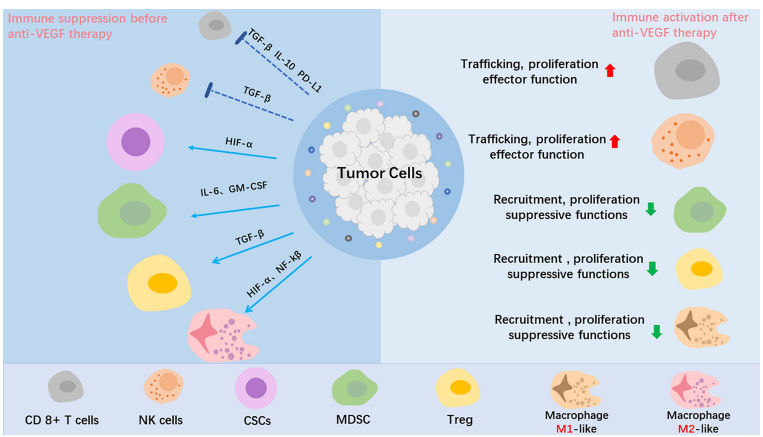

FIGURE 2 | The role of anti-VEGF treatment in the tumor microenvironment (TME). Tumor angiogenesis creates a hypoxic tumor microenvironment, which impedes T-effector cells、NK cells and DC cells infiltration into tumor, mediates tumor cell de-differentiation into CSCs, promotes proliferation of immunosuppressive cells, including Tregs and MDSCs, and polarizes TAMs to the immune inhibitory M2-like phenotype. After anti-VEGF treatment, the anti-tumor factors increase, and the pro-tumor factors are decreased. In summary, anti-VEGF treatment alleviate the immunosuppressive tumor microenvironment and improve cancer immunotherapy.

due to a lack of PD-L1 and the inhibitory effect in the TME. Facing a complex TME, the key strategy is to inhibit angiogenesis, and an effective immune response (41).

Anti-Angiogenesis Produces Vessel Normalization and Stimulates Immune Responses

The formation of blood vessels in malignant tumors is largely caused by hypoxia and the excessive secretion of VEGF. Anti-angiogenic therapy for VEGF or VEGFR-2 can increase the transport of T cells to the tumor, thereby reducing immunosuppressive cytokines and regulatory T cells, which may help overcome resistance to checkpoint inhibitors' medicinal properties (30). A case study of immune checkpoint inhibitors combined with anti-angiogenic drugs in the treatment of metastatic renal cell carcinoma demonstrated that antigen-specific T cell migration and expression of MHC-1 and PD-L1 were increased. Furthermore, anti-tumor activity was enhanced with less toxicity (42). Tumor blood vessels were found to be highly abnormal, with tumor vessels showing structural abnormalities, leading to hypoxia, acidity, and a high interstitial fluid pressure microenvironment. These microenvironmental abnormalities can affect immune cell proliferation, infiltration, survival, and function (43). Myeloid-derived suppressor cells (MDSCs) are one of the most important stromal cells of the TME, and protect tumor cells from the host immune system by suppressing T-cell function (44). There is evidence to support the hypothesis that anti-angiogenic therapy and immunotherapy act synergistically (45). GM-CSF, a potent cytokine promoting the differentiation of myeloid cells such as dendritic cells, macrophages and granulocytes, which elicits antitumor immunity by enhance tumor antigen presentation to T cells, has been proven to be effective across numerous clinical trials (46–50).

Another study has reported that binding of tumor-derived VEGF to VEGFR on CD34+ bone marrow progenitor cells reduces the differentiation of these cells into dendritic cells, thus limiting the efficacy of GM-CSF-related immunotherapy (51). And Sylvie et al. also included that human GFs *in vitro* actively inhibit the differentiation of monocyte-derived dendritic cells through the secretion of IL-6 and VEGF, limiting the immunotherapy of GM-CSF (52). Furthermore, it also promotes proliferation of immunosuppressive cells, such as Tregs and MDSCs, and inhibits DC maturation, and restricts the development of T lymphocytes from the lymphoid progenitors (30, 53–55). A study (56) on three different NSCLC animal models demonstrated that combining adoptive transfer of cytokine-induced killer (CIK) cells with recombinant human endostatin significantly inhibited angiogenesis and tumor growth, whereas neither was effective when used alone.

Blocking VEGF Induced Immune Checkpoint Expression

Lydia Meder et al. conducted an experiment on five groups on the combined use of vehicle, IgG, VEGF inhibitor, PD-L1 inhibitor, VEGF inhibitor, and PD-L1 inhibitor in a mouse model of small cell lung cancer. The results indicate that treatment with VEGF, compared to any other treatment methods, the combination of inhibitor and PD-L1 inhibitor greatly improved PFS and OS in mice (57). S. Yasuda et al. reported that in a mouse model of colon cancer, the combined use of PD-1 inhibitors and VEGFR2 inhibitors demonstrated no obvious toxicity. Compared to the control group, the experimental group drugs were found to better inhibit tumor growth. The author believes that the combined use of inhibitors can produce a synergistic anti-tumor effect in the body through a variety of mechanisms, including anti-VEGFR2 therapy resulted in a significant decrease of tumor micro vessels as well as reducing tumor vasculature and anti-PD-1 mAb treatment enhanced the infiltration of T cells into tumors. And that the two drugs are not mutually exclusive (58). Since immunotherapy has been proved to be effective against CSCs and the immunosuppressive TME, it is reasonable to surmise that a combination of anti-angiogenesis and immunotherapies would have a synergistic effect against recalcitrant tumors. Indeed, studies have shown that (38) targeting the angiogenic factor VEGF, as well as its receptors, stimulates onco-immunity, since VEGF is known to be involved in the immune escape of tumors. The VEGF signaling pathway can abrogate the effects of anti-tumor therapy *via* various mechanisms. Usually, is LFA1 that can interact on ICAM1. LFA1 is expressed on lymphocytes and it is a crucial for T cell entry into mammalian lymph nodes and tissues while ICAM1 on tumor target cells or endothelial cells (59). Previous study showed that clustering of ICAM-1 was indeed prevented by VEGF and a reduced induction of ICAM-1 and VCAM-1 mRNA transcripts by TNF in the presence of VEGF (60). VEGF can also block T-cell activation and induce apoptosis *via* the Fas/FasL pathway (61). Therefore, blocking VEGF and its receptor can help stimulate immune responses and improve immunotherapy outcomes. Studies on tumor-bearing mouse models have demonstrated that (62, 63) multi-targeted anti-angiogenic tyrosine kinase inhibitors (TKIs) increased tumor infiltration of CD8+ and CD4+ T cells by downregulating PD-1 expression, and decreased the number and activity of Tregs and MDSCs (64). Similarly, sunitinib inhibited the expansion of Tregs and MDSCs in patients with renal cell carcinoma (30, 63, 65). The VEGFR2-targeting TKI cabozantinib was also associated with a reduction in the number of Tregs and MDSCs, and simultaneously promoted tumor infiltration of CD4+ and CD8+ T lymphocytes, both alone and in combination with the anti-cancer vaccine MVA/rF-CEA/TRICOM (65). VEGFR1/R2 and soluble chimeric VEGF receptor, can bind to VEGF with high affinity and efficiently play an anti-angiogenic therapy function. In animal experiments, the combination of sVEGFR1/R2 therapy and GM-CSF–secreting tumor cell immunotherapy can remarkably prolong the survival of tumor model mice (66, 67). Similarly, the combination of cabozantinib and MVA/rF-CEA/TRICOM was found to significantly inhibit growth of MC38-CEA tumors in a mouse model (65). In a mouse model of colon cancer, anti-PD-1 monoclonal antibodies and VEGFR2 resulted in significantly greater tumor inhibition compared to either monotherapy (58).

CLINICAL USE OF ANTIANGIOGENIC DRUGS AND ICBS AGAINST TUMORS

The relationship between angiogenesis and immune therapy has been suggested to be a complicated interplay (68). Anti-angiogenic agents are known to stimulate the immune system and improve the immune suppression environment (69). Furthermore, immunotherapy can also cause anti-angiogenesis effects, and there is a synergistic relationship between the two treatment methods (39). Tumor cells can evade T cell-mediated killing by up-regulating the interaction of PD-L1 with the inhibitory receptor PD-1 that is expressed on tumor-infiltrating T cells. Thus, it is inevitable that patients develop resistance to immune checkpoint inhibitors due to a lack of PD-L1 and the inhibitory effect in the tumor microenvironment. The therapy should inhibit angiogenesis, on the other hand trigger anti-tumor immunity (41). The formation of blood vessels in malignant tumors is mainly caused by hypoxia and excessive secretion of vascular endothelial growth factor (VEGF). Recently, an accumulating number of clinical trials have been conducted to explore the efficacy of the combination of anti-angiogenesis and immunotherapy (**Table 1**).

Clinical Trials on NSCLC

In a phase 3 clinical trial IMpower150 (NCT02366143), 1202 patients with metastatic non-squamous NSCLC (ns-NSCLC) were treated with a combination of Atezolizumab to Bevacizumab-based chemotherapy, including three groups: (1) Atezolizumab, Carboplatin, and Paclitaxel (ACP); (2) Atezolizumab, Bevacizumab, Carboplatin and Paclitaxel (ABCP); (3) Bevacizumab, Carboplatin and Paclitaxel (BCP). The results demonstrated that the ABCP group had significantly improved PFS and OS, with an average of 8.3 and 19.2 months, respectively, both of which were better than the control group (70). Subgroup analysis was performed according to the status of EGFR, results of which indicated that the PFS of ABCP group (n=356) and BCP group (n=336) in EGFR wild-type (WT) population were 11.3 months and 6.8 months, respectively. Furthermore, 124/1202 EGFR-positive patients were randomized to three groups, including the ABCP (n=34), ACP (n=45), or BCP (n=45). The median OS was not estimated in the ABCP, but it was 21.4 months in the ACP group and 18.7 months in BCP group (71). In addition, patients with advanced NSCLC receiving treatment with a combination of Nivolumab and Bevacizumab were recruited for a phase 1 study (NCT01454102), which aimed to evaluate whether the combination therapy improves PFS and OS. The experimental results indicate that the combined treatment group had significant safety, and the incidence of grade 3 and above adverse reactions is low. Therefore, it has shown excellent therapeutic effects compared to the single-agent treatment group (72). The combined treatment group had a median PFS of 37.1 weeks; however, in the Nivolumab monotherapy group, the median PFS of squamous cell carcinoma was 16 weeks, and the median PFS of non-squamous cell carcinoma was 21.4 weeks. Additionally, the median OS of the combined treatment group was 86.7 weeks, which is much larger than that of the monotherapy group (73). In 2019, results of the phase 1 study (NCT02443324) were reported. Among the total 27 enrolled patients with previously treated advanced NSCLC that received Ramucirumab plus Pembrolizumab, 8 patients achieved an objective response. Results also demonstrated that the disease control rate was 86%, with a median PFS and OS of 9.7 and 26.2 months, respectively (74). Another phase 1 study (NCT02572687) indicated that the combination of Ramucirumab plus Durvalumab led to an enhancement of preliminary antitumor activity in heavy pre-treated NSCLC patients with a median PFS of 1.7 months and OS of 12.4 months (75).

Clinical Trials on RCC

A first randomized phase 2 IMmotion150 study (NCT01984242) for patients with previously untreated mRCC treated with Atezolizumab combination Bevacizumab or single Atezolizumab or single sunitinib showed that the PFS of this combination group significantly improved within the population, whatever the PD-L1 status (76). Immunotherapy with PD-1 and PD-L1 inhibitors or combined with antiangiogenic therapy (i.e. VEGF inhibitors or CTLA-4 antibodies) has become a first line therapy for advanced RCC patients (77). Nivolumab plus Ipilimumab in a phase 3 trial (NCT02231749) has provided significant benefits in untreated intermediate and poor-risk RCC patients with a higher 18-month OS rate of 75% and objective responses rate (ORR) of 42%, compared to sunitinib with 18-month OS rate of 60% and ORR of 27% (78). In 2018, an open-label, dose-finding and dose-expansion multicenter phase 1 study (NCT02493751) confirmed the disease control rate (DCR) of 78% with the security in the combination therapy of axitinib plus Avelumab in advanced RCC patients (79). Another phase 3 study (NCT02684006) validated that the combination of Avelumab plus axitinib enhanced the curative effect in patients with advanced RCC, leading to remarkable improvement in median PFS (13.8 months) and ORR (51.4%), compared to treatment with sunitinib (8.4 months and 25.7%, respectively) (80). In 2020, a pivotal phase 3 study (NCT02853331) demonstrated that Avelumab or Pembrolizumab Plus axitinib were more efficacious than sunitinib, a previous standard of care. This study recruited 861 metastatic renal cell carcinoma (mRCC) patients with results showing an improvement in PFS, a high response rate, and a low rate of intrinsic resistance (81). Recently, a phase 1b/2 study (NCT03136627) of Tivozanib combined with Nivolumab in patients with mRCC has been completed. The results demonstrated a promising antitumor efficacy with ORR of 56%, DCR of 96% and median PFS of 18.9 months (82).

Clinical Trials on HCC

Phase 1 study (NCT02942329) of the VEGFR2 inhibitor apatinib plus anti-PD1 antibody SHR-1210 in patients with advanced hepatocellular carcinoma (HCC) has demonstrated manageable toxicity and encouraged clinical activity at recommended single-agent doses of both drugs (83). A phase 1b clinical trial (NCT02715531) proved that combination of Bevacizumab and Atezolizumab profoundly improved the therapeutic effect

TABLE 1 | Principal clinical trials for the approval of antiangiogenic and or immunotherapy agents.

Drug	Indication	Phase	Pivotal study	PFS (Months)	OS (Months)	ORR	First posted	Recruitment status
Atezolizumab + Bevacizumab	NSCLC	3	NCT02366143	8.3 vs 6.8	19.2 vs 14.7	NA	2015	Completed
Bevacizumab + Nivolumab	NSCLC	1	NCT01454102	9.3 vs 4.0	21.7 vs 14.1	8.0% vs 10.0%	2011	Completed
Ramucirumab + Pembrolizumab	NSCLC	1	NCT02443324	9.7	26.2	30.0%	2015	Active, not recruiting
Ramucirumab + Durvalumab	NSCLC	1	NCT02572687	2.7	11.0	11.0%	2015	Completed
Bevacizumab + Atezolizumab	RCC	2	NCT01984242	11.7 vs 8.4 vs 6.1	NA	32.0% vs 29.0% vs 25.0%	2013	Completed
Nivolumab + Ipilimumab	RCC	3	NCT02231749	11.6 vs 8.4	NA vs 26.0	9.0% vs 1.0%	2014	Active, not recruiting
Axitinib + Avelumab	RCC	1	NCT02493751	NA	NA	27.0% vs 4.0%	2015	Completed
Axitinib + Avelumab	RCC	3	NCT02684006	13.8 vs 8.4	11.6 vs 10.7	55.2% vs 25.5%	2016	Active, not recruiting
Pembrolizumab + Axitinib	RCC	3	NCT02853331	17.1 vs. 11.1	NA	60.0% vs. 38.5%	2016	Active, not recruiting
Tivozanib + Nivolumab	RCC	1/2	NCT03136627	18.9%	NA	56.0%	2017	Completed
Apatinib + SHR-1210	HCC	1	NCT02942329	2.9	11.4	30.8%	2016	Unknown
Bevacizumab + Atezolizumab	HCC	1	NCT02715531	5.6 vs 3.4	NA	36.0%	2016	Completed
Nivolumab + Ipilimumab	HCC	1/2	NCT01658878	NA	22.8 vs 12.5 vs 12.7	32.0% vs 27.0% vs 29.0%	2012	Active, not recruiting
Lenvatinib + Pembrolizumab	HCC	1	NCT03006926	8.6	22.0	36.0%	2016	Active, not recruiting
Bevacizumab + Atezolizumab	HCC	3	NCT03434379	NA	NA	NA	2018	Active, not recruiting
Bevacizumab + Dacarbazine	Melanoma	2	NCT01164007	5.5	11.4	18.9%	2010	Completed
Bevacizumab + Ipilimumab	Melanoma	1	NCT00790010	9.0	25.1	19.6%	2008	Active, not recruiting
Axitinib + Toripalimab	Melanoma	1	NCT03086174	7.5	NA	67.5%	2017	Active, not recruiting
Bevacizumab + Atezolizumab	CRC	2	NCT0287319	4.4 vs 3.3	NA	NA	Unknown	Unknown
Bevacizumab + Nivolumab	CRC	2	NCT04072198	NA	NA	NA	2019	Recruiting

NSCLC, non-small cell lung cancer; RCC, renal cell cancer; HCC, hepatocellular carcinoma; CRC, colorectal cancer; ORR, objective responses rate; RFS, progression-free survival; OS, overall survival. NA, Not available.

compared to the standard-of-care sorafenib in a phase 3 trial with ORR and DCR of 62% and 78%, respectively. With regards to safety, the combination group demonstrated tolerable safety, with serious adverse events (AEs) rate of only 8% (84). CheckMate040 is a phase 1/2 randomized clinical trial (NCT01658878) which comprised of 148 HCC patients that were randomized 1:1:1 into three dosing arms (Nivolumab, alone or in combination with ipilimumab). These cohort results suggest that Nivolumab, plus Ipilimumab, may provide an improved ORR and OS, especially in arm A (lower dose Nivolumab and higher dose Ipilimumab), relative to anti-PD-L1 monotherapy (85). The combination of lenvatinib plus Pembrolizumab for unresectable HCC (uHCC) patients in the Phase 1b trial (NCT03006926) represented a promising antitumor activity with an ORR of 46.0%, and a median PFS of 9.3 months (86). Moreover, an ongoing double-blind randomized controlled phase 3 study (NCT03713593) of lenvatinib plus Pembrolizumab treatment of uHCC is currently being undertaken (77). Imbrave150 (NCT03434379), a randomized, multicenter phase 3 clinical study aims to evaluate the efficacy and safety of Atezolizumab plus Bevacizumab versus Sorafenib among patients with advanced HCC. The results indicated that, among 501 patients (336 in the combination group and 165 in the Sorafenib group) with HCC, the combination group showed a remarkable improvement in median PFS and OS with tolerated and controllable toxicity, compared to the Sorafenib group (87).

Clinical Trials on Melanoma and CRC

Dacarbazine in combination with Bevacizumab was studied in a phase 2 study (NCT01164007) of 40 unresectable/metastatic melanoma patients. The results from this study indicated that the treatment had an ORR of 18.9% and a median OS of 11.4 months, with no new toxicity (88). Preliminary results from the phase 1 clinical trial (NCT00790010) showed that Ipilimumab (CTLA-4 antibody) plus Bevacizumab (VEGF inhibitors) in patients with metastatic melanoma (MM) had favorable clinical outcomes, for reasons of increasing tumor vascular expression of ICAM-1 and VCAM-1 and lymphocyte infiltration in tumors (89). Another open-label phase 1b trial (NCT03086174) validated the efficacy of axitinib in combination with Toripalimab among patients with advanced melanoma with an ORR of 48.3% and a median PFS of 7.5 months (90). In addition, a phase 2 study (NCT0287319) in 133 mCRC patients also demonstrated that the addition of Atezolizumab to Bevacizumab, as well as capecitabine, improved the median

PFS of 4.4 months compared to that of 3.3 months in the modified intent-to-treat analysis (mITT) analysis group (91). Another open-label, multicenter phase 2 trial (NCT04072198) of FOLFOXIRI/Bevacizumab, in association with Nivolumab, was conducted in patients with mCRC. The results demonstrated that the combination was generally well tolerated, with an acceptable toxicity profile without any unexpected findings (92).

FUTURE PROSPECTS

Anti-tumor angiogenesis was found to be favorable to T-cell infiltration and drug delivery to the tumor, thereby enhancing the efficacy of immunotherapy. Additionally, immunotherapy can also increase tumor vascular normalization and form positive feedback to anti-angiogenesis. Therefore, the combination of anti-angiogenic agents and immunotherapy provides a new therapeutic approach for tumor patients. A large number of studies have demonstrated that the combination therapy has good clinical application prospects. However, the relationship between tumor angiogenesis and immune response is intricate, and some tough problems still need to be solved for future practical application.

Firstly, there is no way to identify tumor patients that can benefit from combination therapy (93), and anti-angiogenesis therapy has a lack of biomarkers, as mentioned above. In order to address the problem, oncologists have to identify the biomarkers that can be associated with patient groups that would be advantaged with this therapy. Secondly, the dose of each drug, the optimal sequence, and the time of the combination also remain significant. The high or low dose, simultaneous or sequential treatment, will have an effect on the efficacy of the combination therapy. Furthermore, studies have demonstrated that high doses of anti-angiogenic drugs can directly damage tumor blood vessels, which results in more serious disturbances of tumor microenvironment, such as hypoxia and immunosuppression (94). Therefore, it is necessary to choose the appropriate drug dosage, and optimize the schedule of tumor immunotherapy and anti-angiogenesis therapy in order to obtain improved anticancer efficacy. Moreover, the most frequent side effect of anti-angiogenic is hypertension (95). Therefore, primary or acquired resistance, including non-upregulation VEGF in tumors, changes in the TME, the presence of CSCs, and the patient with hypertension contribute to anti-angiogenesis failure (16). Besides, resistance to immunotherapy, including lack of tumor-infiltrating lymphocytes in the tumor, accumulating immunosuppressive cells in the TME and secreting immunosuppressive cytokines in the tumor cells, contributes significantly to failure of immunotherapy.

AUTHOR CONTRIBUTIONS

FL and JH contributed to the study design. HH and YC were responsible for data collection. ST, YH, and SF drafted and prepared the manuscript. SW worked for the table and figures. All authors participated in the data interpretation and contributed to the manuscript writing with important intellectual input. All authors approved the final version of the manuscript.

REFERENCES

1. Soria J-C, Mauguen A, Reck M, Sandler A, Saijo N, Johnson D, et al. Systematic Review and Meta-Analysis of Randomised, Phase Ii/Iii Trials Adding Bevacizumab to Platinum-Based Chemotherapy as First-Line Treatment in Patients With Advanced Non-Small-Cell Lung Cancer. *Ann Oncol* (2012) 24(1):20–30. doi: 10.1093/annonc/mds590
2. Reck M, Kaiser R, Mellemgaard A, Douillard J, Orlov S, Krzakowski M, et al. Docetaxel Plus Nintedanib Versus Docetaxel Plus Placebo in Patients With Previously Treated Non-Small-Cell Lung Cancer (Lume-Lung 1): A Phase 3, Double-Blind, Randomised Controlled Trial. *Lancet Oncol* (2014) 15(2):143–55. doi: 10.1016/s1470-2045(13)70586-2
3. Garon EB, Ciuleanu T-E, Arrieta O, Prabhash K, Syrigos KN, Goksel T, et al. Ramucirumab Plus Docetaxel Versus Placebo Plus Docetaxel for Second-Line Treatment of Stage Iv Non-Small-Cell Lung Cancer After Disease Progression on Platinum-Based Therapy (Revel): A Multicentre, Double-Blind, Randomised Phase 3 Trial. *Lancet* (2014) 384(9944):665–73. doi: 10.1016/S0140-6736(14)60845-X
4. Pàez-Ribes M, Allen E, Hudock J, Takeda T, Okuyama H, Viñals F, et al. Antiangiogenic Therapy Elicits Malignant Progression of Tumors to Increased Local Invasion and Distant Metastasis. *Cancer Cell* (2009) 15 (3):220–31. doi: 10.1016/j.ccr.2009.01.027
5. Kindler HL, Niedzwiecki D, Hollis D, Sutherland S, Schrag D, Hurwitz H, et al. Gemcitabine Plus Bevacizumab Compared With Gemcitabine Plus Placebo in Patients With Advanced Pancreatic Cancer: Phase III Trial of the Cancer and Leukemia Group B (Calgb 80303). *J Clin Oncol* (2010) 28 (22):3617. doi: 10.1200/JCO.2010.28.1386
6. Keunen O, Johansson M, Oudin A, Sanzey M, Rahim SAA, Fack F, et al. Anti-Vegf Treatment Reduces Blood Supply and Increases Tumor Cell Invasion in Glioblastoma. *Proc Natl Acad Sci* (2011) 108(9):3749–54. doi: 10.1073/pnas.1014480108
7. Ebos JM, Lee CR, Cruz-Munoz W, Bjarnason GA, Christensen JG, Kerbel RS. Accelerated Metastasis After Short-Term Treatment With a Potent Inhibitor of Tumor Angiogenesis. *Cancer Cell* (2009) 15(3):232–9. doi: 10.1016/j.ccr.2009.01.021
8. Ramadan W, Zaher D, Altaie A, Talaat I, Elmoselhi A. Potential Therapeutic Strategies for Lung and Breast Cancers Through Understanding the Anti-Angiogenesis Resistance Mechanisms. *Int J Mol Sci* (2020) 21(2):565. doi: 10.3390/ijms21020565
9. Missiaen R, Mazzone M, Bergers G. The Reciprocal Function and Regulation of Tumor Vessels and Immune Cells Offers New Therapeutic Opportunities in Cancer. *Semin Cancer Biol* (2018) 52:107–16. doi: 10.1016/j.semcancer.2018.06.002
10. Craven K, Gore J, Korc M. Overview of Pre-Clinical and Clinical Studies Targeting Angiogenesis in Pancreatic Ductal Adenocarcinoma. *Cancer Lett* (2016) 381(1):201–10. doi: 10.1016/j.canlet.2015.11.047
11. Ioannidou E, Moschetta M, Shah S, Parker J, Ozturk M, Pappas-Gogos G, et al. Angiogenesis and Anti-Angiogenic Treatment in Prostate Cancer: Mechanisms of Action and Molecular Targets. *Int J Mol Sci* (2021) 22 (18):9926. doi: 10.3390/ijms22189926
12. Kerbel R. Reappraising Antiangiogenic Therapy for Breast Cancer. *Breast (Edinburgh Scotland)* (2011) 20 Suppl 3(0 3):S56–60. doi: 10.1016/s0960-9776(11)70295-8
13. Ahir B, Engelhard H, Lakka S. Tumor Development and Angiogenesis in Adult Brain Tumor: Glioblastoma. *Mol Neurobiol* (2020) 57(5):2461–78. doi: 10.1007/s12035-020-01892-8
14. Cascone T, Herynk M, Xu L, Du Z, Kadara H, Nilsson M, et al. Upregulated Stromal Egfr and Vascular Remodeling in Mouse Xenograft Models of

Angiogenesis Inhibitor-Resistant Human Lung Adenocarcinoma. *J Clin Invest* (2011) 121(4):1313–28. doi: 10.1172/jci42405
15. Huijbers E, van Beijnum J, Thijssen V, Sabrkhany S, Nowak-Sliwinska P, Griffioen A. Role of the Tumor Stroma in Resistance to Anti-Angiogenic Therapy. *Drug Resist Updat: Rev Comment Antimicrob Anticancer Chemother* (2016) 25:26–37. doi: 10.1016/j.drup.2016.02.002
16. Chandra A, Rick J, Yagnik G, Aghi MK. Autophagy as a Mechanism for Anti-Angiogenic Therapy Resistance. *Semin Cancer Biol* (2020) 66:75–88. doi: 10.1016/j.semcancer.2019.08.031
17. Li C, Teixeira A, Zhu H, Ten Dijke P. Cancer Associated-Fibroblast-Derived Exosomes in Cancer Progression. *Mol Cancer* (2021) 20(1):154. doi: 10.1186/s12943-021-01463-y
18. Mao X, Xu J, Wang W, Liang C, Hua J, Liu J, et al. Crosstalk Between Cancer-Associated Fibroblasts and Immune Cells in the Tumor Microenvironment: New Findings and Future Perspectives. *Mol Cancer* (2021) 20(1):131. doi: 10.1186/s12943-021-01428-1
19. Deepak K, Vempati R, Nagaraju G, Dasari V, Nagini S, Rao D, et al. S NTumor Microenvironment: Challenges and Opportunities in Targeting Metastasis of Triple Negative Breast Cancer. *Pharmacol Res* (2020) 153:104683. doi: 10.1016/j.phrs.2020.104683
20. Zhang H, Wang Z, Peng Q, Liu Y-Y, Zhang W, Wu L, et al. Tumor Refractoriness to Endostatin Anti-Angiogenesis Is Associated With the Recruitment of Cd11b+ Gr1+ Myeloid Cells and Inflammatory Cytokines. *Tumori J* (2013) 99(6):723–33. doi: 10.1700/1390.15462
21. Wang Z, Li Z, Wang Y, Cao D, Wang X, Jiang M, et al. Versican Silencing Improves the Antitumor Efficacy of Endostatin by Alleviating Its Induced Inflammatory and Immunosuppressive Changes in the Tumor Microenvironment. *Oncol Rep* (2015) 33(6):2981–91. doi: 10.3892/or.2015.3903
22. Wang L, Wang J, Li Z, Liu Y, Jiang M, Li Y, et al. Silencing Stem Cell Factor Attenuates Stemness and Inhibits Migration of Cancer Stem Cells Derived From Lewis Lung Carcinoma Cells. *Tumor Biol* (2016) 37(6):7213–27. doi: 10.1007/s13277-015-4577-6
23. Wang L, Guo H, Lin C, Yang L, Wang X. Enrichment and Characterization of Cancer Stem–Like Cells From a Cervical Cancer Cell Line. *Mol Med Rep* (2014) 9(6):2117–23. doi: 10.3892/mmr.2014.2063
24. Lin C, Wang L, Wang H, Yang L, Guo H, Wang X. Tanshinone Iia Inhibits Breast Cancer Stem Cells Growth *In Vitro* and *In Vivo* Through Attenuation of Il-6/Stat3/Nf-Kb Signaling Pathways. *J Cell Biochem* (2013) 114(9):2061–70. doi: 10.1002/jcb.24553
25. Cao L, Fan X, Jing W, Liang Y, Chen R, Liu Y, et al. Osteopontin Promotes a Cancer Stem Cell-Like Phenotype in Hepatocellular Carcinoma Cells *Via* an Integrin–Nf-κb–Hif-1α Pathway. *Oncotarget* (2015) 6(9):6627. doi: 10.18632/oncotarget.3113
26. Santoyo-Ramos P, Likhatcheva M, García-Zepeda EA, Castañeda-Patlán MC, Robles-Flores M. Hypoxia-Inducible Factors Modulate the Stemness and Malignancy of Colon Cancer Cells by Playing Opposite Roles in Canonical Wnt Signaling. *PloS One* (2014) 9(11):e112580. doi: 10.1371/journal.pone.0112580
27. Zhang L, Huang R, Shen Y, Liu J, Wu Y, Jin J, et al. Viaenhanced Anti-Tumor Efficacy by Inhibiting Hif-1α to Reprogram Tams Core-Satellite Upconverting Nanoparticles With Curcumin Mediated Photodynamic Therapy. *Biomater Sci* (2021) 9:6403–15. doi: 10.1039/d1bm00675d
28. Zahavi D, Weiner L. Tumor Mechanisms of Resistance to Immune Attack. *Prog Mol Biol Trans Sci* (2019) 164:61–100. doi: 10.1016/bs.pmbts.2019.03.009
29. Whiteside T. Immune Suppression in Cancer: Effects on Immune Cells, Mechanisms and Future Therapeutic Intervention. *Semin Cancer Biol* (2006) 16(1):3–15. doi: 10.1016/j.semcancer.2005.07.008
30. Finke JH, Rini B, Ireland J, Rayman P, Richmond A, Golshayan A, et al. Sunitinib Reverses Type-1 Immune Suppression and Decreases T-Regulatory Cells in Renal Cell Carcinoma Patients. *Clin Cancer Res* (2008) 14(20):6674–82. doi: 10.1158/1078-0432.CCR-07-5212
31. Noguera-Troise I, Daly C, Papadopoulos NJ, Coetzee S, Boland P, Gale NW, et al. Blockade of Dll4 Inhibits Tumour Growth by Promoting Non-Productive Angiogenesis. *Nature* (2006) 444(7122):1032. doi: 10.1038/nature05355
32. Welford AF, Biziato D, Coffelt SB, Nucera S, Fisher M, Pucci F, et al. Tie2-Expressing Macrophages Limit the Therapeutic Efficacy of the Vascular-Disrupting Agent Combretastatin A4 Phosphate in Mice. *J Clin Invest* (2011) 121(5):1969–73. doi: 10.1172/JCI44562
33. Huang J, Soffer SZ, Kim ES, McCrudden KW, Huang J, New T, et al. Vascular Remodeling Marks Tumors That Recur During Chronic Suppression of Angiogenesis11nih U10 Ca13539-27, Subcontract 6641 (Jk), Nih 1 R01 Ca08895101-A1 (Dy), Pediatric Cancer Foundation, and Sorkin Gift Fund. Note: J. Huang and Sz Soffer Contributed Equally to This Work. *Mol Cancer Res* (2004) 2(1):36–42.
34. Wu X, Giobbie-Hurder A, Liao X, Connelly C, Connolly E, Li J, et al. Angiopoietin-2 as a Biomarker and Target for Immune Checkpoint Therapy. *Cancer Immunol Res* (2017) 5(1):17–28. doi: 10.1158/2326-6066.Cir-16-0206
35. Schmittnaegel M, Rigamonti N, Kadioglu E, Cassará A, Wyser Rmili C, Kiialainen A, et al. Dual Angiopoietin-2 and Vegfa Inhibition Elicits Antitumor Immunity That Is Enhanced by Pd-1 Checkpoint Blockade. *Sci Trans Med* (2017) 9(385):eaak9670. doi: 10.1126/scitranslmed.aak9670
36. Tobias J, Steinberger P, Drinić M, Wiedermann U. Emerging Targets for Anticancer Vaccination: Pd-1. *ESMO Open* (2021) 6(5):100278. doi: 10.1016/j.esmoop.2021.100278
37. Shin C, Kim S, Jo Y. Extending Traditional Antibody Therapies: Novel Discoveries in Immunotherapy and Clinical Applications. *Mol Ther Oncolytics* (2021) 22:166–79. doi: 10.1016/j.omto.2021.08.005
38. Ohm J, Carbone D. Vegf as a Mediator of Tumor-Associated Immunodeficiency. *Immunol Res* (2001) 23:263–72. doi: 10.1385/ir:23:2-3:263
39. Garber K. Promising Early Results for Immunotherapy-Antiangiogenesis Combination. *J Natl Cancer Inst* (2014) 106(11):dju392. doi: 10.1093/jnci/dju392
40. Woo S, Turnis M, Goldberg M, Bankoti J, Selby M, Nirschl C, et al. Immune Inhibitory Molecules Lag-3 and Pd-1 Synergistically Regulate T-Cell Function to Promote Tumoral Immune Escape. *Cancer Res* (2012) 72(4):917–27. doi: 10.1158/0008-5472.Can-11-1620
41. De Palma M, Biziato D, Petrova TV. Microenvironmental Regulation of Tumour Angiogenesis. *Nat Rev Cancer* (2017) 17(8):457–74. doi: 10.1038/nrc.2017.51
42. Wallin J, Bendell J, Funke R, Sznol M, Korski K, Jones S, et al. Atezolizumab in Combination With Bevacizumab Enhances Antigen-Specific T-Cell Migration in Metastatic Renal Cell Carcinoma. *Nat Commun* (2016) 7:12624. doi: 10.1038/ncomms12624
43. Huang Y, Goel S, Duda D, Fukumura D, Jain R. Vascular Normalization as an Emerging Strategy to Enhance Cancer Immunotherapy. *Cancer Res* (2013) 73(10):2943–8. doi: 10.1158/0008-5472.Can-12-4354
44. Hinshaw D, Shevde L. The Tumor Microenvironment Innately Modulates Cancer Progression. *Cancer Res* (2019) 79(18):4557–66. doi: 10.1158/0008-5472.Can-18-3962
45. Khan K, Kerbel R. Improving Immunotherapy Outcomes With Anti-Angiogenic Treatments and Vice Versa. *Nat Rev Clin Oncol* (2018) 15(5):310–24. doi: 10.1038/nrclinonc.2018.9
46. Soiffer R, Hodi F, Haluska F, Jung K, Gillessen S, Singer S, et al. Vaccination With Irradiated, Autologous Melanoma Cells Engineered to Secrete Granulocyte-Macrophage Colony-Stimulating Factor by Adenoviral-Mediated Gene Transfer Augments Antitumor Immunity in Patients With Metastatic Melanoma. *J Clin Oncol: Off J Am Soc Clin Oncol* (2003) 21(17):3343–50. doi: 10.1200/jco.2003.07.005
47. Dranoff G, Jaffee E, Lazenby A, Golumbek P, Levitsky H, Brose K, et al. Vaccination With Irradiated Tumor Cells Engineered to Secrete Murine Granulocyte-Macrophage Colony-Stimulating Factor Stimulates Potent, Specific, and Long-Lasting Anti-Tumor Immunity. *Proc Natl Acad Sci USA* (1993) 90(8):3539–43. doi: 10.1073/pnas.90.8.3539
48. Jaffee E, Hruban R, Biedrzycki B, Laheru D, Schepers K, Sauter P, et al. Novel Allogeneic Granulocyte-Macrophage Colony-Stimulating Factor-Secreting Tumor Vaccine for Pancreatic Cancer: A Phase I Trial of Safety and Immune Activation. *J Clin Oncol: Off J Am Soc Clin Oncol* (2001) 19(1):145–56. doi: 10.1200/jco.2001.19.1.145
49. Nemunaitis J. Gvax (Gmcsf Gene Modified Tumor Vaccine) in Advanced Stage Non Small Cell Lung Cancer. *J Control Release: Off J Control Release Soc* (2003) 91:225–31. doi: 10.1016/s0168-3659(03)00210-4
50. Salgia R, Lynch T, Skarin A, Lucca J, Lynch C, Jung K, et al. Vaccination With Irradiated Autologous Tumor Cells Engineered to Secrete Granulocyte-

Macrophage Colony-Stimulating Factor Augments Antitumor Immunity in Some Patients With Metastatic Non-Small-Cell Lung Carcinoma. *J Clin Oncol: Off J Am Soc Clin Oncol* (2003) 21(4):624–30. doi: 10.1200/jco.2003.03.091

51. Dikov M, Ohm J, Ray N, Tchekneva E, Burlison J, Moghanaki D, et al. Differential Roles of Vascular Endothelial Growth Factor Receptors 1 and 2 in Dendritic Cell Differentiation. *J Immunol (Baltimore Md: 1950)* (2005) 174 (1):215–22. doi: 10.4049/jimmunol.174.1.215
52. Séguier S, Tartour E, Guérin C, Couty L, Lemitre M, Lallement L, et al. Inhibition of the Differentiation of Monocyte-Derived Dendritic Cells by Human Gingival Fibroblasts. *PloS One* (2013) 8(8):e70937. doi: 10.1371/journal.pone.0070937
53. Gabrilovich D, Ishida T, Oyama T, Ran S, Kravtsov V, Nadaf S, et al. Vascular Endothelial Growth Factor Inhibits the Development of Dendritic Cells and Dramatically Affects the Differentiation of Multiple Hematopoietic Lineages in Vivo: Presented in Part at the Keystone Symposium "Cellular and Molecular Biology of Dendritic Cells", Santa Fe, Nm, March 3-9, 1998, and at the Annual Meeting of the American Association for Cancer Research, March 28-April 1, 1998. *Blood* (1998) 92(11):4150–66. doi: 10.1182/blood.v92.11.4150
54. Gabrilovich DI, Chen HL, Girgis KR, Cunningham HT, Meny GM, Nadaf S, et al. Production of Vascular Endothelial Growth Factor by Human Tumors Inhibits the Functional Maturation of Dendritic Cells. *Nat Med* (1996) 2 (10):1096. doi: 10.1038/nm1096-1096
55. Ohm JE, Gabrilovich DI, Sempowski GD, Kisseleva E, Parman KS, Nadaf S, et al. Vegf Inhibits T-Cell Development and May Contribute to Tumor-Induced Immune Suppression. *Blood* (2003) 101(12):4878–86. doi: 10.1182/blood-2002-07-1956
56. Shi S, Wang R, Chen Y, Song H, Chen L, Huang G. Combining Antiangiogenic Therapy With Adoptive Cell Immunotherapy Exerts Better Antitumor Effects in Non-Small Cell Lung Cancer Models. *PloS One* (2013) 8 (6):e65757. doi: 10.1371/journal.pone.0065757
57. Meder L, Schuldt P, Thelen M, Schmitt A, Dietlein F, Klein S, et al. Combined Vegf and Pd-L1 Blockade Displays Synergistic Treatment Effects in an Autochthonous Mouse Model of Small Cell Lung Cancer. *Cancer Res* (2018) 78(15):4270–81. doi: 10.1158/0008-5472.Can-17-2176
58. Yasuda S, Sho M, Yamato I, Yoshiji H, Wakatsuki K, Nishiwada S, et al. Simultaneous Blockade of Programmed Death 1 and Vascular Endothelial Growth Factor Receptor 2 (Vegfr2) Induces Synergistic Anti-Tumour Effect in Vivo. *Clin Exp Immunol* (2013) 172(3):500–6. doi: 10.1111/cei.12069
59. Gérard A, Cope A, Kemper C, Alon R, Köchl R. Lfa-1 in T Cell Priming, Differentiation, and Effector Functions. *Trends Immunol* (2021) 42(8):706–22. doi: 10.1016/j.it.2021.06.004
60. Bouzin C, Brouet A, De Vriese J, DeWever J, Feron O. Effects of Vascular Endothelial Growth Factor on the Lymphocyte-Endothelium Interactions: Identification of Caveolin-1 and Nitric Oxide as Control Points of Endothelial Cell Anergy. *J Immunol* (2007) 178(3):1505–11. doi: 10.4049/jimmunol.178.3.1505
61. Motz GT, Santoro SP, Wang L-P, Garrabrant T, Lastra RR, Hagemann IS, et al. Tumor Endothelium Fasl Establishes a Selective Immune Barrier Promoting Tolerance in Tumors. *Nat Med* (2014) 20(6):607. doi: 10.1038/nm.3541
62. Ko JS, Zea AH, Rini BI, Ireland JL, Elson P, Cohen P, et al. Sunitinib Mediates Reversal of Myeloid-Derived Suppressor Cell Accumulation in Renal Cell Carcinoma Patients. *Clin Cancer Res* (2009) 15(6):2148–57. doi: 10.1158/1078-0432.CCR-08-1332
63. Voron T, Colussi O, Marcheteau E, Pernot S, Nizard M, Pointet A-L, et al. Vegf-A Modulates Expression of Inhibitory Checkpoints on Cd8+ T Cells in Tumors. *J Exp Med* (2015) 212(2):139–48. doi: 10.1084/jem.20140559
64. Terme M, Pernot S, Marcheteau E, Sandoval F, Benhamouda N, Colussi O, et al. Vegfa-Vegfr Pathway Blockade Inhibits Tumor-Induced Regulatory T-Cell Proliferation in Colorectal Cancer. *Cancer Res* (2013) 73(2):539–49. doi: 10.1158/0008-5472.CAN-12-2325
65. Kwilas AR, Ardiani A, Donahue RN, Aftab DT, Hodge JW. Dual Effects of a Targeted Small-Molecule Inhibitor (Cabozantinib) on Immune-Mediated Killing of Tumor Cells and Immune Tumor Microenvironment Permissiveness When Combined With a Cancer Vaccine. *J Trans Med* (2014) 12(1):294. doi: 10.1186/s12967-014-0294-y
66. Li B, Lalani A, Harding T, Luan B, Koprivnikar K, Huan Tu G, et al. Vascular Endothelial Growth Factor Blockade Reduces Intratumoral Regulatory T Cells and Enhances the Efficacy of a Gm-Csf-Secreting Cancer Immunotherapy. *Clin Cancer Res: An Off J Am Assoc Cancer Res* (2006) 12(22):6808–16. doi: 10.1158/1078-0432.Ccr-06-1558
67. Holash J, Davis S, Papadopoulos N, Croll S, Ho L, Russell M, et al. Vegf-Trap: A Vegf Blocker With Potent Antitumor Effects. *Proc Natl Acad Sci USA* (2002) 99(17):11393–8. doi: 10.1073/pnas.172398299
68. Mortara L, Benest A, Bates D, Noonan D. Can the Co-Dependence of the Immune System and Angiogenesis Facilitate Pharmacological Targeting of Tumours? *Curr Opin Pharmacol* (2017) 35:66–74. doi: 10.1016/j.coph.2017.05.009
69. Wu J, Zhao X, Sun Q, Jiang Y, Zhang W, Luo J, et al. Synergic Effect of Pd-1 Blockade and Endostar on the Pi3k/Akt/Mtor-Mediated Autophagy and Angiogenesis in Lewis Lung Carcinoma Mouse Model. *Biomed Pharmacother = Biomed Pharmacother* (2020) 125:109746. doi: 10.1016/j.biopha.2019.109746
70. Socinski MA, Jotte RM, Cappuzzo F, Orlandi F, Stroyakovskiy D, Nogami N, et al. Atezolizumab for First-Line Treatment of Metastatic Nonsquamous Nsclc. *N Engl J Med* (2018) 378(24):2288–301. doi: 10.1056/NEJMoa1716948
71. Reck M, Mok TSK, Nishio M, Jotte RM, Cappuzzo F, Orlandi F, et al. Atezolizumab Plus Bevacizumab and Chemotherapy in Non-Small-Cell Lung Cancer (Impower150): Key Subgroup Analyses of Patients With Egfr Mutations or Baseline Liver Metastases in a Randomised, Open-Label Phase 3 Trial. *Lancet Respir Med* (2019) 7(5):387–401. doi: 10.1016/s2213-2600(19)30084-0
72. Hellmann M, Rizvi N, Goldman J, Gettinger S, Borghaei H, Brahmer J, et al. Nivolumab Plus Ipilimumab as First-Line Treatment for Advanced Non-Small-Cell Lung Cancer (Checkmate 012): Results of an Open-Label, Phase 1, Multicohort Study. *Lancet Oncol* (2017) 18(1):31–41. doi: 10.1016/s1470-2045(16)30624-6
73. Rizvi N, Antonia S. F Shepherd. Nivolumab (Anti-Pd-1; Bms-936558, Ono-4538) Maintenance as Monotherapy or in Combination With Bevacizumab (Bev) for Non-Small Cell Lung Cancer (Nsclc) Previously Treated With Chemotherapy: Metastatic Non-Small Cell Lung Cancer. *Int J Radiat Oncol• Biol• Phys* (2014) 90(5):S32. doi: 10.1016/j.ijrobp.2014.08.206
74. Herbst RS, Arkenau H-T, Santana-Davila R, Calvo E, Paz-Ares L, Cassier PA, et al. Ramucirumab Plus Pembrolizumab in Patients With Previously Treated Advanced Non-Small-Cell Lung Cancer, Gastro-Oesophageal Cancer, or Urothelial Carcinomas (Jvdf): A Multicohort, Non-Randomised, Open-Label, Phase 1a/B Trial. *Lancet Oncol* (2019) 20(8):1109–23. doi: 10.1016/s1470-2045(19)30458-9
75. Bang YJ, Golan T, Dahan L, Fu S, Moreno V, Park K, et al. Ramucirumab and Durvalumab for Previously Treated, Advanced Non-Small-Cell Lung Cancer, Gastric/Gastro-Oesophageal Junction Adenocarcinoma, or Hepatocellular Carcinoma: An Open-Label, Phase Ia/B Study (Jvdj). *Eur J Cancer* (2020) 137:272–84. doi: 10.1016/j.ejca.2020.06.007
76. McDermott DF, Huseni MA, Atkins MB, Motzer RJ, Rini BI, Escudier B, et al. Clinical Activity and Molecular Correlates of Response to Atezolizumab Alone or in Combination With Bevacizumab Versus Sunitinib in Renal Cell Carcinoma. *Nat Med* (2018) 24(6):749–57. doi: 10.1038/s41591-018-0053-3
77. Chambers A, Kundranda M, Rao S, Mahmoud F, Niu J. Anti-Angiogenesis Revisited: Combination With Immunotherapy in Solid Tumors. *Curr Oncol Rep* (2021) 23(9):100. doi: 10.1007/s11912-021-01099-7
78. Motzer RJ, Tannir NM, McDermott DF, Aren Frontera O, Melichar B, Choueiri TK, et al. Nivolumab Plus Ipilimumab Versus Sunitinib in Advanced Renal-Cell Carcinoma. *N Engl J Med* (2018) 378(14):1277–90. doi: 10.1056/NEJMoa1712126
79. Choueiri TK, Larkin J, Oya M, Thistlethwaite F, Martignoni M, Nathan P, et al. Preliminary Results for Avelumab Plus Axitinib as First-Line Therapy in Patients With Advanced Clear-Cell Renal-Cell Carcinoma (Javelin Renal 100): An Open-Label, Dose-Finding and Dose-Expansion, Phase 1b Trial. *Lancet Oncol* (2018) 19(4):451–60. doi: 10.1016/s1470-2045(18)30107-4
80. Motzer RJ, Penkov K, Haanen J, Rini B, Albiges L, Campbell MT, et al. Avelumab Plus Axitinib Versus Sunitinib for Advanced Renal-Cell Carcinoma. *N Engl J Med* (2019) 380(12):1103–15. doi: 10.1056/NEJMoa1816047
81. Grimm MO, Leucht K, Grunwald V, Foller S. New First Line Treatment Options of Clear Cell Renal Cell Cancer Patients With Pd-1 or Pd-L1

Immune-Checkpoint Inhibitor-Based Combination Therapies. *J Clin Med* (2020) 9(2):565. doi: 10.3390/jcm9020565
82. Albiges L, Barthelemy P, Gross-Goupil M, Negrier S, Needle MN, Escudier B. Tinivo: Safety and Efficacy of Tivozanib-Nivolumab Combination Therapy in Patients With Metastatic Renal Cell Carcinoma. *Ann Oncol* (2021) 32(1):97–102. doi: 10.1016/j.annonc.2020.09.021
83. Xu J, Zhang Y, Jia R, Yue C, Chang L, Liu R, et al. Anti-Pd-1 Antibody Shr-1210 Combined With Apatinib for Advanced Hepatocellular Carcinoma, Gastric, or Esophagogastric Junction Cancer: An Open-Label, Dose Escalation and Expansion Study. *Clin Cancer Res* (2019) 25(2):515–23. doi: 10.1158/1078-0432.CCR-18-2484
84. Lee MS, Ryoo B-Y, Hsu C-H, Numata K, Stein S, Verret W, et al. Atezolizumab With or Without Bevacizumab in Unresectable Hepatocellular Carcinoma (Go30140): An Open-Label, Multicentre, Phase 1b Study. *Lancet Oncol* (2020) 21(6):808–20. doi: 10.1016/s1470-2045(20)30156-x
85. Yau T, Kang YK, Kim TY, El-Khoueiry AB, Santoro A, Sangro B, et al. Efficacy and Safety of Nivolumab Plus Ipilimumab in Patients With Advanced Hepatocellular Carcinoma Previously Treated With Sorafenib: The Checkmate 040 Randomized Clinical Trial. *JAMA Oncol* (2020) 6(11): e204564. doi: 10.1001/jamaoncol.2020.4564
86. Finn RS, Ikeda M, Zhu AX, Sung MW, Baron AD. Phase Ib Study of Lenvatinib Plus Pembrolizumab in Patients With Unresectable Hepatocellular Carcinoma. *J Clin Oncol* (2020) 38(26):2960–70. doi: 10.1200/JCO.20.00808
87. Galle PR, Finn RS, Qin S, Ikeda M, Zhu AX, Kim T-Y, et al. Patient-Reported Outcomes With Atezolizumab Plus Bevacizumab Versus Sorafenib in Patients With Unresectable Hepatocellular Carcinoma (Imbrave150): An Open-Label, Randomised, Phase 3 Trial. *Lancet Oncol* (2021) 22(7):991–1001. doi: 10.1016/s1470-2045(21)00151-0
88. Ferrucci PF, Minchella I, Mosconi M, Gandini S, Verrecchia F, Cocorocchio E, et al. Dacarbazine in Combination With Bevacizumab for the Treatment of Unresectable/Metastatic Melanoma: A Phase II Study. *Melanoma Res* (2015) 25(3):239–45. doi: 10.1097/CMR.0000000000000146
89. Wu X, Giobbie-Hurder A, Liao X, Lawrence D, McDermott D, Zhou J, et al. Vegf Neutralization Plus Ctla-4 Blockade Alters Soluble and Cellular Factors Associated With Enhancing Lymphocyte Infiltration and Humoral Recognition in Melanoma. *Cancer Immunol Res* (2016) 4(10):858–68. doi: 10.1158/2326-6066.CIR-16-0084
90. Sheng X, Yan X, Chi Z, Si L, Cui C, Tang B. Axitinib in Combination With Toripalimab, a Humanized Immunoglobulin G 4 Monoclonal Antibody Against Programmed Cell Death-1, in Patients With Metastatic Mucosal Melanoma: An Open-Label Phase Ib Trial. *J Clin Oncol* (2019) 37(32):2987–99. doi: 10.1200/JCO.19
91. Mettu NB, Twohy E, Ou F-S, Halfdanarson TR, Lenz HJ, Breakstone R. Bacci: A Phase Ii Randomized, Double-Blind, Multicenter, Placebocontrolled Study of Capecitabine (C) Bevacizumab (B) Plus Atezolizumab (a) or Placebo (P) in Refractory Metastatic Colorectal Cancer (Mcrc): An Accru Network Study. *Ann Oncol* (2019) 30(Supplement 5):203. doi: 10.1093/annonc/mdz246.011
92. Damato A, Berselli A, Iachetta F, Romagnani A, Larocca M, Arias AG. Preliminary Safety Analysis of Phase Ii Open-Label Nivacor Trial (Goirc-03-2018) in Patients With Advanced Colorectal Cancer Ras or Braf Mutated. *J Clin Oncol* (2021) 39:37. doi: 10.1200/jco.2021.39.3_suppl.37
93. Ramjiawan RR, Griffioen AW, Duda DG. Anti-Angiogenesis for Cancer Revisited: Is There a Role for Combinations With Immunotherapy? *Angiogenesis* (2017) 20(2):185–204. doi: 10.1007/s10456-017-9552-y
94. Jain RK. Antiangiogenesis Strategies Revisited: From Starving Tumors to Alleviating Hypoxia. *Cancer Cell* (2014) 26(5):605–22. doi: 10.1016/j.ccell.2014.10.006
95. des Guetz G, Uzzan B, Chouahnia K, Morère J. Cardiovascular Toxicity of Anti-Angiogenic Drugs. *Target Oncol* (2011) 6(4):197–202. doi: 10.1007/s11523-011-0204-7

Conflict of Interest: The authors declare that the research was conducted in the absence of any commercial or financial relationships that could be construed as a potential conflict of interest.

Publisher's Note: All claims expressed in this article are solely those of the authors and do not necessarily represent those of their affiliated organizations, or those of the publisher, the editors and the reviewers. Any product that may be evaluated in this article, or claim that may be made by its manufacturer, is not guaranteed or endorsed by the publisher.

Copyright © 2022 Hu, Chen, Tan, Wu, Huang, Fu, Luo and He. This is an open-access article distributed under the terms of the Creative Commons Attribution License (CC BY). The use, distribution or reproduction in other forums is permitted, provided the original author(s) and the copyright owner(s) are credited and that the original publication in this journal is cited, in accordance with accepted academic practice. No use, distribution or reproduction is permitted which does not comply with these terms.

frontiers | Frontiers in Immunology

PERSPECTIVE
published: 12 May 2022
doi: 10.3389/fimmu.2022.892543

On the Prognostic Power of Tumor-Infiltrating Lymphocytes – A Critical Commentary

Zeev Elkoshi *

Research and Development Department, Taro Pharmaceutical Industries Ltd, Haifa, Israel

Tumor-infiltrating lymphocytes are extensively used as prognostic biomarkers in cancer. Regulatory T cells (Tregs) or CD8+ T cells frequencies in tumor site, or their ratio, are the most common markers used to assess prognosis. This work offers a possible explanation for the opposite correlations between intra-tumoral Tregs and survival, associated with different types of cancer. The complexity involved with the selection of a preferred marker, including the effect of variability, is presented and discussed. The lymphocytes frequency ratio is proposed as the marker of choice in most types of cancer. The ratio correlates directly with survival, irrespective of cancer type and is also less variable than the frequencies of each of the two lymphocytes, if these frequencies correlate with each other in the tumor microenvironment. However, if the frequency of one of the two lymphocytes is highly variable, abandoning the ratio in favor of the lymphocyte with less variable frequency will improve correlation with survival, especially when the intra-tumoral frequencies of the two species are inversely correlated. It is plausible, that the best prognostic marker selected this way, will be also be the best predictor of checkpoint inhibitor therapy success.

Keywords: tumor-infiltrating lymphocytes, regulatory T cells, CD8+ T cells, cancer prognosis, CD8/Treg, Treg

OPEN ACCESS

Edited by:
Alexandr Bazhin, LMU Munich University Hospital, Germany

Reviewed by:
Rainer Christoph Miksch, Ludwig Maximilian University of Munich, Germany

***Correspondence:**
Zeev Elkoshi
zeev.elkoshi@gmail.com

Specialty section:
This article was submitted to Cancer Immunity and Immunotherapy, a section of the journal Frontiers in Immunology

Received: *09 March 2022*
Accepted: *11 April 2022*
Published: *12 May 2022*

Citation:
Elkoshi Z (2022) On the Prognostic Power of Tumor-Infiltrating Lymphocytes – A Critical Commentary. Front. Immunol. 13:892543. doi: 10.3389/fimmu.2022.892543

INTRODUCTION

Tumor-infiltrating lymphocytes can affect cancer progression. Tumor-infiltrating lymphocytes may generally be classified as tumor-suppressive or tumor-promoting lymphocytes.

Cytotoxic CD8+ T cells play a major role in sustaining anti-cancer immunity by attacking cancer cells directly (through FAS-mediated apoptosis and perforin-mediated cytolysis) (1). Within the tumor microenvironment (TME), regulatory T cells (Tregs) are the major tumor-suppressive lymphocytes (2). Regulatory T cells suppress the anti-cancer activities of CD8+ T cells and of CD4+ T cells and dendritic cells (DCs) that mediate CD8+ T cell activation. Diverse contact-dependent and cytokine-mediated mechanisms are employed by Tregs for this purpose, as thoroughly reviewed by Han et al. (3). For example, perforin and granzyme expressed by Tregs in the TME (but not by naïve Tregs) trigger lysis of effector T cells (and of NK cells) (4). In addition, CD39 and CD73 expressed on Treg cells catalyze adenosine generation which suppresses the anti-tumor function of other T cells (5). It is not surprising therefore, that CD8+ and regulatory T cells are vastly used as markers for cancer prognosis. This commentary provides a possible explanation for the opposite correlations between intra-tumoral Tregs and survival, affiliated with different types of cancer.

It also proposes simple rules for the selection of preferred prognostic biomarkers, considering the variability in frequency and function of intra-tumoral lymphocytes.

INTRA-TUMOR ACCUMULATION OF Tregs MAY CORRELATE WITH A BETTER OR WORSE PROGNOSIS, DEPENDING ON CANCER TYPE. A POSSIBLE EXPLANATION

Shang et al. performed a meta-analysis to assess the prognostic value of Tregs (FoxP3+ T cells) across different types of cancer (6). Seventeen types of cancer and 15,512 cancer cases were analyzed. Using intra-tumoral Tregs as a marker, and a 95% confidence interval, cervical cancer, lung cancer, renal cancer, ovarian cancer, hepatocellular carcinoma, melanoma, and pancreatic cancer, positively correlated with a shorter survival while colorectal cancer, head and neck cancer, endometrial cancer, and esophageal cancer correlated with a longer survival compared to cancer-specific mean values.

The present work proposes an explanation for the direct or inverse correlations of intra-tumoral Tregs with survival, observed in different cancer types. The clue for this puzzle lies in the opposite effects of CD8+ T cells and Tregs on cancer growth, coupled with different penetration rates of the two lymphocytes into the TME. In some types of cancer, impairment of CD8+ T cell anti-cancer activity in the TME also affects the relation between Tregs accumulation in tumor and cancer prognosis.

Suppose that intra-tumoral cell frequencies of CD8+ T cells and Tregs correlate directly with each other. Suppose that Treg frequency is used as a marker. Any increase in intra-tumoral Treg cell number will be associated with an increase in CD8+ cell number. Since CD8+ T cells have a positive effect on survival, prognosis will be better than expected if the two frequencies were independent of each other. Accordingly, the hazard ratio (HR) will be smaller than expected if correlation between the frequencies is not assumed.

Consider the opposite scenario, when intra-tumor frequencies of the two lymphocytes inversely correlate with each other. Suppose that Treg frequency is used as a marker. Any increase in intra-tumoral Treg cell number will be associated with a decrease in CD8+ cell number. Since CD8+ T cells have a positive effect on survival, prognosis will be worse than expected if the two lymphocytes were independent of each other. The hazard ratio (HR) in this case will be larger than expected if correlation between the frequencies is not assumed.

Inspecting published experimental data, it seems that the effect of intra-tumoral Tregs on CD8+ tumor infiltration depends on the specific type of cancer. As will be demonstrated below, in cancer types presenting HR < 1, an increased intra-tumoral Tregs is involved with an increased infiltration of CD8+ T cells. On the other hand, in many cancer types presenting HR>1, an increased intra-tumoral Tregs is involved with a decreased infiltration of CD8+ T. In line with this, in several types of cancer with HR >1, CD8+/Treg frequency ratio is reduced at higher tumor grades. In addition, in several cancer types with HR > 1, an impaired cytotoxic function of CD8+ T cells has been reported. Each of these properties contributes to the effect of intra-tumoral Tregs on survival. The examples below illustrate these points.

Hazard Ratio < 1

Colorectal Cancer (CRC)

Sideras et al. reported a positive (though not statistically significant) effect of tumor penetration by FoxP3 cells on survival of CRC patients with liver metastases, after metastatectomy. At the same time, the intra-tumoral CD8/FoxP3 cell ratio was an independent positive predictor of survival (7). Similar results were observed by Suzuki et al. (8). Assuming a pro-cancer role for Tregs and an anti-cancer role for CD8+ T cells, such an event is possible only if the two lymphocytes infiltrate simultaneously into the tumor, where the positive effect of CD8+ T cells overweighs the negative effect of FoxP3+ T cells on cancer prognosis. In accordance with this, several works demonstrated a positive correlation between the frequencies of intra-tumoral CD8+ T cell and Tregs in colorectal cancer (9–12). In addition, CD8+ T cell densities at high tumor stages were similar to these at lower tumor stages (the difference was statistically non-significant), while Treg cell densities at high tumor stages were statistically significantly lower compared to lower stages (T_{3+4} vs. T_{1+2}; $P = 0.007$) (11). This behavior however did not repeat using the AJCC staging system. At AJCC stage III, both CD8+ and Treg densities were reduced compared to their values at AJCC stage II, but the reduction in CD8+ T cell density was larger (11).

Head and Neck Cancer

Echarti et al. compared lymphocyte densities in head and neck tumor tissue samples with different degrees of lymphocyte infiltration (13). The authors noticed that CD8+ and FoxP3+ T cells infiltration occurred simultaneously. However, the CD8+/FoxP3 frequency ratio was higher in tumor epithelia than in stroma indicating a higher influx of CD8+ cells than Tregs into tumor epithelia. This difference in flow rate may contribute to the beneficial effect of intra-tumoral Tregs on the prognosis of head and neck carcinoma.

Hypopharyngeal Squamous Cell Carcinoma (HSCC)

Wang et al. noticed a beneficial effect of both tumor-infiltrating Tregs and of the CD8/FoxP3 density ratio on the survival of HSCC patients (14).The simultaneous validity of these two observations can hold only if the positive effect of CD8+ T cells overweighs the negative effect of Tregs on prognosis, considering the opposite effects of the two lymphocytes on tumor growth.

Ovarian Cancer (Advanced Stage)

In advanced stage ovarian cancer, the presence of CD8+ cells, FoxP3+Treg or a high CD8/FoxP3 frequency ratio in tumor tissue was associated with an increased disease specific survival (15).

Similarly, disease-specific survival was positively associated with the markers CD8 and FoxP3 in high-grade serous tumors from optimally debulked patients (16). These scenarios can hold only if the beneficial effect of tumor-infiltrated CD8+ T cells on patients survival, more than compensate for the detrimental effect of tumor-infiltrating Tregs on survival.

Hazard Ratio > 1

Lung Cancer

An inverse correlation between CD8+ T cells and Tregs intra-tumor frequencies was reported in lung adenocarcinoma tumors, whereby CD8+ T cell frequency reduced while Tregs frequency increased at the tumor site compared to non-involved lung tissue (17). Jackute et al. reported an increase in both CD8+ cells and Tregs numbers in non-small cell lung cancer tumors, in comparison to controls, but the increase in Treg cells number was double the increase in the number of CD8+ T cells (18). In a mouse model of pulmonary adenocarcinoma, Tregs accumulated over the time in tumor tissues and induced tumor growth, while CD8+ T cells restrained this growth (19). In addition, Tregs were elevated in the circulation of patients with untreated extensive stage small cell lung cancer, compared to healthy controls. These circulating Tregs negatively correlated with the percentage of proliferative CD8+ T cells in peripheral blood (20).

Renal Cell Carcinoma (RCC)

Using specimens collected from RCC patients, Kawashima et al. performed RNA sequencing of both CD8+ T cells and CD4+ T cells based on the expression patterns of PD-1 and TIM-3 in tumor and adjacent normal tissue. Among these T cells, a sub-population of regulatory CD4+ T cells (Tregs) and a subpopulation of *exhausted* CD8+ T cellswere identified. These two subpopulations accumulated more in high-grade RCC tumors than in low-grade tumors (21). It turns out that RCC high-grade tumors are infiltrated more by Tregs and less by active (unexhausted) CD8+ T cells than low-grade tumors.

Endometrial Cancer

The infiltration of CD8+ T cells and Tregs into endometrial cancer tumors was evaluated by Yamagami et al. using immunohistochemistry. Both CD8+ and Treg cell counts as well as the Treg/CD8+ count ratio increased with higher tumor grades, implying a larger increase in Treg frequency compared to CD8+ frequency at higher tumor grades. Disease free survival (DFS) was shorter in patients with high Treg counts or a high Treg/CD8 count ratio (22) [in opposite to the pooled analysis by Shang et al. (6)]. In addition, it was reported that endometrial cancer cells suppressed CD8+ T cell cytotoxicity (23). This effect counteracts the effect of the increased number of CD8+ T cells and further explains the association between high tumor infiltration by Treg cells and shorter survival of endometrial cancer patients.

Cervical Cancer

In a study including 115 cervical cancer patients, the mean frequencies of both, CD8+ T cells and Tregs, increased considerably in tumor tissue compared to cervical tissues excised from women with no cervical abnormalities. However, the increase in Tregs frequency was double the increase in CD8+ frequency. In this study, both, low FoxP3 frequency and high CD8+/FoxP3 frequency ratio in tumor tissue correlated with a longer survival (24). A study by Shah et al. confirmed the negative effect of high intra-tumoral Tregs on the survival of cervical cancer patients (25). The higher influx of Tregs into tumor tissue compared to that of CD8+ cells may explain the negative correlation between high intra-tumoral Tregs and survival in cervical cancer.

Ovarian Cancer

Adams et al. found that high frequency of intra-tumoral FoxP3+ T cells in ovarian adenocarcinoma specimens was statistically significantly associated with diminished long-term survival. They noticed that patients who had tumors with a high frequency of intraepithelial CD8+ cells and a low frequency of FoxP3+ T cells had a 5-year survival rate of 64.3%, while patients with high frequency of intraepithelial CD8+ T cells and high frequency of FoxP3+ T cells had a much lower survival rate of 32.1% (26). It is clear that here, the negative effect of intra-tumoral Tregs on patients survival, overcomes the positive effect of CD8+ T cells. As aforementioned, in *advanced* ovarian cancer, intra-tumoral high Tregs frequency is associated with *improved* survival. A change in the relative tumor penetration rates of CD8+ T cells and Tregs, between advanced and early cancers, may be the cause for this discrepancy. Such a change, however, is not documented in the literature.

Hepatocellular Carcinoma (HCC)

In a pooled analysis of HCC studies, high intra-tumoral infiltration of Tregs was associated with a mean HR value of 1.894 (95% CI: 1.658 – 2.164) for overall survival, while high infiltration of CD8+ T cells was associated with a mean HR value of 0.676 (95% CI: 0.540 – 0.845) for overall survival (27). An increased frequency of Tregs together with a decreased frequency of CD8+ T cells was observed in HCC tumor regions (relative to healthy tissue) (28, 29). In addition, higher histologic grades of HCC tumors were associated with a higher FoxP3/CD8 frequency ratio (30). An impairment of intra-tumoral CD8+ cell cytotoxic function by HCC intra-tumoral Tregs was also reported (28).The association between high infiltration of Tregs on the one hand, and low infiltration of CD8+ cells on the other hand, coupled with a decreased activity of intra-tumoral CD8+ cells, contribute to the positive correlation between high intra-tumoral Tregs and poor survival in HCC.

Pancreatic Cancer

Two meta-analyses have shown a high negative impact of intra-tumoral Tregs on the prognosis of pancreatic cancer (6, 31). The relative numbers of intra-tumoral CD4+CD25+Foxp3+ Tregs and CD8+ T cells were negatively correlated in pancreatic ductal adenocarcinoma (32).

These results are summarized in **Table 1**.

TABLE 1 | Hazard ratios associated with Tregs infiltration and the related lymphocyte frequencies in the TME.

Cancer Type	HR associated with high tumor infiltration by Tregs	Reference	Intra-tumoral CD8+ T cells	Intra-tumoral Treg cells	References
Colorectal cancer	HR < 1	(6)(*)	CD8+ and Treg tumor frequencies are positively correlated. CD8+ effect overweighs Tregs effect.	CD8+ and Treg tumor frequenciesare positively correlated. CD8+ effect overweighs Tregs effect.	(7–12)
Colorectal cancer	HR < 1	(6)(*)	Intra-tumoral CD8+ density is independent of tumor stage	Intra-tumoral Treg density is lower at higher tumor stages	(11)
Head and neck cancer	HR < 1	(6)(*)	Tumor frequencies of CD8+ and Tregs are positively correlated. CD8+ effect overweighs the effect of Tregs.CD8+/Treg frequency ratio is higher in tumor epithelia than in stroma	Tumor frequencies of CD8+ and Tregs are positively correlated. CD8+ effect overweighs the effect of Tregs. CD8+/Treg frequency ratio is higher in tumor epithelia than in stroma	(13, 14)
Ovarian cancer (advanced stage)	HR < 1	(15, 16)	Both CD8+ and Tregs infiltrate into tumor simultaneously. CD8+ effect overweighsTregs effect	CD8+ and Tregs infiltrate into tumor simultaneously. CD8+ effect overweighs Tregs effect	(15, 16)
Ovarian cancer	HR > 1	(26)	Intra-tumoral Tregs effect overweighs intra-tumoral CD8+ effect	Intra-tumoral Tregs effect overweighs intra-tumoral CD8+ effect	(26)
Lung cancer	HR > 1	(6)(*)	Intra-tumoral CD8+ frequency is lower relative to normal tissue	Intra-tumoral Treg frequency is higher relative to normal tissue	(17)
Lung cancer	HR > 1	(6)(*)	Intra-tumor Tregs number is higher than CD8+ number (both are higher compared to normal tissue)	Intra-tumor Treg number is higher than CD8+ number (both are higher compared to normal tissue)	(18)
Lung cancer	HR > 1	(6)(*)	Percentage of proliferative *circulating* CD8+ inversely correlate with *circulating* Tregs	*Circulating* Tregs elevated and inversely correlate with percentage of proliferative *circulating* CD8+	(20)
Renal cell carcinoma	HR > 1	(6)(*)	Active CD8+ frequency is lower in high-grade tumors	Treg frequency is higher in high-grade tumors	(21)
Endometrial cancer	HR > 1	(22)	CD8+ frequency increases but less than Treg frequency at higher tumor grades. Endometrial cancer cells suppress CD8+ activity	Treg frequency increases more than CD8+ frequency at higher tumor grades	(22, 23)
Cervical cancer	HR > 1	(24, 25)	Both CD8+ and Treg frequencies increase in tumor compared to normal tissue. CD8+ increase is half the increase in Tregs frequency	Both CD8+ and Treg frequencies increase in tumor compared to normal tissue.Treg frequency increase is double the increase in CD8+ frequency	(24)
Hepatocellular carcinoma	HR > 1	(27)(*)	CD8+ frequency in tumor is reduced and CD8+ function is impaired. CD8+/Treg frequency ratio is lower at higher tumor grades	Tregs frequency in tumor is increased. CD8+/Treg frequency ratio is lower at higher tumor grades	(28–30)
Pancreatic cancer	HR > 1	(6)(*) (31)(*)	Intra-tumoral CD8+ and Treg numbers were negatively correlated	Intra-tumoral CD8+ and Treg numbers were negatively correlated	(32)

HR, hazard ratio (mortality hazard associated with Tregs infiltration into the TME, compared to cancer-specific mean values).
(*)The reference presents mean values obtained by a pooled analysis of the variables.

TUMOR-INFILTRATING CD8+ T CELLS, Treg CELLS OR CD8+/Treg RATIO: WHICH IS THE PREFERRED PROGNOSTIC MARKER?

Selecting the best prognostic marker is important not only for improving cancer prognosis. A better prognostic marker may better correlate with the response to checkpoint inhibitor therapy.

By the earlier discussion, it is clear that survival is a function of both intra-tumoral lymphocytes, Tregs and CD8+ cells. However, due to the opposite effects of these two lymphocytes on survival, it seems that the frequency ratio would better correlate with survival, than the frequency of each of the single species. In addition, the use of the CD8/Treg frequency ratio as a marker is expected to correlate directly with cancer prognosis, *irrespective* of cancer type or stage, unlike a prognosis based on a the frequency of CD8+ cells or Tregs.

However, more confounding factors are involved in the process of selecting the "the best" marker. In particular, it should be realized that the addition of any extra variable may affect variability. In fact, when x and y are two correlated random variables, the variance (σ) of {x/y}can be approximated by (33):

$$\sigma(x/y) \sim \left(\mu_x^2/\mu_y^2\right)\left\{\sigma_x^2/\mu_x^2 - 2\mathrm{Cov}(x,y)/\mu_x\mu_y + \sigma_y^2/\mu_y^2\right\} \quad (1)$$

Where: σ = variance; Cov = covariance; μ = arithmetic mean;

By eq. 1, when x and y directly correlate with each other (Cov> 0), the variance of {x/y} is lower compared to the variance involved with independent (uncorrelated) variables (Cov=0), assuming fixed μ_x, μ_y, σ_x, σ_y values. Under the same assumption, when x and y are inversely correlated (Cov< 0), the variance of {x/y}is higher compared to the variance involved with independent variables.

Thus, the prognostic power of the ratio is inherently poorer when CD8+ cell and Treg frequencies are inversely correlated, compared to a situation when they are directly correlated, assuming all other variables in eq. 1 are fixed.

When HR decreases with a higher Tregs intra-tumoral frequency, the two lymphocytes intra-tumoral frequencies necessarily correlate directly with each other (Cov>1).

TABLE 2 | A summary table of (a) mortality hazard ratios associated with the use of different intra-tumoral markers; (b) the preferred markers under different relationships between lymphocyte-related variances.

	Tregs	CD8+/Tregs	CD8+
frequencies inversely correlate with each other	HR > 1	HR < 1	HR < 1
frequencies directly correlate with each other {TIR(CD8) >TIR(Treg)}	HR < 1	HR < 1	HR < 1
frequencies directly correlate with each other {TIR(CD8) <TIR(Treg)}	HR > 1	HR < 1	HR > 1
σ_{CD8} and σ_{Treg} are of comparable size, or are unknown	–	preferred	–
$\sigma_{CD8}>>\sigma_{Treg}$	preferred	–	–
$\sigma_{CD8}<<\sigma_{Treg}$	–	–	preferred

TIR(X), tumor infiltration rate (X); σ_x, intra-tumoral variance of specie X; HR, hazard ratio associated with an increase in the marker's value.

Both lymphocytes infiltrate simultaneously into the tumor tissue, but CD8+ T cells infiltrate faster than Tregs, resulting in improved prognosis. **Table 1** includes 3 types of cancer with HR < 1. Indeed, in CRC (9–12), in head and neck cancer (13, 14), and in advanced ovarian cancer (15, 16), the tumoral frequencies of the two species positively correlate with each other (comparing tumors of different grades or comparing tumor with normal tissue).

When HR increases with higher frequencies of intra-tumoral Tregs, the two lymphocyte frequencies either inversely correlate with each other (Tregs frequency increases while CD8+ cells frequency decreases) (Cov<1), or they are directly correlated (Cov>1), however in the last scenario Tregs are expected to infiltrate faster than CD8+ T cells into the tumor site, affecting an increase in HR this way. **Table 1** includes 7 types of cancer with HR > 1. In lung adenocarcinoma (17), renal cell carcinoma (21), HCC (28, 29), and pancreatic cancer (32), the frequencies of Tregs and CD8+ (or active CD8+) are inversely correlated. In ovarian cancer (26), and cervical cancer (24) these frequencies are directly correlated. In endometrial cancer, even though the frequencies directly correlate with each other (22), the tumor microenvironment downregulates the activity of CD8+ T cell (23), and the number of *active* CD8+ T cells plausibly decreases.

Consequently, for most types of cancer listed in Tab. 1, when intra-tumoral *Tregs* frequency is used as a marker for cancer prognosis, equation 2 holds:

$$\{\sigma_{HR}, \text{when HR} > 1\} > \{\sigma_{HR}, \text{when HR} < 1\} \quad (2)$$

Where HR is the mortality hazard ratio affected by an increase in intra-tumoral Tregs frequency.

Inspection of the data presented in Shang et al. meta-analysis (6) (which is based on Tregs as a marker) confirms eq. 2 for *all* cancer types: within this list of 11 types of cancers, any cancer type with HR > 1, presents a larger variance than any cancer type with HR < 1.It should be realized that the hazard involved with an increase in Tregs frequency is different from the hazard involved with an increase in the lymphocytes frequency ratio. Thus, eq. 2 does not hold when the lymphocytes frequency ratio is used as a marker.

As mentioned above, dendritic cells and effector CD4+ T cells also affect survival, since both types of cells are involved in priming cytotoxic reaction (34). In addition, effector CD4+ T cells may demonstrate direct cytotoxicity (35).The control of dendritic cells and CD4+T effector cells by regulatory T cells adds to the complexity involved with the prediction of prognosis.

Due to these intricate relationships it seems that no single marker would fit all types of cancer and all patient subpopulations as "the best" prognostic marker.

Having said that, the frequency ratio of the two lymphocytes (CD8+/Treg or Treg/CD8+) demonstrates good correlation with survival in many types of cancer. A good correlation of the ratio with survival was observed in lung adenocarcinoma (17), cervical cancer (24), type I endometrial cancer (36), ovarian cancer (37, 38), colorectal cancer (7, 8), endometrial cancer (overall survival) (22), and breast cancer (39). In some of these studies (7, 8, 24, 37, 38) the frequency ratio was found superior to the single lymphocyte frequencies (one of them or both) as a prognostic marker. Moreover, {PD1+Tregs/PD1+CD8+T cells} ratio was found superior to all other markers in predicting the efficacy of programmed cell death protein 1 (PD-1) blockade therapies (40).

However, the frequency ratio did not correlate with survival in three clinical studies: in type II endometrial cancer study (36), in a CRC study (41), and in endometrial cancer study (DFS) (22). In addition, a meta-analysis of 21 ovarian cancer studies did not show a correlation of the ratio with survival (42).

Taken together, the use of the lymphocytes frequency ratio as a marker is recommended when the frequency variances of the two lymphocytes within the tumor site are of comparable size, or when their values are unknown. However, if one lymphocyte presents highly variable frequency or function, the other specie should be preferred as a marker. In such a case, the lymphocyte frequency ratio may demonstrate high variability and may poorly correlate with survival, especially when the intra-tumoral frequencies of the two species inversely correlate with each other.

SUMMARY

This commentary provides a possible explanation for the opposite correlations between intra-tumoral Tregs and survival, associated with different types of cancer. For most types of cancer, it also explains the higher variances of hazard ratios (σ_{HR}) observed in cancer types with HR>1 compared to cancer types with HR<1, when Tregs frequency in the tumor microenvironment is used as a marker for cancer prognosis. The complexity involved with the selection of a preferred prognostic marker is presented and discussed. The lymphocytes frequency ratio is proposed as the marker of choice, in the absence of data regarding the variances of the two lymphocytes (frequency or function) within the tumor

microenvironment, or if the two variances are of comparable size. If the intra-tumoral frequency of one of these two species exhibits high variability, the low variable lymphocyte should be preferred, over both, the highly variable lymphocyte and the frequency ratio, especially when the intra-tumoral frequencies of the two lymphocytes inversely correlate with each other. The best prognostic marker selected this way, may also be the best predictor for checkpoint inhibitor therapy of cancer. **Table 2** summarizes these results.

AUTHOR CONTRIBUTIONS

The author confirms being the sole contributor of this work and has approved it for publication.

REFERENCES

1. van den Broek ME, Kägi D, Ossendorp F, Toes R, Vamvakas S, Lutz WK, et al. Decreased Tumor Surveillance in Perforin-Deficient Mice. *J Exp Med* (1996) 184(5):1781–90. doi: 10.1084/jem.184.5.1781
2. Li C, Jiang P, Wei S, Xu X, Wang J. Regulatory T Cells in Tumor Microenvironment: New Mechanisms, Potential Therapeutic Strategies and Future Prospects. *Mol Cancer* (2020) 19(1):116. doi: 10.1186/s12943-020-01234-1
3. Han S, Toker A, Liu ZQ, Ohashi PS. Turning the Tide Against Regulatory T Cells. *Front Oncol* (2019) 9:279. doi: 10.3389/fonc.2019.00279
4. Cao X, Cai SF, Fehniger TA, Song J, Collins LI, Piwnica-Worms DR, et al. Granzyme B and Perforin are Important for Regulatory T Cell-Mediated Suppression of Tumor.Clearance. *Immunity* (2007) 27(4):635–46. doi: 10.1016/j.immuni.2007.08.014
5. Deaglio S, Dwyer KM, Gao W, Friedman D, Usheva A, Erat A, et al. Adenosine Generation Catalyzed by CD39 and CD73 Expressed on Regulatory T Cells Mediates Immune Suppression. *J Exp Med* (2007) 204 (6):1257–65. doi: 10.1084/jem.20062512
6. Shang B, Liu Y, Jiang SJ, Liu Y. Prognostic Value of Tumor-Infiltrating FoxP3 + Regulatory T Cells in Cancers: A Systematic Review and Meta-Analysis. *Sci Rep* (2015) 5:15179. doi: 10.1038/srep15179
7. Sideras K, Galjart B, Vasaturo A, Pedroza-Gonzalez A, Biermann K, Mancham S, et al. Prognostic Value of Intra-Tumoral CD8+/FoxP3+ Lymphocyte Ratio in Patients With Resected Colorectal Cancer Liver Metastasis. *J Surg Oncol* (2018) 118(1):68–76. doi: 10.1002/jso.25091
8. Suzuki H, Chikazawa N, Tasaka T, Wada J, Yamasaki A, Kitaura Y, et al. IntratumoralCD8(+) T/FOXP3 (+) Cell Ratio Is a Predictive Marker for Survival in Patients With Colorectal Cancer. *Cancer Immunol Immun* (2010) 59(5):653–61. doi: 10.1007/s00262-009-0781-9
9. Ling A, Edin S, Wikberg ML, Öberg Å, Palmqvist R. The Intratumoural Subsite and Relation of CD8(+) and FOXP3(+) T Lymphocytes in Colorectal Cancer Provide Important Prognostic Clues. *Br J Cancer* (2014) 110 (10):2551–9. doi: 10.1038/bjc.2014.161
10. Frey DM, Droeser RA, Viehl CT, Zlobec I, Lugli A, Zingg U, et al. High Frequency of Tumor-Infiltrating FOXP3(+) Regulatory T Cells Predicts Improved Survival in Mismatch Repair-Proficient Colorectal Cancer Patients. *Int J Cancer* (2010) 126(11):2635–43. doi: 10.1002/ijc.24989
11. Salama P, Phillips M, Grieu F, Morris M, Zeps N, Joseph D, et al. Tumor-Infiltrating FOXP3+ T Regulatory Cells Show Strong Prognostic Significance in Colorectal Cancer. *J Clin Oncol* (2009) 27(2):186–92. doi: 10.1200/JCO.2008.18.7229
12. Lee WS, Kang M, Baek JH, Lee JI, Ha SY. Clinical Impact of Tumor-Infiltrating Lymphocytes for Survival in Curatively Resected Stage IV Colon Cancer With Isolated Liver or Lung Metastasis. *Ann Surg Oncol* (2013) 20 (2):697–702. doi: 10.1245/s10434-012-2752-1
13. Echarti A, Hecht M, Büttner-Herold M, Haderlein M, Hartmann A, Fietkau R, et al. CD8+ and Regulatory T Cells Differentiate Tumor Immune Phenotypes and Predict Survival in Locally Advanced Head and Neck Cancer. *Cancers (Basel)* (2019) 11(9):1398. doi: 10.3390/cancers11091398
14. Wang J, Tian S, Sun J, Zhang J, Lin L, Hu C. The Presence of Tumour-Infiltrating Lymphocytes (TILs) and the Ratios Between Different Subsets Serve as Prognostic Factors in Advanced Hypopharyngeal Squamous Cell Carcinoma. *BMC Cancer* (2020) 20(1):731. doi: 10.1186/s12885-020-07234-0
15. Leffers N, Gooden MJ, de Jong RA, Hoogeboom BN, ten Hoor KA, Hollema H, et al. Prognostic Significance of Tumor-Infiltrating T-Lymphocytes in Primary and Metastatic Lesions of Advanced Stage Ovarian Cancer. *Cancer Immunol Immun* (2009) 58(3):449–59. doi: 10.1007/s00262-008-0583-5
16. Milne K, Köbel M, Kalloger SE, Barnes RO, Gao D, Gilks CB, et al. Systematic Analysis of Immune Infiltrates in High-Grade Serous Ovarian Cancer Reveals CD20, FoxP3 and TIA-1 as Positive Prognostic Factors. *PloS One* (2009) 4(7): e6412. doi: 10.1371/journal.pone.0006412
17. Lavin Y, Kobayashi S, Leader A, Amir ED, Elefant N, Bigenwald C, et al. Innate Immune Landscape in Early Lung Adenocarcinoma by Paired Single-Cell Analyses. *Cell* (2017) 169(4):750–65.e17. doi: 10.1016/j.cell.2017.04.014
18. Jackute J, Zemaitis M, Pranys D, Sitkauskiene B, Miliauskas S, Bajoriunas V, et al. The Prognostic Influence of Tumor Infiltrating Foxp3(+)CD4(+), CD4(+) and CD8(+) T Cells in Resected Non-Small Cell Lung Cancer. *J Inflammation (Lond)* (2015) 12:63. doi: 10.1186/s12950-015-0108-x
19. Ganesan AP, Johansson M, Ruffell B, Yagui-Beltrán A, Lau J, Jablons DM, et al. Tumor-Infiltrating Regulatory T Cells Inhibit Endogenous Cytotoxic T Cell Responses to Lung Adenocarcinoma. *J Immunol* (2013) 191(4):2009–17. doi: 10.4049/jimmunol.1301317
20. An N, Wang H, Jia W, Jing W, Liu C, Zhu H, et al. The Prognostic Role of Circulating CD8+ T Cell Proliferation in Patients With Untreated Extensive Stage Small Cell Lung Cancer. *J Transl Med* (2019) 17(1):402. doi: 10.1186/s12967-019-02160-7
21. Kawashima A, Kanazawa T, Kidani Y, Yoshida T, Hirata M, Nishida K, et al. Tumour Grade Significantly Correlates With Total Dysfunction of Tumour Tissue-Infiltrating Lymphocytes in Renal Cell Carcinoma. *Sci Rep* (2020) 10 (1):6220. doi: 10.1038/s41598-020-63060-1
22. Yamagami W, Susumu N, Tanaka H, Hirasawa A, Banno K, Suzuki N, et al. Immunofluorescence-Detected Infiltration of CD4+FOXP3+ Regulatory T Cells Is Relevant to the Prognosis of Patients With Endometrial Cancer. *Int J Gynecol Cancer* (2011) 21(9):1628–34. doi: 10.1097/IGC.0b013e31822c271f
23. Patel MV, Shen Z, Rodriguez-Garcia M, Usherwood EJ, Tafe LJ, Wira CR. Endometrial Cancer Suppresses CD8+ T Cell-Mediated Cytotoxicity in Postmenopausal Women. *Front Immunol* (2021) 12:657326. doi: 10.3389/fimmu.2021.657326
24. Jordanova ES, Gorter A, Ayachi O, Prins F, Durrant LG, Kenter GG, et al. Human Leukocyte Antigen Class I, MHC Class I Chain-Related Molecule A, and CD8+/regulatory T-Cell Ratio: Which Variable Determines Survival of Cervical Cancer Patients? *Clin Cancer Res* (2008) 14(7):2028–35. doi: 10.1158/1078-0432.CCR-07-4554
25. Shah W, Yan X, Jing L, Zhou Y, Chen H, Wang Y. A Reversed CD4/CD8 Ratio of Tumor-Infiltrating Lymphocytes and a High Percentage of CD4(+)FOXP3 (+) Regulatory T Cells Are Significantly Associated With Clinical Outcome in Squamous Cell Carcinoma of the Cervix. *Cell Mol Immunol* (2011) 8(1):59–66. doi: 10.1038/cmi.2010.56
26. Adams SF, Levine DA, Cadungog MG, Hammond R, Facciabene A, Olvera N, et al. Intraepithelial T Cells and Tumor Proliferation: Impact on the Benefit From Surgical Cytoreduction in Advanced Serous Ovarian Cancer. *Cancer* (2009) 115(13):2891–902. doi: 10.1002/cncr.24317
27. Ding W, Xu X, Qian Y, Xue W, Wang Y, Du J, et al. Prognostic Value of Tumor-Infiltrating Lymphocytes in Hepatocellular Carcinoma: A Meta-Analysis. *Med (Baltimore)* (2018) 97(50):e13301. doi: 10.1097/MD.0000000000013301
28. Fu J, Xu D, Liu Z, Shi M, Zhao P, Fu B, et al. Increased Regulatory T Cells Correlate With CD8 T-Cell Impairment and Poor Survival in Hepatocellular Carcinoma Patients. *Gastroenterology* (2007) 132(7):2328–39. doi: 10.1053/j.gastro.2007.03.102
29. Huang Y, Wang FM, Wang T, Wang YJ, Zhu ZY, Gao YT, et al. Tumor-Infiltrating Foxp3+ Tregs and CD8+ T Cells Affect the Prognosis of Hepatocellular Carcinoma Patients. *Digestion* (2012) 86(4):329–37. doi: 10.1159/000342801

30. Mathai AM, Kapadia MJ, Alexander J, Kernochan LE, Swanson PE, Yeh MM. Role of Foxp3-Positive Tumor-Infiltrating Lymphocytes in the Histologic Features and Clinical Outcomes of Hepatocellular Carcinoma. *Am J Surg Pathol* (2012) 36(7):980–6. doi: 10.1097/PAS.0b013e31824e9b7c
31. Hu L, Zhu M, Shen Y, Zhong Z, Wu B. The Prognostic Value of Intratumoral and Peritumoral Tumor-Infiltrating FoxP3+Treg Cells in of Pancreatic Adenocarcinoma: A Meta-Analysis. *World J Surg Oncol* (2021) 19(1):300. doi: 10.1186/s12957-021-02420-1
32. Tang Y, Xu X, Guo S, Zhang C, Tang Y, Tian Y, et al. An Increased Abundance of Tumor-Infiltrating Regulatory T Cells Is Correlated With the Progression and Prognosis of Pancreatic Ductal Adenocarcinoma. *PloS One* (2014) 9(3): e91551. doi: 10.1371/journal.pone.0091551
33. Stuart A, Ord JK. *Kendall's Advanced Theory of Statistics. 6th Edition* Vol. 1: Distribution Theory. Edward Arnold, London: (1998). p. 351.
34. Elkoshi Z. Cancer and Autoimmune Diseases: A Tale of Two Immunological Opposites? *Front Immunol* (2022) 13:821598. doi: 10.3389/fimmu 2022.821598
35. Oh DY, Fong L. Cytotoxic CD4+ T Cells in Cancer: Expanding the Immune Effector Toolbox. *Immunity* (2021) 54(12):2701–11. doi: 10.1016/ j.immuni.2021.11.015
36. de Jong RA, Leffers N, Boezen HM, ten Hoor KA, van der Zee AG, Hollema H, et al. Presence of Tumor-Infiltrating Lymphocytes Is an Independent Prognostic Factor in Type I and II Endometrial Cancer. *Gynecol Oncol* (2009) 114(1):105–10. doi: 10.1016/j.ygyno.2009.03.022
37. Preston CC, Maurer MJ, Oberg AL, Visscher DW, Kalli KR, Hartmann LC, et al. The Ratios of CD8+ T Cells to CD4+CD25+ FOXP3+ and FOXP3- T Cells Correlate With Poor Clinical Outcome in Human Serous Ovarian Cancer. *PloS One* (2013) 8(11):e80063. doi: 10.1371/journal.pone.0080063
38. Sato E, Olson SH, Ahn J, Bundy B, Nishikawa H, Qian F, et al. Intraepithelial CD8+ Tumor-Infiltrating Lymphocytes and a High CD8+/regulatory T Cell Ratio are Associated With Favorable Prognosis in Ovarian Cancer. *Proc Natl Acad Sci USA* (2005) 102(51):18538–43. doi: 10.1073/pnas.0509182102
39. Peng GL, Li L, Guo YW, Yu P, Yin XJ, Wang S, et al. CD8+ Cytotoxic and FoxP3+ Regulatory T Lymphocytes Serve as Prognostic Factors in Breast Cancer. *Am J Transl Res* (2019) 11(8):5039–53.
40. Kumagai S, Togashi Y, Kamada T, Sugiyama E, Nishinakamura H, Takeuchi Y, et al. The PD-1 Expression Balance Between Effector and Regulatory T Cells Predicts the Clinical Efficacy of PD-1 Blockade Therapies. *Nat Immunol* (2020) 21(11):1346–58. doi: 10.1038/s41590-020-0769-3
41. Loddenkemper C, Schernus M, Noutsias M, Stein H, Thiel E, Nagorsen D. *In Situ* Analysis of FOXP3+ Regulatory T Cells in Human Colorectal Cancer. *J Transl Med* (2006) 4:52. doi: 10.1186/1479-5876-4-52
42. Li J, Wang J, Chen R, Bai Y, Lu X. The Prognostic Value of Tumor-Infiltrating T Lymphocytes in Ovarian Cancer. *Oncotarget* (2017) 8(9):15621–31. doi: 10.18632/oncotarget.14919

Author Disclaimer: The views and opinions expressed, and/or conclusions drawn, in this article are those of the author and do not necessarily reflect those of Taro Pharmaceutical Industries Ltd., its affiliates, directors or employees.

Conflict of Interest: The author is an employee of Taro Pharmaceutics, Israel.

Publisher's Note: All claims expressed in this article are solely those of the authors and do not necessarily represent those of their affiliated organizations, or those of the publisher, the editors and the reviewers. Any product that may be evaluated in this article, or claim that may be made by its manufacturer, is not guaranteed or endorsed by the publisher.

Copyright © 2022 Elkoshi. This is an open-access article distributed under the terms of the Creative Commons Attribution License (CC BY). The use, distribution or reproduction in other forums is permitted, provided the original author(s) and the copyright owner(s) are credited and that the original publication in this journal is cited, in accordance with accepted academic practice. No use, distribution or reproduction is permitted which does not comply with these terms.

frontiers | Frontiers in Immunology

REVIEW
published: 10 June 2022
doi: 10.3389/fimmu.2022.859633

Next-Generation Anti-Angiogenic Therapies as a Future Prospect for Glioma Immunotherapy; From Bench to Bedside

Parisa Shamshiripour[1,2], Fahimeh Hajiahmadi[2], Shahla Lotfi[2], Niloofar Robab Esmaeili[3], Amir Zare[1,4], Mahzad Akbarpour[5,6] and Davoud Ahmadvand[2,7]**

[1] Faculty of Medicine, Iran University of Medical Sciences, Tehran, Iran, [2] Department of Molecular Imaging, Faculty of Advanced Technologies in Medicine, Iran University of Medical Sciences, Tehran, Iran, [3] Department of Biomedical Engineering, Amirkabir University of Technology (Tehran Polytechnic), Tehran, Iran, [4] Department of Surgery, School of Medicine, Iran University of Medical Sciences, Tehran, Iran, [5] Advanced Cellular Therapeutics Facility, David and Etta Jonas Center for Cellular Therapy, Hematopoietic Cellular Therapy Program, The University of Chicago Medical Center, Chicago, IL, United States, [6] Immunology Board for Transplantation and Cell-Based Therapeutics (Immuno-TACT), Universal Science and Education Research Network (USERN), Tehran, Iran, [7] Neuroscience Research Center, Iran University of Medical Sciences, Tehran, Iran

OPEN ACCESS

Edited by:
Pravin Kaumaya, The Ohio State University, United States

Reviewed by:
Domenico Ribatti, University of Bari Aldo Moro, Italy
Eiichi Ishikawa, University of Tsukuba, Japan

***Correspondence:**
Davoud Ahmadvand
d.ahmadvand@iums.ac.ir
Mahzad Akbarpour
Mahzad.Akbarpour@uchospitals.edu

Specialty section:
This article was submitted to Cancer Immunity and Immunotherapy, a section of the journal Frontiers in Immunology

Received: *21 January 2022*
Accepted: *24 March 2022*
Published: *10 June 2022*

Citation:
Shamshiripour P, Hajiahmadi F, Lotfi S, Esmaeili NR, Zare A, Akbarpour M and Ahmadvand D (2022) Next-Generation Anti-Angiogenic Therapies as a Future Prospect for Glioma Immunotherapy; From Bench to Bedside. Front. Immunol. 13:859633. doi: 10.3389/fimmu.2022.859633

Glioblastoma (grade IV glioma) is the most aggressive histopathological subtype of glial tumors with inordinate microvascular proliferation as one of its key pathological features. Extensive angiogenesis in the tumor microenvironment supplies oxygen and nutrients to tumoral cells; retains their survival under hypoxic conditions; and induces an immunosuppressive microenvironment. Anti-angiogenesis therapy for high-grade gliomas has long been studied as an adjuvant immunotherapy strategy to overcome tumor growth. In the current review, we discussed the underlying molecular mechanisms contributing to glioblastoma aberrant angiogenesis. Further, we discussed clinical applications of monoclonal antibodies, tyrosine kinase inhibitors, and aptamers as three major subgroups of anti-angiogenic immunotherapeutics and their limitations. Moreover, we reviewed clinical and preclinical applications of small interfering RNAs (siRNAs) as the next-generation anti-angiogenic therapeutics and summarized their potential advantages and limitations. siRNAs may serve as next-generation anti-angiogenic therapeutics for glioma. Additionally, application of nanoparticles as a delivery vehicle could increase their selectivity and lower their off-target effects.

Keywords: glioma, immunotherapy, anti-angiogenesis therapy, tyrosine kinase inhibitors, monoclonal antibodies, siRNAs

INTRODUCTION

Brain gliomas are a major neurooncological challenge because of high mortality, morbidity and recurrence rates. Among the glial neoplasms of the brain, glioma grade IV or glioblastoma multiform (GBM) is the most frequent and deadliest. Despite the current advances in development of novel therapeutic strategies for gliomas, the prognosis of patients suffering high-

grade gliomas is very poor. Up to present, aggressive surgery (ideally gross total resection of the tumor bulk), Temozolomide (TMZ) chemotherapy, and radiation therapy are the standalone and gold standard of care for GBM, based on the National Comprehensive Cancer Network (NCCN) guidelines. Meanwhile, many patients receiving the standard of care experience recurrence and disease-specific survival and progression-free survival for GBM patients are very poor. Extensively aggregating focally anastomosing capillaries forming glomeruloid vessel-like structures which are supported by basal lamina and pericytes and are devoid of astrocytic end-feet is a key histopathological characteristic of GBM (1). Hence, anti-angiogenic therapy is one of the well-known adjuvant therapy strategies for GBM. Proposing that vascular-reach tumor such as GBM depend on neovessel formation for survival and nutrient supply, inhibiting tumor angiogenesis is one of the key treatment strategies that could help combat glioma growth and also increase the patients' quality of life due to symptom alleviation and reduction of peritumoral edema. Additionally, tumor aberrant angiogenesis supports the immunosuppressive tumor microenvironment (TME) in GBM and hence, reducing the angiogenic signals in the TME could enhance anti-tumor immune responses. However, the hypoxia caused by the severe reduction of tumor vasculature after anti-angiogenic therapy, contributes to activation of compensatory signals which resist against anti-angiogenic therapies and maintain tumor angiogenesis. Herein, we critically discuss the major contributing mechanisms to tumor angiogenesis and resistance to anti-angiogenic therapeutics and also discuss the novel advances in the field of designing anti-angiogenic therapeutics for GBM. We provide a detailed discussion on antibody-based anti-angiogenic therapies; small peptides; tyrosine kinase inhibitors and oligonucleotide-based therapeutics (e.g. aptamers and siRNAs) and critically review their potential challenges, safety, efficacy and future perspective. Furthermore, we explore the challenges of BBB for targeted brain delivery and strategies to overcome comprising passive and active targeting of both biological and synthetic nano-carriers.

BIOLOGY OF GBM ANGIOGENESIS AND RESISTANCE MECHANISMS TO ANTI-ANGIOGENIC THERAPY

Of all brain tumors, gliomas make up about 70% of brain neoplastic lesions. The prognosis of patients with high-grade gliomas is very poor despite development of advanced neurosurgical approaches. Glioma angiogenesis has long been considered to be a key controller of tumor progression and acquisition of aggressive phenotypes. Tumor aberrant angiogenesis was first described by Folkman et al. (2). Currently, several contributing cellular and molecular mechanisms have been proposed for incremental angiogenesis in GBM tumors, the most stated of which are as follows: (1) Hypoxia: The extensive cellular proliferation in tumoral bulk of the GBM, causes severe hypoxia, nutrient-deprivation and also induces secretion of angiogenic cytokines (**Figure 1**) and Matrix Metalloproteinases (MMPs). Consequently, neo-angiogenesis forming haphazard blood vessels lacking normal vessels structure speeds-up due to extracellular matrix (ECM) degradation. Quiescent endothelial cells (ECs) get activated *via* complex downstream signaling pathways induced by the TME cytokines, and ECs extensively proliferate and sprout in a complex TME comprising pericytes, reactive astrocytes, glioma-associated macrophages (GAMs), tumoral cells and ECs. Propagation of newly-formed vessel buds are enhanced by the interactions of binding proteins (e.g. $\alpha v\beta 5$ and $\alpha v\beta 3$ integrins) and furthermore, pericytes and smooth muscle cells eventually surround the newly lumenized tubes and stabilize their basement membranes. In the proangiogenic and proinflammatory TME of the GBM, extensive proliferation of ECs leads to formation of leaky and abnormal blood vessels. However, the haphazard vessels formed are not able to efficiently deliver the nutrients and oxygen demand of the proliferating tumor bulk and also are not efficient for delivering the chemotherapeutics. (2) Vasculogenic Mimicry (VM) of Cancer Stem Cells (CSCs): firstly, Maniotis et al. reported melanoma cells forming tube-like structure with no vascular endothelial cells containing red blood cells and this type of vessel formation was therefore named vasculogenic mimicry (3). Tumor-initiating cells have high dedifferentiation plasticity and can Trans-differentiate to vessel-like structures (identified by accumulation of RBCs and CD31/CD34-negative and PAS-positive cells) supported by glycoproteins comprising type I, IV, and VI collagen, and laminin Ln5 and its cleavage products, $\gamma 2x$ and $\gamma 2'$ (4, 5). These vessel-like structures eventually merge with micro-vessels formed by angiogenesis or vascularization to retain blood supply and nutrient delivery and also play pivotal roles in tumor metastasis by shedding tumoral cells directly into the bloodstream. Epithelial-Mesenchymal Transition (EMT) and VE-cadherin/EphA2/MMP signaling pathway are key players to facilitate VM. Additionally, adenosine/STAT3/IL-6 pathway, MAPK/ERK pathway, Wnt/β-catenin, Notch, Wnt, Hedgehog, Hippo signaling pathway are also key triggers for VM due to their pivotal roles in generating CSCs. Hypoxic TME is a key trigger for GBM angiogenesis. The major contributing TME cytokines in VM are summarized in **Figure 1** (6). Over production of HIF1α in the TME increases BCL9 expression, mediating activation of β-catenin-mediated transcriptional activity at hypoxic tumor tissues, and facilitates VM. Tight junction proteins are negatively regulated by overexpression of CSCs markers (Twist and Snail) enhancing the migration capacity of endothelial cells (7). Moreover, the ECM is degraded by overproduction of matrix metalloproteinase such as MMP9 mediating EphA2/MMP signaling pathway. Afterwards, the newly-proliferated cancer stem cells form vessel-like structures in order to support tumor oxygen delivery. (3) Infiltration of Bone Marrow-Derived Mesenchymal Cells (BM-MCs): BM-MCs infiltrate into tumor tissues *via* chemo-attraction (e.g. by CX3CL1) and secrete pro-angiogenic and pro-inflammatory cytokines (e.g. HIF1α, VEGF and IL6). The recruited

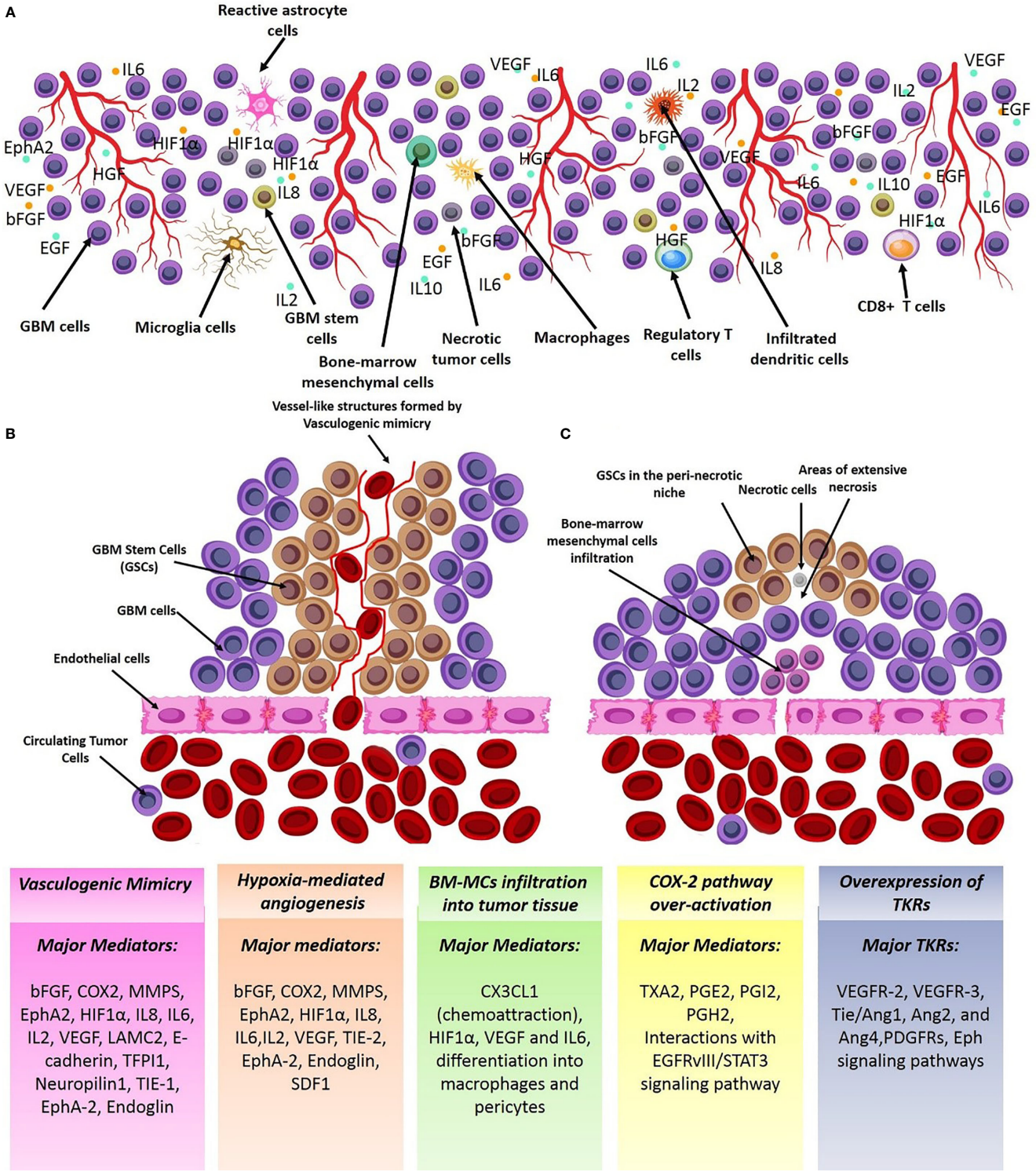

FIGURE 1 | Major mechanisms of GBM angiogenesis. **(A)** Cellular schema of the angiogenic tumor microenvironment (TME) of GBM. GBM TME consists numerous cell sources (e.g. immune cells, GBM cells, astrocytes, macroglia/macrophages, and astrocytes) which support the angiogenic TME by overproducing angiogenic cytokines. **(B)** Vasculogenic mimicry; GSCs form vessel-like structures which invade to tumoral endothelia to get nutrient and oxygen supply. **(C)** Chemical attraction and infiltration of angiogenic clones of BMSCs in the tumor tissue by TME chemotactic signals. Some of the vectors used to design this figure were downloaded from Vecteezy under a free license.

tumor-associated BMDCs may differentiate into macrophages and pericytes. Macrophages in the TME modulate the pro- and anti-angiogenic balance by cytokine production and pericytes, derived from PDGFRβ+ BMDCs, can enhance the ECs survival and also provide an extensive mechanical support to maintain the vessels (**Figure 1**) (8). (4) Over-activation of Cyclooxygenase-2 (COX-2) hydroperoxidase pathway: COXs, checkpoint enzymes of prostanoids production, have two mammalian isoforms. COX-1 regulates the homeostatic synthesis of prostanoids expressed in the most tissues and retains the physiological functions of prostanoids at target organs. COX-2, also known as prostaglandin G/H synthase, is expressed at extremely low levels in physiological circumstances, and the robust increase in COX2 expression reflects severe inflammatory responses to tissue injuries and other detrimental stimuli such as tumorigenesis. COX2 activation results in an eventual overproduction of prostaglandin E2 (PGE2), thromboxane A 2 (TXA2) and prostaglandin I2 (PGI2). TXA2 facilitates ECs migration and proliferation and PGI2 is involved in multiple angiogenesis-related processes (e.g. ECs sprouting, ECs proliferation and vessel permeability; **Figure 2**). PGE2 facilitates glioma angiogenesis *via* protein kinase C activation (PKC) by activating G-protein-coupled receptors. Additionally, the interactions of Epidermal Growth Factor Receptors (EGFR)/Signal transducer and activator of transcription 3 (STAT3) or the epidermal growth factor receptor variant III (EGFRvIII)/STAT3 signaling axes with COX2 downstream pathways contributes to glioma angiogenesis (**Figure 2**) (9). (5) Overexpression of tyrosine kinase receptors (TKRs): Over-activation of TKRs are thought to be of the key players in oncogenesis. Major TKRs families which are extensively involved in tumor angiogenesis are thought to be the VEGF receptors (VEGFRs), the Tie receptors platelet-derived growth factor (PDGF) receptors and Eph receptors. VEGFR-2 and VEGFR-3 act in order to facilitate and drive angiogenesis, whereas VEGFR-1 restricts the angiogenic response and is said to be a key player in tissue remodeling acting to recruit macrophages. Under physiological circumstances, stimulation of VEGFR-2 contributes to angiogenesis of blood vascular ECs, however, activating VEGFR-3 elicits a similar response for lymphatic ECs. During the cancer pathogenesis, VEGFR2 is extremely overexpressed. Tie2/Ang1, Ang2, and Ang4 interactions also play pivotal roles in EC survival, stabilization and remodeling of blood and lymphatic vessels. The PDGF receptors mediate vascular wall stabilization by mural cells (e.g. pericytes and smooth muscle cells), and the Eph receptors contribute in determining arterial versus venous identity. The TKRs downstream signaling pathways contributing to glioma aberrant angiogenesis are depicted in detail in **Figure 2**. Over-activation of mitogen-activated protein kinase (MAPK) and Phosphoinositide 3-kinase (PI3K)-Akt signaling pathways eventually result in sustained angiogenesis, cellular proliferation and evasion from apoptosis (10).

Although the normalized tumor vasculature after anti-angiogenic therapy with a high dose interrupted protocol which is conventionally used as an adjuvant therapy for GBM with Tyrosine Kinase Inhibitors (TKIs) or monoclonal antibodies (mAbs) provides a transient window period for more efficient chemotherapy, high dose systemic consumption of mAbs or TKIs can cause tumor escape and acquisition of resistance to anti-angiogenic therapies (**Figures 1**, **2**). Previous studies have identified several mechanisms for tumor escape from anti-angiogenic therapy which include: (1) over-activation of compensatory angiogenic signaling pathways: In the hypoxic GBM TME with few remaining vessels after angiogenesis blockade, cells rewire their signaling pathways to activate compensatory signals comprising the Hypoxia-inducible factor signaling pathway, Notch signaling pathway, and Ang2/Tie2 signaling pathway (**Figure 2**). (2) Immunological escape: Briefly, pro-angiogenic signals produced by TIE2+ monocytes, GAMs, reactive astrocytes and CD11b+ myeloid cells, neutrophils and T helper-17 cytokines enhance infiltration of the pro-angiogenic clones of BM-DSCs and result in tumor angiogenesis. (3) Increased pericyte coverage: after anti-angiogenic therapy, extensive pericyte coverage may also be another contributing mechanism to maintain the survival of ECs. (4) Vessel co-option and perivascular invasion: Invasion of tumoral cells to co-opt with the vessels in the tumoral tissues is a well-known characteristic of aggressive tumors which facilitates nutrient delivery and oxygenation of the rapidly-expanding tumor tissue. The exact molecular mechanisms mediating vessel co-option are not yet fully-described however previous evidence highlights the role of Bradykinin/bradykinin receptor-2 (B2R) signaling pathway, CXCR4/SDF-1α pathway, MDGI/FABP3 signaling pathway, EGFRvIII signaling pathway, and Olig2/Wnt7a signaling pathway (11). It is noteworthy to note that increased pericyte coverage in the co-opted blood vessels supports survival of ECs under anti-angiogenic therapy by promoting an autocrine VEGF-A signaling and consequently, vessel co-option was previously noted as an indicator of poor clinical response to anti-angiogenic therapy in many cancers including breast, colorectal, lung and pancreatic cancer, GBM, melanoma, hepatocellular carcinoma, and renal cell carcinoma (12). Hence, the modulating molecular targets of vessel-cooption serve a potent future perspective for generating more efficient anti-angiogenic drugs for cancer therapy and also as a mechanism to enhance tumor chemo-sensitization. Co-option of tumoral cells to tumor vessels is also another compensatory mechanism to get oxygen and nutrient supply which supports the survival of tumoral ECs. (5) VM; as previously described. (6) Autophagy process: Both selective and non-selective autophagy mechanisms are ways to provide energy for tumoral cells in order to maintain their survival under hypoxic or anoxic conditions through both HIF-1 dependent/independent mechanisms. A well-known strategy to overcome anti-angiogenesis therapy resistance is to pursue low dose and continuous inhibition rather than disrupted high dose consumption. A future perspective therefore proposed is to use slow-releasing nanoparticles as vehicles for anti-angiogenic compounds.

OPTIMIZATION STRATEGIES FOR ANTI-ANGIOGENESIS DRUG DESIGNING

The primary objective of anti-angiogenic therapy for GBM is to normalize the tumor vasculature rather than eliminating

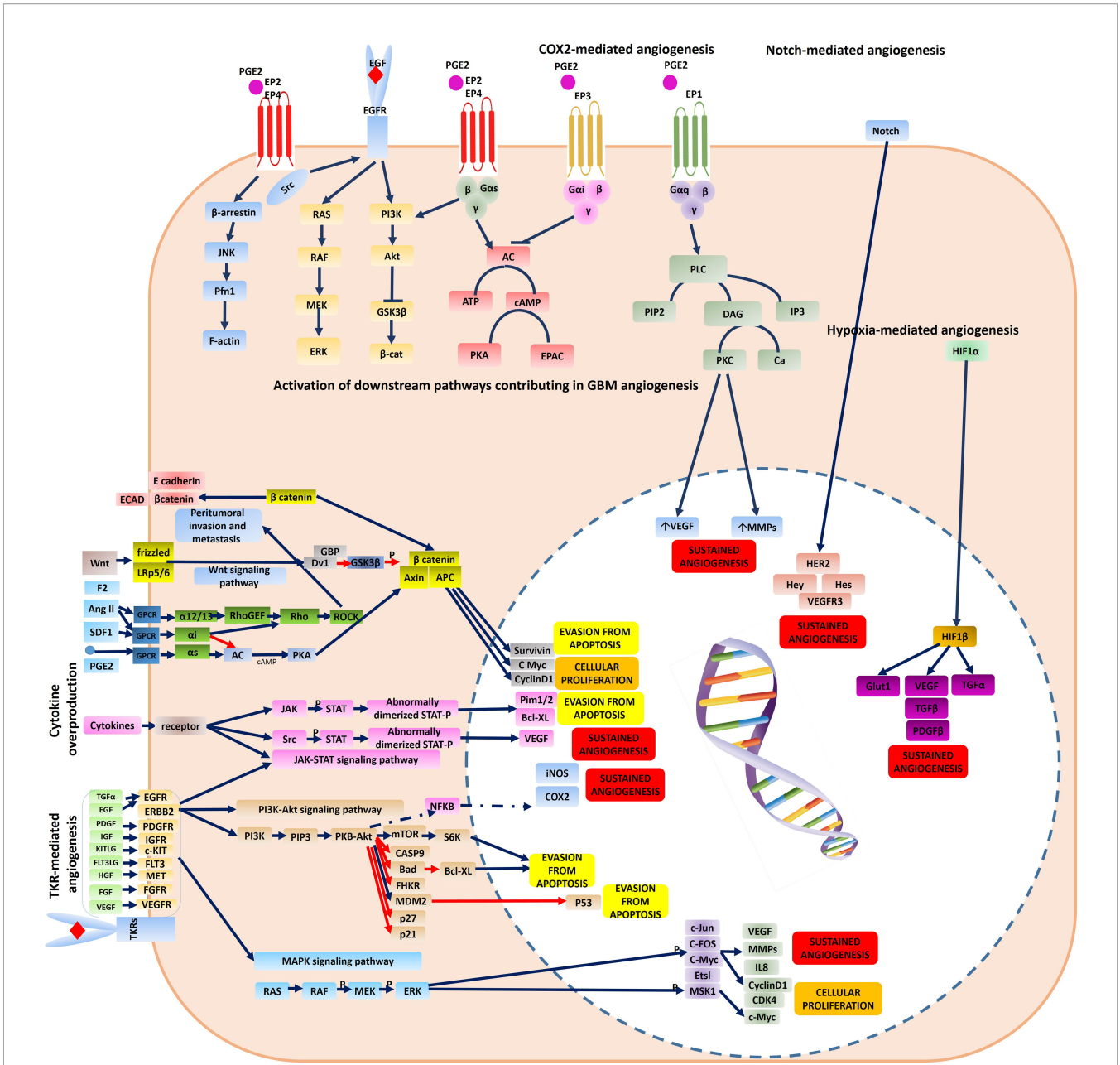

FIGURE 2 | Molecular mechanisms contributing to tumor angiogenesis and resistance to anti-angiogenic therapy in a GBM cell. The major molecular pathways responsible for GBM angiogenesis comprise: (1) TKR-mediated angiogenesis *via* activation of downstream signaling pathways (PI3K-Akt signaling pathway, and MAPK signaling pathway) (2) cytokine-mediated angiogenesis *via* activation of downstream signaling pathways (JAK-STAT signaling pathway) (3) SDF1, ANG2 as compensatory mechanisms (4) Hypoxia-mediated angiogenesis *via* activation of HIF1α signaling pathway (5) COX2-mediated angiogenesis *via* activation of G-protein- coupled receptors mediating activation of protein-kinase C (PKC) and also its interactions with EGFR signaling (6) Notch-mediated angiogenesis. Some of the vectors used to design this figure were downloaded from Vecteezy under a free license.

all the tumoral vessels. Normalized tumor vasculature serves as a window for more effective chemotherapy and enhance tumor delivery of therapeutic agents. An ideal anti-angiogenic drug should have the following characteristics: (1) Target multiple signaling pathways (2) cause minimal drug-induced resistance (3) increase endogenous anti-angiogenesis substances (4) have minimal off-target effects (5) high selectivity (6) and limited systemic toxicity.

Anti-angiogenic therapeutics are categorized as tabulated in **Table 1**.

ANTI-ANGIOGENIC mAbs; CURRENT STATUS, CHALLENGES AND FUTURE PERSPECTIVE

Currently, the clinical applicability of a large number of mAbs for GBM is under evaluation however major challenges exist to optimize the efficacy of anti-angiogenic therapy with mAbs which include: (1) Low tumor accumulation rates: low absolute tumor accumulation of the large molecules of intact mAbs are due to increased interstitial fluid pressure (IFP). The increased IFP and extensive peritumoral edema impair the trans-capillary transport of mAbs into the tumor tissue. High IFP slows the diffusion constants and forms a "binding site barrier" that causes uneven tumor penetration and hence mAbs tend to bind to the first antigen molecules they encounter. (2) Low concentration in tumor tissue due to the Blood-Brain Barrier (BBB): Prolonged high dose consumption of mAbs to overcome the BBB challenge insert systemic AEs and enhances acquisition of resistance to anti-angiogenic therapy due to extensive tumor hypoxia after angiogenesis blockade. (3) Long circulation time (days to weeks) resulting in dose-limiting toxicities (4) slow tumor uptake (5) heterogeneity in the expression of targeting antigens in the tumor tissue. Due to the aforementioned limitations of intact mAbs, there is a rising tendency to use antibody fragments with smaller molecular sizes (e.g. minibodies, diabodies, single-chain fragment variable, camelid antibodies, and small peptides) for future clinical applications. As a future perspective, camelid antibodies, also named as noanobodies or single-domain antibodies, are completely devoid of light chain and have only one single VH domain termed VHH in the antigen binding regions (13). Previously, we have successfully generated combined Mucin-1 (MUC1)-specific nanobody-tagged polyethylene glycol (PEG)-polyethylenimine polyplex targeting and transcriptional targeting of tBid transgene for directed killing of MUC1 over-expressing tumor cells (14). Production of camelid antibodies is a future perspective for antibody-based knockdown of tumor angiogenesis by phage display technologies with particular advantages comprising (1) small molecular size of about 10-15 KDs (2) robust kinetics and behavior (3) high affinity (4) high specificity and (5) better tissue penetration due to smaller size and (6) ability to deliver therapeutic cargos. Investigating the *in-vivo* efficacy of nano-bodies to successfully penetrate the BBB and deliver their cargo to the region of interest in the brain with high affinity for tumoral cells is a potential future perspective. Muruganandam et al. reported that two llama single-domain antibodies were selected, sequenced, subcloned, and expressed as fusion proteins with c-Myc-His5 tags which selectively bind to human cerebromicrovascular endothelial cells and transmigrate across an *in vitro* human BBB model (15). Additionally, Wouters et al. also reported successful generation of an anti-transferrin receptor nano-body that can reach the brain *via* receptor-mediated transcytosis after peripheral administration (16). Moreover, Li et al. also reported successful generation of two novel single-domain antibodies (VHHs or nano-bodies) against extracellular amyloid deposits and intracellular tau neurofibrillary tangles and reported gradual extravasation of the VHHs across the BBB, diffusion in the parenchyma and labeling of amyloid deposits and neurofibrillary tangles in transgenic Alzheimer's disease mice models (17). Moreover, Farrington et al. (18), M Vandesquille et al. (19), and Rutgers et al. (20) also reported that camelid antibodies pass through the BBB. In a review by GAO Et Al the potential mechanisms by which the nano-bodies pass through the BBB are completely discussed (21). We are currently investigating the BBB penetration of some VHH clones by phage display strategy as an experimental project and aim to examine the efficacy of VHH nano-bodies as carriers for brain

TABLE 1 | Major categories of anti-angiogenic immunotherapeutics.

Anti-angiogenic immunotherapeutic	Major category	Examples
Intracellular Tyrosine Kinase Inhibitors (TKIs)	TKIs	mTOR inhibitors, protein kinase C inhibitors
Membrane TKIs		Sunitinib, Sorafenib
Ligand TKIs		VEGF inhibitors such as Bevacizumab; also categorized as a mAB
decoy receptors	decoy receptors	aflibercept
Matrix metalloproteinase inhibitors (MMPIs)	MMPIs	Marimastat
matrix-derived inhibitors	Endogenous angiogenic substance inhibitors	Konstatin,thrombospondin1-2, endostatin, endorphin, arsenic
non-matrix-derived inhibitors		angiostatin, antithrombin, TIMP 4, vasostatin
integrin antagonists	integrin antagonists	Vitaxin (integrin $\alpha5\beta3$ mAB), Anti-integrin $\alpha5\beta1$ blocking peptides, Cilengitide (integrin $\alpha5\beta3$ and integrin $\alpha5\beta5$; a cyclic RGD pentapeptide),
Cytokine/chemokine inhibitors	Cytokine/chemokine inhibitors	tumor necrosis factor (TNF) inhibitors, IL2 inhibitors, or α/β interferon (INF α/β) inhibitors
aptamers	aptamers	Pegabtanib
Monoclonal antibodies (mAbs; targeting angiogenic cytokines or TKRs)	mAbs	Tanibirumab, Cetuximab, Onartuzumab

delivery as a future perspective. Despite previous evidence suggesting that nano-bodies may cross the BBB by direct penetration or RMT, yet future research may shed light to the exact molecular mechanisms mediating BBB penetration of VHHs and their efficacy to target tumoral tissues in the brain. Novel technologies developed for high-yield production of recombinant mAbs by cloning of immunoglobulin gene segments and producing libraries of antibodies (e.g. repertoire cloning, CRISPR/Cas9 and phage display) has attracted much attention in the recent years compared to the traditional methods (e.g. chimeric antibodies, and hybridoma technologies) Traditional methods are less efficient and may cause adverse events (AEs) such as human anti-mouse antibodies (HAMA) formation. Consequently, phage display technologies can be a potential future perspective to cross the blood-brain-barrier with nano-ligand drug carriers in clinics to optimize the drug delivery process for neurological disorders and brain tumors (22). The aforementioned technologies enables the scientific committee to engineer the mAbs with modified amino acid (AA) sequences to achieve the desired characteristics. Production of fully-humanized antibody fragments with modifiable AA sequences are the goal for novel anti-body-based products which can be achieved by newer antibody engineering techniques (e.g. phage display, transgenic mice and single B cell cloning; **Figure 3**). Small peptides are also potentially more advantageous to intact mAbs due to faster clearance rates and tumor penetration. However, one of the major drawbacks of peptides is that a slight change in their AA composition causes major conformation modification which results in huge changes in their relative affinity. Consequently, they are relatively less potent for designing novel therapeutic conjugates than mAbs.

CLINICAL TRIAL PIPELINES OF ANTI-ANGIOGENIC mABS/FUSION PROTEINS FOR GBM

As summarized in **Table 2**, the majority of previous evidence suggests poor clinical applicability of mAbs for GBM. However, Bevacizumab (BV), a humanized anti-VEGF mAB targeting circulating VEGF, is now broadly used as an FDA-approved adjuvant immunotherapy for recurrent GBM. A major concern for using BV in patients suffering GBM at childbearing ages is that it may impair fertility. Other serious systemic adverse events (AEs) of BV include gastrointestinal perforation, thromboembolic events, renal injury, and impairment of wound healing process which may increase the risk of post-surgical infections, Posterior Reversible Encephalopathy Syndrome (PRES), congestive heart failure and hypertension. Aflibercept: Aflibercept is an IV-injected soluble decoy receptor (a decoy fusion protein of domain 2 of VEGFR-1 and domain 3 of VEGFR-2 with the Fc fragment of IgG1) binds to VEGF-A, VEGF-B, and PGF with greater affinities than their native receptors (e.g.VEGFR family). Hence, it traps the soluble VEGF preventing its interaction with VEGFR family to activate downstream angiogenic pathways. The phase II trials of Aflibercept in patients with recurrent GBM reported moderate toxicity, including fatigue, hypertension, lymphopenia, CNS ischemia and systemic hemorrhage. In addition, in another trial of TMZ-resistant malignant gliomas, moderate toxicity was also reported with major adverse events being fatigue, hypertension, hand-foot syndrome, lymphopenia, thrombosis, proteinuria, CNS ischemia and systemic hemorrhage. Further, a phase I clinical evidence suggested that Aflibercept in

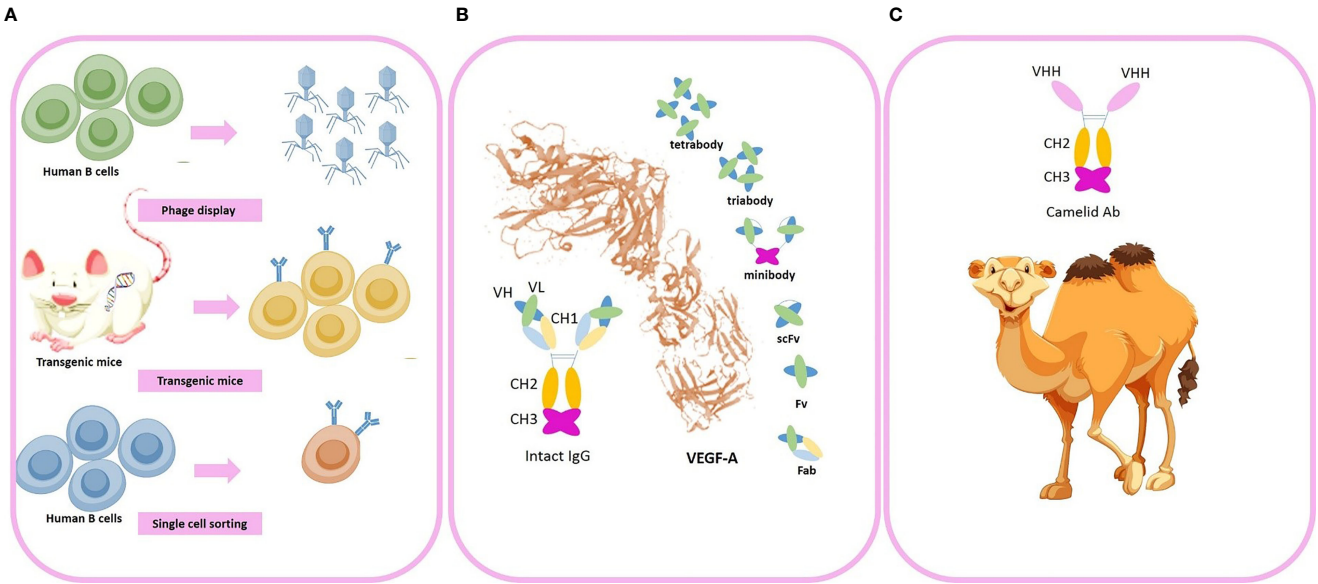

FIGURE 3 | Novel advances in generation of anti-angiogenic monoclonal antibodies (mAbs). **(A)** Novel strategies used for industrial production of engineered fully-humanized mAbs comprising (1) phage display technologies (2) transgenic mice (3) single-cell sorting. **(B)** An intact mAb and antibody fragments (i.e. minibody, tirabody, tetrabody, and scFv) **(C)** camelid antibodies. Some of the vectors used to design this figure were downloaded from Vecteezy under a free license.

TABLE 2 | Clinical trials on mAbs/fusion proteins for GBM.

mAB	Co-therapy	Target	Phase	Antibody type	Ref.
Aflibercept	–	VEGF-A, VEGF-B, PGF	II	Fully-humanized IgG	(23, 24)
	+TMZ		I		(25)
	+ radiation therapy+ TMZ		I		(26)
Tanibirumab	–	VEGFR2	II	Fully-humanized IgG	(27)
			I		(28)
Cetuximab	–	EGFR	II	Fully-humanized IgG	(29)
Onartuzumab	+Bevacizumab	c-MET	II	Fully-humanized IgG	(30)

combination with TMZ was well tolerated and the dose-limiting toxicities reported were thrombotic microangiopathy and thrombocytopenia in the dose escalation study. Although the monotherapy of Aflibercept may cause moderate systemic toxicities, potential advantages of adding Aflibercept to TMZ chemotherapy still needs further clinical investigations (23–26). Tanibirumab: In a phase I investigation, Tanibirumab was considered tolerable and had modest clinical efficacy for refractory solid tumors. Furthermore, the results of a phase IIa clinical study of Tanibirumab in patients with recurrent GBM revealed that Tanibirumab is safe and a common AE of Tanibirumab was cutaneous hemangiomas (27, 28). Cetuximab: Cetuximab is an EGFR inhibitor, a fully humanized mAB, with FDA-approval for patients with K-Ras wild-type, EGFR-expressing colorectal cancer, metastatic colorectal cancer and advanced squamous cell carcinoma of the head and neck in combination with radiation therapy. Results of a phase II clinical trial suggested that cetuximab had both minor toxicities and minor clinical benefits in progressive malignant gliomas (29). Two serious AEs of Cetuximab reported in patients with head and neck squamous were heart attacks and sudden deaths. Onartuzumab: Onartuzumab is a fully-humanized and monovalent antibody against c-met. A phase II trial reported adding Onartuzumab to BV had no further clinical benefits compared to BV alone (30).

ANTI-ANGIOGENIC TYROSINE KINASE INHIBITORS (TKIS); CURRENT STATUS, CHALLENGES AND FUTURE PERSPECTIVE

TKs are a group of phosphorylating enzymes which activate a variety of downstream pathways resulting in a biological response (e.g. cellular proliferation, differentiation, migration, survival, vessel formation or permeability). TKs can be further categorized as Receptor-Tyrosine Kinases (RTKs) and non-Receptor-Tyrosine Kinases (nRTKs). RTKs transduce extracellular signals into cells, while nRTKs reform intracellular communications. The downstream pathways of the overexpressed TKRs result in glioma angiogenesis and proliferation (**Figure 2**). Up to the present, a large number of TKIs are under clinical investigation for GBM. TKIs, as small hydrophobic molecules, can pass through the cellular membranes and inhibit the functions of multiple downstream pathway, whereas mAbs are extracellular antagonists of specific protein targets. Therefore, the majority of anti-angiogenic TKIs have multiple targets of several signaling pathways (e.g. VEGFRs EGFRs, FGFRs and PDGFRs) despite mAbs. Therefore, TKIs are more potent to reduce tumor angiogenesis than single-targeted blockade with mAbs. However, due to limited selectivity of TKIs, the off-target effects and systemic AEs are major challenges of TKIs. Despite the overproduction of TKRs in cancer cells and tumor ECs, TKs are expressed in lower levels in all cells. Consequently, inhibition of TKs can result in the impairment of important hemostatic or endocrine organs functions (e.g. thyroid gland or kidney). Nephrotic syndrome and hypothyroidism are rare but possible off-target effects of TKIs. Moreover, TKIs administration impairs the wound healing process due to a significant reduction in growth factors and may also cause bleedings due to impaired platelet interaction with ECs. In addition, the tumor heterogeneity affects the efficacy of TKIs. Taken together, accumulating evidence suggests that there are still many concerns about TKIs, including systemic AEs and low selectivity. Previously, it was taught that TKIs and mAbs do not insert cytotoxic effects on normal endothelia due to the quiescent state of adulthood ECs and only target tumor angiogenesis. However, some further investigations unveiled that anti-angiogenic therapy reduces survival and renewal capacity of normal ECs *via* growth factor signaling pathways. Hence, the development of novel anti-angiogenic agents with lower off-target effects can help reduce the side effects of systemic administration of TKIs or mAbs.

CLINICAL TRIAL PIPELINES OF ANTI-ANGIOGENIC TKIs FOR GBM

Table 3 summarizes some previous clinical trial pipelines of Antiangiogenic TKIs on GBM. Axitinib: Axitinib showed a manageable toxicity profile and the most frequent grade III/IV AEs were fatigue, diarrhea and oral hyperesthesia. Axitinib had objective response rates as a monotherapy compared with BV or lomustine (28% in axitinib-treated individuals and 23% in BV or lomustine-treated group) in a phase II trial. Another phase II trial suggested that Axitinib increases the response rate and progression-free survival in recurrent GBM, but the combination therapy of lomustine and Axitinib did not show any promising priorities compared to Axitinib monotherapy. The results of another phase II trial testing clinical efficacy and

TABLE 3 | Clinical trials on TKRs for GBM.

TKI	Co-therapy	Target	Phase	Ref.
Axitinib	–	VEGFR1, VEGFR2, VEGFR3	II	(31)
	+ lomustine			(32)
	+ avelumab			(33)
Cabozantinib	+TMZ+RT	RET, MET, VEGFR1, VEGFR2, VEGFR3, KIT, TRKB, FLT-3, AXL, TIE-2	I	(34)
Lenvatinib	+ everolimus	VEGFR1, VEGFR2, VEGFR3, FGFR1, FGFR2, FGFR3, PDGFRα, KIT, RET	I/II	(35)
Nintedanib	–	FGFR1, FGFR2, FGFR3, PDGFRα/β, VEGFR1, VEGFR2, VEGFR3, FLT3	II	(36, 37)
Pazopanib	+ lapatinib	VEGFR1, VEGFR2, VEGFR3, PDGFRα/β, FGFR 1/3, KIT, LCK, FMS, Itk	I/II	(38, 39)
	–		II	(40)
Sunitinib	–	PDGFRα/β, VEGFR1, VEGFR2, VEGFR3, c-KIT, FLT3, CSF-1R, RET	II	(41–45)
	+irinitecan		I	(46, 47)
Ponatinib	–	BCR-ABL, BCR-ABL T315I, VEGFR, PDGFR, FGFR, EPHR, SRC family kinases, KIT, RET, TIE2, FLT3	II	(48)
Regorafenib	–	VEGFR1, VEGFR2, VEGFR3, BCR-ABL, B-RAF, B-RAF(V600E),c-KIT, PDGFRα/β, RET, FGFR1/2, TIE2, Eph2A	II	(49)
Sorafenib	+RT*	B/C-RAF, B-RAF(V600E), KIT, FLT3, RET, VEGFR1, VEGFR2, VEGFR3, PDGFRβ	I/II	(50)
	–			(51)
Vandetanib		\	I/II	(52)
	+RT*	EGFR, VEGFR1, VEGFR2, VEGFR3, RET, BRK, TIE2, EPHRs, SRC kinases	I/II	(53)
	fractionated radiosurgery			(54)

**RT, Radiation therapy; VEGFR, VEGF receptor; PDGFR, Platelet-derived growth factor receptor; CSFR, Colony stimulating factor receptor.*

safety of Axitinib+Avelumab were not justifying for further clinical investigations (31–33). Cabozantinib: Phase I clinical investigations of Cabozantinib concurrent with chemradiation therapy in newly diagnosed patients with high-grade gliomas were well-tolerated and also showed promising results (34). Lenvatinib: in a phase I/II study for recurrent and refractory pediatric CNS tumors, the clinical efficacy and safety of Lenvatinib+ everolimus was investigated (35). Nintedanib: phase II clinical study of Nintedanib in recurrent high-grade gliomas showed promising results regardless of previous BV therapy. However, in another phase II clinical trial, Nintedanib showed minimal clinical anti-tumor activity despite its perfect safety profile with no grade III/IV AEs (36, 37). phase I/II trial in adult patients with relapsed malignant glioma, and the results showed limited efficacy. Also, monotherapy of Pazopanib did not associate with any significant survival benefits in a phase II investigation in patients with recurrent GBM (38–40). Sunitinib: monotherapy of Sunitinib showed insufficient activity as a monotherapy regimen in recurrent high-grade gliomas. The combination therapy of Sunitinib and Irinotecan showed moderate toxicity and limited anti-tumor activity (41–47). Ponatinib: Ponatinib administration in patients with BV-refractory GBMs showed minimal clinical efficacy (48). Regorafenib: The results of comparing Regorafenib with Lomustine in patients with relapsed GBM was promising with an encouraging overall survival benefit (49). Sorafenib: Sorafenib combined with radiation therapy and TMZ showed significant AEs and resulted in moderate clinical outcomes (50, 51). Vandetanib: Seizures were a major concern as a serious AE in Vandetanib monotherapy, and Vandetanib did not show significant anti-tumor activity in patients with recurrent malignant glioma (52–54).

ANTI-ANGIOGENIC APTAMERS

Aptamers are single-stranded short oligonucleotides with architectural folding to bind their targets (mostly proteins) with high specificity and affinity. Aptamers can be designed to target a wide range of biological targets (e.g. whole cells, nucleic acids, proteins, and peptides). Compared to mAbs, aptamers are advantageous in many aspects, which comprise (1) minimal immunogenicity (2) minimized toxicity (3) easy and fast *in-vitro* production without need for hosting animals (4) smaller size (8-15KD compared to 150 KD for mAbs) (5) higher tumor permeability (6) easy site-directed modifications (7) ability to be conjugated with broad ranges of tags (8) high chemical compatibility in organic and biological solutions (pH ranges:4-8.5 active temperature up to 95°C) and (9) lower cost. Design and discovery of aptamers is performed by Systematic Evolution of Ligands by Exponential Enrichment (SELEX) strategy, which includes a random synthesis step followed by selection, amplification and mutation steps. Potential challenges faced for clinical applications of aptamers are: (1) degradation by endogenous nucleases resulting in low stability in biofluids which can be further improved by backbone modifications (e.g. sugar modifications) or using spiegelmer®s. (2) Relatively high renal filtration rates. A possible strategy to overcome this challenge is PEGylation. The first anti-angiogenic aptamer FDA-approved for age-related macular degeneration was Pegaptanib-sodium (Macugen; Pfizer/Eyetech) (55). As a future perspective, aptamers can be used as theranostic agents delivering the cargo of interest to tumor site. Yet, further clinical investigations are required to shed light on the efficacy and safety of anti-angiogenic aptamers for GBM.

THE BBB HURDLE; STRATEGIES TO OVERCOME FOR GBM ANTI-ANGIOGENIC THERAPY

The BBB functions as a selective barrier to import nutrients so as to maintain neuronal survival and limit the passage of neurotoxins or infectious particles. The main element of BBB functions is the presence of dozens of tight junction proteins resulting in low para-cellular permeability (e.g. cluadins 3, 5, 12, ZO1 and occludin). However, several subsidiary mechanisms also maintain the appropriate BBB functions in physiological conditions including (1) high Transendothelial Endothelial Electrical Resistance (TEER) (2) low transcytosis/pinocytosis rates (3) lack of fenestrations in the apical surface of brain microvessels (4) size selectivity for diffusion of small molecules (e.g. lipophilic small molecules, O2, and CO2). (5) carrier-mediated transport of larger nutrients such as glucose, amino-acids, ketones, nucleosides and neurotransmitters (6) receptor-mediated transcytosis of specific proteins (e.g. transferrin, or insulin) (7) and efflux of toxic metabolites, xenobiotics, and chemo-agents (56). In the TME of GBM however, the BBB disruption is due to the following cellular or molecular mechanisms: (1) imbalance of tight junction proteins due to alterations in the synthesis, trafficking, or post-transcriptional modifications (2) secretion of multiple pro-inflammatory cytokines (3) extensive edema and increased interstitial fluid pressure (4) lower capability of tumor-reactive astrocytes to support normal BBB functions (5) active degeneration of the BBB tight junction proteins by invasion of glioma cells to tumor ECs (6) leaky and haphazard nature of glioma microvessels with suboptimal delivery functions (i.e. to deliver chemoagents or TKIs). Accumulating evidence suggests that the impaired BBB in GBM pathogenesis provides an important area of research to enhance drug delivery strategies for BBB penetration. This section is devoted to a detailed and critical literature review on the BBB targeting strategies previously reported. (1) Passive targeting: Nano-carriers (NCs) can passively target neoplastic tissues through Enhanced Permeability and Retention (EPR) effect. EPR and passive targeting is highly dependent NCs characteristics such as size, shape, spatial characteristics and surface charge as well as the tumor biology, itself. Previously, numerous passively-targeted NCs have been commercialized comprising Doxil™, Abraxane™, Marqibo™, DaunoXome™, and Onivyde™ in the US; Myocet™ and Mepact™; Genexol-PM™; and SMANCS™ however, there is a rising tendency to increase the accumulation rates and enhance tissue-specific-targeting by active strategies. (2) Active targeting: several Moieties can be used to actively deliver the siRNA cargo through the BBB, including receptor substrates, cell-penetrating peptides, mAbs, aptamers, monosaccharides, polysaccharides, proteins, peptides and surface modifications. Receptor-Mediated Transcytosis (RMT) is one of the most frequently used strategies to transfer the cargos of interest into the brain. The most common RMT targets are the transferrin receptor (TfR), low-density lipoprotein (LDL) receptor, insulin receptor, ApoE receptors growth factors, biotin-binding proteins, insulin, lactoferrin, and EGFR variants (**Figure 4**).

RNA INTERFERENCE: A FUTURE PERSPECTIVE FOR GBM ANTI- ANGIOGENIC THERAPY

Small interfering RNAs (siRNAs); known as 20-25 base pairs-in-length double-stranded non-coding RNAs; interfere expression of mRNAs. They are known as post-transcriptional silencers of a specific gene target by assembly of the RNA-induced silencing complex (RISC). This causes cleavage of the target mRNA molecules and its further degradation by cellular exonucleases (57). Molecular therapy using siRNA has indicated promising results in treating diseases caused by abnormal gene overexpression or mutation-based diseases. Naked siRNAs are unstable, and their physicochemical features (e.g. size and charge) may prevent them from crossing the BBB and the blood-tumor barrier (BTB). Additionally, they can potentiate immune responses when systemically administered and also may be entrapped by the reticuloendothelial system. Meanwhile, siRNAs loaded in tumor-targeted nanoparticles display many benefits, including minimal recognition by the immune system, more blood stability, high specificity and low off-target effects. Consequently, nanotechnology could aid development of novel and effective delivery systems that can enhance targeted delivery siRNAs and also protect them from degradation, rapid cellular washout and systemic clearance. When loaded in nano-carriers as a nanopelex, they are advantageous to mAbs/TKIs in several aspects as follows: (1) Firstly, siRNAs can be encapsulated into various nano-vehicles to mediate active transport of the nano-vehicle-siRNA complexes (nanoplexes) to targeted cells. Hence, nanoplexes may show higher tumor penetrance compared to intact mAbs (2) the nanovehicles' characteristics can be engineered to pass through the BBB more efficiently (e.g., by consumption of a BBB-penetrating peptide which mediates active transport of nano-vehicle) (3) circulation time, pharmacodynamics and pharmacokinetics of the nanoplexes is modifiable (4) Developing multidisciplinary treatment strategies (e.g., loading multiple siRNAs, chemo agents and also radio-active isotopes into a single nano-vehicle to increase the synergic potential) (5) siRNAs have relatively lower systemic adverse events due to precise tumor targeting (e.g. by loading tumor-specific Abs on the nanoparticle's surface). (6) Sustained and long release of siRNAs from engineered nano-vehicles reduces the injection frequency and increases the treatment efficacy (7) High selectivity of targeted nanoplexes to target a specific organ as well as a specific gene target reduces "off-target effects" compared to TKIs (8) need for relatively lower doses due to slow and targeted release which reduces tumor acquired resistance. To date, various carriers have been used for siRNA delivery to combat the main obstacles in GBM comprising liposomes, polymeric nanoparticles, gold nanoparticles and exosomes. Up to the present, only two clinical trials have been published on siRNA therapy for solid tumors (e.g. glioma), which are summarized in **Table 4**. Delivery of EphA2

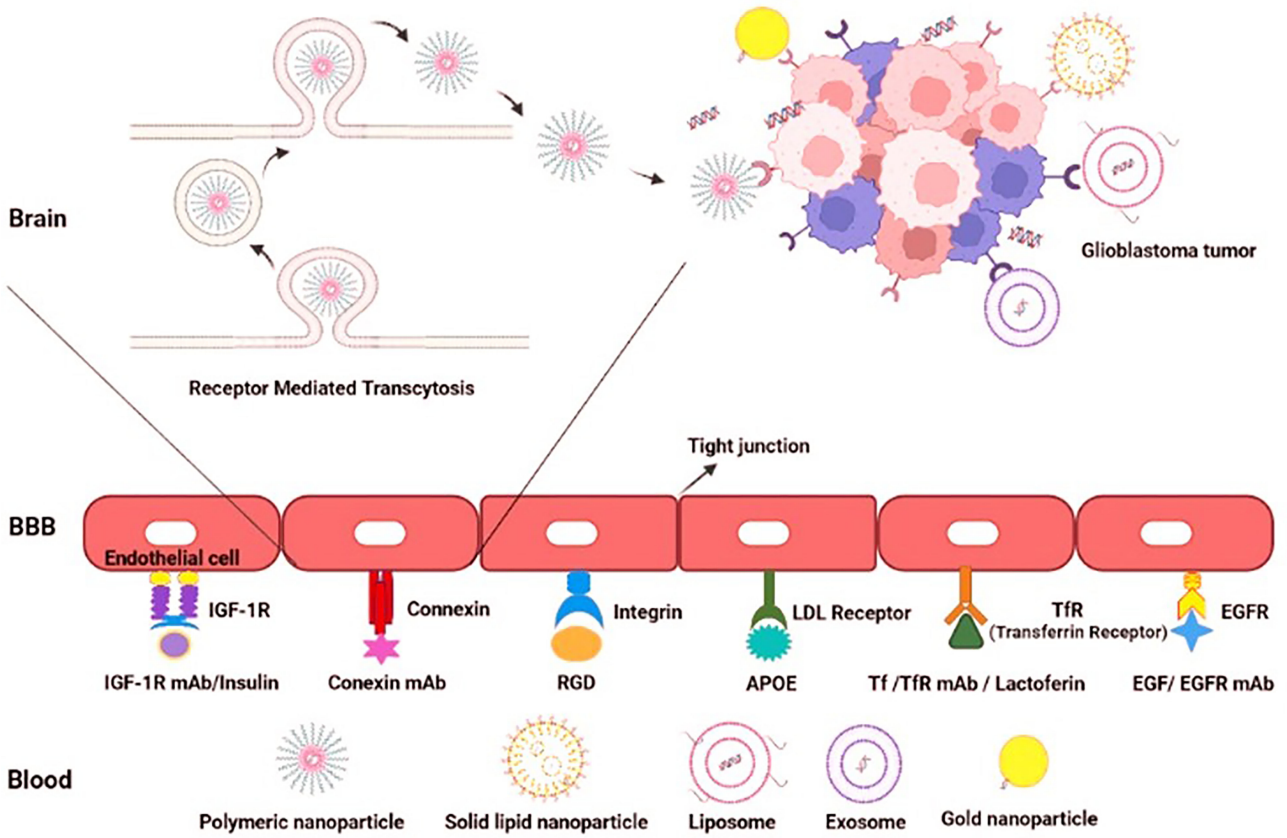

FIGURE 4 | Active targeting to overcome the BBB hurdle for drug delivery in GBM. Active targeting using receptor-mediated transcytosis by using a diverse range of nano-carriers.

TABLE 4 | Clinical trials on siRNAs for GBM.

SiRNA complex	Study phase	summary	Ref.
DOPC-encapsulated EphA2 siRNA	I	This first phase study examines the side effects and best dose of EphA2 siRNA in the treatment of patients with metastatic solid tumors or recurrent cases. DOPC-encapsulated siRNA slows the growth of tumor cells by targeting EphA2.	(58)
Bcl2L12 siRNA conjugated with gold nanoparticles	0	A potential treatment for GBM involves the use of RNA-interfering spherical nucleic acids that penetrate the brain and consist of nuclei of gold nanoparticles covalently bonded to small interfering RNA (siRNA) oligonucleotides.	(59)

siRNA *via* neutral liposomes (1,2-dioleoyl-sn-glycero-3-phosphatidylcholine or DOPC) in patients with advanced/recurrent neoplasms showed an acceptable safety profile. Moreover, delivery of Bcl2L12 siRNA-conjugated with gold nanoparticles penetrating BBB were promising and showed minimal toxicity (58, 59). Herein, we highlight the recent advances developing nano-carriers for siRNA delivery to GBM.

NANOVEHICLES FOR SIRNA DELIVERY ACROSS THE BBB

The synthesis strategy, size/charge optimization or conjugation strategies should be modulated for generating BBB penetrating nano-carriers with robust drug delivery properties. Previous literature suggests nano-carriers can be designed to pass through the BBB successfully (e.g., exosomes (60), liposomes (61–63), and even gold nanoparticles (64–66). An optimal nano-carrier for delivery of siRNAs should have the following characteristics; (1) protection drugs from degradation (2) low-immunogenic properties (3) high uptake rates by target cells (4) acceptable blood circulation time (5) rapid and high accumulation at target organs (6) a long and controlled release pattern to obtain a permanent and effective gene-silencing response. Potential challenges of using synthetic nano-carriers also comprise (1) low blood circulation time (2) rapid entrapment in filter organs and recognition by the immune system causing fast clearance and (3) immunogenicity.

Consequently, various strategies have been utilized to prolong nano-carriers' circulation time in the peripheral blood (e.g. by grafting biocompatible hydrophilic polymers like polyethylene glycol or PEG). PEGylation, impairs the opsonin proteins binding to nano-carriers and protects them from recognition by reticuloendothelial system. Moreover, PEGylation can effectively prevent nanoparticles from aggregation and the endosomal release due to its esteric barrier nature and also lowers the immunogenicity of the synthetic nanocarriers. Hence, the nano-carriers can accumulate in the tumor milieu in higher concentrations. Herein, we discuss the previous attempts using nanocarriers for siRNA delivery to GBM. Previously reported nanocarriers for siRNA delivery to GBM comprise the following:

(1) Cationic liposomes: One of the most frequently used nano-carriers for gene delivery is liposome. The liposome-siRNA complex is also named as a lipoplex. Due to the negatively-charged nature of oligonucleotides, cationic lipids have attracted much attention and have advantageous properties for optimization of gene delivery process in cancers which comprise (1) easy synthesis (2) surface-modifiable domains which facilitates engineering and targeting properties (3) high and efficient loading of nucleic acids through electrostatic interactions (4) the excess cationic coats also facilitate vectors binding to negatively charged cell membranes (5) interruption of endosomal membrane to improve cytoplasmic delivery of nucleic acids. Major hurdles that limits the advantages of lipoplexes for high yield siRNA delivery comprise (1) aqueous instability of suspensions limiting the shelf life of produced siRNA-nanoparticles (2) electrostatic attraction force also is a challenge for optimized synthesis and design of lipoplexes which directly impacts the therapeutic efficacy. A balance of strong enough to protect nucleic acids from degradation during transportation and weak enough to allow for timely release of the payload of nucleic acids within target cells should be maintained. Mounting the previous evidence, cationic liposomes functionalized with two receptor-specific peptides, including Angiopep-2 and neuropilin-1 has been developed for glioma targeting and BBB penetration, respectively. They reported successful knockdown of VEGF and inhibition of glioma growth by loading VEGF-siRNA and docetaxel in the Angiopep-2 and neuropilin-1 targeting liposomes (67). Wei et al. developed an effective siRNA delivery system through T7 peptide-conjugated cationic liposomes (named as T7-LPC/siRNA NPs) as a targeted drug delivery system for transferrin receptor-mediated active targeting for GMB therapy (68). Another hurdle in using liposomes for gene delivery purposes is the loading efficacy. Development of hybrid nano-systems or introducing different alkyl chains in the same lipid with varying lengths in the hydrophobic domain are possible strategies to overcome the loading efficacy and transfection challenge. (2) Polymeric nanoparticles: Polymeric nanoparticles offer high yield transfection and are advantageous for many reasons comprising unlimited gene packing and the ability of polyplexes to be extensively modified *via* multiple modifiable moieties. In addition, polymers with specific functional groups such as positively charged or pH-sensitive moieties promote the endosomal escape of encapsulated therapeutic agents into the cytoplasm. Among the cationic polymers previously suggested for targeted drug delivery to brain, Poly (lactic-co-glycolic acid) PLGA, poly (glycolic acid) PGA, and poly (lactic acid) PLA are frequently reported. PLGA and PLA has been approved by the US Food and Drug Administration (FDA) for clinical use in humans therefore can be considered as a safe option for brain drug delivery. Kozielski et al. developed a biodegradable polymer consisting two monomers (1) bis(2-hydroxyethyl) disulfide (BR6) and (2) 4-amino-1-butanol (S4) to deliver siRNAs targeting GBM-promoting genes (e.g. Survivin, EGFR, NKCC1, YAP1, and Robo1) with promising results (69). Polyamidoamine (PAMAM) dendrimers are one of the most frequently used cationic polymers, which comprise of a variety of surface functional groups (-OH, -COOH, -NH2). Moreover, these nanoparticles has a pH-sensitive property due to the existence of protonated amine groups in an acidic condition, which imparts electrostatic repulsion between the polymer chains. These attractive features provide a versatile carrier for controlled siRNA delivery in GBM. One example was a PAMAM-dendrimer carrier with a RGD receptor-specific anchored to the surface, which was designed for the delivery of siRNA plus doxorubicin (DOX) against GBM. Peptides containing an arginine-glycine-aspartic acid (RGD) can be detected by the integrin receptors, especially $\alpha v\beta 3$, which are often overexpressed in tumor cells, but rarely identified in normal tissue cells. Previous evidence suggested that these pH-sensitive effectively penetrate the BBB and co-deliver Doxorubicin and c-Myc-siRNAs in order to suppress GBM progression (70). Gold nanoparticles: Gold nanoparticles are reliable drug delivery systems for loading siRNAs conjugated covalently or by electrostatic conjugation onto their surface. The free thiol groups also can be used for surface modifications and bio-conjugation of targeting moieties to gold nanoparticles. Promising results have been reported by using synthetized gold-liposome nanoparticles functionalized with ApoE and rabies virus glycoprotein (RVG) as the targeting peptides for brain delivery (71). Solid Lipid Nanoparticles (SLNs): SLNs are also considered as promising nano-carriers for gene delivery because of their lipid nature, biodegradability and bio-compatibility. Due to their promising properties for oligonucleotide delivery, SLNs have been used for generation of the COVID19 vaccine; Pfizer recently. Neves et al. prepared a solid lipid nanoparticles (SLNs) functionalized with ApoE to improve brain drug delivery. Confocal images and flow-cytometry results indicated an increase in brain cellular uptake compared to the non-conjugated SLNs (72). Super-paramagnetic iron oxide nanoparticles (SPIONPs): SPIONPs have a wide range of clinical utilities (e.g. theranostic applications and hyperthermia). When external magnetic field is applied, SPIONPs can be used for efficient and targeted delivery of the loaded cargos with potential advantages such as high stability and increased blood circulation. Previously,

EGFR-conjugated superparamagnetic iron oxide nanoparticles (SPIONPs) were loaded with survivin siRNAs (apoptosis-related inhibitors) and doxorubicin with promising results (73). Biological nanocarriers such as exosomes: Exosomes are natural drug delivery systems (40–100 nm) with advantageous properties for either active or passive targeting secreted by various cell types and are able to transfer different types of biological molecules (e.g. mRNAs and small RNAs). They can be obtained from autologous dendritic cells (DCs), Chimeric Antigen Receptor T cells (CAR T cells), stromal/stem cells (bone-marrow derived mesenchymal stem cells, placenta derived mesenchymal stem cells or adipose tissue mesenchymal stem cells), Natural Killer Cells (NK cells), CAR NK cells or NK T cells. To focus on the biogenesis process, one of the major exosome formation mechanisms is the endosomal sorting complexes required for transport (ESCRT) pathway however ESCRT-independent pathways may also be responsible for EV formation. Consequently, ESCRT proteins and their accessory proteins (Alix, TSG101, HSC70, and HSP90β) are noted as positive EV markers for characterization however the Tetraspanin transmembrane proteins family (e.g. CD63, CD81, and CD9) are also of the frequent markers used for EV characterization and validation of EV purification procedures (**Figure 5**) (74). Encapsulated drugs in exosomes have demonstrated multiple advantages compared to synthetic nanoparticles, including (1) more biocompatibility due to human-derived nature and better membrane fusion (2) unique proteo-lipid structure which stabilizes exosomes in blood circulation and increases their shelf-life (3) minimal recognition by the mononuclear phagocytic system (MPS) and immunogenicity (4) easy and fast production from cell culture media; a byproduct of cell-therapy facilities (5) intrinsic anti-cancer cargos of exosomes derived from mesenchymal cells or dendritic cells (e.g., miRNAs, proteins, mRNAs, or DNA fragments). Added to the mentioned advantages, exosomes may have the ability to cross different biological barriers (e.g. the BBB) (75). Despite the potential advantages of exosomes as biological nanocarriers,

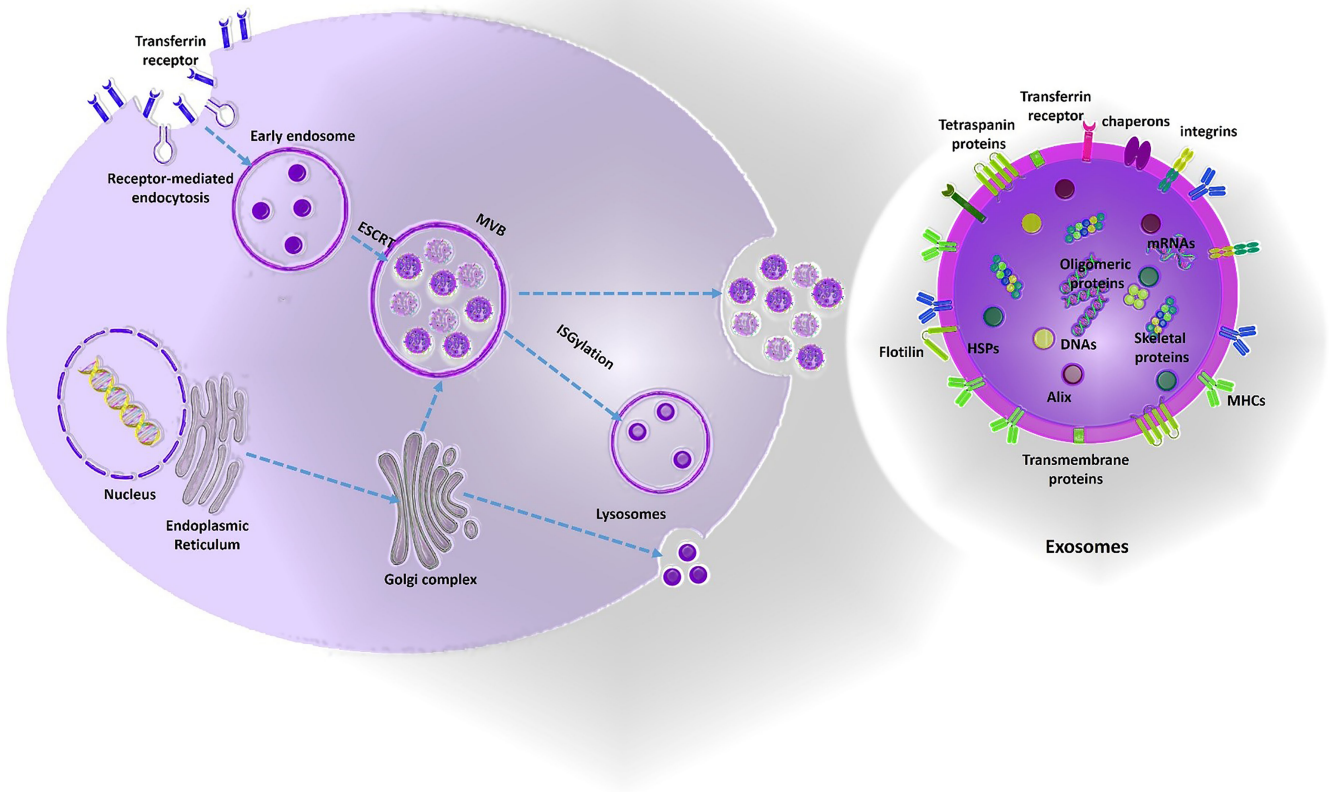

FIGURE 5 | Exosomes biogenesis. Mainly, exosomes are produced by ESCRT- dependent mechanisms from early endosomes into the multivesicular bodies (MVBs). Exosomes contain the members of tetraspanin protein family and ESCRT proteins and their accessory proteins as positive markers for EV characterization. Moreover, exosomes also contain signaling cargos which mediate paracrine interaction of cells (DNAs, proteins, and also RNAs). Exomes are potent engineerable biological nano-carriers which pass through the BBB and can be used as a trojan horse to deliver the drugs to the brain. Some of the vectors used to design this figure were downloaded from Vecteezy under a free license.

scale up process for high yield and purified exosome production faces many potential challenges. Major industrial-Scale exosome isolation methods depend on ultracentrifugation and ultrafiltration and both methods are time-consuming and have low yield for clinical applications (76). Mounting the previous evidence, Erviti et al. prepared engineered Lamp2b expressing self-derived dendritic cell exosomes for siRNA delivery to target the neuron-specific RVG peptide which is preferably expressed in the neurons, microglia, oligodendrocytes in the brain leading to a knockdown rate of 60% at mRNA level and 62% at protein-level for BACE1 (77). Another hurdle to use exosomes for siRNA delivery is the loading efficacy which does not exceed 20-30% in most of the previous studies. Modifying the siRNAs by adding hydrophobic tags (e.g. cholesterol tags) is a potential strategy to overcome the loading efficacy challenge (78).

CONCLUSIONS

Next-Generation Anti-Angiogenic Therapies

Tumor angiogenesis is a vital mechanism for maintaining tumor cell survival, providing nutrients, and oxygen uptake. Inhibition of tumor angiogenesis can act as a highly effective mechanism to combat vascular-rich tumors such as GBM. So far, extensive research has been focused on the production of novel anti-angiogenic drugs for gliomas, most of them were focused on mAbs and TKIs. Clinical application of intact mAbs faces many challenges, including low penetration into solid tumor tissues, failure to cross the BBB due to its large size, and systemic side effects. Despite the advantages of TKIs compared to mAbs (i.e., including smaller size and targeting angiogenesis *via* several molecular pathways), they also have disadvantages such as low selectivity. TKs are expressed in numerous cell types and systemic inhibition of TKs increases the risk of major systemic toxicities. Moreover, acquired resistance to anti-angiogenic TKIs is another challenge which limits their clinical advantages as adjuvants to radiation therapy or chemotherapy as a post-surgical management strategy (79). As a future perspective, siRNAs are potent effective silencers of tumor angiogenic gene expression for GBM. Exosomes obtained from various cell sources comprising autologous dendritic cells (DCs), Chimeric Antigen Receptor T cells (CAR T cells), stromal/stem cells (bone-marrow derived mesenchymal stem cells, placenta derived mesenchymal stem cells or adipose tissue mesenchymal stem cells), Natural Killer Cells (NK cells), CAR NK cells or NK T cells can serve as potent biological nano-carriers for efficient and targeted drug delivery to GBM with modifiable surface characteristics for a precisely targeted therapy with minimal systemic adverse side effects (80). Moreover, exosomes can also be used to minimize the AEs of chemo agents by targeting them directly to the tumor site with priorities to synthetic nanocarriers such as liposomes due to their human-derived and biological nature (81). Additionally, using nanobodies as an immunotaregting strategy could aid deliver the cargo of interest to tumor site with minimal systemic adverse events and optimal passage through the BBB (82).

Combination Therapy; a Future Perspective to Improve Anti-Angiogenic Therapy Efficacy

As another future perspective, adjuvant combination immunotherapies may aid increase the efficacy of anti-angiogenic therapy for GBM which comprise immune checkpoint blockade (83) and DC vaccination. Moreover, using anti-angiogenic agents which target multiple downstream angiogenic signaling pathways or using a combination of antiangiogenic agents may help reduce therapy resistance and also using long-release nanoparticles to maintain the antiangiogenic properties at a low permanent concentration rather than using high dose interrupted systemic injections of mAbs/TKIs may also be effective strategies to overcome therapy resistance (84, 85). Combination therapies of antiangiogenic agents with chemoagents are also a future perspective to obtain a permanent anti-tumor response (86). In addition, anti-angiogenic therapy could serve as a potential complementary treatment adjuvant to many anti-cancer immunotherapies comprising DC therapy or adoptive T/CART cells transfer. Previous literature suggests that there is a substantial relationship between tumor aberrant angiogenesis and cytotoxic T cells functions as well as dynamics of DC maturation. Anti-angiogensis therapy empowers anti-tumor immune response and therfore using anti-angiogenic agents as adjuvants to immune therapy may be a future perspective for more efficient treatment of the GBM. In addition to increasing knowledge about developing safe and efficient nano-carriers for effective siRNA delivery, the identification of novel strategies to overcome the BBB hurdle such as using focused ultrasound will also enhance our ability to target GBM (87). Generating multidisciplinary nanoplexes delivering anti-cancer agents (e.g. chemoagents) and antiangiogenic therapeutic cargos could be a future perspective to combat glioma angiogenesis with minimal systemic adverse events and high potency in the future. Up to present numerous multidisciplinary nanoplexes are being tested in preclinical grades which could serve as potential clinical-grade next-generation anti-angiogenic therapeutics for GBM (88–98). Future work will shed light to the clinical applicability of active targeting using RMT to overcome the BBB hurdle for GBM drug delivery (99–103).

Optimizing Carrier Design for Potent Drug Delivery Through the BBB

Despite accumulating preclinical evidence on designing BBB penetrating vehicles, still a major hurdle for successful delivery of anti-angiogenic agents to brain in clinical settings is the BBB. Despite accumulating preclinical evidence on designing BBB penetrating vehicles, still a major hurdle for successful delivery of anti-angiogenic agents to brain in clinical settings is the BBB. Up to present, numerous strategies have been introduced to overcome the BBB hurdle comprising: Convection enhanced delivery (CED), chemical permeation using vasoactive agents and hyperosmotic Manitol, physical permeation by applying external magnetic fields for magnetic vehicles, using

intraoperative drug-coated wafers or intraventricular injections. However, a major shortcoming for the aforementioned methods is the infection risk. One of the most promising methods which could serve as a future prospect is active targeting *via* RMT. Future work will shed light to the clinical applicability of active targeting using RMT to overcome the BBB hurdle for GBM drug delivery.

AUTHOR CONTRIBUTIONS

PS and SL conceptualized and wrote the manuscript. FHA and NE also participated in writing up the paper. AZ guided the surgical aspects. MA and DA conceptualized, supervised and wrote the manuscript. All the authors have read and approved the final draft.

REFERENCES

1. Rojiani AM, Dorovini-Zis K. Glomeruloid Vascular Structures in Glioblastoma Multiforme: An Immunohistochemical and Ultrastructural Study. *J Neurosurg* (1996) 85(6):1078–84. doi: 10.3171/jns.1996.85.6.1078
2. Folkman J. Tumor Angiogenesis. *Adv Cancer Res* (1974) 19:331–58. doi: 10.1016/S0065-230X(08)60058-5
3. Maniotis AJ, Folberg R, Hess A, Seftor EA, Gardner LM, Pe'er J, et al. Vascular Channel Formation by Human Melanoma Cells *In Vivo* and *In Vitro*: Vasculogenic Mimicry. *Am J Pathol* (1999) 155(3):739–52. doi: 10.1016/S0002-9440(10)65173-5
4. Hao X, Sun B, Zhang S, Zhao X. Correlation between the Expression of Collgen Iv, Vegf and Vasculogenic Mimicry. *Zhonghua Zhong Liu Za Zhi* (2003) 25(6):524–6.
5. Xiang T, Lin Y-X, Ma W, Zhang H-J, Chen K-M, He G-P, et al. Vasculogenic Mimicry Formation in Ebv-Associated Epithelial Malignancies. *Nat Commun* (2018) 9(1):1–15. doi: 10.1038/s41467-018-07308-5
6. Liu X-m, Zhang Q-p, Mu Y-g, Zhang X-h, Sai K, Pang JC-S, et al. Clinical Significance of Vasculogenic Mimicry in Human Gliomas. *J Neurooncol* (2011) 105(2):173–9. doi: 10.1007/s11060-011-0578-5
7. Wei X, Chen Y, Jiang X, Peng M, Liu Y, Mo Y, et al. Mechanisms of Vasculogenic Mimicry in Hypoxic Tumor Microenvironments. *Mol Cancer* (2021) 20(1):1–18. doi: 10.1186/s12943-020-01288-1
8. Birnbaum T, Roider J, Schankin CJ, Padovan CS, Schichor C, Goldbrunner R, et al. Malignant Gliomas Actively Recruit Bone Marrow Stromal Cells by Secreting Angiogenic Cytokines. *J Neurooncol* (2007) 83(3):241–7. doi: 10.1007/s11060-007-9332-4
9. Onguru O, Gamsizkan M, Ulutin C, Gunhan O. Cyclooxygenase-2 (Cox-2) Expression and Angiogenesis in Glioblastoma. *Neuropathology* (2008) 28 (1):29–34. doi: 10.1111/j.1440-1789.2007.00828.x
10. Kim G, Ko YT. Small Molecule Tyrosine Kinase Inhibitors in Glioblastoma. *Arch Pharm Res* (2020) 43(4):385–94. doi: 10.1007/s12272-020-01232-3
11. Seano G, Jain RK. Vessel Co-Option in Glioblastoma: Emerging Insights and Opportunities. *Angiogenesis* (2020) 23(1):9–16. doi: 10.1007/s10456-019-09691-z
12. Kuczynski EA, Reynolds AR. Vessel Co-Option and Resistance to Anti-Angiogenic Therapy. *Angiogenesis* (2020) 23(1):55–74. doi: 10.1007/s10456-019-09698-6
13. Rahbarizadeh F, Ahmadvand D, Sharifzadeh Z. Nanobody; an Old Concept and New Vehicle for Immunotargeting. *Immunol Invest* (2011) 40(3):299–338. doi: 10.3109/08820139.2010.542228
14. Sadeqzadeh E, Rahbarizadeh F, Ahmadvand D, Rasaee MJ, Parhamifar L, Moghimi SM. Combined Muc1-Specific Nanobody-Tagged Peg-Polyethylenimine Polyplex Targeting and Transcriptional Targeting of Tbid Transgene for Directed Killing of Muc1 over-Expressing Tumour Cells. *J Control Release* (2011) 156(1):85–91. doi: 10.1016/j.jconrel.2011.06.022
15. Muruganandam A, Tanha J, Narang S, Stanimirovic D. Selection of Phage-Displayed Llama Single-Domain Antibodies That Transmigrate across Human Blood-Brain Barrier Endothelium. *FASEB J* (2002) 16(2):1–22. doi: 10.1096/fj.01-0343fje
16. Wouters Y, Jaspers T, De Strooper B, Dewilde M. Identification and *In Vivo* Characterization of a Brain-Penetrating Nanobody. *Fluids Barriers CNS* (2020) 17(1):1–10. doi: 10.1186/s12987-020-00226-z
17. Li T, Vandesquille M, Koukouli F, Dudeffant C, Youssef I, Lenormand P, et al. Camelid Single-Domain Antibodies: A Versatile Tool for *In Vivo* Imaging of Extracellular and Intracellular Brain Targets. *J Control Release* (2016) 243:1–10. doi: 10.1016/j.jconrel.2016.09.019
18. Farrington GK, Caram-Salas N, Haqqani AS, Brunette E, Eldredge J, Pepinsky B, et al. A Novel Platform for Engineering Blood-Brain Barrier-Crossing Bispecific Biologics. *FASEB J* (2014) 28(11):4764–78. doi: 10.1096/fj.14-253369
19. Vandesquille M, Li T, Po C, Ganneau C, Lenormand P, Dudeffant C, et al. Chemically-Defined Camelid Antibody Bioconjugate for the Magnetic Resonance Imaging of Alzheimer's Disease. *MAbs* (2017). doi: 10.1080/19420862.2017.1342914
20. Rutgers K, Nabuurs R, Van den Berg S, Schenk G, Rotman M, Verrips C, et al. Transmigration of Beta Amyloid Specific Heavy Chain Antibody Fragments across the in Vitro Blood–Brain Barrier. *Neuroscience* (2011) 190:37–42. doi: 10.1016/j.neuroscience.2011.05.076
21. Gao Y, Zhu J, Lu H. Single Domain Antibody-Based Vectors in the Delivery of Biologics across the Blood–Brain Barrier: A Review. *Drug Deliv Trans Res* (2021) 11(5):1818–28. doi: 10.1007/s13346-020-00873-7
22. Wu L-P, Ahmadvand D, Su J, Hall A, Tan X, Farhangrazi ZS, et al. Crossing the Blood-Brain-Barrier with Nanoligand Drug Carriers Self-Assembled from a Phage Display Peptide. *Nat Commun* (2019) 10(1):1–16. doi: 10.1038/s41467-019-12554-2
23. De Groot JF, Lamborn KR, Chang SM, Gilbert MR, Cloughesy TF, Aldape K, et al. Phase Ii Study of Aflibercept in Recurrent Malignant Glioma: A North American Brain Tumor Consortium Study. *J Clin Oncol* (2011) 29(19):2689. doi: 10.1200/JCO.2010.34.1636
24. De Groot J, Wen P, Lamborn K, Chang S, Cloughesy T, Chen A, et al. Phase Ii Single Arm Trial of Aflibercept in Patients with Recurrent Temozolomide-Resistant Glioblastoma: Nabtc 0601. *J Clin Oncol* (2008) 26(15_suppl):2020. doi: 10.1200/jco.2008.26.15_suppl.2020
25. De Groot J, Cloughesy T, Lieberman F, Chang S, Omuro A, Drappatz J, et al. Phase I Study of Aflibercept (Vegf Trap) and Temozolomide in Newly Diagnosed, High-Grade Glioma. *J Clin Oncol* (2011) 29(15_suppl):2043. doi: 10.1200/jco.2011.29.15_suppl.2043
26. Nayak L, de Groot J, Wefel JS, Cloughesy TF, Lieberman F, Chang SM, et al. Phase I Trial of Aflibercept (Vegf Trap) with Radiation Therapy and Concomitant and Adjuvant Temozolomide in Patients with High-Grade Gliomas. *J Neurooncol* (2017) 132(1):181–8. doi: 10.1007/s11060-016-2357-9
27. Cher L, Nowak A, Iatropoulos G, Lee WS, Lee SY, Shim SR, et al. Actr-75. A Multicenter, 3-Arm, Open-Label, Phase Iia Clinical Trial to Evaluate Safety and Efficacy of Tanibirumab (Vegfr2 Mab), in Patients with Recurrent Gbm Assessed with K-Trans and Initial Area under the Gadolinium Concentration-Time Curve (Iaugc). *Neuro Oncol* (2017) 19(Suppl 6):17. doi: 10.1093/neuonc/nox168.062
28. Lee SJ, Lee SY, Lee WS, Yoo JS, Sun J-M, Lee J, et al. Phase I Trial and Pharmacokinetic Study of Tanibirumab, a Fully Human Monoclonal Antibody to Vascular Endothelial Growth Factor Receptor 2, in Patients with Refractory Solid Tumors. *Invest New Drugs* (2017) 35(6):782–90. doi: 10.1007/s10637-017-0463-y
29. Neyns B, Sadones J, Joosens E, Bouttens F, Verbeke L, Baurain J-F, et al. Stratified Phase Ii Trial of Cetuximab in Patients with Recurrent High-Grade Glioma. *Ann Oncol* (2009) 20(9):1596–603. doi: 10.1093/annonc/mdp032
30. Cloughesy T, Finocchiaro G, Belda-Iniesta C, Recht L, Brandes AA, Pineda E, et al. Randomized, Double-Blind, Placebo-Controlled, Multicenter Phase Ii Study of Onartuzumab Plus Bevacizumab Versus Placebo Plus Bevacizumab in Patients with Recurrent Glioblastoma: Efficacy, Safety, and Hepatocyte Growth Factor and O (6)-Methylguanine-DNA Methyltransferase Biomarker Analyses. *J Clin Oncol* (2017) 35(3):343–51. doi: 10.1200/JCO.2015.64.7685
31. Duerinck J, Du Four S, Vandervorst F, D'Haene N, Le Mercier M, Michotte A, et al. Randomized Phase Ii Study of Axitinib Versus Physicians Best

Alternative Choice of Therapy in Patients with Recurrent Glioblastoma. *J Neurooncol* (2016) 128(1):147–55. doi: 10.1007/s11060-016-2092-2
32. Duerinck J, Du Four S, Bouttens F, Andre C, Verschaeve V, Van Fraeyenhove F, et al. Randomized Phase Ii Trial Comparing Axitinib with the Combination of Axitinib and Lomustine in Patients with Recurrent Glioblastoma. *J Neurooncol* (2018) 136(1):115–25. doi: 10.1007/s11060-017-2629-z
33. Awada G, Salama LB, De Cremer J, Schwarze JK, Fischbuch L, Seynaeve L, et al. Axitinib Plus Avelumab in the Treatment of Recurrent Glioblastoma: A Stratified, Open-Label, Single-Center Phase 2 Clinical Trial (Gliavax). *J Immunother Cancer* (2020) 8 (2). doi: 10.1136/jitc-2020-001146
34. Schiff D, Desjardins A, Cloughesy T, Mikkelsen T, Glantz M, Chamberlain MC, et al. Phase 1 Dose Escalation Trial of the Safety and Pharmacokinetics of Cabozantinib Concurrent with Temozolomide and Radiotherapy or Temozolomide After Radiotherapy in Newly Diagnosed Patients with High-Grade Gliomas. *Cancer* (2016) 122(4):582–7. doi: 10.1002/cncr.29798
35. Dela Cruz FS, Fox E, Muscal JA, Kirov I, Geller JI, DuBois SG, et al. A Phase I/Ii Study of Lenvatinib (Len) Plus Everolimus (Eve) in Recurrent and Refractory Pediatric Solid Tumors, Including Cns Tumors. *J Clin Oncol* (2020) 38(15_suppl):10527. doi: 10.1200/JCO.2020.38.15_suppl.10527
36. Norden AD, Schiff D, Ahluwalia MS, Lesser GJ, Nayak L, Lee EQ, et al. Phase Ii Trial of Triple Tyrosine Kinase Receptor Inhibitor Nintedanib in Recurrent High-Grade Gliomas. *J Neurooncol* (2015) 121(2):297–302. doi: 10.1007/s11060-014-1631-y
37. Muhic A, Poulsen HS, Sorensen M, Grunnet K, Lassen U. Phase Ii Open-Label Study of Nintedanib in Patients with Recurrent Glioblastoma Multiforme. *J Neurooncol* (2013) 111(2):205–12. doi: 10.1007/s11060-012-1009-y
38. Reardon DA, Groves MD, Wen PY, Nabors L, Mikkelsen T, Rosenfeld S, et al. A Phase I/Ii Trial of Pazopanib in Combination with Lapatinib in Adult Patients with Relapsed Malignant Glioma. *Clin Cancer Res* (2013) 19 (4):900–8. doi: 10.1158/1078-0432.CCR-12-1707
39. Frentzas S, Groves M, Barriuso J, Harris D, Reardon D, Curtis M, et al. Pazopanib and Lapatinib in Patients with Relapsed Malignant Glioma: Results of a Phase I/Ii Study. *J Clin Oncol* (2009) 27(15_suppl):2040–. doi: 10.1200/jco.2009.27.15_suppl.2040
40. Iwamoto FM, Lamborn KR, Robins HI, Mehta MP, Chang SM, Butowski NA, et al. Phase II Trial of Pazopanib (Gw786034), an Oral Multi-Targeted Angiogenesis Inhibitor, for Adults with Recurrent Glioblastoma (North American Brain Tumor Consortium Study 06-02). *Neuro Oncol* (2010) 12 (8):855–61. doi: 10.1093/neuonc/noq025
41. Neyns B, Sadones J, Chaskis C, Dujardin M, Everaert H, Lv S, et al. Phase II Study of Sunitinib Malate in Patients with Recurrent High-Grade Glioma. *J Neurooncol* (2011) 103(3):491–501. doi: 10.1007/s11060-010-0402-7
42. Pan E, Yu D, Yue B, Potthast L, Chowdhary S, Smith P, et al. A Prospective Phase II Single-Institution Trial of Sunitinib for Recurrent Malignant Glioma. *J Neurooncol* (2012) 110(1):111–8. doi: 10.1007/s11060-012-0943-z
43. Chaskis C, Sadones J, Michotte A, Dujardin M, Everaert H, Neyns B. A Phase II Trial of Sunitinib in Patients with Recurrent High-Grade Glioma. *J Clin Oncol* (2008) 26(15_suppl):13001. doi: 10.1200/jco.2008.26.15_suppl.13001
44. Wetmore C, Daryani VM, Billups CA, Boyett JM, Leary S, Tanos R, et al. Phase Ii Evaluation of Sunitinib in the Treatment of Recurrent or Refractory High-Grade Glioma or Ependymoma in Children: A Children's Oncology Group Study Acns1021. *Cancer Med* (2016) 5(7):1416–24. doi: 10.1002/cam4.713
45. Neyns B, Chaskis C, Dujardin M, Everaert H, Sadones J, Nupponen N, et al. Phase Ii Trial of Sunitinib Malate in Patients with Temozolomide Refractory Recurrent High-Grade Glioma. *J Clin Oncol* (2009) 27(15_suppl):2038. doi: 10.1200/jco.2009.27.15_suppl.2038
46. Reardon DA, Vredenburgh JJ, Coan A, Desjardins A, Peters KB, Gururangan S, et al. Phase I Study of Sunitinib and Irinotecan for Patients with Recurrent Malignant Glioma. *J Neurooncol* (2011) 105(3):621–7. doi: 10.1007/s11060-011-0631-4
47. Friedman H, Vredenburgh J, Desjardins A, Janney D, Peters K, Friedman A, et al. A Phase I Study of Sunitinib Plus Irinotecan in the Treatment of Patients with Recurrent Malignant Glioma. *J Clin Oncol* (2009) 27 (15_suppl):e13024–e. doi: 10.1200/jco.2009.27.15_suppl.e13024
48. Lee EQ, Muzikansky A, Duda DG, Gaffey S, Dietrich J, Nayak L, et al. Phase Ii Trial of Ponatinib in Patients with Bevacizumab-Refractory Glioblastoma. *Cancer Med* (2019) 8(13):5988–94. doi: 10.1002/cam4.2505
49. Lombardi G, De Salvo GL, Brandes AA, Eoli M, Rudà R, Faedi M, et al. Regorafenib Compared with Lomustine in Patients with Relapsed Glioblastoma (Regoma): A Multicentre, Open-Label, Randomised, Controlled, Phase 2 Trial. *Lancet Oncol* (2019) 20(1):110–9. doi: 10.1016/S1470-2045(18)30675-2
50. Hottinger A, Aissa AB, Espeli V, Squiban D, Dunkel N, Vargas M, et al. Phase I Study of Sorafenib Combined with Radiation Therapy and Temozolomide as First-Line Treatment of High-Grade Glioma. *Br J Cancer* (2014) 110(11):2655–61. doi: 10.1038/bjc.2014.209
51. Nabors L, Supko J, Rosenfeld M, Chamberlain M, Phuphanich S, Batchelor T, et al. Phase I Trial of Sorafenib in Patients with Recurrent or Progressive Malignant Glioma. *Neuro Oncol* (2011) 13(12):1324–30. doi: 10.1093/neuonc/nor145
52. Kreisl TN, McNeill KA, Sul J, Iwamoto FM, Shih J, Fine HA. A Phase I/Ii Trial of Vandetanib for Patients with Recurrent Malignant Glioma. *Neuro Oncol* (2012) 14(12):1519–26. doi: 10.1093/neuonc/nos265
53. Broniscer A, Baker JN, Tagen M, Onar-Thomas A, Gilbertson RJ, Davidoff AM, et al. Phase I Study of Vandetanib During and after Radiotherapy in Children with Diffuse Intrinsic Pontine Glioma. *J Clin Oncol* (2010) 28 (31):4762. doi: 10.1200/JCO.2010.30.3545
54. Fields EC, Damek D, Gaspar LE, Liu AK, Kavanagh BD, Waziri A, et al. Phase I Dose Escalation Trial of Vandetanib with Fractionated Radiosurgery in Patients with Recurrent Malignant Gliomas. *Int J Radiat Oncol Biol Phys* (2012) 82(1):51–7. doi: 10.1016/j.ijrobp.2010.09.008
55. Moshfeghi AA, Puliafito CA. Pegaptanib Sodium for the Treatment of Neovascular Age-Related Macular Degeneration. *Expert Opin Invest Drugs* (2005) 14(5):671–82. doi: 10.1517/13543784.14.5.671
56. Harder BG, Blomquist MR, Wang J, Kim AJ, Woodworth GF, Winkles JA, et al. Developments in Blood-Brain Barrier Penetrance and Drug Repurposing for Improved Treatment of Glioblastoma. *Front Oncol* (2018) 8:462. doi: 10.3389/fonc.2018.00462
57. Mocellin S, Provenzano M. RNA Interference: Learning Gene Knock-Down from Cell Physiology. *J Trans Med* (2004) 2(1):1–6.
58. Available at: https://clinicaltrials.gov/ct2/show/NCT01591356.
59. Kumthekar P, Ko CH, Paunesku T, Dixit K, Sonabend AM, Bloch O, et al. A First-in-Human Phase 0 Clinical Study of Rna Interference–Based Spherical Nucleic Acids in Patients with Recurrent Glioblastoma. *Sci Trans Med* (2021) 13(584):eabb3945. doi: 10.1126/scitranslmed.abb3945
60. Chen CC, Liu L, Ma F, Wong CW, Guo XE, Chacko JV, et al. Elucidation of Exosome Migration across the Blood–Brain Barrier Model *In Vitro*. *Cell Mol Bioeng* (2016) 9(4):509–29. doi: 10.1007/s12195-016-0458-3
61. Gao J-Q, Lv Q, Li L-M, Tang X-J, Li F-Z, Hu Y-L, et al. Glioma Targeting and Blood–Brain Barrier Penetration by Dual-Targeting Doxorubincin Liposomes. *Biomaterials* (2013) 34(22):5628–39. doi: 10.1016/j.biomaterials.2013.03.097
62. Vieira DB, Gamarra LF. Getting into the Brain: Liposome-Based Strategies for Effective Drug Delivery across the Blood–Brain Barrier. *Int J Nanomed* (2016) 11:5381. doi: 10.2147/IJN.S117210
63. Agrawal M, Tripathi DK, Saraf S, Saraf S, Antimisiaris SG, Mourtas S, et al. Recent Advancements in Liposomes Targeting Strategies to Cross Blood-Brain Barrier (Bbb) for the Treatment of Alzheimer's Disease. *J Control Release* (2017) 260:61–77. doi: 10.1016/j.jconrel.2017.05.019
64. Khongkow M, Yata T, Boonrungsiman S, Ruktanonchai UR, Graham D, Namdee K. Surface Modification of Gold Nanoparticles with Neuron-Targeted Exosome for Enhanced Blood–Brain Barrier Penetration. *Sci Rep* (2019) 9(1):1–9. doi: 10.1038/s41598-019-44569-6
65. Cheng Y, Dai Q, Morshed RA, Fan X, Wegscheid ML, Wainwright DA, et al. Blood-Brain Barrier Permeable Gold Nanoparticles: An Efficient Delivery Platform for Enhanced Malignant Glioma Therapy and Imaging. *Small* (2014) 10(24):5137–50. doi: 10.1002/smll.201400654
66. Sokolova V, Mekky G, van der Meer SB, Seeds MC, Atala AJ, Epple M. Transport of Ultrasmall Gold Nanoparticles (2 Nm) across the Blood–Brain Barrier in a Six-Cell Brain Spheroid Model. *Sci Rep* (2020) 10(1):1–12. doi: 10.1038/s41598-020-75125-2

67. Yang Z-z, Gao W, Liu Y-j, Pang N, Qi X-r. Delivering siRNA and Chemotherapeutic Molecules across Bbb and Btb for Intracranial Glioblastoma Therapy. *Mol Pharm* (2017) 14(4):1012–22. doi: 10.1021/acs.molpharmaceut.6b00819
68. Wei L, Guo X-Y, Yang T, Yu M-Z, Chen D-W, Wang J-C. Brain Tumor-Targeted Therapy by Systemic Delivery of Sirna with Transferrin Receptor-Mediated Core-Shell Nanoparticles. *Int J Pharm* (2016) 510(1):394–405. doi: 10.1016/j.ijpharm.2016.06.127
69. Kozielski KL, Ruiz-Valls A, Tzeng SY, Guerrero-Cázares H, Rui Y, Li Y, et al. Cancer-Selective Nanoparticles for Combinatorial Sirna Delivery to Primary Human Gbm *In Vitro* and *In Vivo*. *Biomaterials* (2019) 209:79–87. doi: 10.1016/j.biomaterials.2019.04.020
70. Zhou J, Wu J, Hafdi N, Behr J-P, Erbacher P, Peng L. Pamam Dendrimers for Efficient Sirna Delivery and Potent Gene Silencing. *Chem Commun* (2006) 22):2362–4. doi: 10.1039/b601381c
71. Grafals-Ruiz N, Rios-Vicil CI, Lozada-Delgado EL, Quinones-Diaz BI, Noriega-Rivera RA, Martínez-Zayas G, et al. Brain Targeted Gold Liposomes Improve RNAi Delivery for Glioblastoma. *Int J Nanomed* (2020) 15:2809. doi: 10.2147/IJN.S241055
72. Neves AR, Queiroz JF, Lima SAC, Reis S. Apo E-Functionalization of Solid Lipid Nanoparticles Enhances Brain Drug Delivery: Uptake Mechanism and Transport Pathways. *Bioconjug Chem* (2017) 28(4):995–1004. doi: 10.1021/acs.bioconjchem.6b00705
73. Wang X, Li R, Zhu Y, Wang Z, Zhang H, Cui L, et al. Active Targeting Co-Delivery of Therapeutic Sur Sirna and an Antineoplastic Drug *Via* Epidermal Growth Factor Receptor-Mediated Magnetic Nanoparticles for Synergistic Programmed Cell Death in Glioblastoma Stem Cells. *Mater Chem Front* (2020) 4(2):574–88. doi: 10.1039/C9QM00666D
74. Hessvik NP, Llorente A. Current Knowledge on Exosome Biogenesis and Release. *Cell Mol Life Sci* (2018) 75(2):193–208. doi: 10.1007/s00018-017-2595-9
75. Batrakova EV, Kim MS. Using Exosomes, Naturally-Equipped Nanocarriers, for Drug Delivery. *J Control Release* (2015) 219:396–405. doi: 10.1016/j.jconrel.2015.07.030
76. Wang J, Chen D, Ho EA. Challenges in the Development and Establishment of Exosome-Based Drug Delivery Systems. *J Control Release* (2021) 329:894–906. doi: 10.1016/j.jconrel.2020.10.020
77. Alvarez-Erviti L, Seow Y, Yin H, Betts C, Lakhal S, Wood MJ. Delivery of Sirna to the Mouse Brain by Systemic Injection of Targeted Exosomes. *Nat Biotechnol* (2011) 29(4):341–5. doi: 10.1038/nbt.1807
78. Didiot M-C, Hall LM, Coles AH, Haraszti RA, Godinho BM, Chase K, et al. Exosome-Mediated Delivery of Hydrophobically Modified siRNA for Huntingtin mRNA Silencing. *Mol Ther* (2016) 24(10):1836–47. doi: 10.1038/mt.2016.126
79. Nakada M, Kita D, Watanabe T, Hayashi Y, Hamada J-i. The Mechanism of Chemoresistance against Tyrosine Kinase Inhibitors in Malignant Glioma. *Brain tumor Pathol* (2014) 31(3):198–207. doi: 10.1007/s10014-013-0174-9
80. Basu B, Ghosh MK. Extracellular Vesicles in Glioma: From Diagnosis to Therapy. *BioEssays* (2019) 41(7):1800245. doi: 10.1002/bies.201800245
81. Wibroe PP, Ahmadvand D, Oghabian MA, Yaghmur A, Moghimi SM. An Integrated Assessment of Morphology, Size, and Complement Activation of the Pegylated Liposomal Doxorubicin Products Doxil®, Caelyx®, Doxorubicin, and Sinadoxosome. *J Controlled Release* (2016) 221:1–8. doi: 10.1016/j.jconrel.2015.11.021
82. Jamnani FR, Rahbarizadeh F, Shokrgozar MA, Ahmadvand D, Mahboudi F, Sharifzadeh Z. Targeting High Affinity and Epitope-Distinct Oligoclonal Nanobodies to Her2 over-Expressing Tumor Cells. *Exp Cell Res* (2012) 318 (10):1112–24. doi: 10.1016/j.yexcr.2012.03.004
83. Mougel A, Terme M, Tanchot C. Therapeutic Cancer Vaccine and Combinations with Antiangiogenic Therapies and Immune Checkpoint Blockade. *Front Immunol* (2019) 10:467. doi: 10.3389/fimmu.2019.00467
84. Kuesters GM, Campbell RB. Conjugation of Bevacizumab to Cationic Liposomes Enhances Their Tumor-Targeting Potential. *Nanomedicine* (2010) 5(2):181–92. doi: 10.2217/nnm.09.105
85. Khodabakhsh F, Muyldermans S, Behdani M, Kazemi-Lomedasht F. Liposomal Delivery of Vascular Endothelial Growth Factor/Receptors and Their Inhibitors. *J Drug Target* (2020) 28(4):379–85. doi: 10.1080/1061186X.2019.1693578
86. Francesconi AB, Dupre S, Matos M, Martin D, Hughes BG, Wyld DK, et al. Carboplatin and Etoposide Combined with Bevacizumab for the Treatment of Recurrent Glioblastoma Multiforme. *J Clin Neurosci* (2010) 17(8):970–4. doi: 10.1016/j.jocn.2009.12.009
87. Liu H-L, Hsu P-H, Lin C-Y, Huang C-W, Chai W-Y, Chu P-C, et al. Focused Ultrasound Enhances Central Nervous System Delivery of Bevacizumab for Malignant Glioma Treatment. *Radiology* (2016) 281(1):99–108. doi: 10.1148/radiol.2016152444
88. Liu H-M, Zhang Y-F, Xie Y-D, Cai Y-F, Li B-Y, Li W, et al. Hypoxia-Responsive Ionizable Liposome Delivery Sirna for Glioma Therapy. *Int J Nanomed* (2017) 12:1065. doi: 10.2147/IJN.S125286
89. Bruun J, Larsen TB, Jølck RI, Eliasen R, Holm R, Gjetting T, et al. Investigation of Enzyme-Sensitive Lipid Nanoparticles for Delivery of Sirna to Blood–Brain Barrier and Glioma Cells. *Int J Nanomed* (2015) 10:5995. doi: 10.2147/IJN.S87334
90. Kato T, Natsume A, Toda H, Iwamizu H, Sugita T, Hachisu R, et al. Efficient Delivery of Liposome-Mediated Mgmt-Sirna Reinforces the Cytotoxity of Temozolomide in Gbm-Initiating Cells. *Gene Ther* (2010) 17(11):1363–71. doi: 10.1038/gt.2010.88
91. Saw PE, Zhang A, Nie Y, Zhang L, Xu Y, Xu X. Tumor-Associated Fibronectin Targeted Liposomal Nanoplatform for Cyclophilin a Sirna Delivery and Targeted Malignant Glioblastoma Therapy. *Front Pharmacol* (2018) 1194. doi: 10.3389/fphar.2018.01194
92. Liu X, Madhankumar A, Slagle-Webb B, Sheehan JM, Surguladze N, Connor JR. Heavy Chain Ferritin Sirna Delivered by Cationic Liposomes Increases Sensitivity of Cancer Cells to Chemotherapeutic Agents. *Cancer Res* (2011) 71(6):2240–9. doi: 10.1158/0008-5472.CAN-10-1375
93. Ye C, Pan B, Xu H, Zhao Z, Shen J, Lu J, et al. Co-Delivery of Golph3 siRNA and Gefitinib by Cationic Lipid-Plga Nanoparticles Improves Egfr-Targeted Therapy for Glioma. *J Mol Med* (2019) 97(11):1575–88. doi: 10.1007/s00109-019-01843-4
94. Ravi V, Madhankumar AB, Abraham T, Slagle-Webb B, Connor JR. Liposomal Delivery of Ferritin Heavy Chain 1 (Fth1) Sirna in Patient Xenograft Derived Glioblastoma Initiating Cells Suggests Different Sensitivities to Radiation and Distinct Survival Mechanisms. *PloS One* (2019) 14(9):e0221952. doi: 10.1371/journal.pone.0221952
95. Costa PM, Cardoso AL, Mendonça LS, Serani A, Custódia C, Conceição M, et al. Tumor-Targeted Chlorotoxin-Coupled Nanoparticles for Nucleic Acid Delivery to Glioblastoma Cells: A Promising System for Glioblastoma Treatment. *Mol Ther Nucleic Acids* (2013) 2:e100. doi: 10.1038/mtna.2013.30
96. Cheng D, Cao N, Chen J, Yu X, Shuai X. Multifunctional Nanocarrier Mediated Co-Delivery of Doxorubicin and Sirna for Synergistic Enhancement of Glioma Apoptosis in Rat. *Biomaterials* (2012) 33 (4):1170–9. doi: 10.1016/j.biomaterials.2011.10.057
97. Kim S-S, Harford JB, Moghe M, Rait A, Pirollo KF, Chang EH. Targeted Nanocomplex Carrying Sirna against Malat1 Sensitizes Glioblastoma to Temozolomide. *Nucleic Acids Res* (2018) 46(3):1424–40. doi: 10.1093/nar/gkx1221
98. Linder B, Weirauch U, Ewe A, Uhmann A, Seifert V, Mittelbronn M, et al. Therapeutic Targeting of Stat3 Using Lipopolyplex Nanoparticle-Formulated Sirna in a Syngeneic Orthotopic Mouse Glioma Model. *Cancers* (2019) 11(3):333. doi: 10.3390/cancers11030333
99. Jain A, Jain SK. Ligand-Appended Bbb-Targeted Nanocarriers (Labtns). *Crit Rev Ther Drug Carrier Syst* (2015) 32(2). doi: 10.1615/CritRevTherDrugCarrierSyst.2015010903
100. Li J, Wang F, Sun D, Wang R. A Review of the Ligands and Related Targeting Strategies for Active Targeting of Paclitaxel to Tumours. *J Drug Target* (2016) 24(7):590–602. doi: 10.3109/1061186X.2016.1154561
101. Rabiei M, Kashanian S, Samavati SS, Jamasb S, McInnes SJ. Active Targeting Towards and inside the Brain Based on Nanoparticles: A Review. *Curr Pharm Biotechnol* (2020) 21(5):374–83. doi: 10.2174/1389201020666191203094057
102. Mojarad-Jabali S, Farshbaf M, Walker PR, Hemmati S, Fatahi Y, Zakeri-Milani P, et al. An Update on Actively Targeted Liposomes in Advanced Drug Delivery to Glioma. *Int J Pharm* (2021) 602:120645. doi: 10.1016/j.ijpharm.2021.120645

103. Béduneau A, Saulnier P, Benoit J-P. Active Targeting of Brain Tumors Using Nanocarriers. *Biomaterials* (2007) 28(33):4947–67. doi: 10.1016/j.biomaterials.2007.06.011

Conflict of Interest: The authors declare that the research was conducted in the absence of any commercial or financial relationships that could be construed as a potential conflict of interest.

Publisher's Note: All claims expressed in this article are solely those of the authors and do not necessarily represent those of their affiliated organizations, or those of the publisher, the editors and the reviewers. Any product that may be evaluated in this article, or claim that may be made by its manufacturer, is not guaranteed or endorsed by the publisher.

Copyright © 2022 Shamshiripour, Hajiahmadi, Lotfi, Esmaeili, Zare, Akbarpour and Ahmadvand. This is an open-access article distributed under the terms of the Creative Commons Attribution License (CC BY). The use, distribution or reproduction in other forums is permitted, provided the original author(s) and the copyright owner(s) are credited and that the original publication in this journal is cited, in accordance with accepted academic practice. No use, distribution or reproduction is permitted which does not comply with these terms.

frontiers | Frontiers in Immunology

TYPE Original Research
PUBLISHED 26 July 2022
DOI 10.3389/fimmu.2022.934387

Check for updates

OPEN ACCESS

EDITED BY
Mohammad Taheri,
University Hospital Jena, Germany

REVIEWED BY
Yanlong Liu,
Harbin Medical University Cancer Hospital, China
Jie Luo,
University of Michigan, United States

*CORRESPONDENCE
Enyang Zhao
lspzey@sina.com
Xuedong Li
h06370@hrbmu.edu.cn

†These authors have contributed equally to this work

SPECIALTY SECTION
This article was submitted to Cancer Immunity and Immunotherapy, a section of the journal Frontiers in Immunology

RECEIVED 02 May 2022
ACCEPTED 30 June 2022
PUBLISHED 26 July 2022

CITATION
Zhang W, Liu Z, Wang J, Geng B, Hou W, Zhao E and Li X (2022) The clinical significance, immune infiltration, and tumor mutational burden of angiogenesis-associated lncRNAs in kidney renal clear cell carcinoma.
Front. Immunol. 13:934387.
doi: 10.3389/fimmu.2022.934387

COPYRIGHT
© 2022 Zhang, Liu, Wang, Geng, Hou, Zhao and Li. This is an open-access article distributed under the terms of the Creative Commons Attribution License (CC BY). The use, distribution or reproduction in other forums is permitted, provided the original author (s) and the copyright owner(s) are credited and that the original publication in this journal is cited, in accordance with accepted academic practice. No use, distribution or reproduction is permitted which does not comply with these terms.

The clinical significance, immune infiltration, and tumor mutational burden of angiogenesis-associated lncRNAs in kidney renal clear cell carcinoma

Wei Zhang†, Zhiming Liu†, Jinpeng Wang†, Bo Geng†, Wenbin Hou, Enyang Zhao* and Xuedong Li*

Department of Urology, The Second Affiliated Hospital of Harbin Medical University, Harbin, China

Background: Poor prognosis of kidney renal clear cell carcinoma (KIRC) is often related to angiogenesis. The lncRNAs that regulate angiogenesis could also affect the prognosis of KIRC. It is meaningful for us to use lncRNAs related to angiogenesis to construct a generic, individualized prognostic signature for patients with KIRC.

Methods: We identified eight angiogenesis-associated genes (AAGs) by differential expression analysis and univariate Cox regression from The Cancer Genome Atlas dataset, including 537 KIRC samples and 72 normal samples. In total, 23 prognostic lncRNAs were screened out after Pearson correlation analysis and univariate Cox regression analysis. Then, we performed least absolute shrinkage and selection operator (LASSO) regression and multivariate Cox regression to establish a four-AAG-related lncRNA prognostic signature.

Results: The risk score was calculated for each KIRC patients by using a four-AAG-related lncRNA prognostic signature. We divided the KIRC patients into high- and low-risk groups by the median of the risk score. It was confirmed that the AAG-related lncRNA prognostic signature has good prognostic value for KIRC patients by time-dependent receiver operating characteristic and Kaplan–Meier survival analysis. We identified 3,399 differentially expressed genes between the high- and low-risk groups and performed their functional enrichment analyses. The AAG-related lncRNA prognostic signature was an independent prognostic predictor for KIRC patients and was used to perform a combined nomogram. We reevaluated them in terms of survival, clinic characteristics, tumor-infiltrating immune cells and tumor mutation burden.

Conclusion: Our research indicates that the AAG-related lncRNA prognostic signature is a promising and potential independent prognostic indicator for KIRC patients. Then, it could offer new insights into the prognosis assessment and potential treatment strategies of KIRC patients.

KEYWORDS

angiogenesis-associated genes, lncRNA, KIRC, independent prognostic predictor, treatment biomarkers

Introduction

Renal cell carcinoma (RCC) is the third most common urologic cancer, with an annual global incidence of more than 400,000 and a mortality rate of more than 170,000 (1). RCC is classified into different histopathological subtypes based on a specific molecular pattern. KIRC is the most common histopathological subtype, accounting for 75% of all RCC cases (2). KIRC could not be diagnosed early, resulting in the poor efficacy of conventional treatment and low survival rate (3). Molecularly targeted therapies, including anti-vascular endothelial growth factors, have made therapeutic advances, but improving patients' overall survival (OS) and progression-free survival (PFS) remains a major challenge (4, 5). The development and metastasis of malignant tumors require the establishment of an adequate blood supply, that is, tumor angiogenesis (6). During angiogenesis, pro-angiogenic growth factors are highly expressed in tumor cells (7). Therefore, it is necessary to identify some new effective angiogenic gene signatures for KIRC.

lncRNAs have been found to play key roles in cell growth, cell cycle, apoptosis, cell differentiation, cell invasion, and metastasis (8–11). Abnormally expressed lncRNAs are closely related to various diseases, such as tumor occurrence and development (12–15). Recently, some independent studies have shown that dysregulation of lncRNAs affects tumor angiogenesis (16, 17). The lncRNA RPL34-AS1 regulates the angiogenic gene VEGFA to promote proliferation and angiogenesis in glioma (18). The lncRNA MALAT1 affects the miR-101-3p/STC1 axis to promote the development of colon cancer (19). Currently, few studies have explored the underlying mechanisms of angiogenic lncRNAs for the initiation, progression, and treatment of KIRC. Therefore, exploring unclear correlations between angiogenesis-related genes and lncRNAs may help identify biomarkers as useful therapeutic targets for KIRC.

In this research, we constructed a new AAG-related lncRNA prognostic signature from the TCGA dataset for the KIRC. We used the ROC analysis to confirm that the signature has a high prognostic value. The prognostic signature of AAG-related lncRNAs was well validated in different clinical features and stratified analyses. The AAG-related lncRNA prognostic signature was closely related with tumor-infiltrating immune cells (TICs) and tumor mutation burden (TMB). The AAG-related lncRNA prognostic signature will provide a theoretical basis for better realization of precision targeted therapy in clinical practice with KIRC patients.

Materials and methods

Data acquisition

The transcriptome RNA-seq data of 609 KIRC cases (KIRC samples, 537 cases; normal samples, 72 cases) and related clinical information were obtained from The Cancer Genome Atlas (TCGA) dataset (https://portal.gdc.cancer.gov/). To ensure valid analyses, we retained samples with survival time ≥30 days. In total, 36 AAGs were obtained from the MSigDB Team (Hallmark Gene set) (20) (Supplementary Table S1).

Eight AAGs in KIRC acquisition

The 14 AAGs which were differentially and highly expressed in KIRC that were in tumor samples relative to normal samples were determined ($p < 0.05$, logFC > 1) (Supplementary Table S2). According to the 14 AAGs, the univariate Cox regression analysis by R package "survival" (21) ($p < 0.05$) showed the eight AAGs which were significantly correlated with KIRC prognosis.

Four AAG-related lncRNAs of prognostic signature obtainment

To identify AAG-related lncRNAs, we firstly acquired all lncRNA expression data according to the GENCODE project (http://www.gencodegenes.org) in the TCGA dataset. We used the Pearson correlation analysis to identify the AAG-related

lncRNAs between AAGs and all lncRNAs based on the correlation coefficient and *p*-values (|Corpearson| > 0.5 and $p < 0.01$). Then, we identified 23 AAG-related lncRNAs by univariate Cox regression ($p < 0.001$). We used the R package "glmnet" (22) with the minimum 10-fold cross-validation (23) to perform the LASSO regression. Lastly, we used multivariate Cox regression to obtain an AAG-related lncRNA prognostic signature for the KIRC patients involving four AAG-related lncRNAs ($p < 0.05$).

RNA extraction and quantitative real-time PCR

We extracted total RNA from 786O and 293T cells by the TRIzol reagent (Life Technologies, Thermo Fisher Scientific, USA). We used All-in-one First Strand cDNA Synthesis Kit (Seven Bio Inc., Beijing, China) to synthesize the complementary DNA and used 2× SYBR Green qPCR MasterMix (Seven Bio Inc., Beijing, China) to perform quantitative real-time PCR (qRT-PCR) following the standard protocol (24). The forward primer for AC093278.2 was 5′-GCAAGCTTTGTGGGAAGG AA-3′, and the reverse primer for AC093278.2 was 5′-TGGGC AATAGAGGCACTTGA-3′. The forward primer for NNT-AS1 was 5′-CTGGAATCCCTGCTACTCAGGA-3′, and the reverse primer for NNT-AS1 was 5′-GCCATGTGATATGCCTGCTC-3′. The forward primer for CYTOR was 5′-TGGGAATGGAGG GAAATAAA-3′, and the reverse primer for CYTOR was 5′-C CAGGAACTGTGCTGTGAAG-3′. The forward primer for NUP50-DT was 5′-CTGGAAGTTAGAGCTGAGGAAGTT-3′, and the reverse primer for NUP-50DT was 5′-GGGAAATAA TAAGGGCTCAGGAAGG-3′. The forward primer for GAPDH was 5′-CATGTTCGTCATGGGTGTGAA-3′, and the reverse primer for GAPDH was 5′-GGCATGGACTGTGGTCATGA G-3′. GAPDH served as the control. The relative expression was calculated by the $2^{-\triangle\triangle Ct}$ method.

Non-negative matrix factorization clustering

KIRC samples were clustered by applying non-negative matrix factorization (NMF) clustering algorithm *via* the R package "NMF" to explore potential subgroups (25). We set the number of clusters k from 2 to 9. Lastly, due to the cophenetic correlation coefficients, the best $k = 2$ was chosen.

Screening of prognostic-related lncRNAs and verification of a prognostic model

The risk score is the lncRNA expression for each prognosis multiplied by the lncRNA coefficient for each prognosis: risk score = AC093278.2 × (-0.351782815872485) + NNT-AS1× (-0.336893752787579) + CYTOR × (0.256677130521836) + NUP50-DT × (0.584700743765635). KIRC patients were divided into high- and low-risk groups according to the median cutoff of the risk score from the R packages "survival", "pheatmap" (26), and "ggupbr" (27). We used the Kaplan–Meier survival curve analysis with log-rank test and time-dependent ROC analysis to analyze OS and to evaluate the accuracy of model predictions. Principal component analysis (PCA) has demonstrated the expression of KIRC samples. Chi-square test was used to analyze the relationship between clinical characteristics and prognostic models. We performed univariate and multivariate Cox regression analyses between the risk score and clinical characteristics to confirm that the prognostic model was an independent predictor of clinical prognosis. In addition, a nomogram was established, using the independent prognostic predictors, by the R package "rms" (26).

GO and KEGG enrichment analysis

Gene Ontology (GO) and Kyoto Encyclopedia of Genes and Genomes (KEGG) enrichment analyses were performed by the R packages "clusterProfiler" (28), "enrichplot" (28), and "ggplot2" (29). Both *p*- and *q*-values <0.05 were considered significantly enriched.

Immune microenvironment analysis

The CIBERSORT algorithm was used to acquire the TICs content of the tumor gene expression dataset. Then, we tested the difference between risk groups defined by the prognostic signature using a two-sample *t*-test. Moreover, the R package "ggpubr" (27) was used to exhibit the relationship between immune checkpoints and different risk groups.

Mutation analysis

We achieved the mutation data of KIRC patients from the TCGA dataset (https://portal.gdc.cancer.gov/). Then, we used the R package "maftools" (30) to analyze and summarize the data containing somatic variants. The TMB score was measured by the formula: (total mutation/total covered bases) × 10^6.

Statistical analysis

The prognostic differences between the groups were examined using the Kaplan–Meier survival curves analysis, and the *p*-value was checked in the log-rank test. Univariate and multivariate Cox regression analyses were conducted to

illustrate the relationship between the risk score and clinical characteristics. The ROC curves evaluated the value of the risk score for prognosis prediction, and we used the area under the ROC curve as an indicator of prognostic accuracy. Pearson's correlation test was used for correlation analysis. We used R software (version 4.0.3) for statistical analysis and used Strawberry Perl programming language (version 5.30.1) for data processing (***p < 0.001, **p < 0.01, and *p < 0.05).

Results

Identification of eight AAGs in KIRC patients

Firstly, we acquired the transcriptome profiling data through the KIRC projects of the TCGA dataset, including 537 KIRC samples and 72 normal samples. Next, we used Ensemble's gene transfer format file to annotate the data and then extracted the expression matrix of 36 AAGs from TCGA. In total, 14 different AAGs which were differentially and highly expressed in KIRC were identified due to their expression levels in the KIRC samples and the normal samples (Figures 1A, B). The 14 different AAGs included CCND2, COL3A1, COL5A2, FSTL1, JAG2, MSX1, NRP1, PF4, PGLYRP1, POSTEN, PRG2, TIMP1, VCAN, and VEGFA ($p < 0.05$, logFC>1). The correlations among these 14 AAGs are shown in Figure 1C. Lastly, we used univariate Cox regression analysis to evaluate the prognostic effect of 14 AAGs. The forest plot showed that JAG2 and NRP1 were protective factors with hazard ratio (HR) <1 ($p<0.05$), while COL5A2, MSX1, PF4, PRG2, TIMP1, and VCAN were risk factors with HR > 1 ($p < 0.05$) in KIRC patients (Figure 1D). The abovementioned results showed that the eight AAGs played an essential biological role in the development of KIRC patients.

Exploration of the prognostic AAG-related lncRNAs in KIRC

According to the eight AAGs, we used the Pearson coefficient and p-value (|Corpearson| > 0.5 and $p < 0.01$) to acquire the AAGs significantly related to lncRNAs. The Sankey diagram showed the relationship between AAGs and 47 targeted lncRNAs (Figure 2A). The 47 AAG-related lncRNAs were included in the univariate Cox regression analysis, and 23 prognostic lncRNAs demonstrated their prognostic roles ($p < 0.001$) (Figure 2B). To construct the AAG-related lncRNA prognostic signature for forecasting the OS of KIRC patients, we performed a LASSO Cox regression analysis due to the 23 AAG-related prognostic lncRNAs, and it generated the AAG-related lncRNA prognostic signature which contains nine AAG-related lncRNAs and the coefficient of each (Figures 2C, D). Lastly, we used the multivariate Cox regression to screen the AAG-related lncRNAs with the greatest prognostic value. The four AAG-related lncRNAs include AC093278.2, NNT-AS1, CYTOR, and NUP50-DT ($p<0.05$) that were identified to construct the prognostic model for KIRC patients (Figure 2E). The correlations among these four AAG-related lncRNAs are shown in Figure 2F.

Exploration of the expression of the four AAG-related lncRNAs in KIRC

We compared the expression levels of four AAG-related lncRNAs in KIRC and normal samples through the TCGA dataset and found that AC093278.2 and CYTOR showed higher expression levels in the KIRC samples compared to the normal samples, while NNT-AS1 and NUP50-DT showed lower expression levels in the KIRC samples compared to the normal samples (Figure 3A). The expression levels of four AAG-related lncRNAs in 786O and 293T cells were evaluated by qRT-PCR analysis and found to be consistent with the TCGA results (Figure 3B).

Two molecular subgroups of KIRC divided from NMF clustering

We selected AAG-related lncRNAs with significant survival differences from the results of the univariate Cox regression analysis to explore the potential molecular subgroups of KIRC. A total of 528 KIRC patients with 23 lncRNAs were used in the NMF consensus clustering analysis. Moreover, $k = 2$ was determined as the optimal k value by cophenetic correlation coefficients (Figures 4A–C). The KIRC samples were divided into cluster 1 ($n = 340$) and cluster 2 ($n = 188$) (Figure 4D). We found significant differences in the gene expression profiles between cluster 1 and cluster 2 by PCA (Figure 4E). Moreover, the Kaplan–Meier survival curves showed that cluster 1 had a better OS than cluster 2 in KIRC patients ($p < 0.001$) (Figure 4F). The abovementioned results not only showed that the KIRC patients could be divided into two subgroups but also identified their differences in OS. Our results showed that subgroups defined by AAG-related lncRNA expression had a close relationship with the heterogeneity of KIRC patients.

Construction and validation of the AAG-related lncRNA prognostic model in KIRC

Excluding the KIRC samples with incomplete clinical information, the coefficients of four AAG-related prognostic lncRNAs were used to calculate the risk score of each patient. According to the determined cutoff point, there were 264 cases in the high-risk group and the low-risk group, respectively. The

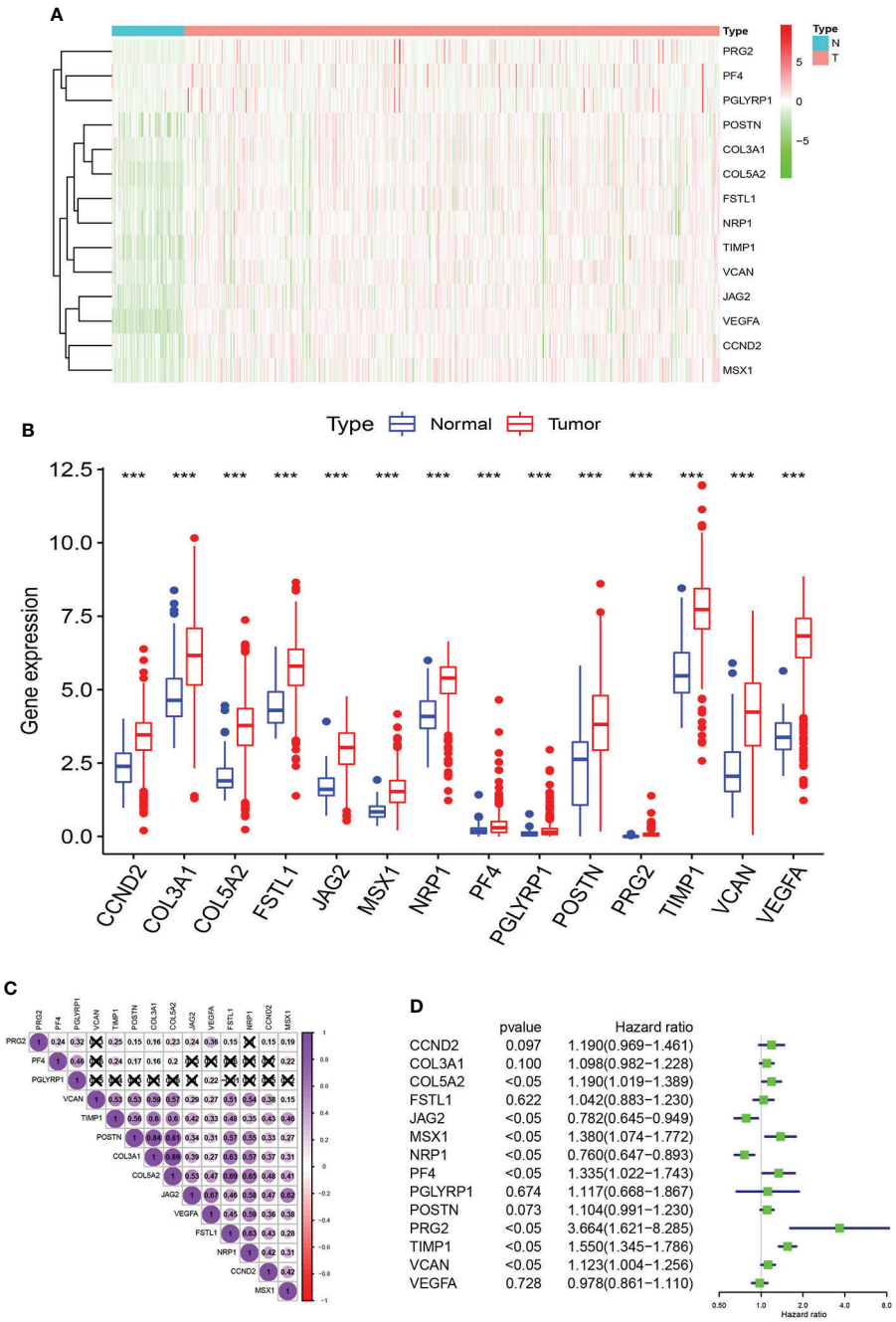

FIGURE 1
AAGs screening. Heat map **(A)** and box plot **(B)** showing the expression distributions of differentially expressed genes between KIRC and normal samples of the AAGs. **(C)** Correlation analysis of the 14 AAGs. **(D)** Univariate Cox regression analysis of 14 AAGs. The meaning of the symbol *** is p<0.001.

Kaplan–Meier analysis showed that low-risk KIRC patients had a higher OS than high-risk KIRC patients ($p < 0.001$; Figure 5A). The risk scores and survival of each case showed that the clinical outcomes of patients in the low-risk group were better than those in the high-risk group (Figure 5B). Moreover, the four AAG-related prognostic lncRNAs showed great AUC values in a time-dependent ROC analysis (Figure 5C), which meant that the AAG-related lncRNA prognostic model had better prediction ability of the 1-, 3-, and 5-year OS. The Kaplan–Meier survival curves showed that not only the high expression of AC093278.2 and NNT-AS1 but also the low expression of CYTOR and NUP50-DT were

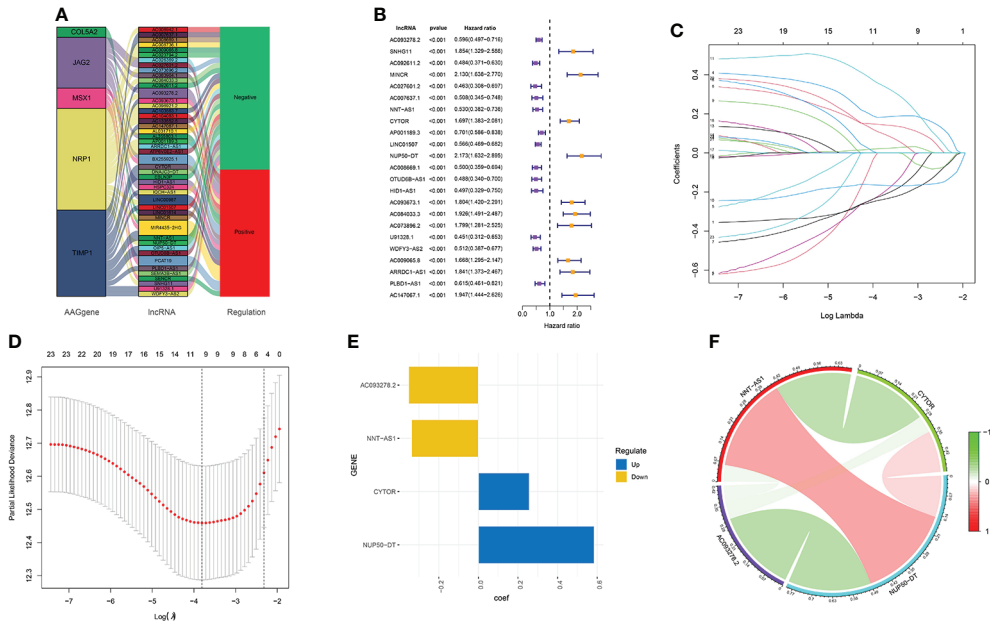

FIGURE 2
Screening of the four AAG-related prognostic lncRNAs. **(A)** Association between AAGs and targeted lncRNAs. **(B)** Univariate Cox regression analysis of 23 AAG-related lncRNAs ($p < 0.001$). **(C)** LASSO coefficient profiles of 23 AAG-related lncRNAs. **(D)** LASSO regression with 10-fold cross-validation obtained nine AAG-related lncRNAs using a minimum lambda value. **(E)** Multivariate Cox regression of the four prognostic AAG-related lncRNAs. **(F)** Correlation analysis of the four AAG-related lncRNAs.

associated with better OS in the TCGA dataset (Supplementary Figure S1). Different distribution patterns between the high- and low-risk groups were detected by PCA. The PCA results based on the prognostic model genome showed a significant difference between the high-risk and the low-risk groups (Figure 5D), while we did not detect a significant separation on the basis of the AAG-related lncRNAs and the genome-wide expression profiles (Figures 5E, F). To sum up, the four AAG-related prognostic lncRNAs performed well in the prediction of OS in KIRC patients.

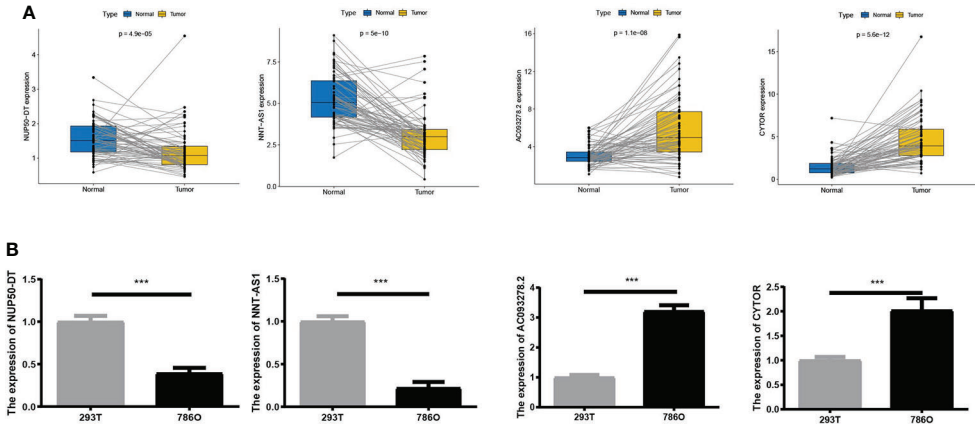

FIGURE 3
(A) Expression of four lncRNAs in KIRC and normal samples from The Cancer Genome Atlas. **(B)** A qRT-PCR analysis was conducted to detect the expression levels of four lncRNAs among 786O and 293T cells. The meaning of the symbol *** is p<0.001.

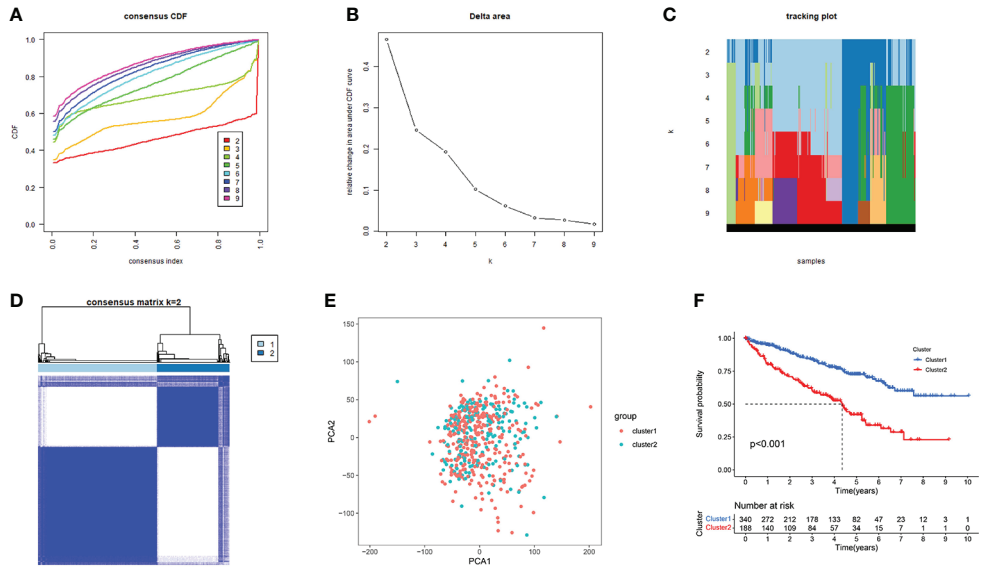

FIGURE 4
Consensus clusters by 23 AAG-related lncRNAs. **(A)** Consensus clustering cumulative distribution function (CDF) for k = 2 to 9. **(B)** Relative change in area under the CDF curve for k = 2 to 9. **(C)** Tracking plot for k = 2 to 9. **(D)** Consensus clustering matrix for k = 2. **(E)** Principal component analysis of the gene expression profiles. **(F)** Kaplan–Meier curve showing a different prognosis between the two clusters.

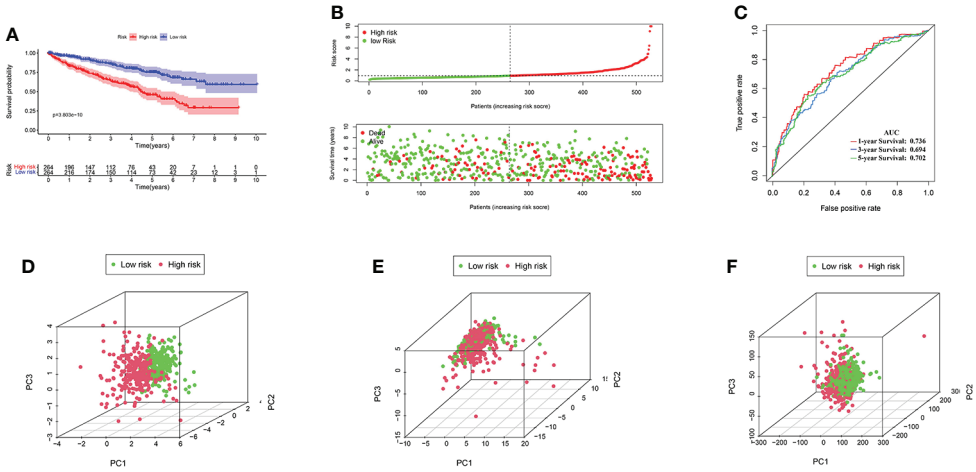

FIGURE 5
(A) KIRC patients in the high-risk group had a worse overall survival than the low-risk group by Kaplan–Meier curves. **(B)** The distribution of risk score and survival times of KIRC patients. **(C)** Receiver operating characteristic analysis of the angiogenesis-associated gene (AAG)-related lncRNA prognostic signature for predicting the 1/3/5-year survival. **(D)** Principal component analysis among high- and low-risk groups based on the four prognostic AAG-related lncRNA sets. **(E)** PCA among high- and low-risk groups based on all the AAG-related lncRNA sets. **(F)** PCA among high- and low-risk groups based on the whole gene sets.

Clinical evaluation by the AAG-related lncRNA prognostic model

The heat map shows the relationship between the risk score of KIRC and clinical characteristics (Supplementary Figure S2A). Then, consequent scatter diagrams obtained by the Wilcoxon signed-rank test showed that tumor grade, clinical stage, T stage, N stage, and M stage (Supplementary Figures S2B–F) were positively related to the risk score, while age and gender (Supplementary Figures S2G,H) were not significantly

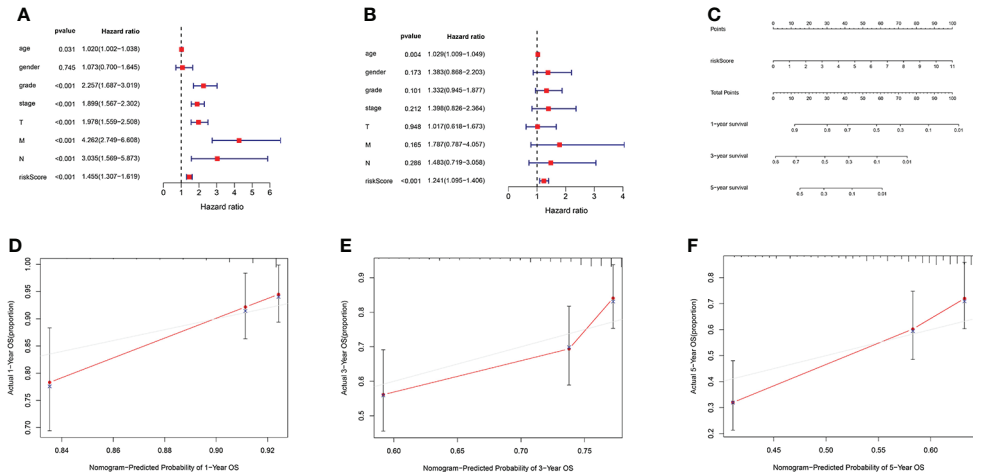

FIGURE 6
(A) Forest plot for univariate Cox regression analysis showing that grade, stage, T stage, M stage, N stage, and risk score were prognostic risk-related variables ($p < 0.001$). **(B)** Forest plot for multivariate Cox regression analysis showing that only the risk score was the independent prognostic factor ($p < 0.001$). **(C)** Nomogram integrating the risk score of four AAG-related lncRNAs. **(D–F)** Calibration curve analysis of the nomogram for predicting the 1-, 3-, and 5-year overall survival in The Cancer Genome Atlas dataset.

related to the risk score. The abovementioned results confirmed that KIRC had a higher risk score and a higher degree of malignancy, regardless of age and gender.

The AAG-related lncRNA prognostic signature was an independent prognostic predictor for KIRC patients

We used univariate and multivariate Cox regression analyses to assess independent prognostic predictors in KIRC patients. The univariate Cox regression analysis showed that the AAG-related lncRNA prognostic signature had a close relationship with OS (HR: 1.324, 95% CI: 1.211–1.449, $p < 0.001$) (Figure 6A), and the multivariate Cox regression analysis also further showed that the AAG-related lncRNA prognostic signature was remarkably associated with OS (HR: 1.160, 95% CI: 1.041–1.293, $p < 0.001$) (Figure 6B). We established a nomogram using the AAG-related lncRNA prognostic signature screened by univariate and multivariate Cox regression analyses (Figure 6C). The calibration plots showed high concordance in predicting the 1-, 3-, and 5-year OS in KIRC patients (Figures 6D–F). These results showed that, as the only independent prognostic predictor, the AAG-related lncRNA prognostic signature may be useful for clinical prognostic evaluation.

Pathway and process enrichment analysis

To explore the potential biological pathway and process involved in the molecular heterogeneity between the high- and low-risk groups, we identified 3,399 differentially expressed genes (DEGs) [|log2 (fold change)| > 2 and $p < 0.05$] between the high- and low-risk groups in KIRC patients. GO enrichment analysis and KEGG pathway analysis of DEGs were adopted. We found that the top five GO terms for biological processes were response to oxidative stress, viral process, positive regulation of cell adhesion, positive regulation of response to external stimulus, and positive regulation of cell activation. The top five GO terms for cellular components were cell–substrate junction, focal adhesion, cell leading edge, vesicle lumen, and cytoplasmic vesicle lumen. The top five GO terms for molecular functions were cadherin binding, actin binding, ubiquitin-like protein ligase binding, structural constituent of ribosome, and antigen binding (Figure 7A). According to the KEGG analysis, the top five pathways included pathways of neurodegeneration-multiple disease, Alzheimer disease, amyotrophic lateral sclerosis, Huntington's disease, and Parkinson's disease (Figure 7B). These abovementioned results may give us some insights into the cellular biological effects related to the AAG-related lncRNA prognostic signature.

The relationship between immune microenvironment and risk score

To explore the relationship between the immune microenvironment and risk score, we analyzed the proportion of tumor-infiltrating immune groups by CIBERSORT algorithm and constructed 21 immune cell profiles in the KIRC samples (Supplementary Figure S3). We combined correlation analysis ($p < 0.01$) (Figure 8A) and difference analysis ($p < 0.01$) (Figure 8B)

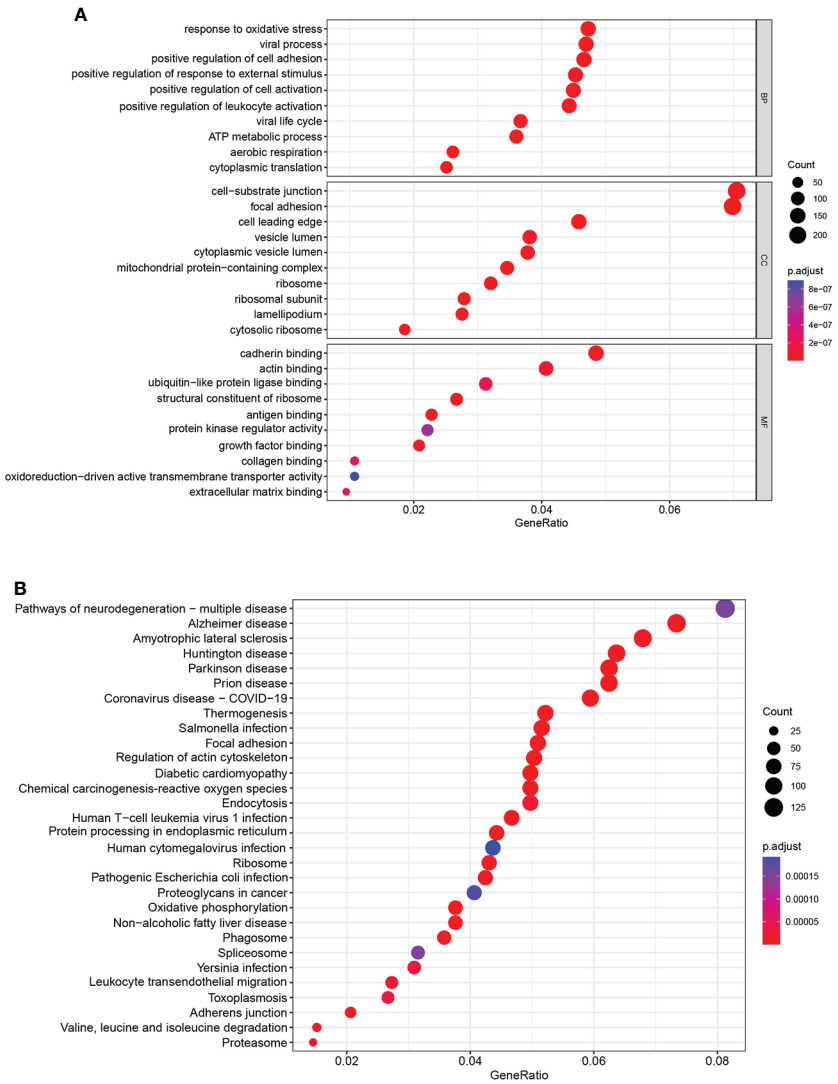

FIGURE 7
Functional enrichment analysis. **(A)** Gene Ontology analysis of DEGs revealed the enriched biological processes, cell components, and molecular functions. **(B)** Kyoto Encyclopedia of Genes and Genomes pathway analysis of DEGs revealed the enriched signaling pathways.

to obtain a total of five TICs associated with the AAG-related lncRNA prognostic signature risk score (Figure 8C). Among them, CD4 memory-activated T cells, follicular helper T cells, and regulatory T cells (Tregs) had a positive correlation with the risk score, while CD4 memory resting T cells and resting mast cells were negatively correlated with risk score. Moreover, compared with the low-risk group, the high-risk group had relatively higher expression levels of immune checkpoints, including IL6, CXCR4, CD276, TGFB1, CTLA4, LAG3, CD274, and CD4 (Figure 8D). The abovementioned results suggested that different risk groups had a specific relationship with immune microenvironment. We could formulate treatment methods for KIRC patients with different risk groups through the differences between different risk groups and the immune microenvironment.

The relationship between risk score and TMB

In the high-risk group, we listed the 20 most frequent mutant genes, including VHL, PBRM1, TTN, SETD2, BAP1, MTOR, HMCN1, MUC16, PTEN, SPEN, KDM5C, DNAH9, FLG, ROS1, XIRP2, ABCC6, ANK2, CELSR1, RYR3, and TP53 and the interaction among them (Figures 9A, B), while in the low-risk group, PBRM1, VHL, ANK3, ARID1A, KIF13A, AFF3,

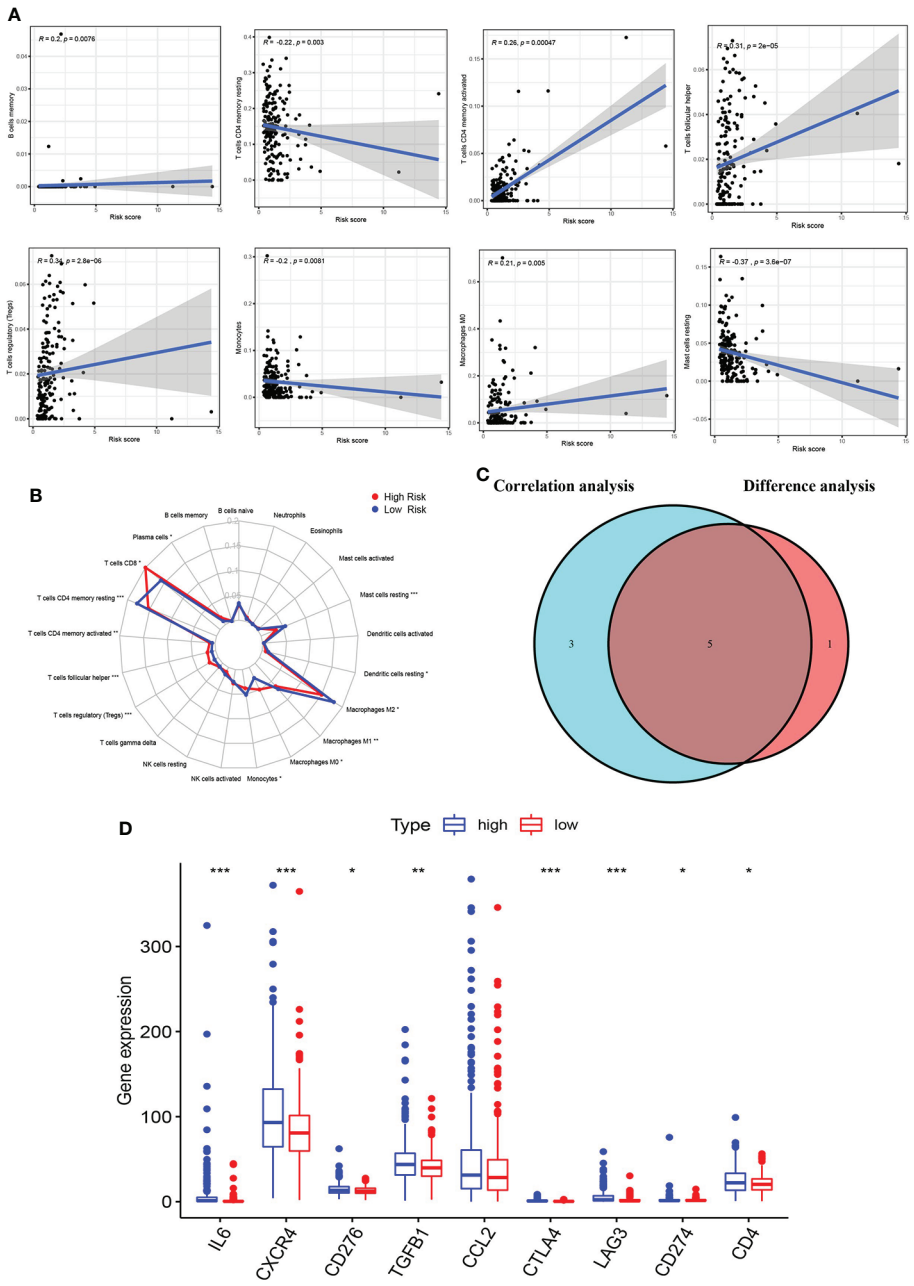

FIGURE 8
Correlation of immune microenvironment with risk score. **(A)** Scatter plot showing eight significantly correlated TICs ($p < 0.01$). The blue line in each plot was a fitted linear model indicating the proportion of tropism of the immune cell along with risk score, and Pearson coefficient was used for the correlation test. **(B)** Radar plot showing differences in TICs between the high- and low-risk groups as measured by Wilcoxon rank-sum test. **(C)** Venn diagram showing that the 5 TICs were associated with the risk score jointly determined by the difference and correlation tests shown in the scatter and radar charts, respectively ($p < 0.01$). **(D)** Box plot showing the correlation between immune checkpoint and risk score. The meaning of the symbol *** is p<0.001.

ALMS1, CSMD3, DNMT3A, INPP5F, INPPL1, KIF1B, LRP1B, NEB, NOS1, NSD1, PDGFRA, POLR2B, POCK1, and RP1 were the 20 most frequent mutant genes, and their interactions are shown in Figures 9C, D. A summary of variant classification, variant type, SNV class, and variants per sample in the high- and low-risk groups is shown in Supplementary Figure S4. In Figures 9E, F, the analysis showed that the high-risk KIRC patients had higher TMB with shorter OS. These data were consistent with previous results obtained with Kaplan–Meier survival curves for the high- and low-risk groups.

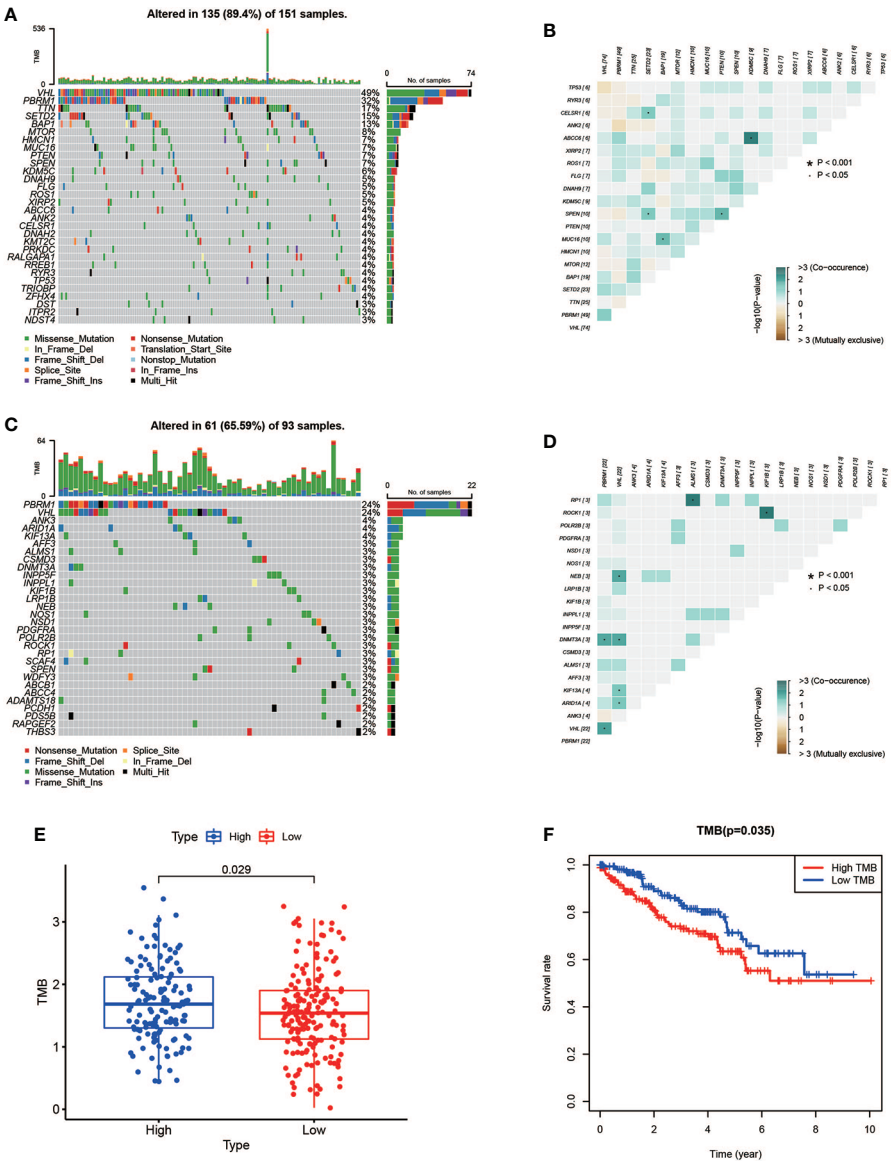

FIGURE 9
Mutation profile and relationship between tumor mutation burden (TMB) and risk score. **(A, B)** Mutation profile of the high-risk group and interaction among 20 most frequent mutant genes. **(C, D)** Mutation profile of the low-risk group and interaction among 20 most frequent mutant genes. **(E)** Relationship between TMB and risk score. **(F)** Association of TMB and overall survival in KIRC patients.

Conclusion

Briefly, we constructed a novel prognostic signature of four AAG-related lncRNAs (AC093278.2, NNT-AS1, CYTOR, and NUP50-DT) for KIRC patients. A series of analyses were performed, and the results indicated that the newly constructed prognostic signature could be a potential predictor for KIRC patients. In summary, our study indicates that the prognostic signature has close relationships with clinical characteristics, TICs, and TMB, which may help to offer a more individualized treatment for KIRC patients.

Discussion

As one of the most prevalent primary malignant tumors of the urinary system, KIRC has the characteristics of high heterogeneity, poor prognosis, and distant metastasis (4, 31,

32). It is critical to explore the potential predictor for KIRC treatment and prognosis. Angiogenesis is a complex consequence of co-regulation between pro-angiogenic and anti-angiogenic factors, and it is disrupted and dysregulated in cancer (33). Angiogenesis is an important process in cancer pathogenesis and therapy. lncRNAs play an important role in angiogenesis, so new therapeutic targets and drug candidates are needed to inhibit angiogenesis (10).

Recent studies have shown that the lncRNA PAARH promotes hepatocellular carcinoma (HCC) angiogenesis by activating HIF-1α/VEGF signaling (34). JAG1 is involved in angiogenesis, and Linc-OIP5 may regulate JAG1 signaling through YAP1 signaling (35). The lncRNA H22954 inhibits angiogenesis in acute myeloid leukemia by downregulating PDGFA expression (36). The lncRNA MIR31HG accelerates colorectal cancer progression by targeting miR-361-3p to regulate glycolysis and angiogenesis (37). The abovementioned results indicate that lncRNAs regulate angiogenesis, thereby further achieving the effect of tumor treatment, which has attracted more and more attention. So, we constructed a signature based on AAG-related lncRNAs to achieve better personalized treatment and predict the prognosis of KIRC patients.

We constructed the prognostic signature by using four AAG-related lncRNAs (AC093278.2, CYTOR, NNT-AS1, and NUP50-DT) from 537 KIRC patients. Several of these lncRNAs were reported to be associated with cancer progression. lncRNA CYTOR promotes HCC proliferation by targeting the microRNA-125a-5p/LASP1 axis (38). lncRNA NNT-AS1 promotes estrogen-mediated endometrial carcinoma proliferation by regulating miR-30c/NPM1 (39). The lncRNA NNT-AS1 promotes KIRC progression through the miR-137/YBX-1 pathway (40). These results demonstrate that lncRNAs which construct the signature are involved in tumor progression, but there are fewer reports related to angiogenesis. The prognostic signature also provides some theoretical suggestions for these lncRNAs as potential targets and drug candidates for anti-vascular therapy of tumors.

In our study, the ROC analysis result confirmed that the signature had a high prognostic value. In total, 3,399 DEGs were identified between the high- and low-risk groups; then, GO and KEGG analyses were performed. In addition, the signature showed a significant correlation with clinical characteristics, further supporting its prognostic value. We also identified that the AAG-related lncRNAs can potentially be utilized as an independent predictor for the OS in the TCGA dataset. The nomogram composed of the signature showed a high performance in 1, 3, and 5 years, which may help in the analysis of the prognosis of KIRC patients and the choice of treatment. Moreover, the prognostic signature was closely associated with TICs and TMB, suggesting that they could potentially help clinicians design effective individual therapy for KIRC patients.

Although we used a large number of TCGA dataset, our research still had some limitations. We extensively explored the expression and potential prognostic capabilities of the AAG-related lncRNA prognostic signature in KIRC and the roles of these lncRNAs on angiogenesis in KIRC, but the drug-resistant KIRC has not been specifically elucidated. We will also further study the specific mechanism of these lncRNAs affecting angiogenesis in future studies so as to provide a theoretical basis for these lncRNAs to become therapeutic targets as soon as possible.

Data availability statement

The transcriptome RNA-seq data of KIRC samples and related clinical information were obtained from the TCGA dataset (https://portal.gdc.cancer.gov/). All lncRNAs expression data in the TCGA dataset were according to the GENCODE project (http://www.gencodegenes.org). The mutation data of KIRC patients were from the TCGA dataset (https://portal.gdc.cancer.gov/).

Author contributions

WZ and ZL were the first to design the study. JW and BG drafted the manuscript. WZ and WH provided technical assistance for the continuation of the experiment. ZL, EZ, and XL participated in the production and improvement of tables and figures. All authors contributed to the article and approved the submitted version.

Funding

This work was funded by the Scientific Research Project of Heilongjiang Provincial Health and Family Planning Commission (2017-070) and the Second Affiliated Hospital of Harbin Medical University First-Class Discipline First-Class Specialist Construction Project (100123).

Conflict of interest

The authors declare that the research was conducted in the absence of any commercial or financial relationships that could be construed as a potential conflict of interest.

The reviewer YL declared a shared parent affiliation with the authors to the handling editor at the time of the review.

Publisher's note

All claims expressed in this article are solely those of the authors and do not necessarily represent those of their affiliated organizations, or those of the publisher, the editors and the reviewers. Any product that may be evaluated in this article, or claim that may be made by its manufacturer, is not guaranteed or endorsed by the publisher.

Supplementary material

The Supplementary Material for this article can be found online at: https://www.frontiersin.org/articles/10.3389/fimmu.2022.934387/full#supplementary-material

SUPPLEMENTARY FIGURE 1
The KIRC patients with different expression levels of the four AAG-related lncRNAs had different overall survival by Kaplan–Meier curves.

SUPPLEMENTARY FIGURE 2
Prognostic signature of clinical evaluation. A heat map **(A)** along with a scatter diagram showing that grade **(B)**, stage **(C)**, T stage **(D)**, N stage **(E)**, and M stage **(F)** were significantly associated with the risk score, while age **(G)** and gender **(H)** were not significantly related to the risk score.

SUPPLEMENTARY FIGURE 3
Distribution of tumor-infiltrating immune cells (TICs) in KIRC and correlation analysis. **(A)** Bar plot showing the distribution of TICs in KIRC. **(B)** Correlation analysis of the 21 TICs in KIRC.

SUPPLEMENTARY FIGURE 4
(A) Summary of variant classification, variant type, SNV class, and variants per sample in the high-risk group. **(B)** Summary of variant classification, variant type, SNV class, and variants per sample in the low-risk group.

References

1. Bray F, Ferlay J, Soerjomataram I, Siegel RL, Torre LA, Jemal A. Global cancer statistics 2018: GLOBOCAN estimates of incidence and mortality worldwide for 36 cancers in 185 countries. *CA Cancer J Clin* (2018) 68(6):394–424. doi: 10.3322/caac.21492

2. Lalani AA, McGregor BA, Albiges L, Choueiri TK, Motzer R, Powles T, et al. Systemic treatment of metastatic clear cell renal cell carcinoma in 2018: Current paradigms, use of immunotherapy, and future directions. *Eur Urol* (2019) 75 (1):100–10. doi: 10.1016/j.eururo.2018.10.010

3. Bai S, Wu Y, Yan Y, Shao S, Zhang J, Liu J, et al. Construct a circRNA/miRNA/mRNA regulatory network to explore potential pathogenesis and therapy options of clear cell renal cell carcinoma. *Sci Rep* (2020) 10(1):13659. doi: 10.1038/s41598-020-70484-2

4. Sun Z, Tao W, Guo X, Jing C, Zhang M, Wang Z, et al. Construction of a lactate-related prognostic signature for predicting prognosis, tumor microenvironment, and immune response in kidney renal clear cell carcinoma. *Front Immunol* (2022) 13:818984. doi: 10.3389/fimmu.2022.818984

5. Liu D, Shu G, Jin F, Qi J, Xu X, Du Y, et al. ROS-responsive chitosan-SS31 prodrug for AKI therapy via rapid distribution in the kidney and long-term retention in the renal tubule. *Sci Adv* (2020) 6(41). doi: 10.1126/sciadv.abb7422

6. Zheng W, Zhang S, Guo H, Chen X, Huang Z, Jiang S, et al. Multi-omics analysis of tumor angiogenesis characteristics and potential epigenetic regulation mechanisms in renal clear cell carcinoma. *Cell Commun Signal* (2021) 19(1):39. doi: 10.1186/s12964-021-00728-9

7. Han B, Zhang H, Tian R, Liu H, Wang Z, Wang Z, et al. Exosomal EPHA2 derived from highly metastatic breast cancer cells promotes angiogenesis by activating the AMPK signaling pathway through ephrin A1-EPHA2 forward signaling. *Theranostics* (2022) 12(9):4127–46. doi: 10.7150/thno.72404

8. Kopp F, Mendell JT. Functional classification and experimental dissection of long noncoding RNAs. *Cell* (2018) 172(3):393–407. doi: 10.1016/j.cell.2018.01.011

9. Shuai Y, Ma Z, Lu J, Feng J. LncRNA SNHG15: A new budding star in human cancers. *Cell Prolif* (2020) 53(1):e12716. doi: 10.1111/cpr.12716

10. Kumar MM, Goyal R. LncRNA as a therapeutic target for angiogenesis. *Curr Top Med Chem* (2017) 17(15):1750–7. doi: 10.2174/1568026617666161116144744

11. Sun J, Sun X, Hu S, Wang M, Ma N, Chen J, et al. Long noncoding RNA SNHG1 silencing accelerates hepatocyte-like cell differentiation of bone marrow-derived mesenchymal stem cells to alleviate cirrhosis *via* the microRNA-15a/SMURF1/UVRAG axis. *Cell Death Discov* (2022) 8(1):77. doi: 10.1038/s41420-022-00850-8

12. Fang Y, Fullwood MJ. Roles, functions, and mechanisms of long non-coding RNAs in cancer. *Genomics Proteomics Bioinf* (2016) 14(1):42–54. doi: 10.1016/j.gpb.2015.09.006

13. Mercer TR, Dinger ME, Mattick JS. Long non-coding RNAs: insights into functions. *Nat Rev Genet* (2009) 10(3):155–9. doi: 10.1038/nrg2521

14. Zhou Y, Wang L, Zhang W, Ma J, Zhang Z, Yang M, et al. Identification of epithelial mesenchymal transition-related lncRNAs associated with prognosis and tumor immune microenvironment of hepatocellular carcinoma. *Dis Markers 2022* (2022) p:6335155. doi: 10.1155/2022/6335155

15. Shree B, Tripathi S, Sharma V. Transforming growth factor-Beta-Regulated LncRNA-MUF promotes invasion by modulating the miR-34a Snail1 axis in glioblastoma multiforme. *Front Oncol* (2021) 11:788755. doi: 10.3389/fonc.2021.788755

16. Xu Y, Leng K, Yao Y, Kang P, Liao G, Han Y, et al. A circular RNA, cholangiocarcinoma-associated circular RNA 1, contributes to cholangiocarcinoma progression, induces angiogenesis, and disrupts vascular endothelial barriers. *Hepatology* (2021) 73(4):1419–35. doi: 10.1002/hep.31493

17. Niu Y, Bao L, Chen Y, Wang C, Luo M, Zhang B, et al. HIF2-induced long noncoding RNA RAB11B-AS1 promotes hypoxia-mediated angiogenesis and breast cancer metastasis. *Cancer Res* (2020) 80(5):964–75. doi: 10.1158/0008-5472.CAN-19-1532

18. Zhang D, Jiang H, Ye J, Gao M, Wang X, Lu E, et al. A novel lncRNA, RPL34-AS1, promotes proliferation and angiogenesis in glioma by regulating VEGFA. *J Cancer* (2021) 12(20):6189–97. doi: 10.7150/jca.59337

19. Luan C, Li Y, Liu Z, Zhao C. Long noncoding RNA MALAT1 promotes the development of colon cancer by regulating miR-101-3p/STC1 axis. *Onco Targets Ther* (2020) 13:3653–65. doi: 10.2147/OTT.S242300

20. Qing X, Xu W, Liu S, Chen Z, Ye C, Zhang Y. Molecular characteristics, clinical significance, and cancer immune interactions of angiogenesis-associated genes in gastric cancer. *Front Immunol* (2022) 13:843077. doi: 10.3389/fimmu.2022.843077

21. Diboun I, Wernisch L, Orengo CA, Koltzenburg M. Microarray analysis after RNA amplification can detect pronounced differences in gene expression using limma. *BMC Genomics* (2006) 7:252. doi: 10.1186/1471-2164-7-252

22. Friedman J, Hastie T, Tibshirani R. Regularization paths for generalized linear models via coordinate descent. *J Stat Softw* (2010) 33(1):1–22. doi: 10.18637/jss.v033.i01

23. Tao C, Huang K, Shi J, Hu Q, Li K, Zhu X. Genomics and prognosis analysis of epithelial-mesenchymal transition in glioma. *Front Oncol* (2020) 10:183. doi: 10.3389/fonc.2020.00183

24. Xu J, Liu Y, Liu J, Xu T, Cheng G, Shou Y, et al. The identification of critical m(6)A RNA methylation regulators as malignant prognosis factors in prostate adenocarcinoma. *Front Genet* (2020) 11:602485. doi: 10.3389/fgene.2020.602485

25. Gaujoux R, Seoighe C. A flexible r package for nonnegative matrix factorization. *BMC Bioinf* (2010) 11:367. doi: 10.1186/1471-2105-11-367

26. Zhang Z, Lin E, Zhuang H, Xie L, Feng X, Liu J, et al. Construction of a novel gene-based model for prognosis prediction of clear cell renal cell carcinoma. *Cancer Cell Int* (2020) 20:27. doi: 10.1186/s12935-020-1113-6

27. Whitehead MJ, McCanney GA, Willison HJ, Barnett SC. MyelinJ: an ImageJ macro for high throughput analysis of myelinating cultures. *Bioinformatics* (2019) 35(21):4528–30. doi: 10.1093/bioinformatics/btz403

28. Yu G, Wang LG, Han Y, He QY. clusterProfiler: an r package for comparing biological themes among gene clusters. *OMICS* (2012) 16(5):284–7. doi: 10.1089/omi.2011.0118

29. Wang J, Yang J. Identification of significant genes with a poor prognosis in skin cutaneous malignant melanoma based on a bioinformatics analysis. *Ann Transl Med* (2022) 10(8):448. doi: 10.21037/atm-22-1163

30. Mayakonda A, Lin DC, Assenov Y, Plass C, Koeffler HP. Maftools: efficient and comprehensive analysis of somatic variants in cancer. *Genome Res* (2018) 28 (11):1747–56. doi: 10.1101/gr.239244.118

31. Poplawski P, Boguslawska J, Hanusek K, Piekielko-Witkowska A. Nucleolar proteins and non-coding RNAs: Roles in renal cancer. *Int J Mol Sci* (2021) 22(23). doi: 10.3390/ijms222313126

32. Liu H, Yang Y. Identification of mast cell-based molecular subtypes and a predictive signature in clear cell renal cell carcinoma. *Front Mol Biosci* (2021) 8:719982. doi: 10.3389/fmolb.2021.719982

33. Che X, Su W, Li X, Liu N, Wang Q, Wu G. Angiogenesis pathway in kidney renal clear cell carcinoma and its prognostic value for cancer risk prediction. *Front Med (Lausanne)* (2021) 8:731214. doi: 10.3389/fmed.2021.731214

34. Wei H, Xu Z, Chen L, Wei Q, Huang Z, Liu G, et al. Long non-coding RNA PAARH promotes hepatocellular carcinoma progression and angiogenesis via upregulating HOTTIP and activating HIF-1alpha/VEGF signaling. *Cell Death Dis* (2022) 13(2):102. doi: 10.1038/s41419-022-04505-5

35. Zhu Q, Li Y, Dong X, Yang Y, Wang H, Guo S. Linc-OIP5 loss regulates migration and invasion in MDA-MB-231 breast cancer cells by inhibiting YAP1/JAG1 signaling. *Oncol Lett* (2020) 19(1):103–12. doi: 10.3892/ol.2019.11071

36. Li X, Rong J, Li T, Zhou Y, Qi X. LncRNA H22954 inhibits angiogenesis in acute myeloid leukemia through a PDGFA-dependent mechanism. *Recent Pat Anticancer Drug Discov* (2022) 17:427–34. doi: 10.2174/1871526522666220321154949

37. Guo T, Liu D, Peng S, Wang M, Li Y. A positive feedback loop of lncRNA MIR31HG-miR-361-3p -YY1 accelerates colorectal cancer progression through modulating proliferation, angiogenesis, and glycolysis. *Front Oncol* (2021) 11:684984. doi: 10.3389/fonc.2021.684984

38. Liu Y, Geng X. Long non-coding RNA (lncRNA) CYTOR promotes hepatocellular carcinoma proliferation by targeting the microRNA-125a-5p/LASP1 axis. *Bioengineered* (2022) 13(2):3666–79. doi: 10.1080/21655979.2021.2024328

39. Shen J, Yuan Z, Sheng J, Feng X, Wang H, Wang Y, et al. Long non-coding RNA NNT-AS1 positively regulates NPM1 expression to affect the proliferation of estrogen-mediated endometrial carcinoma by interacting. *J Cancer* (2022) 13(1):112–23. doi: 10.7150/jca.62630

40. Zhou Y, Zhang Z, Wo M, Xu W. The long non-coding RNA NNT-AS1 promotes clear cell renal cell carcinoma progression *via* regulation of the miR-137/y-box binding protein 1 axis. *Bioengineered* (2021) 12(1):8994–9005. doi: 10.1080/21655979.2021.1992330

frontiers | Frontiers in Immunology

TYPE Original Research
PUBLISHED 20 October 2022
DOI 10.3389/fimmu.2022.940635

Check for updates

OPEN ACCESS

EDITED BY
Christoph F. A. Vogel,
University of California, Davis,
United States

REVIEWED BY
Pramod Darvin,
Queen Mary University of London,
United Kingdom
Concetta Saponaro,
Bari John Paul II Cancer Institute
(IRCCS), Italy
Jabed Iqbal,
Singapore General Hospital, Singapore
Carmen Gómez De León,
Universidad Nacional Autónoma de
México, Mexico

*CORRESPONDENCE
Sheng Chen
0456177@fudan.edu.cn

SPECIALTY SECTION
This article was submitted to
Cancer Immunity
and Immunotherapy,
a section of the journal
Frontiers in Immunology

RECEIVED 10 May 2022
ACCEPTED 05 October 2022
PUBLISHED 20 October 2022

CITATION
Wang R-X, Ji P, Gong Y, Shao Z-M and
Chen S (2022) SDF-1 expression and
tumor-infiltrating lymphocytes identify
clinical subtypes of triple-negative
breast cancer with different responses
to neoadjuvant chemotherapy
and survival.
Front. Immunol. 13:940635.
doi: 10.3389/fimmu.2022.940635

COPYRIGHT
© 2022 Wang, Ji, Gong, Shao and
Chen. This is an open-access article
distributed under the terms of the
Creative Commons Attribution License
(CC BY). The use, distribution or
reproduction in other forums is
permitted, provided the original
author(s) and the copyright owner(s)
are credited and that the original
publication in this journal is cited, in
accordance with accepted academic
practice. No use, distribution or
reproduction is permitted which does
not comply with these terms.

SDF-1 expression and tumor-infiltrating lymphocytes identify clinical subtypes of triple-negative breast cancer with different responses to neoadjuvant chemotherapy and survival

Ruo-Xi Wang[1,2], Peng Ji[1,2], Yue Gong[1,2], Zhi-Ming Shao[1,2,3] and Sheng Chen[1,2]*

[1]Department of Breast Surgery, Cancer Institute, Fudan University Shanghai Cancer Center, Shanghai, China, [2]Department of Oncology, Shanghai Medical College, Fudan University, Shanghai, China, [3]Institutes of Biomedical Science, Fudan University, Shanghai, China

Background: In this study, we investigated the prediction and prognostic value of SDF-1 for triple-negative breast cancer (TNBC) patients who underwent neoadjuvant chemotherapy (NAC) following standard radical surgery.

Methods: A total of 303 TNBC patients were included in this study. The NAC regimen was weekly paclitaxel plus carboplatin (PC) for all patients. SDF-1 and CXCR4 expression were measured at baseline and surgery *via* enzyme-linked immunosorbent assay (ELISA) and immunohistochemistry (IHC), respectively. Correlations between variables and treatment response were studied, and Cox proportional hazards regression analysis was implemented for prognostic evaluation.

Results: Of the 303 patients, 103 (34.0%) experienced pathological complete response (pCR) after completion of NAC. Serum SDF-1 expression before NAC was significantly correlated with the abundance of TILs. A higher pCR rate was more likely to be observed in patients with lower serum SDF-1 levels before NAC (P=0.001, OR=0.997, 95% CI: 0.996-0.999) and higher levels of TILs (P=0.005). In the multivariate survival model for nonpCR patients, serum SDF-1 expression at surgery served as an independent prognostic value for survival (high level, HR=1.980, 95% CI: 1.170-3.350, low level was used as a reference; P=0.011). Additionally, the predictive and prognostic value of serum SDF-1 expression was significant in patients with high abundance of TILs but not in patients with low abundance of TILs.

Conclusions: This study contributes to the clarification of the value of serum SDF-1 to predict pCR and survival for TNBC patients who underwent NAC. This new serum marker, together with TILs, might help identify clinical subtypes of

TNBC with different treatment responses and survival and play an important role in tailoring and modifying the NAC strategy for advanced TNBCs in the future.

KEYWORDS

breast cancer, neoadjuvant chemotherapy, SDF-1, TILs, pathological complete response

Background

Triple-negative breast cancer (TNBC) is a type of breast cancer that exhibits low expression of estrogen receptor (ER), progesterone receptor (PgR), and human epidermal growth factor receptor-2 (HER2) (1). TNBC accounts for 15-20% of all breast cancers and has an aggressive tumor biology. Neoadjuvant chemotherapy (NAC), also known as preoperative chemotherapy, followed by definitive surgery is a standard of care for locally advanced TNBC and early-stage TNBC with relatively large tumor sizes. The outcome of NAC is usually assessed based on the pathological response of surgical specimens and has a significant impact on patient survival. Patients who achieve a pathological complete response (pCR) have a relatively lower risk of disease recurrence or death than patients with residual disease after NAC (2, 3). Although the

definition of pCR varies across different studies, it has been accepted that the ideal definition should be absence of invasive cancer within both breast and nodes. In earlier studies, analyses were performed based on biological variables (such as ER, PR) through classical cutoffs to predict pCR, however, new biomarkers with more sensitivity and accuracy for early prediction of pCR are still needed.

TNBC is a heterogeneous disease comprising multiple subtypes with different biological behaviors and clinical outcomes (4). However, due to clinical accessibility and convenience, the genomic features of TNBC are still not mature enough to enable the prediction of treatment response. Recent studies have reported numerous biomarkers (e.g., tumor size, node status, Ki-67, HER2) and imaging-based metrics (e.g., magnetic resonance imaging [MRI] and positron emission tomography) for the prediction of pCR (5, 6); however, most efforts with traditional biomarkers measured prior to chemotherapy lack accuracy, and most efforts focusing on monitoring changes in morphological characteristics are indicative only of a late-stage response (7–10).

Stromal cell-derived factor-1 (SDF-1), also known as CXC motif chemokine ligand-12 (CXCL12), which binds to the CXC receptors 4 and 7, is ubiquitously expressed in almost all organs and involved in several aspects of tumor progression, including angiogenesis, metastasis, and survival (11). Some studies have shown that high expression of SDF-1 in cancer cells attracts CXCR4-positive cells, such as cancer-associated fibroblasts (CAFs) or tumor infiltrating lymphocytes (TILs), to the tumor sites and converts the tumor microenvironment (TME) to immune tolerance (12–14). Since TILs are a reliable marker of chemotherapy efficacy and are associated with clinical outcomes in breast cancer (15–17), it is plausible that SDF-1 might also play an essential role in the response to NAC according to environment-mediated drug resistance.

In this study, we analyzed the correlation of SDF-1 and TILs at different time points during NAC and aimed to demonstrate the predictive and prognostic performance of SDF-1 in chemo-naive and chemo-resistant TNBC.

Patients and methods

Study population

We retrospectively collected data from 303 patients with TNBC for this study according to inclusive and exclusive criteria reported in previous studies (18). TNBC was defined as ER-, PgR-, and HER2–. The cutoff values for ER positivity and PgR positivity were 1% of positive tumor cells with nuclear staining. HER2 was evaluated as 0, 1+, 2+, or 3+ using circumferential membrane-bound staining. Positivity for HER2 (HER2+) was considered as 3 + using immunohistochemistry (IHC) or as positive on fluorescence *in situ* hybridization (FISH), whereas cases with 0 to 1 + or 2 + using IHC but without FISH detection were regarded as negative for HER2 (HER2–). All patients were treated with six cycles of weekly PC (paclitaxel [80 mg/m^2] and carboplatin [AUC 2 mg*min/ml] on Days 1, 8, and 15 of a 28-day cycle) followed by surgical resection of the primary breast and axillary lymph node at Shanghai Cancer Hospital between January 2009 and July 2015. Subsequently, patients with pCR received two additional cycles of the same regimen, whereas those who failed to reach pCR received three cycles of anthracycline-containing chemotherapy. Radiation therapy was performed at the discretion of the treating radiologist and was based on disease status before NAC. Patients treated with any other pre-operative treatment including radiotherapy, target

therapy, endocrine therapy or chemotherapy were excluded from the study.

Response and survival evaluation

pCR was defined as no residual invasive cancer in either the breast or lymph nodes. Patients with ductal carcinoma *in situ* (DCIS) only were also considered pCR responders. Patients were followed up every three months in the first two years after the operation and every six months after the first two years after the operation. Disease-free survival was calculated from the date of surgery to the date of disease relapse (local or distant relapse or death from any cause). Patients without events or death were censored at the last follow-up.

ELISA and immunohistochemistry

Peripheral blood samples were collected prior to the start of NAC (at baseline) and after the completion of NAC (at surgery). Blood samples were centrifuged at 1800 rpm for 15 min at 4°C, and serum was transferred to tubes and stored at −80°C until the time of analysis. The serum SDF-1 levels were blindly evaluated concurrently by using a quantitative sandwich ELISA kit (RAB0123-1KT, Sigma–Aldrich) according to a standard protocol. For each serum sample, measurement was repeated at three time points, and the final result was marked as the average level. The inter- and intra-assay coefficients of variation for SDF-1 were 3.5–5.2% and 3.3–6.2%, respectively. The detection range was 93.75-6000 pg/mL. IHC was performed on formalin-fixed, paraffin-embedded tissue sections collected from core-needle biopsy and residual tumor specimens using a two-step protocol (GTVisionIII) to evaluate CXCR4 expression. The antibody was purchased from Cell Signaling Technology (AB124824, Abcam). As a negative control, the primary antibody was omitted and replaced by 1% BSA-PBS. The immunostained slides were evaluated independently by two pathologists. The H score was used to define the positivity of variables (19). An H score of < 100 was defined as negative, whereas an H score > 100 was considered positive. The assessment of unstained TILs was based on the recommendation of an International TIL Working Group (20). TILs were evaluated within the stromal compartment close to the invasive tumor and reported as the percentage of stromal TILs. Representative pathological images (200X) are shown in Figure 1.

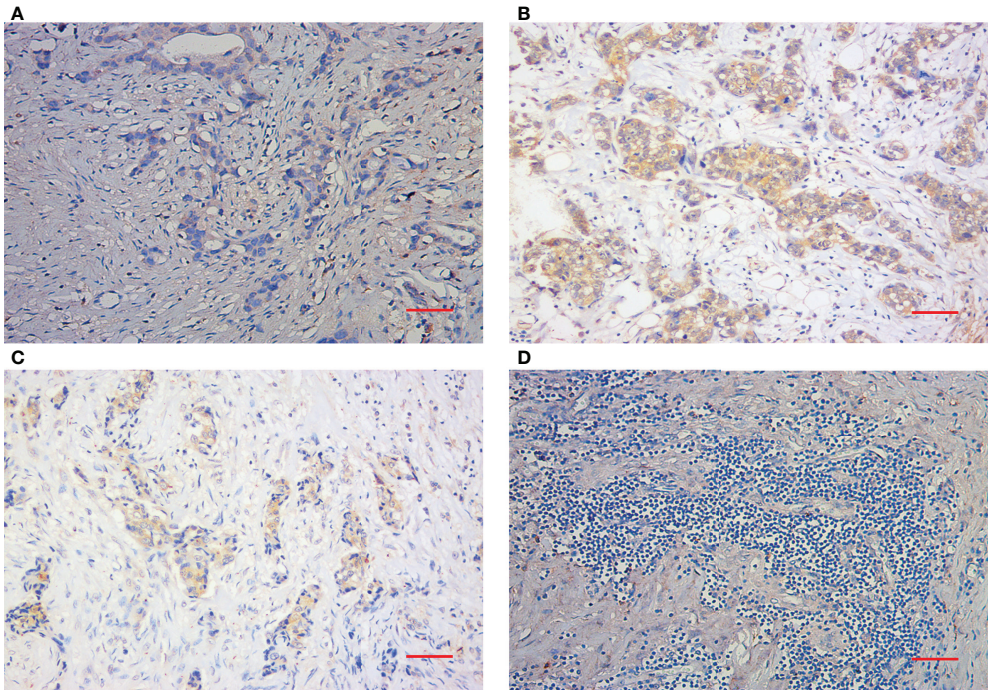

FIGURE 1
Immunohistochemical staining of TILs and CXCR4. **(A)** Representative IHC images of negative CXCR4 staining (200X). **(B)** Representative IHC images of positive CXCR4 staining. **(C)** Representative IHC images of low TIL staining. **(D)** Representative IHC images of high TIL staining (200X). Scale bar (Red): 50 μm.

Statistical analysis

The two-tailed Student's T test was used to compare differences in SDF-1 expression between the two groups. The chi-squared test was used to evaluate the relationships between patient characteristics and pathological response. Variables that significantly predicted pCR in the chi-square test were entered into the multivariate analyses using a logistic regression model. Univariate and multivariate survival analyses were performed using the Cox regression model. Survival curves were estimated using the Kaplan–Meier method, and the log-rank test was used to test for differences between groups. All statistical tests were two-sided, and P values less than 0.05 were considered significant. All analyses were performed with SPSS (version 19.0, SPSS Company, Chicago, IL, USA).

Results

Patient characteristics

Table 1 shows the main characteristics of all patients. The median age of the 303 patients was 50 years (range, 27-74 years). A total of 159 patients were premenopausal at diagnosis, whereas 144 patients were postmenopausal. All patients were diagnosed with T stage between T2-T4, whereas 82.8% of all patients had positive nodes before NAC. TILs in the stromal area of the tumor bed were counted according to the recommendation by an International TIL Working Group (20), whereas TILs outside of the tumor border were excluded. Patients were classified into the high TIL group with the recommended cutoff of 50%. A total of 133 patients (43.9%) had high levels of TILs, and 170 patients

TABLE 1 Patient characteristics and observed pathological complete response (pCR).

Characteristics	Number of patients (%)	Number of pCR (%)	Chi-Square P value	Multivariate P value	Exp. OR (95%CI)
Age			0.564	–	
<40	60 (19.8)	23 (38.3)			
40-59	194 (64.0)	66 (34.0)			
60+	49 (16.2)	14 (28.6)			
Menopausal status			0.817	–	
Pre	159 (52.5)	55 (34.6)			
Post	144 (47.5)	48 (33.3)			
Tumor stage			0.026	0.034	
T2	150 (49.5)	62 (41.3)			Ref.
T3	100 (33.0)	28 (28.0)			0.510 (0.275-0.947)
T4	53 (17.5)	13 (24.5)			0.449 (0.210-0.962)
Node status			0.917	–	
–	52 (17.2)	18 (34.6)			
+	251 (82.8)	85 (33.9)			
TILs			<0.001	<0.001	
<50%	170 (56.1)	41 (24.1)			Ref.
≥50%	133 (43.9)	62 (46.6)			4.607 (1.530-4.442)
Ki-67 expression			<0.001	0.001	
<20%	107 (35.3)	22 (20.6)			Ref.
≥20%	196 (64.7)	81 (41.3)			2.618 (1.456-4.707)
Serum SDF-1 (pg/ml)			<0.001	0.005	
<200.0	68 (22.4)	36 (52.9)			Ref.
200-299.9	55 (18.2)	23 (41.8)			0.515 (0.233-1.136)
300-399.9	69 (22.8)	19 (27.5)			0.304 (0.142-0.650)
400-499.9	51 (16.8)	13 (25.5)			0.318 (0.136-0.743)
≥500	60 (19.8)	12 (20)			0.264 (0.114-0.609)
CXCR4 expression			0.421	–	
Negative	117 (38.6)	43 (36.8)			
Positive	186 (61.4)	60 (32.3)			

pCR, pathological complete response; OR, odds ratio; CI, confidence interval; TILs, tumor-infiltrating lymphocytes; SDF-1, stromal cell-derived factor-1; Ref., reference.

(56.1%) had low levels of TILs. Serum SDF-1 expression was detected according to ELISA prior to NAC. The median level was 329.0 pg/ml (range: 100.0 pg/ml-1158.3 pg/ml). A total of 186 patients were identified as CXCR4 positive through IHC, whereas the remaining 117 patients were CXCR4 negative. Supplemental Figure 1 shows the distribution of SDF-1 expression among different characteristics. SDF-1 expression was similar in patients with different ages, menopausal statuses, tumor stages, and Ki67 levels; however, high expression of SDF-1 was observed in patients with low levels of TILs (mean level 376.3 ± 188.1 vs. 315.3 ± 182.7, P=0.0048) and in patients with high expression of CXCR4 (mean level 295.4 ± 161.3 vs. 383.6 ± 195.7, P<0.001).

Variables that predict pCR

Among the 303 patients, the overall pCR rate was 34.0% (103/303). The correlations between multiple patient characteristics and pCR were analyzed (Table 1). In univariate analysis, the primary T stage (P=0.026), TILs (P<0.001), Ki-67 expression (P<0.001), and serum SDF-1 (P<0.001) were identified as pCR predictors, and we found no significant differences in pCR according to patient age, menopausal status, node status, and CXCR4 expression. In the multivariate logistic regression model, SDF-1 was independently correlated with pCR (P=0.005). TILs were also independently correlated with pCR (P<0.001). The OR of TILs ≥50% was 4.607 (95% CI: 1.530-4.442, P<0.001, TILs <50% as reference). Tumor T stage and Ki-67 expression were also independent predictors of pCR (P=0.034, OR=0.510 for T3, and OR=0.449 for T4, T2 as reference; and P=0.001, HR=2.618 for high Ki67, low Ki-67 as reference, respectively). The ROC curves of the pCR predictors are shown in Figure 2A. The AUCs were 0.657, 0.624, 0.606, and 0.585 for SDF-1, TILs, Ki67, and T stage, respectively.

Serum SDF-1, TILs, and treatment response

The pCR rates were 52.9%, 41.8%, 27.5%, 25.5%, and 20% according to different SDF-1 levels (<200.0 pg/ml, 200-299.9, 300-399.9 pg/ml, 400-499.9 pg/ml, and ≥500.0 pg/ml, respectively). A higher pCR possibility was more likely observed in patients with lower levels of SDF-1, especially in patients with SDF-1 expression of <300.0 pg/ml. According to the ROC curve of SDF-1 (AUC=0.657, 95% CI: 0.592-0.722), the cutoff value of SDF-1 to predict pCR was 328.25 pg/ml, with the largest sum of sensitivity and specificity. For the sake of convenience, we set the cutoff as 300.0 pg/ml. The pCR rate was 48.0% in patients with low SDF-1 expression and 24.4% in patients with high SDF-1 expression (P<0.001, Figure 2B). The correlation between the serum SDF-1 levels, TILs, and tumor regression (according to MP grades) is also shown in Figures 2C, D). Low levels of SDF-1 and high levels of TILs were significantly correlated with a relatively better response. For instance, the proportion of patients with poor response (MP 1, 2) was almost doubled in both high SDF-1 (22.2%, compared to 10.6% in low SDF-1) and low TILs (23.5%, compared to 9.8% in high TILs).

We also investigated the performance of SDF-1 at different TIL levels. Supplementary Table 1 shows that the subgroup according to SDF-1 and TIL level (SDF-1 low/TILs-high, SDF-1 low/TILs-low, SDF-1 high/TILs-high and SDF-1 high/TILs-low) is independently correlated to pCR. Interestingly, the difference in the pCR rate between low and high SDF-1 levels was only significant in patients with high TILs (63.5% vs. 31.4%, P<0.001) but not in patients with low TILs (31.7% vs. 20.0%, P=0.089) (Figure 2E). The distribution of tumor regression also showed a similar phenomenon, indicating that patients with high TILs and low SDF-1 experienced a favorable response to NAC (Figure 2F).

We also analyzed the change in serum SDF-1 before and after NAC. The mean value of SDF-1 (pg/ml) in nonpCR patients was 380.9 (95% CI: 355.2-406.6) at baseline and 392.2 (95% CI: 361.6-422.7) at surgery, whereas the mean value of SDF-1 (pg/ml) in pCR patients was 288.6 (95% CI: 253.4-323.8) at baseline and 206.4 (95% CI: 184.1-228.7) at surgery. The reduction in SDF-1 before and after NAC was correlated with pathological response, as the mean reduction was -11.3 (95% CI: -47.4-24.5) (pg/ml) in nonpCR patients and 82.2 (95% CI: 49.7-114.8) (pg/ml) in pCR patients (P=0.004). In subgroup analyses, a significant difference in SDF-1 reduction between pCR and nonpCR responders was only observed in patients with high TILs (Supplementary Figure 2).

SDF-1 and patient survival

For all patients in this study, the median follow-up time was 50 months. Among the 103 patients who achieved pCR, only 4 developed disease recurrence or metastasis. However, in the remaining 200 patients in the nonpCR group, 71 had cases of event or death (35.1%). Therefore, we developed survival analyses in only 200 nonpCR responders.

A Cox regression model was used to detect the prognostic biomarker in univariate and multivariate analyses (Table 2). Residual tumor size (P=0.018), residual involved nodes (P<0.001), tumor Ki-67 (P<0.001), serum SDF-1 at baseline (P=0.046), serum SDF-1 at surgery (P<0.001), and TILs at surgery (P<0.001) were significant predictors of DFS and entered the multivariate Cox regression model with forward

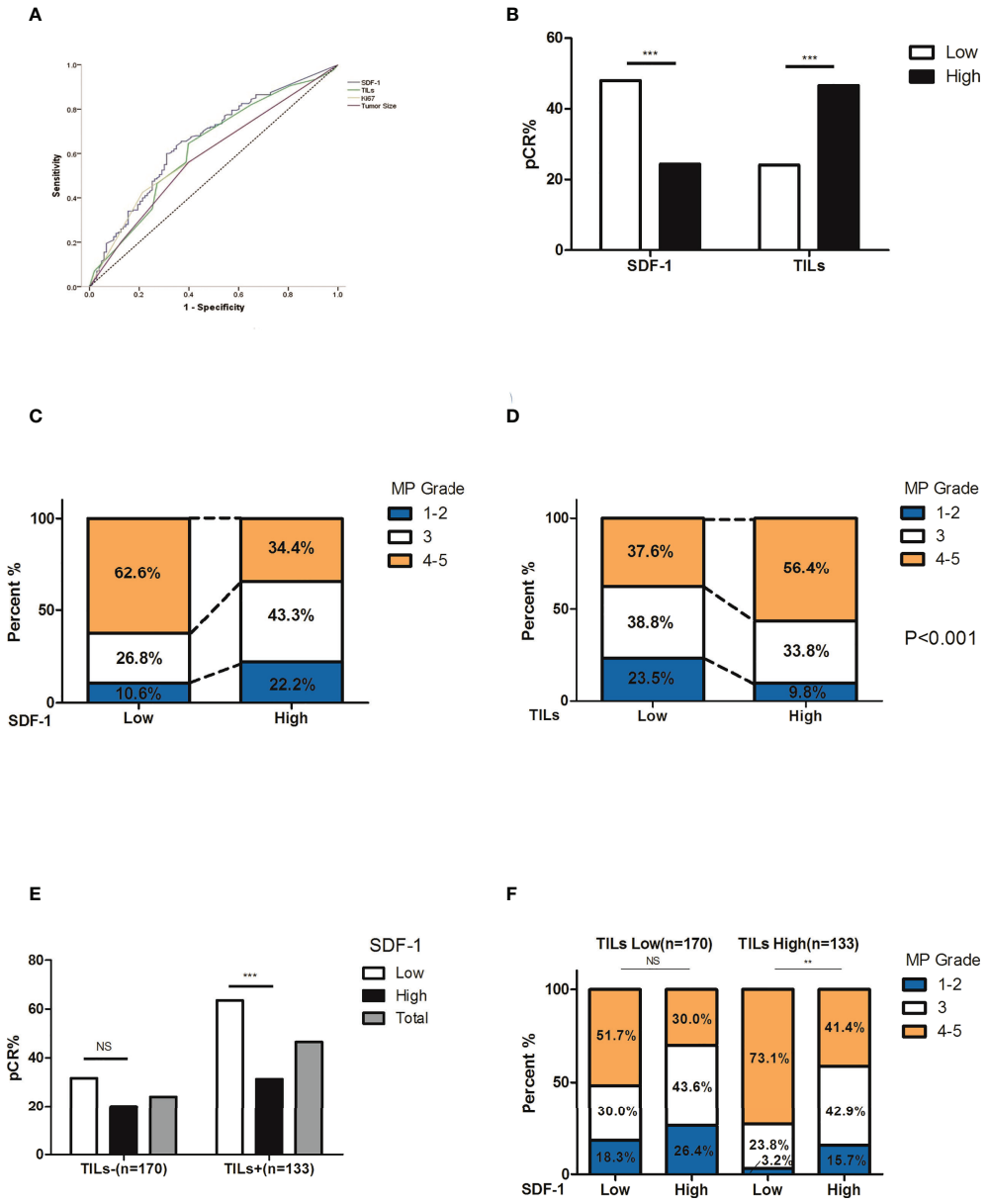

FIGURE 2
Correlation between treatment response and its predictors. **(A)** ROC curve of pCR predictors. The AUCs were 0.657, 0.624, 0.606, and 0.585 for SDF-1, TILs, Ki67, and T stage, respectively. **(B)** The rate of pCR and SDF-1 expression. The pCR rate was 48.0% in patients with low SDF-1 expression and 24.4% in patients with high SDF-1 expression (P<0.001). **(C)** The correlation between the SDF-1 levels and tumor regression (according to MP grades). Notably, there was a higher proportion of favorable responses in SDF-1-low patients. **(D)** The correlation between TILs and tumor regression (according to MP grades). Notably, there was a higher proportion of favorable responses in SDF-1 high expression patients. **(E)** The correlation between SDF-1 and pCR according to different TIL levels. The pCR rate in patients with high TILs was 63.5% for low SDF-1 and 31.4% for high SDF-1 (P<0.001). The pCR rate in patients with low TILs was 31.7% for low SDF-1 and 20.0% for high SDF-1 (P=0.089). **(F)** The correlation between SDF-1 and tumor regression (according to MP grades) according to different TIL levels. Notably, patients with high TILs and low SDF-1 levels experienced a favorable response to NAC. (NS, not significant; **P<0.01, ***P<0.001).

selection. In the multivariate Cox regression model, both SDF-1 and TIL expression at surgery were independent predictors for DFS (SDF-1: P=0.011; HR=1.980, 95% CI: 1.170-3.350, low level as reference; TILs: P=0.012; HR=0.487, 95% CI: 0.278-0.855, low level as reference). However, serum SDF-1 at baseline failed to show independent prognostic value (P=0.559). The survival distribution by Kaplan–Meier survival curve is shown in Figure 3. Higher DFS was observed in nonpCR patients with

TABLE 2 Univariate and multivariate survival analysis of non-pCR patients.

Factors	Disease-free survival		
	Univariate	Multivariate	
	P	P	HR (95% CI)
Age			
<40 vs. 40-60 vs.≥60	0.448	–	–
Menopausal status			
Pre vs. Post	0.350	–	–
Initial tumor status			
T2 vs. T3 vs. T4	0.163	–	–
Residual tumor size			
≤2cm vs. 2-5cm vs. >5cm	<0.001	0.018	Ref. 0.802 (0.419-1.535) 1.774 (0.993-3.168)
Residual involved nodes			
0 vs. 1-3 vs. ≥4	<0.001	<0.001	Ref. 0.862 (0.397-1.870) 2.685 (1.387-5.196)
Vascular invasion			
Negative vs. Positive	0.981	–	–
Grade			
I - II vs. III	0.051	–	–
Ki-67			
<20% vs.≥20%	<0.001	0.203	–
Serum SDF-1 at baseline			
Low vs. High	0.046	0.559	–
Serum SDF-1 at surgery			
Low vs. High	<0.001	0.011	Ref. 1.980 (1.170-3.350)
CXCR4 at baseline			
- vs.+	0.111	–	–
CXCR4 at surgery			
- vs. +	0.188	–	–
TILs at baseline			
Low vs. High	0.218	–	–
TILs at surgery			
Low vs. High	<0.001	0.012	Ref 0.487 (0.278-0.855)

HR, hazard ratio; CI, confidence interval; SDF-1, stromal cell-derived factor-1; TILs, tumor-infiltrating lymphocytes; Ref., reference.

low SDF-1 (Figure 3A Log-rank test P<0.001) and high TILs at surgery (Figure 3B Log-rank test P<0.001). We also demonstrated DFS according to SDF-1 expression in different subgroups of TIL levels (Figures 3C, D). Different levels of SDF-1 expression showed significant differences in the survival of patients with high TILs (log-rank test P=0.001), with 3-year DFS rates of 93% and 71% in patients with low SDF-1 and high SDF-1, respectively. However, SDF-1 expression failed to show prognostic value in patients with low TILs (log-rank test P=0.257), since patients in this subgroup had experienced similar unfavorable outcomes. The 3-year DFS was 65% and 50% in patients with low SDF-1 and high SDF-1, respectively.

Discussion

At present, the optimal chemotherapy regimen for TNBC remains controversial; therefore, it is managed with standard chemotherapy, including paclitaxel in combination with anthracycline or platinum drugs. Compared with other breast

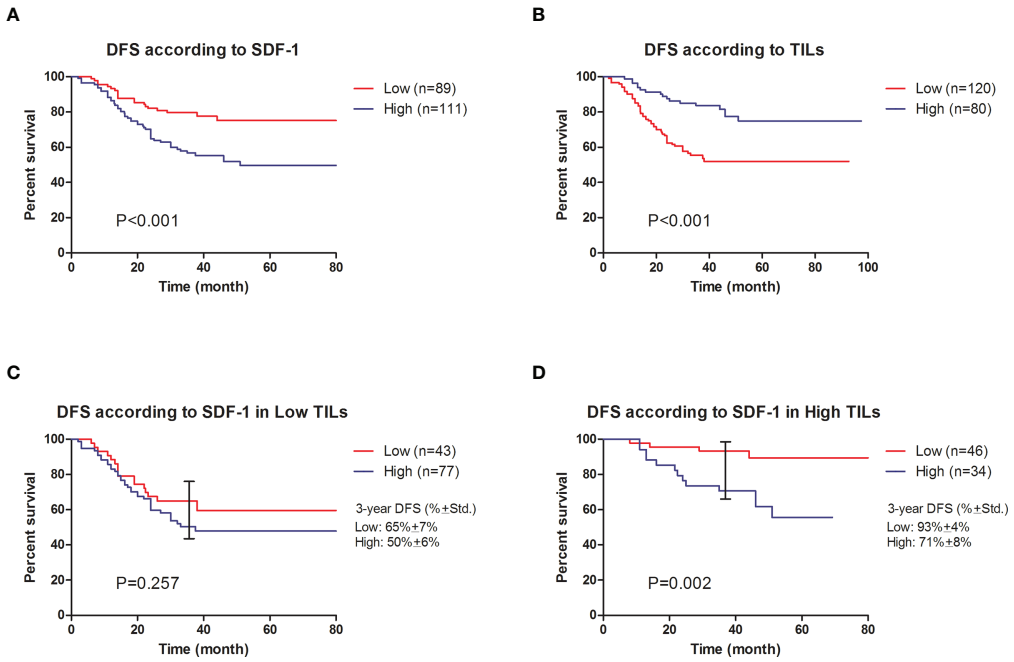

FIGURE 3
Cumulative disease-free survival of nonpCR patients after NAC. **(A)** DFS according to SDF-1 expression (log-rank test P<0.001). **(B)** DFS according to TIL expression (log-rank test P<0.001). **(C)** DFS according to SDF-1 expression in low TIL patients (log-rank test P=0.257. The observed 3-year DFS rates were 65% ± 7% and 50% ± 6% in the low SDF-1 and high SDF-1 groups, respectively. **(D)** DFS according to SDF-1 expression in high TIL patients (log-rank test P=0.002). The observed 3-year DFS rates were 93% ± 4% and 71% ± 8% in the low SDF-1 and high SDF-1 groups, respectively.

cancer subtypes, TNBC has a higher possibility of achieving pCR; however, this advantage is not clearly translated into improved overall survival due to the poor outcomes of nonpCR responders (21). Thus, it is important to identify sensitive responders. In recent studies, numerous biomarkers (e.g., tumor size, lymph node status, Ki-67, HER2, etc.) and imaging-based metrics (e.g., MRI and PET) have been studied for the prediction of pCR and survival (5, 6); however, reliable predictive and prognostic biological markers remain limited. In this study, we demonstrated that serum SDF-1 serves as a biomarker for predicting the treatment response and survival of TNBC patients who underwent NAC.

SDF-1 is a class of stromal cell-derived factors belonging to the chemokine CXC family systematically named CXCL12. It is a self-stable chemokine that marks CXCR4 and encodes a polypeptide of 89 amino acid residues (22). SDF-1 activates downstream signaling pathways, such as PAM and ERK1/2, and enhances cancer cell survival, proliferation, and chemotaxis by binding to its receptor CXCR4 (23). Previous studies have shown that high expression of SDF-1/CXCR4 is correlated with poor survival in various tumors, such as colorectal cancer (24), prostate cancer (25), pancreatic cancer (26), and breast cancer (27). However, limited data have reported the value of SDF-1/CXCR4 in predicting chemotherapy response. Karin Tamas et al. (28) reported that CXCR4 and SDF-1 are highly expressed in primary rectal tumors of patients presenting with metastatic disease, while radiochemotherapy and bevacizumab further upregulate CXCL12 expression; however, there were no differences in CXCR4 or CXCL12 expression at baseline between patients who had (n=9) vs did not have (n=30) a pCR. In contrast, Kim et al. (29) reported that unregulated expression of SDF-1α (P=0.016), after neoadjuvant chemoradiotherapy for rectal cancer, was significantly associated with treatment resistance. Our study presented new evidence that in TNBC, expression of SDF-1 in serum samples could identify chemosensitive tumors. To the best of our knowledge, no previous reports have identified the mechanism of acquiring chemotherapy resistance *via* upregulation of SDF-1 expression in breast cancer.

The expression of SDF-1 was significantly upregulated in myofibroblasts associated with invasive breast cancer compared with myofibroblasts obtained from normal breast tissue. Further evidence of SDF-1 production by stromal cells associated with breast cancer was provided by Orimo et al. (30). The mechanisms governing the stable regulation of SDF-1 in breast cancer-associated myofibroblasts have not been established; however, it is speculated that destruction of tumor cells by chemotherapeutic agents may release tumor-associated

antigens, triggering an immune response that regulates SDF-1, which is particularly strong in patients whose immune systems are sensitive to certain tumor antigens before the onset of chemotherapy. Therefore, SDF-1 expression level might reflect the sensitivity of patients' immune reaction to chemotherapy. It is also supported by our analysis that the reduction of SDF-1 was extremely high in pCR patients compared to nonpCR patients, indicating that regulation of SDF-1 was correlated with chemosensitivity.

Furthermore, we demonstrated that SDF-1 expression in patients with residual tumors was correlated with survival. It is suggested that residual chemotherapy-resistant disease after NAC is a substitute for chemotherapy-resistant micrometastases, which can eventually develop into clinically obvious metastatic breast cancer. Because TNBC is initially sensitive to NAC, residual tumors are generally more aggressive, which leads to poor prognosis and shorter RFS and OS (31, 32). In addition, some reports suggest that residual cancer cells in TNBC are a heterogeneous population, including subtypes with different outcomes (33). Therefore, the expression of SDF-1 in residual cancer cells may reflect a subtype of TNBC with stronger invasive behavior, leading to poor survival.

Interestingly, the predictive and prognostic value of SDF-1 was only significant in patients with high TILs but not in patients with low TILs, suggesting that TILs might play an important role in the interaction between SDF-1 and tumors. In recent years, many investigations have noted that TILs are important predictive and prognostic biomarkers in breast cancer patients. Carsten Denkert et al. (34) reported that the presence of tumor-associated lymphocytes in breast cancer is an independent predictor of response to anthracycline/taxane NAC in the cohort from the GeparDuo and GeparTrio study. Dieci et al. (17) also presented data that the presence of TILs in residual disease after NAC is associated with better prognosis in TNBC patients. These studies have led to the hypothesis that the pretreatment host response enhances the ability of chemotherapy to eliminate cancer cells, and the chemo-induced antitumor immune response might also influence patient survival (35). This hypothesis is strongly supported by our study, as TILs have also shown predictive and prognostic value in multivariate analyses. Since the SDF-1/CXCR4 axis plays a crucial role in recruiting immune cells such as MDSCs and Tregs to the tumor microenvironment (36, 37), we speculate that upregulation of SDF-1 expression may induce chemoresistance in TNBC *via* infiltration of immune cells. Further investigation of the relationship between SDF-1 and the precision subtyping of TILs is needed in our future study.

There are several limitations in this study. This was a retrospective study including 303 patients in single institution. Due to the relatively small sample size, we were not able to validate the cutoff values and establish a nomogram to predict pCR and survival. Additionally, the expression of SDF-1 was only detected at two time points, and it will be necessary to evaluate the change in SDF-1 at different periods of NAC, and the method used for choosing the cut-off point need to be further validated. It is also not clear at present whether our observation is restricted to NAC therapies in this study (paclitaxel and carboplatin) or may be a general feature of chemotherapy response.

In conclusion, the current study highlighted the utility of serum SDF-1 and established this as a potential predictive and prognostic marker in TNBC. We have presented that SDF-1, together with TILs, might help to identify patients who would benefit from chemotherapy and patients who need further intensified treatment strategies. Collectively, these biomarkers might help to shape preoperative and postoperative treatment strategies targeting SDF-1 and immune cells for the improvement of pCR rates and prevention of disease relapse in nonpCR patients.

Data availability statement

The raw data supporting the conclusions of this article will be made available by the authors, without undue reservation.

Ethics statement

The studies involving human participants were reviewed and approved by Shanghai Cancer Center Ethical Committee. The patients/participants provided their written informed consent to participate in this study.

Author contributions

R-XW and SC contributed to the conception of the study, data analysis and interpretation, and writing the manuscript. PJ and YG made tissue sections and participated in ELISA and immunohistochemical analysis. SC and Z-MS contributed to the collection and assembly of data. All authors contributed to the article and approved the submitted version.

Funding

This research was supported by the National Natural Science Foundation of China (81872134). The funders had no role in the study design, data collection and analysis, decision to publish, or preparation of the manuscript.

Acknowledgments

The authors are grateful to Yin Zhou, Guang-Yu Liu, and Can-Ming Chen for their excellent data management.

Conflict of interest

The authors declare that the research was conducted in the absence of any commercial or financial relationships that could be construed as a potential conflict of interest.

Publisher's note

All claims expressed in this article are solely those of the authors and do not necessarily represent those of their affiliated organizations, or those of the publisher, the editors and the reviewers. Any product that may be evaluated in this article, or claim that may be made by its manufacturer, is not guaranteed or endorsed by the publisher.

Supplementary material

The Supplementary Material for this article can be found online at: https://www.frontiersin.org/articles/10.3389/fimmu.2022.940635/full#supplementary-material

SUPPLEMENTARY FIGURE 1
Correlation between SDF-1 expression and other variables. SDF-1 expression was similar in patients with different ages, menopausal statuses, tumor stages, and Ki67 levels; however, high expression of SDF-1 was observed in patients with low levels of TILs (mean level 376.3 + 188.1 vs. 315.3 + 182.7, P=0.0048) and in patients with high expression of CXCR4 (mean level 295.4 + 161.3 vs. 383.6 + 195.7, P<0.001).

SUPPLEMENTARY FIGURE 2
Reduction in SDF-1 expression during NAC. The mean value of SDF-1 (pg/ml) in nonpCR patients was 380.9 (95% CI: 355.2-406.6) at baseline and 392.2 (95% CI: 361.6-422.7) at surgery, whereas the mean value of SDF-1 (pg/ml) in pCR patients was 288.6 (95% CI: 253.4-323.8) at baseline and 206.4 (95% CI: 184.1-228.7) at surgery. The reduction in SDF-1 before and after NAC was correlated with pathological response, as the mean reduction was -11.3 (95% CI: -47.4-24.5) (pg/ml) in nonpCR patients and 82.2 (95% CI: 49.7-114.8) (pg/ml) in pCR patients (P=0.004). In subgroup analyses, a significant difference in SDF-1 reduction between pCR and nonpCR responders was only observed in patients with high TILs.

References

1. Bauer KR, Brown M, Cress RD, Parise CA, Caggiano V. Descriptive analysis of estrogen receptor (ER)-negative, progesterone receptor (PR)-negative, and HER2-negative invasive breast cancer, the so-called triple-negative phenotype: a population-based study from the California cancer registry. *Cancer* (2007) 109 (9):1721–8. doi: 10.1002/cncr.22618

2. Kong X, Moran MS, Zhang N, Haffty B, Yang Q. Meta-analysis confirms achieving pathological complete response after neoadjuvant chemotherapy predicts favourable prognosis for breast cancer patients. *Eur J Cancer* (2011) 47(14):2084–90. doi: 10.1016/j.ejca.2011.06.014

3. Prowell TM, Pazdur R. Pathological complete response and accelerated drug approval in early breast cancer. *N Engl J Med* (2012) 366(26):2438–41. doi: 10.1056/NEJMp1205737

4. Lehmann BD, Bauer JA, Chen X, Sanders ME, Chakravarthy AB, Shyr Y, et al. Identification of human triple-negative breast cancer subtypes and preclinical models for selection of targeted therapies. *J Clin Invest* (2011) 121(7):2750–67. doi: 10.1172/JCI45014

5. Yankeelov TE, Atuegwu N, Hormuth D, Weis JA, Barnes SL, Miga MI, et al. Clinically relevant modeling of tumor growth and treatment response. *Sci Trans Med* (2013) 5(187):187ps189. doi: 10.1126/scitranslmed.3005686

6. Weis JA, Miga MI, Arlinghaus LR, Li X, Abramson V, Chakravarthy AB, et al. Predicting the response of breast cancer to neoadjuvant therapy using a mechanically coupled reaction-diffusion model. *Cancer Res* (2015) 75(22):4697–707. doi: 10.1158/0008-5472.CAN-14-2945

7. Kim KI, Lee KH, Kim TR, Chun YS, Lee TH, Park HK. Ki-67 as a predictor of response to neoadjuvant chemotherapy in breast cancer patients. *J Breast Cancer* (2014) 17(1):40–6. doi: 10.4048/jbc.2014.17.1.40

8. Rouzier R, Pusztai L, Delaloge S, Gonzalez-Angulo AM, Andre F, Hess KR, et al. Nomograms to predict pathologic complete response and metastasis-free survival after preoperative chemotherapy for breast cancer. *J Clin Oncol Off J Am Soc Clin Oncol* (2005) 23(33):8331–9. doi: 10.1200/JCO.2005.01.2898

9. Hayashi Y, Takei H, Nozu S, Tochigi Y, Ichikawa A, Kobayashi N, et al. Analysis of complete response by MRI following neoadjuvant chemotherapy predicts pathological tumor responses differently for molecular subtypes of breast cancer. *Oncol Lett* (2013) 5(1):83–9. doi: 10.3892/ol.2012.1004

10. Liu Q, Wang C, Li P, Liu J, Huang G, Song S. The role of (18)F-FDG PET/CT and MRI in assessing pathological complete response to neoadjuvant chemotherapy in patients with breast cancer: A systematic review and meta-analysis. *BioMed Res Int* (2016) 2016:3746232. doi: 10.1155/2016/1235429

11. Balkwill F. Cancer and the chemokine network. *Nat Rev Cancer* (2004) 4 (7):540–50. doi: 10.1038/nrc1388

12. Righi E, Kashiwagi S, Yuan J, Santosuosso M, Leblanc P, Ingraham R, et al. et al. CXCL12/CXCR4 blockade induces multimodal antitumor effects that prolong survival in an immunocompetent mouse model of ovarian cancer. *Cancer Res* (2011) 71(16):5522–34. doi: 10.1158/0008-5472.CAN-10-3143

13. Feig C, Jones JO, Kraman M, Wells RJ, Deonarine A, Chan DS, et al. Targeting CXCL12 from FAP-expressing carcinoma-associated fibroblasts synergizes with anti-PD-L1 immunotherapy in pancreatic cancer. *Proc Natl Acad Sci USA* (2013) 110(50):20212–7. doi: 10.1073/pnas.1320318110

14. Li X, Bu W, Meng L, Liu X, Wang S, Jiang L, et al. CXCL12/CXCR4 pathway orchestrates CSC-like properties by CAF recruited tumor associated macrophage in OSCC. *Exp Cell Res* (2019) 378(2):131–8. doi: 10.1016/j.yexcr.2019.03.013

15. Garcia-Martinez E, Gil GL, Benito AC, Gonzalez-Billalabeitia E, Conesa MA, Garcia Garcia T, et al. Tumor-infiltrating immune cell profiles and their change after neoadjuvant chemotherapy predict response and prognosis of breast cancer. *Breast Cancer Res* (2014) 16(6):488. doi: 10.1186/s13058-014-0488-5

16. Adams S, Gray RJ, Demaria S, Goldstein L, Perez EA, Shulman LN, et al. Prognostic value of tumor-infiltrating lymphocytes in triple-negative breast cancers from two phase III randomized adjuvant breast cancer trials: ECOG 2197 and ECOG 1199. *J Clin Oncol* (2014) 32(27):2959–66. doi: 10.1200/JCO.2013.55.0491

17. Dieci MV, Criscitiello C, Goubar A, Viale G, Conte P, Guarneri V, et al. Prognostic value of tumor-infiltrating lymphocytes on residual disease after primary chemotherapy for triple-negative breast cancer: a retrospective multicenter study. *Ann Oncol* (2015) 26(7):1518. doi: 10.1093/annonc/mdv241

18. Chen XS, Nie XQ, Chen CM, Wu JY, Wu J, Lu JS, et al. Weekly paclitaxel plus carboplatin is an effective nonanthracycline-containing regimen as neoadjuvant chemotherapy for breast cancer. *Ann Oncol Off J Eur Soc Med Oncol / ESMO* (2010) 21(5):961–7. doi: 10.1093/annonc/mdq041

19. Wang RX, Chen S, Huang L, Shao ZM. Predictive and prognostic value of matrix metalloproteinase (MMP) - 9 in neoadjuvant chemotherapy for triple-negative breast cancer patients. *BMC Cancer* (2018) 18(1):909. doi: 10.1186/s12885-018-4822-7

20. Salgado R, Denkert C, Demaria S, Sirtaine N, Klauschen F, Pruneri G, et al. The evaluation of tumor-infiltrating lymphocytes (TILs) in breast cancer: recommendations by an international TILs working group 2014. *Ann Oncol Off J Eur Soc Med Oncol / ESMO* (2015) 26(2):259–71. doi: 10.1093/annonc/mdu450

21. Carey LA, Dees EC, Sawyer L, Gatti L, Moore DT, Collichio F, et al. The triple negative paradox: primary tumor chemosensitivity of breast cancer subtypes. *Clin Cancer Res an Off J Am Assoc Cancer Res* (2007) 13(8):2329–34. doi: 10.1158/1078-0432.CCR-06-1109

22. Fernandez EJ, Lolis E. Structure, function, and inhibition of chemokines. *Annu Rev Pharmacol Toxicol* (2002) 42:469–99. doi: 10.1146/annurev.pharmtox.42.091901.115838

23. Scala S. Molecular pathways: Targeting the CXCR4-CXCL12 axis–untapped potential in the tumor microenvironment. *Clin Cancer Res* (2015) 21(19):4278–85. doi: 10.1158/1078-0432.CCR-14-0914

24. Akishima-Fukasawa Y, Nakanishi Y, Ino Y, Moriya Y, Kanai Y, Hirohashi S. Prognostic significance of CXCL12 expression in patients with colorectal carcinoma. *Am J Clin Pathol* (2009) 132(2):202–10. doi: 10.1309/AJCPK35VZJEWCUTL

25. Parol-Kulczyk M, Gzil A, Ligmanowska J, Grzanka D. Prognostic significance of SDF-1 chemokine and its receptors CXCR4 and CXCR7 involved in EMT of prostate cancer. *Cytokine* (2022) 150:155778. doi: 10.1016/j.cyto.2021.155778

26. Kato T, Matsuo Y, Ueda G, Murase H, Aoyama Y, Omi K, et al. Enhanced CXCL12/CXCR4 signaling increases tumor progression in radiationresistant pancreatic cancer. *Oncol Rep* (2022) 47(4):68. doi: 10.3892/or.2022.8279

27. Kato M, Kitayama J, Kazama S, Nagawa H. Expression pattern of CXC chemokine receptor-4 is correlated with lymph node metastasis in human invasive ductal carcinoma. *Breast Cancer Res* (2003) 5(5):R144–50. doi: 10.1186/bcr627

28. Tamas K, Domanska UM, van Dijk TH, Timmer-Bosscha H, Havenga K, Karrenbeld A, et al. CXCR4 and CXCL12 expression in rectal tumors of stage IV patients before and after local radiotherapy and systemic neoadjuvant treatment. *Curr Pharm Des* (2015) 21(17):2276–83. doi: 10.2174/1381612821666150105155615

29. Kim HJ, Bae SB, Jeong D, Kim ES, Kim CN, Park DG, et al. Upregulation of stromal cell-derived factor 1alpha expression is associated with the resistance to neoadjuvant chemoradiotherapy of locally advanced rectal cancer: angiogenic markers of neoadjuvant chemoradiation. *Oncol Rep* (2014) 32(6):2493–500. doi: 10.3892/or.2014.3504

30. Orimo A, Gupta PB, Sgroi DC, Arenzana-Seisdedos F, Delaunay T, Naeem R, et al. Stromal fibroblasts present in invasive human breast carcinomas promote tumor growth and angiogenesis through elevated SDF-1/CXCL12 secretion. *Cell* (2005) 121(3):335–48. doi: 10.1016/j.cell.2005.02.034

31. Nahleh Z. neoadjuvant chemotherapy for "triple negative" breast cancer: a review of current practice and future outlook. *Med Oncol* (2010) 27(2):531–9. doi: 10.1007/s12032-009-9244-6

32. Keam B, Im SA, Lee KH, Han SW, Oh DY, Kim JH, et al. et al. ki-67 can be used for further classification of triple negative breast cancer into two subtypes with different response and prognosis. *Breast Cancer Res* (2011) 13(2):R22. doi: 10.1186/bcr2834

33. Cheang MC, Voduc D, Bajdik C, Leung S, McKinney S, Chia SK, et al. Basal-like breast cancer defined by five biomarkers has superior prognostic value than triple-negative phenotype. *Clin Cancer Res* (2008) 14(5):1368–76. doi: 10.1158/1078-0432.CCR-07-1658

34. Denkert C, Loibl S, Noske A, Roller M, Muller BM, Komor M, et al. Tumor-associated lymphocytes as an independent predictor of response to neoadjuvant chemotherapy in breast cancer. *J Clin Oncol* (2010) 28(1):105–13. doi: 10.1200/JCO.2009.23.7370

35. Zitvogel L, Apetoh L, Ghiringhelli F, Andre F, Tesniere A, Kroemer G. The anticancer immune response: indispensable for therapeutic success? *J Clin Invest* (2008) 118(6):1991–2001. doi: 10.1172/JCI35180

36. Takahashi R, Amano H, Ito Y, Eshima K, Satoh T, Iwamura M, et al. Microsomal prostaglandin e synthase-1 promotes lung metastasis *via* SDF-1/CXCR4-mediated recruitment of CD11b(+)Gr1(+)MDSCs from bone marrow. *BioMed Pharmacother* (2020) 121:109581. doi: 10.1016/j.biopha.2019.109581

37. Costa A, Kieffer Y, Scholer-Dahirel A, Pelon F, Bourachot B, Cardon M, et al. Fibroblast heterogeneity and immunosuppressive environment in human breast cancer. *Cancer Cell* (2018) 33(3):463–79.e410. doi: 10.1016/j.ccell.2018.01.011

frontiers | Frontiers in Immunology

TYPE Original Research
PUBLISHED 16 March 2023
DOI 10.3389/fimmu.2023.1165101

Check for updates

OPEN ACCESS

EDITED BY
Xin Lu,
University of Notre Dame, United States

REVIEWED BY
Jun Yan,
Southern Medical University, China
Dawei Li,
Fudan University, China

*CORRESPONDENCE
Bo Feng
fb11427@rjh.com.cn
Xiao Yang
yxrjmis@alumni.sjtu.edu.cn
Sen Zhang
zhangsen6886@163.com

†These authors have contributed equally to this work

SPECIALTY SECTION
This article was submitted to Cancer Immunity and Immunotherapy, a section of the journal Frontiers in Immunology

RECEIVED 13 February 2023
ACCEPTED 06 March 2023
PUBLISHED 16 March 2023

CITATION
Xu X, Ding C, Zhong H, Qin W, Shu D, Yu M, Abuduaini N, Zhang S, Yang X and Feng B (2023) Integrative analysis revealed that distinct cuprotosis patterns reshaped tumor microenvironment and responses to immunotherapy of colorectal cancer. *Front. Immunol.* 14:1165101. doi: 10.3389/fimmu.2023.1165101

COPYRIGHT
© 2023 Xu, Ding, Zhong, Qin, Shu, Yu, Abuduaini, Zhang, Yang and Feng. This is an open-access article distributed under the terms of the Creative Commons Attribution License (CC BY). The use, distribution or reproduction in other forums is permitted, provided the original author(s) and the copyright owner(s) are credited and that the original publication in this journal is cited, in accordance with accepted academic practice. No use, distribution or reproduction is permitted which does not comply with these terms.

Integrative analysis revealed that distinct cuprotosis patterns reshaped tumor microenvironment and responses to immunotherapy of colorectal cancer

Ximo Xu†, Chengsheng Ding†, Hao Zhong†, Wei Qin†, Duohuo Shu, Mengqin Yu, Naijipu Abuduaini, Sen Zhang*, Xiao Yang* and Bo Feng*

Department of General Surgery, Ruijin Hospital, Shanghai Jiao Tong University School of Medicine, Shanghai, China

Background: Cuprotosis is a novel form of programmed cell death that involves direct targeting of key enzymes in the tricarboxylic acid (TCA) cycle by excess copper and may result in mitochondrial metabolic dysfunction. However, whether cuprotosis may mediate the tumor microenvironment (TME) and immune regulation in colorectal cancer (CRC) remains unclear.

Methods: Ten cuprotosis-related genes were selected and unsupervised consensus clustering was performed to identify the cuprotosis patterns and the correlated TME characteristics. Using principal component analysis, a COPsig score was established to quantify cuprotosis patterns in individual patients. The top 9 most important cuprotosis signature genes were analyzed using single-cell transcriptome data.

Results: Three distinct cuprotosis patterns were identified. The TME cell infiltration characteristics of three patterns were associated with immune-excluded, immune-desert, and immune-inflamed phenotype, respectively. Based on individual cuprotosis patterns, patients were assigned into high and low COPsig score groups. Patients with a higher COPsig score were characterized by longer overall survival time, lower immune cell as well as stromal infiltration, and greater tumor mutational burden. Moreover, further analysis demonstrated that CRC patients with a higher COPsig score were more likely to respond to immune checkpoint inhibitors and 5-fluorouracil chemotherapy. Single-cell transcriptome analysis indicated that cuprotosis signature genes recruited tumor-associated macrophages to TME through the regulation of TCA and the metabolism of glutamine and fatty acid, thus influencing the prognosis of CRC patients.

Conclusion: This study indicated that distinct cuprotosis patterns laid a solid foundation to the explanation of heterogeneity and complexity of individual TME, thus guiding more effective immunotherapy as well as adjuvant chemotherapy strategies.

KEYWORDS

cuprotosis, colorectal cancer, tumor microenvironment, immune checkpoint inhibitor, prognosis

Introduction

Colorectal cancer (CRC) is one of the most prevalent malignancies and remains the leading cause of cancer death worldwide, with more than 30% of patients suffering from recurrence, metastasis, and death within a 5-year treatment (1, 2). Currently, immunotherapy, which makes use of immune checkpoint inhibitors (ICIs), including anti-PD-1/CTLA-4, is popular worldwide, with good results in treating non-small cell lung cancer (3, 4). Moreover, studies have demonstrated that this effective treatment has the potential to achieve a durable response in CRC as well (5, 6). Recently, the concept of tumor microenvironment (TME) has been proposed and widely appreciated as a result of the increasing knowledge of diversity and complexity of tumor components. TME is the environment where the tumor is located and various immune cells, stromal cells, extracellular matrix (ECM) molecules, and cytokines coexist (7–9). As a result of their interaction with the TME components, tumor cells show a variety of changes in biological behavior, such as the stimulation of proliferation and angiogenesis, apoptosis inhibition, and hypoxia avoidance. Emerging evidence indicates that TME appears to play a critical role in tumor progression, immune escape, and response to immunotherapy (10–12). The prediction of ICI response based on the characteristics of TME cell infiltration is a promising way to improve the current ICIs' effect and develop new immunotherapeutic approaches (13–16). Therefore, a comprehensive analysis of different TME patterns may help identify distinct tumor immune phenotypes and further guide and predict the selection of ICIs (16, 17).

Copper is an essential metal ion that is required for many cellular functions, including energy production and antioxidant defense. However, when copper levels become excessive, it can lead to the production of reactive oxygen species (ROS) through Fenton chemistry, which can cause oxidative damage to cellular components. This oxidative stress can activate a number of cell death pathways, including apoptosis, necrosis, and autophagy, ultimately leading to cell death (18). Copper-induced cell death, also named cuprotosis, refers to the direct targeting of copper to the key lapidated enzyme of the tricarboxylic acid (TCA) cycle and thus is responsible for the dysfunction of mitochondrial metabolism (19). A great deal of progress has been made in immunometabolism in recent years, and there is substantial evidence that both the dysfunction of mitochondrial metabolism and ROS are associated with immune response (20–23). Therefore, a comprehensive understanding of whether cuprotosis is associated with TME and the response of ICIs in CRC will help deepen our understanding of it and provide new strategies for immunotherapy.

In this study, the genomic and clinical information of 1,226 CRC samples was synthesized to investigate the copper death patterns, and the correlation between the cuprotosis patterns and their related TME infiltration characteristics. Three distinct cuprotosis patterns were identified by the unsupervised consensus clustering, and we found that the TME cell infiltration characteristics of the three patterns were associated with immune-excluded, immune-desert, and immune-inflamed phenotype, respectively. Then, we established a scoring scheme to quantify the cuprotosis patterns in individual CRC patients and to predict the response to ICIs and adjuvant chemotherapy.

Materials and methods

Source and preprocess of publicly attainable colorectal expression datasets

The publicly attainable NCBI Gene Expression Omnibus (GEO) datasets (https://www.ncbi.nlm.nih.gov/geo/) and the Cancer Genome Atlas (TCGA) (https://cancergenome.nih.gov/) were used to retrospectively collect the gene expression and clinical characteristics of CRC samples. No further evaluation was conducted for samples who had no survival information. A total of 4 eligible CRC cohorts (GSE103479, GSE39582, TCGA-COAD, and TCGA-READ) were enrolled in this study for further analysis. As for the datasets in TCGA, RNA sequencing data of gene expression (FPKM value) were downloaded from the Genomic Data Commons (GDC) using TCGAbiolinks, an R package that was specifically developed to allow integration of GDC data (24). The FPKM values were then converted to transcripts per kilobase million (TPM) values. The "Combat" algorithm of the R package sva was used to correct the batch effect among the different datasets (25). The genomic mutation data [somatic mutation and copy number variation (CNV)] of TCGA-COAD and TCGA-READ were curated from GDC.

Unsupervised consensus clustering for 10 cuprotosis regulation genes

Ten cuprotosis-related genes (CRGs) were extracted from the meta-cohort. Unsupervised clustering analysis was applied to identify different cuprotosis patterns and classify patients for further study based on their expression of 10 CRGs. In a consistent clustering algorithm, cluster number and the stability of each cluster are determined (26). The above steps were implemented following the ConsensusClusterPlus package, and 1,000 times repetitions were conducted to ensure the stability of classification (27).

Functional annotation and gene set variation analysis

Gene set variation analysis (GSVA) enrichment analysis was performed by using the "GSVA" R package, in order to investigate the heterology of the different cuprotosis patterns. As a non-parametric and unsupervised approach to explore the variations in pathway and biological process activity, GSVA is generally employed in estimating the samples of an expression dataset (28). GSVA was performed using gene sets "c2.cp.kegg.v7.5.1.symbols" downloaded from MSigDB, as implemented in the GSVA package (version 1.42.0).

Analysis of TME immune cell infiltration and the immune response predictor

ssGSEA (single sample gene set enrichment analysis) (29), EPIC (30), xCELL (31), and MCPcounter (32) algorithms were performed to quantify the relative abundance of TME immune cell infiltration as well as assess the immune function in the CRC patients. The ESTIMATE (33) algorithm was performed to estimate the immune and stromal cells in CRC. The ESTIMATE algorithm helps us predict the infiltration level of immune cells and stromal cells by calculating the immune and stromal scores. The tumor immune dysfunction and exclusion (TIDE) algorithm, including two major mechanisms of tumor immune escape, T-cell dysfunction and T-cell exclusion, was utilized to evaluate the TME and predict response to treatment with ICIs (34). Higher TIDE scores indicate a lower response rate to ICI treatment as tumor cells tend to induce immune escape.

Identification of differentially expressed genes between distinct cuprotosis patterns

By examining the expression of 10 CRGs, we categorized samples into three different cuprotosis patterns, in order to identify CRGs. With the "limma" R package, we applied the empirical Bayesian algorithm to ascertain differentially expressed genes (DEGs) between distinct cuprotosis patterns (35). To determine the DEGs, an adjusted p-value < 0.05 was employed.

Generation of COPsig sore

A COPsig score system was established to quantify the cuprotosis level of individual CRC patients. First, COP gene signatures A and B corresponded to DEGs that appeared to be positively and negatively correlated with the clusters of COP genes, respectively. Then, the dimensionality of COP gene signature A and B was reduced by performing the Boruta algorithm (36), and principal component 1 was adopted as the feature score by applying the PCA. As a last step, we determined the COPsig score group for each CRC patient using an approach similar to the gene expression grading index (37):

$$\text{COPsig} \cdot \text{score} = \sum PC1_A \cdot \sum PC1_B$$

Cancer cell line data and chemotherapeutic response prediction

On the basis of the Genomics of Drug Sensitivity in Cancer (GDSC, https://www.cancerrxgene.org/), the largest publicly available pharmacogenomic database, we predicted the response to chemotherapy for each CRC sample. Two commonly used chemotherapy drugs, 5-fluorouracil (5-FU) and paclitaxel, were selected. Using the R package "pRRrophic", the estimation of half-maximal inhibitory concentration (IC_{50}) for each sample was determined by ridge regression, and Prediction accuracy is measured by 10-fold cross-validation based on the GDSC training dataset.

The Broad Institute-Cancer Cell Line Encyclopedia (CCLE, https://portals.broadinstitute.org/ccle/data) project compiled expression profile and mutation data of human cancer cell lines (CCLs) (38). From the Cancer Therapeutics Response Portal (CTRP) (39) and PRISM Repurposing dataset (19Q4, https://depmap.org/portal/download/Drugsensitivity), drug sensitivity data for CCLs were obtained. Based on CTRP data, 481 compounds were tested across 835 CCLs, while 1,448 compounds over 482 CCLs were contained in the PRISM dataset. In both datasets, a value for area under the curve (AUC) indicates the level of sensitivity to the treatment, with lower AUC values representing greater sensitivity. According to the suggestion of Yang et al. (40), compounds with NAs in more than 20% of samples and cell lines from hematopoietic and lymphoid tissues were excluded. Next, AUC values were imputed through K nearest neighbor (k-NN) imputation. Finally, for further analysis of CTRP and PRISM, CCLE molecular data were used.

Genomic and clinical data collection for the ICI cohort

Four immunotherapeutic cohorts with gene expression and clinical data were enrolled in our study. Metastatic melanoma received either pembrolizumab or nivolumab (41), non-small cell lung cancer patients were administered either nivolumab or pembrolizumab (42), patients with urothelial cancer received

anti-PD1/PD-L1 therapy (43), and urothelium cancers were treated with atezolizumab, an anti-PD-L1 antibody (IMvigor210 cohort) (17). The gene expression profiles were collated and transformed into TPM format for further analysis.

Single-cell RNA sequencing analysis

GSE132257, which contained single-cell RNA sequencing (scRNA-seq) data of five CRC samples, was downloaded from the GEO database. We first filtered and standardized the scRNA-seq data using the "Seurat" R package. After standardization, the 1,500 genes with the largest variance were reserved for subsequent analysis. PCA was then conducted to reduce dimensionality of data. t-SNE was applied to sort cells into different clusters. The cell annotation of each cluster was conducted by the "SingleR" R package with reference to CellMarker (44). In order to calculate the activity of senescence-related model genes in cells, we utilized the "AUCell" R package to calculate the AUC of each cell with reference to model genes and then mapped the AUC to the corresponding cells. Cells that express more genes from the senescence-related model will exhibit higher AUC values than cells expressing fewer genes. The "NicheNet" R package was utilized to infer the interactions between epithelial cells (tumor cells) and surrounding cells (45). Genes that are expressed in larger than 10% cells of clusters were considered for ligand–receptor interactions. In paired ligand–receptor activity analysis, we extracted top 100 ligands and top 1,000 targets of DEGs of "sender cell" and "affected cell", respectively.

Statistical analysis

All the statistical analyses were generated by R software (version 4.1.2). All statistical p-values were two-sided, and p-value < 0.05 was considered statistically significant. A univariate Cox regression model was utilized to calculate the hazard ratios (HRs) for CRGs and cuprotosis phenotype-related genes. Patients with complete clinical information were included, and a multivariate Cox regression model was established to ascertain the independent prognostic risk factors. The results of multivariate and univariate prognostic analysis were visualized by applying the forest plot R package. Spearman correlation analysis and distance correlation analysis was used to calculate the correlation coefficient. Based on the median COPsig scores, the sample was divided into two groups: the high and low scoring groups. Differences between three or more groups were compared using one-way ANOVA and Kruskal–Wallis tests (46). The waterfall function in the maftools package was employed to display mutations in the TCGA-CRC cohort (47). Using the R package "Rcircos", the CNV landscapes of 10 cuprotosis-regulated genes in human chromosomes were plotted.

Cell line culture and quantitative real-time polymerase chain reaction

The CRC cell lines HT-29, HCT116, RKO, SW480, and SW620 and the normal cell line NCM460 were purchased from the China Center for Type Culture Collection (CCTCC; Shanghai, China) and cultured in RPMI-1640 (Gibco, Grand Island, NY, USA), supplemented with 10% fetal bovine serum and 1% penicillin–streptomycin (Gibco). All cells were incubated at 37°C in humidified air with 5% CO_2. The total RNA of each cell line was extracted by FastPure® Cell/Tissue Total RNA Isolation Kit V2 (Vazyme, China). Then, the NanoDrop 2000 spectrophotometer (Thermo) was used to quantify RNA. After reverse transcription of RNA to cDNA by HiScript® RT SuperMix for qPCR with gDNA wiper (Vazyme, China), we performed quantitative real-time polymerase chain reaction (RT-qPCR) on cDNA using ChamQ Universal SYBR qPCR Master Mix (Vazyme, China). The cycler protocol is as follows: Stage 1: 30 s at 95°C; Stage 2: 40 cycles of 10 s at 95°C and 30 s at 60°C; and Stage 3: 15 s at 95°C, 60 s at 60°C, and 15 s at 95°C. GAPDH was exploited as an internal reference. The mRNA relative expressions of CRGs were calculated by the $2^{-\Delta\Delta Ct}$ method. The primer sequences used for analysis are listed in Table S1.

Tissue microarray and immunohistochemistry

The CRC tissues (n = 80) and matched adjacent normal tissues (n = 80) were collected from the Department of General Surgery, Ruijin Hospital, Shanghai Jiao Tong University School of Medicine. All patients signed written informed consent before the study. The immunohistochemical assay was conducted as previously described (48). Two pathologists, blinded to clinical information, analyzed the relative intensity of specimens using ImageJ software (National Institutes of Health, USA).

Western blotting

Proteins were electrophoresed with 4%–20% SDS-PAGE gels and transferred to polyvinylidene difluoride membranes. The membrane was blocked with 5% BSA for 1 h at room temperature and incubated overnight at 4°C in primary antibody diluent. Then, the membrane was incubated with secondary antibody for 1 h at room temperature. All bands were measured and analyzed by Quantity One software (Bio-Rad, Hercules, CA, USA). The primary antibody was anti-PDHA1 (1 μg/ml, A13687, ABclonal, CHN). The secondary antibodies such as horseradish peroxidase (HRP)-conjugated anti-rabbit (A6154) and anti-mouse (A4416) antibodies were from Sigma-Aldrich.

Results

Landscape of genetic variation of cuprotosis-regulated genes in colorectal cancer

In this study, a total of 10 CRGs were finally identified. We first examined the expression levels of 10 CRGs in pan-cancer. We

found that in the majority of carcinomas, the CRGs were poorly expressed in tumors, except for CDKN2A (Figure 1A). Then, we demonstrated the CNV and somatic mutations of 10 CRGs in CRC. Among the 399 samples, 9.33% underwent genetic alteration of CRGs, principally including missense mutation, frame shift deletions, and nonsense mutation (Figure S1A). It was observed that LIAS showed the highest mutation frequency, followed by LIPT1, while neither FDX1 nor CDKN2A showed any mutation in the CRC samples (Figure 1B). Next, we investigated the CNV frequency mutations of CRGs, and six genes showed a CNV mutation. DLD and PDHB had a wide amplification in copy number. On the contrary, CDKN2A and LIAS were focused on the prevalent CNV deletions (Figure 1C). The location of CNV alterations of 10 CRGs on chromosomes is demonstrated in Figure 1D. Moreover, further analysis was made to investigate the mRNA expression level of CRGs between normal and CRC samples, and we found that the expressions of FDX1, DLD, DLAT, PDHB, and MTF1 were significantly decreased, whereas LIPT1, GLS, and CDKN2A were significantly upregulated in tumor samples (Figure 1E). The expression level of CRGs with CNV amplification was higher in CRC samples compared to normal samples (e.g., GLS and PDHA1), while the expression level of LIAS was relatively decreased in tumor samples (Figures 1D, E). In addition, Spearman correlation analysis was performed to evaluate the mutual regulation between the CRGs (Figure S1B). CDKN2A showed a significantly negative correlation with most other CRGs. The univariate and multivariate Cox model were established to ascertain whether CRGs were independent risk factors for prognosis in CRC patients. The forest plots showed that CDKN2A and GLS could be considered as a risk factor for CRC patients and correlated with a markedly shorter overall survival (Figure S1C,D). Thus, in the above analyses, we observed a very heterogeneous landscape of genetic and expressional changes in CRGs between normal and CRC samples. Accordingly, the imbalance in CRG expression was crucial to the occurrence and progression of CRC.

Cuprotosis patterns mediated by 10 CRGs

Four datasets (GSE103479, GSE39582, TCGA-COAD, and TCGA-READ cohort) with available survival information and clinical annotations were merged in one meta-cohort. The CRG network revealed a landscape of CRG interactions, gene connection, and their prognosis significance for CRC patients (Figure 2A). The illustration indicated that the cross-talk among the CRGs probably plays a pivotal role in different cuprotosis patterns and was involved in CRC development and progression. Based on the above hypothesis, we stratified the samples with quantitatively distinct cuprotosis patterns according to the expression levels of 10 CRGs utilizing the R package of ConsensusClusterPlus. Three different cuprotosis patterns were eventually identified using unsupervised clustering, including 406 cases in COPcluster C1, 206 cases in COPcluster C2, and 614 cases in COPcluster C3 (Figures 2B, C). Then, we performed a prognosis analysis for the three main cuprotosis clusters; the results demonstrated that COPcluster C3 showed a prominent survival advantage, while COPcluster C2 was the least likely to survive in the meta-cohort (Figure 2D). Moreover, the unsupervised clustering discovered three totally different patterns of cuprotosis in the meta-cohort (Figures 2E, F). There was significant distinction in the CRG transcriptional profile among the three different cuprotosis patterns (Figure 2F).

The cuprotosis patterns characterized by distinct immune landscape

In order to investigate the molecular mechanisms among the three different cuprotosis patterns, GSVA enrichment analysis was performed on the KEGG gene set. We found that all the three clusters were markedly enriched in the immune signaling pathway, including the T-cell receptor signaling pathway, the B-cell receptor signaling pathway, and the Toll-like receptor signaling pathway. However, COPcluster C1 and COPcluster C2 were simultaneously enriched in stromal elements such as ECM–receptor interaction and cell adhesion molecules cams (Figures 3A, B). To clarify and compare the 23 immune infiltration cell subpopulations of each cluster, we then constructed a boxplot with ssGSEA. To our surprise, subpopulation analysis of TME cell infiltration indicated that the vast majority of immune cells, such as active $CD4^+$ cells, eosinophils, and activated B cells, were enriched in COPcluster C1 and C3, with the least enrichment in COPcluster C2 (Figure 3C). Nevertheless, patients in COPcluster C3 and C2 had a longer median overall survival, while those in COPcluster C2 did not show a matching prognosis advantage (Figure 2D). In addition, the ESTIMATE algorithm was used to evaluate the immune cell infiltration level (Immune Score) and stromal cell infiltration level (Stromal Score) across three different cuprotosis patterns. Further analysis revealed that COPcluster C3 exhibited the lowest immune score, followed by C2 and C1 (Figure S1E). Meanwhile, COPcluster C1 and C2 had a much higher stromal score than COPcluster C3 (Figure S1F). According to previous studies, immune-excluded tumor phenotype exhibited an abundance of immune cells. Rather than penetrating tumor parenchyma, these immune cells remained in the stroma surrounding tumor cell nests (49). Thus, we hypothesized that the abundant stromal component in COPcluster C1 and C2 inhibited potential antitumor immune response. Subsequent TME analysis demonstrated that stromal activation was significantly enhanced in COPcluster C1 and C2, including the activity of epithelial–mesenchymal transition (EMT), transforming growth factor beta (TGF-β). Moreover, previous studies proposed a novel concept, TMEscore (TMEscore A – TMEscore B), representing the signature of tumor immune microenvironment (17). In our study, we found a relatively lower TMEscore B as well as a markedly higher TMEscore in COPcluster C3 (Figure 3D). As a result of the above findings, we confirmed that the three cuprotosis patterns developed significantly different characterizations of TME cell infiltration. COPcluster C1 was considered as an immune-excluded phenotype, characterized by diminished immune cell infiltration and stromal activation. COPcluster C2 was classified as immune-desert phenotype, characterized by immunosuppression, while COPcluster C3 was

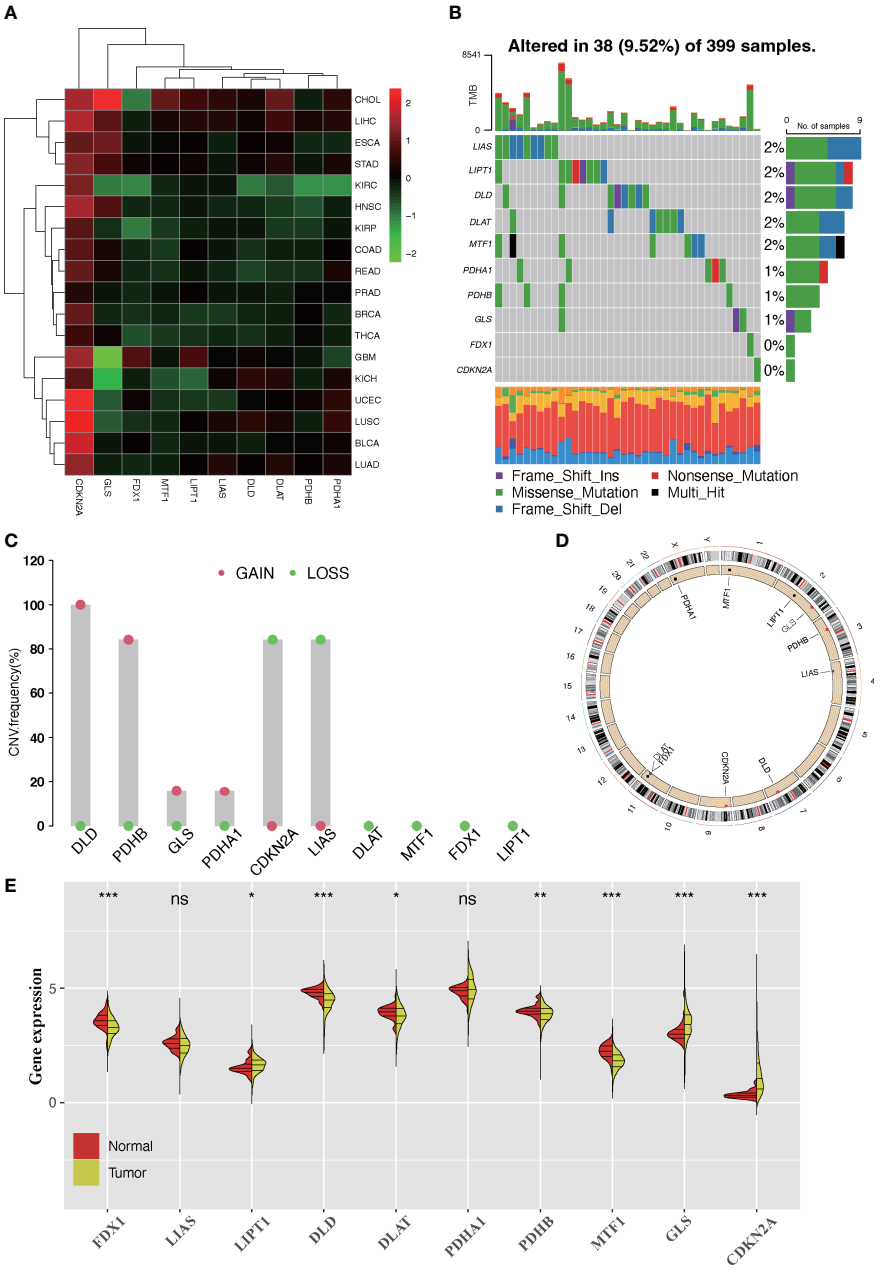

FIGURE 1
Landscape of expression and genetic alteration of cuprotosis-related genes (CRGs) in colorectal cancer. **(A)** The fold changes of the expression level alterations of CRGs in 18 cancer types, with red representing upregulated genes and green representing downregulated genes in the heatmap. **(B)** Thirty-eight of the 399 CRC patients developed genetic mutation of 10 CRGs. Each column represented an individual patient. The upper barplot showed the tumor mutational burden. The right barplot showed the frequency of each variant type. **(C)** The CNV frequency mutations of 10 CRGs. Alteration frequency was represented by the column height. Green dots represented the deletion frequency. Red dots represented the amplification frequency. **(D)** The location of CNV alteration of 10 CRGs on chromosomes. **(E)** The difference of mRNA expression level of 10 CRGs between normal and tumor CRC samples (TCGA-COAD and TCGA-READ). The asterisks represent the statistical *p*-value (ns: $p > 0.05$; *$p < 0.05$; **$p < 0.01$; ***$p < 0.001$).

considered as an immune-infiltrated phenotype, marked by immune cell infiltration and immune activation.

We then further explored the specific correlations between CRGs and TME immune cell infiltration by Spearman's correlation analysis (Figure S2A). We found that high expression of CDKN2A and MTF1 was associated with abundant immune cell infiltration, whereas PDHA1, LIPT1, LIAS, GLS, FDX1, and DLAT expression exhibited a negative correlation with the immunocyte infiltration. Among these CRGs, the relatively high level of negative correlation between PDHA1 and immune cell infiltration attracted our attention. Based on the PDHA1 expression level, the CRC samples were assigned into high- and low-expression groups according to the best cutoff of 6.68376. There was significant prognostic difference between the two groups of patients (Figure S2B). The results of GSVA indicated that patients with a low PDHA1 level were more likely to be associated with enrichment of immune-related signaling pathway such as

10.3389/fimmu.2023.1165101

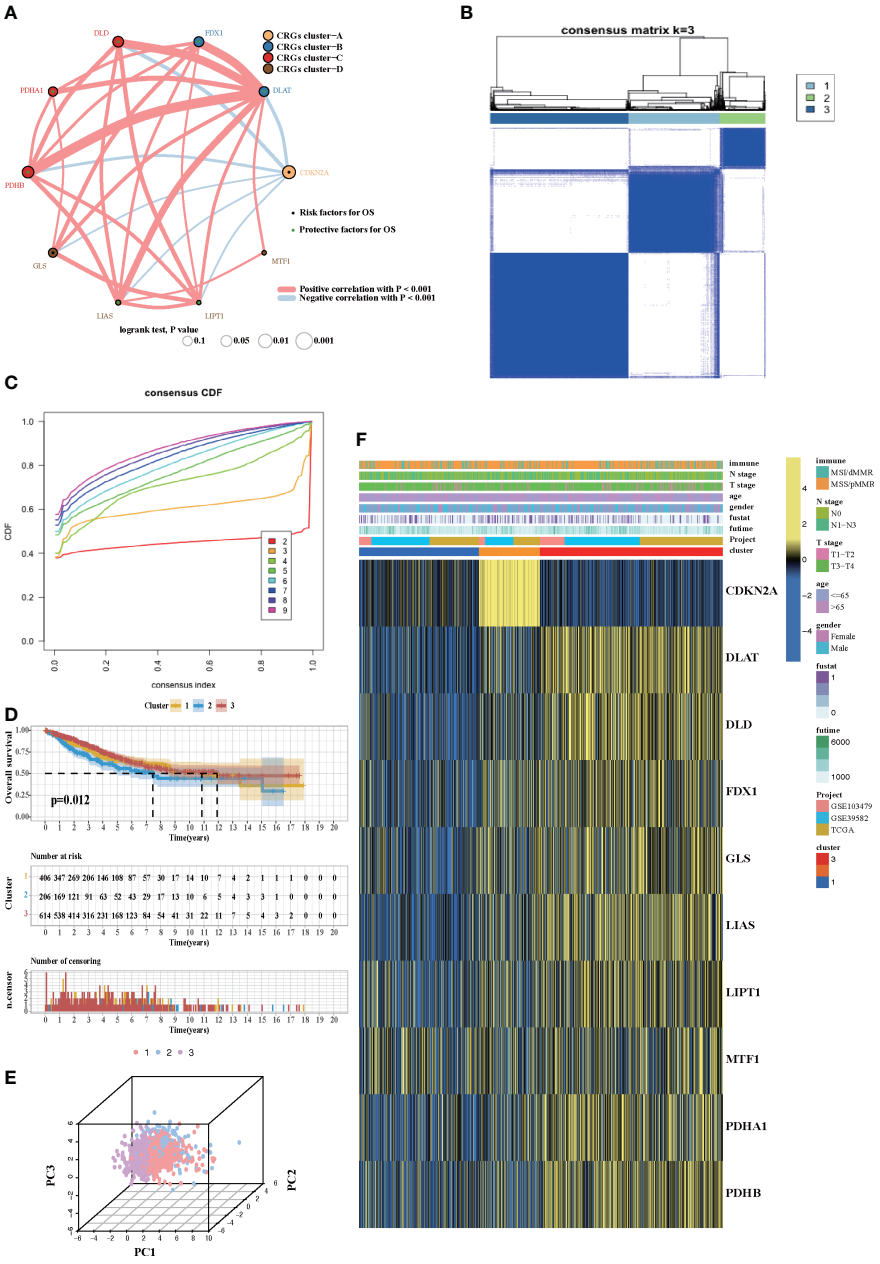

FIGURE 2
Cuprotosis patterns in CRC patients. **(A)** The network between 10 CRGs in CRC patients. The size of the circle corresponded to the effect of each gene on the patients' prognosis, and the range of values was scaled by log-rank test. Protective factor for patients' OS was illustrated by a green dot, and risk factors was illustrated by a black dot. The lines showed the interaction of each gene, and the thickness represented the correlation strength. Blue lines indicated negative correlation, and red lines indicated positive correlation. The CRG cluster A–D was marked with yellow, blue, red, and brown, respectively. **(B)** Unsupervised consensus clustering for 10 CRGs in the meta-cohort and the consensus matrices for k = 3. **(C)** Consensus values range from 0 to 1. **(D)** Kaplan–Meier curves for the three cuprotosis patterns based on 1,226 CRC patients from the meta-cohort, including 406 samples in COPcluster C1, 206 samples in COPcluster C2, and 614 samples in COPcluster C3 (log-rank test). The COPcluster C3 showed a significantly better prognosis than the other two COPclusters. **(E)** The transcriptome profiles of three cuprotosis patterns were analyzed by principal component analysis, revealing a striking difference in transcriptome profiles between different patterns. **(F)** Expression heatmap of three COPclusters of 10 CRGs in the meta-cohort. Immune subtype, age, gender, N stage, T stage, and prognosis were annotated. Yellow represents a high expression of CRGs, and blue represents a low expression.

natural killer cell, Toll-like receptor, and B cell response signaling pathways (Figure S2C). ESTIMATE algorithm was then used to quantify the overall immune cell infiltration between low and high PDHA1 samples. The results demonstrated that low expression of PDHA1 exhibited higher immune scores, which meant that the tumors with low PDHA1 expression were surrounded by more immunocyte components, thus confirming our above findings (Figure S2D). Additionally, we discovered that tumors with low expression levels of PDHA1 had significantly higher infiltration of 23 TME immune cells (Figure S2E). Furthermore, considering that

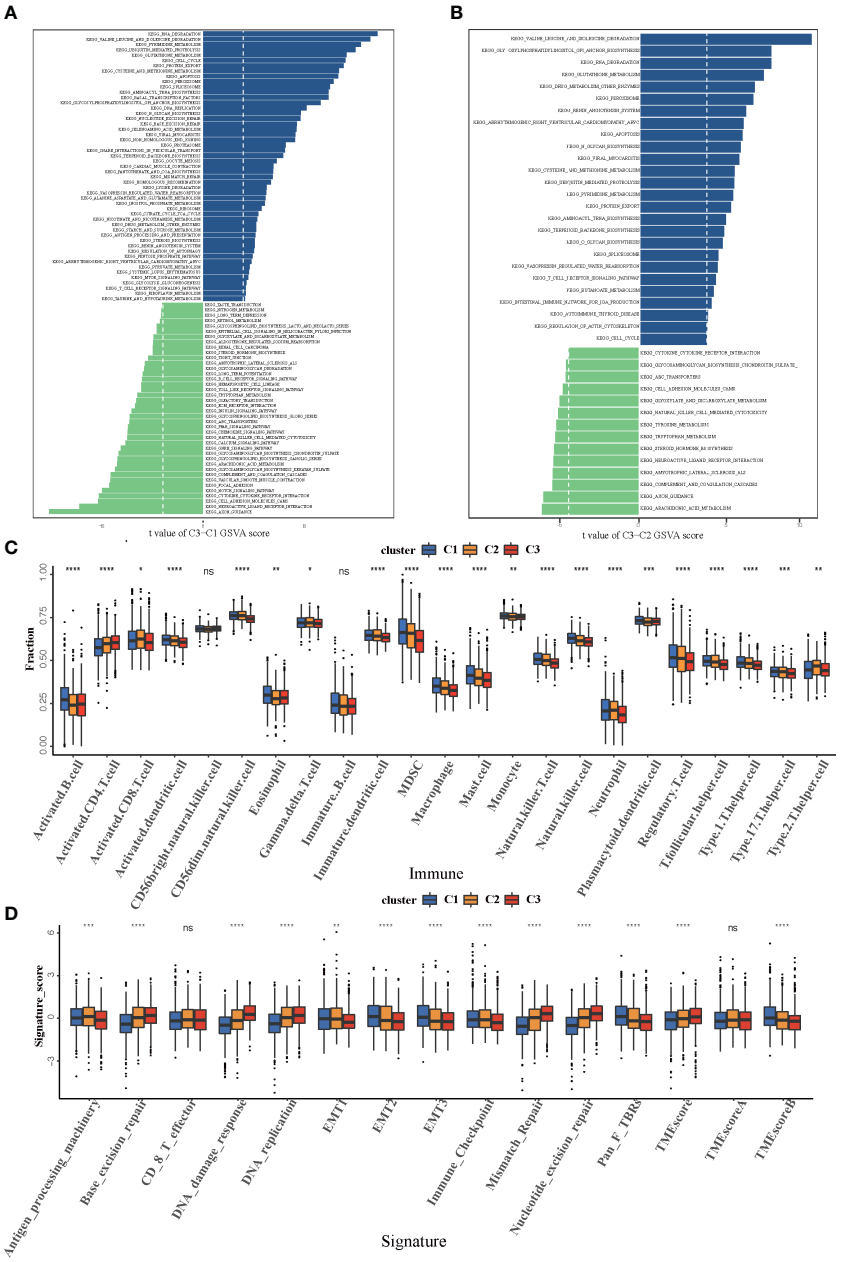

FIGURE 3
Biological and TME infiltration characteristics of each cuprotosis pattern. **(A, B)** Barplot depicting the GSVA score of representative KEGG pathways curated from MSigDB in three cuprotosis patterns. **(A)** COPcluster C3 *vs*. COPcluster C1. **(B)** COPcluster C3 *vs*. COPcluster C2. **(C)** The fraction of TME cell infiltration of three cuprotosis patterns using the ssGSEA algorithm. The top end, median line, and bottom end of the box represent the 25%, 50%, and 75% value, respectively. The black dots show outliers. The asterisks illustrate the statistical *p*-value (*$p < 0.05$, **$p < 0.01$, ***$p < 0.001$, ****$p < 0.0001$, ns $p > 0.05$). **(D)** The fraction of different signatures (immune-relevant signature, mismatch-relevant signature, and stromal-relevant signature) and TMEscore. The line in the box represents the median value. The bottom and top of the boxes are the 25th and 75th percentiles (interquartile range). The whiskers encompass 1.5 times the interquartile range. The asterisks illustrate the statistical *p*-value (*$p < 0.05$, **$p < 0.01$, ***$p < 0.001$, ****$p < 0.0001$, ns $p > 0.05$).

PD-L1 and CTLA-4 are well-proven biomarkers for predicting the response of anti-PD-1/PD-L1 and anti-CTLA-4 treatment, we compared the expression levels of CD274 (known as PD-L1) and CTLA-4 between the different PDHA1 expression subtypes. It is not surprising that CD274 and CTLA-4 expression were significantly upregulated while the expression of PDHA1 was low (Figures S2F, G). Taken together, we could speculate that the PDHA1-mediated cuprotosis process might promote tumor TME immune cell infiltration, thus enhancing the intratumoral antitumor immune response. Furthermore, PDHA1 might mediate the regulation of PD-L1 and CTLA-4, thereby influencing the sensitivity of patients to immunotherapy.

Cuprotosis phenotype-related DEGs in colorectal cancer

Although samples were classified into three different cuprotosis patterns, the potential genetic alterations and expression disturbances in these phenotypes remained unclear. Based on these queries, we further investigated the underlying cuprotosis-related transcriptional expression change across three cuprotosis patterns in CRC. For each of the three cuprotosis patterns, the Limma package was applied to identify overlapping DEGs. A total of 1,727 DEGs representing the crucial distinct indices of the three cuprotosis patterns were selected and illustrated in the Venn diagram (Figure 4A). Afterwards, in order to screen for DEGs associated with patients' prognosis, a univariate Cox analysis was performed, which resulted in 375 genes. To further validate the biological process of CRGs, we subsequently performed an unsupervised clustering analysis based on the selected 375 CRGs to classify the samples into different genomic subtypes. The stratifications assigned samples into three subgroups consistent with the clustering grouping of cuprotosis patterns, and we named the three distinct subgroups COP gene clusters A–C (Figures 4B-D). The results demonstrated that three different cuprotosis patterns did exist in CRC. We found that patients with relatively advanced T stage and N stage were probably represented by COP gene cluster C, while patients with MSI/dMMR were more likely to be characterized by COP gene clusters A and B (Figure 4D). Among 1,226 colorectal patients, 556 were found to be clustered in the COP gene cluster A, which was linked to a better prognosis. While a worse survival outcome was observed for patients in gene cluster C, an intermediate prognosis was observed in gene cluster, with a total of 462 patients aggregated (Figure 4E). The expression level of the 10 CRGs among the three gene clusters was compared and is shown in Figure 4F. We observed significant differences in CRG expression between the three gene clusters, which was also in accordance with the expected results of cuprotosis patterns.

Construction of COPsig score and exploration of its clinical relevance

Despite our findings indicating that cuprotosis patterns were involved in prognosis and immune infiltration, these analyses are based only on patient populations and cannot accurately predict the signatures of cuprotosis in individual tumors. We thus formulated a scoring scheme known as the COPsig score, which hinged on the identified cuprotosis-related signature genes, to classify the patterns of cuprotosis in individual colorectal patient. Due to the complexity of cuprotosis quantification, an alluvial diagram could be used to illustrate the workflow of COPsig score construction (Figure 4G). Meanwhile, we calculated the COPsig score in the ICI cohort in the same manner, to confirm our results. Kruskal–Wallis test revealed a prominent difference between COPsig score and COP gene clusters. Gene cluster B showed a higher median COPsig score, indicating that high COPsig scores were likely to be associated with immune activation-related signatures, whereas gene clusters A and C illustrated a relatively lower median COPsig score (Figures 4H, I). In particular, COPcluster C3 had a significantly higher COPsig score compared to other clusters and COPcluster C1 presented the lowest COPsig score (Figure 5A). We then ought to ascertain the prognostic capacity of the COPsig score to predict oncological outcomes by assigning patients into high or low scoring groups with a cutoff of 0.658 (see *Materials and Methods*). As anticipated, patients with a high COPsig score were markedly related to a better prognosis (Figure 5B). As an additional step in validating the COPsig score, we used the three CRC cohorts mentioned above to determine the relationship between the COPsig score and patient prognosis (GSE103479, GSE39582, and TCGA-CRC). In a similar manner to the results above, high COPsig scores were significantly correlated with better survival outcomes (Figures S3A–C). Based on the univariate and multivariate Cox regression model analysis considering patient age, gender, T stage, N stage, and COPsig score, COPsig score was found to serve as a reliable and independent protective factor for assessing patient survival outcomes (Figures S3D, S4E). According to the analysis of the relevant components of TME, a significant association was revealed between low COPsig score and stromal-related pathways in both the meta-cohort and the ICI cohort (Figures 5C, D). To better characterize the cuprotosis signature, we also examined the correlation between the signatures and COPsig scores. According to the heatmap of correlation matrix, COPsig score was negatively correlated with immune activation process, EMT, and stromal-related features, but was positively correlated with DNA repair signatures in both the meta-cohort and the ICI cohort (Figure 5E). Moreover, the ESTIMATE algorithm was used to further examine the immune characteristics of high and low COPsig scores. We could find that in both the meta-cohort and the ICI cohort, low COPsig scores were strongly associated with high immune scores and stromal scores (Figures S4A–D). Next, we performed xCell, MCPcounter, single-sample gene set enrichment analysis (ssGSEA), and EPIC algorithm, in order to illustrate the immune landscape of high and low COPsig scores. As shown in Figure S4E, F, abundant immune cell infiltration could be found in the low COPsig score group, and the level of immune infiltration was negatively correlated with the COPsig scores. In light of the above findings, low COPsig scores were significantly associated with immune activation and stromal activation. The COPsig score could be used to distinguish individual colorectal tumors' patterns of cuprotosis and further characterize the TME immune cell infiltration. In addition, high COPsig scores were strongly correlated with better survival outcomes, creating an accurate predictor of CRC patient prognosis.

Then, using the Maftools package, the distribution differences of somatic mutation between high and low COPsig scores in the TCGA-CRC cohort were analyzed. The high COPsig score group had a greater tumor mutation burden than the low COPsig score group. Mutational landscapes revealed that APC (81% *vs.* 62%) and tp53 (58% *vs.* 45%) were more susceptible to somatic mutations in the high COPsig score group (chi-square test, $p < 0.05$, Figures S3F, G). The TMB quantification analysis supported the hypothesis that high COPsig score tumors correlated markedly with a higher TMB

10.3389/fimmu.2023.1165101

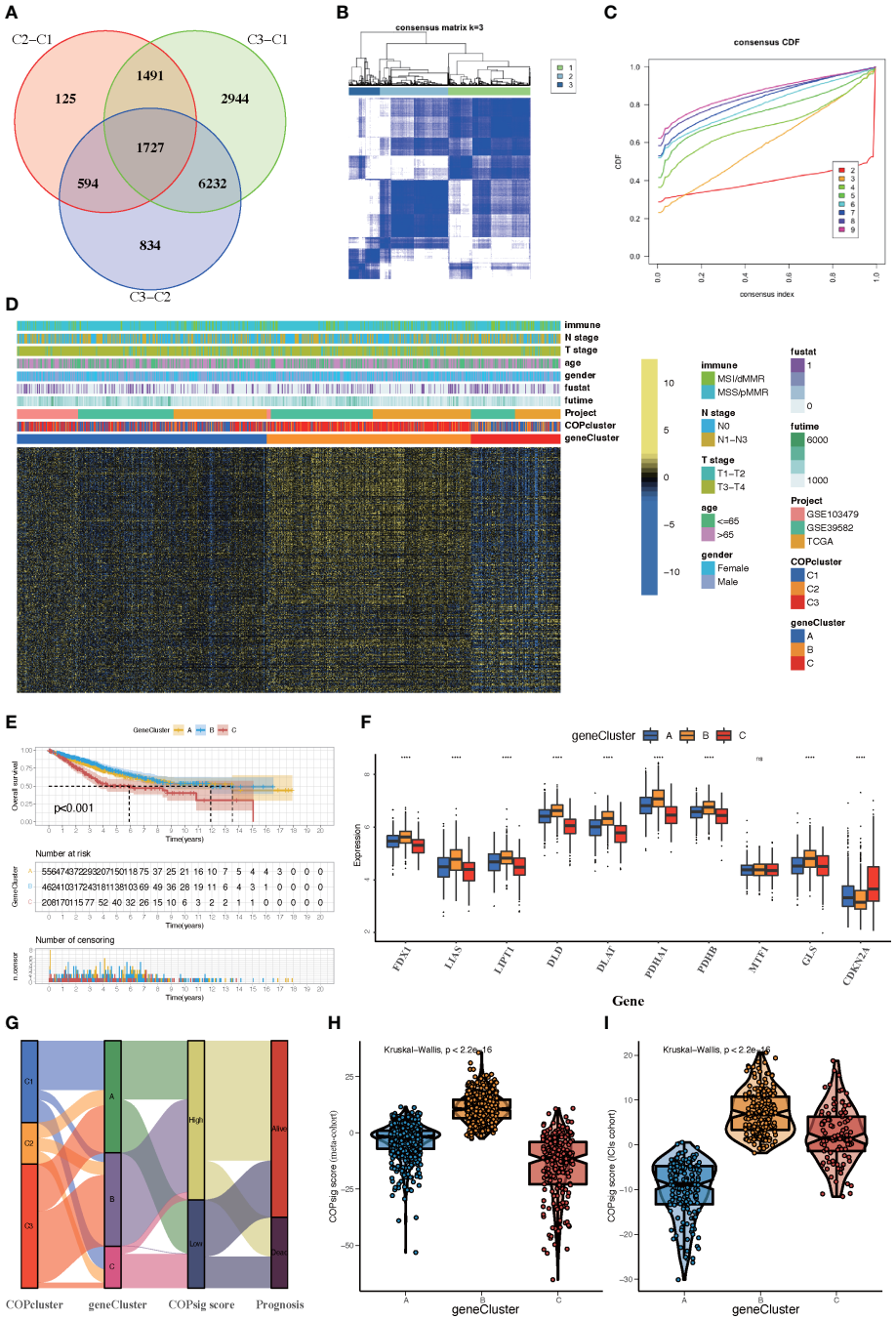

FIGURE 4
Construction of COP gene clusters and COPsig score. **(A)** A total of 1,727 cuprotosis-related differentially expressed genes (DEGs) between three cuprotosis patterns were illustrated in the Venn diagram. **(B)** Unsupervised consensus clustering for 375 prognosis-related DEGs in the meta-cohort and the consensus matrices for $k = 3$. **(C)** Consensus values range from 0 to 1. **(D)** Expression heatmap of three COP gene clusters of 375 DEGs. Immune subtype, COPcluster, age, gender, N stage, T stage, and prognosis were annotated. Yellow represents a high expression of DEGs, and blue represents a low expression. **(E)** Kaplan–Meier curves for the three COP gene clusters, including 556 samples in gene cluster A, 462 samples in gene cluster B, and 208 samples in gene cluster C (log-rank test). Gene cluster A showed a significantly better prognosis than the other two gene clusters. **(F)** The expression level of 10 CRGs in three gene clusters. The line in the box represents the median value. The bottom and top of the boxes are the 25th and 75th percentiles (interquartile range). The whiskers encompass 1.5 times the interquartile range. The asterisks illustrate the statistical *p*-value (*$p < 0.05$, **$p < 0.01$, ***$p < 0.001$, ****$p < 0.0001$, ns $p > 0.05$). **(G)** Alluvial diagram showing the changes in COPclusters, gene clusters, COPsig score, and patients' prognosis. **(H, I)** Differences in COPsig score among three COP gene clusters in the meta-cohort **(H)** and the ICI cohort **(I)**. The Kruskal–Wallis test was used to compare the statistical difference between three gene clusters ($p < 0.001$).

10.3389/fimmu.2023.1165101

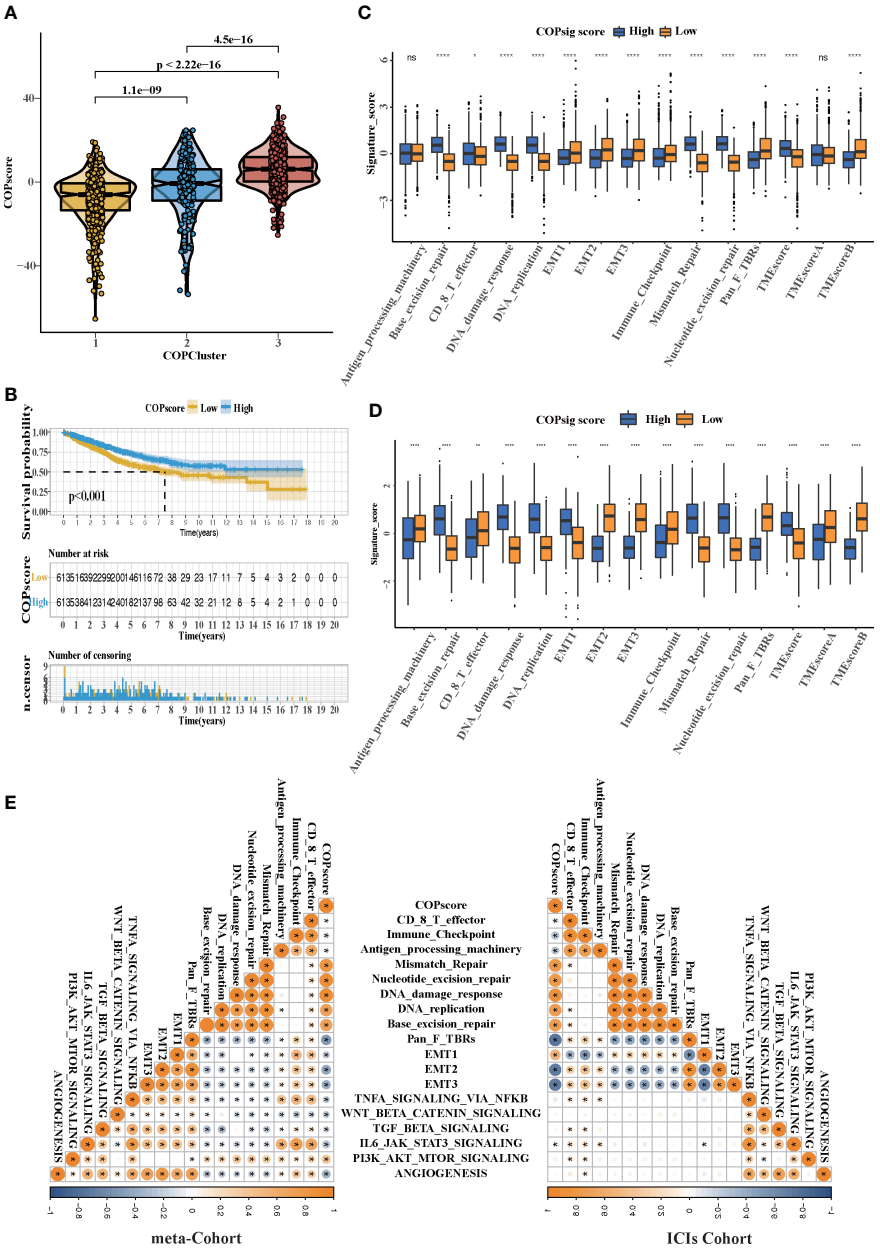

FIGURE 5
The TME cell infiltration characteristics in the high and low COPsig score groups. **(A)** Differences in COPsig score among three COPclusters in the meta-cohort. The Kruskal–Wallis test was used to compare the statistical difference between three gene clusters ($p < 0.001$). **(B)** Kaplan–Meier curves for the two COPsig score groups, including 789 samples in the high COPsig score group, and 437 samples in the low COPsig score group (log-rank test). The high COPsig score group showed a significant better prognosis. **(C)** The fraction of TME cell infiltration of the high and low COPsig score groups using the ssGSEA algorithm. The top end, median line, and bottom end of the box represent the 25%, 50%, and 75% values, respectively. The black dots show outliers. The asterisks illustrate the statistical p-value (*$p < 0.05$, **$p < 0.01$, ***$p < 0.001$, ****$p < 0.0001$, ns $p > 0.05$). **(D)** The fraction of different signatures (immune-relevant signature, mismatch-relevant signature, and stromal-relevant signature) and TMEscore. The line in the box represents the median value. The bottom and top of the boxes are the 25th and 75th percentiles (interquartile range). The whiskers encompass 1.5 times the interquartile range. The asterisks illustrate the statistical p-value (*$p < 0.05$, **$p < 0.01$, ***$p < 0.001$, ****$p < 0.0001$, ns $p > 0.05$). **(E)** Correlations between COPsig score and the known biological gene signatures in the meta-cohort and the ICI cohort using Spearman analysis. Negative correlation was marked with blue and positive correlation was marked with orange.

(Figure S3H). Increasing evidence indicated that patients with high TMB status appear to respond to immunotherapy with durable clinical effects. In summary, the above results inferred that the differences in tumor cuprotosis patterns might act as a critical factor mediating clinical responses to immunotherapy. The COPsig scores were found to be able to indirectly predict immunotherapy, as well.

Implications of COPsig scores in the prediction of immune response and drug sensitivity

There is no doubt that anti-CTLA-4/PD-1 therapy has made a significant breakthrough in antitumor therapy. TIDE, a newly

identified immune response predictor, is widely used and is strongly recommended in addition to some of the well-known TMB, PD-L1, and MSI measures (50, 51) According to our analysis, both in the meta-cohort and the ICI cohort, the TIDE value significantly declined in the high COPsig group ($p < 0.01$ in the meta-cohort, $p < 0.001$ in the ICI cohort, Figures 6A, B). It appeared from these findings that the expression of tumor-specific cuprotosis patterns played a critical role in regulating immune responses. As COPsig score offered a robust correlation with immune response, we next investigated whether COPsig score could predict patient response to ICI therapy in four immunotherapy cohorts. We found that in the ICI cohort, patients were assigned into two groups (Figures 6C, D). Patients with a high COPsig score were proven to have significant benefit and immune response to ICI treatment (response rate: 30% *vs.* 18%, Figure 6E). Figure 6F also illustrates that patients who received CR/PR tended to have a higher COPsig score ($p = 0.0012$).

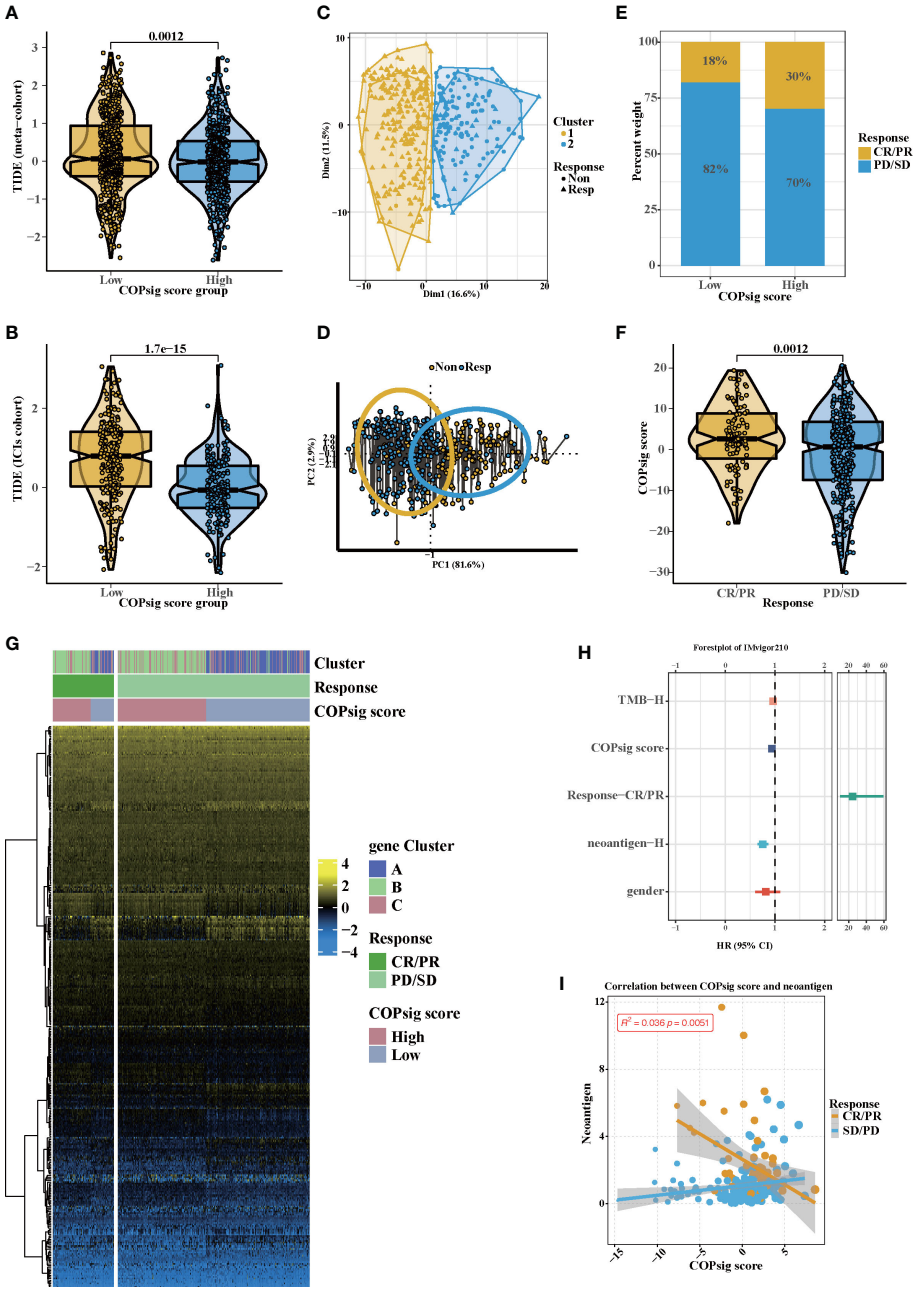

FIGURE 6
Potential immunotherapy in high and low COPsig score group. (A, B) The relative distribution of TIDE was compared between COPsig score high vs. low groups in meta-cohort **(A)** and ICIs cohort **(B)**, respectively. **(C, D)** Principal component analysis of the ICIs cohort and the response to ICIs. **(E, F)** The fraction of patients with immunotherapy response (ICIs cohort) in low and high COPsig score groups **(E)**. The COPsig score of CR/PR and PD/SD patients in ICIs cohort **(F)**. **(G)** Expression heatmap in meta-cohort. Gene clusters, response, COPsig score, were annotated. Yellow represented a high expression, and blue represented a low expression. **(H)** Univariate cox regression model estimating clinical prognosis significance between TMB, COPsig score, response, neoantigen and gender. **(I)** correlation between COPsig score and neoantigen in CR/PR. Yellow represented CR/PR patients, blue represented SD/PD patients.

A heatmap illustrated the gene expression difference between the high and low COPsig score groups, which might be correlated with the response of ICIs (Figure 6G). Then, we established a univariate Cox model to predict whether COPsig score was an impact factor for patient prognosis (Figure 6H). The results showed that COPsig score, neoantigen, TMB, and gender were protective factors, while response to ICIs was a risk factor for patients' long-term survival. Moreover, for patients who benefited from ICIs, COPsig score was significantly negatively correlated with neoantigen expression, while COPsig score was positively correlated with neoantigen expression in the PD/SD group, which confirmed the above results (Figure 6I).

Since chemotherapy is the most common form of treatment for CRC, we assessed the effect of two chemo drugs: 5-FU and paclitaxel. The ridge regression model was then trained by ridge regression on the GDSC cell line dataset and proven accurate by 10-fold cross-validation. Based on our predictive models of these two drugs, we estimated the IC_{50} for each sample in the meta-cohort. There was a significant difference between low and high COPsig scores for the two chemo drugs, with the high COPsig score group being more sensitive to commonly administered chemotherapy ($p < 0.001$ for 5-FU and paclitaxel, Figures 7A, B). Furthermore, the correlation analysis demonstrated that the IC_{50} values of both drugs were markedly negatively correlated with the COPsig score as well (Figures 7C, D).

Then, a drug response prediction model was built using the CTRP and PRISM datasets that contain gene expression profiles and drug sensitivity profiles for hundreds of CCLs. Compounds with NAs in more than 20% of samples and cell lines from hematopoietic and lymphoid tissues were excluded. Moreover, NAs were filled using the k-NN algorithm. Ultimately, the analysis was then carried out using 680 CCLs (containing 354 compounds) from the CTRP dataset and 480 CCLs (containing 1,285 compounds) from the PRISM dataset, respectively. Afterwards, in order to predict the response for each compound in each sample, the pRRophetic package with the ridge-regression model was utilized to obtain an estimated AUC value based on the expression profile. Next, the correlation between AUC values and COPsig scores was analyzed using Spearman correlation analysis, and we select the compounds with the top five and the bottom five Spearman's r value in CTRP and PRISM datasets, respectively (Figures 7E, F). We found that 5-FU showed a higher drug sensitivity in high COPsig score patients, which further confirmed the above results. In general, our results strongly indicated that the COPsig score had a direct link with the response to immunotherapy and chemotherapy.

Cuprotosis signature genes in single-cell transcriptomic data

Random forest algorithm was utilized to screen out the top nine important genes among the cuprotosis signature genes for further analysis (Figure 8A). After rigorous data normalization and filtering, 6,490 cells were retained for further analysis. In the following step, we used graph-based clustering to separate the cells into 12 clusters after normalizing them using principal component analysis (Figure S5A). These clusters can be assigned to cell lines by marker genes or DEGs (Figures 8B, S5B). According to the AUC values, two peaks of all cells were observed, whereas 3,918 cells had relatively higher AUC values (Figures 8C, S4C). The stacking map showed that there were more macrophages in the AUC_low group, which were consistent with our results of bulk RNA-seq analysis (Figure 8D). Moreover, GSVA indicated that cell adhesion pathways and immune-related pathways were enriched in the AUC_high group, which further confirmed the results of bulk RNA-seq analysis (Figure S5D). We next used CellChat and NicheNet to identify the expression of ligands at different cell interfaces and thus predict the cross-talk of the top 15 active ligand and relative receptors (Figures 8E, F). The results indicated that TNFSF12 interacted with TNFRSF12A on macrophage cells and thus potentially targeted ID2, IER2, and SDC4. In addition, interactions related to cell adhesion such as MDK–SDC4 and cytokine interactions such as CXCL2–CXCR4 were observed (Figure S5E). Previous studies have confirmed that cytokines such as CXCL2 and CXCR4 can recruit macrophages (52–54). Therefore, we hypothesized that cuprotosis signature genes might affect TME through the recruitment of macrophages, thereby influencing the prognosis of colorectal patients and the response to immunotherapy. Since cuprotosis influences the TCA cycle, we then explored the difference in metabolism pathways between AUC_high and AUC_low groups. As illustrated, TCA-associated genes observed a preference correlated with the AUC_low group, and enriched TCA pathway, glycolysis pathway, and oxidative phosphorylation pathway could be found in the AUC_low group (Figures 8G, S5F, G). Taken together, our findings indicate that cuprotosis signature might recruit macrophages and thus developed interaction networks with surrounding cells, which potentially induced cellular senescence and promoted the remodeling of the TME.

PDHA1 was downregulated in CRC and associated with worse prognosis

Since cuprotosis patterns might influence the prognosis of CRC patients, RT-PCR was performed to examine the relative expression of CRGs in CRC cell lines and the normal cell line (Figures 9A-J). Similar to our previous results, the mRNA expressions of CDKN2A, GLS, and LIPT1 were upregulated in CRC, whereas the expressions of other CRGs were downregulated. As a crucial gene in the glucose metabolism reprogram of tumor cells, there is growing evidence that PDHA1 might act as a prognostic and immune-related biomarker and negatively associated with immune cell infiltration in TME (55). Western blotting confirmed that PDHA1 expression in normal colon cells was higher than that in CRC cells (Figure 9K). In order to confirm the relationship between PDHA1 and prognosis of CRC patients, we enrolled 80 CRC patients from our center. The expression level of PDHA1 was examined by immunohistochemistry. Compared with normal tissues, the expression level of PDHA1 in tumor tissues was significantly lower (Figure 9L, $p < 0.001$). The tumor

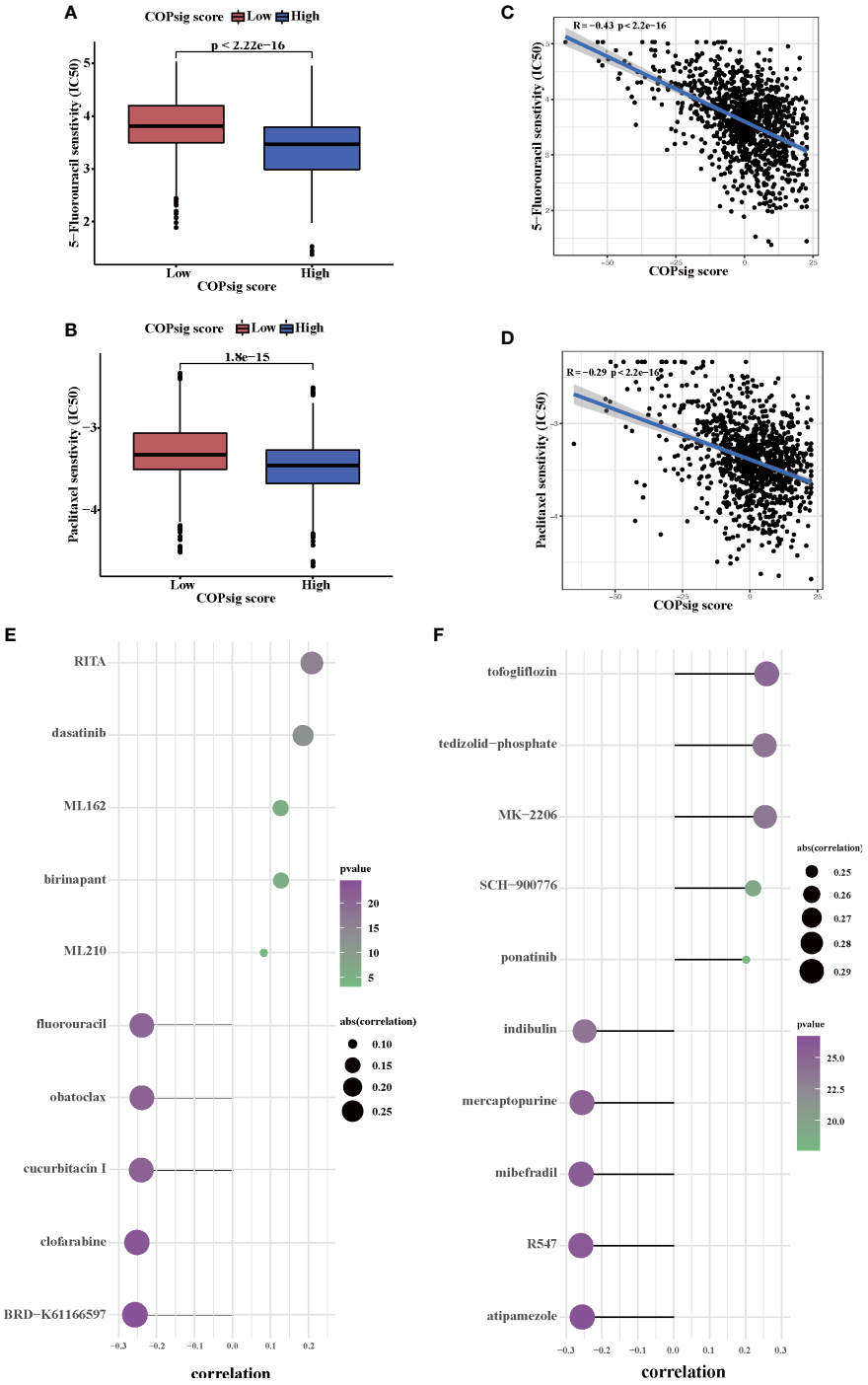

FIGURE 7
Chemotherapy response in the high and low COPsig score groups. **(A, B)** The differences of response to 5-FU **(E)** and paclitaxel **(F)** between the high and low COPsig score groups. **(C, D)** The correlation between COPsig scores of patients and the estimated IC_{50} value of 5-FU **(C)** and paclitaxel **(D)**. **(E)** The results of Spearman's correlation analysis of 10 CTRP-derived compounds. **(F)** The results of Spearman's correlation analysis of 10 PRISM-derived compounds.

samples were then divided into PDHA1-high (n = 15) and PDHA1-low (n = 65) groups according to the relative intensity. Kaplan–Meier analysis indicated that CRC patients in the PDHA1-low group had a lower disease-free survival rate (Figure 9M). Our findings further validated the results of Bulk-RNAseq analysis and demonstrated that PDHA1 was a potential prognostic biomarker for CRC patients.

Discussion

Copper-induced cell death, also named cuprotosis, is a novel discovered type of programmed cell death, which refers to the direct binding of copper to the lipoylated proteins of the TCA cycle, further inducing mitochondrial dysfunction and ROS accumulation

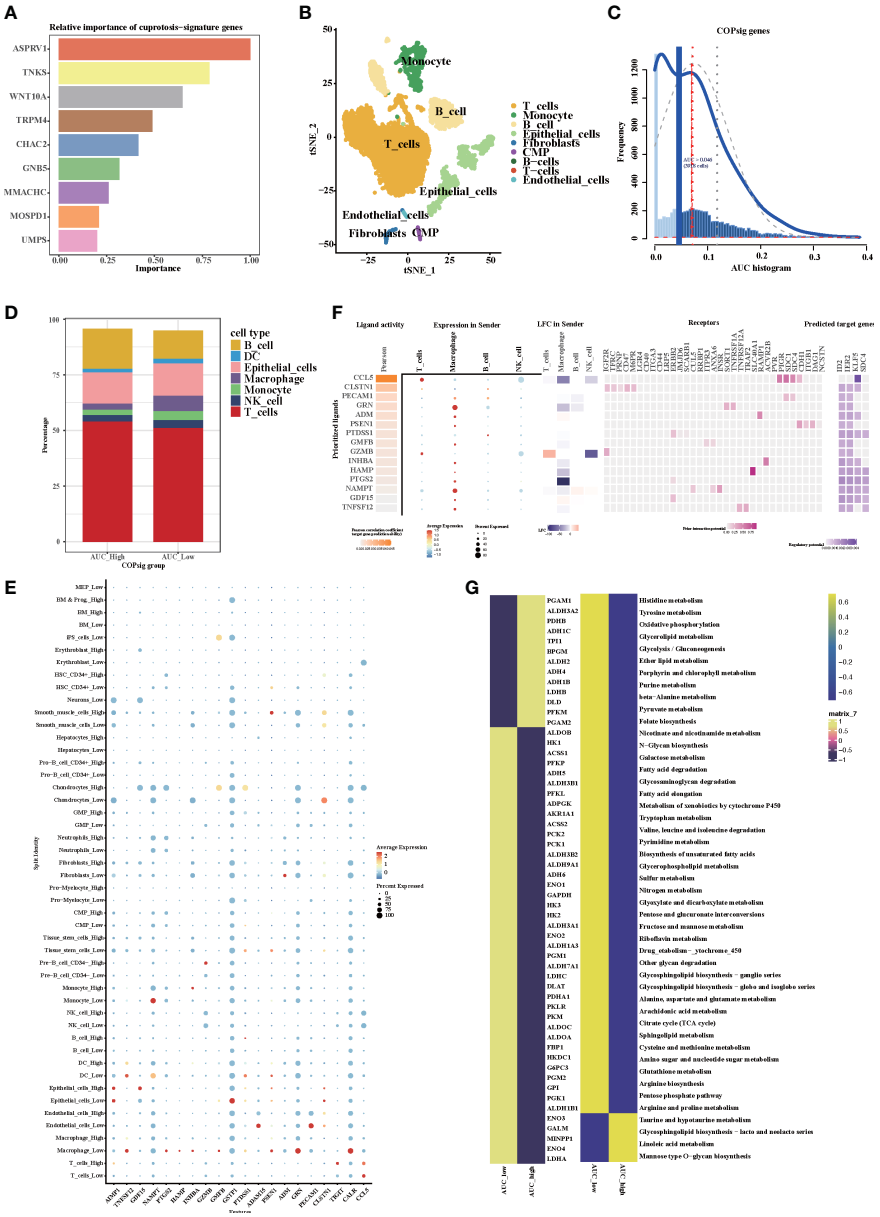

FIGURE 8
The expression of cuproptosis signature genes in TME by single-cell transcriptome analysis. **(A)** Relative importance of cuproptosis signature genes analyzed by random forest algorithm. **(B)** The t-SNE (t-distributed stochastic neighbor embedding) plot of 6,490 cells grouped into 12 clusters. **(C)** The threshold was chosen as 0.046 and the AUCell score of 3,918 cells exceeded the threshold value. **(D)** Percentage of each distinct cells in the high and low AUCell score groups. **(E)** Heatmap shows the expression of the top 20 active ligands in cells of the high and low AUCell score groups. The size of the dot represents the percent expressed. Red represents high expression; blue represents low expression. **(F)** Expression of the first 15 active ligands in different cells, as well as their interacting receptors and downstream potential target genes. **(G)** Metabolic differences in the high and low AUCell score groups.

(18, 19). Mounting evidence has shown that not only mitochondrial dysfunction and ROS accumulation, but also programmed cell death pathway, are associated with the TME and immune response (20–22, 56). Therefore, clarifying the role of cuproptosis patterns in TME cell infiltration could shed light on the mechanism of cuproptosis patterns in antitumor immune responses, as well as facilitate an effective immunotherapy strategy.

In the present study, we examined the 10 CRGs and identified three different cuproptosis patterns. Distinct patterns of TME cell infiltration characteristics can be distinguished through these three patterns. COPcluster C1 was considered as an immune-excluded phenotype, characterized by the presence of abundant immune cell and stromal infiltration, together with EMT and TGF-β signaling pathway activation. COPcluster C2 was classified as the immune-desert phenotype, characterized by immunosuppression. COPcluster C3 was considered as an immune-infiltrated phenotype, marked by immune cell infiltration and immune activation. Lots of evidence have reported that TME, particularly the infiltrating immune and stromal cells, are strongly correlated to tumor progression and immunotherapeutic response (14, 57, 58).

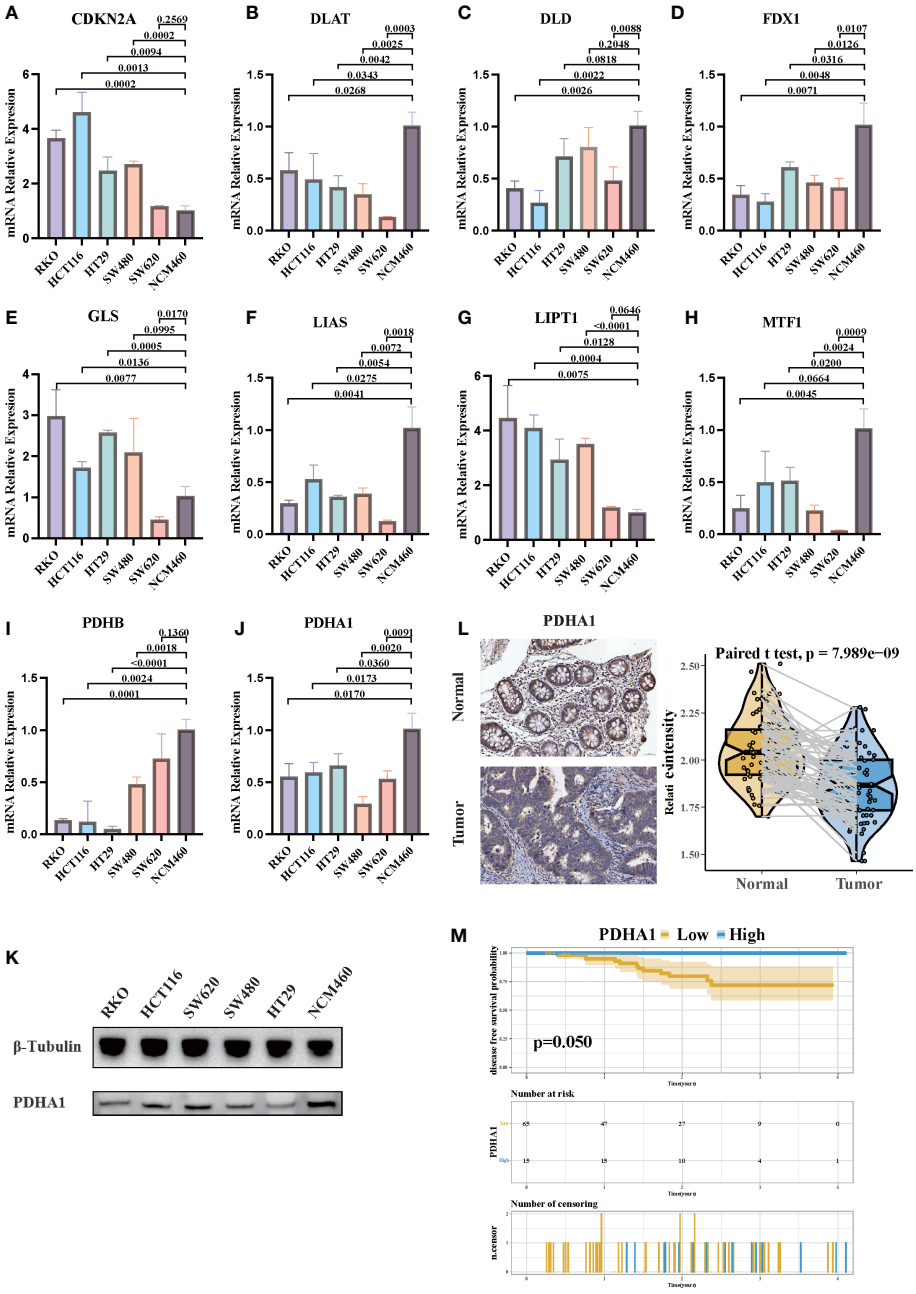

FIGURE 9
The expression of CRGs in CRC cell lines and tissues. **(A-J)** The mRNA relative expression of each CRG in 5 CRC cell lines and normal colon cell line. The asterisks illustrated the statistical *p*-value. **(K)** Western blotting results of PDHA1 protein levels in five CRC cell lines and the normal colon cell line. **(L)** PDHA1 was downregulated in colorectal cancer tissues compared to normal tissues, as examined by immunohistochemistry. **(M)** Kaplan–Meier analysis of the disease-free survival rate of CRC patients, which is stratified according to the expression of PDHA1.

The presence of immune cells such as CD4+/CD8+ T-cell infiltrating tumors is correlated with the likelihood of an immune response (59). Conversely, immune cells can be surrounded by a dense stroma, maintaining a nest around tumor cells instead of penetrating the parenchyma. This weakens the antitumor immune response. The antitumor immune response is thus diminished. Moreover, recent studies have provided evidence that the infiltration of lymphocytes into tumor parenchyma is hindered by activation of EMT and TGF-β pathways (60, 61). Collectively, our findings were consistent with the above definitions, which corroborated the accuracy of our immunophenotype classification of the three cuprotosis patterns. Meanwhile, we speculated that CRC patients with COPcluster C3 patterns might benefit from ICI treatment and have a better prognosis.

Moreover, in the present study, differences in mRNA transcriptome between distinct cuprotosis patterns have been demonstrated to be significantly associated with immune-related biological pathways. The DEGs were considered as cuprotosis-related signature genes. In accordance with the results of cuprotosis pattern clustering, three genomic clusters based on

cuprotosis signature genes were identified and strongly correlated with different prognosis and TME landscapes. A comprehensive evaluation of cuprotosis modification patterns will help us to better understand the infiltration features of TME cells and thus predict the response to immunotherapy. Therefore, in order to provide more accurate guidance on individual treatment strategies, we developed a quantitative system called "COPsig score" to identify different cuprotosis patterns. The results indicated that the cuprotosis patterns characterized by the immune-excluded phenotype showed a lower COPsig score, while the pattern characterized by the immune-inflamed phenotype had a higher COPsig score. Further analysis elucidated that COPsig score was an independent prognosis biomarker in CRC. According to recent studies, patients with low TIDE scores and high TMB are more likely to benefit from ICIs, while EMT and TGF-β pathway activation might play a critical role in resistance to ICIs (34, 60, 62, 63). The activation of EMT and TGF-β pathways, higher stromal scores, higher TIDE scores, and lower TMB were found in the low COPsig score group. Indeed, in the four independent ICI cohorts, the COPsig score was confirmed to be valuable for predicting the response to immunotherapy. The COPsig score showed a significant difference between responders and non-responders.

5-FU is an anti-metabolic drug with substitution of fluorine for hydrogen at the C-5 position of uracil, which has been broadly used since 1957 for the treatment of different types of cancer (64). To improve the efficacy and reduce toxic effects, 5-FU is often used in combination with other chemotherapeutic agents. Some studies have shown that combination chemotherapy with 5-FU can significantly prolong the survival time and relieve symptoms of CRC patients. For example, a randomized controlled trial of 423 CRC patients showed that combination treatment with 5-FU and oxaliplatin can significantly prolong the progression-free survival and overall survival of patients (65). Another clinical study of 572 patients with advanced CRC also showed that combination treatment with 5-FU and irinotecan can significantly improve the survival rate and relieve symptoms (66). However, the response rate to 5-FU-based chemotherapy is still low and the development of chemoresistance often hampers the benefit of the therapy (67, 68). Hence, the identification and validation predictive biomarkers for 5-FU-based chemotherapy might improve the prognosis of CRC patients in the future. Interestingly, recent studies have found that the activation of ferroptosis is associated with chemosensitization to 5-FU (69). We speculated that copper-induced cell death, as a type of programmed cell death as well, might be associated with the chemosensitivity of 5-FU. Our results indicated that 5-FU showed a higher drug sensitivity in high COPsig score patients in two datasets. The findings above substantiated our speculation that cuprotosis patterns could potentially be employed in clinical practice to pinpoint immune phenotypes and guide therapeutic strategies.

Tumor-associated macrophages (TAMs) in TME promote tumor development, invasion, metastasis, immune suppression, angiogenesis, and drug resistance, thereby affecting patient prognosis and playing a crucial role in regulating complex immune responses (70–73). In our study, the expression level of cuprotosis signature genes was related to the number of TAM infiltrations. Moreover, the expression of TNFSF12 was higher in the low AUCell score group, associated with tumor proliferation, invasion, migration, and angiogenesis (74). Potentially targeted gene SDC4, a transmembrane heparan sulfate proteoglycan, is considered as a central mediator of growth factors, ECM molecules, and cytoskeletal signaling proteins (75–77). Furthermore, it seems that SDC4 might be a valuable target for cancer diagnosis and treatment, since it is significantly reduced by trastuzumab and panitumumab (78, 79). Research has shown that metabolism can regulate the differentiation, mobilization, and function of TAMs, such as the glycolysis process leading to the recruitment of macrophages and polarization towards the M2 phenotype (80). Furthermore, M2 TAMs are associated with fatty acid and glutamine metabolism (81). According to our results, it was proposed that cuprotosis signature genes influenced TCA and increased glutamine and fatty acid metabolism, thereby recruiting M2 TAMs to TME and influencing the prognosis of CRC patients.

The PDHA1 gene encodes the alpha subunit of the human pyruvate dehydrogenase complex, which plays a crucial role in catalyzing the conversion of pyruvate to acetyl-CoA, an important step in the citric acid cycle and a major pathway for cellular energy production. There is a complex relationship between the PDHA1 gene and cancer. On the one hand, the PDHA1-encoded pyruvate dehydrogenase complex plays an important role in energy metabolism, and the expression level of PDHA1 is closely associated with cell proliferation and energy metabolism in some cancers, suggesting that it may promote tumor growth and metastasis. On the other hand, mutations or deletions of the PDHA1 gene have also been found, suggesting that PDHA1 may act as a potential tumor suppressor gene. Several studies have found that the expression level of the PDHA1 gene is elevated in various cancers such as ovarian cancer, and high expression levels are closely related to the malignancy and prognosis of tumors. In addition, the PDHA1 gene is involved in regulating the oxidative stress response of tumor cells, enabling them to acquire stronger antioxidant capabilities and survival advantages, thereby promoting tumor cell growth and metastasis (82, 83). Some studies have also suggested that the PDHA1 gene may act as a potential tumor suppressor gene in gastric and renal cell carcinoma, and its mutations or deletions can lead to disruptions in cellular energy metabolism and inhibition of autophagy and apoptosis, and promote tumor formation and development (84, 85). However, the relationship between PDHA1 and the prognosis of CRC patients is still unclear. In our study, we found that PDHA1 might act as a tumor suppressor in CRC. The lower expression level of PDHA1 was consistent with worse prognosis of CRC patients. Furthermore, lower PDHA1 expression is associated with higher PD-L1 and CTLA-4 expression levels, as well as increased immune cell infiltration, suggesting that PDHA1 may be involved in the remodeling of the colorectal TME, and may therefore affect the efficacy of immune therapy.

Taken together, the COPsig score could be clinically applied for the comprehensive evaluation of the cuprotosis patterns and the corresponding TME infiltration characteristics in individual CRC patients. Thus, it is possible to determine the immunophenotype of

the tumor and devise a more effective therapeutic strategy. Moreover, as an independent prognostic biomarker, the COPsig score could predict not only patient survival but also the response to adjuvant chemotherapy and immunotherapy. Furthermore, we found that by changing the cuprotosis patterns, the TME infiltration characteristics subsequently changed, which was the transformation of immune-excluded and immune-desert phenotypes to the immune-inflamed phenotype, thus improving the response to ICIs.

The limitations of this study should not be neglected. First, although we reviewed the literature and selected 10 genes recognized as CRGs, other potential genes may exist since the concept of cuprotosis was somewhat novel and there are few relevant studies. Second, the evidence level of our study was relatively low due to the retrospective nature of the ICI dataset as well as the absence of appropriate ICI-based CRC datasets. Third, the follow-up time of enrolled CRC patients was relatively short, as 18 out of 65 PDHA1-low patients had less than 1 year of follow-up, which resulted in imperfect results of Kaplan–Meier analysis.

Conclusion

Collectively, our works led to a better understanding of the regulation mechanisms underlying cuprotosis patterns on CRC TME cell infiltration. The distinct cuprotosis patterns laid a solid foundation to the explanation of heterogeneity and complexity of individual TME, thus guiding more effective immunotherapy as well as adjuvant chemotherapy strategies.

Data availability statement

The datasets presented in this study can be found in online repositories. The names of the repository/repositories and accession number(s) can be found within the article/Supplementary Materials.

Ethics statement

The studies involving human participants were reviewed and approved by Committee of Ruijin Hospital. The patients/participants provided their written informed consent to participate in this study.

Author contributions

XX, CD, HZ and WQ performed the bioinformatic analysis. DS, MY and NA checked the manuscript and the language. SZ, XY and BF designed the study. All authors contributed to the article and approved the submitted version.

Funding

This work was supported by National Facility for Translational Medicine (Shanghai, China) (TMSK-2021-503) to BF and National Natural Science Foundation of China (82103207) to SZ.

Acknowledgments

We would like to thank Wenrui Zhang for assistance with thoughtful discussion.

Conflict of interest

The authors declare that the research was conducted in the absence of any commercial or financial relationships that could be construed as a potential conflict of interest.

Publisher's note

All claims expressed in this article are solely those of the authors and do not necessarily represent those of their affiliated organizations, or those of the publisher, the editors and the reviewers. Any product that may be evaluated in this article, or claim that may be made by its manufacturer, is not guaranteed or endorsed by the publisher.

Supplementary material

The Supplementary Material for this article can be found online at: https://www.frontiersin.org/articles/10.3389/fimmu.2023.1165101/full#supplementary-material

References

1. Sung H, Ferlay J, Siegel RL, Laversanne M, Soerjomataram I, Jemal A, et al. Global cancer statistics 2020: GLOBOCAN estimates of incidence and mortality worldwide for 36 cancers in 185 countries. *CA Cancer J Clin* (2021) 71(3):209–49. doi: 10.3322/caac.21660

2. Schmoll HJ, Van Cutsem E, Stein A, Valentini V, Glimelius B, Haustermans K, et al. ESMO consensus guidelines for management of patients with colon and rectal cancer. a personalized approach to clinical decision making. *Ann Oncol* (2012) 23 (10):2479–516. doi: 10.1093/annonc/mds236

3. Carlino MS, Larkin J, Long GV. Immune checkpoint inhibitors in melanoma. *Lancet* (2021) 398(10304):1002–14. doi: 10.1016/S0140-6736(21)01206-X

4. Shankar B, Zhang J, Naqash AR, Forde PM, Feliciano JL, Marrone KA, et al. Multisystem immune-related adverse events associated with immune checkpoint inhibitors for treatment of non-small cell lung cancer. *JAMA Oncol* (2020) 6 (12):1952–6. doi: 10.1001/jamaoncol.2020.5012

5. Le DT, Durham JN, Smith KN, Wang H, Bartlett BR, Aulakh LK, et al. Mismatch repair deficiency predicts response of solid tumors to PD-1 blockade. *Science* (2017) 357(6349):409–13. doi: 10.1126/science.aan6733

6. Andre T, Shiu KK, Kim TW, Jensen BV, Jensen LH, Punt C, et al. Pembrolizumab in microsatellite-Instability-High advanced colorectal cancer. *N Engl J Med* (2020) 383 (23):2207–18. doi: 10.1056/NEJMoa2017699

7. Hanahan D, Coussens LM. Accessories to the crime: functions of cells recruited to the tumor microenvironment. *Cancer Cell* (2012) 21(3):309–22. doi: 10.1016/j.ccr.2012.02.022

8. Fridman WH, Zitvogel L, Sautes-Fridman C, Kroemer G. The immune contexture in cancer prognosis and treatment. *Nat Rev Clin Oncol* (2017) 14 (12):717–34. doi: 10.1038/nrclinonc.2017.101

9. Turley SJ, Cremasco V, Astarita JL. Immunological hallmarks of stromal cells in the tumour microenvironment. *Nat Rev Immunol* (2015) 15(11):669–82. doi: 10.1038/nri3902

10. Quail DF, Joyce JA. Microenvironmental regulation of tumor progression and metastasis. *Nat Med* (2013) 19(11):1423–37. doi: 10.1038/nm.3394

11. Lan Y, Moustafa M, Knoll M, Xu C, Furkel J, Lazorchak A, et al. Simultaneous targeting of TGF-beta/PD-L1 synergizes with radiotherapy by reprogramming the tumor microenvironment to overcome immune evasion. *Cancer Cell* (2021) 39 (10):1388–403 e10. doi: 10.1016/j.ccell.2021.08.008

12. Pitt JM, Marabelle A, Eggermont A, Soria JC, Kroemer G, Zitvogel L, et al. Targeting the tumor microenvironment: removing obstruction to anticancer immune responses and immunotherapy. *Ann Oncol* (2016) 27(8):1482–92. doi: 10.1093/annonc/mdw168

13. Ali HR, Chlon L, Pharoah PDP, Markowetz F, Caldas C. Patterns of immune infiltration in breast cancer and their clinical implications: A gene-Expression-Based retrospective study. *PloS Med* (2016) 13(12):e1002194. doi: 10.1371/journal.pmed.1002194

14. Galon J, Bruni D. Approaches to treat immune hot, altered and cold tumours with combination immunotherapies. *Nat Rev Drug Discovery* (2019) 18(3):197–218. doi: 10.1038/s41573-018-0007-y

15. Bejarano L, Jordao MJC, Joyce JA. Therapeutic targeting of the tumor microenvironment. *Cancer Discovery* (2021) 11(4):933–59. doi: 10.1158/2159-8290.CD-20-1808

16. Binnewies M, Roberts EW, Kersten K, Chan V, Fearon DF, Merad M, et al. Understanding the tumor immune microenvironment (TIME) for effective therapy. *Nat Med* (2018) 24(5):541–50. doi: 10.1038/s41591-018-0014-x

17. Mariathasan S, Turley SJ, Nickles D, Castiglioni A, Yuen K, Wang Y, et al. TGFbeta attenuates tumour response to PD-L1 blockade by contributing to exclusion of T cells. *Nature* (2018) 554(7693):544–8. doi: 10.1038/nature25501

18. Saporito-Magrina CM, Musacco-Sebio RN, Andrieux G, Kook L, Orrego MT, Tuttolomondo MV, et al. Copper-induced cell death and the protective role of glutathione: the implication of impaired protein folding rather than oxidative stress. *Metallomics* (2018) 10(12):1743–54. doi: 10.1039/C8MT00182K

19. Tsvetkov P. Copper induces cell death by targeting lipoylated TCA cycle proteins. *Science* (2022) 376(6592):470. doi: 10.1126/science.abf0529

20. O'Neill LA, Kishton RJ, Rathmell J. A guide to immunometabolism for immunologists. . *Nat Rev Immunol* (2016) 16(9):553–65. doi: 10.1038/nri.2016.70

21. Soto-Heredero G, Gomez de Las Heras MM, Gabande-Rodriguez E, Gabandé-Rodríguez E, Oller J, Mittelbrunn M, et al. Glycolysis - a key player in the inflammatory response. *FEBS J* (2020) 287(16):3350–69. doi: 10.1111/febs.15327

22. Lloberas J, Munoz JP, Hernandez-Alvarez MI, Cardona PJ, Zorzano A, Celada A, et al. Macrophage mitochondrial MFN2 (mitofusin 2) links immune stress and immune response through reactive oxygen species (ROS) production. *Autophagy* (2020) 16(12):2307–9. doi: 10.1080/15548627.2020.1839191

23. Peng HY, Lucavs J, Ballard D, Das JK, Kumar A, Wang L, et al. Metabolic reprogramming and reactive oxygen species in T cell immunity. *Front Immunol* (2021) 12:652687. doi: 10.3389/fimmu.2021.652687

24. Colaprico A, Silva TC, Olsen C, Garofano L, Cava C, Garolini D, et al. TCGAbiolinks: an R/Bioconductor package for integrative analysis of TCGA data. *Nucleic Acids Res* (2016) 44(8):e71. doi: 10.1093/nar/gkv1507

25. Dai W, Li Y, Mo S, Feng Y, Zhang L, Xu Y, et al. A robust gene signature for the prediction of early relapse in stage I-III colon cancer. *Mol Oncol* (2018) 12(4):463–75. doi: 10.1002/1878-0261.12175

26. Wong J, Hartigan J. Algorithm as 136: A k-means clustering algorithm. *J R Stat Society* (1979) 28(1):100–8.

27. Wilkerson MD, Hayes DN. ConsensusClusterPlus: a class discovery tool with confidence assessments and item tracking. *Bioinformatics* (2010) 26(12):1572–3. doi: 10.1093/bioinformatics/btq170

28. Hanzelmann S, Castelo R, Guinney J. GSVA: gene set variation analysis for microarray and RNA-seq data. *BMC Bioinf* (2013) 14:7. doi: 10.1186/1471-2105-14-7

29. Charoentong P, Finotello F, Angelova M, Mayer C, Efremova M, Rieder D, et al. Pan-cancer immunogenomic analyses reveal genotype-immunophenotype relationships and predictors of response to checkpoint blockade. *Cell Rep* (2017) 18 (1):248–62. doi: 10.1016/j.celrep.2016.12.019

30. Yeo JG, Wasser M, Kumar P, Pan L, Poh SL, Ally F, et al. The extended polydimensional immunome characterization (EPIC) web-based reference and discovery tool for cytometry data. *Nat Biotechnol* (2020) 38(6):679–84. doi: 10.1038/s41587-020-0532-1

31. Aran D, Hu Z, Butte AJ. xCell: digitally portraying the tissue cellular heterogeneity landscape. *Genome Biol* (2017) 18(1):220. doi: 10.1186/s13059-017-1349-1

32. Becht E, Giraldo NA, Lacroix L, Buttard B, Elarouci N, Petitprez F, et al. Estimating the population abundance of tissue-infiltrating immune and stromal cell populations using gene expression. *Genome Biol* (2016) 17(1):218. doi: 10.1186/s13059-016-1070-5

33. Yoshihara K, Shahmoradgoli M, Martinez E, Vegesna R, Kim H, Torres-Garcia W, et al. Inferring tumour purity and stromal and immune cell admixture from expression data. *Nat Commun* (2013) 4:2612. doi: 10.1038/ncomms3612

34. Jiang P, Gu S, Pan D, Fu J, Sahu A, Hu X, et al. Signatures of T cell dysfunction and exclusion predict cancer immunotherapy response. *Nat Med* (2018) 24(10):1550–8. doi: 10.1038/s41591-018-0136-1

35. Ritchie ME, Phipson B, Wu D, Hu Y, Law CW, Shi W, et al. Limma powers differential expression analyses for RNA-sequencing and microarray studies. *Nucleic Acids Res* (2015) 43(7):e47. doi: 10.1093/nar/gkv007

36. Kursa MB, Rudnicki WR. Feature selection with the boruta package. *J Stat Software* (2010) 36(11):1–13. doi: 10.18637/jss.v036.i11

37. Sotiriou C, Wirapati P, Loi S, Fox S, Smeds J, Nordgren H, et al. Gene expression profiling in breast cancer: understanding the molecular basis of histologic grade to improve prognosis. *J Natl Cancer Inst* (2006) 98(4):262–72. doi: 10.1093/jnci/djj052

38. Ghandi M, Huang FW, Jane-Valbuena J, Kryukov GV, Lo CC, McDonald ER 3rd, et al. Next-generation characterization of the cancer cell line encyclopedia. *Nature* (2019) 569(7757):503–8. doi: 10.1038/s41586-019-1186-3

39. Rees MG, Seashore-Ludlow B, Cheah JH, Adams DJ, Price EV, Gill S, et al. Correlating chemical sensitivity and basal gene expression reveals mechanism of action. *Nat Chem Biol* (2016) 12(2):109–16. doi: 10.1038/nchembio.1986

40. Yang C, Huang X, Li Y, Chen J, Lv Y, Dai S. Prognosis and personalized treatment prediction in TP53-mutant hepatocellular carcinoma: an in silico strategy towards precision oncology. *Brief Bioinform* (2021) 22(3):bbaa164. doi: 10.1093/bib/bbaa164

41. Hugo W, Zaretsky JM, Sun L, Song C, Moreno BH, Hu-Lieskovan S, et al. Genomic and transcriptomic features of response to anti-PD-1 therapy in metastatic melanoma. *Cell* (2016) 165(1):35–44. doi: 10.1016/j.cell.2016.02.065

42. Cho JW, Hong MH, Ha SJ, Kim YJ, Cho BC, Lee I, et al. Genome-wide identification of differentially methylated promoters and enhancers associated with response to anti-PD-1 therapy in non-small cell lung cancer. *Exp Mol Med* (2020) 52 (9):1550–63. doi: 10.1038/s12276-020-00493-8

43. Rose TL, Weir WH, Mayhew GM, Shibata Y, Eulitt P, Uronis JM, et al. Fibroblast growth factor receptor 3 alterations and response to immune checkpoint inhibition in metastatic urothelial cancer: a real world experience. *Br J Cancer* (2021) 125(9):1251–60. doi: 10.1038/s41416-021-01488-6

44. Aran D, Looney AP, Liu L, Wu E, Fong V, Hsu A, et al. Reference-based analysis of lung single-cell sequencing reveals a transitional profibrotic macrophage. *Nat Immunol* (2019) 20(2):163–72. doi: 10.1038/s41590-018-0276-y

45. Browaeys R, Saelens W, Saeys Y. NicheNet: modeling intercellular communication by linking ligands to target genes. *Nat Methods* (2020) 17(2):159–62. doi: 10.1038/s41592-019-0667-5

46. Hazra A, Gogtay N. Biostatistics series module 3: Comparing groups: Numerical variables. *Indian J Dermatol* (2016) 61(3):251–60. doi: 10.4103/0019-5154.182416

47. Mayakonda A, Lin DC, Assenov Y, Plass C, Koeffler HP. Maftools: efficient and comprehensive analysis of somatic variants in cancer. *Genome Res* (2018) 28(11):1747–56. doi: 10.1101/gr.239244.118

48. Yang X, Zhang S, He C, Xue P, Zhang L, He Z, et al. METTL14 suppresses proliferation and metastasis of colorectal cancer by down-regulating oncogenic long non-coding RNA XIST. *Mol Cancer* (2020) 19(1):46. doi: 10.1186/s12943-020-1146-4

49. Chen DS, Mellman I. Elements of cancer immunity and the cancer-immune set point. *Nature* (2017) 541(7637):321–30. doi: 10.1038/nature21349

50. Chen H, Yang M, Wang Q, Song F, Li X, Chen K. The new identified biomarkers determine sensitivity to immune check-point blockade therapies in melanoma. *Oncoimmunology* (2019) 8(8):1608132. doi: 10.1080/2162402X.2019.1608132

51. Chen H, Chong W, Wu Q, Yao Y, Mao M, Wang X. Association of LRP1B mutation with tumor mutation burden and outcomes in melanoma and non-small cell lung cancer patients treated with immune check-point blockades. *Front Immunol* (2019) 10:1113. doi: 10.3389/fimmu.2019.01113

52. Wree A, McGeough MD, Inzaugarat ME, Eguchi A, Schuster S, Johnson CD, et al. NLRP3 inflammasome driven liver injury and fibrosis: Roles of IL-17 and TNF in mice. *Hepatology* (2018) 67(2):736–49. doi: 10.1002/hep.29523

53. Zhang N, Ma Q, You Y, Xia X, Xie C, Huang Y, et al. CXCR4-dependent macrophage-to-fibroblast signaling contributes to cardiac diastolic dysfunction in heart failure with preserved ejection fraction. *Int J Biol Sci* (2022) 18(3):1271–87. doi: 10.7150/ijbs.65802

54. Susek KH, Karvouni M, Alici E, Lundqvist A. The role of CXC chemokine receptors 1-4 on immune cells in the tumor microenvironment. *Front Immunol* (2018) 9:2159. doi: 10.3389/fimmu.2018.02159

55. Deng L, Jiang A, Zeng H, Peng X, Song L. Comprehensive analyses of PDHA1 that serves as a predictive biomarker for immunotherapy response in cancer. *Front Pharmacol* (2022) 13:947372. doi: 10.3389/fphar.2022.947372

56. Yatim N, Cullen S, Albert ML. Dying cells actively regulate adaptive immune responses. *Nat Rev Immunol* (2017) 17(4):262–75. doi: 10.1038/nri.2017.9

57. Ren B, Cui M, Yang G, Wang H, Feng M, You L, et al. Tumor microenvironment participates in metastasis of pancreatic cancer. *Mol Cancer* (2018) 17(1):108. doi: 10.1186/s12943-018-0858-1

58. Xu Q, Chen S, Hu Y, Huang W. Landscape of immune microenvironment under immune cell infiltration pattern in breast cancer. *Front Immunol* (2021) 12:711433. doi: 10.3389/fimmu.2021.711433

59. Topalian SL, Taube JM, Anders RA, Pardoll DM. Mechanism-driven biomarkers to guide immune checkpoint blockade in cancer therapy. *Nat Rev Cancer* (2016) 16(5):275–87. doi: 10.1038/nrc.2016.36

60. Tauriello DVF, Palomo-Ponce S, Stork D, Berenguer-Llergo A, Badia-Ramentol J, Iglesias M, et al. TGFbeta drives immune evasion in genetically reconstituted colon cancer metastasis. *Nature* (2018) 554(7693):538–43. doi: 10.1038/nature25492

61. Bai X, Yi M, Jiao Y, Chu Q, Wu K. Blocking TGF-beta signaling to enhance the efficacy of immune checkpoint inhibitor. *Onco Targets Ther* (2019) 12:9527–38. doi: 10.2147/OTT.S224013

62. Liu L, Bai X, Wang J, Tang XR, Wu DH, Du SS, et al. Combination of TMB and CNA stratifies prognostic and predictive responses to immunotherapy across metastatic cancer. *Clin Cancer Res* (2019) 25(24):7413–23. doi: 10.1158/1078-0432.CCR-19-0558

63. Voron T, Marcheteau E, Pernot S, Colussi O, Tartour E, Taieb J, et al. Control of the immune response by pro-angiogenic factors. *Front Oncol* (2014) 4:70. doi: 10.3389/fonc.2014.00070

64. Vertessy BG, Toth J. Keeping uracil out of DNA: physiological role, structure and catalytic mechanism of dUTPases. *Acc Chem Res* (2009) 42(1):97–106. doi: 10.1021/ar800114w

65. Grothey A, Sargent D, Goldberg RM, Schmoll HJ. Survival of patients with advanced colorectal cancer improves with the availability of fluorouracil-leucovorin, irinotecan, and oxaliplatin in the course of treatment. *J Clin Oncol* (2004) 22(7):1209–14. doi: 10.1200/JCO.2004.11.037

66. Van Cutsem E, Rivera F, Berry S, Kretzschmar A, Michael M, DiBartolomeo M, et al. Safety and efficacy of first-line bevacizumab with FOLFOX, XELOX, FOLFIRI and fluoropyrimidines in metastatic colorectal cancer: the BEAT study. *Ann Oncol* (2009) 20(11):1842–7. doi: 10.1093/annonc/mdp233

67. Vodenkova S, Buchler T, Cervena K, Veskrnova V, Vodicka P, Vymetalkova V., et al. 5-fluorouracil and other fluoropyrimidines in colorectal cancer: Past, present and future. *Pharmacol Ther* (2020) 206:107447. doi: 10.1016/j.pharmthera.2019.107447

68. Sethy C, Kundu CN. 5-fluorouracil (5-FU) resistance and the new strategy to enhance the sensitivity against cancer: Implication of DNA repair inhibition. *BioMed Pharmacother* (2021) 137:111285. doi: 10.1016/j.biopha.2021.111285

69. Sharma P, Shimura T, Banwait JK, Goel A. Andrographis-mediated chemosensitization through activation of ferroptosis and suppression of beta-catenin/Wnt-signaling pathways in colorectal cancer. *Carcinogenesis* (2020) 41(10):1385–94. doi: 10.1093/carcin/bgaa090

70. Goswami KK, Ghosh T, Ghosh S, Sarkar M, Bose A, Baral R, et al. Tumor promoting role of anti-tumor macrophages in tumor microenvironment. *Cell Immunol* (2017) 316:1–10. doi: 10.1016/j.cellimm.2017.04.005

71. Chanmee T, Ontong P, Konno K, Itano N. Tumor-associated macrophages as major players in the tumor microenvironment. *Cancers (Basel)* (2014) 6(3):1670–90. doi: 10.3390/cancers6031670

72. Van Overmeire E, Laoui D, Keirsse J, Van Ginderachter JA, Sarukhan A. Mechanisms driving macrophage diversity and specialization in distinct tumor microenvironments and parallelisms with other tissues. *Front Immunol* (2014) 5:127. doi: 10.3389/fimmu.2014.00127

73. Newell P, Cottam B, Savage T, Hammill C, Wolf R, Bifulco C, et al. Circulating and intratumoral macrophages in patients with hepatocellular carcinoma: correlation with therapeutic approach. *Am J Surg* (2013) 205(5):534–40. doi: 10.1016/j.amjsurg.2013.02.002

74. Hu G, Zeng W, Xia Y. TWEAK/Fn14 signaling in tumors. *Tumour Biol* (2017) 39(6):1010428317714624. doi: 10.1177/1010428317714624

75. Karamanos NK, Piperigkou Z, Theocharis AD, Watanabe H, Franchi M, Baud S, et al. Proteoglycan chemical diversity drives multifunctional cell regulation and therapeutics. *Chem Rev* (2018) 118(18):9152–232. doi: 10.1021/acs.chemrev.8b00354

76. Onyeisi JOS, Pernambuco Filho PCA, Mesquita APS, Azevedo LC, Nader HB, Lopes CC, et al. Effects of syndecan-4 gene silencing by micro RNA interference in anoikis resistant endothelial cells: Syndecan-4 silencing and anoikis resistance. *Int J Biochem Cell Biol* (2020) 128:105848. doi: 10.1016/j.biocel.2020.105848

77. Cavalheiro RP, Lima MA, Jarrouge-Boucas TR, Viana GM, Lopes CC, Coulson-Thomas VJ, et al. Coupling of vinculin to f-actin demands syndecan-4 proteoglycan. *Matrix Biol* (2017) 63:23–37. doi: 10.1016/j.matbio.2016.12.006

78. Onyeisi JOS, Castanho de Almeida Pernambuco Filho P, de Araujo Lopes S, de Araujo Lopes S, Nader HB, Lopes CC, et al. Heparan sulfate proteoglycans as trastuzumab targets in anoikis-resistant endothelial cells. *J Cell Biochem* (2019) 120 (8):13826–40. doi: 10.1002/jcb.28656

79. Gialeli C, Theocharis AD, Kletsas D, Tzanakakis GN, Karamanos NK. Expression of matrix macromolecules and functional properties of EGF-responsive colon cancer cells are inhibited by panitumumab. *Invest New Drugs* (2013) 31(3):516–24. doi: 10.1007/s10637-012-9875-x

80. Colegio OR, Chu NQ, Szabo AL, Chu T, Rhebergen AM, Jairam V, et al. Functional polarization of tumour-associated macrophages by tumour-derived lactic acid. *Nature* (2014) 513(7519):559–63. doi: 10.1038/nature13490

81. Choi J, Stradmann-Bellinghausen B, Yakubov E, Savaskan NE, Régnier-Vigouroux A. Glioblastoma cells induce differential glutamatergic gene expressions in human tumor-associated microglia/macrophages and monocyte-derived macrophages. *Cancer Biol Ther* (2015) 16(8):1205–13. doi: 10.1080/15384047.2015.1056406

82. Dan L, Wang C, Ma P, Yu Q, Gu M, Dong L, et al. PGC1α promotes cholangiocarcinoma metastasis by upregulating PDHA1 and MPC1 expression to reverse the warburg effect. *Cell Death Dis* (2018) 9(5):466. doi: 10.1038/s41419-018-0494-0

83. Li Y, Huang R, Li X, Li X, Yu D, Zhang M, et al. Decreased expression of pyruvate dehydrogenase A1 predicts an unfavorable prognosis in ovarian carcinoma. *Am J Cancer Res* (2016) 6(9):2076–87.

84. Lin CS, Lee HT, Lee MH, Pan SC, Ke CY, Chiu AW, et al. Role of mitochondrial DNA copy number alteration in human renal cell carcinoma. *Int J Mol Sci* (2016) 17 (6):814. doi: 10.3390/ijms17060814

85. Liu Z, Yu M, Fei B, Fang X, Ma T, Wang D, et al. miR–21–5p targets PDHA1 to regulate glycolysis and cancer progression in gastric cancer. *Oncol Rep* (2018) 40 (5):2955–63. doi: 10.3892/or.2018.6695

frontiers | Frontiers in Immunology

TYPE Original Research
PUBLISHED 15 May 2023
DOI 10.3389/fimmu.2023.1189161

Check for updates

OPEN ACCESS

EDITED BY
Xi Cheng,
Shanghai Jiao Tong University, China

REVIEWED BY
Xin Yu,
Merck, United States
Azam Roohi,
Tehran University of Medical Sciences, Iran

*CORRESPONDENCE
Yulian Wu
yulianwu@zju.edu.cn
Xifeng Wu
xifengw@zju.edu.cn

†These authors have contributed equally to this work

RECEIVED 18 March 2023
ACCEPTED 03 May 2023
PUBLISHED 15 May 2023

CITATION
Pan S, Zhao W, Li Y, Ying Z, Luo Y, Wang Q, Li X, Lu W, Dong X, Wu Y and Wu X (2023) Prediction of risk and overall survival of pancreatic cancer from blood soluble immune checkpoint-related proteins. *Front. Immunol.* 14:1189161. doi: 10.3389/fimmu.2023.1189161

COPYRIGHT
© 2023 Pan, Zhao, Li, Ying, Luo, Wang, Li, Lu, Dong, Wu and Wu. This is an open-access article distributed under the terms of the Creative Commons Attribution License (CC BY). The use, distribution or reproduction in other forums is permitted, provided the original author(s) and the copyright owner(s) are credited and that the original publication in this journal is cited, in accordance with accepted academic practice. No use, distribution or reproduction is permitted which does not comply with these terms.

Prediction of risk and overall survival of pancreatic cancer from blood soluble immune checkpoint-related proteins

Sai Pan[1,2†], Wenting Zhao[1,2†], Yizhan Li[1,2], Zhijun Ying[1,2], Yihong Luo[1,2], Qinchuan Wang[1,2,3], Xiawei Li[4], Wenjie Lu[4], Xin Dong[4], Yulian Wu[4*] and Xifeng Wu[1,2*]

[1]Center for Biostatistics, Bioinformatics and Big Data, The Second Affiliated Hospital and School of Public Health, Zhejiang University School of Medicine, Hangzhou, Zhejiang, China, [2]The Key Laboratory of Intelligent Preventive Medicine of Zhejiang Province, Hangzhou, Zhejiang, China, [3]Department of Surgical Oncology, The Affiliated Sir Run Run Shaw Hospital, Zhejiang University School of Medicine, Hangzhou, Zhejiang, China, [4]Department of Hepato-Pancreato-Biliary Surgery, The Second Affiliated Hospital, Zhejiang University School of Medicine, Hangzhou, Zhejiang, China

Background: Immune checkpoint inhibition holds promise as a novel treatment for pancreatic ductal adenocarcinoma (PDAC). The clinical significance of soluble immune checkpoint (ICK) related proteins have not yet fully explored in PDAC.

Methods: We comprehensively profiled 14 soluble ICK-related proteins in plasma in 70 PDAC patients and 70 matched healthy controls. Epidemiological data of all subjects were obtained through structured interviews, and patients' clinical data were retrieved from electronical health records. We evaluated the associations between the biomarkers with the risk of PDAC using unconditional multivariate logistic regression. Consensus clustering (k-means algorithm) with significant biomarkers was performed to identify immune subtypes in PDAC patients. Prediction models for overall survival (OS) in PDAC patients were developed using multivariate Cox proportional hazards regression. Harrell's concordance index (C-index), time-dependent receiver operating characteristic (ROC) curve and calibration curve were utilized to evaluate performance of prediction models. Gene expressions of the identified ICK-related proteins in tumors from TCGA were analyzed to provide insight into underlying mechanisms.

Results: Soluble BTLA, CD28, CD137, GITR and LAG-3 were significantly upregulated in PDAC patients (all $q < 0.05$), and elevation of each of them was correlated with PDAC increased risk (all $p < 0.05$). PDAC patients were classified into soluble immune-high and soluble immune-low subtypes, using these 5 biomarkers. Patients in soluble immune-high subtype had significantly poorer OS than those in soluble immune-low subtype (log-rank p = 9.7E-03). The model with clinical variables and soluble immune subtypes had excellent predictive power (C-index = 0.809) for the OS of PDAC patients. Furthermore, the immune subtypes identified with corresponding genes' expression in PDAC tumor samples in TCGA showed an opposite correlation with OS to that of immune subtypes based on blood soluble ICK-related proteins (log-rank p =0.02). The

immune-high subtype tumors displayed higher cytolytic activity (CYT) score than immune-low subtype tumors (p < 2E-16).

Conclusion: Five soluble ICK-related proteins were identified to be significantly associated with the risk and prognosis of PDAC. Patients who were classified as soluble immune-low subtype based on these biomarkers had better overall survival than those of the soluble immune-high subtype.

KEYWORDS

soluble immune checkpoint-related protein, pancreatic cancer, immune subtype, survival, prediction model

1 Introduction

Pancreatic ductal adenocarcinoma (PDAC) remains one of the most lethal malignancies worldwide and ranks as the third leading cause of cancer death in the US (1, 2). The 5-year survival rate for PDAC remains low (less than 10%) over the past 4 decades, and it decreases to less than 1% in advanced patients (2, 3). Treatment for PDAC is currently limited to surgery and chemotherapy while efficacious strategies are desperately needed to improve the dismal prognosis of PDAC patients.

Molecular subtyping of PDAC is still in its infancy largely because there has been no clinically relevant molecular subtype that alternates treatment decision (4), unlike other solid tumors such as non-small cell lung cancer (5). *KRAS*, *TP53* and *CDKN2A* mutations, loss of *SMAD4* expression and *BRCA1/2* mutations were reported in PDAC patients (6). A transcriptomic subtyping was thus established by Bailey et al. (7), where PDAC patients were classified into four subtypes: squamous, pancreatic progenitor, immunogenic and ADEX (aberrantly differentiated endocrine exocrine). However, limited evidence of treatment responses based on these subtypes were reported in PDAC, especially for immunotherapy.

Immunotherapy in PDAC remains challenging due to multiple immune resistance mechanisms (8). Tumor-cell-intrinsic *KRAS* mutations could orchestrate a network of immune suppression in tumor microenvironment (TME) (9). Immune checkpoint blockade has been limited in the treatment of naïve PDAC patients due to factors such as the lack of activated T effector and TCR (T Cell Receptor) clonality (10), low MHC-I (Major Histocompatibility Complex-I) expression (11), low to moderate mutational burden limiting antigenic targets (12), and TME mediated suppression of T cell priming and function. Therefore, only small fraction (<1%) of PDAC patients responded to anti-PD1 for hypermutated MSI-H (Microsatellite Instability- High) tumors, let alone anti-CTLA4 or anti-PD-L1 therapies (13). Identifying the mechanisms of immune suppression and how to sensitize PDAC to immune checkpoint inhibitors are two major challenges of the immunotherapy in PDAC.

Soluble forms of membrane-bound receptors/ligands are generated by cleavage of membrane proteins or by alternative splicing from tumor cells/immune cells in TME or circulation (14). Soluble immune checkpoint proteins have been identified to be associated with advanced stage, survival and treatment response in multiple types of cancer (14). Soluble PD-1 and PD-L1 (sPD1 and sPD-L1) were identified as biomarkers of systemic inflammation in 41 advanced PDAC patients (15). Another study reported that soluble PD-1, PD-L1, BTLA, BTN3A1, and pan-BTN3As levels in plasma could predict survival in 59 PDAC patients, suggesting that these soluble immune checkpoint (ICK)-related proteins could be involved in anti-tumor immunity in PDAC (16). Studies also indicated that soluble ICK-related proteins might alter anti-tumor immunity by combining with corresponding immune checkpoint receptors/ligands, thereby influencing the outcomes of patients (14, 17). Nevertheless, the value of soluble ICK-related proteins in the diagnosis, prognosis and treatment of PDAC remains obscure. In present study, we implemented a two-stage study to systematically investigate the role of soluble ICK-related proteins in the prediction of cancer risk and overall survival in the patients of PDAC.

Abbreviations: PDAC, Pancreatic Ductal Adenocarcinoma; OS, Overall Survival; MSI-H, Microsatellite Instability- High; TME, Tumor Microenvironment; TCR, T Cell Receptor; ICK, Immune Checkpoint (ICK); SAHZU, The Second Affiliated Hospital, Zhejiang University; TCGA-PAAD, The Cancer Genome Atlas Pancreatic Adenocarcinoma; BMI, Body Mass Index; EDTA, Ethylenediaminetetraacetic acid; LLOQ, Lower Limit Of Quantification (LLOQ); RECIST1.1, Response Evaluation Criteria in Solid Tumours 1.1; PFS, Progression-free survival; FDR, False discovery rate; PCA, Principal component analysis; CYT, Cytolytic activity; ERCP, Endoscopic retrograde cholangiopancreatography; PTCD, Percutaneous transhepatic bile duct drainage; OR, Odds Ratio; HR, Hazard Ratio; BTLA, B- and T-lymphocyte attenuator; HVEM, Herpesvirus Entry Mediator; GITR, Glucocorticoid-induced TNFR-related protein; HCC, Hepatocellular Carcinoma; TNFRSF9, Tumor Necrosis Factor Receptor Superfamily Member 9.

2 Materials and methods

2.1 Study design and participants

This study was approved by the Institutional Review Board of The Second Affiliated Hospital, Zhejiang University (SAHZU). At enrollment, a written informed consent was signed by all the

participant and corresponding blood samples and clinical data were collected.

A schematic design of this study is illustrated in Figure S1. First, we systemically profiled the plasma levels of soluble ICK-related proteins in 70 PDAC patients and 70 matched healthy controls from SAHZU. The taxonomy of PDAC based on soluble ICK-related proteins was established. Second, we performed *in silico* functional validation of our taxonomy by exploring the transcriptomic levels of corresponding ICK genes in The Cancer Genome Atlas Pancreatic Adenocarcinoma (TCGA-PAAD) dataset.

PDAC patients were consecutively recruited from an ongoing pancreatic cancer cohort at SAHZU initiated in August, 2020. Patients who met the following criteria were included: 1. Pathologically (biopsy or fine-needle aspiration cytology) confirmed PDAC; 2. Informed consent or waiver of consent provided by each patient; 3. Follow-up information available. The exclusion criteria were as follows: 1. Patients had any prior treatment at the time of enrollment; 2. Non-PDAC or multiple cancer; 3. Failure to provide informed consent. Healthy controls without cancer diagnosis were recruited from an ongoing cohort on health individuals at SAHZU. To reduce the confounding effect, PDAC patients and healthy controls were matched with age (± 5 years) and sex using the propensity matching method (PSM) at the ratio of 1.

In addition, gene expression and phenotype data of PDAC tumor samples were retrieved from TCGA-PAAD cohort at GDC Data Portal (https://portal.gdc.cancer.gov/) (accessed July 6, 2022).

2.2 Baseline data collection

Epidemiological data were collected by SAHZU interviewers through face-to-face interview. Information on weight at 3 years before diagnosis (for patients) or enrollment (for controls), height, history of diabetes (yes/no), smoking status was recorded. Body Mass Index (BMI) was calculated by dividing weight by height squared (kg/m^2), and it was categorized according to the WHO guideline: underweight and normal weight (< 25 kg/m^2), overweight (≥ 25 kg/m^2 but <30 kg/m^2) or obese(≥30 kg/m^2). A smoker was defined as an individual who had smoked at least 100 cigarettes in his or her lifetime; otherwise defined as a non-smoker. The clinical, pathological, and laboratory test data were retrieved from electronic medical records at SAHZU. Serum CA 19-9 levels at diagnosis (for patients) or at health checkups (for controls) were obtained. PDAC patients were staged by physicians in charge and pathologists according to the NCCN Guidelines for Pancreatic Adenocarcinoma (version 1.2022).

2.3 Sample collection and assessment of soluble ICK-related proteins

After the interview, 20 ml of venous blood from each participant was collected in EDTA (Ethylenediaminetetraacetic acid) tubes by phlebotomists and transported through cold chain to the laboratory in SAHZU. After centrifugation, plasma was aliquoted and stored under -80°C freezer until use. The plasma levels of 14 soluble ICK-related proteins (BTLA, LAG-3, GITR, IDO, PD-L2, PD-L1, PD-1, HVEM, TIM-3, CD28, CD27, CD80, CD137 and CTLA-4) were measured using multiplex assay kits (Thermo Fisher, USA) in a Luminex FLEXMAP 3D® instrument (Luminex Corp, USA). Laboratory personnel were blinded to the case-control status of the samples. The manufacture's protocol was followed for the assay procedure, which was described in our previous study (18). The lower limit of quantification (LLOQ) of each analyte was listed in Table S1.

2.4 Patient follow-up and outcomes

PDAC patients were regularly reviewed for vital status and disease progression every three months for the first two years, and twice a year thereafter. Death was confirmed on a death certificate from an attended hospital. Disease progression was measured by RECIST1.1 (Response Evaluation Criteria in Solid Tumours 1.1). Overall survival (OS) was defined as duration from the date of diagnosis to death of any cause or last follow-up. Progression-free survival (PFS) was defined as the duration from the date of diagnosis until disease progression or death, whichever occurred first. The loss to follow-up patients were censored. All patients were followed up for survival status until December, 2022.

2.5 Statistical analysis

Categorical variables were described as frequency and percentage [n (%)]. Continuous variables were described as mean (standard deviation, SD) or median [25th and 75th percentiles (Q1-Q3)]. Categorical variables were compared by Pearson's χ^2-test, and Wilcoxon rank-sum test or Student's t-test was used to compare continuous variables. Unconditional logistic regression was performed to estimate the associations between each biomarker and PDAC risk with adjustment for age, sex, BMI, smoking status and history of diabetes. All biomarkers were considered as continuous variables and log-transformed to reduce skewness. False discovery rate (FDR) adjustment was applied to *p*-values (reported as *q*-values) to decrease the probability of Type I errors (19).

Unsupervised consensus clustering was employed on PDAC samples (both blood and tumor samples) using R package ConsensusClusterPlus (version 1.62.0) (20). K-means algorithm was used with 1,000 iterations to ensure the classification stability. The optimum number of clusters (k) was determined based on the proportion of ambiguously clustered pairs (PAC) and cumulative distribution function (CDF). Principal component analysis (PCA) was performed to show the distribution difference between the clusters. To reduce bias, for the soluble immune checkpoint-related proteins included in this study, we treated them as continuous variates in the consensus clustering analysis. For the covariates in the multivariate models, we used commonly accepted cut-off points.

Kaplan-Meier curve with log-rank test were used for comparing survival differences. Multivariate Cox proportional hazards regression models were developed by adding variables of interest sequentially to evaluate the effect on the outcomes of PDAC. Model 1 included clinical

variables (sex, age, BMI, smoking status, diabetes and stage), followed by adding CA19-9 in model 2, or adding immune subtypes in model 3. The treatment (including surgery, chemotherapy, radiation, etc.) for PDAC subjects was not included in multivariate Cox model for its correlation with tumor stage. For instance, patients with resectable disease usually received surgery or surgery plus chemotherapy, whereas patients with locally advanced disease usually received palliative chemotherapy (21). Furthermore, as a sensitivity analysis, we included treatment information in the multivariate Cox model, and the results remain consistent. Time-dependent ROC (receiver operator characteristic) curve and Harrell's concordance index (C-index) and were used to evaluate the discrimination of models. The calibration of each model was evaluated by calibration curve with 1,000 bootstrap resampling. The overall performance of the models was assessed by Brier score at a given time-point and integrated Brier score (IBS) at all available times (22). The gene expression data was downloaded from TCGA datasets. Cytolytic activity (CYT) was evaluated as the geometric mean of *GZMA* and *PRF1* expression according to a previous study (23).

We performed all statistical analysis in R (version 4.2.0). All statistical tests were two sided, and the significance level is 0.05.

3 Results

3.1 Participant characteristics

The baseline characteristics of all subjects, including 70 PDAC patients and 70 healthy controls was summarized in Table 1. All the participants of this study were Han Chinese. Over half of the participants were males. The mean ages of PDAC patients and healthy controls were 65.16 and 63.80 years, respectively. Over a third of participants were smokers with slightly more smokers in patients. Diabetes and serum CA19-9 were significantly different between PDAC patients and healthy controls ($p < 0.001$). Most patients were diagnosed at an advanced stage, in which more than half presented with metastatic disease. Serum CA19-9 levels were not elevated (below 37 U/mL) in 17 (24.29%) patients at diagnosis. Thirty-three (47.14%) patients died during the follow-up. The median follow-up time was 8.2 months (range: 0.3-28.1). Among all PDAC patients, 6 patients received radical surgery, 22 patients received radical surgery and chemotherapy, 28 patients received palliative chemotherapy, 9 patients received other treatment (palliative surgery, high-intensity focused ultrasound, ERCP (Endoscopic retrograde cholangiopancreatography) and PTCD (Percutaneous transhepatic bile duct drainage)), and 5 patients did not receive any treatment.

3.2 Associations between soluble ICK-related proteins and PDAC risk

The distributions of 14 soluble immune checkpoint-related proteins (median and Q1-Q3) were listed in Table 2. Soluble HVEM and PD-L1 were excluded from the subsequent analysis because most of the measurements were below the LLOQ.

We identified that sBTLA, sCD28, sCD137, sGITR, and sLAG-3 were significantly increased in PDAC patients as compared to those in healthy controls (Figure 1A, Table 2, all $q < 0.05$). Logistic regression adjusted for age, sex, BMI, smoking and diabetes indicated that these 5 biomarkers were significantly associated with PDAC risk (Figure 1B, Table S2, all $q < 0.05$). Among them, sCD28 was the most significantly associated biomarker with PDAC risk (Odds ratio (OR) = 2.11, 95% CI: 1.39-3.39).

3.3 Association of soluble ICK-related proteins taxonomy and prognosis of PDAC

Unsupervised consensus clustering was performed in PDAC patients based on the levels of the 5 identified biomarkers (sBTLA, sCD28, sCD137, sGITR and sLAG-3). We found that when k = 2, the slope of the CDF curve was flat and relative area change was large (Figure 2A, Figure S2); PCA outputted k=2. Thus, we classify the PDAC patients into 2 clusters. There were 33 and 37 cases in cluster 1 and 2, respectively. PCA analysis showed obvious segregation between the two clusters (Figure 2B). The two clusters also had striking different profiles of the 5 biomarkers. Cluster 1 displayed a higher relative abundance of the biomarkers compared to cluster 2 (Figure 2C). Thus, we designated these two clusters as soluble immune-high (cluster 1) and soluble immune-low (cluster 2) subtype. The relationships between the immune subtype and clinicopathologic characteristics were investigated, but there were no significant differences other than vital status (Figure 2C, Table S3). We also compared the OS between the two soluble immune subtypes, and showed that the OS was remarkably shorter in soluble immune-high subtype than that of soluble immune-low subtype (log-rank p = 9.7E-03) (Figure 2D). Furthermore, the multivariate Cox regression model indicated that soluble immune subtype was an independent predictor of OS (Hazard ratio (HR) = 3.46, 95% CI: 1.47-8.12) (Figure 2E).

3.4 Predictive models for OS in PDAC

We developed three multivariate Cox proportional hazards regression models to predict the OS of PDAC patients (Table 3). In model 1 (clinical variables only), locally advanced and metastatic patients showed significantly poorer OS compared to resectable patients (HR = 5.12, 95% CI: 1.87-13.99; HR = 6.24, 95% CI: 2.37-16.42, respectively). In model 2 (clinical variables + CA19-9), CA19-9 elevation was not statistically associated with OS. In model 3 (model 1 + soluble immune subtypes), patients of soluble immune-low subtype showed significantly better OS compared to patients of soluble immune-high subtype (HR = 3.46, 95% CI: 1.47-8.12). As shown in Figure 3A and Table 4, model 3 demonstrated better discrimination than the other two models. The C-index of model 3 was the highest (0.809, 95% CI: 0.733-0.885), followed by model 2 (0.764, 95% CI: 0.686-0.842), and model 1 (0.763, 95% CI: 0.690-0.836). The area under the curve (AUC) of model 3 was also the highest among the three models, which was 0.822, 0.786 and 0.769 at 6, 12 and 18 months,

10.3389/fimmu.2023.1189161

TABLE 1 Host characteristics of all participants.

Characteristics		Controls, n (%)	Cases, n (%)	*p*
n		70	70	
Age, mean (SD)		63.80 (9.62)	65.16 (10.13)	0.42
Sex				1.00
	Female	31 (44.29)	31 (44.29)	
	Male	39 (55.71)	39 (55.71)	
BMI, mean (SD)		24.25 (2.90)	23.55 (2.77)	0.15
Smoking				0.73
	No	42 (60.00)	39 (55.71)	
	Yes	28 (40.00)	31 (44.29)	
Diabetes				<0.001
	No	66 (94.29)	47 (67.14)	
	Yes	4 (5.71)	23 (32.86)	
Tumor location				–
	Head	–	39 (55.71)	
	Neck	–	5 (7.14)	
	Body	–	6 (8.57)	
	Tail	–	20 (28.57)	
T stage				–
	T1	–	2 (2.86)	
	T2	–	27 (38.57)	
	T3	–	23 (32.86)	
	T4	–	18 (25.71)	
N stage				–
	N0	–	39 (55.71)	
	N1	–	15 (21.43)	
	N2	–	16 (22.86)	
M stage				–
	M0	–	45 (64.29)	
	M1	–	25 (35.71)	
Stage				–
	Resectable	–	28 (40.00)	
	Locally advanced	–	17 (24.29)	
	Metastatic	–	25 (35.71)	
CA19-9 (U/ml)				<0.001
	Normal (<37 U/ml)	70 (100.0)	17 (24.29)	
	Elevated (≥37 U/ml)	0 (0.0)	53 (75.71)	
Treatment				NA
	Radical surgery only	–	6 (8.60)	

(Continued)

TABLE 1 Continued

Characteristics		Controls, n (%)	Cases, n (%)	*p*
	Radical surgery plus chemotherapy	–	22 (31.40)	
	Palliative chemotherapy	–	28 (40.00)	
	*Others	–	9 (12.90)	
	None	–	5 (7.10)	

*Others indicate palliative surgery, high-intensity focused ultrasound, ERCP and PTCD.
SD, standard deviation.

respectively. The calibration curve of model 3 for the prediction of 6-, 12- and 18-month OS showed promising agreement between the predicted and actual results (Figure 3B). Brier score of model 3 was the lowest among the three models at 6, 12 and 18 months, and IBS was the same (Table 4). Collectively, these results indicated that model 3 outperformed the models without soluble immune subtype as covariate and thus could be a useful predictive model for OS in PDAC patients.

3.5 Identification of distinct immune checkpoints subtypes in TCGA-PAAD cohort

Immune checkpoint genes' expression in TCGA-PAAD cohort was employed to further validate and explore the immune subtypes in PDAC. The demographic and clinical information of PDAC samples were listed in Table S4. Based on the expression levels of *BTLA*, *CD28*, *TNFRSF9* (gene coding for CD137), *TNFRSF18* (gene coding for GITR) and *LAG3*, two different patterns were determined by unsupervised consensus clustering (Figure S3), including immune-low (cluster 1, n = 95) and immune-high (cluster 2, n = 51) subtypes (Figures 4A–C, Table S5). Interestingly, patients in the immune-low subtype demonstrated significantly poorer OS compared to the patients in the immune-high subtype (log-rank $p = 0.02$) (Figure 4D). Besides, we found that the CYT score was significantly higher in immune-high subtype than that in immune-low subtype ($p < 2E\text{-}16$) (Figure 4E).

4 Discussion

We identified immune subtypes of PDAC based on soluble ICK-related proteins, established survival predictive models combining the biomarkers and clinical variables, and successfully applied in the PDAC patients. We found that soluble BTLA, CD28,

TABLE 2 Plasma levels of soluble immune checkpoint-related proteins in cases and controls.

Markers	Controls (n=70)	Cases (n=70)	*p*	q^b
	Median (IQR) pg/ml	Median (IQR) pg/ml		
BTLA	508.53 (306.86-748.43)	642.74 (409.05-1009.30)	**0.02**	**0.04**
CD27	103.02 (60.39-177.17)	127.48 (49.39-358.83)	0.13	0.19
CD28	32.47 (29.67-52.20)	54.84 (32.47-125.98)	**4.20E-04**	**5.04E-03**
CD80	129.39 (78.23-239.56)	131.73 (53.42-356.89)	0.54	0.59
CD137	40.82 (28.77-63.13)	68.61 (36.58-124.93)	**4.72E-03**	**1.42E-02**
CTLA-4	20.00 (14.83-25.30)	27.23 (13.09-47.52)	0.09	0.15
HVEM[a]	15.01 (15.01-15.01)	15.01 (15.01-15.01)	–	–
GITR	21.48 (13.01-34.03)	33.69 (21.21-51.01)	**2.90E-03**	**1.16E-02**
IDO	23.73 (14.43-31.44)	24.28 (16.08-47.82)	0.19	0.23
LAG-3	15.11 (11.02-22.24)	22.33 (14.68-37.26)	**1.61E-03**	**9.66E-03**
PD-1	51.49 (31.25-80.63)	55.86 (33.60-110.77)	0.18	0.23
PD-L1[a]	3.49 (3.49-3.49)	3.49 (3.49-3.49)	–	–
PD-L2	2990.45 (2044.44-3643.34)	2849.28 (2051.36-5299.90)	0.61	0.61
TIM-3	622.85 (460.61-923.06)	807.28 (435.30-1520.76)	0.06	0.12

[a]Soluble HVEM and PD-L1 were not included in the subsequent analysis for most measurements below the LLOQ.
[b]FDR-correction was applied.
The bold values means significant p value.

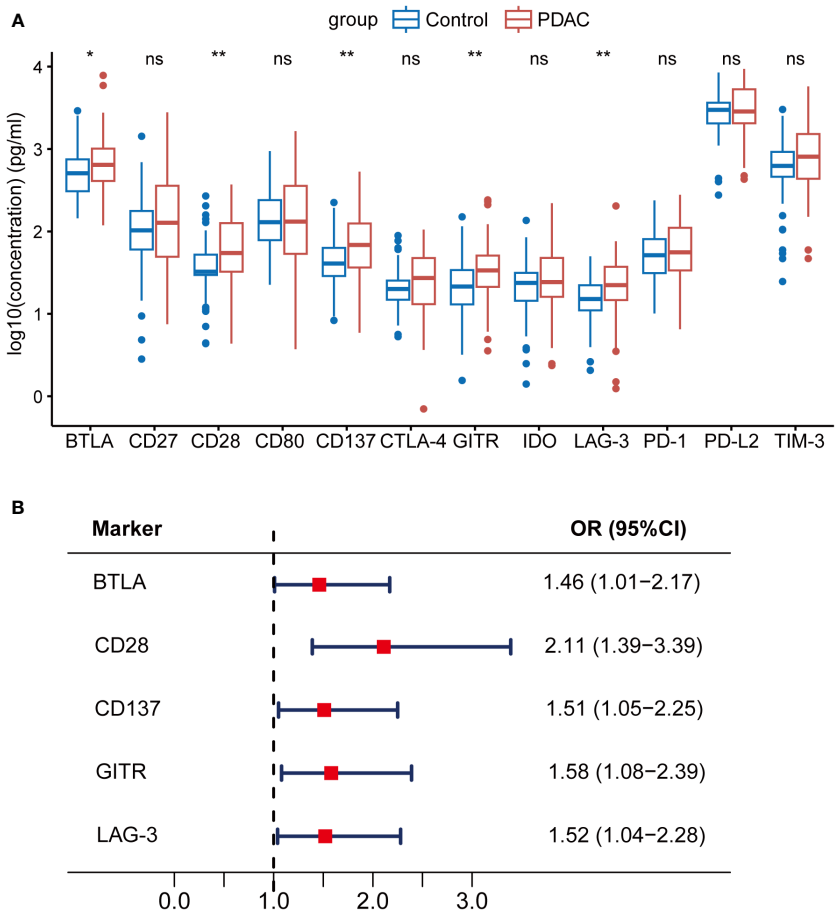

FIGURE 1
Associations between soluble immune checkpoint-related proteins and PDAC risk. sBTLA, sCD28, sCD137, sGITR, and sLAG-3 were significantly increased in PDAC patients compared to healthy controls. **(A)** Comparison of 12 soluble immune checkpoint-related proteins between PDAC patients (n=70) and healthy controls (n=70). **(B)** Forest plot of multivariable-adjusted ORs of the 5 biomarkers in unconditional logistic regression analysis. The vertical dash line indicates an OR of 1.0. The solid square with horizontal lines corresponding to the ORs and 95% CIs. PDAC, pancreatic ductal adenocarcinoma; OR, odds ratio; CI, confidence interval. $*q$ <0.05; $**q$ <0.01; 'ns' indicated not significant.

CD137, GITR, and LAG-3 were significantly associated with PDAC risk, and these biomarkers could further classify PDAC patients into soluble immune-high and soluble immune-low subtypes. Our multivariate model including the soluble immune subtypes performed better than a similar model using CA19-9 in predicting overall survival of the PDAC patients. Functional analysis employing transcriptomic data from TCGA validated that the expression of the five ICK genes could also stratify the PDAC tumor samples into two clusters. The patients with high soluble immune checkpoint-related proteins levels (soluble immune-high) had significantly poorer OS than the patients with low levels (soluble immune-low). Interestingly, the association with OS in tumoral transcriptomic levels of corresponding genes was opposite from what was observed in the blood soluble protein levels, indicating the distinct roles of soluble ICK-related proteins versus tumoral ICK related proteins in the development of PDAC. Our findings illustrated the values of soluble ICK-related proteins in the risk and prognosis prediction of PDAC.

To our knowledge, soluble ICK-related proteins have not been jointly assessed for their combined contribution to PDAC patients' survival. Our results defined two robust soluble immune subtypes based on 5 soluble ICK-related proteins, which could successfully predict survival of PDAC patients in the multivariate Cox regression model. The 5 biomarkers were all high in soluble immune-high subtype and were all low in soluble immune-low subtype, which suggested a common function in interfering anti-tumor immunity and regulation of these immune proteins in PDAC. In transcriptomic subtyping, the CYT score in the immune-low subtype was significantly lower compared with that in the immune-high subtype, indicating that tumors in the immune-low subtype lack $CD8^+$ T cells or have $CD8^+$ T cell anergy (23). Thus, the prognosis of the patient with immune-low subtype was poor. Interestingly, our cohort showed an opposite result where soluble immune-high subtype had poorer OS compared to soluble immune-low subtype. This discrepancy was also observed in solid tumor patients treated with anti-PD-1/PD-L1, where plasma sBTLA, sCD28, sGITR and sLAG-3 levels were significantly lower in the durable benefit group, but the corresponding genes expression levels were higher than the non-durable clinical benefit group (24). Furthermore, the upregulated

10.3389/fimmu.2023.1189161

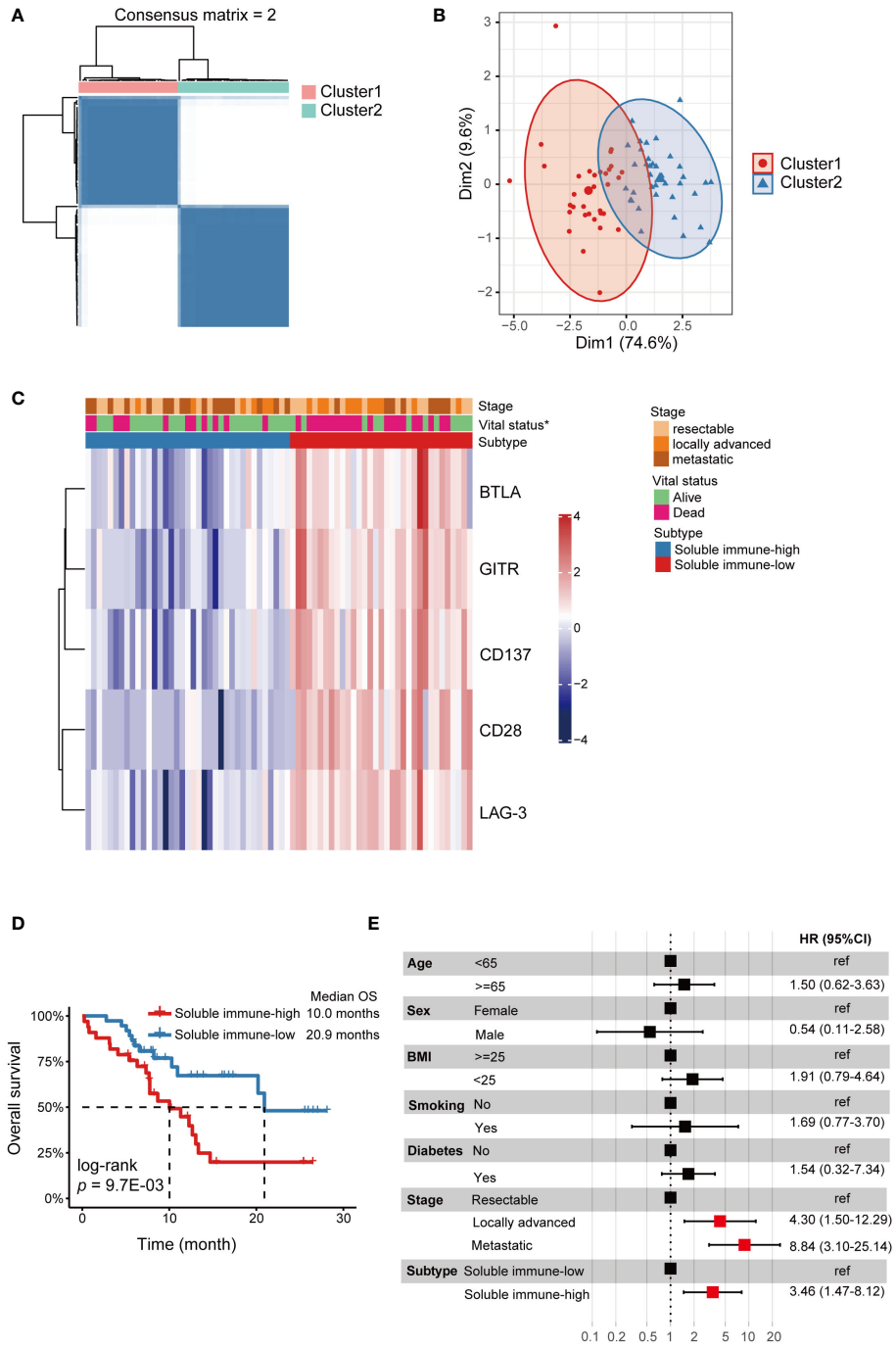

FIGURE 2
Identification of soluble immune checkpoint-related proteins-based subtypes in PDAC. Soluble immune subtypes based on soluble immune checkpoint-related proteins were associated with outcomes of PDAC patients. **(A)** Consensus clustering matrix for k=2 based on the plasma levels of soluble immune checkpoint-related proteins by unsupervised consensus clustering method (k-means). **(B)** PCA showed obvious segregation between the two clusters. **(C)** Heatmap for the associations between the clusters and clinicopathological characteristics. Subtype, age, BMI, smoke, tumor location, N stage, M stage, stage and vital status were used as annotations. $*p$ <0.05. **(D)** Kaplan-Meier curve showed that OS of the soluble immune-high subtype patients was significantly poorer than those in the soluble immune-low subtype. **(E)** Forest plot of multivariate Cox regression analysis. Covariates were age, sex, BMI, smoking, diabetes, stage and subtype. The vertical dash line indicates an HR of 1.0. The solid square with horizontal lines corresponding to the HRs and 95% CIs. PDAC, pancreatic ductal adenocarcinoma; PCA, principal component analysis; OS, overall survival; HR, hazards ratio; CI, confidence interval.

genes expression group showed significantly increased fractions of $CD8^+$ T cells (24). Soluble ICK-proteins could competitively interfere with the interactions of their corresponding receptors/ligands in the membrane of immune/tumor cells, which could subsequently alter the anti-tumor immunity and cancer outcomes (12, 15). Further studies focus on the blood, tumoral and immune

10.3389/fimmu.2023.1189161

TABLE 3 Multivariate Cox regression models in prediction of overall survival in PDAC patients.

Variables	Model 1	Model 2	Model 3
	HR (95% CI)	HR (95% CI)	HR (95% CI)
Age			
<65	1 (reference)	1 (reference)	1 (reference)
>=65	2.00 (0.85-4.71)	2.20 (0.91-5.36)	1.50 (0.62-3.63)
Sex			
Female	1 (reference)	1 (reference)	1 (reference)
Male	0.47 (0.10-2.14)	0.44 (0.09-2.04)	0.54 (0.11-2.58)
BMI			
<25	1 (reference)	1 (reference)	1 (reference)
>=25	1.40 (0.62-3.17)	1.54 (0.66-3.59)	1.91 (0.79-4.64)
Diabetes			
No	1 (reference)	1 (reference)	1 (reference)
Yes	1.62 (0.72-3.62)	1.60 (0.72-3.56)	1.69 (0.77-3.70)
Smoking			
No	1 (reference)	1 (reference)	1 (reference)
Yes	1.67 (0.36-7.76)	1.84 (0.39-8.69)	1.54 (0.32-7.34)
Stage			
Resectable	1 (reference)	1 (reference)	1 (reference)
Locally advanced	5.12 (1.87-13.99)	5.10 (1.86-14.00)	4.30 (1.50-12.29)
Metastatic	6.24 (2.37-16.42)	6.87 (2.52-18.70)	8.84 (3.10-25.14)
CA19-9			
Normal	–	1 (reference)	–
Elevated	–	1.47 (0.55-3.94)	–
Subtype			
Soluble immune-low	–	–	1 (reference)
Soluble immune-high	–	–	3.46 (1.47-8.12)

Model1: epidemiology variables, Model 2: epidemiology variables + CA19-9, Model 3: epidemiology variables + immune subtype.

cellular levels of immune checkpoint-related proteins in a same cohort is warranted to validate our findings and also to explore the potential mechanisms underlying the discrepancy.

CD28 is a major co-stimulatory receptor constitutively expressed on naïve T cells that induces T cell differentiation and proliferation upon ligation by CD80 or CD86 on antigen-presenting cells (25). sCD28 could be derived from alternatively spliced transcripts in resting T cells. One of the sCD28 variants has intensities similar to membrane CD28, suggesting it may participates in immune regulation (26). We found that sCD28 was most strongly associated with PDAC risk, and high plasma sCD28 concentrations associated with poor OS in PDAC patients. This was consistent with findings in hepatocellular carcinoma (HCC), in which high baseline levels of sCD28 predicted a significantly greater HCC cumulative rate (27). Whereas treatment-induced survival benefit was strongly correlated with decreased sCD28 levels (28). Also, sCD28 levels were higher in breast cancer patients than in healthy controls (29). sCD28 was found to inhibit CD28 signaling by competing for B7 ligands, thereby impairing T-cell activation (30, 31). Besides, sCD28 could lead to dendritic cells-induced IL-6 production in *in vitro* cultures (32). IL-6 was a driver of tumorigenesis and metastasis in PDAC (33). Overall, sCD28 is a useful biomarker for clinical outcome in PDAC patients, though more validation is required.

CD137 is an important costimulatory molecule expressed on the surface of activated $CD8^+$ T cells (34). The interaction of CD137/CD137L led to T cell activation and survival, thereby enhancing antitumor immunity. CD137 agonist antibodies had shown therapeutic effects in pancreatic cancer alone or in combination with other agents including PD-1 checkpoint inhibitors (35–37). In our study, high levels of sCD137 were associated with increased PDAC risk and shorter OS in PDAC patients. Previous studies had

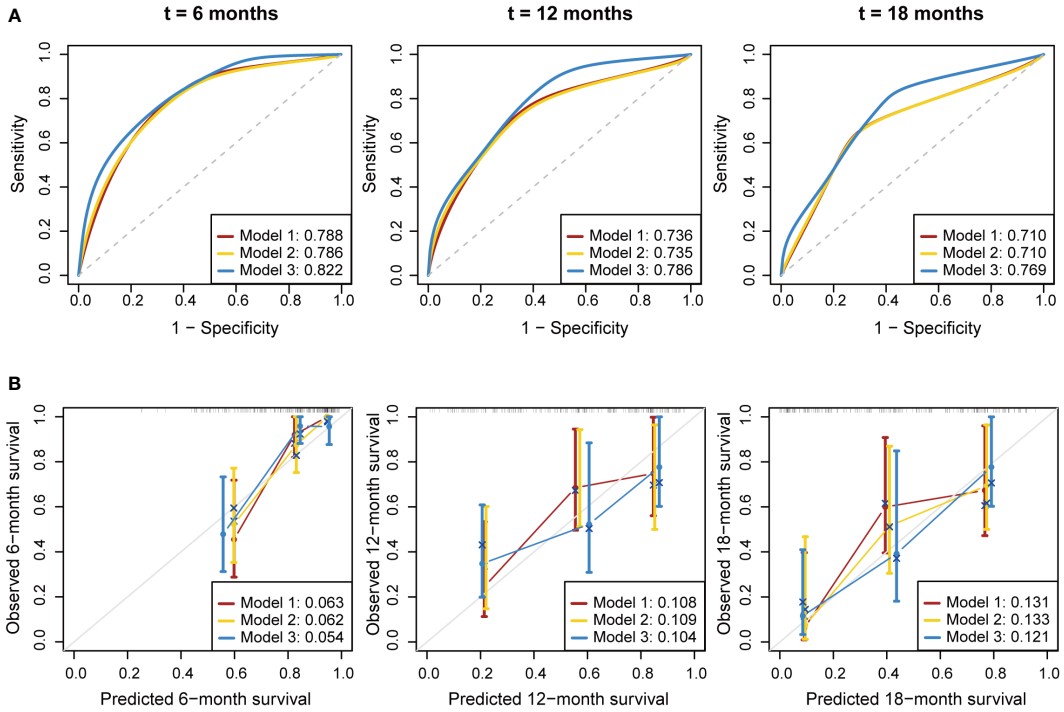

FIGURE 3
Performance evaluation for the predictive models. Multivariate Cox proportional hazards models were established to predict the overall survival of PDAC patients. **(A)** Time-dependent ROC curve of the three prognostic models at 6, 12 and 18 months. **(B)** Calibration curve of the three prognostic models at 6, 12 and 18 months. Bier score was used to quantify the prediction error. The gray line indicated the ideal reference line. ROC, receiver operating characteristic; AUC, area under curve.

reported that sCD137 was overexpressed in NSCLC patients and CLL patients compared with the control group (38, 39). Moreover, uveal melanoma patients with fast-progressive disease had higher levels of sCD137 as compared to slow progressors and long survivors (40). Soluble CD137 was generated by alternately splicing of *TNFRSF9* (Tumor Necrosis Factor Receptor Superfamily Member 9) in activated T cells (41), which could not only block CD137-CD137L interactions but directly suppress effector T cells via CD137L, thereby preventing co-stimulation of T lymphocytes (42). In addition, Labiano et al. (43) found that cell lines from hepatocellular tumors, lung, renal, and melanoma selectively expressed sCD137 but not membrane-bound CD137 (mCD137) under hypoxia condition, suggesting sCD137 was beneficial for tumor survival. Taken together, the results indicated that sCD137 could be an inhibitor of effector T cells, which could help immune evasion and survival of tumor.

LAG-3, is one of suppressive immune checkpoints expressed on the surface of T cells, which has been reported to be associated with

TABLE 4 Predictive evaluation metrics of different models.

Metrics	Model 1	Model 2	Model 3
C-index (95%CI)	0.763 (0.690-0.836)	0.764 (0.686-0.842)	0.809 (0.733-0.885)
AUC			
6 months	0.788	0.786	0.822
12 months	0.736	0.735	0.786
18 months	0.710	0.710	0.769
IBS	0.156	0.157	0.145
Brier score			
6 months	0.063	0.062	0.054
12 months	0.108	0.109	0.104
18 months	0.131	0.133	0.121

*model 1 (clinical variables only, including sex, age, BMI, smoking status, diabetes and stage), model 2 (clinical variables + CA19-9), model 3 (model 1 + soluble immune subtypes).

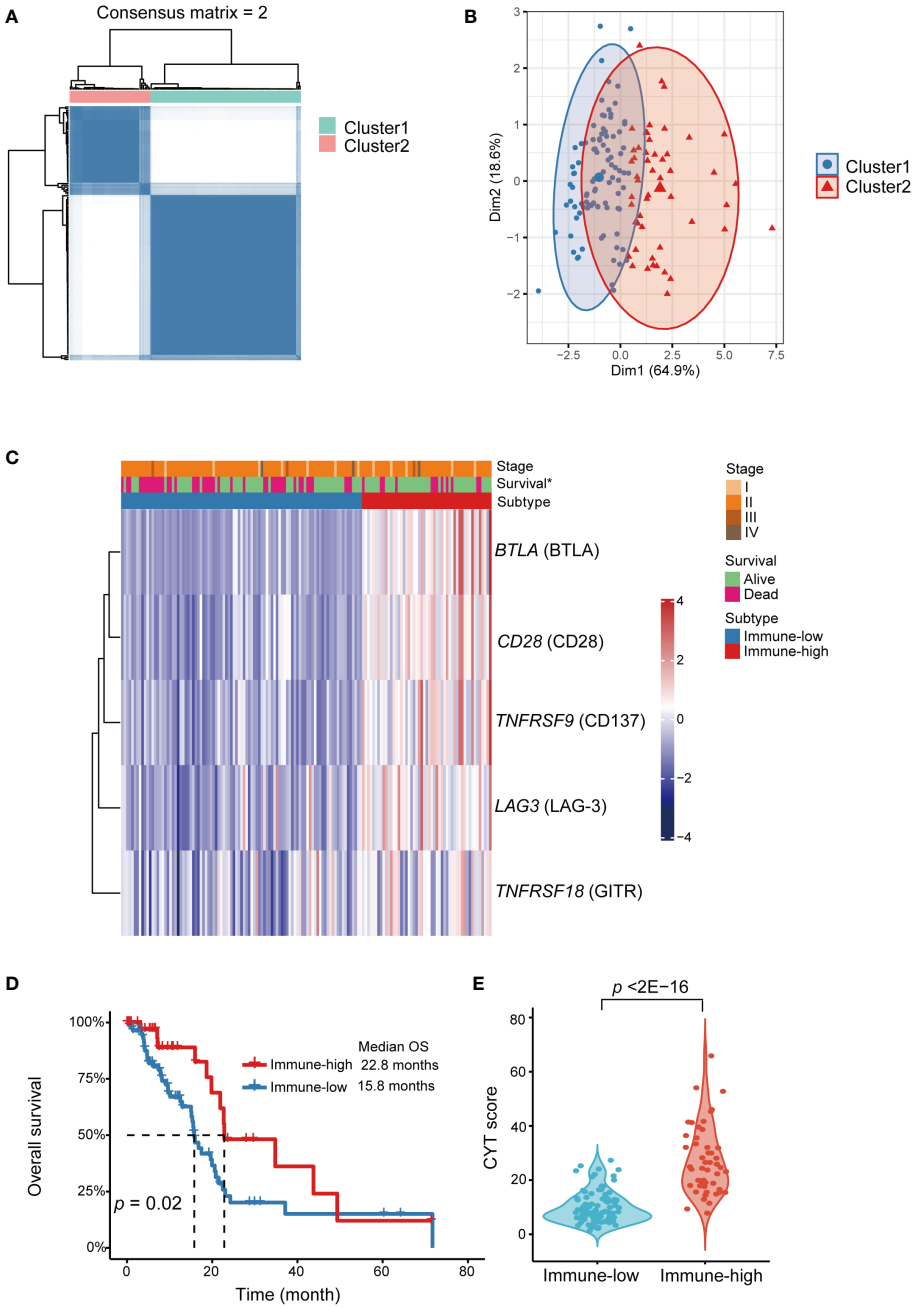

FIGURE 4
Identification of immune checkpoint genes expression subtypes in TCGA-PAAD cohort. Functional explorations of our immune subtypes applying transcriptomic data from TCGA PAAD dataset. **(A)** Consensus clustering matrix for k=2 based on the expression levels of immune checkpoint by unsupervised consensus clustering method (k-means). **(B)** PCA showed obvious segregation between the two clusters. **(C)** Heatmap for the associations between the clusters and clinicopathological characteristics. Subtype, age, sex, smoking, diabetes, stage, grade and vital status were used as annotations. $*p$ <0.05. **(D)** Kaplan-Meier curve showed that OS of the immune-low subtype patients was significantly poorer than those in the immune-high subtype. **(E)** Comparison of CYT score between two subtypes. PDAC, pancreatic ductal adenocarcinoma; PCA, principal component analysis; OS, overall survival; CYT, cytolytic activity.

reduced survival in pancreatic cancer (44). LAG-3 antagonist in combination with other immunologic agents increased antitumor immunity and achieved durable remission in PDAC (37). After T cell activation, LAG-3 cleavage was increased, resulting in the release of sLAG-3 (45). Our results indicated that high levels of sLAG-3 were associated with increased risk and reduced OS of PDAC patients. Similar findings on the associations of sLAG-3 with poor survival in CLL patients had been reported (46). Also, high sLAG-3 levels were also found to be predictive of poor prognosis in several solid tumors, including melanoma (47), NSCLC (48), and HNSCC (49). However, in gastric cancer, sLAG-3 could positively regulate and enhance the anti-tumor immunity of $CD8^+$T cells and

secretion of IL-12 and IFN-γ, thereby improve the survival of patients (50). The discrepancy may stem from the distinct immune contextures and mechanisms among different cancer types (51).

GITR is another novel stimulatory immune checkpoint in NK cells and T cells, whose agonism could promote anti-tumor immunity by reducing the regulatory T cells and stimulating the proliferation and activation of effector T cells (52). sGITR elevation was associated with increased risk and reduced OS of PDAC in our study. The result was partially supported by a study indicating high GITR expression in tumor was associated with poor relapse-free survival in a cohort of breast cancer patients (53). Our previous study also indicated that sGITR was associated with increased risk of biochemical recurrence and progression of prostate cancer (54). Therefore, GITR has gain increasing interest of research as a promising target of immunotherapy (55). Also, BTLA is an important co-inhibitory molecule on the surface of antigen presenting cells, which could interact with its ligand HVEM to suppress the T cell activity (56). sBTLA is identified correlating with increased cancer risk and reduced OS of PDAC in our study. High level of sBTLA was found to be associated with reduced survival in ccRCC and pancreatic cancer (16, 18), which was consistent with our findings. sBTLA could interact with membrane HVEM on tumor cells, thereby blocking BTLA/HVEM axis and promoting tumor growth via the ERK1/2 pathway (57). This study partially explained the mechanism of sBTLA associated poor survival in PDAC patients.

Our study has several strengths like multiplex soluble ICK-related proteins profiling, establishing the immune subtypes and prediction models of PDAC based on soluble ICK-related proteins, and a novel approach that significantly increased predictivity of survival in PDAC patients. However, the study has several limitations. First, our 70 cases of PDAC sample size were relatively small although the study was well designed and all the participants were strictly matched to avoid potential confounding factors. Second, we did not evaluate corresponding genes' expression in tumors and peripheral blood mononuclear cells. Instead, we applied the immune checkpoint and cytolytic activity genes expression in TCGA database to decipher potential mechanisms. Third, the study was a retrospective study in a single institution, more independent validations were required.

5 Conclusion

In this study, we established soluble immune subtypes of PDAC based on soluble ICK-related proteins for the first time. We further established predictive model using the soluble immune subtypes and clinical variables. PDAC patients who were classified as soluble immune-low subtype had better OS than those of the soluble immune-high subtype. Our findings indicated that immune-high PDAC patients may be more suitable for immune checkpoint blockade therapy. Future studies may apply the immune subtypes in prospective settings to examine the accuracy of survival predictions and treatment outcomes of immunotherapy of PDAC patients.

Data availability statement

The original contributions presented in the study are included in the article/Supplementary Material. Further inquiries can be directed to the corresponding authors.

Ethics statement

The studies involving human participants were reviewed and approved by Institutional Review Board of The Second Affiliated Hospital, Zhejiang University. The patients/participants provided their written informed consent to participate in this study.

Author contributions

XW involved in conception and design; SP, QW and WZ involved in development of methodology; XL, WL, XD, YW and SP participated in acquisition of data (acquired and managed patients, provided facilities, etc.); SP, YzL, ZY, YhL and YW involved in analysis and interpretation of data (e.g., statistical analysis, biostatistics, computational analysis); QW, SP, WZ and XW drafted the manuscript and all the authors participant in the revision of the manuscript; XW, YW involved in study supervision.

Funding

This work was funded by Key Laboratory of Intelligent Preventive Medicine of Zhejiang Province (2020E10004), Leading Innovative and Entrepreneur Team Introduction Program of Zhejiang (2019R01007) and Key Research and Development Program of Zhejiang Province (2020393822), Nature and Science Fund Public Program of Zhejiang Province (LGF22H160008).

Acknowledgments

We would like to thank the excellent work of the field team and laboratory staff for patient recruitment and for collection and/or processing of clinical/epidemiological information and biological specimens.

Conflict of interest

The authors declare that the research was conducted in the absence of any commercial or financial relationships that could be construed as a potential conflict of interest.

Publisher's note

All claims expressed in this article are solely those of the authors and do not necessarily represent those of their affiliated organizations, or those of the publisher, the editors and the reviewers. Any product that may be evaluated in this article, or claim that may be made by its manufacturer, is not guaranteed or endorsed by the publisher.

Supplementary material

The Supplementary Material for this article can be found online at: https://www.frontiersin.org/articles/10.3389/fimmu.2023.1189161/full#supplementary-material

References

1. Siegel RL, Miller KD, Wagle NS, Jemal A. Cancer statistics, 2023. *CA Cancer J Clin* (2023) 73(1):17–48. doi: 10.3322/caac.21763

2. Sung H, Ferlay J, Siegel RL, Laversanne M, Soerjomataram I, Jemal A, et al. Global cancer statistics 2020: globocan estimates of incidence and mortality worldwide for 36 cancers in 185 countries. *CA: A Cancer J Clin* (2021) 71(3):209–49. doi: 10.3322/caac.21660

3. Bengtsson A, Andersson R, Ansari D. The actual 5-year survivors of pancreatic ductal adenocarcinoma based on real-world data. *Sci Rep* (2020) 10(1):16425. doi: 10.1038/s41598-020-73525-y

4. Collisson EA, Bailey P, Chang DK, Biankin AV. Molecular subtypes of pancreatic cancer. *Nat Rev Gastroenterol Hepatol* (2019) 16(4):207–20. doi: 10.1038/s41575-019-0109-y

5. Cancer Genome Atlas Research N. Comprehensive molecular profiling of lung adenocarcinoma. *Nature* (2014) 511(7511):543–50. doi: 10.1038/nature13385

6. Jones S, Zhang X, Parsons DW, Lin JC, Leary RJ, Angenendt P, et al. Core signaling pathways in human pancreatic cancers revealed by global genomic analyses. *Science* (2008) 321(5897):1801–6. doi: 10.1126/science.1164368

7. Bailey P, Chang DK, Nones K, Johns AL, Patch AM, Gingras MC, et al. Genomic analyses identify molecular subtypes of pancreatic cancer. *Nature* (2016) 531(7592):47–52. doi: 10.1038/nature16965

8. Bear AS, Vonderheide RH, O'Hara MH. Challenges and opportunities for pancreatic cancer immunotherapy. *Cancer Cell* (2020) 38(6):788–802. doi: 10.1016/j.ccell.2020.08.004

9. Collins MA, Bednar F, Zhang Y, Brisset JC, Galban S, Galban CJ, et al. Oncogenic kras is required for both the initiation and maintenance of pancreatic cancer in mice. *J Clin Invest* (2012) 122(2):639–53. doi: 10.1172/JCI59227

10. Clark CE, Hingorani SR, Mick R, Combs C, Tuveson DA, Vonderheide RH. Dynamics of the immune reaction to pancreatic cancer from inception to invasion. *Cancer Res* (2007) 67(19):9518–27. doi: 10.1158/0008-5472.CAN-07-0175

11. Yamamoto K, Venida A, Yano J, Biancur DE, Kakiuchi M, Gupta S, et al. Autophagy promotes immune evasion of pancreatic cancer by degrading mhc-I. *Nature* (2020) 581(7806):100–5. doi: 10.1038/s41586-020-2229-5

12. Alexandrov LB, Nik-Zainal S, Wedge DC, Aparicio SA, Behjati S, Biankin AV, et al. Signatures of mutational processes in human cancer. *Nature* (2013) 500(7463):415–21. doi: 10.1038/nature12477

13. Le DT, Durham JN, Smith KN, Wang H, Bartlett BR, Aulakh LK, et al. Mismatch repair deficiency predicts response of solid tumors to pd-1 blockade. *Science* (2017) 357(6349):409–13. doi: 10.1126/science.aan6733

14. Gu D, Ao X, Yang Y, Chen Z, Xu X. Soluble immune checkpoints in cancer: production, function and biological significance. *J Immunother Cancer* (2018) 6(1):132. doi: 10.1186/s40425-018-0449-0

15. Kruger S, Legenstein ML, Rosgen V, Haas M, Modest DP, Westphalen CB, et al. Serum levels of soluble programmed death protein 1 (Spd-1) and soluble programmed death ligand 1 (Spd-L1) in advanced pancreatic cancer. *Oncoimmunology* (2017) 6(5):e1310358. doi: 10.1080/2162402X.2017.1310358

16. Bian B, Fanale D, Dusetti N, Roque J, Pastor S, Chretien AS, et al. Prognostic significance of circulating pd-1, pd-L1, pan-Btn3as, Btn3a1 and btla in patients with pancreatic adenocarcinoma. *Oncoimmunology* (2019) 8(4):e1561120. doi: 10.1080/2162402X.2018.1561120

17. Khan M, Zhao Z, Arooj S, Fu Y, Liao G. Soluble pd-1: predictive, prognostic, and therapeutic value for cancer immunotherapy. *Front Immunol* (2020) 11:587460. doi: 10.3389/fimmu.2020.587460

18. Wang Q, Zhang J, Tu H, Liang D, Chang D, Ye Y, et al. Soluble immune checkpoint-related proteins as predictors of tumor recurrence, survival, and T cell phenotypes in clear cell renal cell carcinoma patients. *J immunotherapy Cancer* (2019) 7(1):1–9. doi: 10.1186/s40425-019-0810-y

19. Benjamini Y, Hochberg Y. Controlling the false discovery rate: a practical and powerful approach to multiple testing. *J R Stat Society: Ser B (Methodological)* (1995) 57(1):289–300. doi: 10.1111/j.2517-6161.1995.tb02031.x

20. Wilkerson MD, Hayes DN. Consensusclusterplus: a class discovery tool with confidence assessments and item tracking. *Bioinformatics* (2010) 26(12):1572–3. doi: 10.1093/bioinformatics/btq170

21. Mizrahi JD, Surana R, Valle JW, Shroff RT. Pancreatic cancer. *Lancet* (2020) 395(10242):2008–20. doi: 10.1016/S0140-6736(20)30974-0

22. Steyerberg EW, Vickers AJ, Cook NR, Gerds T, Gonen M, Obuchowski N, et al. Assessing the performance of prediction models: a framework for traditional and novel measures. *Epidemiology* (2010) 21(1):128–38. doi: 10.1097/EDE.0b013e3181c30fb2

23. Rooney MS, Shukla SA, Wu CJ, Getz G, Hacohen N. Molecular and genetic properties of tumors associated with local immune cytolytic activity. *Cell* (2015) 160(1-2):48–61. doi: 10.1016/j.cell.2014.12.033

24. Li Y, Wang J, Wu L, Li X, Zhang X, Zhang G, et al. Diversity of dominant peripheral T cell receptor clone and soluble immune checkpoint proteins associated with clinical outcomes following immune checkpoint inhibitor treatment in advanced cancers. *Front Immunol* (2021) 12:649343. doi: 10.3389/fimmu.2021.649343

25. Esensten JH, Helou YA, Chopra G, Weiss A, Bluestone JA. Cd28 costimulation: from mechanism to therapy. *Immunity* (2016) 44(5):973–88. doi: 10.1016/j.immuni.2016.04.020

26. Magistrelli G, Jeannin P, Elson G, Gauchat JF, Nguyen TN, Bonnefoy JY, et al. Identification of three alternatively spliced variants of human Cd28 mrna. *Biochem Biophys Res Commun* (1999) 259(1):34–7. doi: 10.1006/bbrc.1999.0725

27. Dong MP, Thuy LTT, Hoang DV, Hai H, Hoang TH, Sato-Matsubara M, et al. Soluble immune checkpoint protein Cd27 is a novel prognostic biomarker of hepatocellular carcinoma development in hepatitis c virus-sustained virological response patients. *Am J Pathol* (2022) 192(10):1379–96. doi: 10.1016/j.ajpath.2022.07.003

28. Qin SK, Li Q, Ming Xu J, Liang J, Cheng Y, Fan Y, et al. Icaritin-induced immunomodulatory efficacy in advanced hepatitis b virus-related hepatocellular carcinoma: immunodynamic biomarkers and overall survival. *Cancer Sci* (2020) 111(11):4218–31. doi: 10.1111/cas.14641

29. Isitmangil G, Gurleyik G, Aker FV, Coskun C, Kucukhuseyin O, Arikan S, et al. Association of Ctla4 and Cd28 gene variants and circulating levels of their proteins in patients with breast cancer. *In Vivo* (2016) 30(4):485–93.

30. Sakthivel P, Shively V, Kakoulidou M, Pearce W, Lefvert AK. The soluble forms of Cd28, Cd86 and ctla-4 constitute possible immunological markers in patients with abdominal aortic aneurysm. *J Intern Med* (2007) 261(4):399–407. doi: 10.1111/j.1365-2796.2007.01773.x

31. Pyo JY, Yoon T, Ahn SS, Song JJ, Park YB, Lee SW. Soluble immune checkpoint molecules in patients with antineutrophil cytoplasmic antibody-associated vasculitis. *Sci Rep* (2022) 12(1):21319. doi: 10.1038/s41598-022-25466-x

32. Sun Z, Yi L, Tao H, Huang J, Jin Z, Xiao Y, et al. Enhancement of soluble Cd28 levels in the serum of graves' disease. *Cent Eur J Immunol* (2014) 39(2):216–22. doi: 10.5114/ceji.2014.43726

33. van Duijneveldt G, Griffin MDW, Putoczki TL. Emerging roles for the il-6 family of cytokines in pancreatic cancer. *Clin Sci (Lond)* (2020) 134(16):2091–115. doi: 10.1042/CS20191211

34. Croft M. Co-Stimulatory members of the tnfr family: keys to effective T-cell immunity? *Nat Rev Immunol* (2003) 3(8):609–20. doi: 10.1038/nri1148

35. Muth ST, Saung MT, Blair AB, Henderson MG, Thomas DL2nd, Zheng L. Cd137 agonist-based combination immunotherapy enhances activated, effector

memory T cells and prolongs survival in pancreatic adenocarcinoma. *Cancer Lett* (2021) 499:99–108. doi: 10.1016/j.canlet.2020.11.041

36. Li K, Tandurella JA, Gai J, Zhu Q, Lim SJ, Thomas DL2nd, et al. Multi-omic analyses of changes in the tumor microenvironment of pancreatic adenocarcinoma following neoadjuvant treatment with anti-Pd-1 therapy. *Cancer Cell* (2022) 40 (11):1374–91 e7. doi: 10.1016/j.ccell.2022.10.001

37. Gulhati P, Schalck A, Jiang S, Shang X, Wu CJ, Hou P, et al. Targeting T cell checkpoints 41bb and Lag3 and myeloid cell Cxcr1/Cxcr2 results in antitumor immunity and durable response in pancreatic cancer. *Nat Cancer* (2023) 4(1):62–80. doi: 10.1038/s43018-022-00500-z

38. Peng Y, Zhang C, Rui Z, Tang W, Xu Y, Tao X, et al. A comprehensive profiling of soluble immune checkpoints from the sera of patients with non-small cell lung cancer. *J Clin Lab Anal* (2022) 36(2):e24224. doi: 10.1002/jcla.24224

39. Furtner M, Straub RH, Kruger S, Schwarz H. Levels of soluble Cd137 are enhanced in sera of leukemia and lymphoma patients and are strongly associated with chronic lymphocytic leukemia. *Leukemia* (2005) 19(5):883–5. doi: 10.1038/sj.leu.2403675

40. Rossi E, Zizzari IG, Di Filippo A, Acampora A, Pagliara MM, Sammarco MG, et al. Circulating immune profile can predict survival of metastatic uveal melanoma patients: results of an exploratory study. *Hum Vaccin Immunother* (2022) 18 (3):2034377. doi: 10.1080/21645515.2022.2034377

41. Michel J, Langstein J, Hofstadter F, Schwarz H. A soluble form of Cd137 (Ila/4-1bb), a member of the tnf receptor family, is released by activated lymphocytes and is detectable in sera of patients with rheumatoid arthritis. *Eur J Immunol* (1998) 28 (1):290–5. doi: 10.1002/(SICI)1521-4141(199801)28:01<290::AID-IMMU290>3.0.CO;2-S

42. Kachapati K, Bednar KJ, Adams DE, Wu Y, Mittler RS, Jordan MB, et al. Recombinant soluble Cd137 prevents type one diabetes in nonobese diabetic mice. *J Autoimmun* (2013) 47:94–103. doi: 10.1016/j.jaut.2013.09.002

43. Labiano S, Palazon A, Bolanos E, Azpilikueta A, Sanchez-Paulete AR, Morales-Kastresana A, et al. Hypoxia-induced soluble Cd137 in malignant cells blocks Cd137l-costimulation as an immune escape mechanism. *Oncoimmunology* (2016) 5(1): e1062967. doi: 10.1080/2162402X.2015.1062967

44. Seifert L, Plesca I, Muller L, Sommer U, Heiduk M, von Renesse J, et al. Lag-3-Expressing tumor-infiltrating T cells are associated with reduced disease-free survival in pancreatic cancer. *Cancers (Basel)* (2021) 13(6):1297. doi: 10.3390/cancers13061297

45. Li N, Workman CJ, Martin SM, Vignali DA. Biochemical analysis of the regulatory T cell protein lymphocyte activation gene-3 (Lag-3; Cd223). *J Immunol* (2004) 173(11):6806–12. doi: 10.4049/jimmunol.173.11.6806

46. Shapiro M, Herishanu Y, Katz BZ, Dezorella N, Sun C, Kay S, et al. Lymphocyte activation gene 3: a novel therapeutic target in chronic lymphocytic leukemia. *Haematologica* (2017) 102(5):874–82. doi: 10.3324/haematol.2016.148965

47. Machiraju D, Wiecken M, Lang N, Hulsmeyer I, Roth J, Schank TE, et al. Soluble immune checkpoints and T-cell subsets in blood as biomarkers for resistance to immunotherapy in melanoma patients. *Oncoimmunology* (2021) 10(1):1926762. doi: 10.1080/2162402X.2021.1926762

48. Montalban-Hernandez K, Casalvilla-Duenas JC, Cruz-Castellanos P, Gutierrez-Sainz L, Lozano-Rodriguez R, Avendano-Ortiz J, et al. Identification of Ssiglec5 and Slag3 as new relapse predictors in lung cancer. *Biomedicines* (2022) 10(5):1047. doi: 10.3390/biomedicines10051047

49. Botticelli A, Zizzari IG, Scagnoli S, Pomati G, Strigari L, Cirillo A, et al. The role of soluble Lag3 and soluble immune checkpoints profile in advanced head and neck cancer: a pilot study. *J Pers Med* (2021) 11(7):651. doi: 10.3390/jpm11070651

50. Li N, Jilisihan B, Wang W, Tang Y, Keyoumu S. Soluble Lag3 acts as a potential prognostic marker of gastric cancer and its positive correlation with Cd8+T cell frequency and secretion of il-12 and inf-gamma in peripheral blood. *Cancer biomark* (2018) 23(3):341–51. doi: 10.3233/CBM-181278

51. Fridman WH, Pages F, Sautes-Fridman C, Galon J. The immune contexture in human tumours: impact on clinical outcome. *Nat Rev Cancer* (2012) 12(4):298–306. doi: 10.1038/nrc3245

52. Zappasodi R, Sirard C, Li Y, Budhu S, Abu-Akeel M, Liu C, et al. Rational design of anti-Gitr-Based combination immunotherapy. *Nat Med* (2019) 25(5):759–66. doi: 10.1038/s41591-019-0420-8

53. Zhu MMT, Burugu S, Gao D, Yu J, Kos Z, Leung S, et al. Evaluation of glucocorticoid-induced tnf receptor (Gitr) expression in breast cancer and across multiple tumor types. *Mod Pathol* (2020) 33(9):1753–63. doi: 10.1038/s41379-020-0550-z

54. Wang Q, Ye Y, Yu H, Lin SH, Tu H, Liang D, et al. Immune checkpoint-related serum proteins and genetic variants predict outcomes of localized prostate cancer, a cohort study. *Cancer Immunol Immunother* (2021) 70(3):701–12. doi: 10.1007/s00262-020-02718-1

55. Richards DM, Marschall V, Billian-Frey K, Heinonen K, Merz C, Redondo Muller M, et al. Hera-gitrl activates T cells and promotes anti-tumor efficacy independent of fcgammar-binding functionality. *J Immunother Cancer* (2019) 7 (1):191. doi: 10.1186/s40425-019-0671-4

56. Ning Z, Liu K, Xiong H. Roles of btla in immunity and immune disorders. *Front Immunol* (2021) 12:654960. doi: 10.3389/fimmu.2021.654960

57. Cheng T-Y, Liu Y-J, Yan H, Xi Y-B, Duan L-Q, Wang Y, et al. Tumor cell-intrinsic btla receptor inhibits the proliferation of tumor cells Via Erk1/2. *Cells* (2022) 11(24):4021. doi: 10.3390/cells11244021

frontiers | Frontiers in Immunology

TYPE Mini Review
PUBLISHED 15 May 2023
DOI 10.3389/fimmu.2023.1175343

Check for updates

OPEN ACCESS

EDITED BY
Xi Cheng,
Shanghai Jiao Tong University, China

REVIEWED BY
Bo Feng,
Shanghai Jiao Tong University, China
Cheng-Cheng Zhang,
Army Medical University, China

*CORRESPONDENCE
Wei Zhang
weizhang2000cn@163.com
Guanyu Yu
yuguanyu0451@163.com
Fuao Cao
caofuao@gmail.com

†These authors have contributed equally to this work

RECEIVED 27 February 2023
ACCEPTED 24 April 2023
PUBLISHED 15 May 2023

CITATION
Wen R, Zhou L, Peng Z, Fan H, Zhang T, Jia H, Gao X, Hao L, Lou Z, Cao F, Yu G and Zhang W (2023) Single-cell sequencing technology in colorectal cancer: a new technology to disclose the tumor heterogeneity and target precise treatment.
Front. Immunol. 14:1175343.
doi: 10.3389/fimmu.2023.1175343

COPYRIGHT
© 2023 Wen, Zhou, Peng, Fan, Zhang, Jia, Gao, Hao, Lou, Cao, Yu and Zhang. This is an open-access article distributed under the terms of the Creative Commons Attribution License (CC BY). The use, distribution or reproduction in other forums is permitted, provided the original author(s) and the copyright owner(s) are credited and that the original publication in this journal is cited, in accordance with accepted academic practice. No use, distribution or reproduction is permitted which does not comply with these terms.

Single-cell sequencing technology in colorectal cancer: a new technology to disclose the tumor heterogeneity and target precise treatment

Rongbo Wen†, Leqi Zhou†, Zhiying Peng†, Hao Fan, Tianshuai Zhang, Hang Jia, Xianhua Gao, Liqiang Hao, Zheng Lou, Fuao Cao*, Guanyu Yu* and Wei Zhang*

Department of Colorectal Surgery, Changhai Hospital, Naval Medical University, Shanghai, China

Colorectal Cancer (CRC) is one of the most common gastrointestinal tumors, and its high tumor heterogeneity makes traditional sequencing methods incapable of obtaining information about the heterogeneity of individual cancer cells in CRC. Therefore, single-cell sequencing technology can be applied to better analyze the differences in genetic and protein information between cells, to obtain genomic sequence information of single cells, and to more thoroughly analyze the cellular characteristics and interactions in the CRC microenvironment. This will provide a more comprehensive understanding of colorectal cancer development and metastasis and indicate the treatment plan and prognosis. In this study, we review the application of single-cell sequencing to analyze the tumor microenvironment of CRC, explore the mechanisms involved in CRC metastasis and progression, and provide a reference for potential treatment options.

KEYWORDS

colorectal cancer, single-cell sequencing, tumor heterogeneity, tumor microenvironment, precise treatment

1 Introduction

Colorectal cancer (CRC) is one of the most common gastrointestinal tumors and is reported to have the third-highest morbidity and second-highest mortality worldwide (1). Additionally, approximately 50% of patients are diagnosed with metastatic CRC (mCRC) at the first visit, and the 5-year survival rate is no more than 50% (2). Tumor heterogeneity is a result of differences in genetic and molecular characteristics between individual cancer cells due to different degrees of cell differentiation in the same tumor tissue (3). The tumor microenvironment (TME) interacts with tumor heterogeneity to promote differentiation into different cell subtypes and metastatic spread, thus participating in the cancer

development process (4, 5). CRC is highly heterogeneous; however, traditional sequencing methods target the entire tumor tissue, which can only reflect the total characteristics of the cell population and cannot obtain information on cell heterogeneity (6). Single-cell sequencing (SCS) sequences single cells at the genome or transcriptome level to obtain genomic, transcriptomic, or other information about individual cells, thereby revealing cell population differences and evolutionary relationships (7, 8). Therefore, studies conducted on individual cells can be more precisely localized to cell-to-cell interactions and are more conducive to detecting heterogeneity among individual cancer cells, thus exploring the complex heterogeneous mechanisms involved in the development of CRC, further clarifying diagnosis, improving prognostic analysis, and monitoring drug efficacy. Recently, SCS technology has been applicated in more and more studies and reported to help achieve considerable breakthrough in many other tumors including lung cancer, breast cancer and prostate cancer (9–11). Here, we review the studies of SCS in colorectal cancer and provide researchers with a reference for better understanding the tumor characteristics from multiple dimensions (Table 1) exploring its clinical application potential, and directing precise treatment.

2 Application of SCS for in-depth analysis of CRC TME

The TME is a complex integrated system composed of tumor cells, various cytokines, chemokines, and multiple stromal cells, including immune inflammatory cells, cancer-associated fibroblasts, and endothelial cells. These can be divided into immune microenvironments, which are dominated by immune cells, and non-immune microenvironments, which are dominated by fibroblasts (27). Tumor cells are closely related to TME. Tumor cells can influence its microenvironment by releasing cell signaling molecules to promote tumor angiogenesis and induce immune tolerance, while immune cells in the microenvironment can influence tumor cells growth and development. Several studies have shown that changes of TME are closely related to cancer development, invasion, and metastasis, and immunotherapy efficacy can be predicted by distinguishing different TME subtypes (28–30). Therefore, the application of SCS technology for in-depth analysis of the CRC TME is a hot research area, and many research results have laid the foundation for future molecular typing and treatment of CRC.

2.1 Tumor cells

CRC is characterized by genomic instability, epigenetic abnormalities, and abnormal gene expression (31). This has led to high tumor heterogeneity in patients with CRC. Tumor heterogeneity in CRC can be divided into inter- and intra-tumor heterogeneity. CRC inter-tumor heterogeneity may originate from human embryonic development, where different embryonic layers develop as proximal and distal colon, and hypermutated tumors with microsatellite instability (MSI) are often located in the proximal colon, while tumors in the distal colon or rectum usually exhibit microsatellite stability (MSS) and chromosomal instability (CIN) (32). CRC intra-tumor heterogeneity (ITH) may also occur due to differences in cancer cells and TME within the tumor, further complicating the development of new therapeutic strategies and biomarker identification (33). ITH is detectable within a single tumor in which cancer cell subpopulations with different genome features coexist in a patient in different tumor areas or may differ over time (34–36). Exploring the ITH within single tumor is the advantage of SCS technology.

CRC cells are similar to normal cells to some extent but exhibit individualized phenotypic diversity at the same time. Through analyzing the single-cell RNA sequencing (scRNA-seq) data of metastatic CRC patients, Lee HO et al. found that the differentiation trajectory of CRC cells was similar to that of normal epithelial cells, with aggregation of tumor cells with normal stem cell-like/transporter-amplified cell populations. This suggests that tumor epithelial cells have regenerative and proliferative potential, while clustering analysis showed that tumor epithelial cells have highly variable transcriptional status and individual variability (12). Another study also confirmed the similarity between CRC-like organs and normal-like organs at the patient-derived tumor organoids (tumor PDOs) level, but with molecular phenotypic diversity. scRNA-seq analysis of paired cancer and normal tissue organoid models from patients with MSS sporadic early-onset CRC (EOCRC) resulted in the observation of significant molecular phenotypic diversity, including PTPRK-RSPO3 fusions, and RSPO fusion organoids were similar to normal colon organoids with high BMP2 and low PTK7 expression, which confirms the similarity between RSPO fusion organs and normal organs (13). In addition, a study confirmed the heterogeneity of copy number alterations in tumor PDO by single-cell karyotype sequencing and showed that monoclonal lines evolved new karyotypes over time *in vitro*, suggesting that chromosomal instability and karyotype evolution persist in human colon cancer carcinoids (14). In another study using tumor PDOs and biopsy tumors, it was demonstrated that karyotypic alterations of varying complexities are prevalent and can occur within several cell generations (37). Both studies corroborate the existence of complex karyotypic alterations and evolution in CRC, resulting in high intratumoral heterogeneity.

Meanwhile, RNA metabolic markers and RNA velocity assessments revealed CRC cell development trajectories along the mitogen-activated protein kinase (MAPK) pathway in tumor PDOs, whereas normal colon organoid cells develop along a hierarchy of WNT activity, highlighting that cancer cell development is a driver of non-genetic cancer cell heterogeneity and that changes in trajectories affect the effectiveness of targeted therapies (15). Roerink et al. concluded that CRC cells exhibit extensive mutational diversity and carry several times more somatic mutations than normal colorectal cells. Most mutations are acquired during the final dominant clonal expansion of cancer cells and are caused by mutations that are absent in normal colorectal cells. Specific somatic mutations can result in different responses to chemotherapy and targeted therapy (16). This suggests that CRC cell development, clonal expansion, and mutations

TABLE 1 Overview of key findings in CRC SCS technology.

Type of Sample	Species	Cell Infiltration	Lineages represented	Key finding	Sequencing Technology	Reference
CRC tissues and nonmalignant colon tissues	Human	Tumor tissues: • SPP1 + macrophages • Th17 cells • Treg cells • CD8 + T cells • Myofibroblasts • IgG+ plasma cells Normal mucosa: • γδT cells • Matrix fibroblasts • CD4 + T cells • IgA+ plasma cells	Epithelia, immune	• An overall increase in myeloid cells and an overall decrease in B cells were observed in tumor tissue compared to normal tissue. • Human colon cancer cells have a multilineage differentiation process of normal colonic epithelial cells. • Myofibroblasts stimulate tumor growth through extensive tissue remodeling and support cancer stem cell survival through Wnt signaling. • The marked expansion of SPP1 + macrophages may play a central role in immunosuppression and tumor progression through osteopontin, and patients with high levels of SPP 1 + expression have a poor prognosis. • T cell subtypes are evenly distributed in normal and tumor tissues: Th17 and Treg cells are mainly distributed in tumor tissues, and γδT cells are abundant in normal mucosa.	10X Chromium	(12)
Paired cancer and normal organoids from microsatellite-stable EOCRC patients	Human			• The observation of molecular phenotypic diversity, including PTPRK-RSPO3 fusions. • Discovery of the similarity between RSPO fusion-like organs and normal-like organs, with high BMP2 and low PTK7 expression.	WES, WGS, 10X Chromium	(13)
Tumor PDOs	Human			• Discovery of the heterogeneity of copy number alterations in tumor PDOs. • Chromosomal instability and karyotype evolution persist in human colon cancer carcinoids.	scKaryo-seq	(14)
Fresh normal colon and colorectal cancer tissues	Human	Definition of six transcriptome-based states of CRC cells: • Stem/TA-like • Goblet cell-like • TC1-4 Be found in colorectal polyp and cancer cell: • Stem/TA-like TC1-4	Epithelia, immune	• Definiton of patient-overarching colorectal cancer cell clusters characterized by differential activities of oncogenic signaling pathways such as mitogen-activated protein kinase and oncogenic traits such as replication stress. • CRC cell development trajectories follow the MAPK pathway in tumor organoids. • The targeting of EGFR-BRAF-MEK in tumor organoids depends on acquired KRAS/BRAF mutations and induced cellular plasticity rather than the default developmental trajectory that affects signal transduction and gene expression.	10X Chromium	(15)
CRC tissues and adjacent normal intestinal crypts	Human			• CRC cells carry several times more somatic mutations than normal colorectal cells, which is more likely acquired during the final dominant clonal expansion of the cancer. • Genetic diversification of each cancer is accompanied by pervasive, stable and inherited differences in the biological states of individual cancer cells.	single-cell genome sequencing, WGS	(16)
Lung cancer, CRC, ovary cancer and breast cancer tissues	Human	• B cells • Treg cells • CD8+ T cells CD4+ T cells	Endothelia, immune	• T cells are the most common cell type found in tumor tissue. • Tissue specificity of endothelial cells is restricted to normal tissue. • Fibroblasts are a cell type shared by a variety of tissues, showing the highest cancer type specificity. • Colon-specific subsets mainly exist in normal tissue.	10X Chromium CITE-seq	(17)

(Continued)

TABLE 1 Continued

Type of Sample	Species	Cell Infiltration	Lineages represented	Key finding	Sequencing Technology	Reference
				• Dendritic cells and T cells present low -tissue-specific. • B cells, except plasma cells in mucosa-rich normal colon, all other tumors are rich in B cells. • In myeloid cells, other myeloid cell subsets exist in all cancer types, except for the resident alveolar macrophages.		
CRC tissues, Liver metastasis tissues and adjacent tissues	Human Mouse	CRLM: • CD8+ T cells • CD4+ T cells • NK cells • B cells Liver Metastasis: • SPP1+ macrophages • MRC1+ macrophages • CCL18+ macrophages	Immune	• Further developed scMetabolism, a computational pipeline to quantify single-cell metabolism, and observed that these macrophages have enhanced metabolic activity. • Provided a single-cell and spatial map of colorectal liver metastases and identified highly metabolically activated MRC 1 + CCL 18 + m2-like macrophages at the metastatic site. • Efficient neoadjuvant chemotherapy can slow the metabolic activation, increasing the possibility of targeting metabolic pathways in metastasis.	10X Chromium	(18)
CRC tissues and adjacent normal tissues	Human	• Tumor tissues: • CTLA4+ Tregs • CTLA4- Tregs • Th 1/Th 17 cells with high CXCL13 expression • Macrophages Adjacent normal tissues: • Naive T cells (CD8-TCF 7 and CD4-CCR 7) • Tex cells (CD8-HAVCR2)	Immune	• CXCL13 + T cells may perform similar functions in microsatellite unstable (MSI) tumors and are associated with a high response rate to checkpoint blockade. • Discovery of reduction of antigen presentation and anti-tumor immunity of CD40 + and CD27 + cells in tumors. • Communication between non-immune cells and immune cells expanded significantly in the tumor.	10X Chromium	(19)
CRC tissues and liver metastasis	Human	• B cells(early tumor) • Plasma cells (advanced tumor): IgA+IGLC2+ plasma cells	Immune	• B cells in early CRC tumors are predominantly pre-B-like cells with tumor suppression capacity, whereas B cells in advanced CRC tumors develop as plasma cells. • The interaction between CCL 8 + cycling B cells and CCR 5 + T cells may play an antitumor role in advanced CRC. • T-cell anti-tumor responses are activated in CRC tumors, and in the tumor microenvironment, T-cell responses are attenuated by myeloid cells.	Smart-seq2 DNBelab C4	(20)
CRC tissues and adjacent normal tissues	Human	• CD8+ Tem cells • Tex cells • Effector T cells • Th17 cells • Th1-like cells with high expression of CXCL13 • Intraepithelial	Immune, endothelia	• Together, the tumor microenvironment and TCR affected the transformation of tumor-infiltrating CD8 effector memory T cells to exhausted T cells and effector T cells. • Among CRC patients, MSI/dMMR patients showed a significantly better therapeutic response to immune checkpoint inhibitors than did MSS patients. • Intraepithelial lymphocytes and Th 17 cells were more enriched in CRC patients than in liver and lung cancer.	Smart-seq2	(21)

(Continued)

TABLE 1 Continued

Type of Sample	Species	Cell Infiltration	Lineages represented	Key finding	Sequencing Technology	Reference
		lymphocytes (CD160+)				
CRC tissues, liver metastasis tissues, blood and adjacent normal tissues	Human	• CD8+T cells a. IEL b. Tex c. MAIT • CD4+T cells a. Th17 b. Th1-like c. IL10+ Treg d. CTLA4+ Treg • Macrophages a. FCN1+ RTM b. C1QC+ TAM c. NLRP3+ RTM d. PLTP+ RTM e. CXCL12+ RTM f. MKI67+ TAM g. SPP1+ TAM • DCs a. LAMP3+ cDC b. CD1C+ cDC2 c. DC3 d. FCN1+ cDC2 e. TIMP1+ cDC2	Immune	• The CD8+ Texs are malignancy-related and TCR-dependent. • Primary CRC tumors with Liv.Mets may exhibit a stronger immunosuppressive niche compared to non-metastatic CRC tumors. • SPP1+ is mainly found in Liv.Mets as well as the potent phagocytosis of C1QC+ and may play an important role in tumor metastasis. • Proinflammatory DC3 is phenotypically formed by cancer cells in the CRLM.	Smart-seq2	(22)
CRC tissues	Human Mouse	• Treg cells • CD8+ T cells	Immune	• Intratumoral Tregs are characterized by low activity of the MondoA-thiokycin interacting protein (TXNIP) axis and increased glucose uptake. • Inhibition of the MondoA-TXNIP axis promotes glucose uptake and glycolysis, inducing Th 17-like Tregs with high glycolysis, thereby promoting Th 17 inflammation, promoting interleukin 17A-induced CD8+ T cell exhaustion, and driving colorectal cancer. • IL-17A blockers can be coordinated with PD-1 inhibitors in treating AOM-DSS-induced colorectal cancer.	Smart-seq2	(23)
CRC tissues and adjacent normal tissues	Human Mouse	• C1QC+ TAMs • SPP1+ TAMs • Tem cells • Trm cells • DCs • Bhlhe40+ TH1-like cells • CD8+ Tm cells	Immune, mesenchyme	• C1QC+ TAM interacts with a variety of T cells and plays the function of cell phagocytosis and antigen presentation. • SPP1+ TAM mainly interacts with fibroblasts to play the function of promoting angiogenesis and promoting tumor metastasis. • The anti-CSF1R blocking antibody affects the proliferation of macrophages during the cell cycle, specifically deleting a percentage of macrophages with C1QC+ TAM features, but not on macrophages with SPP1+ TAM features. • α CD40 agonists can exert their immunotherapeutic effects by activating DC cells, promoting Bhlhe40 + Th 1 cells, enhancing the migration ability of Tem cells between lymph nodes and tumors and the conversion ability between Tem cells and Trm cell groups.	Smart-seq2	(24)

(Continued)

TABLE 1 Continued

Type of Sample	Species	Cell Infiltration	Lineages represented	Key finding	Sequencing Technology	Reference
CRC tissues	Human Mouse	• ILC1s • ILC2s(ILC2-A, ILC2-B, ILC2-C) • ILC3s • ILCregs	Immune	• ILC1s express inhibitory receptors and undergo inhibitory functional turnover in late CRC. • ILC2-C can promote tumor progression. HS3ST1 and PD1 are highly expressed in ILC2 in advanced CRC tumors, and lack of HS3ST1 or PD1 in ILC2s inhibited tumor growth. • ILC3s transdifferentiate into ILCregs during CRC progression, and ILCregs promotes tumor growth.	10X Chromium	(25)
CRC tissues	Human	• CSCs	Epithelia, Stem cells	• Rare CSCs in CRCs exist in a dormant state and possess high stemness and high WNT, TGF-β and YAP/HIPPO signaling and are able to maintain short telomeres without cell proliferation.	10X Chromium Smart-seq2	(26)

continue to drive intratumor heterogeneity in CRC, making chemotherapy and targeted therapy difficult and promoting drug resistance in patients.

To deeply explore CRC intra-tumor heterogeneity, a study performed optimized single-cell multi-omics sequencing, including DNA, DNA methylation, and transcriptome sequencing, on CRC patients with CRC. This showed that DNA methylation levels in CRC cells were lower than those in normal epithelial cells adjacent to the cancer cells, with different methylation levels varying from different spectra in the same tumor tissue, suggesting that methylation heterogeneity mainly results from differences in DNA methylation between different subclones within the same patient's tumor. This study also elucidated the demethylation characteristics of CRC, where the degree of demethylation was consistent within each subtype but varied across subtypes. Interestingly, long interspersed nuclear element 1 (LINE-1, L1) shows stronger demethylation than L2 in cancer cells, in contrast to embryonic development, suggesting that abnormal demethylation processes may arise in the L1 and heterochromatin regions during tumorigenesis and progression, breaking the normal developmental pattern (38).

2.2 Immune cells

2.2.1 T cell

Various immune cells in the TME interact with tumor cells and mediate immune tolerance to tumors, affecting tumor progression and metastasis, and thus immunotherapy efficacy. T cells, one of the major cellular components involved in the body's immune response and the most common cell type in tumor tissue (17), can kill tumor cells. In order to escape the pursuit of T cells, tumor cells could produce some inhibitory signals on their own surface, and inhibit the immune function of T cells through immune checkpoint (39). Ever since Allison et al. discovered the immunosuppressive effects of CTLA4 on T cells in 1996, immunotherapy drugs, notably immune checkpoint inhibitors (ICIs), have taken off and become a lifesaving drug for tumor patients (40). Various ICIs have been applicated in cancer immunotherapy, including PD1/PDL1 and CTLA4 (41, 42).

However, the efficacy of immunotherapy in patients with CRC is not as good today. Thus, an increasing number of studies have been conducted to analyze the TME in depth using SCS technology.

Several studies have mapped the global cellular landscape in CRC, with an overall increase in myeloid cells and an overall decrease in B-cell numbers observed in tumor tissues compared to normal tissues, suggesting a redirected immune response. This indicates that the immune response undergoes dynamic changes during cancer development and that the transcriptional profile of cancer cells is similar to that of normal human differentiation, with genetic alterations creating an immunosuppressive microenvironment directed by regulatory T cells (Tregs), myofibroblasts, and myeloid cells (12, 18–20). Meanwhile, T cell subtypes are unevenly distributed in normal and tumor tissues, Th17 and Treg cells are mainly distributed in tumor tissues, while γδT cells are more abundant in normal mucosa. The TME and T-cell receptors (TCR) affect the transformation of tumor-infiltrating CD8+ effector memory T cells (Tems) into exhausted T cells (Texs) and effective T cells (Teffs), indicating the transformation of the organism from mucosal immunity to inhibiting cellular immunity (12, 21).

A study analyzing CD45+ cells from multiple matched tissues of patients with untreated primary hepatocellular carcinoma (HCC), CRC, and CRC liver metastases (CLM) found that Texs and activated Tregs originate from primary CRC tumors with a malignancy-related phenotype and are TCR-dependent. There is a high degree of TCR sharing between Tems and Texs. Natural killer (NK) cells and mucosa-associated T cells are mainly derived from the liver tissue at metastatic foci, and their phenotypes are associated with the liver TME (22). Another study similarly found decreased B-cell antigen presentation as well as tumor-specific Tregs and their two subtypes, proliferative exhausted T cells and a predominance of naive T cells (CD8-TCF7 and CD4-CCR7) in adjacent tissues and exhausted T cells in tumors (CD8-HAVCR2). Th1/Th17 cells with high CXCL13 expression are preferentially enriched in patients with a high tumor mutational burden (TMB) and respond well to immunotherapy (19), suggesting that CXCL13+ T cells may perform functions similar to those of MSI tumors and are associated with a high response rate to checkpoint blockade. The results of these two studies are consistent, suggesting that the exhausted T cell phenotype is associated with malignancy and that CXCL13+ T cells may be associated with

immunotherapy. Moreover, CXCL13 expression accurately identifies both tumor-specific T cell clones that are terminally differentiated and highly exhausted and tumor-specific T cell precursor cell clones that are abundantly present in responding tumors after immune checkpoint blockade (ICB) treatment, demonstrating that tumor-specific CXCL13+CD8+ T cells play a key role in the treatment process and that the degree of infiltration before treatment can predict ICB efficacy (43).

It was also found that in tissue samples from CRC patients, impaired T cell proliferation and activation were associated with ZFP91, which disrupts the metabolic pathways and antitumor activity of tumor-infiltrating T cells, suggesting that targeting ZFP91 may improve the effectiveness of tumor immunotherapy (44). The transcription factor TCF-1 is critical for Treg development and function and primarily inhibits the transcription of genes that co-bind with FOXP3. Deficiency of TCF-1 could activate Treg cells and make Th17 cells acquire the intestinal homing characteristics, leading to more dangerous and dramatic CRC, and the specific TCF-1 expression of Tregs regulates inflammation and CD8+ T cell toxicity and may determine the prognosis of CRC (45). Similarly, the glucose-responsive transcription factor MondoA is highly expressed in Tregs, and inhibition of the MondoA-TXNIP axis promotes glucose uptake and glycolysis, inducing highly glycolytic Th17-like Tregs, which promotes Th17 inflammation and CRC development (23).

2.2.2 Cancer-associated fibroblasts

In addition to T cells, the most common cells in the TME, cancer-associated fibroblasts (CAF), and tumor-associated macrophages (TAMs), are also being explored and analyzed with the development of SCS technology.

Somatic copy number alterations (SCNAs) are prevalent in the TME and immune cells, fibroblasts, and endothelial cells in the normal tissues of each individual, and the proportion of fibroblasts with genomic copy number variants is much higher in tumor tissues than in adjacent issues, so that it can predict the prognosis of CRC by screening the differentially expressed genes of CAFs in tumor tissues. Five genes (BGN, RCN3, TAGLN, MYL9, and TPM2) have been identified as specific CAFs biomarkers of poor prognosis in CRC (46). Fibroblasts are a cell type common to multiple tissues and exhibit the highest cancer-type specificity (17). In addition, myofibroblasts have been shown to stimulate tumor growth through extensive tissue remodeling and support cancer stem cell survival through WNT signaling (12), indicating that fibroblasts also play a role in promoting tumor growth, and that genetic alterations in fibroblasts could incur CRC *via* paracrine signaling in epithelial cells (47).

2.2.3 Tumor-associated macrophages

TAMs are infiltrating macrophages in tumor tissue, mainly derived from monocyte differentiation. TAMs can interact with tumor cells through exosomes or secrete multiple cytokines to promote tumor cell proliferation, invasion, migration, and angiogenesis.

TAMs recruit Tregs through chemokine CCL2 secretion, which inhibits the antitumor immune response of T cells and interferes with immune cell interactions, thus leading to an immunosuppressive microenvironment in CRC (48). TAMs in CRC can be divided into two cell groups, SPP1+ TAM and C1QC + TAM. C1QC+ TAM interacts with various T cells and performs cytophagic and antigen-presenting functions, whereas SPP1+ TAM interacts mainly with fibroblasts and performs pro-angiogenic and tumor-promoting functions (24). Single-cell analysis of CLM samples showed that a subpopulation of dendritic cells (DC3s) and SPP1+ macrophages is associated with malignancy and plays a critical role in liver metastasis (22). Additionally, a study detected numerous immunosuppressive cells in CRC liver metastatic tumors, with a dramatic increase in SPP1+ macrophages and MRC1+ CCL18+ macrophages and an enrichment of neutrophils as potential participants in liver metastases (18). A previous study also showed that significant expansion of SPP1+ macrophages may play a central role in immunosuppression and tumor progression through bone bridge proteins and that CRC patients with high SPP1 + expression levels have a poorer prognosis (12). These studies confirm the role of SPP1+ macrophages in promoting CRC progression and the potential suppressive TME in liver metastasis. In addition, one study showed that the density of TAMs was not associated with survival in patients with CLM, but the area and circumference of TAMs were significantly higher in CLMs, while larger morphologies of TAMs were mostly observed in patients with a poorer prognosis (49), which demonstrated the strong prognostic significance of the morphological representation of TAM.

2.2.4 Intrinsic lymph-like cell

Intrinsic lymphocytes (ILCs) are located on the mucosal surface and include NK cells; helper classes ILC1s, ILC2s, and ILC3s; and lymphoid tissue-inducing (LTi) cells that enhance the immune response, maintain mucosal integrity, and sustain tissue homeostasis (25, 50).

One study analyzed tumor-infiltrating ILCs during CRC progression using scRNA-seq and classified them into six clusters. ILC1 expressed inhibitory receptors and underwent an inhibitory functional transformation in advanced CRC, and ILC2 was divided into three subgroups (ILC2-A, -B, and -C), of which the ILC2-C subgroup promoted tumor progression. HS3ST1 and PD1 are highly expressed in ILC2 of advanced CRC In addition, ILC3 transdifferentiates into ILCregs during CRC progression and promotes tumor growth. Notably, the TGF-β signaling pathway initiated the conversion of ILC3 to ILCregs. Therefore, this study suggests that interfering with ILC conversion may be a potential strategy for CRC immunotherapy (25). Moreover, another study reported single-cell characteristics of blood and intestinal helper ILC subtypes in healthy conditions and CRC, where the healthy intestine contained ILC1s, ILC3s, and ILC3/NKs, but not ILC2s, while additional tumor-specific ILC1 and ILC2 subtypes were identified in CRC patients. SLAMF1 (signaling lymphocyte-activating molecule family member 1, CD150) was selectively expressed on tumor-specific ILCs, and higher levels of SLAMF1+ ILCs were observed in the blood of patients with CRC. The survival rate of patients with CRC in the high SLAMF1 group was significantly higher than that in the low SLAMF1 group, indicating that SLAMF1 is an antitumor biomarker of CRC (50).

3 Application of SCS to explore mechanisms affecting CRC metastasis & progression

3.1 CRC liver metastasis

CLM is the leading cause of death from CRC and a major factor in reducing the survival time of CRC patients (51). Besides the rapid metastatic spread of cancer cells, TME with liver metastasis exhibits a highly immunosuppressive phenotype (52). A previous study observed a dramatic increase in SPP1+ and MRC1+ CCL18+ macrophages in metastatic tumors, which corroborated the potentially suppressive TME in liver metastases. Meanwhile, TAM may be suppressed in metastatic tumors, liver metastatic cells may preferentially reprogram macrophages and induce their specific functional states, and metastatic tumor cells in liver metastases preferentially express the ligand CD47 and thus may recruit or activate MRC1+ CCL18+ macrophages through the corresponding receptor SIRPA, suggesting that specific macrophage subpopulations may play a fundamental role in the formation of premetastatic niche in CLM (18).

In addition, studies have revealed rare mutations in metastatic tumors and defined two separate cell populations by analyzing single-cell sequencing data from primary and metastatic foci in patients with CRC and liver metastases, suggesting different evolutionary trajectories between primary and metastatic tumor cells. Meanwhile, extensive WES data reflect different mutant allele frequencies between primary and metastatic foci. TP53, APC, and SNVs in SMAD4 show an increase in variant allele frequency (VAF) in metastatic samples (53).

3.2 Cancer stem cells

Cancer stem cells (CSCs) are thought to proliferate extensively and drive tumor growth, indicating that malignant cell populations in tumors are generated by CSCs (54). A previous study found that each tumor gland was derived from a stem cell by genomic analysis of 349 individual tumor glands, and they found that after initial transformation, CRC tumors grew primarily as a single expansion comprising many intermixed subclones, and it was then proposed that most of the mutations driving tumor growth occurred during early tumor expansion and led to clonal diversity and intra-tumor heterogeneity (55).

Currently, it has been suggested that CSCs may contribute to tumor progression and drug resistance. By single-cell sequencing of telomerase and transcriptome in 8 primary foci of untreated CRC, it was shown that CSCs can be remodeled into cancer epithelial cells and both of them retain the important signaling pathway such as WNT, TGF-β, and HIPPO/YAP. In addition, proliferating tumor epithelial cells were found to be derived from resting CSCs, which are related to the recurrence and metastasis of tumors, and resting CSCs may develop drug resistance through mutations (26).

3.3 CRC genomic/chromosomal mutations

Continued high-frequency chromosomal instability (CIN) has a dramatic impact on tumor evolution and treatment response. A previous study showed that CIN is prevalent in CRC, and single-cell karyotyping sequencing confirmed the heterogeneity of copy number alterations in tumor PDOs and showed that monoclonal lines evolved new karyotypes over time *in vitro* (14). Abnormal DNA methylation at the chromosomal level has also been found in CRC cells, where six chromosomes (chromosomes 4, 5, 8, 13, 18, and X) tend to undergo intense DNA demethylation, with three hypomethylated chromosomes (chromosomes 8, 13, and 18) (46), which confirms that CRC is characterized by genomic instability.

In addition, it has been found that CRC cells usually develop along the mitogen-activated protein kinase (MAPK) pathway, while MAPK activity will drive the cellular trajectory of cancer cells, and the targeting of EGFR-BRAF-MEK in tumor-like organs depends on acquired KRAS/BRAF mutations and induced cellular plasticity, which affects signal transduction and gene expression (15). Furthermore, a study showed a significantly increased somatic mutation rate in CRC cells compared to normal colorectal cells; the presence of driver mutations such as BRAF (V600E), PIK3CA (E81K), and ACVR2A (protein truncated small indel); as well as MLH1 methylation and genetic diversification in each cancer, accompanied by generalized, stable and genetic differences (16).

4 Application of SCS to explore and improve CRC treatment

4.1 Immunotherapy targets

Current immunotherapies for metastatic CRC are effective only in tumors with high microsatellite instability or mismatch repair defects. As tumor cells can determine their immune microenvironment and often form an immunosuppressive microenvironment (12), current immune checkpoint inhibitors (ICIs) are not effective against tumors with proficient mismatch repair (pMMR), MSS, or low-frequency microsatellite instability (MSI-L) (called pMMR-MSI-L tumors) (56). Therefore, finding new immunotherapy targets or improving current immunotherapy to expand the range of CRC immunotherapies has become an area of research interest.

A study found that T-cell antigen receptor-dependent cytoplasmic translocation of ZFP91 promotes the assembly of the PP2A complex, thereby limiting mTORC1-mediated metabolic reprogramming, suggesting that ZFP91 interferes with the metabolic and functional state of T cells in the TME, suggesting that targeting ZFP91 may improve the efficacy of CRC immunotherapy (44).

In addition, a study indicated that anti-CSF1R treatment preferentially depletes macrophages with inflammatory features but avoids macrophage populations expressing pro-angiogenic/

tumorigenic genes in mice and humans. Treatment with CD40 agonist antibodies preferentially activates conventional dendritic cell (cDC) populations with increased Bhlhe40+ Th1-like cells and CD8+ memory T cells and identified key cellular interactions that regulate tumor immunity and mechanisms for myeloid-targeted immunotherapy currently in clinical trials (24).

4.2 Causes of chemotherapy sensitivity

Currently, the primary treatment for CRC is surgical resection combined with radiotherapy, chemotherapy, and targeted therapy. However, some patients undergoing chemotherapy may develop drug resistance, resulting in reduced efficacy.

One study developed a scMetabolism system to provide a single-cell and spatial atlas of colorectal liver metastases and identified highly metabolically activated MRC1+ CCL18+ M2-like macrophages at metastatic sites. Efficient neoadjuvant chemotherapy can slow metabolic activation and increase the possibility of targeting metabolic pathways in metastases (18).

In addition, another study confirmed the strong response of the CMS2 epithelial/typical group to EGFR and HER2 inhibitors by translating consensus molecular typing (CMS) preclinical models of developing cancer cells adapted to CMS classifiers combined with high-throughput drug sensitivity screening and revealed that cells with CMS1 microsatellite instability/immunity and CMS4 mesenchymal phenotypes were strongly sensitive to HSP90 inhibitors. A combination of 5-fluorouracil and HSP90 inhibitor has the potential to relieve drug resistance and improve treatment efficacy in a CMS4 patient-derived xenograft (PDX) model (57).

5 Summary

Tumor heterogeneity is widespread in CRC patients, and cluster analysis shows that tumor epithelial cells are individualized for each patient and are highly mutated Various immune cells and inflammatory chemokines in the TME interact and influence each other to promote tumor progression, thus affecting tumor recurrence and treatment response and adversely affecting the prognosis of CRC patients. While the impact of the TME on CRC can be fully investigated by obtaining information on cancer cell characteristics through SCS, it is also possible to identify relevant predictive markers for CRC prognosis and potential immunotherapeutic targets through SCS, thus improving patient prognosis and therapeutic effects. In addition, the use of SCS technology for drug development and for addressing the problem of chemotherapy resistance in some patients is now emerging (31). It is expected to be applied in precision medicine to develop and personalize cancer medical treatments, providing a more accurate diagnosis and the best-individualized treatment plan for cancer patients.

However, SCS technology still has some limitations in current platform. First, SCS technology requires high levels of sample preparation and sample quality, including cell quantity and activity, which increased the combined cost. Second, although the number of cells that can be detected from SCS has increased from 10~100 to tens of thousands with the development of technology, the tedious process still results in the loss of some cell populations, which can bias the results. In addition, SCS technology lacks of spatial information. Thus, a combination of multiple sequencing methods including bulk sequencing, spatial transcriptomics and SCS technology could be a solution and future direction of development.

Author contributions

WZ, GY and FC designed the research. RW, LZ and ZP made substantial contributions to acquisition, analysis and interpretation of data, and wrote the manuscript. HF, TZ, HJ, XG, ZL and LH coordinated and were involved in acquisition, interpretation of the data. WZ, GY and FC revised it critically for important intellectual content and gave final approval of the version to be published.

Funding

National Natural Science Foundation of China(82072750, 82203137), Natural Science Fund of Shanghai(20ZR1457200), Shanghai Sailing Program(21YF1459300), 71st Batch of China Postdoctoral Science Foundation (48804), and Excellent doctoral dissertation training program of Naval Medical University.

Conflict of interest

The authors declare that the research was conducted in the absence of any commercial or financial relationships that could be construed as a potential conflict of interest.

Publisher's note

All claims expressed in this article are solely those of the authors and do not necessarily represent those of their affiliated organizations, or those of the publisher, the editors and the reviewers. Any product that may be evaluated in this article, or claim that may be made by its manufacturer, is not guaranteed or endorsed by the publisher.

References

1. Sung H, Ferlay J, Siegel RL, Laversanne M, Soerjomataram I, Jemal A, et al. Global cancer statistics 2020: GLOBOCAN estimates of incidence and mortality worldwide for 36 cancers in 185 countries. *CA Cancer J Clin* (2021) 71(3):209–49. doi: 10.3322/caac.21660

2. Engstrand J, Nilsson H, Stromberg C, Jonas E, Freedman J. Colorectal cancer liver metastases - a population-based study on incidence, management and survival. *BMC Cancer* (2018) 18(1):78. doi: 10.1186/s12885-017-3925-x

3. Zhang Y, Song J, Zhao Z, Yang M, Chen M, Liu C, et al. Single-cell transcriptome analysis reveals tumor immune microenvironment heterogenicity and granulocytes enrichment in colorectal cancer liver metastases. *Cancer Lett* (2020) 470:84–94. doi: 10.1016/j.canlet.2019.10.016

4. Hui L, Chen Y. Tumor microenvironment: sanctuary of the devil. *Cancer Lett* (2015) 368(1):7–13. doi: 10.1016/j.canlet.2015.07.039

5. Wu T, Dai Y. Tumor microenvironment and therapeutic response. *Cancer Lett* (2017) 387:61–8. doi: 10.1016/j.canlet.2016.01.043

6. Kulkarni A, Anderson AG, Merullo DP, Konopka G. Beyond bulk: a review of single cell transcriptomics methodologies and applications. *Curr Opin Biotechnol* (2019) 58:129–36. doi: 10.1016/j.copbio.2019.03.001

7. Gawad C, Koh W, Quake SR. Single-cell genome sequencing: current state of the science. *Nat Rev Genet* (2016) 17(3):175–88. doi: 10.1038/nrg.2015.16

8. Lawson DA, Kessenbrock K, Davis RT, Pervolarakis N, Werb Z. Tumour heterogeneity and metastasis at single-cell resolution. *Nat Cell Biol* (2018) 20 (12):1349–60. doi: 10.1038/s41556-018-0236-7

9. Kim C, Gao R, Sei E, Brandt R, Hartman J, Hatschek T, et al. Chemoresistance evolution in triple-negative breast cancer delineated by single-cell sequencing. *Cell* (2018) 173(4):879–93.e13. doi: 10.1016/j.cell.2018.03.041

10. Guo X, Zhang Y, Zheng L, Zheng C, Song J, Zhang Q, et al. Global characterization of T cells in non-small-cell lung cancer by single-cell sequencing. *Nat Med* (2018) 24(7):978–85. doi: 10.1038/s41591-018-0045-3

11. Karthaus WR, Hofree M, Choi D, Linton EL, Turkekul M, Bejnood A, et al. Regenerative potential of prostate luminal cells revealed by single-cell analysis. *Science* (2020) 368(6490):497–505. doi: 10.1126/science.aay0267

12. Lee HO, Hong Y, Etlioglu HE, Cho YB, Pomella V, Van den Bosch B, et al. Lineage-dependent gene expression programs influence the immune landscape of colorectal cancer. *Nat Genet* (2020) 52(6):594–603. doi: 10.1038/s41588-020-0636-z

13. Yan HHN, Siu HC, Ho SL, Yue SSK, Gao Y, Tsui WY, et al. Organoid cultures of early-onset colorectal cancers reveal distinct and rare genetic profiles. *Gut* (2020) 69 (12):2165–79. doi: 10.1136/gutjnl-2019-320019

14. Bolhaqueiro ACF, Ponsioen B, Bakker B, Klaasen SJ, Kucukkose E, van Jaarsveld RH, et al. Ongoing chromosomal instability and karyotype evolution in human colorectal cancer organoids. *Nat Genet* (2019) 51(5):824–34. doi: 10.1038/s41588-019-0399-6

15. Uhlitz F, Bischoff P, Peidli S, Sieber A, Trinks A, Luthen M, et al. Mitogen-activated protein kinase activity drives cell trajectories in colorectal cancer. *EMBO Mol Med* (2021) 13(10):e14123. doi: 10.15252/emmm.202114123

16. Roerink SF, Sasaki N, Lee-Six H, Young MD, Alexandrov LB, Behjati S, et al. Intra-tumour diversification in colorectal cancer at the single-cell level. *Nature* (2018) 556(7702):457–62. doi: 10.1038/s41586-018-0024-3

17. Qian J, Olbrecht S, Boeckx B, Vos H, Laoui D, Etlioglu E, et al. A pan-cancer blueprint of the heterogeneous tumor microenvironment revealed by single-cell profiling. *Cell Res* (2020) 30(9):745–62. doi: 10.1038/s41422-020-0355-0

18. Wu Y, Yang S, Ma J, Chen Z, Song G, Rao D, et al. Spatiotemporal immune landscape of colorectal cancer liver metastasis at single-cell level. *Cancer Discov* (2022) 12(1):134–53. doi: 10.1158/2159-8290.CD-21-0316

19. Mei Y, Xiao W, Hu H, Lu G, Chen L, Sun Z, et al. Single-cell analyses reveal suppressive tumor microenvironment of human colorectal cancer. *Clin Transl Med* (2021) 11(6):e422. doi: 10.1002/ctm2.422

20. Wang W, Zhong Y, Zhuang Z, Xie J, Lu Y, Huang C, et al. Multiregion single-cell sequencing reveals the transcriptional landscape of the immune microenvironment of colorectal cancer. *Clin Transl Med* (2021) 11(1):e253. doi: 10.1002/ctm2.253

21. Zhang L, Yu X, Zheng L, Zhang Y, Li Y, Fang Q, et al. Lineage tracking reveals dynamic relationships of T cells in colorectal cancer. *Nature* (2018) 564(7735):268–72. doi: 10.1038/s41586-018-0694-x

22. Liu Y, Zhang Q, Xing B, Luo N, Gao R, Yu K, et al. Immune phenotypic linkage between colorectal cancer and liver metastasis. *Cancer Cell* (2022) 40(4):424–37.e5. doi: 10.1016/j.ccell.2022.02.013

23. Lu Y, Li Y, Liu Q, Tian N, Du P, Zhu F, et al. MondoA-Thioredoxin-Interacting protein axis maintains regulatory T-cell identity and function in colorectal cancer microenvironment. *Gastroenterology* (2021) 161(2):575–91.e16. doi: 10.1053/j.gastro.2021.04.041

24. Zhang L, Li Z, Skrzypczynska KM, Fang Q, Zhang W, O'Brien SA, et al. Single-cell analyses inform mechanisms of myeloid-targeted therapies in colon cancer. *Cell* (2020) 181(2):442–59.e29. doi: 10.1016/j.cell.2020.03.048

25. Wang S, Qu Y, Xia P, Chen Y, Zhu X, Zhang J, et al. Transdifferentiation of tumor infiltrating innate lymphoid cells during progression of colorectal cancer. *Cell Res* (2020) 30(7):610–22. doi: 10.1038/s41422-020-0312-y

26. Wang H, Gong P, Chen T, Gao S, Wu Z, Wang X, et al. Colorectal cancer stem cell states uncovered by simultaneous single-cell analysis of transcriptome and telomeres. *Advanced Sci (Weinheim Baden-Wurttemberg Germany)* (2021) 8 (8):2004320. doi: 10.1002/advs.202004320

27. Huang HW, Chang CC, Wang CS, Lin KH. Association between inflammation and function of cell adhesion molecules influence on gastrointestinal cancer development. *Cells* (2021) 10(1):67. doi: 10.3390/cells10010067

28. Bader JE, Voss K, Rathmell JC. Targeting metabolism to improve the tumor microenvironment for cancer immunotherapy. *Mol Cell* (2020) 78(6):1019–33. doi: 10.1016/j.molcel.2020.05.034

29. Bagaev A, Kotlov N, Nomie K, Svekolkin V, Gafurov A, Isaeva O, et al. Conserved pan-cancer microenvironment subtypes predict response to immunotherapy. *Cancer Cell* (2021) 39(6):845–65 e7. doi: 10.1016/j.ccell.2021.04.014

30. Schulz M, Salamero-Boix A, Niesel K, Alekseeva T, Sevenich L. Microenvironmental regulation of tumor progression and therapeutic response in brain metastasis. *Front Immunol* (2019) 10. doi: 10.3389/fimmu.2019.01713

31. Angius A, Scanu AM, Arru C, Muroni MR, Carru C, Porcu A, et al. A portrait of intratumoral genomic and transcriptomic heterogeneity at single-cell level in colorectal cancer. *Medicina (Kaunas Lithuania)* (2021) 57(11):1257. doi: 10.3390/medicina57111257

32. Cancer Genome Atlas N. Comprehensive molecular characterization of human colon and rectal cancer. *Nature* (2012) 487(7407):330–7. doi: 10.1038/nature11252

33. Molinari C, Marisi G, Passardi A, Matteucci L, De Maio G, Ulivi P. Heterogeneity in colorectal cancer: a challenge for personalized medicine? *Int J Mol Sci* (2018) 19(12):3733. doi: 10.3390/ijms19123733

34. Navin N, Kendall J, Troge J, Andrews P, Rodgers L, McIndoo J, et al. Tumour evolution inferred by single-cell sequencing. *Nature* (2011) 472(7341):90–4. doi: 10.1038/nature09807

35. Gerlinger M, Rowan AJ, Horswell S, Math M, Larkin J, Endesfelder D, et al. Intratumor heterogeneity and branched evolution revealed by multiregion sequencing. *N Engl J Med* (2012) 366(10):883–92. doi: 10.1056/NEJMoa1113205

36. Driessens G, Beck B, Caauwe A, Simons BD, Blanpain C. Defining the mode of tumour growth by clonal analysis. *Nature* (2012) 488(7412):527–30. doi: 10.1038/nature11344

37. Bollen Y, Stelloo E, Van Leenen P, van den Bos M, Ponsioen B, Lu B, et al. Reconstructing single-cell karyotype alterations in colorectal cancer identifies punctuated and gradual diversification patterns. *Nat Genet* (2021) 53(8):1187–95. doi: 10.1038/s41588-021-00891-2

38. Bian S, Hou Y, Zhou X, Li X, Yong J, Wang Y, et al. Single-cell multiomics sequencing and analyses of human colorectal cancer. *Science* (2018) 362(6418):1060–3. doi: 10.1126/science.aao3791

39. Chen DS, Mellman I. Oncology meets immunology: the cancer-immunity cycle. *Immunity* (2013) 39(1):1–10. doi: 10.1016/j.immuni.2013.07.012

40. Leach DR, Krummel MF, Allison JP. Enhancement of antitumor immunity by CTLA-4 blockade. *Science* (1996) 271(5256):1734–6. doi: 10.1126/science.271.5256.1734

41. Mellman I, Coukos G, Dranoff G. Cancer immunotherapy comes of age. *Nature* (2011) 480(7378):480–9. doi: 10.1038/nature10673

42. Pardoll DM. The blockade of immune checkpoints in cancer immunotherapy. *Nat Rev Cancer* (2012) 12(4):252–64. doi: 10.1038/nrc3239

43. Liu B, Zhang Y, Wang D, Hu X, Zhang Z. Single-cell meta-analyses reveal responses of tumor-reactive CXCL13(+) T cells to immune-checkpoint blockade. *Nat Cancer* (2022) 3(9):1123–36. doi: 10.1038/s43018-022-00433-7

44. Wang F, Zhang Y, Yu X, Teng XL, Ding R, Hu Z, et al. ZFP91 disturbs metabolic fitness and antitumor activity of tumor-infiltrating T cells. *J Clin Invest* (2021) 131(19): e144318. doi: 10.1172/JCI144318

45. Osman A, Yan B, Li Y, Pavelko KD, Quandt J, Saadalla A, et al. TCF-1 controls t (reg) cell functions that regulate inflammation, CD8(+) T cell cytotoxicity and severity of colon cancer. *Nat Immunol* (2021) 22(9):1152–62. doi: 10.1038/s41590-021-00987-1

46. Zhou Y, Bian S, Zhou X, Cui Y, Wang W, Wen L, et al. Single-cell multiomics sequencing reveals prevalent genomic alterations in tumor stromal cells of human colorectal cancer. *Cancer Cell* (2020) 38(6):818–28.e5. doi: 10.1016/j.ccell.2020.09.015

47. Roulis M, Kaklamanos A, Schernthanner M, Bielecki P, Zhao J, Kaffe E, et al. Paracrine orchestration of intestinal tumorigenesis by a mesenchymal niche. *Nature* (2020) 580(7804):524–9. doi: 10.1038/s41586-020-2166-3

48. Wang H, Tian T, Zhang J. Tumor-associated macrophages (TAMs) in colorectal cancer (CRC): from mechanism to therapy and prognosis. *Int J Mol Sci* (2021) 22 (16):8470. doi: 10.3390/ijms22168470

49. Donadon M, Torzilli G, Cortese N, Soldani C, Di Tommaso L, Franceschini B, et al. Macrophage morphology correlates with single-cell diversity and prognosis in

colorectal liver metastasis. *J Exp Med* (2020) 217(11):e20191847. doi: 10.1084/jem.20191847

50. Qi J, Crinier A, Escaliere B, Ye Y, Wang Z, Zhang T, et al. Single-cell transcriptomic landscape reveals tumor specific innate lymphoid cells associated with colorectal cancer progression. *Cell Rep Med* (2021) 2(8):100353. doi: 10.1016/j.xcrm.2021.100353

51. Dekker E, Tanis PJ, Vleugels JLA, Kasi PM, Wallace MB. Colorectal cancer. *Lancet* (2019) 394(10207):1467–80. doi: 10.1016/S0140-6736(19)32319-0

52. Zhou SN, Pan WT, Pan MX, Luo QY, Zhang L, Lin JZ, et al. Comparison of immune microenvironment between colon and liver metastatic tissue in colon cancer patients with liver metastasis. *Digestive Dis Sci* (2021) 66(2):474–82. doi: 10.1007/s10620-020-06203-8

53. Tang J, Tu K, Lu K, Zhang J, Luo K, Jin H, et al. Single-cell exome sequencing reveals multiple subclones in metastatic colorectal carcinoma. *Genome Med* (2021) 13 (1):148. doi: 10.1186/s13073-021-00962-3

54. Frank MH, Wilson BJ, Gold JS, Frank NY. Clinical implications of colorectal cancer stem cells in the age of single-cell omics and targeted therapies. *Gastroenterology* (2021) 160(6):1947–60. doi: 10.1053/j.gastro.2020.12.080

55. Sottoriva A, Kang H, Ma Z, Graham TA, Salomon MP, Zhao J, et al. A big bang model of human colorectal tumor growth. *Nat Genet* (2015) 47(3):209–16. doi: 10.1038/ng.3214

56. Ganesh K, Stadler ZK, Cercek A, Mendelsohn RB, Shia J, Segal NH, et al. Immunotherapy in colorectal cancer: rationale, challenges and potential. *Nat Rev Gastroenterol Hepatol* (2019) 16(6):361–75. doi: 10.1038/s41575-019-0126-x

57. Sveen A, Bruun J, Eide PW, Eilertsen IA, Ramirez L, Murumagi A, et al. Colorectal cancer consensus molecular subtypes translated to preclinical models uncover potentially targetable cancer cell dependencies. *Clin Cancer Res* (2018) 24 (4):794–806. doi: 10.1158/1078-0432.CCR-17-1234

frontiers | Frontiers in Immunology

TYPE Original Research
PUBLISHED 25 May 2023
DOI 10.3389/fimmu.2023.1182409

Check for updates

OPEN ACCESS

EDITED BY
Xi Cheng,
Shanghai Jiao Tong University, China

REVIEWED BY
Sanbin Wang,
The 920th Hospital of Joint Logistics Support Force, China
Juan José Lasarte,
University of Navarra, Spain
Qiang Wang,
Shandong Second Provincial General Hospital, China

*CORRESPONDENCE
Cheng Qian
cqian8634@gmail.com
Zhi Yang
yz2003can@126.com

†These authors have contributed equally to this work

RECEIVED 08 March 2023
ACCEPTED 09 May 2023
PUBLISHED 25 May 2023

CITATION
Zhang C, Wang L, Zhang Q, Shen J, Huang X, Wang M, Huang Y, Chen J, Xu Y, Zhao W, Qi Y, Li Y, Ou Y, Yang Z and Qian C (2023) Screening and characterization of the scFv for chimeric antigen receptor T cells targeting CEA-positive carcinoma.
Front. Immunol. 14:1182409.
doi: 10.3389/fimmu.2023.1182409

COPYRIGHT
© 2023 Zhang, Wang, Zhang, Shen, Huang, Wang, Huang, Chen, Xu, Zhao, Qi, Li, Ou, Yang and Qian. This is an open-access article distributed under the terms of the Creative Commons Attribution License (CC BY). The use, distribution or reproduction in other forums is permitted, provided the original author(s) and the copyright owner(s) are credited and that the original publication in this journal is cited, in accordance with accepted academic practice. No use, distribution or reproduction is permitted which does not comply with these terms.

Screening and characterization of the scFv for chimeric antigen receptor T cells targeting CEA-positive carcinoma

Chengcheng Zhang[1†], Linling Wang[2†], Qianzhen Zhang[2], Junjie Shen[2], Xia Huang[2], Meiling Wang[2], Yi Huang[2], Jun Chen[2], Yanmin Xu[2], Wenxu Zhao[2], Yanan Qi[2], Yunyan Li[2], Yanjiao Ou[1], Zhi Yang[2*] and Cheng Qian[2*]

[1]Department of Hepatobiliary Surgery, Southwest Hospital, Army Medical University, Chongqing, China, [2]Chongqing Key Laboratory of Gene and Cell Therapy, Institute of Precision Medicine and Biotechnology, Chongqing Precision Biotech Co. Ltd., Chongqing, China

Introduction: Chimeric antigen receptor T (CAR-T) cell therapy presents a promising treatment option for various cancers, including solid tumors. Carcinoembryonic antigen (CEA) is an attractive target due to its high expression in many tumors, particularly gastrointestinal cancers, while limited expression in normal adult tissues. In our previous clinical study, we reported a 70% disease control rate with no severe side effects using a humanized CEA-targeting CAR-T cell. However, the selection of the appropriate single-chain variable fragment (scFv) significantly affects the therapeutic efficacy of CAR-T cells by defining their specific behavior towards the target antigen. Therefore, this study aimed to identify the optimal scFv and investigate its biological functions to further optimize the therapeutic potential of CAR-T cells targeting CEA-positive carcinoma.

Methods: We screened four reported humanized or fully human anti-CEA antibodies (M5A, hMN-14, BW431/26, and C2-45), and inserted them into a 3rd-generation CAR structure. We purified the scFvs and measured the affinity. We monitored CAR-T cell phenotype and scFv binding stability to CEA antigen through flow cytometry. We performed repeated CEA antigen stimulation assays to compare the proliferation potential and response of the four CAR-T cells, then further evaluated the anti-tumor efficacy of CAR-T cells ex vivo and in vivo.

Results: M5A and hMN-14 CARs displayed higher affinity and more stable CEA binding ability than BW431/26 and C2-45 CARs. During CAR-T cell production culture, hMN-14 CAR-T cells exhibit a larger proportion of memory-like T cells, while M5A CAR-T cells showed a more differentiated phenotype, suggesting a greater tonic signal of M5A scFv. M5A, hMN-14, and BW431/26 CAR-T cells exhibited effective tumor cell lysis and IFN-γ release when cocultured with CEA-positive tumor cells *in vitro*, correlating with the abundance of CEA expression in target cells. While C2-45 resulted in almost no tumor lysis or IFN-γ release. In a repeat CEA antigen stimulation assay, M5A showed the best cell proliferation and cytokine secretion levels. In a mouse xenograft model, M5A CAR-T cells displayed better antitumor efficacy without preconditioning.

Discussion: Our findings suggest that scFvs derived from different antibodies have distinctive characteristics, and stable expression and appropriate affinity are critical for robust antitumor efficacy. This study highlights the importance of selecting an optimal scFv in CAR-T cell design for effective CEA-targeted therapy. The identified optimal scFv, M5A, could be potentially applied in future clinical trials of CAR-T cell therapy targeting CEA-positive carcinoma.

KEYWORDS

chimeric antigen receptor T cells, carcinoembryonic antigen, single-chain fragment variable, affinity, cell therapy

Introduction

Chimeric antigen receptor T lymphocyte (CAR-T) therapy has shown encouraging and convincing antitumor effects with a high complete remission (CR) rate in refractory and relapsed hematological malignancies, especially leukemia (1, 2). Breakthroughs are also being attempted in solid tumors (3–5). Carcinoembryonic antigen (CEA) is an early tumor-specific marker for human colon cancer (6). Subsequent studies have shown that CEA is expressed in several types of solid tumors, such as colorectal, gastric, lung, breast, pancreatic, and ovarian carcinomas (7). CEA serves as a tumor marker for screening, diagnosis, and prognosis prediction in many cancers (8–13). Its safety and feasibility as a target for chimeric antigen receptor T (CAR-T) cell therapy have been demonstrated in multiple preclinical and clinical trials for the treatment of CEA-positive solid tumors (14–20).

The potential for off-target and on-target/off-tumor side effects are major concerns of CAR-T therapy (21, 22). Although CEA, as a tumor-associated antigen, is highly expressed in malignant tumors, it is also physiologically expressed at low levels in some normal tissues, such as the tongue epithelium, tracheal mucosa, and gastrointestinal tract (23). Thus, the influence of CAR-T cells on these normal tissues must be considered. Amino acid mutations of monoclonal antibodies have generated a series of antibodies with different affinities but targeting the same epitope (24). Among these antibodies, scFvs with decreased affinity were found to exhibit potent antitumor efficacy and better safety in related CAR-T cells (25, 26). However, scFvs derived from different hybridomas targeting diverse epitopes have produced conflicting results regarding CAR-T cell therapy. High-affinity scFvs resulted in better tumor eradication (27, 28). Thus, the selection of appropriate epitopes and affinity for CEA-targeted CAR-T cells is crucial in reducing adverse reactions while improving efficacy.

Murine scFvs are likely to induce humoral (e.g., human anti-mouse antibodies, HAMA) and cellular anti-CAR immune responses, leading to lethal events such as anaphylaxis and attenuated CAR-T efficacy. (29, 30). The humanization of scFvs significantly reduced the immunogenicity and increased the persistence and safety of CAR-T cells compared to those of murine CAR-T cells (31). Humanized CAR-T cells have shown superior clinical therapeutic efficacy (32) and sustained antitumor ability in patients who relapsed after murine CAR-T cell treatment (33, 34). Therefore, humanization is a critical factor in scFv selection for CAR-T cell therapy.

T-cell exhaustion attenuates the efficacy of CAR-T cells and shortens their persistence *in vivo*. Several scFvs even exhibit early exhaustion due to scFv clustering, CAR-dependent tonic signal, and antigen-independent signal transduction (35). It has been reported that CARs with different scFvs have different cell phenotypes and functions (36). Therefore, screening for scFvs with low self-activation and sustained function is necessary to prevent T-cell exhaustion and ensure optimal CAR-T cell therapy.

In this study, we selected four humanized monoclonal antibodies (M5A, hMN-14, C2-45, and BW431/26) based on the binding domain position, humanization status, serum CEA blockade efficacy, reported affinity, and application frequency. We inserted the VH and VL domains of these four mAbs into a 3rd-generation CAR backbone (scFv-G4h-28TM-28BBZ) to evaluate and compare the phenotype, CAR expression level, proliferation, and function of each CAR-T cell type. Additionally, we measured the affinity of each scFv and performed assays to assess cytolysis targeting CEA-positive cells *in vitro* and potent control of tumors *in vivo*. Our findings highlight the distinct features and functions of each scFv targeting CEA, providing improved strategies to enhance the clinical efficacy of CEA-targeted CAR-T therapy.

Materials and methods

scFv purification and affinity measurement

The His-tagged sequence of each of the 4 scFvs was inserted into a plasmid and transfected into HEK293 cells. The supernatant was collected after 6 days. Purification was conducted through filtration (0.22 μm) and absorption (nickel column). The purity of the purified protein was greater than 95%. The concentration was measured by the Bradford method. scFv affinity was measured using a FortéBio Octet Red 96 biolayer interferometry system (Pall, CA, U.S.). The detailed protocol followed the published literature (37). Anti-human IgG Fc (AHC) biosensors (Pall FortéBio, 1512121) were purchased and applied for measurement. Fc-tagged recombinant CEA (15 μg/ml; CEA-Fc, 11077-H03H-50,

Sino Biological Inc.) was precoated on the biosensor. scFv was diluted twice in a gradient of 5 concentrations, with phosphate-buffered saline (PBS) as the negative control. Binding kinetics were calculated using FortéBio Data Analysis software (version 7.1) for y-axis alignment, reference subtraction, interstep correction, and Savitzky–Golay filtering. The association (kon, 1/Ms) and dissociation (koff, 1/s) rate constants were determined by fitting the association and dissociation data to a 1:1 model. The binding affinity (K_D, nM) was calculated as koff/kon (Figure 1). The experiment was conducted three independent times.

Tumor cell lines and CEA-expressing HEK293T cells

Cell lines with high (LS174T and LoVo), moderate (HT-29 and Caco-2), low (MCF7), and negative (RKO and SW620) CEA expressions were purchased from ATCC and cultured according to the corresponding protocols. STR identification of the main cell lines was carried out. CEA expression in each cell line was confirmed before the experiment. The pCMV-CEACAM5-GFP plasmid was obtained from Sino Biological Inc. (HG11077-ACG) and transfected into HEK293T cells to obtain cells with different CEA expression levels. Then, 6 μg, 3 μg, and 1.5 μg of the plasmid were transfected into HEK293T cells to produce high, medium, and low CEA expression, respectively. CEA expression in these HEK293T cells was confirmed by FACS, and the cells were used for cytolytic assays. Untransfected HEK293T cells were used as a control.

Generation of lentivirus and CAR-T cells

Four reported humanized scFvs (M5A, hMN-14, BW431/26, and C2-45) were synthesized (GenScript, China) and inserted into the pCDH lentiviral vector linked to the IgG4 hinge (G4h), CD28 transmembrane domain (28TM), CD28 intracellular signaling domains, 4-1BB intracellular signaling domains, and CD3 zeta ITAM domains. The EF1α promoter was used to drive CAR expression. The GFP sequence was also inserted downstream of each CAR-T sequence using the 2A protein (Figure 2A). Lentivirus was collected and purified from the supernatant of transfected HEK293T cells. To generate CAR-T cells, fresh primary human lymphocytes were obtained from healthy volunteer donors and cultured in GT-T561 (Takara) medium supplemented with 10% fetal bovine serum (FBS; Gibco). PBMCs were activated with immobilized GMP anti-CD3 (MACS, 170-076-116) and anti-CD28 (MACS, 170-076-117) antibodies. Then, the cells were transduced in 6-well plates (1×10^6 cells per well, the multiplicity of infection of 3-5 per well) in the presence of polybrene. T cells were stimulated and expanded with IL-2 (100 U/ml) after viral transduction.

Flow cytometric detection and analysis

We applied BD FACSCalibur and BD FACSAria II instruments for FCM detection. BD FACSDiva software and FlowJo software were used for analysis. FCM detection was performed according to the schedule shown in Figure 2C. CD3, CD4, CD8, and CAR

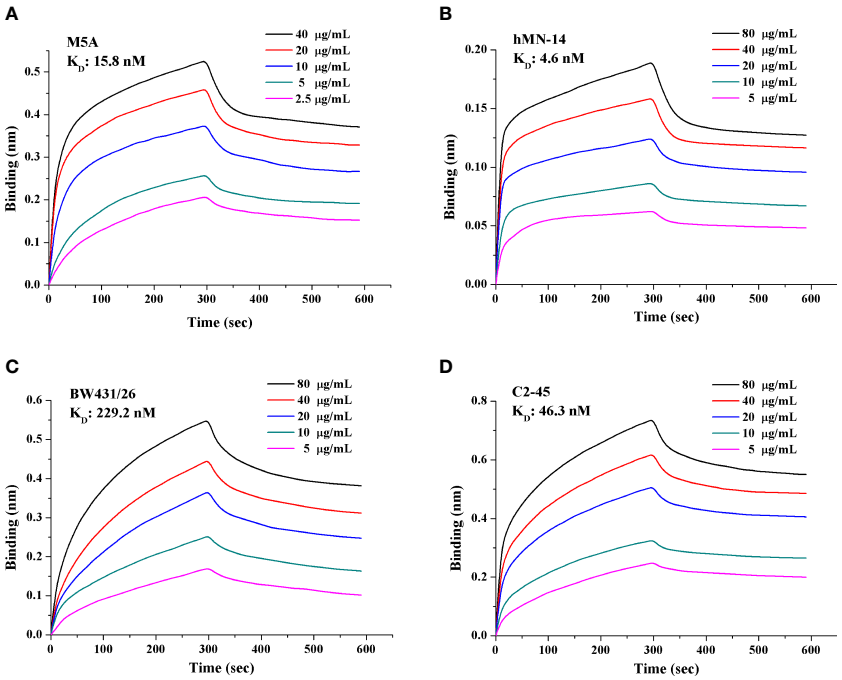

FIGURE 1
Affinity and binding kinetics of each scFv targeting CEA. The K_D of each scFv was obtained and calculated based on a gradient of 5 concentrations. **(A)** M5A, **(B)** hMN-14, **(C)** BW431/26, and **(D)** C2-45. A lower K_D value indicates higher affinity. Each experiment was conducted three independent times (n=3).

expression were evaluated on days 6, 10, and 14, and memory T subsets were evaluated on days 10 and 14. We used His-tagged recombinant CEACAM5 (CEA-His; Sino Biological Inc., 11077-H08H-50) and biotin-protein L (GenScript, M00097) for specific detection of CAR expression. The following antibodies were used: anti-CD3-PE-Cy7 (BioLegend, 300420), anti-CD4-BUV395 (BD, 564724), anti-CD8-BV510 (BioLegend, 344732), anti-CD25-BV421 (BioLegend, 302630), anti-CD45RA-BV421 (BioLegend, 304130), anti-CD45RO-PerCP-Cy5.5 (BioLegend, 304222), AF-647-conjugated IgG fraction of mouse monoclonal anti-biotin (Jackson, 200-602-211) and anti-CD197-PE (BioLegend, 353204).

CAR-T cell response to repeat CEA stimulation

Six-well plates were coated with the CEACAM5 protein (Human, Recombinant Fc Tag). On day 0, 2.5×10^6 viable CAR-T cells were plated into the CEA-coated plates and cultured with 10% FBS medium in the absence of cytokines. The culture supernatant was collected on day 1 for measurement of secreted IFN-γ and IL-2 levels by ELISA. The expression of CD25 in CAR-T cells was measured after 48 hours of culture in CEA-coated plates. The medium was supplemented according to the growth of the cells, and the cells were counted every two days using AO/PI staining to evaluate cell proliferation. The proportion of CAR-positive cells was indicated by the rate of GFP-positive cells. The stimulation was repeated every 7 days until the GFP-positive CAR-T cells stopped expanding. The fold expansion of CAR-T cells was calculated, and after repeated stimulation, cumulative proliferation was analyzed.

In vitro cytolytic assay

The cytolytic assay was conducted with an ACEA xCELLigence RTCA MP instrument and related protocols. Data were recorded based on cell attachment to the plate. In brief, tumor cells attached to the plate and induced an increase in the electrical index of the plate. When CAR-T cells were added and eliminated these attached tumor cells, the electrical index was altered and recorded. On the first day, $2\text{-}5\times10^4$ tumor cells were added to each well of a 96-well plate. The electrical index was recorded every 15 minutes to monitor the attachment of tumor cells. Twenty-four hours later, CAR-T cells were added to each well at a certain E:T ratio. The electrical index was measured over the next 24 hours. Two replicates of each well were established. The specific cytolysis percentage was calculated based on the attenuation of the electrical index compared to the baseline index before the addition of CAR-T cells: % specific lysis = (baseline index - real-time index)/baseline index. Supernatants were collected 24 hours after the addition of CAR-T cells. These specimens were stored at -80°C and subjected to ELISA (IFN-γ, BD Biosciences, 4316955) with a related protocol.

Mouse xenograft studies

At 6-8 weeks of age, female NOD.Cg-PrkdcscidIL2rgtm1Sug/JicCrl (NOG) mice (Vital River Laboratory Animal Technology Co., Ltd.; Beijing, China) were injected subcutaneously with 1×10^6 (per mouse) LoVo cells and fed in a specific pathogen-free (SPF) environment at the animal facility of Southwest Hospital. The mice received humane care according to the criteria outlined in the "Guide for the Care and Use of Laboratory Animals" prepared by the National Academy of Sciences. Tumor volumes and tumor bioluminescence were confirmed before CAR-T cell infusion. After that, the mice were randomly and equally assigned to groups (n=4). Each mouse was injected with 1×10^7 CAR-T cells *via* the tail vein 6 days after LoVo cell implantation. Tumor volumes were measured every 3-4 days and calculated with the following equation: volume= length × width × width/2. The mice were imaged weekly. During tumor volume measurement and bioluminescence detection, the evaluator was blinded to the group allocations. After the experiment, only living mice were included in the statistical analyses. Tumor volumes and tumor bioluminescence were compared among groups.

Statistical analysis

Statistical analyses were performed with SPSS software (version 13.0) and GraphPad Prism software (version 8). Student's t-test was used for comparisons between the two groups. ANOVA (randomized block design) was applied for comparisons among more than two groups. One-way ANOVA and Student's t-test were applied for the comparison of tumor volumes among groups. The Shapiro–Wilk test was applied to confirm whether the data analyzed were normally distributed, and the F test was used to compare variances. In the figures, the data are presented as the means ± SDs or means ± SEMs, and the mean values were calculated from at least three independent experiments. The significance of differences was defined as follows: ns = not significant; * = $p < 0.05$; ** = $p < 0.01$; *** = $p < 0.001$.

Results

scFvs derived from M5A and hMN-14 showed higher affinity

We obtained and purified the scFv of each mAb with a purity of greater than 95%. The affinity of each scFv was measured with a gradient of 5 concentrations, and the K_D value was calculated (Figure 1). M5A (15.8 nM, Figure 1A) and hMN-14 (4.6 nM,

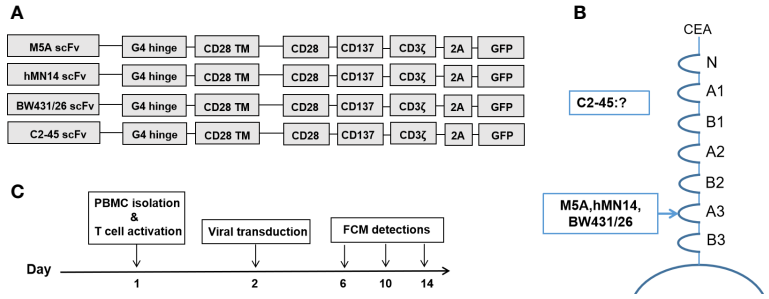

FIGURE 2
CAR structures and detection schedule during CAR-T cell culture. **(A)** Structures of the 4 CARs with the corresponding scFvs. **(B)** The binding domain of CEA in each scFv is shown. **(C)** Preparation and FCM detection schedule of CAR-T cells.

Figure 1B) showed higher affinity for CEA than BW431/26 (229.2 nM, Figure 1C) and C2-45 (46.3 nM, Figure 1D).

Generation and detection of CAR-T cells

Four scFvs derived from each mAb were generated and inserted into a 3rd-generation CAR backbone (Figure 2A). The CEA binding site for each mAb is shown (Figure 2B). The binding site of C2-45 was not identified, while the other three mAbs bound to the A3 domain of CEA (38, 39). The procedures for cell preparation were formulated, and FCM detection was performed on days 6, 10, and 14 (Figure 2C).

M5A and hMN-14 CAR showed more stable and sustained binding to the CEA protein

CAR expression was evaluated according to the schedule on days 6, 10, and 14. The expression of all CARs was stably detected with protein L and GFP at every time point (Figure 3A). When CEA-His was used to determine the proportion of CAR-positive cells, M5A and hMN-14 maintained stable detectability (Figures 3A, B). However, for BW431/26 CAR, the proportion of CAR-positive cells detected by CEA-His was significantly different from that detected by GFP and PL, especially on days

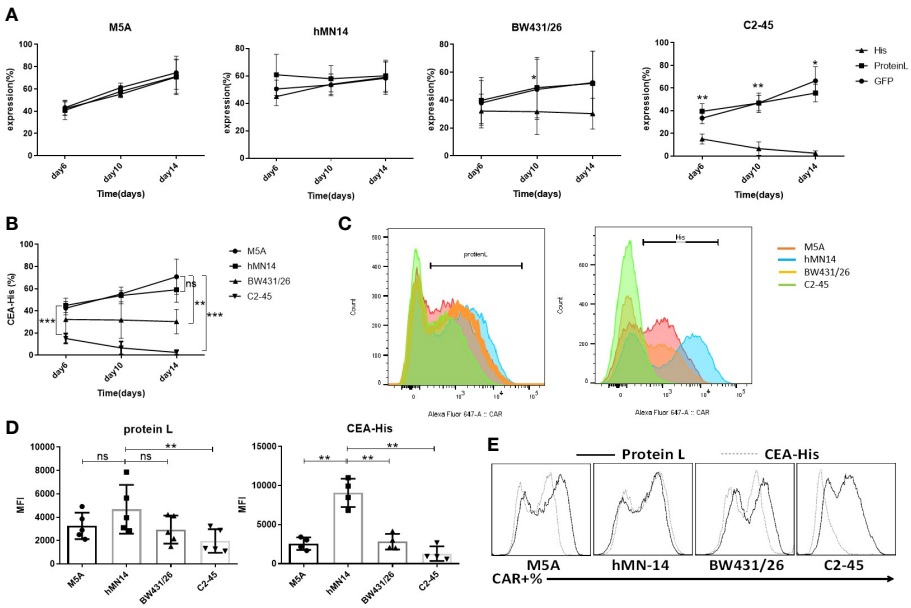

FIGURE 3
Comparison of the detection and expression of several scFvs CAR by flow cytometry. **(A)** The expression of the 4 CAR scFvs on the same cells was evaluated on days 6, 10, and 14 of cell culture using three methods: CEA-His, protein L and GFP. The values are presented as the mean ± SD of four independent experiments derived from 4 different donors (n=4). **(B)** When CAR expression was detected using CEA-His, the results for the 4 types of CAR-T cells were compared. hMN-14, BW431/26 and C2-45 CAR-T cells were compared to M5A cells. The values are presented as the mean ± SD of four independent experiments (n=4). **(C)** Representative FCM results for protein L and CEA-His in the 4 types of CAR-T cells. **(D)** The MFI of protein L and CEA-His was also measured and compared on day 10 of cell culture. The data are presented as the mean ± SD of five independent experiments (protein L) (n=5) and four independent experiments (CEA-His) (n=4). **(E)** HEK293T cells were transduced with each CAR viral vector, and CAR expression was measured by assessment of protein L and CEA-His. Representative FCM results from three independent experiments are shown (n=3). Statistical analysis was performed by a paired t-test. * = $p < 0.05$; ** = $p < 0.01$; and ns, not significant.

10 and 14. In addition, C2-45 was barely detected by CEA-His on days 10 and 14 (Figures 3A, B). The results showed that the binding of CEA-His to the BW431/26 and C2-45 CARs was significantly lower than that to the M5A and hMN-14 CARs, and showed decreasing trend with the extension of culture time (Figure 3B). We speculated that the difference in the original affinity of scFv for CEA was a possible reason for the difference in CAR binding. Moreover, the different influences of the antigen-recognition domain on each scFv changed the binding ability. The results were replicated in multiple donors (Figure 3C). The mean fluorescence intensity (MFI) was also measured and compared on day 10 of cell culture, and the MFI of the hMN-14 CAR, especially that bound to CEA-His, remained stronger (Figure 3D). The strongest affinity was one of the main contributions. To exclude T-cell-related expression bias, we separately transduced HEK293T cells with a lentivirus expressing each CAR. CAR expression was similar to that in T cells (Figure 3E).

M5A CAR-T cells displayed higher proliferation but a more differentiated phenotype than other CAR-T cells

To determine whether different scFv CARs affect the cellular status, including the proliferative capacity and cell phenotype, the cell numbers were determined every four days, and the cell but M5A CAR-T cells displayed greater proliferation than the other CAR-T cells on day 14 (Figure 4A). However, the percentages of CD4 to CD8 were not different (Figure 4B). Memory T subsets were evaluated on days 10 and 14. M5A CAR-T cells contained more T_{cm} and fewer T_{ef} cells on day 10 of *in vitro* culture, while the T_{ef} population was increased on day 14 (Figure 4C). Based on the differences in cell proliferation and memory T-cell subsets, we confirmed that the M5A CAR induced enhanced promoting effects on cell proliferation and differentiation of memory T cells into effector cells at later culture time points, and the proliferation advantage was related to CAR rather than untransduced T cells.

M5A CAR-T cells were less exhausted and secreted more cytokines in the CEA repeated stimulation assay

Because minor differences were observed among all 4 CAR-T cell phenotypes after cell culture, we performed repeated antigen stimulation assays to compare proliferation and cytokine secretion. The 4 CAR-T cell lines were repeatedly stimulated with CEA coated on the culture plate every 7 days. T cells were counted, and CAR expression was assayed every 2-3 days. Seven days after the first stimulation, the proportion of CAR-positive T cells among M5A CAR-T cells was significantly greater than that among the other CAR-T cells (Figure 5A). After the second stimulation, the population of CAR-T cells increased only among M5A CAR-T cells and gradually decreased in the other CAR-T cell populations (Figure 5B), M5A activated stronger intracellular signals to induce CAR-T cell responses. In addition, M5A CAR-T cells exhibited

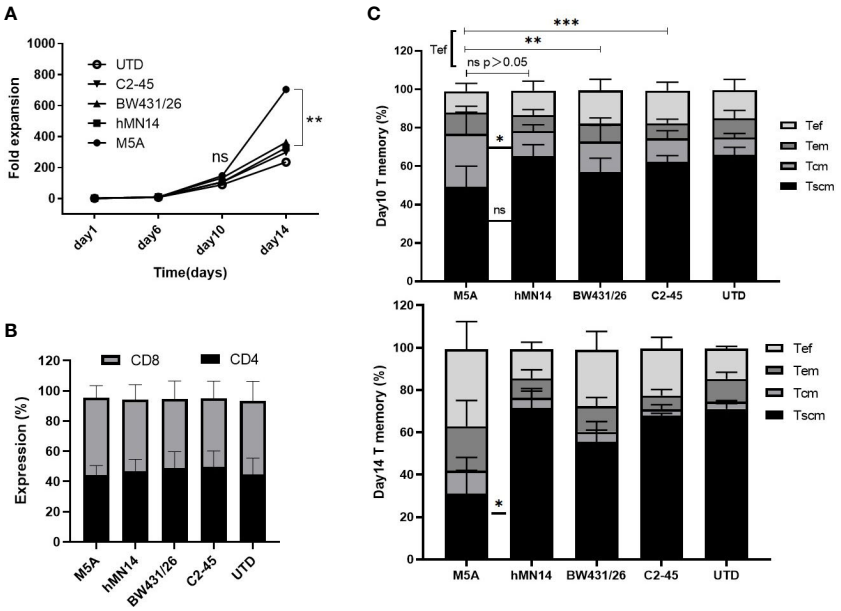

FIGURE 4
The proliferation and T-cell subsets of several types of CAR-T cells during culture. **(A)** Several types of CAR-T cells were cultured *in vitro* for two weeks and counted every four days by AO/PI staining. The fold expansion was calculated to evaluate the proliferative capacity. **(B)** The CD4-positive and CD8-positive populations in cultured cells were measured and compared. **(C)** The expression of CD45RA, CD45RO, and CCR7 was measured to determine the differentiation state of memory T-cell subsets by flow cytometry on day 10 and day 14: Tscm (CD45RA+CD197+), Tcm (CD45RA-CD45RO+CD197+), Tem (CD45RA-CD45RO+CD197-), and Tef (CD45RA+CD197-). All data were obtained from five independent experiments derived from 5 different donors (n=5). Statistical analysis was performed with a paired t-test in **(A, C)** and for **(B)** by one-way ANOVA in **(B)**. * = $p < 0.05$; ** = $p < 0.01$; *** = $p < 0.001$; and ns, not significant.

10.3389/fimmu.2023.1182409

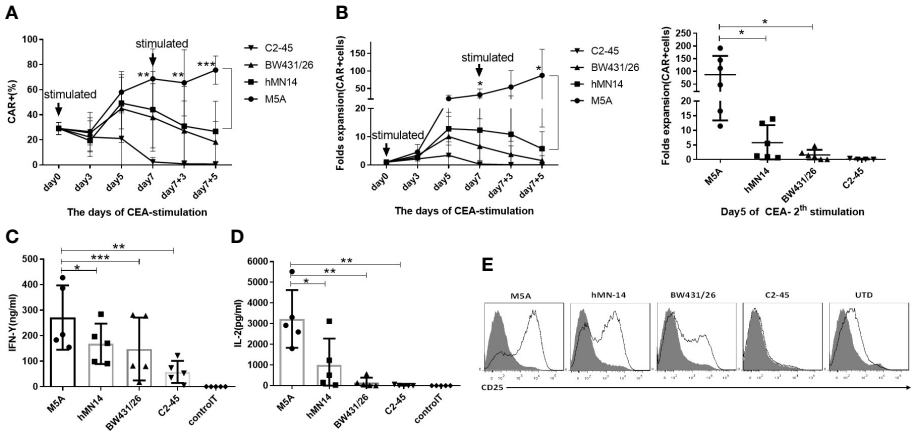

FIGURE 5
Evaluation of the CAR-T cell response to repeated CEA stimulation. All groups were compared with M5A (paired t-test). **(A)** Several types of CAR-T cells were incubated in 6-well plates coated with the CEACAM5 protein every seven days (1st and 2nd stimulation), and the percentage of CAR-positive cells was determined every 2-3 days by monitoring GFP expression. The values are presented as the mean ± SD of six independent experiments derived from 6 different donors (n=6) from different donors. **(B)** After two rounds of stimulation with CEA in the absence of cytokines, CAR-positive cells were counted, and the fold expansion was calculated by assessment of CAR-positive cells. The values are presented as the mean ± SD of six independent experiments (n=6) with technical duplicates. **(C, D)** The culture supernatant was collected 24 hours after CEA stimulation to measure the levels of secreted IFN-γ and IL-2 by ELISA. The values are presented as the mean ± SD of five independent experiments (n=5). **(E)** The CD25 expression of several scFvs CAR-T cells was detected 48 hours after CEA stimulation. Representative FCM results from three independent experiments are shown (n=3). Statistical analysis was performed by paired t-test. * = $p < 0.05$, ** = $p < 0.01$, *** = $p < 0.001$ and ns, not significant.

significantly greater cytokine secretion (IFN-γ and IL-2) than the other CAR-T cells (Figures 5C, D), that could also triggered M5A to gain more cell expansion. After the first stimulation, the phenotypic analysis revealed significantly upregulated expression of CD25 in M5A CAR-T cells. In contrast, C2-45 CAR-T cells barely responded to antigen stimulation, and CD25 was barely expressed (Figure 5E).

CARs with scFvs with different affinities discriminated between cells expressing different levels of CEA

First, we performed cytolytic assays to compare the tumor elimination properties of the 4 types of CAR-T cells in a tumor cell line with high CEA expression (Supplementary Figure S1). CAR-T cells were cocultured with high-CEA-expression LoVo cells at effector:-target (E:T) ratios of 1:1 and 1:2 for 48 hours. All 3 tested CAR-T cells lysed LoVo cells in a concentration- and time-dependent manner. M5A and hMN-14 CAR-T cells showed better specific lysis ability and higher IFN-γ levels than the other 2 types of CAR-T cells. hMN-14 CAR-T cells exhibited the highest level of IL-2 secretion (Supplementary Figure S1). C2-45 CAR cells exhibited weaker tumoricidal capacity and little cytokine secretion. Considering the weak effects of C2-45, we did not use the C2-45 CAR in further experiments or comparisons.

To further discriminate the function of these CAR-T cells, we evaluated several tumor cell lines with different levels of CEA expression. First, the expression of CEA in tumor cell lines was measured (Supplementary Figure S2). Then, after 24 hours of coculture of CAR-T cells with tumor cells, IFN-γ secretion was measured by ELISA. IFN-γ secretion was significantly higher in cell lines with high CEA expression (LoVo and LS174T) (Figure 6A). In cell lines with moderate or low CEA expression (HT-29, Caco-2, and MCF7), IFN-γ secretion was significantly lower, but the M5A and hMN-14 CAR-T cells showed a slight advantage. In CEA-negative cell lines (RKO and SW620), none of the 3 CAR-T cells exhibited obvious effects on cytokine secretion.

Next, we used a real-time, quantitative cell analysis system (xCELLigence RTCA System, Agilent) to determine the cytolytic activity of CAR-T cells against tumor cells with different levels of CEA expression. After 8 hours of coculture at an E:T ratio of 6:1, M5A, hMN-14, and BW431/26 CAR-T cells showed diverse cytolytic activity against tumor cell lines with different levels of CEA expression: high (LoVo and LS174T) and moderate or low (HT-29, Caco-2, and MCF7) (Figure 6B). M5A, hMN-14 and BW431/26 CAR-T cells showed high cytolytic activity against cells with high CEA expression, and M5A showed a slight advantage. The cytolytic activity of CAR-T cells against cell lines with moderate or low CEA expression gradually decreased, but M5A showed more stable cytolytic activity (Figure 6B). The preferential cytolytic activity of M5A was also confirmed in cytolytic assays with different E:T ratios and incubation times (Figures 6C, D). To further study the responses of several CAR-T scFvs to different CEA expression levels, we conducted cytolytic assays targeting HEK293T cells with exogenous expression of CEA. HEK293T cells were transfected with increasing concentrations of the CEA expression plasmid, and CEA expression was measured (Figure 6E). M5A also showed superior cytolytic activity against both high- and low-CEA-expressing HEK293T cells (Figure 6F). In addition, the cytolytic activity of M5A was confirmed at different E:T ratios (Figure 6G). The results showed that the cytolytic effect of

10.3389/fimmu.2023.1182409

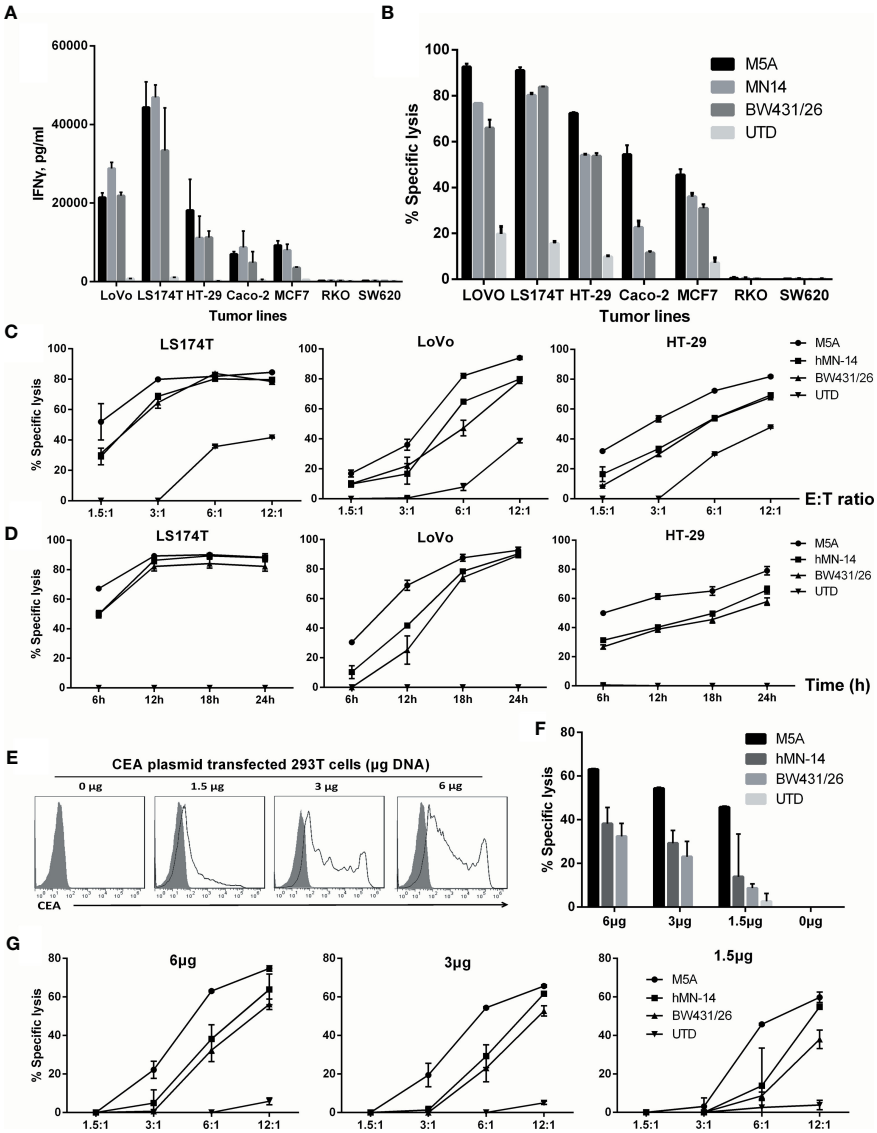

FIGURE 6
Comparison of the specific cytolytic activity of several types of CAR-T cells based on time and concentration. **(A)** IFN-γ was measured by ELISA in culture supernatants collected after 24 hours of coculture. **(B)** Specific cytolytic activity of CAR-T cells. Several types of CAR-T cells were incubated with tumor cell lines with different CEA expression levels for 8 hours at an E:T ratio of 6:1. Cytolysis at different E:T ratios after 8 hours **(C)** and at an E:T ratio of 3:1 after different durations **(D)** is shown. **(E)** HEK293T cells were transduced with different concentrations of a DNA plasmid expressing CEA. Membrane CEA expression was detected. **(F, G)** Specific cytolysis of each HEK293T cell line was measured. The other two groups were compared with M5A (ANOVA, randomized block design).

CAR-T cells was significantly enhanced with increasing CEA expression on the HEK293T cell surface.

M5A CAR-T cells had greater antitumor activity *in vivo*

We evaluated the antitumor activity of M5A, hMN-14, and BW431/26 CAR-T cells *in vivo* in a LoVo cell xenograft model. NOG mice were injected i.v. with 1×10^6 LoVo cells genetically modified to express firefly luciferase. Six days later, the mice were injected intravenously (i.v.) with 1×10^7 CAR-T cells without any preconditioning treatment. Control mice were injected with 1×10^7 T cells with no CAR. The tumor burden was monitored by serial bioluminescence imaging every 7 days (Figure 7A). M5A CAR-T cells showed superior tumor suppression compared with that of the other CAR-T cells (Figure 7B). M5A CAR-T cells consistently exhibited preferential tumor suppression and were superior to BW431/26 and UTD ($p < 0.001$). According to the actual measurements on day 27, the tumor volume increased in the following order: M5A<hMN-14<BW431/26<UTD (Figure 7B). These results indicated optimal tumor suppression by M5A CAR-

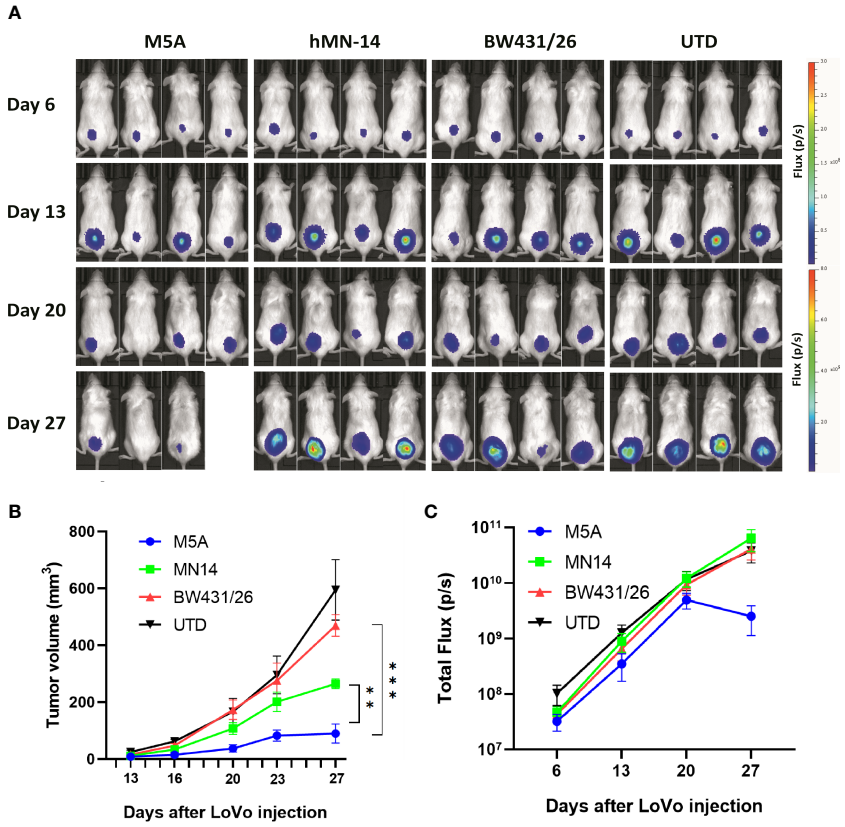

FIGURE 7
M5A CAR-T cells exhibited superior tumor suppression in the xenograft model in NOG mice. **(A)** Each mouse was implanted with 1× 10^6 LoVo cells (Luc$^+$) on day 1 and injected i.v. with 1 × 10^7 CAR-T cells on day 7. Mice were imaged weekly. **(B)** Tumor growth was assessed by calculating the tumor volume. The values are presented as the means ± SEMs. The growth of tumors treated with M5A CAR-T cells was potently controlled compared with that of tumors in the other groups. **(C)** The total bioluminescence values were also recorded and compared. The values are presented as the means ± SEMs. Statistical analysis was performed by one-way ANOVA. * = $p < 0.05$; ** = $p < 0.01$; and ns, not significant.

T cells. The total bioluminescence flux is shown in Figure 7C, and the values indicate a decreasing trend only in the M5A group and no significant difference in the other groups.

Discussion

CEA is highly expressed in various types of solid tumors, especially some gastrointestinal tumors. Its high expression in tumors and detectability in serum make it a valuable tumor biomarker for clinical diagnosis. CEA expression is undetectable in most normal tissues, except for the surface epithelium of the tongue, the tracheal mucosa, and specific locations in the gastrointestinal tract, where it is expressed at low levels (23). The reactivity of CAR-T cells toward antigen-expressing cells is affected by the avidity of the CAR, which is based on its affinity and surface expression level. Thus, screening for antibodies with appropriate affinity is very important for the application of CEA-targeting CAR-T cells. BW431/26 is a humanized antibody with moderate affinity for CEA. We enrolled ten CRC patients for CAR-T therapy targeting CEA (NCT02349724) using the BW431/26 antibody as the source of scFv. No off-target or on-target/off-tumor side effects were observed. However, patients achieved only transient disease control, and none achieved remission. During CAR-T cell production, we observed unstable CAR, leading to some canceled infusions due to low CAR-positive rates. We suspected that this CAR instability attenuated the expected outcomes. Therefore, the development of better CAR-T cells with more stable expression and greater antitumor effects will improve clinical outcomes.

CEA-specific antibodies, such as T84.66, hMN-14, C2-45, BW431/26, MFE-23, H10 and F023C5, have been developed (38, 40–45). By analyzing the antigen recognition sites and clinical application specificity, we identified three more antibodies from previously reported sources. M5A, hMN-14, and BW431/26 are humanized mAbs and C2-45 is a fully human mAb derived from KM mice, and these mAbs are less likely than others to induce an immune response. The affinity of the scFv derived from these antibodies was measured using a protein expression system in *Escherichia coli*. All four scFvs bound to the CEA protein with their corresponding affinities, as previously reported. When we confirmed the CEA binding capacity after these scFvs were transduced into T cells, the C2-45-derived scFv showed a very low CEA protein-binding capacity. By increasing the amounts of CEA-his to at least 4 times the recommended dose, the results for BW431/26 and C2-45 showed only small increase, which were still far from the percentage of GFP. Previous studies have also reported that the antigen recognition properties of the scFv incorporated into a CAR can differ from those of the original antibody (46). scFvs expressed in mammalian cells undergo various posttranslational modifications, such as

glycosylation. C2-45 might have undergone an unexpected modification and formed an unexpected structure different from that produced in *E. coli*. In addition, CAR aggregation can cause loss of antigen recognition properties, as well as increased differentiation of CAR-T cells (35). When we compared the Tscm and Tcm populations in C2-45 CAR-T cells with those in untransfected control T cells, there was no difference between the two groups. Therefore, the loss of C2-45 affinity is unlikely to be due to aggregation. The three other scFv-derived CARs retained their CEA binding capacity, M5A and hMN-14 were better than BW431/26.

In contrast to BW431/26, the expression of both M5A and hMN-14 was highly stable. There was no significant difference between M5A and hMN-14 in CAR expression. The structure and posttranslational modification of the scFv are predicted to affect the folding of the related CAR protein, leading to structurally unstable CARs that are degraded intracellularly or aggregated on the T-cell membrane. In the structures of BW431/26, M5A, and hMN-14, the complementarity-determining regions (CDRs) of M5A and hMN-14 were assembled in the same human antibody framework region (FR) and were different from those of BW431/26. The FR has been reported to affect the stability of the scFv structure, CAR expression, and KDR binding (47). Changing the FR of BW431/26 might improve CAR expression and stability.

The affinity of a CAR for antigens has been reported to affect the efficacy of CAR-T cells both *in vivo* and *in vitro* (24). CARs containing scFvs with low affinity have shown superior safety and efficacy compared with those of CARs containing scFvs with high affinity (25). Increasing the affinity did not significantly enhance CAR-T cell function and even worsened the on-target/off-tumor effect (26). However, when comparing scFvs derived from different hybridomas and targeting different epitopes, high-affinity scFvs exhibited superior tumor eradication (27, 28). The benefits of increasing or decreasing scFv affinity are discrepant in different types of CAR-T (48). BW431/26 showed the lowest affinity (229.2 nM), hMN-14 showed the highest affinity (4.6 nM), and M5A showed moderate affinity (15.8 nM). hMN-14 CAR-T cells showed the highest cytokine expression and BW431/26 CAR-T cells showed the lowest cytokine expression *in vitro* when cocultured with target cells. *In vitro*, M5A and hMN-14 CAR-T cells showed comparable cytotoxic activity and slightly higher cytotoxicity than BW431/26 CAR-T cells when cocultured with target cells. However, in the SCID mouse xenograft model, M5A CAR-T cells showed the most potent antitumor effect. These results suggest that appropriate affinity improves CAR-T cell function based on different types of CAR-T.

In summary, we screened and compared four CEA-targeting antibody-derived CAR-T cells. M5A CAR-T cells showed stable CAR expression, moderate affinity, moderate cytokine secretion, and superior antitumor ability *in vivo* and *in vitro*. Further clinical trials will be performed to test the clinical efficacy of these cells.

Data availability statement

The original contributions presented in the study are included in the article/Supplementary Material. Further inquiries can be directed to the corresponding authors.

Ethics statement

The animal study was reviewed and approved by Third military medical university(army medical university).

Author contributions

CQ and ZY designed the experiments. YH, XH, ZY, and WZ constructed the plasmid and packaged the virus. CZ and LW conducted the experiments. QZ, JS, MW, JC, YX, YQ, YL, and YO developed the methodologies. ZY, CZ, and LW analyzed the data and wrote the manuscript. All authors contributed to the article and approved the submitted version.

Funding

This study was supported by the National Natural Science Foundation of China (82127804) and the National Natural Science Foundation of China (81903157).

Acknowledgments

This work was supported by the National Natural Science Foundation of China (82127804) , the National Natural Science Foundation of China (81903157) , and Chongqing Precision Biotech Co., Ltd.

Conflict of interest

Authors LW, QZ, JS, XH, MW, YH, JC, YX, WZ, YQ, YL, and ZY, were employed by the company Chongqing Precision Biotech Co., Ltd. CQ is the chief scientist of this company.

The remaining authors declare that the research was conducted in the absence of any commercial or financial relationships that could be construed as a potential conflict of interest.

Publisher's note

All claims expressed in this article are solely those of the authors and do not necessarily represent those of their affiliated organizations, or those of the publisher, the editors and the reviewers. Any product that may be evaluated in this article, or claim that may be made by its manufacturer, is not guaranteed or endorsed by the publisher.

Supplementary material

The Supplementary Material for this article can be found online at: https://www.frontiersin.org/articles/10.3389/fimmu.2023.1182409/full#supplementary-material

References

1. Porter DL, Hwang WT, Frey NV, Lacey SF, Shaw PA. Loren AW et al. chimeric antigen receptor T cells persist and induce sustained remissions in relapsed refractory chronic lymphocytic leukemia. *Sci Trans Med* (2015) 7(303):303ra139. doi: 10.1126/scitranslmed.aac5415

2. Maude SL, Frey N, Shaw PA, Aplenc R, Barrett DM, Bunin NJ, et al. Chimeric antigen receptor T cells for sustained remissions in leukemia. *New Engl J Med* (2014) 371(16):1507–17. doi: 10.1056/NEJMoa1407222

3. Katz SC, Burga RA, McCormack E, Wang LJ, Mooring W, Point GR, et al. Phase I hepatic immunotherapy for metastases study of intra-arterial chimeric antigen receptor-modified T-cell therapy for CEA+ liver metastases. *Clin Cancer Res Off J Am Assoc Cancer Res* (2015) 21(14):3149–59. doi: 10.1158/1078-0432.CCR-14-1421

4. Ahmed N, Brawley VS, Hegde M, Robertson C, Ghazi A, Gerken C, et al. Human epidermal growth factor receptor 2 (HER2) -specific chimeric antigen receptor-modified T cells for the immunotherapy of HER2-positive sarcoma. *J Clin Oncol Off J Am Soc Clin Oncol* (2015) 33(15):1688–96. doi: 10.1200/JCO.2014.58.0225

5. Louis CU, Savoldo B, Dotti G, Pule M, Yvon E, Myers GD, et al. Antitumor activity and long-term fate of chimeric antigen receptor-positive T cells in patients with neuroblastoma. *Blood* (2011) 118(23):6050–6. doi: 10.1182/blood-2011-05-354449

6. Gold P, Freedman SO. Demonstration of tumor-specific antigens in human colonic carcinomata by immunological tolerance and absorption techniques. *J Exp Med* (1965) 121:439–62. doi: 10.1084/jem.121.3.439

7. Hammarstrom S. The carcinoembryonic antigen (CEA) family: structures, suggested functions and expression in normal and malignant tissues. *Semin Cancer Biol* (1999) 9(2):67–81. doi: 10.1006/scbi.1998.0119

8. Eker B, Ozaslan E, Karaca H, Berk V, Bozkurt O, Inanc M, et al. Factors affecting prognosis in metastatic colorectal cancer patients. *Asian Pac J Cancer Prev* (2015) 16 (7):3015–21. doi: 10.7314/APJCP.2015.16.7.3015

9. Mansour EG, Hastert M, Park CH, Koehler KA, Petrelli M. Tissue and plasma carcinoembryonic antigen in early breast cancer. a prognostic factor. *Cancer* (1983) 51 (7):1243–8. doi: 10.1002/1097-0142(19830401)51:7<1243::aid-cncr2820510712>3.0.co;2-a

10. van Manen L, Groen JV, Putter H, Vahrmeijer AL, Swijnenburg RJ, Bonsing BA, et al. Elevated CEA and CA19-9 serum levels independently predict advanced pancreatic cancer at diagnosis. *Biomarkers* (2020) 25(2):186–93. doi: 10.1080/1354750X.2020.1725786

11. Wu LX, Li XF, Chen HF, Zhu YC, Wang WX, Xu CW, et al. Combined detection of CEA and CA125 for the diagnosis for lung cancer: a meta-analysis. *Cell Mol Biol (Noisy-le-grand)* (2018) 64(15):67–70. doi: 10.14715/cmb/2017.64.15.11

12. Tang S, Zhou F, Sun Y, Wei L, Zhu S, Yang R, et al. CEA in breast ductal secretions as a promising biomarker for the diagnosis of breast cancer: a systematic review and meta-analysis. *Breast Cancer* (2016) 23(6):813–9. doi: 10.1007/s12282-016-0680-9

13. Arnaud JP, Koehl C, Adloff M. Carcinoembryonic antigen (CEA) in diagnosis and prognosis of colorectal carcinoma. *Dis Colon Rectum* (1980) 23(3):141–4. doi: 10.1007/BF02587615

14. Zhang C, Wang Z, Yang Z, Wang M, Li S, Li Y, et al. Phase I escalating-dose trial of CAR-T therapy targeting CEA(+) metastatic colorectal cancers. *Mol Ther J Am Soc Gene Ther* (2017) 25(5):1248–58. doi: 10.1016/j.ymthe.2017.03.010

15. Wang L, Ma N, Okamoto S, Amaishi Y, Sato E, Seo N, et al. Efficient tumor regression by adoptively transferred CEA-specific CAR-T cells associated with symptoms of mild cytokine release syndrome. *Oncoimmunology* (2016) 5(9): e1211218. doi: 10.1080/2162402X.2016.1211218

16. Katz SC, Moody AE, Guha P, Hardaway JC, Prince E, LaPorte J, et al. HITM-SURE: hepatic immunotherapy for metastases phase ib anti-CEA CAR-T study utilizing pressure enabled drug delivery. *J Immunother Cancer* (2020) 8(2):e001097. doi: 10.1136/jitc-2020-001097

17. Katz SC, Hardaway J, Prince E, Guha P, Cunetta M, Moody A, et al. HITM-SIR: phase ib trial of intraarterial chimeric antigen receptor T-cell therapy and selective internal radiation therapy for CEA(+) liver metastases. *Cancer Gene Ther* (2020) 27 (5):341–55. doi: 10.1038/s41417-019-0104-z

18. Holzinger A, Abken H. CAR T cells targeting solid tumors: carcinoembryonic antigen (CEA) proves to be a safe target. *Cancer Immunol Immunother CII* (2017) 66 (11):1505–7. doi: 10.1007/s00262-017-2045-4

19. Chi X, Yang P, Zhang E, Gu J, Xu H, Li M, et al. Significantly increased anti-tumor activity of carcinoembryonic antigen-specific chimeric antigen receptor T cells in combination with recombinant human IL-12. *Cancer Med* (2019) 8(10):4753–65. doi: 10.1002/cam4.2361

20. Cha SE, Kujawski M P, Brown C, Shively JE. Tumor regression and immunity in combination therapy with anti-CEA chimeric antigen receptor T cells and anti-CEA-IL2 immunocytokine. *Oncoimmunology* (2021) 10(1):1899469. doi: 10.1080/2162402X.2021.1899469

21. Morgan RA, Yang JC, Kitano M, Dudley ME, Laurencot CM, Rosenberg SA. Case report of a serious adverse event following the administration of T cells transduced with a chimeric antigen receptor recognizing ERBB2. *Mol Ther J Am Soc Gene Ther* (2010) 18(4):843–51. doi: 10.1038/mt.2010.24

22. Lamers CH, Sleijfer S, van Steenbergen S, van Elzakker P, van Krimpen B, Groot C, et al. Treatment of metastatic renal cell carcinoma with CAIX CAR-engineered T cells: clinical evaluation and management of on-target toxicity. *Mol Ther J Am Soc Gene Ther* (2013) 21(4):904–12. doi: 10.1038/mt.2013.17

23. Nap M, Mollgard K, Burtin P, Fleuren GJ. Immunohistochemistry of carcino-embryonic antigen in the embryo, fetus and adult. *Tumour Biol J Int Soc Oncodevelopmental Biol Med* (1988) 9(2-3):145–53. doi: 10.1159/000217555

24. Carter P, Presta L, Gorman CM, Ridgway JB, Henner D, Wong WL, et al. Humanization of an anti-p185HER2 antibody for human cancer therapy. *Proc Natl Acad Sci United States America* (1992) 89(10):4285–9. doi: 10.1073/pnas.89.10.4285

25. Liu X, Jiang S, Fang C, Yang S, Olalere D, Pequignot EC, et al. Affinity-tuned ErbB2 or EGFR chimeric antigen receptor T cells exhibit an increased therapeutic index against tumors in mice. *Cancer Res* (2015) 75(17):3596–607. doi: 10.1158/0008-5472.CAN-15-0159

26. Chmielewski M, Hombach A, Heuser C, Adams GP, Abken H. T Cell activation by antibody-like immunoreceptors: increase in affinity of the single-chain fragment domain above threshold does not increase T cell activation against antigen-positive target cells but decreases selectivity. *J Immunol* (2004) 173(12):7647–53. doi: 10.4049/jimmunol.173.12.7647

27. Lynn RC, Feng Y, Schutsky K, Poussin M, Kalota A, Dimitrov DS, et al. High-affinity FRbeta-specific CAR T cells eradicate AML and normal myeloid lineage without HSC toxicity. *Leukemia* (2016) 30(6):1355–64. doi: 10.1038/leu.2016.35

28. Hudecek M, Lupo-Stanghellini MT, Kosasih PL, Sommermeyer D, Jensen MC, Rader C, et al. Receptor affinity and extracellular domain modifications affect tumor recognition by ROR1-specific chimeric antigen receptor T cells. *Clin Cancer Res Off J Am Assoc Cancer Res* (2013) 19(12):3153–64. doi: 10.1158/1078-0432.CCR-13-0330

29. Lamers CH, Willemsen R, van Elzakker P, van Steenbergen-Langeveld S, Broertjes M, Oosterwijk-Wakka J, et al. Immune responses to transgene and retroviral vector in patients treated with ex vivo-engineered T cells. *Blood* (2011) 117 (1):72–82. doi: 10.1182/blood-2010-07-294520

30. Maus MV, Haas AR, Beatty GL, Albelda SM, Levine BL, Liu X, et al. T Cells expressing chimeric antigen receptors can cause anaphylaxis in humans. *Cancer Immunol Res* (2013) 1(1):26–31. doi: 10.1158/2326-6066.CIR-13-0006

31. Wu Y, Jiang S, Ying T. From therapeutic antibodies to chimeric antigen receptors (CARs): making better CARs based on antigen-binding domain. *Expert Opin Biol Ther* (2016) 16(12):1469–78. doi: 10.1080/14712598.2016.1235148

32. Heng G, Jia J, Li S, Fu G, Wang M, Qin D, et al. Sustained therapeutic efficacy of humanized anti-CD19 chimeric antigen receptor T cells in Relapsed/Refractory acute lymphoblastic leukemia. *Clin Cancer Res Off J Am Assoc Cancer Res* (2020) 26(7):1606–15. doi: 10.1158/1078-0432.CCR-19-1339

33. Zhao Y, Liu Z, Wang X, Wu H, Zhang J, Yang J, et al. Treatment with humanized selective CD19CAR-T cells shows efficacy in highly treated b-ALL patients who have relapsed after receiving murine-based CD19CAR-T therapies. *Clin Cancer Res Off J Am Assoc Cancer Res* (2019) 25(18):5595–607. doi: 10.1158/1078-0432.CCR-19-0916

34. Li X, Liu MJ, Mou N, Yang ZX, Wang J, Mu J, et al. Efficacy and safety of humanized CD19 CAR-T as a salvage therapy for recurrent CNSL of b-ALL following murine CD19 CAR-T cell therapy. *Oncol Lett* (2021) 22(5):788. doi: 10.3892/ol.2021.13049

35. Long AH, Haso WM, Shern JF, Wanhainen KM, Murgai M, Ingaramo M, et al. 4-1BB costimulation ameliorates T cell exhaustion induced by tonic signaling of chimeric antigen receptors. *Nat Med* (2015) 21(6):581–90. doi: 10.1038/nm.3838

36. Caruso HG, Hurton LV, Najjar A, Rushworth D, Ang S, Olivares S, et al. Tuning sensitivity of CAR to EGFR density limits recognition of normal tissue while maintaining potent antitumor activity. *Cancer Res* (2015) 75(17):3505–18. doi: 10.1158/0008-5472.CAN-15-0139

37. Wang C, Shen M, Gohain N, Tolbert WD, Chen F, Zhang N, et al. Design of a potent antibiotic peptide based on the active region of human defensin 5. *J Med Chem* (2015) 58(7):3083–93. doi: 10.1021/jm501824a

38. Hombach AA, Schildgen V, Heuser C, Finnern R, Gilham DE, Abken H. T Cell activation by antibody-like immunoreceptors: the position of the binding epitope within the target molecule determines the efficiency of activation of redirected T cells. *J Immunol* (2007) 178(7):4650–7. doi: 10.4049/jimmunol.178.7.4650

39. You YH, Hefta LJ, Yazaki PJ, Wu AM, Shively JE. Expression, purification, and characterization of a two domain carcinoembryonic antigen minigene (N-A3) in pichia pastoris. the essential role of the n-domain. *Anticancer Res* (1998) 18(5A):3193–201.

40. Mayer A, Tsiompanou E, O'Malley D, Boxer GM, Bhatia J, Flynn AA, et al. Radioimmunoguided surgery in colorectal cancer using a genetically engineered anti-CEA single-chain fv antibody. *Clin Cancer Res Off J Am Assoc Cancer Res* (2000) 6 (5):1711–9.

41. Behr TM, Salib AL, Liersch T, Behe M, Angerstein C, Blumenthal RD, et al. Radioimmunotherapy of small volume disease of colorectal cancer metastatic to the liver: preclinical evaluation in comparison to standard chemotherapy and initial results of a phase I clinical study. *Clin Cancer Res Off J Am Assoc Cancer Res* (1999) 5(10 Suppl):3232s–42s.

42. Akamatsu Y, Murphy JC, Nolan KF, Thomas P, Kreitman RJ, Leung SO, et al. A single-chain immunotoxin against carcinoembryonic antigen that suppresses growth of colorectal carcinoma cells. *Clin Cancer Res Off J Am Assoc Cancer Res* (1998) 4(11):2825–32.

43. Wong JYC, Chu DZ, Yamauchi DM, Williams LE, Liu A, Wilczynski S, et al. A phase I radioimmunotherapy trial evaluating 90yttrium-labeled anti-carcinoembryonic antigen (CEA) chimeric T84.66 in patients with metastatic CEA-producing malignancies. *Clin Cancer Res Off J Am Assoc Cancer Res* (2000) 6(10):3855–63.

44. Imakiire T, Kuroki M, Shibaguchi H, Abe H, Yamauchi Y, Ueno A, et al. Generation, immunologic characterization and antitumor effects of human monoclonal antibodies for carcinoembryonic antigen. *Int J Cancer* (2004) 108(4):564–70. doi: 10.1002/ijc.11608

45. Oriuchi N, Watanabe N, Kanda H, Hashimoto M, Sugiyama S, Takenoshita S, et al. Antibody-dependent difference in biodistribution of monoclonal antibodies in animal models and humans. *Cancer Immunol Immunother CII* (1998) 46(6):311–7. doi: 10.1007/s002620050492

46. Krokhotin A, Du H, Hirabayashi K, Popov K, Kurokawa T, Wan X, et al. Computationally guided design of single-chain variable fragment improves specificity of chimeric antigen receptors. *Mol Ther Oncolytics* (2019) 15:30–7. doi: 10.1016/j.omto.2019.08.008

47. Fujiwara K, Masutani M, Tachibana M, Okada N. Impact of scFv structure in chimeric antigen receptor on receptor expression efficiency and antigen recognition properties. *Biochem Biophys Res Commun* (2020) 527(2):350–7. doi: 10.1016/j.bbrc.2020.03.071

48. Duan Y, Chen R, Huang Y, Meng X, Chen J, Liao C, et al. Tuning the ignition of CAR: optimizing the affinity of scFv to improve CAR-T therapy. *Cell Mol Life Sci* (2021) 79(1):14. doi: 10.1007/s00018-021-04089-x

frontiers | Frontiers in Immunology

TYPE Mini Review
PUBLISHED 09 June 2023
DOI 10.3389/fimmu.2023.1194590

Check for updates

OPEN ACCESS

EDITED BY
Xi Cheng,
Shanghai Jiao Tong University, China

REVIEWED BY
Jiang Qian,
Fudan University, China
Fu Gui,
Second Affiliated Hospital of Nanchang University, China

*CORRESPONDENCE
Ya Shen
1582026612@qq.com
Jin-di Zhang
158074443@qq.com
Rui-li Wei
ruiliwei@126.com

†These authors have contributed equally to this work and share first authorship

RECEIVED 27 March 2023
ACCEPTED 02 May 2023
PUBLISHED 09 June 2023

CITATION
He L, Mou P, Yang C, Huang C, Shen Y, Zhang J and Wei R (2023) Single-cell sequencing in primary intraocular tumors: understanding heterogeneity, the microenvironment, and drug resistance. *Front. Immunol.* 14:1194590. doi: 10.3389/fimmu.2023.1194590

COPYRIGHT
© 2023 He, Mou, Yang, Huang, Shen, Zhang and Wei. This is an open-access article distributed under the terms of the Creative Commons Attribution License (CC BY). The use, distribution or reproduction in other forums is permitted, provided the original author(s) and the copyright owner(s) are credited and that the original publication in this journal is cited, in accordance with accepted academic practice. No use, distribution or reproduction is permitted which does not comply with these terms.

Single-cell sequencing in primary intraocular tumors: understanding heterogeneity, the microenvironment, and drug resistance

Lin-feng He[1†], Pei Mou[1†], Chun-hui Yang[1†], Cheng Huang[2], Ya Shen[1*], Jin-di Zhang[1*] and Rui-li Wei[1*]

[1]Department of Ophthalmology, Changzheng Hospital of Naval Medical University, Shanghai, China, [2]92882 Troops of the Chinese People's Liberation Army, Qingdao, China

Retinoblastoma (RB) and uveal melanoma (UM) are the most common primary intraocular tumors in children and adults, respectively. Despite continued increases in the likelihood of salvaging the eyeball due to advancements in local tumor control, prognosis remains poor once metastasis has occurred. Traditional sequencing technology obtains averaged information from pooled clusters of diverse cells. In contrast, single-cell sequencing (SCS) allows for investigations of tumor biology at the resolution of the individual cell, providing insights into tumor heterogeneity, microenvironmental properties, and cellular genomic mutations. SCS is a powerful tool that can help identify new biomarkers for diagnosis and targeted therapy, which may in turn greatly improve tumor management. In this review, we focus on the application of SCS for evaluating heterogeneity, microenvironmental characteristics, and drug resistance in patients with RB and UM.

KEYWORDS

single-cell sequencing, retinoblastoma, uveal melanoma, heterogeneity, microenvironment

1 Introduction

Retinoblastoma (RB) and uveal melanoma (UM) are primary intraocular tumors that mainly originate in the retina and uvea, severely impairing visual acuity and threatening patients' lives (1, 2). Although rare, RB is the most common childhood intraocular tumor and tends to disseminate intracranially and distally. The survival outcomes of patients with RB differ substantially between different regions, with a survival rate of just 57.3% at 3 years in low-income countries, and tumor metastasis remains a major cause of death (3). Uveal melanoma (UM) is the most common intraocular tumor in adults, with a propensity to metastasize to the liver (50% of patients may develop metastases within 15 years) coupled with a high mortality rate (4). Meta-analyses have revealed that the median overall survival

is 10.2 months for patients in whom metastasis has occurred, with an extremely poor curative rate (5). To date, enucleation, radiotherapy, and chemotherapy for metastatic intraocular tumors have not effectively improved prognosis among these patients (6). The exact mechanisms underlying the genesis and metastasis of intraocular tumors are not fully understood.

Tumor heterogeneity refers to the different phenotypic profiles and morphologies of distinct tumor cells, and the interaction between the tumor microenvironment (TME) and tumor cells has been shown to influence disease progression, drug resistance, tumor invasion, and prognosis (7). However, traditional bulk sequencing technology is performed using homogenized tissues, which can only provide overall information regarding the pooled cell population and cannot reveal the characteristics of cell heterogeneity. Unlike bulk sequencing, single-cell sequencing (SCS) strategies for genomic, epigenomic, transcriptomic, proteomic, and metabolomic analyses enable researchers to obtain accurate cellular and molecular information concerning individual cells. SCS strategies have revolutionized our understanding of the biological landscape and the dynamics of malignant diseases (8). Therefore, research performed at a single-cell resolution can provide greater insight into cell–cell communication and the heterogeneity of tumor cells. In this review, we summarize the recent progress in obtaining information on RB and UM via SCS, including insights into tumor genesis, heterogeneity, microenvironmental properties, and drug resistance.

2 Tumor heterogeneity

Cells in tumor tissues, which are characterized as diverse and functional diversity under different pathological conditions, are highly heterogeneous, which may influence the therapeutic response to targeted therapy and survival outcomes. The emergence of SCS technology has enabled researchers to evaluate the immense biological complexity of tumors. Liu et al. constructed a cancerous organoid model of RB using genetically engineered human embryonic stem cells with a biallelic mutation in the RB susceptibility gene *RB1*, which was highly consistent with primary RB tumorigenesis, transcriptomic characteristics, and genome-wide methylation (9). Single-cell RNA sequencing (scRNA-seq) analyses of the organoid model revealed four extra cell clusters when compared with human retinal organoids: RB cells, retinoma-like cells, unfolded protein response-related cells, and excessive cone precursors. The cone precursors expressed several cone precursor markers, such as ARR3 and RXRG, suggesting a potential cellular origin for RB. Further investigation using single-cell pseudo-time trajectory analysis confirmed that the maturing cone precursor was the cellular origin of RB in cancerous organoids. Notably, the PI3K-AKT pathway, a key cancer-related signaling pathway in RB tumorigenesis, is dysregulated and its activator, spleen tyrosine kinase (SYK), is significantly upregulated in retinal organoids, which could be the basis for the development of potential drugs targeting SYK (9). Collin et al. performed the first scRNA-seq and single-cell assay for transposase-accessible chromatin sequencing (scATAC-Seq) of primary RB samples from patients (10). A total of 8,086 cells from the two samples were sorted into 18 cell clusters, five of which (i.e., clusters 2, 8, 11, 12, and 14) were in the G2/M phase, and 13 of which (i.e., clusters 0–9, 11, 12, and 14) were identified as cone precursors. The researchers then performed a pseudo-time analysis of cone clusters and suggested that G2/M cone precursors (i.e., clusters 2, 8, 12, and 14) were the cellular origin of RB, corroborating the findings mentioned above. To further explore the molecular mechanisms that cause cone proliferation during the development of the human retina, researchers performed scRNA-Seq and scATAC-Seq of nine retinal samples and two RB samples. Two RB tumor-specific cone subclusters were identified, and each subcluster was characterized by the activation of individual upstream regulators and signaling pathways, leading to the dysregulation of p21 and p53 which further enabled the escape from apoptosis and cell cycle arrest. The authors also proposed that cellular apoptosis is mediated by p53 as the final compromised event in the two subclusters. These findings not only demonstrate tumor heterogeneity in RB, but also provide insight into the potential molecular pathways that could be targeted in the treatment of RB.

Yang et al. sorted 14,739 cells from two RB tumor samples into 10 clusters based on single-cell transcriptomic profiles, observing that the major cell types were cone precursors and RB cells (11). An analysis of the specific developmental trajectory of the RB revealed two subtypes of cone precursors (i.e., clusters 7 and 8) at branch point 2, with RB cells present after two branches. The cell trajectory was separated into five states based on the branches. State 3 launched the delamination of the RB, and state 5 was characterized by the high level of expression of cell cycle-related genes and a gradual shift in the malignancy process. In addition, *UBE2C*, which is abundant in state 5 of RB cell cluster 5, plays a crucial role in RB progression and represents a potential therapeutic target.

Tumor heterogeneity can also be examined from another perspective, focusing on the diversity of the expression and function of tumor subsets. To gain an insight into the intratumoral heterogeneity of RB, a previous group analyzed the single-cell transcriptome and whole exome of patients with RB (12). The authors noted that the principal cell types in RB were cone precursor-like (CP-like) cells and *MKI67*+ cone precursor (*MKI67*+ *CP*) cells, with a few cells maintaining the features of normal retinal photoreceptor cells. Their analysis of RB phenotypes identified the C7 and C10 subtypes of *MKI67*+ CP cells as more malignant, whereas CP-like cells were thought to reflect a transitional state between normal cells and *MKI67*+ CP cells. RB samples presented large clonal heterogeneity and the malignant *MKI67*+ CP cells exhibited greater changes in copy number. Importantly, both tumorigenic cell subpopulations and normal cells were present in RB, and the degree of malignancy in the tumorigenic cell subpopulations varied, which fully supports the intratumoral heterogeneity of RB.

UM is a highly heterogeneous malignant tumor. By performing clustering analysis on six freshly collected primary UM tumor samples, Pandiani et al. found that most cells could be grouped by tumor of origin, supporting the notion of intertumoral heterogeneity (13). Furthermore, unbiased clustering produced 12 clusters; among them, clusters 2, 4, 7, 8, and 10 were related to poor prognosis. Using

single-cell regulatory network inference and clustering technology, they found that clustered regulons (*RELB, HES6, HSF1*, and *MYC*) are associated with a poor prognosis. Depletion of *HES6* (an enhancer of split family basic helix–loop–helix transcription factor 6) has also been shown to weaken disseminative, migratory, and proliferative abilities both *in vitro* and *in vivo* in primary UM. Furthermore, Sun et al. integrated the scRNA-seq dataset from 33 samples (19 patients with primary UM, three patients with metastatic UM, and 11 healthy controls); up to 222,075 cells were classified into 12 clusters, and the UM samples mainly consisted of melanocytes, B cells, T cells, and macrophages (14). Melanocytic carcinogenesis was also accompanied by immune cell infiltration. Researchers have further explored the low immune response in UM, revealing a reduction in the expression of the secreted phosphoprotein 1 signaling pathway gene in melanocytes, which leads to inadequate immune stimulation. In addition, the expression of the major histocompatibility complex class I pathway is increased in T cells, B cells, and macrophages, indicating immune dysfunction in the microenvironment.

Using SCS data from 17 patients with UM, researchers clustered 52,228 cells into 10 clusters (15). Among clusters 1, 3, 5, and 6, a high proportion of metastatic cells was observed. Cluster 5 revealed the most significant differences between primary and metastatic UM, with a high level of expression of GZMB, GPR183, and AREG, which are related to the immune response. In addition, cells in cluster 5 communicated frequently with other cells via the *IL10, SELPLG, EPHB,* and *ITGB2* signaling pathways, which may predict survival outcomes. A previous study analyzed the genomic profiles of two metastatic liver nodules, WL02 and WL03, in a patient with UM (16). Both samples were infiltrated by a high number of hepatic stellates and immune cells. Hepatic stellate and endothelial cells were abundant in WL02, whereas WL03 was enriched with T cells. Tumor cells in WL02 displayed a migratory tendency, with the enrichment of epithelial–mesenchymal transition, myogenesis, coagulation, and hypoxia genes, most of which were in an active proliferative state. These data demonstrate the complexity of UM liver metastases and highlight the importance of a precise assessment of heterogeneity when selecting the most suitable individual therapy for UM.

3 Tumor microenvironment

The TME consists of heterogeneous cells, including tumor cells and the surrounding non-neoplastic cells, such as immune, vascular, and fibroblast cell types. The interaction between tumor cells and their surrounding TME is related to the treatment response and prognosis in patients with malignancies (17). Previous studies have reported the existence of stromal cells in the TME of RB, specifically, retinal astrocytes that stimulate the proliferation of cone-like RB cells and macrophages that enhance RB progression (18–20). However, the molecular interactions between the TME and RB tumor cells are not yet fully understood. Wu et al. used SCS to study the effect of tumor and immune cells on the progression of RB (12). They found that the TME in RB consists of astrocyte-like tumor-associated macrophages (TAMs) and cancer-associated fibroblasts. During the tumor invasion process, the proportion of TAMs is reduced and M1-type macrophages are lost, which acts to suppress TAM-related immune functions and create an immunosuppressive microenvironment. TAMs self-regulate via the inhibition of the *CCL* and GALECTIN signaling pathways, while regulating tumor cells via the *GRN* and *MIF* signaling pathways. These findings provide new molecular insights into the TME of RB.

Accumulating evidence regarding the immune microenvironment has increased attention on pyroptosis, ferroptosis, and necroptosis as potential approaches for tumor management. Xie et al. integrated the SCS datasets of 11 UM samples and sorted the cells into low- and high-necroptosis groups according to the number of necroptosis genes in the individual cells (21). Using comprehensive bioinformatic technologies, they constructed the first necroptosis-associated prognostic model for UM. The high-necroptosis group exhibited stronger immune cell infiltration, including infiltration by M2 macrophages and T cells. Although a high necroptosis score is associated with poor prognosis, evidence to date regarding the value of certain immune checkpoint inhibitors for increasing therapeutic efficacy has been encouraging. Zhang et al. constructed a hypoxia-related prognostic model by integrating scRNA-seq and RNA-seq data (22). They depicted differences in the immune landscape of patients with UM between high- and low-risk groups. Their analyses revealed that follicular helper T cells, CD8+ T cells, activated natural killer (NK) cells, and gamma and delta T cells were significantly increased in high-risk groups, whereas naive B cells, memory resting CD4 T cells, resting mast cells, activated mast cells, resting NK cells, and monocytes were significantly increased in low-risk groups. Another study devised a prognostic model based on immune-related genes, including *S100A13*, *MMP9*, and *SEMA3B*, in which patients were divided into two groups (23). The TME landscape differed significantly between the two groups: antigen-presenting cells and dendritic cells were enriched in the high-risk group, whereas macrophage cells were more abundant in the low-risk group. Functional analysis revealed that knockdown of *S100A13* inhibited UM cell migration and proliferation, with an increase in reactive oxygen species-associated markers, whereas the reactive oxygen species pathway was most abundant in NK cells and platelet cells. These findings may help researchers identify new and efficient targets for immunotherapy.

BRCA1-associated protein 1 (BAP1) may be mutated in UM, leading to metastasis and a poor prognosis. Mutations in BAP1 have been identified in more than 80% of UM cases, and approximately 28% of patients with germline BAP1 alterations are diagnosed with UM, usually leading to metastasis within 5 years (24). Kaler et al. analyzed scRNA-seq data from 11 UM tumor samples and confirmed that BAP1 loss can lead to an increase in PROS1 expression in class 2 UM (characterized by poor prognosis and high metastatic risk) cells while increasing MERTK expression in CD163+ macrophages (25). This in turn stimulates macrophages into an anti-inflammatory M2-polarized state, following which M2-polarized macrophages secrete cytokines that suppress T cells and other types of immune cell. Ultimately, this generates an immunosuppressive microenvironment in UM tissue, which may be associated with therapeutic resistance to tebentafusp. Similarly, Figueiredo et al. found that the loss of BAP1 was related to suppressive immune responses, and that some genes containing

CD38, CD74, and *HLA-DR* established an immunosuppressive axis following the loss of BAP1 (26). Single-cell analysis of five primary UM samples verified this hypothesis and revealed that infiltrating immune cells, including tumor-associated macrophages and regulatory CD8+ T lymphocytes, play a crucial role in generating the immunosuppressive TME in UM. Baqai et al. demonstrated that BAP1 loss in UM is associated with the upregulated expression of cell adhesion molecules (CADMs), such as E-cadherin, CADM1, and syndecan-2 (27). Comparing scRNA-seq data for BAP1 from wild and mutant type UM samples, researchers also reported that the upregulation of CADMS predominantly occurs in UM tumor cells. Interestingly, in the scRNA-seq data, two samples had cells that frequently expressed CADM1; however, not all BAP1 mutant cells exhibited increased levels of E-cadherin or CADM1. These findings provide new insights into the role of BAP1 in the development of UM.

4 Drug resistance

Chemotherapy is an important supplementary treatment for eye protection in patients with RB or UM, and slowing the emergence of chemical resistance remains the top treatment priority. Tumor heterogeneity is the main cause of tumor metastasis and drug resistance. Long-term and extensive use of chemotherapy drugs promotes tumor invasion and metastasis, which can occur easily in drug-resistant cells (28). Carboplatin is widely used to treat RB. A previous study explored the mechanisms of early resistance to carboplatin, which may derive from transcriptomic rearrangement via the PI3K/AKT signaling pathway, including metabolic adaption and the increase in transcription of the *ABCB1* transporter, instead of deriving from a minority of chemoresistant stem cells (29). Their results provide powerful evidence that can aid the development of pharmacological inhibitors, such as *ABCB1* transporter inhibitors, which can mitigate the emergence of drug resistance.

Using SCS technology, researchers have demonstrated that human melanoma cells are characterized by transcriptional variability. Such variability manifests as the infrequent and semi-coordinated transcription of drug resistance markers at a high level in some cells, which may aid in predicting which cells will develop drug resistance. These cells undergo epigenetic reprogramming after treatment with drugs and gradually develop a stable drug-resistant state (30). Rambow et al. demonstrated that the enrichment of neural crest stem cells, which are key drivers of drug resistance, in minimal residual disease in melanoma is mainly caused by *de novo* phenotypic transitions through transcriptional reprogramming, rather than by the enrichment of uncommon pre-existing cells (31).

Immune checkpoint inhibitor therapy has shown excellent efficacy for tumor treatment; nonetheless, recent studies have shown that programmed cell death protein 1 (PD1) and cytotoxic T lymphocyte-associated antigen-4 (CTLA4) blockades for the treatment of metastatic UM are ineffective (32). Using scRNA-seq V(D)J analysis, Durante et al. revealed clonally expanded T cells and/or plasma cells in tumor samples, indicating that tumor-infiltrating immune cells can mount a response and suggesting that poor tumor mutation may not be the only reason for the poor response of UM to checkpoint inhibitors (33). They also found that tumor-infiltrating immune cells in UM samples contained CD8+ T cells, which had not been previously recognized, and that they mainly expressed the checkpoint marker *LAG3* rather than *PD1* or CTLA4. LAG3, a soluble lymphocyte activation gene 3 protein, is an immune checkpoint inhibitor with a strong synergistic effect with PD-1 and may be a promising cancer treatment in the future (34). A previous study also noted that the combination of LAG-3 and PD-1 contributed to meaningful antidrug resistance and antitumor activity in metastatic UM; however, further clinical research is needed (35).

5 Conclusion and discussion

Owing to tremendous advancements in our understanding of RB and UM, strategies for local tumor control and the probability of salvaging the eyeball have vastly improved. However, metastasis remains common, representing a significant barrier to good prognosis (36). The TME affects genesis, progression, metastasis, and response to treatment and has been deemed a therapeutic target in various forms of malignancy. Cancer is a dynamically evolving disease, and tumor cells generally become spatially and temporally heterogeneous, which may be a major obstacle to treatment (37). SCS studies have provided new insights into the inherent complexity of RB and UM as well as their TMEs, which paves the way for early screening, personalized treatment strategies, and survival outcome prediction.

Tissue biopsy is the gold standard for establishing a diagnosis of cancer; however, tissue biopsy of intraocular malignancy is difficult and may increase the risk of extraocular dissemination. Liquid biopsy—a convenient, safe, and repeatable biopsy technology—is increasingly used to detect, analyze, and monitor various types of cancer, including RB and UM (38–40). Recent studies have demonstrated that the aqueous humor can be safely sampled during RB management, and analyses of tumor-derived cell-free DNA and DNA methylation in the aqueous humor can provide insights into the characteristics of RB (41–44). In previous studies, circulating tumor DNA in blood specimens and the aqueous humor as well as soluble human leukocyte antigen and angiopoietin 2 in the aqueous humor were identified as potential prognostic factors for UM (45–48). Researchers have also used SCS technology to study circulating cells in the cerebrospinal fluid, providing a new insight into the diagnosis and therapy of neurologic diseases (49). The combination of SCS and liquid biopsy may represent a new approach for the detection, monitoring, and evaluation of the risk of metastasis in RB and UM.

Despite the advantages of SCS, it has several limitations for the management of intraocular malignancies. First, a sufficient quantity of cells must be sampled to ensure that all cell types can be labeled. However, obtaining intraocular tumor tissue is more difficult than obtaining tissue from solid tumors at other anatomical sites, and there are often insufficient cells in aqueous humor samples. Second, the obtaining and storing of samples requires further refinement to

reduce cellular injury. Third, although the cost of analysis per cell has been reduced to an acceptable level using the current system, the comprehensive sequencing price is extremely high for thousands of cell types in a sample, hindering its broad application in tumor research. Finally, SCS may provide a large amount of information, and to better understand the results and fully quantify biological variations, more advanced and convenient computational strategies are required.

In summary, SCS has provided a promising future for studying tumor heterogeneity and the TME, knowledge of which is crucial for improving our diagnostic methods, biomarkers, therapeutic strategies, and methods of predicting prognosis. The broad use of SCS may improve knowledge regarding intraocular tumors and promote the development of individual therapeutic regimens to prevent tumor metastasis and relapse while improving survival outcomes.

Author contributions

R-lW, J-dZ, and YS designed and supervised the study. L-fH, PM, and C-hY wrote the manuscript. CH helped to conceptualize the manuscript. All authors contributed to the article and approved the submitted version.

Funding

This work was supported by grants from the National Natural Science Foundation of China (81570885 and 81770959), Talent Development Program of Changzheng Hospital (YQ722), Youth Initial Found of Naval Medicine University (2022DN078), and Foundation of Shanghai Health Bureau (201402014).

Conflict of interest

The authors declare that the research was conducted in the absence of any commercial or financial relationships that could be construed as a potential conflict of interest.

Publisher's note

All claims expressed in this article are solely those of the authors and do not necessarily represent those of their affiliated organizations, or those of the publisher, the editors and the reviewers. Any product that may be evaluated in this article, or claim that may be made by its manufacturer, is not guaranteed or endorsed by the publisher.

References

1. Jager MJ, Shields CL, Cebulla CM, Abdel-Rahman MH, Grossniklaus HE, Stern MH, et al. Uveal melanoma. *Nat Rev Dis Primers.* (2020) 6(1):24. doi: 10.1038/s41572-020-0158-0

2. Farhat W, Yeung V, Ross A, Kahale F, Boychev N, Kuang L, et al. Advances in biomaterials for the treatment of retinoblastoma. *Biomater Sci* (2022) 10(19):5391–429. doi: 10.1039/d2bm01005d

3. Global Retinoblastoma Study G. The global retinoblastoma outcome study: a prospective, cluster-based analysis of 4064 patients from 149 countries. *Lancet Glob Health* (2022) 10(8):e1128–e40. doi: 10.1016/S2214-109X(22)00250-9

4. Damato B. Ocular treatment of choroidal melanoma in relation to the prevention of metastatic death - a personal view. *Prog Retin Eye Res* (2018) 66:187–99. doi: 10.1016/j.preteyeres.2018.03.004

5. Khoja L, Atenafu EG, Suciu S, Leyvraz S, Sato T, Marshall E, et al. Meta-analysis in metastatic uveal melanoma to determine progression free and overall survival benchmarks: an international rare cancers initiative (IRCI) ocular melanoma study. *Ann Oncol* (2019) 30(8):1370–80. doi: 10.1093/annonc/mdz176

6. Gu L, Ma G, Li C, Lin J, Zhao G. New insights into the prognosis of intraocular malignancy: interventions for association mechanisms between cancer and diabetes. *Front Oncol* (2022) 12:958170. doi: 10.3389/fonc.2022.958170

7. Wu F, Fan J, He Y, Xiong A, Yu J, Li Y, et al. Single-cell profiling of tumor heterogeneity and the microenvironment in advanced non-small cell lung cancer. *Nat Commun* (2021) 12(1):2540. doi: 10.1038/s41467-021-22801-0

8. Lei Y, Tang R, Xu J, Wang W, Zhang B, Liu J, et al. Applications of single-cell sequencing in cancer research: progress and perspectives. *J Hematol Oncol* (2021) 14 (1):91. doi: 10.1186/s13045-021-01105-2

9. Liu H, Zhang Y, Zhang YY, Li YP, Hua ZQ, Zhang CJ, et al. Human embryonic stem cell-derived organoid retinoblastoma reveals a cancerous origin. *Proc Natl Acad Sci U S A.* (2020) 117(52):33628–38. doi: 10.1073/pnas.2011780117

10. Collin J, Queen R, Zerti D, Steel DH, Bowen C, Parulekar M, et al. Dissecting the transcriptional and chromatin accessibility heterogeneity of proliferating cone precursors in human retinoblastoma tumors by single cell sequencing-opening pathways to new therapeutic strategies? *Invest Ophthalmol Vis Sci* (2021) 62(6):18. doi: 10.1167/iovs.62.6.18

11. Yang J, Li Y, Han Y, Feng Y, Zhou M, Zong C, et al. Single-cell transcriptome profiling reveals intratumoural heterogeneity and malignant progression in retinoblastoma. *Cell Death Dis* (2021) 12(12):1100. doi: 10.1038/s41419-021-04390-4

12. Wu C, Yang J, Xiao W, Jiang Z, Chen S, Guo D, et al. Single-cell characterization of malignant phenotypes and microenvironment alteration in retinoblastoma. *Cell Death Dis* (2022) 13(5):438. doi: 10.1038/s41419-022-04904-8

13. Pandiani C, Strub T, Nottet N, Cheli Y, Gambi G, Bille K, et al. Single-cell RNA sequencing reveals intratumoral heterogeneity in primary uveal melanomas and identifies HES6 as a driver of the metastatic disease. *Cell Death Differ* (2021) 28 (6):1990–2000. doi: 10.1038/s41418-020-00730-7

14. Sun S, Guo B, Xu L, Shi R. Integrated analysis reveals the dysfunction of signaling pathways in uveal melanoma. *BMC Cancer.* (2022) 22(1):734. doi: 10.1186/s12885-022-09822-8

15. Sun S, Shi R, Xu L, Sun F. Identification of heterogeneity and prognostic key genes associated with uveal melanoma using single-cell RNA-sequencing technology. *Melanoma Res* (2022) 32(1):18–26. doi: 10.1097/CMR.0000000000000783

16. Lin W, Beasley AB, Ardakani NM, Denisenko E, Calapre L, Jones M, et al. Intra- and intertumoral heterogeneity of liver metastases in a patient with uveal melanoma revealed by single-cell RNA sequencing. *Cold Spring Harb Mol Case Stud* (2021) 7(5): a006111. doi: 10.1101/mcs.a006111

17. Potter SS. Single-cell RNA sequencing for the study of development, physiology and disease. *Nat Rev Nephrol.* (2018) 14(8):479–92. doi: 10.1038/s41581-018-0021-7

18. Quail DF, Joyce JA. Microenvironmental regulation of tumor progression and metastasis. *Nat Med* (2013) 19(11):1423–37. doi: 10.1038/nm.3394

19. Xu XL, Lee TC, Offor N, Cheng C, Liu A, Fang Y, et al. Tumor-associated retinal astrocytes promote retinoblastoma cell proliferation through production of IGFBP-5. *Am J Pathol* (2010) 177(1):424–35. doi: 10.2353/ajpath.2010.090512

20. Pina Y, Boutrid H, Murray TG, Jager MJ, Cebulla CM, Schefler A, et al. Impact of tumor-associated macrophages in LH(BETA)T(AG) mice on retinal tumor progression: relation to macrophage subtype. *Invest Ophthalmol Vis Sci* (2010) 51 (5):2671–7. doi: 10.1167/iovs.09-4255

21. Xie J, Chen L, Tang Q, Wei W, Cao Y, Wu C, et al. A necroptosis-related prognostic model of uveal melanoma was constructed by single-cell sequencing analysis and weighted Co-expression network analysis based on public databases. *Front Immunol* (2022) 13:847624. doi: 10.3389/fimmu.2022.847624

22. Zhang X, Qiu J, Huang F, Han P, Shan K, Zhang C. Construction and verification of a hypoxia-related nine-gene prognostic model in uveal melanoma based on integrated single-cell and bulk RNA sequencing analyses. *Exp Eye Res* (2022) 223:109214. doi: 10.1016/j.exer.2022.109214

23. Wang W, Zhao H, Wang S. Identification of a novel immune-related gene signature for prognosis and the tumor microenvironment in patients with uveal melanoma combining single-cell and bulk sequencing data. *Front Immunol* (2023) 14:1099071. doi: 10.3389/fimmu.2023.1099071

24. Louie BH, Kurzrock R. BAP1: not just a BRCA1-associated protein. *Cancer Treat Rev* (2020) 90:102091. doi: 10.1016/j.ctrv.2020.102091

25. Kaler CJ, Dollar JJ, Cruz AM, Kuznetsoff JN, Sanchez MI, Decatur CL, et al. BAP1 loss promotes suppressive tumor immune microenvironment via upregulation of PROS1 in class 2 uveal melanomas. *Cancers (Basel)* (2022) 14(15):3678. doi: 10.3390/cancers14153678

26. Figueiredo CR, Kalirai H, Sacco JJ, Azevedo RA, Duckworth A, Slupsky JR, et al. Loss of BAP1 expression is associated with an immunosuppressive microenvironment in uveal melanoma, with implications for immunotherapy development. *J Pathol* (2020) 250(4):420–39. doi: 10.1002/path.5384

27. Baqai U, Purwin TJ, Bechtel N, Chua V, Han A, Hartsough EJ, et al. Multi-omics profiling shows BAP1 loss is associated with upregulated cell adhesion molecules in uveal melanoma. *Mol Cancer Res* (2022) 20(8):1260–71. doi: 10.1158/1541-7786.MCR-21-0657

28. Han Y, Wang D, Peng L, Huang T, He X, Wang J, et al. Single-cell sequencing: a promising approach for uncovering the mechanisms of tumor metastasis. *J Hematol Oncol* (2022) 15(1):59. doi: 10.1186/s13045-022-01280-w

29. Zhang MG, Kuznetsoff JN, Owens DA, Gallo RA, Kalahasty K, Cruz AM, et al. Early mechanisms of chemoresistance in retinoblastoma. *Cancers (Basel)* (2022) 14 (19):4966. doi: 10.3390/cancers14194966

30. Shaffer SM, Dunagin MC, Torborg SR, Torre EA, Emert B, Krepler C, et al. Rare cell variability and drug-induced reprogramming as a mode of cancer drug resistance. *Nature.* (2017) 546(7658):431–5. doi: 10.1038/nature22794

31. Rambow F, Rogiers A, Marin-Bejar O, Aibar S, Femel J, Dewaele M, et al. Toward minimal residual disease-directed therapy in melanoma. *Cell.* (2018) 174 (4):843–55.e19. doi: 10.1016/j.cell.2018.06.025

32. Heppt MV, Steeb T, Schlager JG, Rosumeck S, Dressler C, Ruzicka T, et al. Immune checkpoint blockade for unresectable or metastatic uveal melanoma: a systematic review. *Cancer Treat Rev* (2017) 60:44–52. doi: 10.1016/j.ctrv.2017.08.009

33. Durante MA, Rodriguez DA, Kurtenbach S, Kuznetsov JN, Sanchez MI, Decatur CL, et al. Single-cell analysis reveals new evolutionary complexity in uveal melanoma. *Nat Commun* (2020) 11(1):496. doi: 10.1038/s41467-019-14256-1

34. Andrews LP, Marciscano AE, Drake CG, Vignali DA. LAG3 (CD223) as a cancer immunotherapy target. *Immunol Rev* (2017) 276(1):80–96. doi: 10.1111/imr.12519

35. Atkinson V, Khattak A, Haydon A, Eastgate M, Roy A, Prithviraj P, et al. Eftilagimod alpha, a soluble lymphocyte activation gene-3 (LAG-3) protein plus pembrolizumab in patients with metastatic melanoma. *J Immunother Cancer* (2020) 8(2). doi: 10.1136/jitc-2020-001681

36. Vasalaki M, Fabian ID, Reddy MA, Cohen VM, Sagoo MS. Ocular oncology: advances in retinoblastoma, uveal melanoma and conjunctival melanoma. *Br Med Bull* (2017) 121(1):107–19. doi: 10.1093/bmb/ldw053

37. Dagogo-Jack I, Shaw AT. Tumour heterogeneity and resistance to cancer therapies. *Nat Rev Clin Oncol* (2018) 15(2):81–94. doi: 10.1038/nrclinonc.2017.166

38. Nikanjam M, Kato S, Kurzrock R. Liquid biopsy: current technology and clinical applications. *J Hematol Oncol* (2022) 15(1):131. doi: 10.1186/s13045-022-01351-y

39. de Bruyn DP, Beasley AB, Verdijk RM, van Poppelen NM, Paridaens D, de Keizer ROB, et al. Is tissue still the issue? the promise of liquid biopsy in uveal melanoma. *Biomedicines* (2022) 10(2):506. doi: 10.3390/biomedicines10020506

40. Kim ME, Polski A, Xu L, Prabakar RK, Peng CC, Reid MW, et al. Comprehensive somatic copy number analysis using aqueous humor liquid biopsy for retinoblastoma. *Cancers (Basel)* (2021) 13(13):3340. doi: 10.3390/cancers13133340

41. Li HT, Xu L, Weisenberger DJ, Li M, Zhou W, Peng CC, et al. Characterizing DNA methylation signatures of retinoblastoma using aqueous humor liquid biopsy. *Nat Commun* (2022) 13(1):5523. doi: 10.1038/s41467-022-33248-2

42. Xu L, Kim ME, Polski A, Prabakar RK, Shen L, Peng CC, et al. Establishing the clinical utility of ctDNA analysis for diagnosis, prognosis, and treatment monitoring of retinoblastoma: the aqueous humor liquid biopsy. *Cancers* (2021) 13(6):1282. doi: 10.3390/cancers13061282

43. Berry JL, Xu L, Kooi I, Murphree AL, Prabakar RK, Reid M, et al. Genomic cfDNA analysis of aqueous humor in retinoblastoma predicts eye salvage: the surrogate tumor biopsy for retinoblastoma. *Mol Cancer Res* (2018) 16(11):1701–12. doi: 10.1158/1541-7786.MCR-18-0369

44. Munier FL, Soliman S, Moulin AP, Gaillard MC, Balmer A, Beck-Popovic M. Profiling safety of intravitreal injections for retinoblastoma using an anti-reflux procedure and sterilisation of the needle track. *Br J Ophthalmol* (2012) 96(8):1084–7. doi: 10.1136/bjophthalmol-2011-301016

45. Im DH, Peng CC, Xu L, Kim ME, Ostrow D, Yellapantula V, et al. Potential of aqueous humor as a liquid biopsy for uveal melanoma. *Int J Mol Sci* (2022) 23(11):6226. doi: 10.3390/ijms23116226

46. Wierenga APA, Gezgin G, van Beelen E, Eikmans M, Spruyt-Gerritse M, Brouwer NJ, et al. Soluble HLA in the aqueous humour of uveal melanoma is associated with unfavourable tumour characteristics. *Cancers* (2019) 11(8):1202. doi: 10.3390/cancers11081202

47. Ten Voorde AMW, Wierenga APA, Nell RJ, van der Velden PA, Luyten GPM, Verdijk RM, et al. In uveal melanoma, angiopoietin-2 but not angiopoietin-1 is increased in high-risk tumors, providing a potential druggable target. *Cancers* (2021) 13(16):3986. doi: 10.3390/cancers13163986

48. Bustamante P, Tsering T, Coblentz J, Mastromonaco C, Abdouh M, Fonseca C, et al. Circulating tumor DNA tracking through driver mutations as a liquid biopsy-based biomarker for uveal melanoma. *J Exp Clin Cancer Res* (2021) 40(1):196. doi: 10.1186/s13046-021-01984-w

49. Yekula A, Tracz J, Rincon-Torroella J, Azad T, Bettegowda C. Single-cell RNA sequencing of cerebrospinal fluid as an advanced form of liquid biopsy for neurological disorders. *Brain Sci* (2022) 12(7):812. doi: 10.3390/brainsci12070812

Frontiers in Immunology

Explores novel approaches and diagnoses to treat immune disorders.

The official journal of the International Union of Immunological Societies (IUIS) and the most cited in its field, leading the way for research across basic, translational and clinical immunology.

Discover the latest Research Topics

See more →

Frontiers

Avenue du Tribunal-Fédéral 34
1005 Lausanne, Switzerland
frontiersin.org

Contact us

+41 (0)21 510 17 00
frontiersin.org/about/contact